Vol. 156, January 1, 1984
Complete in one issue

ISSN 0003-2670

ANALYTICA CHIMICA ACTA

International journal devoted to all branches of analytical chemistry

ELSEVIER

ANALYTICA CHIMICA ACTA

International journal devoted to all branches of analytical chemistry
Revue internationale consacrée à tous les domaines de la chimie analytique
Internationale Zeitschrift für alle Gebiete der analytischen Chemie

PUBLICATION SCHEDULE FOR 1984

	J	F	M	A	M	J	J	A	S	O	N	D
Analytica Chimica Acta	156	157/1	157/2	158	159	160	161	162	163	164	165	166

Scope. *Analytica Chimica Acta* publishes original papers, short communications, and reviews dealing with every aspect of modern chemical analysis, both fundamental and applied.

Submission of Papers. Manuscripts (three copies) should be submitted as designated below for rapid and efficient handling:

Papers from the Americas to: Professor Harry L. Pardue, Department of Chemistry, Purdue University, West Lafayette IN 47907, U.S.A.

Papers from all other countries to: Dr. A. M. G. Macdonald, Department of Chemistry, The University, P.O. Box 363 Birmingham B15 2TT, England. Papers dealing particularly with computer techniques to: Professor J. T. Clerc Universität Bern, Pharmazeutisches Institut, Baltzerstrasse 5, CH-3012 Bern, Switzerland.

Submission of an article is understood to imply that the article is original and unpublished and is not being considered for publication elsewhere. Upon acceptance of an article by the journal, authors will be asked to transfer the copyright of the article to the publisher. This transfer will ensure the widest dissemination of information.

Information for Authors. Papers in English, French and German are published. There are no page charges Manuscripts should conform in layout and style to the papers published in this Volume. Authors should consult Vol. 150/2 for detailed information. Reprints of this information are available from the Editors or from: Elsevier Editorial Services Ltd., Mayfield House, 256 Banbury Road, Oxford OX2 7DH (Great Britain).

Reprints. Fifty reprints will be supplied free of charge. Additional reprints (minimum 100) can be ordered. An order form containing price quotations will be sent to the authors together with the proofs of their article.

Advertisements. Advertisement rates are available from the publisher.

Subscriptions. Subscriptions should be sent to: Elsevier Science Publishers B.V., Journals Department, P.O. Box 211, 1000 AE Amsterdam, The Netherlands. Tel: 5803 911, Telex: 18582.

Publication. *Analytica Chimica Acta* appears in 11 volumes in 1984. The subscription for 1984 (Vols. 156–166) is Dfl. 2145.00 plus Dfl. 231.00 (p.p.h.) (total approx. U.S. $950.40). All earlier volumes (Vols. 1–155) except Vols. 23 and 28 are available at Dfl. 200.00 (U.S. $80.00), plus Dfl. 15.00 (U.S. $6.00) p.p.h., per volume.

Our p.p.h. (postage, packing and handling) charge includes surface delivery of all issues, except to subscribers in the U.S.A., Canada and India who receive all issues by air delivery (S.A.L. — Surface Air Lifted) at no extra cost. For the rest of the world, airmail and S.A.L. charges are available upon request.

Claims for issues not received should be made within three months of publication of the issues. If not they cannot be honoured free of charge.

For further information, or a free sample copy of this or any other Elsevier Science Publishers journal, readers in the U.S.A. and Canada can contact the following address: Elsevier Science Publishing Co., Inc., Journal Information Center, 52 Vanderbilt Avenue, New York, NY 10017, U.S.A., Tel: (212) 867-9040.

ANALYTICA CHIMICA ACTA
VOL. 156 (1984)

ANALYTICA CHIMICA ACTA

International journal devoted to all branches of analytical chemistry

ELSEVIER Amsterdam–Oxford–New York–Tokyo

0003-2670/84/$03.0C

Printed in The Netherlands

Analytica Chimica Acta, 156 (1984) 1—8
Elsevier Science Publishers B.V., Amsterdam — Printed in The Netherlands

EVALUATION OF THE OPTIMUM COMPOSITION OF NEUTRAL-CARRIER MEMBRANE ELECTRODES WITH INCORPORATED CATION-EXCHANGER SITES

P. C. MEIER, W. E. MORF, M. LÄUBLI and W. SIMON*

Department of Organic Chemistry, Swiss Federal Institute of Technology (ETH), CH-8092 Zürich (Switzerland)

(Received 29th July 1983)

SUMMARY

Selectivities were measured for membrane electrodes containing a given amount of a neutral carrier (ETH 1692) and varying amounts of the additive potassium tetrakis(*p*-chlorophenyl)borate. The pronounced selectivity changes induced by the additive agreed with a theoretical model. Both theory and experiment confirmed that an optimum composition of the membrane exists. Ideally, sensors for monovalent cations should contain only small amounts of the additive, whereas sensors for divalent cations should contain a molar ratio of additive/carrier of about 0.7 (for 1:2 cation/carrier complexes). Also described are the new desk-computer programs used for the reduction, evaluation, and graphical presentation of ion-selective electrode data.

Neutral-carrier-based liquid membrane electrodes with incorporated anionic sites, e.g., tetraphenylborate ions, were introduced ten years ago [1, 2]. The addition of mobile cation-exchange sites was shown to be favorable in many respects, producing reduction of interferences by lipophilic sample anions, increase of the potentiometric selectivity for divalent over monovalent cations, reduction of the response time, reduction of the electric membrane resistance, and reduction of the activation barrier for the cation-exchange reaction at the membrane/solution interface; reviews have been published [3—5].

Here, a more in-depth investigation of the selectivity-modifying influence of charged components in neutral-carrier-based membrane electrodes is reported. To this end, potentiometric experiments were done on PVC liquid membranes containing *o*-nitrophenyl octyl ether (NPOE) as plasticizer, *N,N*-diisobutyl-*N'*-(*N''*-heptyl-*N''*-methyl)prolylamide-cyclohexane-*cis*-1,2-dicarboxamide (ETH 1692) as ion-selective carrier, and different amounts of the additive potassium-tetrakis(*p*-chlorophenyl)borate (KTpClPB). The experimental results as well as a theoretical treatment of such systems provide documentation that the molar ratio KTpClPB/ETH 1692 strikingly affects the ion selectivity. The evaluation and graphical presentation of numerical data was greatly simplified by custom-tailored computer programs.

0003-2670/84/$03.00

THEORETICAL

The e.m.f. response of liquid-membrane electrodes to samples containing the primary ion I^{z_i} may be described by the approximation

$$E = E_0 + (RT/z_iF) \ln (k_i a_i'/c_i) \tag{1}$$

where the second term corresponds to the interfacial potential difference between sample and ion-selective membrane, and E_0 includes all other potential contributions [3—5] The quantity a_i' is the sensed activity of primary ions in the sample solution, c_i is the concentration of the same species in the membrane surface, k_i is the ionic distribution coefficient, and R, T, and F have their usual meanings.

For cation-selective electrodes based on electrically neutral carrier ligands S, complexes of the type $IS_n^{z_i}$ (stability constant $\beta_{is,n}$) are formed in the membrane. The concentration of exchangeable free cations is then controlled by the complexation equilibria and depends on the concentration of uncomplexed carriers (c_s) and on that of anionic sites R^- in the membrane (c_r). In the absence of interfering ions, the conditions of electroneutrality and of conservation of carriers in the membrane (constant total concentration c_s^{tot}) require that

$$c_i + \sum_n c_{is,n} = c_i(1 + \sum_n \beta_{is,n} c_s^n) = c_r/z_i \tag{2}$$

$$c_s + \sum_n n c_{is,n} = c_s + \sum_n n\beta_{is,n} c_i c_s^n = c_s^{tot} \tag{3}$$

Combination of Eqns. 1—3 leads to the final result for the e.m.f. response

$$E = E_i^0 + (RT/z_iF) \ln a_i' \tag{4}$$

$$\text{with } E_i^0 = E_0 + (RT/z_iF) \ln (z_i K_i/c_r) \tag{5}$$

$$K_i = \sum_n \beta_{is,n} k_i c_s^n + k_i \tag{6}$$

$$c_s = c_s^{tot} - [(\sum_n n c_{is,n})/(c_i + \sum_n c_{is,n})] (c_r/z_i) = c_s^{tot} - \bar{n}_i c_r/z_i \tag{7}$$

where $\bar{n}_i$ is the mean degree of complexation of the primary ion in the membrane surface. If complexes of a given stoichiometry $1{:}n_i$ are presumed to predominate, the following approximation can be derived for the overall distribution parameter [3]

$$K_i \approx \beta_{is} k_i [c_s^{tot} - (n_i c_r/z_i)]^{n_i} + k_i \tag{8}$$

This implies that the extraction-enhancing effect of cation carriers becomes highest for membrane systems with $n_i c_r/z_i \ll c_s^{tot}$, i.e., $K_i \approx \beta_{is} k_i (c_s^{tot})^{n_i}$, but rapidly vanishes for $n_i c_r/z_i \to c_s^{tot}$, i.e., $K_i \approx k_i$.

Analogous expressions hold for the electrode response to separate solutions of interfering cations J^{z_j}, e.g.,

$$K_j = \sum_n \beta_{js,n} k_j c_s^n + k_j \tag{9}$$

$$c_s = c_s^{tot} - \bar{n}_j c_r / z_j \tag{10}$$

Hence the potentiometric selectivity of the sensor for interfering ions relative to the primary ion (K_{ij}^{pot}, separate solution method) is determined as follows [3—5]

$$E = E_i^0 + \frac{RT}{z_i F} \ln[K_{ij}^{pot} a_j^{z_i/z_j}] \tag{11}$$

$$K_{ij}^{pot} = [z_j K_j / c_r]^{z_i/z_j} / [z_i K_i / c_r] \tag{12}$$

Considering Eqns. 6—10, it can be recognized that the cation selectivity of neutral-carrier-based membranes may be highly sensitive to changes in the concentration of anionic membrane components. Generally, stepwise changes in the selectivity coefficients are expected for $c_r \rightarrow c_s^{tot} z_j/\bar{n}_j$ (decrease of K_j and of K_{ij}^{pot}) and for $c_r \rightarrow c_s^{tot} z_i/\bar{n}_i$ (decrease of K_i, increase of K_{ij}^{pot}). An additional selectivity "drift" with varying c_r is superimposed in cases where $z_i \neq z_j$ [3—5] (see Eqn. 12).

The present theoretical analysis may be used to provide detailed information on the optimum composition of neutral carrier membranes yielding the highest possible carrier-induced selectivity for the respective primary ion. Calculations based on Eqns. 1—3, assuming the same $1{:}n$ stoichiometry for all cationic complexes, lead to the following results

electrodes for monovalent cations I^+: $c_r \rightarrow 0$ (all n)

electrodes for divalent cations I^{2+}: $c_r = 1.62\ c_s^{tot}$ ($n = 1$), $c_r = 0.73\ c_s^{tot}$ ($n = 2$), $c_r = 0.46\ c_s^{tot}$ ($n = 3$)

EXPERIMENTAL

Ion-selective liquid membranes were prepared according to the now classical formula [3—5] that typically prescribes 1 wt.-% neutral carrier (ETH 1692), about 65 wt.-% plasticizer (NPOE), about 33 wt.-% PVC, and additive (KTpClPB). The amount of the membrane component KTpClPB, best expressed in mol-% relative to the ligand ETH 1692, was varied, i.e., 0, 52, 61, 63, 77, 91, 97, 105, 151, and 207 mol-%. The procedure, which has been given in detail [6, 7], yields membranes with a diameter of 24 mm and a thickness of 200 μm. Disks of 7-mm diameter were cut from the raw product and were mounted in standard electrode shafts (Philips model IS-561). The e.m.f. measurements for selectivity determinations were effected according to the separate solutions method [8] using 0.1 M solutions of the chlorides of H_3O^+, Li^+, Na^+, K^+, Rb^+, Cs^+, NH_4^+, Mg^{2+}, Ca^{2+}, Sr^{2+}, and Ba^{2+}. The equipment used for the potentiometric measurements was as specified earlier [9].

The membrane containing 91 mol-% KTpClPB was used to obtain an e.m.f. response function in pure magnesium chloride solution. For membranes

containing the synthetic ligand *N,N'*-diheptyl-*N,N'*-dimethyl-succinamide (ETH 1117 [3, 10]) and 71 mol-% KTpClPB, calibration curves for magnesium ions were measured on samples with and without a simulated intracellular background containing 0.01 M NaCl, 0.1 M KCl, and 1 μM $CaCl_2$.

RESULTS AND DISCUSSION

The potentiometric ion selectivities of ten neutral carrier membrane electrodes that differed only in the amount of the membrane component KTpClPB are illustrated in Fig. 1. The selectivity factors K^{pot}_{MgM} determined by the separate solutions method characterize the preference of the sensors for cations M^{z+} over the primary ions Mg^{2+}. Figures 1a and 1b convincingly show that the additive KTpClPB, a lipophilic salt that introduces permanent anionic sites into the membrane, has a decisive effect on the cation-extraction and e.m.f.-response behavior of the electrodes. The most obvious implications are as follows (see Theoretical section). First, the remarkable shifts of the selectivity factors for the alkali metal ions relative to magnesium ion near the additive/ligand ratios of 50 and 100 mol-% indicate that these cations predominantly or at least partly form 1:2 complexes with the carrier ETH 1692. On going from 0 to 207 mol-% KTpClPB, the decrease in the free ligand concentration leads to a significant reduction of the selectivity for alkali ions (near 50 mol-%) and for magnesium ion (near 100 mol-%). Hence the selectivity sequence for alkali metal ions is found to be reversed: the K^{pot}_{MgM} values obtained for membranes with zero mol-% additive reflect the complexation selectivity of the carrier ligands, while the selectivity coefficients induced by 207 mol-% KTpClPB roughly correspond to those of pure liquid ion-exchanger membranes (i.e. without cation carriers) [4, 5, 11]. Secondly, the selectivity factors for calcium, strontium, and barium ions (relative to magnesium ion) are less sensitive to changes in the additive/ligand ratio. This implies that these cations all form complexes of the same stoichiometry (1:2). Thirdly, the carrier membranes with 0—91 mol-% KTpClPB exhibit a striking selectivity for the hydrogen ion and could serve as poor pH sensors. The pronounced selectivity decrease observed near 100 mol-% additive shows that the studied ligand ETH 1692 has a high affinity for protons and undergoes 1:1 complexation with this species.

The experimental evidence given in Fig. 1, as well as the preceding theoretical analysis, for the first time unambiguously proves that one and the same neutral carrier membrane may acquire completely different selectivity characteristics depending on the amount of anionic membrane components. Thus, for neutral or alkaline sample solutions, the membrane evidently prefers Li^+ with <50 mol-% of the additive, Ca^{2+} in the range 50—80 mol-%, and Cs^+ for higher amounts of KTpClPB. If such sensors were designed for monitoring divalent cations, the best membrane (optimum selectivity) would be one containing about 70 mol-% anionic sites (Fig. 1). This nicely conforms to the theoretical predictions.

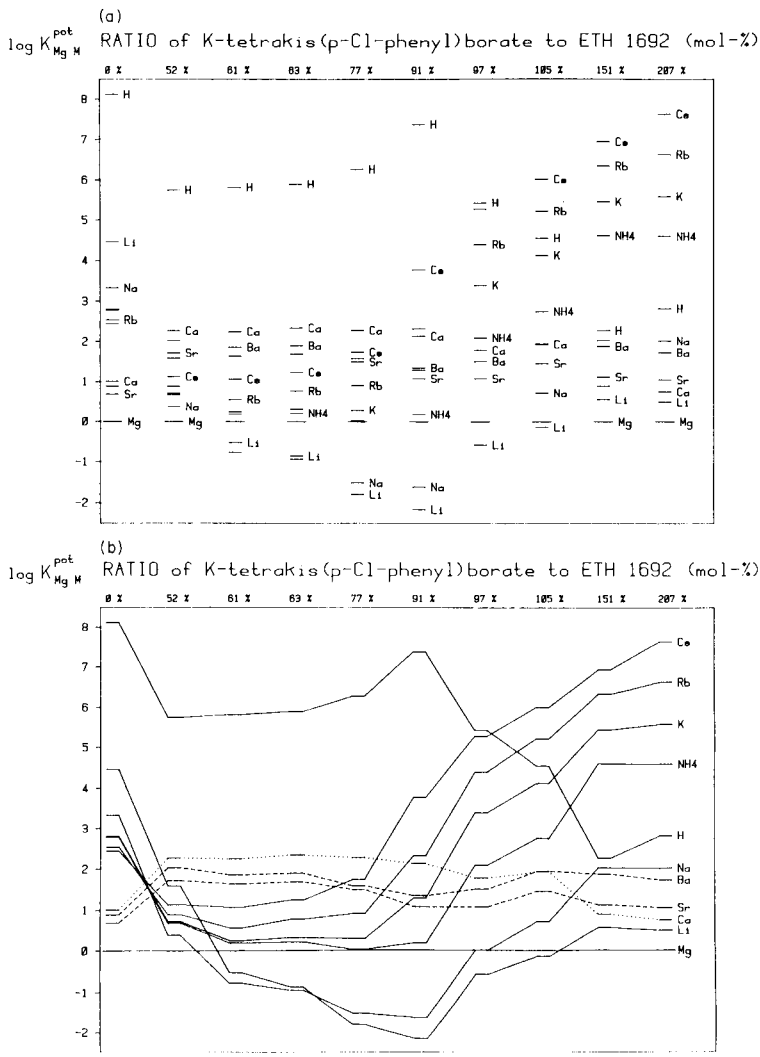

Fig. 1. Selectivity factors K^{pot}_{MgM} for the tested membrane compositions plotted on a logarithmic scale. A computer plot-program was used (a) A routine was invoked to label automatically the selectivity "bars" with the appropriate ion symbols, except where overlapping would occur; there, a manual mode was employed. (b) To make trends more visible, lines are plotted that connect the selectivity bars pertaining to a given ion.

The facts presented bear some important consequences. First, of course, the membrane composition of carrier-based ion-selective electrodes must be chosen very carefully. Secondly, the loss of minute quantities of TpClPB salts and/or ligands from the membrane, as a result of continuous exposure of the electrode to aqueous solutions [3, 12], could drastically alter the selectivity behavior. For example, the selectivity factors K^{pot}_{MgM} given in Fig. 1

for monovalent cations obviously change by a factor of $\approx 10^2$ when the additive/ligand ratio is varied from 91 to 97 mol-%. This difference of 6 mol-% corresponds to a change in the additive or ligand content of only some 10 μg (i.e., 20 nmol) per membrane.

A final experiment was done in order to demonstrate the loss of the ionic membrane component KTpClPB with increasing age of the sensor. To this end, carrier membranes containing 95 and 110 mol-% of the additive were soaked in 0.1 M $MgCl_2$ for one month. After this uninterrupted exposure, the measured potentiometric selectivity coefficients for fresh aqueous solutions indicated a reduction of the content of anionic sites of about 10—15 mol-%. Accordingly, there is a considerable loss of TpClPB salts which finally may limit the lifetime of neutral carrier membrane electrodes for divalent cations.

COMPUTER PROGRAMS FOR EVALUATION AND GRAPHICAL REPRESENTATION OF ION-SELECTIVE ELECTRODE MEASUREMENTS

The data reduction to obtain the selectivity sequences in Fig. 1 was achieved by using an EXTENDED BASIC program written for a desk-top computer (Hewlett-Packard HP-85, configuration: 32 K, Matrix, Printer/Plotter, I/O, and Advanced Programming ROMs, HP-7225 plotter). The program makes use of the Nicolski—Eisenman and the Henderson equations [3—5, 13]. The electrochemical data base contains parts of the NBS activity coefficient tables [14—17] and ionic mobilities from Milazzo [18]; 50 electrolytes are accessible. All calculations involve single-ion activity coefficients as described earlier [4, 13].

The measured e.m.f. values are processed according to the following scheme: (a) the single-ion activity coefficients are calculated; (b) the liquid-junction potentials arising at the reference electrode/sample solution interface are calculated and subtracted from the measured e.m.f. values; (c) the selectivity factors K^{pot} are calculated from such corrected e.m.f. differences (separate solution method) and ordered into a selectivity sequence. Twenty such sequences can be manipulated in the calculator and plotted. An example of the graphical capabilities is given in Fig. 1.

A second program is available that evaluates measured e.m.f. values and plots electrode response curves. Again the e.m.f. values are corrected for liquid-junction potentials and are then plotted versus the logarithm of the primary ion activity. Here a novel interpolation [19] of the activity coefficients recommended by NBS is implemented. Linear regression over a given activity range and fitting of the best Nicolski—Eisenman response curve are possible. The IUPAC-recommended detection limit [8, 20] is also indicated. An example is given in Fig. 2. In the case of the dashed curve, the detection limit is found near $\log a_{Mg} = -4.9$. With $\log K^{pot}_{MgNa} = -2.0$ and $\log K^{pot}_{MgCa} = -0.33$ (known from treatment analogous to Fig. 1) the value $\log K^{pot}_{MgK}$ is optimized to -1.67 to yield the dotted curve (detection limit $\log a_{Mg} = -3.9$,

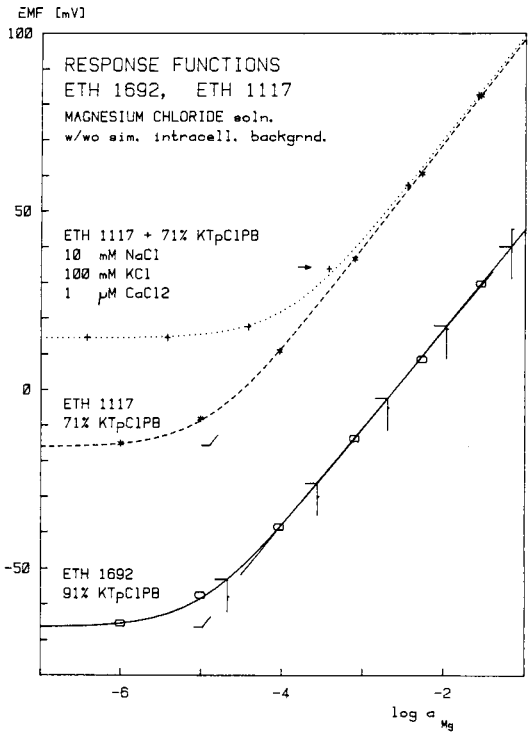

Fig. 2. Electrode response functions. (—) Response for a membrane containing 91 mol-% of KTpClPB and ligand ETH 1692; the function was measured for pure solutions of magnesium chloride at pH 7; the regression line is plotted in the interval $-4.5 < \log a_{Mg} < -1.3$; the detection limit is indicated by the intersection point of the two asymptotes to the Nicolski—Eisenman function. (---) Response to pure solutions of magnesium chloride at pH 7 for a membrane containing 71 mol-% KTpClPB and the ligand ETH 1117 (shifted by +50 mV). (···) Response of the same membrane to magnesium chloride solutions containing a fixed background of 0.01 M NaCl, 0.1 M KCl, and 0.000 001 M $CaCl_2$, also at pH 7.

RSD ± 0.8 mV). For the point marked with an arrow, an analysis suggests that Na^+ contributes 0.12%, K^+ 24.75%, Ca^{2+} 0.03%, and Mg^{2+} only 75.1% towards the sum in the logarithmic term of the Nicolski—Eisenman equation [3—5, 13].

An option of the program is the assessment of ion activities or concentrations from measured e.m.f. values. The e.m.f.s are measured for 5 unknown samples. In an iterative procedure, these are corrected for the liquid-junction potential and compared with the given calibration curve to yield the individual activity or concentration values (see vertical bars in Fig. 2). The programs are available from the authors on request.

This work was partly supported by the Schweizerischer Nationalfonds zur Förderung der wissenschaftlichen Forschung.

REFERENCES

1 W. E. Morf, G. Kahr and W. Simon, Anal. Lett., 7 (1974) 9.
2 W. E. Morf, D. Ammann and W. Simon, Chimia (Switzerland), 28 (1974) 65.
3 D. Ammann, W. E. Morf, P. Anker, P. C. Meier, E. Pretsch and W. Simon, Ion-Selective Electrode Rev., 5 (1983) 3.
4 W. E. Morf, The Principles of Ion-Selective Electrodes and of Membrane Transport, Studies in Analytical Chemistry, Vol. 2, Elsevier, Amsterdam, 1981.
5 W. E. Morf and W. Simon, in H. Freiser (Ed.), Ion-Selective Electrodes in Analytical Chemistry, Vol. 1, Plenum, New York, 1978, Ch. 3.
6 A. Craggs, G. J. Moody and J. D. R. Thomas, J. Chem. Educ., 51 (1974) 541.
7 G. J. Moody and J. D. R. Thomas, in H. Freiser (Ed.), Ion-Selective Electrodes in Analytical Chemistry, Vol. 1, Plenum, New York, 1978, Ch. 4.
8 W. Simon, D. Ammann, M. Oehme and W. E. Morf, Ann. N.Y. Acad. Sci., 307 (1978) 52.
9 P. Anker, E. Wieland, D. Ammann, R. E. Dohner, R. Asper and W. Simon, Anal. Chem. 53 (1981) 1970.
10 D. Erne, N. Stojanac, D. Ammann, P. Hofstetter, E. Pretsch and W. Simon, Helv. Chim. Acta, 63 (1980) 2271.
11 R. Scholer and W. Simon, Helv. Chim. Acta, 55 (1972) 1801.
12 U. Oesch and W. Simon, Anal. Chem., 52 (1980) 692.
13 P. C. Meier, D. Ammann, W. E. Morf and W. Simon, in J. Koryta (Ed.), Medical and Biological Applications of Electrochemical Devices, Wiley-Interscience, Chichester, 1980, Ch. 2.
14 W. J. Hamer and Y.-C. Wu, J. Phys. Chem. Ref. Data, 1 (1972) 1047.
15 R. B. Staples and R. L. Nuttall, J. Phys. Chem. Ref. Data, 6 (1977) 385.
16 R. N. Goldberg and R. L. Nuttall, J. Phys. Chem. Ref. Data, 7 (1978) 263; 8 (1979) 923.
17 R. N. Goldberg, J. Phys. Chem. Ref. Data, 8 (1979) 1005.
18 G. Milazzo, Elektrochemie I, Grundlagen und Anwendungen, Birkhäuser Verlag, Basel, 1980.
19 P. C. Meier, Anal. Chim. Acta, 136 (1982) 363.
20 IUPAC Recommendations for Nomenclature of Ion-Selective Electrodes, Pure Appl. Chem., 48 (1976) 127.

Analytica Chimica Acta, 156 (1984) 9—18
Elsevier Science Publishers B.V., Amsterdam — Printed in The Netherlands

SURFACE STUDIES ON PRECIPITATE-BASED CYANIDE ELECTRODES

E. PUNGOR*, M. GRATZL, L. PÓLOS and K. TÓTH

Institute for General and Analytical Chemistry, Technical University of Budapest (Hungary)

M. F. EBEL, H. EBEL, G. ZUBA and J. WERNISCH

Institut für Angewandte und Technische Physik, Technische Universität Wien (Austria)

(Received 26th July 1983)

SUMMARY

Silver iodide-based electrodes allow indirect measurements of cyanide. Potentiometric investigations and theoretical studies have suggested that a corrosion process is responsible for this cyanide response. Surface analytical methods providing information at different depths are used to investigate mixed membranes of silver iodide/silver sulphide and pure silver iodide membranes. The results prove that in the surface corrosion process the iodide content of the mixed membrane surface decreases. Further, the membrane loses silver sulphide particles from its surface. Finally, a layer enriched with readsorbed iodide is formed on the outermost surface of the membrane. The composition of the surface layer depends on pH and buffer capacity because of the different fluxes of ions observed in the surface layer.

The iodide-selective electrode based on silver iodide can be used to measure cyanide, through sensing the iodide ions generated in a surface reaction

$$AgI + 2CN^- = Ag(CN)_2^- + I^- \quad (1)$$

During this indirect cyanide measurement [1, 2], cyanide ions diffuse from the stirred bulk of the sample solution through the adherent boundary layer to the silver iodide surface, where iodide ions are generated. The reaction products then diffuse back into the bulk of the solution, assuming the simplified Nernst approximation [3]. Stationary conditions are established very quickly and the cyanide activity in the sample bulk is sensed by the electrode through the iodide activity at the membrane surface.

The iodide function of the electrode can be described as $E = E_I^0 - S \ln [I^-]_s$, whereas in presence of cyanide [3], $[I^-]_s \approx [I^-]_b + \frac{1}{2}[CN^-]_b$, thus

$$E \approx E_I^0 - S\,(\ln[I^-]_b + \tfrac{1}{2}[CN^-]_b) \quad (2)$$

where E is the electrode potential, E_I^0 is the standard potential of the electrode with respect to iodide, S is the Nernst factor, square brackets indicate activity, and the indices s and b refer to the electrode surface layer and

0003-2670/84/$03.00

the bulk solution, respectively. The coefficient 1/2 derives from the stoichiometry of Reaction 1. Obviously, this iodide-selective electrode is suitable for measuring cyanide activity either when iodide is absent or when its amount is known and at most equal to that of cyanide; the selectivity coefficient is $K_{CN,I} \approx 2$ [4].

The cyanide sensor outlined above belongs to the group of "corrosion" or "secondary" ion-selective electrodes. Besides this cyanide electrode, several other secondary ion-selective electrodes have been developed, all of which operate on similar principles. Such sensors include the AgI-, AgBr- or AgCl-based electrodes for cyanide, thiosulphate, thiocyanate and ammonia [5]. These electrodes have been the subject of several theoretical studies [3—6] which have provided descriptions more sophisticated than Eqn. 2; these equations agreed well with earlier results derived and checked experimentally for Ag/AgI electrodes of the second kind when dissolved by cyanide [7, 8]. The essence of these results is that the electrode surface is at equilibrium during potentiometric measurements [7, 8], but the system is controlled by diffusion.

Further experimental studies revealed an interesting pH effect [9, 10], which could be interpreted in terms of a stationary (but non-equilibrium) system [10]. It was observed that within the pH range 5—9 the potential of the cyanide electrodes depends not only on the cyanide activity and pH but also strongly on the buffer capacity of the solution. This finding could be interpreted by taking into account the reaction

$$AgI + 2HCN = Ag(CN)_2^- + 2H^+ + I^- \qquad (3)$$

which competes with Reaction 1 at the membrane surface in the pH range mentioned. Clearly, the solution layer in direct contact with the silver iodide surface must be more acidic than the bulk solution. This pH difference between the surface and bulk will obviously be larger as the buffer capacity of the solution diminishes. Thus, the buffer capacity can influence the iodide activity at the membrane surface and so the electrode potential [10].

A special advantage of the secondary (corrosion) ion-selective electrodes is the constant renewal of their sensing surface, caused by continuous dissolution by the component to be measured as in the above reactions. This has the accompanying disadvantage, of course, that the electrodes do not last very long in concentrated solutions.

In order to increase the lifetimes, mixed silver halide/silver sulphide membrane electrodes have been developed [11]. The addition of silver sulphide to the membrane material also improves the mechanical and conductive properties of the electrode. In studies of such electrodes, it has been assumed that the surface becomes covered during use by a porous silver sulphide layer which remains on the membrane while silver iodide is leached out [3, 12]. Accordingly, this porous layer acts as a diffusion barrier, steadily becoming larger. The adherent laminar layer of solution naturally forms an additional diffusion barrier. On the basis of this scheme

[12], the increased lifetime is easily interpreted, as the larger diffusion barrier provides smaller fluxes. However, this steadily thickening porous layer of silver sulphide should cause increasing response times and memory effects. In addition, the continuous renewal of the sensing surface would also become impossible. Yet these latter disadvantages do not appear in practice. For example, the response time of a new silver iodide/silver sulphide electrode increases initially when cyanide is measured, but after a while the response time stabilizes at a level which is still acceptable for practical purposes, i.e., a few seconds at most. The silicone rubber-based silver iodide electrode is an exception in that its response time increases considerably after a short period of use in cyanide solutions [13]. Significant memory effects have not been reported.

To achieve a better understanding of the true characteristics of these mixed salt-based membranes, their surface layers as an effect of corrosion were studied in detail. Indirect methods based on measurement of response times, memory effects or fluxes of components taking part in the corrosion reaction may be measured as functions of corrosion time; from such data obtained under the conditions of actual use, conclusions can be drawn concerning changes of the electrode surface (e.g., whether or not the covering silver sulphide barrier thickens steadily during use). In addition, x-ray fluorescence analysis, electron microscopy and electron spectroscopy offer possibilities for direct observation of the membrane surfaces, providing different types of information. Only some response-time measurements seem to have been done on the corrosion type of electrodes [13]. In the present paper, changes of the surface layer of secondary (corrosion) ion-selective electrodes during potentiometric use were monitored by x-ray fluorescence analysis, electron microscopy and electron spectroscopy. The silver iodide/silver sulphide mixed salt membrane-based electrodes were taken as the model, but pure silver iodide membranes were also studied for comparison.

EXPERIMENTAL

Preparation of the electrode membranes

Home-made membranes (2 mm thick, 7 mm diameter) were used. The silver iodide was prepared by titration of silver nitrate with sodium iodide solution to the end-point while the coprecipitation of AgI/Ag_2S (1:1) was done by titration of silver nitrate with a solution containing NaI and Na_2S in a 1:1 mole ratio also to the end-point. In both cases, a sulphide-selective indicator (Radelkis Type OP-S-7111D) and a silver/silver chloride double-junction reference electrode (Type 8202) were used for end-point detection. After filtering and drying the precipitates were pressed to pellets at 10^9 Pa.

Corrosion of membranes

Corrosion of the membranes was effected at room temperature in 50 ml of cyanide solution stirred magnetically. The vessel was covered to prevent

hydrogen cyanide from volatilizing (this was especially important at pH 7). Significant decrease in the cyanide activity caused by the corrosion reaction was prevented by renewing the corroding cyanide solution every 20 min. The membranes were placed on a thin plastic net 2 cm above the bottom of the vessel. Thus, the membrane was corroded under stirred conditions very similar to those used for real cyanide measurements. After the treatment, the membranes were immediately washed with distilled water. Several of the investigated sets of membranes were built into an electrode body and checked for proper electrochemical operation before and after treatment. The results were satisfactory.

The potassium cyanide solutions used (10^{-1}, 10^{-2}, 10^{-3} M) also contained 10^{-2} M KNO_3 for approximate adjustment of the ionic strength (except for the most concentrated solution). The concentration of Britton—Robinson buffer, if used, was 3.6×10^{-2} M. Reagents of analytical grade and water distilled in quartz equipment were used.

Measurements

The photoelectron spectroscopic investigations (x.p.s.) were done with a Kratos XSAM 800 photoelectron spectrometer; Mg K_α radiation (15 kV, 20 mA) was used. For analysis, the Ag $3d_{5/2}$, I $3d_{5/2}$ and S $2p$ lines were employed. For quantitative analysis [14], the product of peak height and half-width of the photoelectron line was calculated. Additionally, the K $2p$ and N $1s$ lines were investigated but these elements could not be found on the outermost surface. At a rough estimate, a depth of 0.005 μm is available to x.p.s.

The scanning electron micrographs (s.e.m.) were obtained with a JEOL U3 system with wavelength- and energy-dispersive detectors. For quantitative analysis, the standard ZAF program was applied. The estimated depth available to s.e.m. is about 1 μm.

X-ray fluorescence analysis (x.r.f.) was done with a Kevex 700 spectrometer with an energy-dispersive detector and secondary targets. For quantitative analysis, the following radiations were used: the Ag K_α, I K_α and S K_α lines provided information to a depth of approximately 100 μm, and the Ag I_α, I L_α and S L_α lines to a depth of <10 μm. For quantitative analysis, a fundamental parameter algorithm was applied.

To check the loss of silver sulphide from the mixed membranes, some of the pellets were corroded for 2 h in 10^{-1} M potassium cyanide solution as described above. Then the solutions were filtered (Synpor-10, Chemopal, Prague) and the filters were immediately washed with pure 10^{-2} M cyanide solution (to wash out $Ag(CN)_2^-$ before its reduction to silver metal) and then with distilled water. The filters were ashed and then 5 ml of (1:1) nitric acid was added. The solution thus obtained was diluted to 10 ml. The same procedure was also applied to pure silver iodide membranes. The silver content of the final solutions was measured by atomic absorption spectrometry (a.a.s.); a Varian-Techtron AAG instrument was used.

When mixed membrane pellets were placed into a potassium cyanide solution (e.g., 10^{-1} M), corrosion products could be collected on a filter paper. These particles were investigated by s.e.m.

RESULTS AND DISCUSSION

Figures 1—3 show the results of quantitative surface analysis of the corroded mixed membrane electrodes as found by means of x.p.s. and s.e.m. The corrosion was done with 10^{-3} M potassium cyanide solutions at different pH values: pH 7 (Fig. 1), pH 10 (Fig. 2) and pH 7 with Britton—Robinson buffer (Fig. 3). The x.p.s. results obtained after corrosion with cyanide are followed by further results obtained after additional etching with argon ions.

On the basis of these results, the corrosion process accompanying potentiometric measurements can be characterized as follows. Initially, the iodide content of the silver iodide/silver sulphide membranes decreases as expected, but this decrease levels off after a certain period of time. The x.p.s. results show that the final stabilized values of the iodine and sulphur concentrations on the outermost surface are identical for corrosion by a 10^{-3} cyanide solution at pH 7, pH 10 and pH 7 (Britton—Robinson buffer). However, the final stabilized values found for the iodine and sulphur concentrations

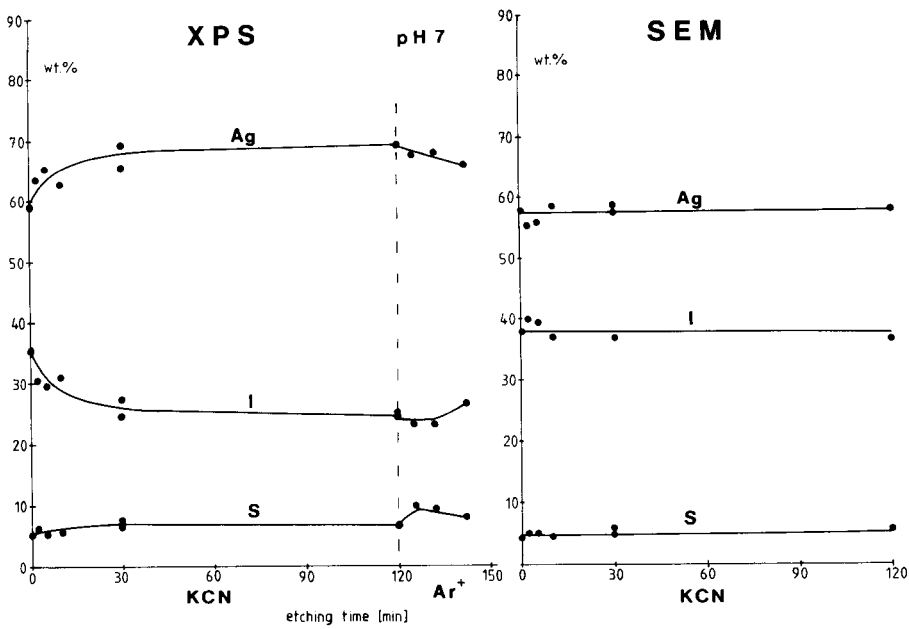

Fig. 1. The elemental composition obtained for silver, iodine and sulphur (% w/w) depending on etching time (min) in 10^{-3} M KCN. The x.p.s. curves are followed by a series obtained by additional etching with argon ions. The results are valid for pH 7.

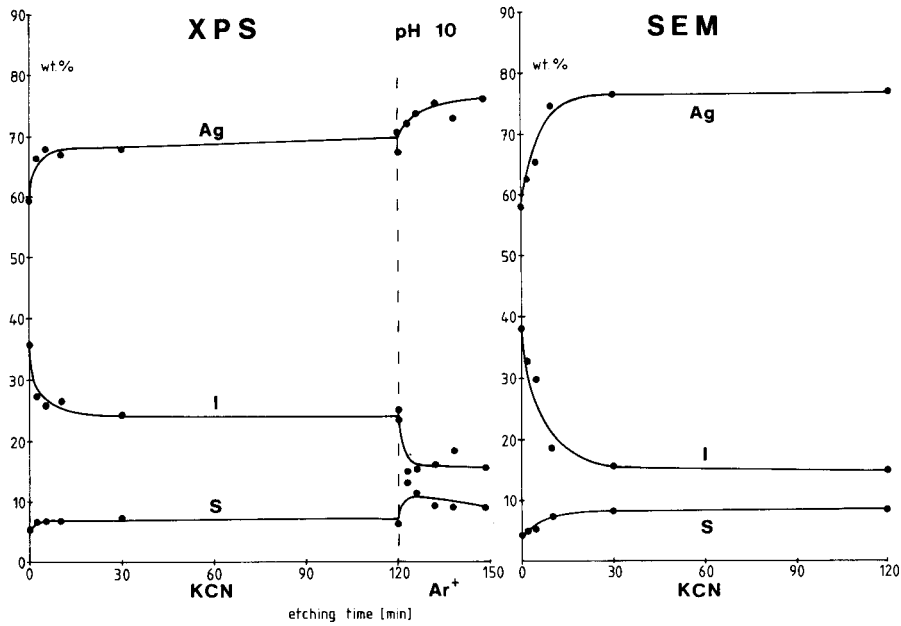

Fig. 2. As Fig. 1, valid for pH 10.

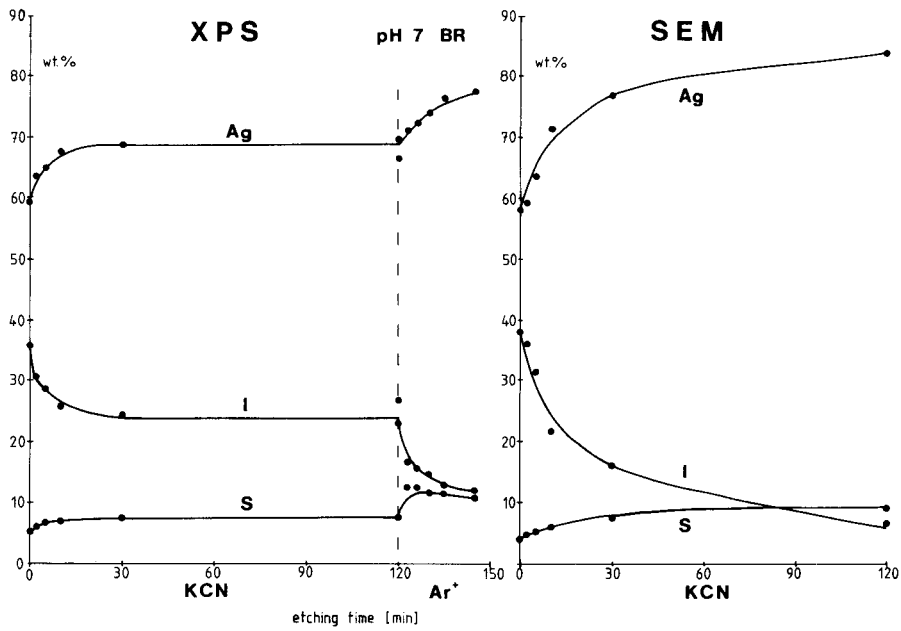

Fig. 3. As Fig. 1, valid for pH 7 with Britton—Robinson buffer.

by s.e.m. are different from those found by x.p.s. and depend on the pH values and the buffer capacity. Argon-ion etching of specimens which had been corroded with cyanide for 120 min causes a change in the surface composition and the x.p.s. results then approach the s.e.m. values. Additional experiments proved that this change in surface composition is not due to selective sputtering.

The results of x.r.f. with the Ag L_α and I L_α lines were in good agreement with the s.e.m. results, whereas the results found with K_α radiation indicated no change of composition.

On the surfaces of the mixed membranes, no changes were observed visually even after treatment for 24 h in 10^{-2} M cyanide. The membrane surface seemed to be as smooth as that of an untreated pellet. However, the electron micrographs of treated pellets (Fig. 4) showed an appreciable change of the membrane surface after treatment; changes were also found on pure silver iodide membranes. Untreated pellets showed no structure apart from the reverse image of the pressing surface. The surface structure of corroded membranes, as seen by s.e.m., seemed to be independent of the time and conditions of corrosion. Finally, the particles which were leached out by the corrosion procedure were identified as silver sulphide, as shown by the elemental micrographs in Fig. 5.

Any consideration of the corrosion process must take into account that the hardness of silver sulphide is about 2 on the Mohs scale [15], whereas that of silver iodide is 1—1.5 [16] at room temperature. Thus it can be assumed that, in the pressing to form the membrane, the harder silver sulphide micro-crystals are surrounded by the softer silver iodide. Accordingly, the AgI/Ag_2S mole ratio influences the stability of the electrode membrane material. If this ratio is low, then Ag_2S crystals are covered with a

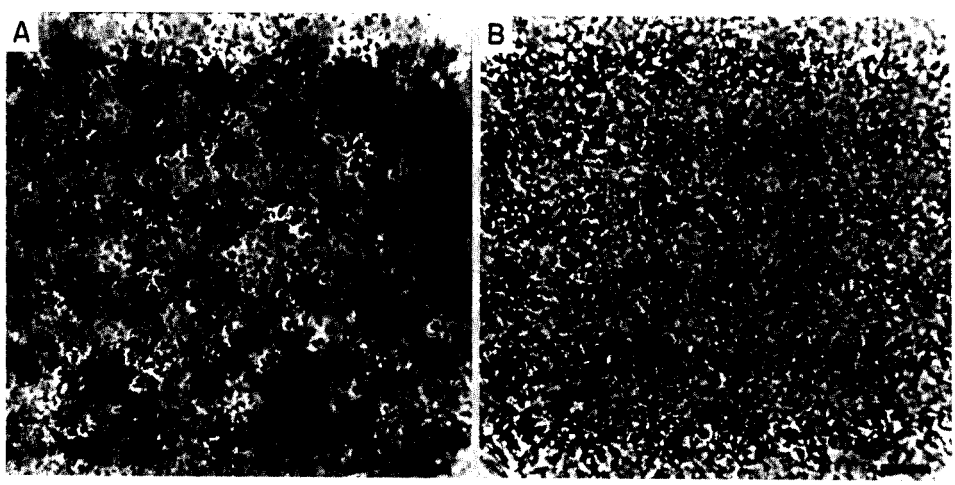

Fig. 4. Secondary electron images of (A) an etched mixed membrane surface and (B) an etched pure silver iodide membrane surface (both at 3000×).

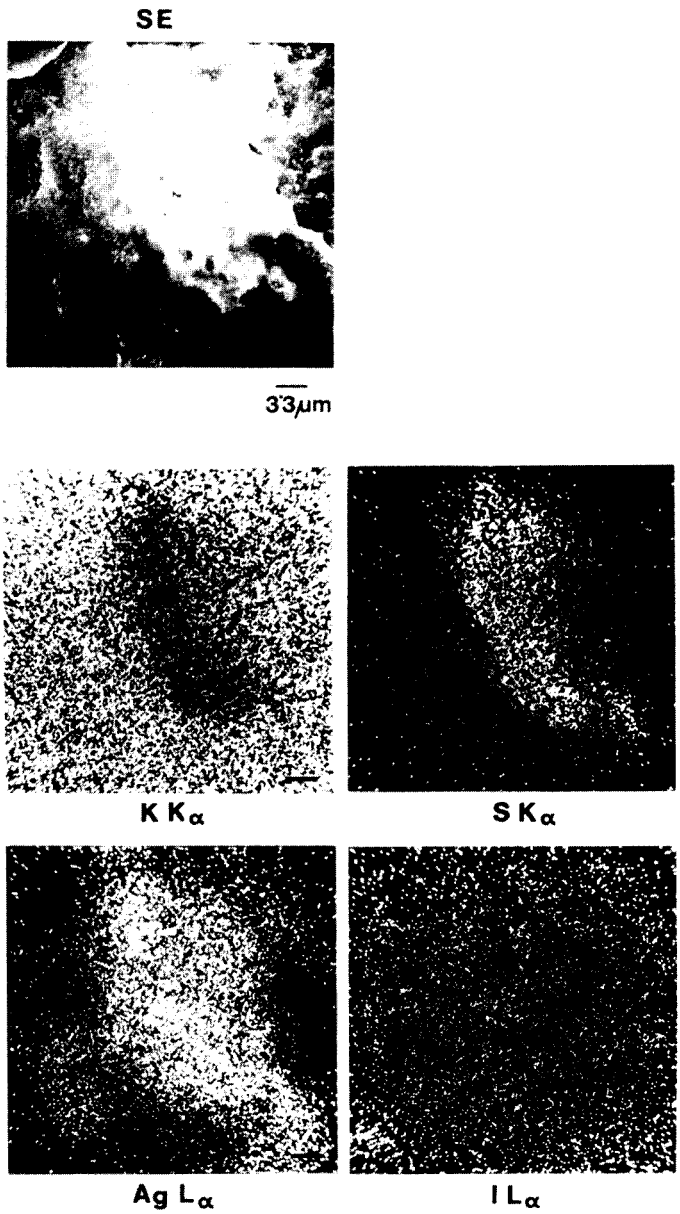

Fig. 5. Secondary electron image (3000×) of an agglomerate of particles leached by the corrosion procedure and the corresponding elemental distributions.

very thin layer of AgI; when the latter is dissolved by cyanide, the remaining Ag_2S skeleton is more resistant to corrosion. If the AgI/Ag_2S mole ratio is high, the silver sulphide crystals become further apart and therefore fall away more easily during corrosion than when the mole ratio is low (see Fig. 5).

The surface layer of the mixed salt membrane thus continuously loses the outermost silver sulphide particles until a statistically constant AgI/Ag_2S ratio is attained at the surface. Thus, the corrosion process produces a diffusion layer with a depth commensurable with the grain size of silver sulphide which is independent of the time of corrosion. This depth is within the possible range of s.e.m. and x.r.f. with L_α radiation.

This picture is supported by the a.a.s. findings. The silver content of the ashed and dissolved filter was significant in the case of AgI/Ag_2S pellets compared to that of silver iodide pellets treated in the same way (see Experimental). This supports the idea that silver sulphide particles are leached from the membrane by corrosion.

The dependence of the surface composition on pH and buffer capacity as shown by the quantitative s.e.m. results (Figs. 1—3) is supported by the fact that the corrosion flux is much less at pH 7 than at pH 10 or at pH 7 with buffering, as expected on the basis of earlier electrochemical findings [10]. During the time period studied, corrosion reaches a depth that can be monitored by x.p.s. but clearly does not proceed to the depth that can be monitored by s.e.m. at pH 7 in unbuffered solution.

More positive e.m.f. values at a given pH correspond to smaller iodide concentrations at the electrode surface. As iodide is generated in Reactions 1 and 3, less iodide at the surface means smaller fluxes of the reacting species, and this in turn causes slower corrosion of the membrane. At neutral pH, the electrode potential is higher for unbuffered solution (Fig. 6) and so corrosion is much slower than at pH 10, or at pH 7 with concentrated Britton—Robinson buffer.

The results corresponding to pure silver iodide pellets can be interpreted in terms of a fraction of the iodide ions leached out by corrosion being re-

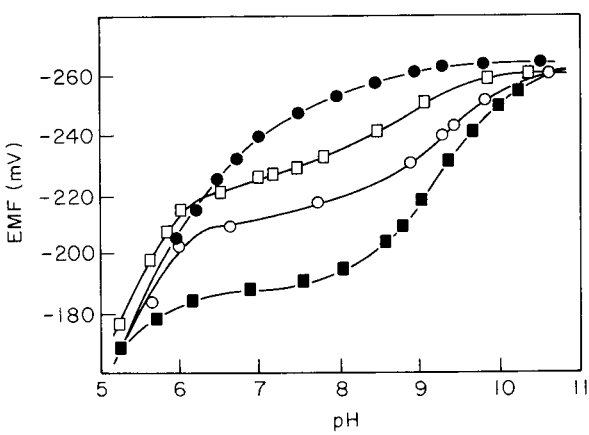

Fig. 6. pH response of a cyanide electrode at different buffer capacities in 10^{-2} M KCN. Concentrations of the Britton—Robinson buffer: (•) 4×10^{-1} M; (□) 4×10^{-3} M; (○) 4×10^{-5} M; (■) unbuffered.

adsorbed onto the membrane surface [17]. This adsorption also occurs during corrosion of mixed membranes and apparently replaces part of the true iodide loss from the membrane surface. The higher iodide content of the outermost surface layer (shown by x.p.s.) supports this view.

Conclusions

The three spectroscopic techniques here employed are very suitable for following the corrosion of silver iodide-based membrane electrodes whether or not silver sulphide is added. The results show that the depth of the silver sulphide layer necessarily covering the membrane after use is in the same range as the mean diameter of micro-crystal grains. Accordingly, significant memory effects and increased response times do not occur when the materials are used as ion-selective membranes. These conclusions are in good agreement with observations reported in the literature. However, it is also advantageous practically that the surface of mixed membranes is steadily renewed during use (with respect to silver iodide as well as sulphide), according to the outlined mechanism of the dynamic equilibrium. The surface layer composition is shown to depend on pH and buffer capacity and this again is in accord with electrochemical behaviour.

The authors thank E. G. Harsanyi for obtaining the atomic absorption results and F. Pal for assistance with membrane preparations. We appreciate the financial support of the "Fonds zur Förderung der wissenschaftlichen Forschung in Osterreich" (Projekt 4272) for purchasing the photoelectron spectrometer.

REFERENCES

1 J. W. Ross, in Proceedings on Ion-Selective Electrodes, Nat. Bur. Stand. U.S. Spec. Publ. 314, Washington, DC, 1969, p. 84.
2 E. Pungor and K. Tóth, Analyst, 95 (1970) 1132.
3 G. P. Bound, B. Fleet, H. von Storp and D. H. Evans, Anal. Chem., 45 (1973) 788.
4 P. L. Bailey, Analysis with Ion-Selective Electrodes, Heyden, London, 1976, p. 93.
5 W. E. Morf, G. Kahr and W. Simon, Anal. Chem., 45 (1974) 1538.
6 A. Hulanicki and A. Lewenstam, Talanta, 24 (1977) 171.
7 W. Jaenicke, Z. Elektrochem., 55 (1951) 648.
8 W. Jaenicke and M. Haase, Z. Elektrochem., 63 (1959) 521.
9 M. Mascini, Anal. Chem., 45 (1973) 615.
10 M. Gratzl, F. Rakiás, G. Horvai, K. Tóth and E. Pungor, Anal. Chim. Acta, 102 (1978) 85.
11 J. W. Ross, J. H. Rieseman and M. S. Frant, U.S. Pat. No. 3874, 16th February, 1971.
12 D. H. Evans, Anal. Chem., 44 (1972) 875.
13 E. Lindner, K. Tóth and E. Pungor, Anal. Chem., 48 (1976) 1071.
14 M. F. Ebel, H. Ebel and K. Hirokawa, Spectrochim. Acta, 378 (1982) 461.
15 J. W. Mellor, A Comprehensive Treatise on Inorganic and Theoretical Chemistry, Vol. III, Longmans, Green and Co., London, 1952, p. 441.
16 P. W. Bridgman, Proc. Am. Acad. Arts Sci., 71 (1973) 387, cited in Gmelin, Silber Teil B2 Verbindungen, Springer Verlag, Berlin, 1974, p. 238.
17 E. G. Harsányi, K. Tóth, L. Pólos and E. Pungor, Anal. Chem., 54 (1982) 1094.

Analytica Chimica Acta, 156 (1984) 19—31
Elsevier Science Publishers B.V., Amsterdam — Printed in The Netherlands

KINETIC INFLUENCES ON STUDIES OF COPPER(II) HYDROLYSIS BY COPPER ION-SELECTIVE ELECTRODE

JANIS GULENS*, PAUL K. LEESON and LUC SÉGUIN[a]

Atomic Energy of Canada Limited, Chalk River Nuclear Laboratories, General Chemistry Branch, Chalk River, Ontario K0J 1J0 (Canada)

(Received 7th June 1983)

SUMMARY

The hydrolysis of micromolar solutions of copper(II) is dominated by the formation of a copper—hydroxy colloid, both in the presence and absence of atmospheric carbon dioxide. Presence of the colloid was inferred from the response of the copper ion-selective electrode and confirmed by light scattering measurements. The colloid is only slowly converted to thermodynamically more stable species, with the result that copper—carbonate complexes are not formed to any significant extent in solutions exposed to atmospheric carbon dioxide. However, copper—carbonate complexes are formed in solutions containing a constant amount of total carbonate. Speciation and complexation capacity measurements should be interpreted with caution because thermodynamic equilibrium may not be attained in solution.

Solid-state ion-selective electrodes are thermodynamic or Nernstian devices whose response is governed by ion-exchange processes between the electrode membrane and the solution [1, 2]. Electrodes based on membranes made from mixed sulfide precipitates, MS—Ag_2S, respond to changes in the activity in solution of the free metal ion, M^{2+} (M = Cu, Pb, Cd) and thus are widely used for speciation studies in systems containing a variety of organic and inorganic ligands [3—12]. Calculation of metal speciation and determination/interpretation of the complexation capacity of natural water samples have been complicated by the complex chemical nature of the organic ligands (humic, fulvic substances) [13, 14], by uncertainties in the values of the thermodynamic constants used in the calculations [10, 11, 15], and by claims that the loss of metal ions from solution by adsorption processes must be taken into account [9, 12]. In addition, electrode response can be affected by certain ligands in solution and by reactions involving the electrode surface [16—19].

A fundamental assumption in speciation measurements and calculations is that all of the species in the system are at thermodynamic equilibrium. It is generally assumed that hydrolysis reactions (particularly those not involving

[a]Present address: Department de Chimie, Université de Montréal, Montréal, Québec H3C 3V1, Canada.

0003-2670/84/$03.00

polynuclear species), and complexation reactions involving labile metal ions are rapid and reversible and thus assumed to be at equilibrium. However, reactions involving precipitation (or dissolution) may involve metastable intermediates or intermediate states and such systems are not at thermodynamic equilibrium [20]. The present paper is concerned with the hydrolysis of micromolar copper solutions; a copper-selective electrode was used in an investigation of a previous claim that the copper-selective electrode responds not only to copper ions but also to cationic copper complexes [21]. It was found that a thermodynamically unstable copper—hydroxy colloid is readily formed in both nitrogen-saturated and air-saturated solutions, and its presence was confirmed by light scattering studies. The rate of conversion of the colloid to thermodynamically more stable species is slow, with the result that electrode response in the range pH 6—10 is not affected by the presence of dissolved carbonate arising from exposure to atmospheric carbon dioxide, i.e. copper—carbonate species are not formed to any significant extent under these conditions. However, copper—carbonate complexes are formed in solutions having a constant amount of total dissolved carbonate. The implications of these findings on the mechanism of electrode response, and on speciation studies in natural waters are discussed.

EXPERIMENTAL

Reagents and apparatus

The E—pH titration curves were done in water-jacketed pyrex cells maintained at 23°C. An Orion Model 91-01 pH electrode, calibrated in freshly prepared pH 6.5 and 9.01 buffers, and an Orion Model 94-29 copper-selective electrode were used, in conjunction with saturated calomel reference electrodes separated from the sample solution by 1 M KNO_3 bridge solutions. Two Orion Model 801 pH meters allowed simultaneous measurement of pH and E, the potential of the copper-selective electrode. A Perkin-Elmer Model MPF-3 fluorescence spectrophotometer was used to measure the intensity of light scattered from 1-cm cells at 90° from the incident beam; the wavelength of the incident and scattered light was 360 nm.

Reagent-grade chemicals and distilled, deionized water were used throughout. To minimize problems of copper contamination, all glassware was soaked in 1 M nitric acid between use. Carbonate-free sodium hydroxide solutions were prepared by dilution of "Dilutit Concentrates" (J. T. Baker) with deaerated water and were stored under a nitrogen atmosphere.

Electrode studies

The copper-selective electrode was always cleaned immediately before use by immersion for 5 min in 0.025 M sulphuric acid followed by thorough rinsing with distilled water. Calibration of the electrode by the standard addition procedure at pH 5—6 showed that Nernstian response (slope of 30.0 ± 0.5 mV/decade) was consistently obtained at copper concentrations

as low as 1×10^{-7} M, with positive deviations from the Nernstian line being observed at lower concentrations. The E—pH titrations, both in the presence and absence of atmospheric carbon dioxide, were normally conducted by increasing the pH of well-stirred copper solutions from an initial pH value of about 5 by the addition of dilute sodium hydroxide solution; occasionally the titration would be started at an initial pH of 10, dilute nitric acid being added to decrease the pH to verify that the same behaviour was observed. Solutions containing fixed amounts of carbonate were titrated from alkaline to acidic conditions under a nitrogen layer, which was stagnant to minimize loss of CO_2. Stable E—pH values were obtained after each addition of titrant within 3 min in solutions containing no carbon dioxide (deaeration with nitrogen) or fixed amounts of carbonate. In the presence of atmospheric carbon dioxide and in the range pH 7—9, the E—pH values were less stable, but reproducible values were obtained after 5 min; further changes in E—pH values with time in this pH range were small and followed the titration curve defined by the points taken at 5 min.

The electrode potentials, measured as a function of pH for a given total copper concentration, Cu_T, were converted to copper ion concentrations by using the relationship:

$$p[Cu^{2+}]_{pH=x} = p[Cu_T]_{pH=5} + \Delta E/30 \quad (1)$$

where ΔE is the difference in electrode potential (in mV) between the solution at pH 5 and pH x. The same relationship was used to obtain values of $p\Sigma Cu^{2+}$.

The "apparent loss of dissolved copper" from solution was measured over the range pH 7—10; aliquots of the solution were transferred to a known volume of acidified 0.1 M sodium nitrate solution and the resultant copper concentration was determined by a copper-selective electrode.

Calculations

Speciation calculations. The equilibrium constants used and reported here are based on activities, not concentrations. Values of activity coefficients, γ_i, for ions of charge Z_i, were calculated as a function of ionic strength, I, by using the Davies equation

$$-\log \gamma_i = 0.5\, Z_i^2\, [I^{1/2}/(1 + I^{1/2}) - 0.3\, I] \quad (2)$$

Speciation calculations were done by using the computer program MINEQL [22].

Equilibrium constants. Values of the hydrolysis constants for Cu(II) were calculated from the E—pH curves by using the following standard procedures. The value of $\bar{n}$ was calculated as the slope of the tangent to the plot of log $[Cu_T]/[Cu^{2+}]$ versus log $[OH^-]$ [23], values of $*\beta_1$ and $*\beta_2$ were calculated from the slope and intercept, respectively, of a plot of $(1 - \bar{n})/\{(2 - \bar{n})\,[OH^-]\}$ versus $\bar{n}/\{(2 - \bar{n})\,[OH^-]^2\}$. Alternatively, the degree of complex formation, ϕ [23] was used; values of $*\beta_1$, and $*\beta_2$ were calculated from the

intercept and slope, respectively, of a plot of $\{[Cu_T] - [Cu^{2+}]\}\{[Cu^{2+}][OH^-]\}^{-1}$ versus $[OH^-]$.

The formation constants for the copper—carbonate complexes, β_1, and β_2, were similarly evaluated from the E—pH curves in solutions containing a constant amount of total dissolved carbonate, C_T. The concentration of the copper—hydroxy complexes simultaneously present in solution was corrected for, using values of log $*\beta_1 = -7.4$, log $*\beta_2 = -16.0$ in the following equations

$$[Cu_T] = [Cu^{2+}] + [CuCO_3] + [Cu(CO_3)_2^{2-}] + [Cu(OH)^+] + [Cu(OH)_2] \quad (3)$$

$$\{([Cu_T] - [Cu^{2+}])[Cu^{2+}]^{-1} - (*\beta_1[H^+] + *\beta_2[H^+]^{-2}\} F(H) = \beta_1 C_T K_1 K_2 + \beta_2 (C_T K_1 K_2)^2 [F(H)]^{-1} \quad (4)$$

where $F(H) = ([H^+]^2 + K_1[H^+] + K_1K_2)$ and K_1, K_2 are the acidity constants for carbonic acid. Values of β_1 and β_2 were calculated from the intercept and slope, respectively, of a plot of Eqn. 4.

Experimental pH values were converted to H^+ and OH^- concentrations ($[H^+]$ and $[OH^-]$, respectively) by using activity coefficients calculated from the Davies equation.

RESULTS AND DISCUSSION

Hydrolysis in absence of carbonate

The change in the potential of the copper-selective electrode as a function of pH for different initial copper concentrations was measured in a 0.1 M sodium nitrate solution that was continuously deaerated with nitrogen (Fig. 1). At copper concentrations $\geqslant 5 \times 10^{-6}$ M, the electrode potential for pH values greater than 8.5 became independent of the total copper concentration, indicating that a solid phase was formed in solution and controlled the concentration of free copper ions. A similar effect has been also reported by other workers at total copper concentrations $\geqslant 1 \times 10^{-6}$ M [10].

The slope of the linear section of the E—pH plots is —60 mV/pH, indicating that the solid is probably $Cu(OH)_2$. The solubility product (based on activities) for the reaction:

$$Cu(OH)_2(s) + 2H^+ \rightleftharpoons Cu^{2+} + 2H_2O \quad (5)$$

is calculated from curves c and d in Fig. 1 to be log $*K_{so} = 10.3$. This value is considerably larger than that commonly used in the literature, log $*K_{so} = 8.6$ [11, 15] but is similar to values obtained by others who also used copper-selective electrodes, log $*K_{so} = 9.6$ ($I = 0.05$) [10] or 10.7 [24].

Schindler et al. [25] have shown that the solubility product of copper hydroxide varies with the molar surface area; some rough calculations based on their formula suggested that the surface area of the present precipitates was about 30×10^3 m^2 with particle diameters [26] of about 4×10^{-9} cm. Light scattering measurements confirmed the presence of a colloidal suspen-

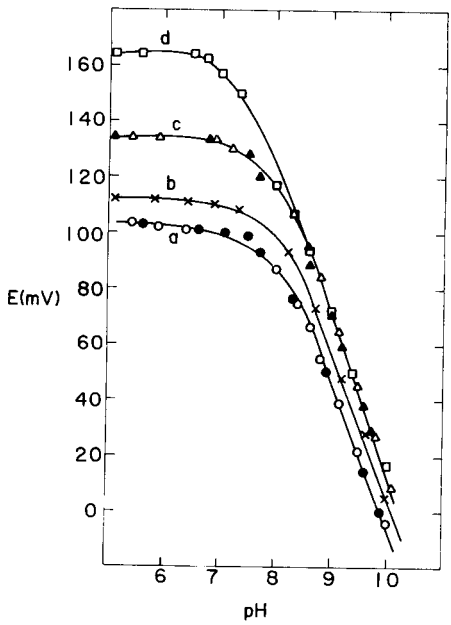

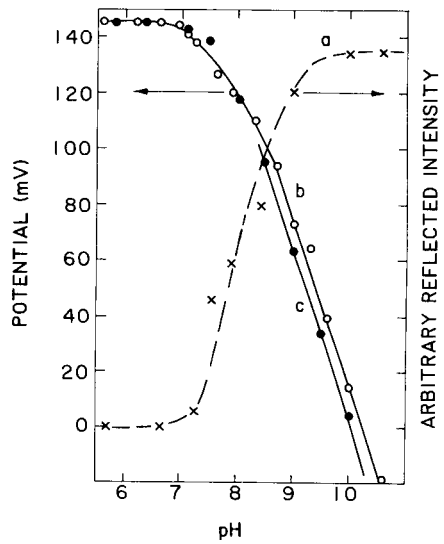

Fig. 1. Copper-selective electrode response as a function of pH in carbonate-free 0.1 M $NaNO_3$ solution under nitrogen. Open and closed symbols represent addition of acid and base, respectively, at initial Cu(II) concentrations of: (a) 5×10^{-7} M; (b) 1×10^{-6} M; (c) 5×10^{-6} M; (d) 5×10^{-5} M.

Fig. 2. Influence of pH, for a 1×10^{-5} M Cu(II) solution in carbonate-free 0.1 M $NaNO_3$ under nitrogen, on: (a) reflected light intensity; (b, c) electrode potential after equilibration times of 5 min and 120 min, respectively.

sion; a significant increase in scattering was observed over the pH range where the potentiometric data indicated the formation of a solid phase in solution (Fig. 2) and scattering was observed even at initial copper concentrations as low as 10^{-6} M. Scattering was not observed when copper ions were absent from these solutions.

The value log $*K_{so}$ = 10.3 was obtained from electrode potentials at total copper concentrations $\geqslant 5 \times 10^{-6}$ M after an equilibration period of 3–5 min following each pH alteration. However, different workers have used different equilibration times in studying the copper-selective electrode response as a function of pH [9—12], and so the electrode potential was monitored as a function of time at constant pH. After 120 min, the resultant potentials (curve c, Fig. 2) were shifted only in the linear region to more negative potentials by about 10 mV, resulting in a new value of log $*K_{so}$ = 10.0; a similar shift was observed in a 10^{-6} M copper solution. The rate of aging and conversion of the colloid to its thermodynamically more stable form is slow under these conditions.

This value of the solubility product is not a "thermodynamic" constant in the usual sense, because the copper—hydroxy colloid is thermodynamically unstable. Thus, the value of $*K_{so}$ is not only time-dependent, but also is influenced by physical parameters that affect the kinetics of colloid formation and growth, such as the concentrations of copper and base, localized pH changes resulting from the addition of alkali, the stirring rate, etc. [25]. Consequently, it is not surprising that there are small differences in the log $*K_{so}$ value reported by various workers who used copper-selective electrodes [10, 24] but it is significant that these earlier values, as well as the present value, are all approximately two orders of magnitude larger than the literature value in common use [11, 15, 27].

Evaluation of $*\beta_1$, $*\beta_2$

Literature values for the conditional formation constant of $Cu(OH)^+$, $*\beta_1$

$$Cu^{2+} + H_2O \rightleftharpoons Cu(OH)^+ + H^+ \qquad (6)$$

range from $10^{-7.4}$ [9—11] to $10^{-7.7}$ [27, 28] to $10^{-8.0}$ [15, 29]. However, there is considerably larger disagreement in the literature regarding the value of the formation constant of the species $Cu(OH)_2(aq)$, $*\beta_2$

$$Cu^{2+} + 2H_2O \rightleftharpoons Cu(OH)_2(aq) + 2H^+ \qquad (7)$$

Vuceta and Morgan [11] presented convincing evidence from copper-selective electrode studies that the value was log $*\beta_2 = -13.7$, whereas later studies, also based on the response of the copper-selective electrode [9, 10, 12], claim that a more appropriate value is log $*\beta_2 \approx -16$. We have calculated values of $*\beta_1$ and $*\beta_2$ from the present E—pH data by using the complex formation function $\bar{n}$, and also the degree of complex formation ϕ [23]. Calculations were restricted to solutions having total copper concentrations of $\leqslant 5 \times 10^{-7}$ M, because of colloid formation at higher concentrations. The values found for log $*\beta_1$ and log $*\beta_2$ range from -7.0 to -7.5, and -15.4 to -23, respectively (Table 1), in agreement with other copper-selective electrode studies (except for the results of Vuceta and Morgan [11]).

Copper speciation as a function of pH was calculated by using the computer program MINEQL [22] and the calculated and measured pCu^{2+} values were compared to establish more precisely the appropriate values of $*\beta_1$ and $*\beta_2$. The calculations were done by using the constants of Eqns. 3 and 4 in Table 2 and variable values of $*\beta_1$ and $*\beta_2$ for total copper concentrations ranging from 1×10^{-7} to 5×10^{-5} M. For a given $*\beta_2$ value, changes in $*\beta_1$ had a relatively minor influence on calculated concentrations and this influence decreased as the total copper concentration increased. The maximum influence of changes in $*\beta_1$ was at pH 8; the difference in calculated pCu^{2+} values using values of $*\beta_1 = 10^{-7.0}$ and $10^{-8.0}$ at pH 8 was 0.5 units at a total copper concentration of 5×10^{-7} M (Fig. 3A) whereas the corresponding difference was only 0.2 units for a total copper concentration of 10^{-5} M.

TABLE 1

Determination of copper hydrolysis constants

Total copper (M)	Method of calculation			
	$\bar{n}$		ϕ	
	$\log {}^*\beta_1$	$\log {}^*\beta_2$	$\log {}^*\beta_1$	$\log {}^*\beta_2$
1×10^{-7}	−7.1	−22.6	−7.1	−15.4
1×10^{-7}	−7.0	−22.6	−7.0	−16.0
5×10^{-7}	−7.5	−23.0	−7.4	−15.8
1×10^{-7} [a]	−7.5	−22.6	−7.5	−16.2

[a]Determined in 10^{-3} M NaCl solution, all others in 10^{-1} M $NaNO_3$.

TABLE 2

Reactions considered in aqueous solution

Reaction	Log equil. constant	Ref.
(1) $Cu^{2+} + H_2O \rightleftharpoons Cu(OH)^+ + H^+$	${}^*\beta_1 = -7.4$	T[a], 9–11
(2) $Cu^{2+} + 2H_2O \rightleftharpoons Cu(OH)_2(aq) + 2H^+$	${}^*\beta_2 = -16.0$	T, 9, 12
(3) $2Cu^{2+} + 2H_2O \rightleftharpoons Cu_2(OH)_2{}^{2+} + 2H^+$	${}^*\beta_{22} = -10.3$	15, 27
(4) $Cu^{2+} + 2H_2O \rightleftharpoons Cu(OH)_2(s) + 2H^+$	$({}^*K_{so})^{-1} = -10.3$	T
(5) $CO_2(g) + H_2O \rightleftharpoons H_2CO_3{}^*$	$K = -5.0$	27
(6) $H_2CO_3{}^* \rightleftharpoons H^+ + HCO_3^-$	$K_1 = -6.3$	27
(7) $HCO_3^- \rightleftharpoons H^+ + CO_3^{2-}$	$K_2 = -10.2$	27
(8) $Cu^{2+} + CO_3^{2-} \rightleftharpoons CuCO_3(aq)$	$\beta_1 = 6.7$	27
(9) $Cu^{2+} + 2CO_3^{2-} \rightleftharpoons Cu(CO_3)_2^{2-}$	$\beta_2 = 9.9$	27
(10) $2Cu^{2+} + 2H_2O + CO_3^{2-} \rightleftharpoons Cu_2(OH)_2CO_3(s) + 2H^+$	$({}^*K_{so})^{-1} = 1.6$	10

[a]This work.

The effect of changes in the value of ${}^*\beta_2$ on copper speciation were much more pronounced. In regions where copper—hydroxy colloids were formed (pH > 8.5, $Cu_T \geqslant 5 \times 10^{-6}$ M), the value $\log {}^*\beta_2 = -15.4$ was an upper limit; calculated pCu^{2+} values did not change as ${}^*\beta_2$ was decreased below this value but became significantly lower when ${}^*\beta_2$ was increased above this value. However, at lower total copper concentrations where colloids were not formed, calculated pCu^{2+} values differed by more than an order of magnitude for pH > 9.5 as ${}^*\beta_2$ ranged from $10^{-15.4}$ to $10^{-17.3}$ (Fig. 3B). The most consistent agreement between calculated and measured pCu^{2+} values for total copper concentrations ranging from 1×10^{-7} to 5×10^{-5} M was obtained when the values used were $\log {}^*\beta_1 = -7.4$ and $\log {}^*\beta_2 = -16.0$. These values agree well with those reported by other workers using copper-selective electrodes [9, 10, 12], and were used for all further calculations (Table 2).

Vuceta and Morgan [11] determined their value of ${}^*\beta_2$ in a 10^{-3} M

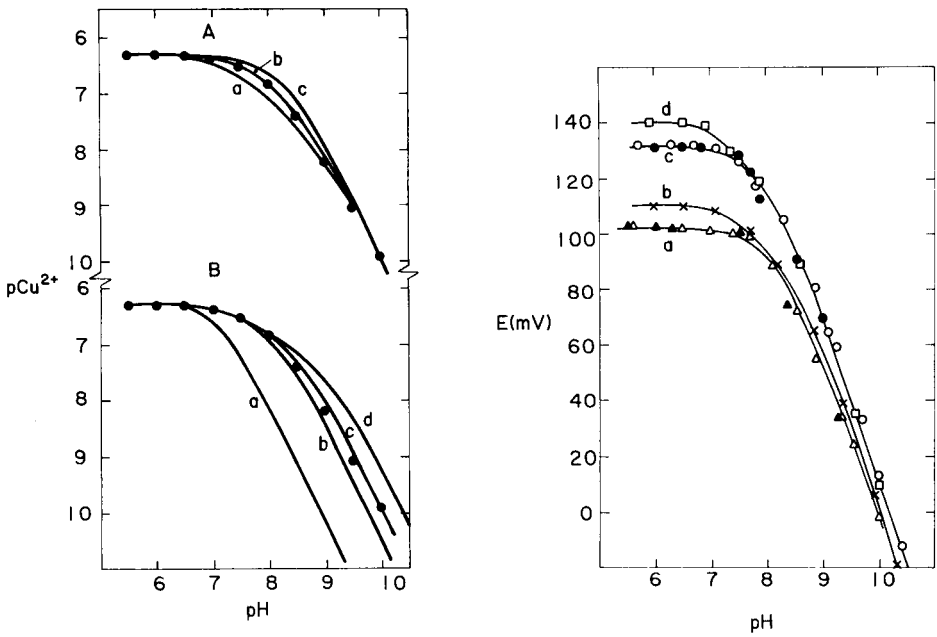

Fig. 3. Comparison of experimental (•) and calculated pCu^{2+} values for a 5×10^{-7} M Cu(II) solution in carbonate-free 0.1 M $NaNO_3$ under nitrogen. pCu^{2+} values were calculated using Eqns. 3 and 4 of Table 2 with: (A) log $*\beta_2$ = −16.0 and log $*\beta_1$ values of (a) −7.0, (b) −7.4, (c) −8.0; (B) log $*\beta_1$ = −7.4 and log $*\beta_2$ values of (a) −13.7, (b) −15.4, (c) −16.0, (d) −17.3.

Fig. 4. Copper-selective electrode response as a function of pH in air-saturated solutions. Open and closed symbols represent addition of acid and base, respectively, at initial Cu(II) concentrations of: (a) 5×10^{-7} M; (b) 1×10^{-6} M; (c) 5×10^{-6} M; (d) 1×10^{-5} M.

chloride solution. Because chloride ions can interfere with the response of the copper-selective electrode at appropriate concentrations [16], Vuceta and Morgan's experiments were repeated to examine if chloride interference could account for the large difference in $*\beta_2$ values. However, it proved impossible to duplicate their results in 10^{-3} M (or 10^{-1} M) chloride solutions, as the electrode response was similar to that observed in corresponding nitrate solutions (Table 1). There is no obvious reason for this discrepancy between the present results and those of Vuceta and Morgan.

It has been claimed that in copper hydrolysis studies, the copper-selective electrode response must be corrected for adsorption losses of dissolved copper species [9, 12]. An "apparent loss of total copper" from solution was found in the present work, but it occurred in the pH region where the copper—hydroxy colloid is formed. It was concluded that the loss is due to adsorption of the copper colloid on the vessel walls, etc.; thus, the electrode response need not be corrected for this effect because it is not "dissolved" copper species that are being lost from solution as had been suggested

[9, 12]. The formation and adsorption reactions of these colloids are rapid and reversible, because the same E—pH curve was re-traced when the direction of the pH titration of a solution was reversed (Fig. 1).

Influence of dissolved carbonate

Copper hydrolysis was also studied in solutions exposed to atmospheric carbon dioxide. The E—pH curves for different initial copper concentrations, (Fig. 4) are virtually identical to those obtained in carbonate-free solutions (Fig. 1) and are also similar to those previously reported [21]. The E—pH curves for total copper concentrations $\geqslant 10^{-6}$ M were independent of copper concentration for pH >8.5, as in the nitrogen-saturated solutions, and formation of a colloidal species in solution was again indicated by light scattering measurements. The same E—pH curve was obtained when the direction of the titration was reversed. When the copper electrode potential was measured as a function of time at a fixed pH, the electrode potentials in the linear region had shifted after 120 min by about 10 mV to more negative values.

The concentration of total dissolved carbonate in a solution exposed to the atmosphere varies from 4×10^{-5} to 6×10^{-2} M as the solution pH is varied from pH 7 to 10, and the corresponding carbonate ion concentration varies from 3×10^{-8} to 3×10^{-2} M [30]. Copper ions form strong complexes with carbonate ions [15, 27] and thus the concentration of free copper ions in a solution exposed to atmospheric carbon dioxide would be expected to be considerably lower than in a nitrogen-saturated solution. However, a comparison of the experimental and calculated pCu^{2+} values for air-saturated solutions (Fig. 5) shows that the measured pCu^{2+} values are orders of magnitude higher for pH > 9 than the values calculated by MINEQL by using Eqns. 1—10 (Table 2). Because of this large discrepancy, and because the same electrode potentials, the same slope (—60 mV/pH) for the linear section of the E—pH curves, and the same light scattering effects were observed whether or not the solutions are exposed to atmospheric carbon dioxide, it can be concluded that copper—carbonate complexes are not formed to any significant extent in solution under these conditions. It can also be concluded that the colloidal species present in these air-saturated solutions is $Cu(OH)_2$.

The finding that significant concentrations of copper—carbonate complexes are not formed (even after 2 h) when the solutions are exposed to atmospheric carbon dioxide was surprising, because the copper—hydroxy colloids are said to be thermodynamically unstable [26]. The influence of copper—carbonate formation on electrode response was studied by repeating the E—pH titrations in solutions containing a fixed amount of total carbonate. The values of the formation constants for the copper—carbonate complexes, determined by applying the degree of complex formation function ϕ [23], were in good agreement with literature values [9, 27] for total carbonate concentrations exceeding 10^{-3} M. Thus, the literature values for

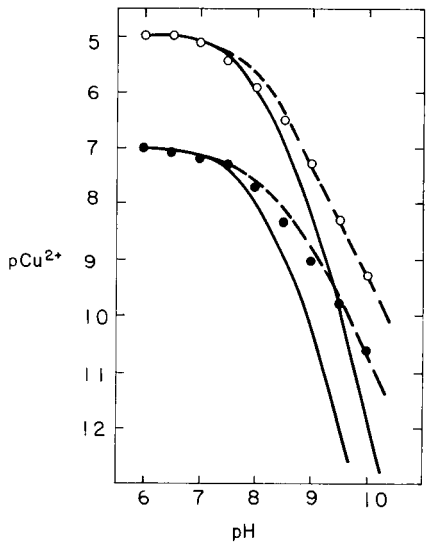

Fig. 5. Comparison of experimental (symbols) and calculated pCu^{2+} values in air-saturated 0.1 M $NaNO_3$ solution for initial copper concentrations of (○) 1×10^{-5} M and (●) 1×10^{-7} M. pCu^{2+} values were calculated using Eqns. 1—10 of Table 2 (—), or only Eqns. 1—4 (- - -).

β_1 and β_2 (Table 2) were used to calculate copper speciation in these solutions; agreement between experimental and calculated pCu^{2+} values is good (Fig. 6). This gives added confidence that the values of the constants in Table 2 are appropriate for the present experimental conditions, thereby further reinforcing the conclusion that copper—carbonate complexes are not formed to a significant extent in air-saturated solutions. It is evident that the total carbonate concentration affects the rate at which copper—carbonate complexes are formed.

Mechanism of electrode response

The response of the Ag_2S—CuS electrode in air-saturated solutions reported here, is very similar to that previously reported where it was concluded that the Ag_2S—CuS electrode was responding to cationic copper complexes [21]. To check this, the electrode potentials measured here were converted to $p\Sigma Cu^{2+}$ values which were then compared with the calculated $p\Sigma Cu^{2+}$ values (Fig. 7). There is poor agreement, for both air-saturated and nitrogen-saturated solutions, between experimental and calculated $p\Sigma Cu^{2+}$ values and trends, whether the values were calculated using the constants given earlier [21] or using the constants in Table 2.

The Ag_2S—CuS electrode is a silver ion sensor and its response to copper or sulfide ions is due to their influence on the silver ion concentration at the electrode surface [1, 2]. This response, and other selectivity and interference effects, is controlled primarily by thermodynamic and occasionally

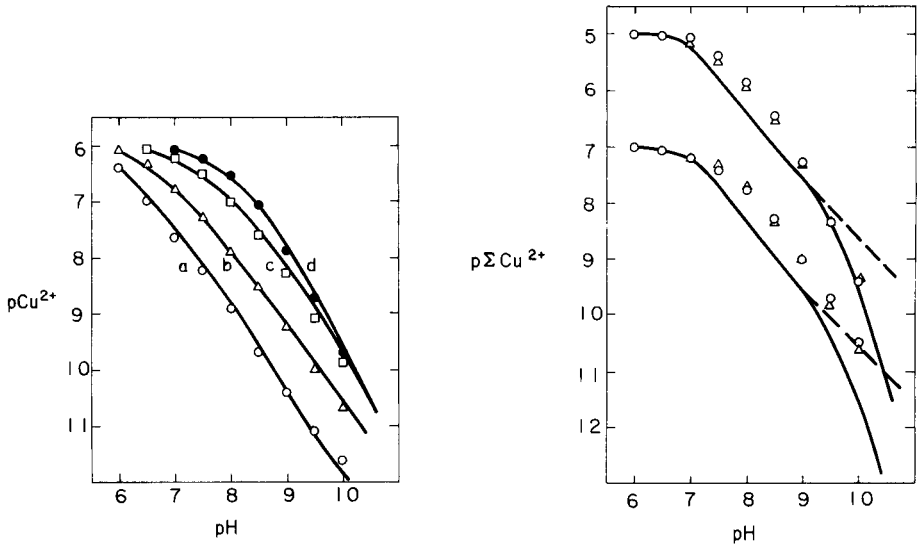

Fig. 6. Comparison of experimental pCu^{2+} values (symbols) with calculated values (solid lines) for 1×10^{-6} M Cu(II) in 0.1 M $NaNO_3$ solutions having a fixed total dissolved carbonate concentration of: (a) 5×10^{-2} M; (b) 1×10^{-2} M; (c) 1×10^{-3} M; (d) 1×10^{-4} M.

Fig. 7. Comparison of experimental $p\Sigma Cu^{2+}$ values in nitrogen-saturated (○) and air-saturated (△) 0.1 M $NaNO_3$ solutions with calculated values. Values of $p\Sigma Cu^{2+}$ were calculated with the constants of Table 2 of ref. [21] and log $*K_{so} = 8.6$, for nitrogen-saturated solutions (- - -) and air-saturated solutions (—).

by kinetic factors [1, 2, 19, 31]. There are no apparent thermodynamic or kinetic reasons why cationic copper complexes should influence the silver ion concentration at the electrode surface, in addition to the influence already exerted by Cu^{2+} ions. The present results show that the kinetic or non-thermodynamic factor influencing the electrode response is the formation of the thermodynamically unstable copper—hydroxy colloid. The presence and influence of this colloid was not recognized previously [21], but when it is taken into account the electrode response can be understood on the basis of conventional thermodynamic principles [1, 2].

Implications for speciation measurements

Ion-selective electrodes should be used with caution for speciation or complexation capacity measurements in natural waters. Evaluations of metal speciation and complexation capacity explicitly assume that thermodynamic equilibrium has been attained in the system. While ion-selective electrodes are thermodynamic devices, the conditions under which they are used more often represent situations controlled by kinetics than by equilibria. Measure-

ments are frequently made by spiking the sample with a metal-ion standard, allowing the system to "equilibrate" briefly and then comparing the response of unspiked and spiked samples. Serious errors may arise if it is not recognized that the spiked sample may not be at equilibrium because of: (i) the possible presence of thermodynamically unstable colloids, (ii) the variation in stability (solubility) of these colloids as a function of time, concentration, stirring rate, etc., and (iii) the influence of the concentration of ligands on the rate at which colloids are converted to stable complexes.

Recent work has shown that metal—humic acid complexes can precipitate from solution [32—35] and that the complexing capacity of soil fulvic acid solutions increases with increasing pH [33, 34]. This latter effect has been ascribed to increased removal of metal ions, including copper, from solution by adsorption onto the precipitated metal—humic acid particles [33, 34]. However, the copper—hydroxy colloids may have a role (as yet undefined) in causing this apparent increase in complexing capacity, because it is known that these colloids can be stabilized by humic substances [35]. The existence of copper—hydroxy—fulvate complexes has already been suggested [6, 33] and the present findings that these copper—hydroxy colloids are readily formed and are relatively stable provide a possible mechanism for the formation of such mixed complexes or precipitates. The existence of copper—hydroxy colloids may also assist in accounting for the low slopes reported for dialysis measurements of copper ions in the presence and absence of soil fulvic acid at pH 7 [33, 36]. It has been observed [9, 12], and confirmed here that the copper—hydroxy colloid is "lost" from solution by adsorption reactions, and thus the analysis of an acidified aliquot of this colloidal solution [33, 36] is not a true measure of the concentration of copper present.

We thank R. E. Jackson, Environment Canada, for providing the MINEQL program, and G. A. Parks, Stanford University, for suggesting the light scattering measurements. This paper was presented in part at the International Symposium on Electroanalysis, Cardiff, Wales, April 5—8, 1983.

REFERENCES

1 R. P. Buck, in H. Freiser (Ed.), Ion-Selective Electrodes in Analytical Chemistry, Vol. 1, Plenum, New York, 1978, Ch. 1.
2 J. W. Ross, in R. A. Durst (Ed.), Ion-Selective Electrodes, Natl. Bur. Stand. (U.S.) Spec. Publ., 1969, Ch. 2.
3 G. A. Bhat, R. A. Saar, R. B. Smart and J. H. Weber, Anal. Chem., 53 (1981) 2275.
4 R. A. Saar and J. H. Weber, Geochim. Cosmochim. Acta, 44 (1980) 1381; Anal. Chem., 52 (1980) 2095; Environ. Sci. Technol., 14 (1980) 877; Can. J. Chem., 57 (1979) 1263.
5 W. T. Bresnahan, C. L. Grant and J. H. Weber, Anal. Chem., 50 (1978) 1675.
6 J. Buffle, Anal. Chim. Acta, 118 (1980) 29.
7 J. Buffle, P. Deladoey, F. L. Greter and W. Haerdi, Anal. Chim. Acta, 116 (1980) 225.

8 J. Buffle, F. L. Greter and W. Haerdi, Anal. Chem., 49 (1977) 216.
9 W. G. Sunda and P. J. Hanson, in E. A. Jenne (Ed.), Chemical Modeling in Aqueous Systems, ACS Symp. Ser. No. 93, 1979, Ch. 8.
10 R. Stella and M. T. Ganzerli-Valentini, Anal. Chem., 51 (1979) 2148.
11 J. Vuceta and J. J. Morgan, Limnol. Oceanogr., 22 (1977) 742.
12 A. J. Paulson and D. R. Kester, J. Solution Chem., 9 (1980) 269.
13 D. S. Gamble and M. Schnitzer, in P. C. Singer (Ed.), Trace Metals and Metal—Organic Interactions in Natural Waters, Ann Arbor Science, Ann Arbor, 1973, Ch. 9.
14 D. S. Gamble, A. W. Underdown and C. H. Langford, Anal. Chem., 52 (1980) 1901.
15 J. O. Leckie and J. A. Davis, in J. O. Nriagu (Ed.), Copper in the Environment, Part 1, Wiley, New York, 1979, Ch. 5.
16 J. C. Westall, F. M. M. Morel and D. N. Hume, Anal. Chem., 51 (1979) 1792.
17 A. Jyo, T. Hashizume and N. Ishibashi, Anal. Chem., 49 (1977) 1868.
18 J. Barica, J. Fish. Res. Board Can., 35 (1978) 141.
19 J. Gulens, Ion-Selective Electrode Rev., 2 (1980) 117.
20 W. Stumm and J. J. Morgan, Aquatic Chemistry, 2nd edn., Wiley, New York, 1981, Ch. 5.
21 R. Wagemann, J. Phys. Chem., 84 (1980) 3433.
22 J. C. Westall, J. L. Zachery and F. M. M. Morel, MINEQL-A Computer Program for the Calculation of Chemical Equilibrium Composition of Aqueous Systems, Tech. Note 18, Dept. Civil Eng., MIT, Cambridge, MA, 1976.
23 F. R. Hartley, C. Burgess and R. M. Alcock, Solution Equilibria, Halsted Press-Wiley, New York, 1980, Ch. 3.
24 G. J. M. Heijne and W. E. van der Linden, Anal. Chim. Acta, 96 (1978) 13.
25 P. Schindler, H. Althaus, F. Hofer and W. Minder, Helv. Chim. Acta, 48 (1965) 1204.
26 W. Stumm and J. J. Morgan, Aquatic Chemistry, 2nd edn., Wiley, New York, 1981, p. 299.
27 R. M. Smith and A. E. Martell, Critical Stability Constants, Vol. 4, Plenum, New York, 1976.
28 R. N. Sylva and M. R. Davidson, J. C. S. Dalton Trans., (1979) 232.
29 C. F. Baes and R. E. Mesmer, The Hydrolysis of Cations, Wiley, New York, 1976, Ch. 12.
30 W. Stumm and J. J. Morgan, Aquatic Chemistry, 2nd edn., Wiley, New York, 1981, p. 180.
31 A. Hulanicki and A. Lewenstam, Talanta, 29 (1982) 661.
32 G. K. Pagenkopf and C. Whitworth, J. Inorg. Nucl. Chem., 43 (1981) 1219.
33 D. P. Rainville and J. H. Weber, Can. J. Chem., 60 (1982) 1.
34 D. K. Ryan and J. H. Weber, Anal. Chem., 54 (1982) 986.
35 P. G. C. Campbell, M. Bisson, R. Gagne and A. Tessier, Anal. Chem., 49 (1977) 2358.
36 R. E. Truitt and J. H. Weber, Anal. Chem., 53 (1981) 337.

Analytica Chimica Acta, 156 (1984) 33—42
Elsevier Science Publishers B.V., Amsterdam — Printed in The Netherlands

ELECTROCHEMICAL STUDIES OF HOMOCYSTEINE AND HOMOCYSTINE AT MERCURY ELECTRODES

A. M. BOND*, S. B. THOMSON and D. J. TUCKER
Division of Chemical and Physical Sciences, Deakin University, Victoria 3217 (Australia)
M. H. BRIGGS
Division of Biological and Health Sciences, Deakin University, Victoria 3217 (Australia)
(Received 3rd August 1983)

SUMMARY

The behaviour of homocysteine and cysteine at mercury electrodes is compared. The one-electron oxidation associated with thiols is shown to be the same for both compounds in acidic phosphate buffer, giving rise to an adsorbed thiol—mercury complex, $(RS)_2Hg$, at the electrode surface. Formation of this complex is utilized in the cathodic stripping voltammetric determination of homocysteine; the detection limit is 10^{-9} M after a deposition time of 90 s at a hanging mercury drop electrode. The similar $E_{1/2}$ values for homocysteine and cysteine mean that prior separation is needed for their individual determination. Amperometric detection with a mercury-coated gold electrode after separation by cation-exchange liquid chromatography provides a method for the simultaneous determination of both compounds. Reduction of homocystine at the mercury electrode is also compared to that of cystine. The more negative reduction potential, and the maximum observed for homocystine on d.c. polarograms, which is not seen for cystine, is attributable to different reaction kinetics at the mercury electrode; the products of both the 2-electron reductions are the corresponding thiol-containing amino acids.

Homocysteine is a product of methionine metabolism not normally detectable in human tissue fluids [1], but in cases of homocystinuria (a block in the metabolic pathway between homocysteine and cystathionine caused by an enzyme deficiency), an accumulation of this thiol-containing amino acid is seen in blood and urine [2, 3]. The physical manifestations of this disease can be extremely severe, including mental retardation, gross skeletal abnormalities and premature vascular disease [4, 5], and the possibility that previously undetected levels of homocyst(e)ine may be found in a sub-clinical group which predispose them toward some effects of this disease warrants the development of a more sensitive method of determination suitable for biological specimens. People at risk from chronic renal failure could also benefit from an enhanced detection of homocyst(e)ine, since a study has shown increased plasma levels of homocystine in over 85% of cases of this disease [6].

Cysteine (R—SH) and homocysteine (R′—SH) have a close structural similarity.

0003-2670/84/$03.00

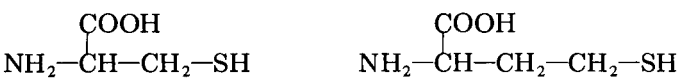

Cysteine Homocysteine

The literature contains numerous references to the anodic reactions of cysteine at mercury [7—12], which involves the formation of an adsorbed species: $Hg(RS)_2$. As a consequence, several electrochemical detectors for cysteine, based on mercury as the working electrode, have been constructed for plasma and urine analysis [13—16], and in two cases, this system has also been utilized to detect the presence of homocysteine [13, 14]. The assumption has been made [13, 14] that the response seen from homocysteine at mercury is due to the same mechanism as for cysteine, although this has not been proved.

In this work, the mechanism of homocysteine has been verified, and the limits of detection of the two thiol-containing compounds by using differential pulse cathodic stripping voltammetry evaluated. Additionally, the feasibility of a chromatographic separation with electrochemical detection has been examined, because separation of the two compounds is necessary prior to detection when they are both present in the same sample, as will usually be the case.

The electrochemical reduction of cystine (R—S—S—R) and homocystine (R′—S—S—R′) has also been compared in this study, because although investigations have shown that cystine reduces at mercury with the formation of two cysteine molecules [7—10], the mechanism of homocystine reduction has yet to be determined. A possible method for determining low concentrations of these species can be based on chemical or electrochemical reduction to produce the thiol [14—16] followed by determination of the thiol.

EXPERIMENTAL

Instrumentation

Direct current (d.c.) and differential pulse (d.p.) polarograms were obtained at a dropping mercury electrode. Other voltammetric (stripping) studies were undertaken with a static mercury drop electrode (Model 303, EG & G Princeton Applied Research) using "medium" sized drops in the hanging mercury drop mode. Cathodic stripping voltammetry (c.s.v.) used the differential pulse setting (d.p.c.s.v.) at a scan rate of 10 mV s^{-1}, with 50-mV pulses every 0.5 s, after a deposition time of 90 s at +0.05 V, with stirring, unless otherwise stated. Potential control and current measurements were made with a Princeton Applied Research Model 174 Polarographic Analyzer, and all electrode potential values were measured versus a Ag/AgCl (3 M KCl) reference electrode. The counter electrode was a platinum wire. The polarograms and voltammograms were recorded on an X-Y recorder (Omnigraphic series 2000, Houston Instruments).

Coulometric studies were undertaken with a Model 173 Princeton Applied

Research Potentiostat/Galvanostat linked with a digital coulometer (Model 179, Princeton Applied Research), using a mercury pool electrode, and same reference and counter electrodes (salt bridge added) as in the other studies.

The ion-exchange chromatographic investigation used an LC-304 series liquid chromatograph with a sample injection loop of 100 μl (Bioanalytical Systems), an eluent flow rate of 0.7 ml min^{-1}, and a 250 mm × 4.6 mm i.d. column packed with Zipax SCX-10 strong cation exchange resin (DuPont). Electrochemical detection of the eluent was done with a flow-through cell (EA 1096/2, Metrohm) equipped with a 3-electrode system; the working electrode was mercury-coated gold (EA 286/3) with a Ag/AgCl reference electrode (3 M KCl) (EA 442) and a glassy carbon counter electrode (EA 286/1). The PAR Model 174 Polarographic Analyzer was used as the amperometric detector.

Chemicals

In all experiments, sodium dihydrogenphosphate (analytical reagent grade; BDH Chemicals) was used at a buffer strength of 0.02 M in distilled water, except for the pH dependence investigations, which also used sodium tetraborate (AR grade; BDH Chemicals). In all cases, the pH was adjusted with orthophosphoric acid (AR grade; BDH Chemicals). Prior to chromatographic work, the buffer was filtered through a 0.45-μm filter (Millipore Corporation). Mercury was triply distilled (Engelhard Pty.). The amino acids used were: L-cysteine, L-cystine and L-homocystine (puriss grade; Fluka), and two D,L-homocysteine samples (one from ICN Life Sciences Group, New York, and the other from Sigma). The 5,5′-dithiobis(2-nitrobenzoic acid) (DTNB) sample was from Sigma.

RESULTS AND DISCUSSION

Thiols

Homocysteine slowly undergoes γ-thiolactone formation on storage [17], necessitating a purity value with respect to the free thiol groups in the two homocysteine samples to be determined. Using the method involving DTNB (Ellmans' reagent) [18—20], the stable cysteine sample was found to have a purity of 98.6%, as expected, while the Sigma homocysteine sample exhibited 95.1% purity and the ICN Life Sciences sample of homocysteine had an apparent purity of 67.2%. These figures compared favourably with electrochemical determination of homocysteine purity (where responses for these samples were compared to cysteine response, which was assumed to be 100% pure). D.c. polarography indicated a purity figure of 95.6% for the Sigma homocysteine sample, whereas polarography, coulometry and a comparison of h.p.l.c. peak heights for the ICN Life Sciences sample of homocysteine gave purity figures of 67.4%, 68.1% and 66.9%, respectively. As a consequence, concentrations of homocysteine samples stated in the following results have been adjusted to allow for the reduced purity.

The d.c. polarograms of cysteine and homocysteine are shown in Fig. 1. As can be seen, they are virtually identical, having similar limiting currents per unit concentration, and shape, as well as both having $E_{1/2}$ values of —0.125 V (drop time 0.5 s). These polarograms also indicate very strong product adsorption accompanying the charge transfer. The indication that the reaction involving these two thiol-containing amino acids and mercury is the same is further supported by Fig. 2. This shows cyclic voltammetric sweeps for cysteine and homocysteine, and again it is seen that the forward (oxidation) scans for both have the same oxidation peak potentials of —0.160 V (scan rate 100 mV s^{-1}). The reduction sweeps for the two amino acids also show a sharply defined symmetrical peak with a reduction peak potential of —0.20 V.

The small peak-to-peak separation, and the sharply defined cathodic peaks are indicative of stripping of a thin film during the reverse scan, which is what is expected for cysteine, because it forms an absorbed species during oxidation [7—12]. The identical behaviour of homocysteine to cysteine in these cases leads to the conclusion that at mercury, therefore, the oxidation reaction causes formation of a layer of the $Hg(RS)_2$ complex

$$Hg + 2RSH \rightarrow Hg(RS)_2 + 2H^+ + 2e^- \quad (1)$$

Figure 3 shows that addition of homocysteine to a solution of cysteine gives the same increased response that addition of cysteine would give. Thus, simultaneous determination of both species is not possible. Comparative coulometric studies of the two thiol-containing amino acids gave results of n = 1.07 for cysteine and n = 1.01 for homocysteine, confirming further

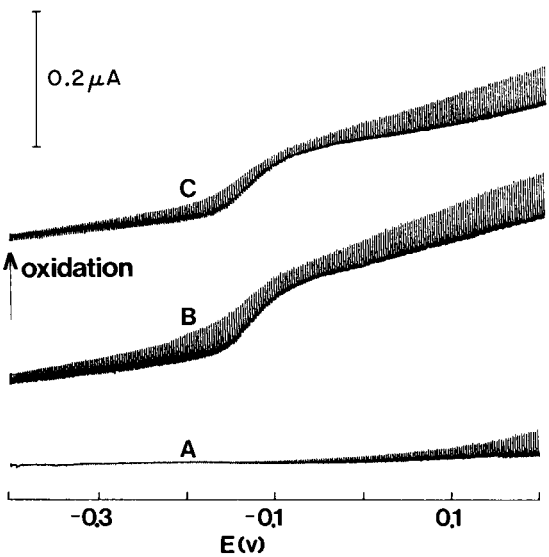

Fig. 1. D.c. polarograms (drop time 0.5 s) of: (A) oxygen-free 0.02 M NaH_2PO_4 buffer, pH 2.2; (B) oxygen-free buffer + 2×10^{-4} M cysteine; (C) oxygen-free buffer + 2×10^{-4} M homocysteine.

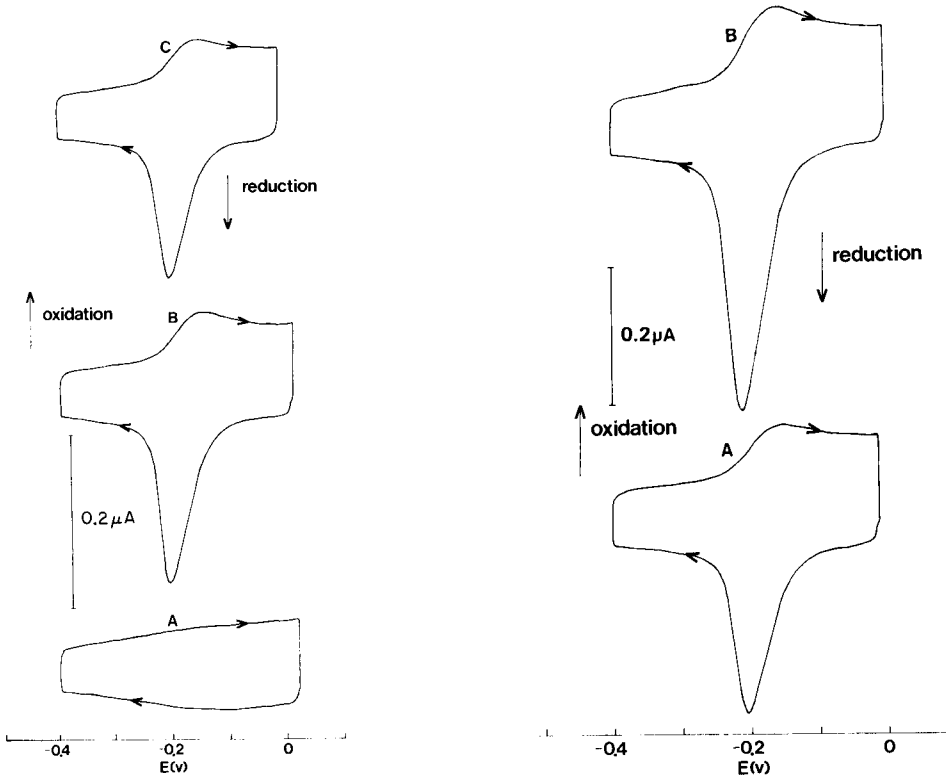

Fig. 2. Cyclic voltammograms (scan rate 100 mV s^{-1}) of: (A) oxygen-free 0.02 M NaH_2PO_4, pH 2.2; (B) oxygen-free buffer + 2 × 10^{-5} M cysteine; (C) oxygen-free buffer + 2 × 10^{-5} M homocysteine.

Fig. 3. Cyclic voltammograms (scan rate 100 mV s^{-1}) of: (A) oxygen-free buffer + 1.3 × 10^{-5} M cysteine; (B) oxygen-free buffer + 1.3 × 10^{-5} M cysteine + 1.3 × 10^{-5} M homocysteine.

that they are both 1-electron reactions per mole of RSH as required for Eqn. 1, and agreeing with coulometric data for cysteine [12].

Differential pulse polarography of the homocysteine sample showed that the detection limit for this compound at mercury is approximately 10^{-6} M. The peak current versus concentration relationship is linear at least over the range 10^{-5}—10^{-4} M (Fig. 4).

Figure 5 represents a plot of buffer pH versus $E_{1/2}$ for homocysteine samples of the same concentration; $E_{1/2}$ becomes more negative as the alkalinity of the buffer is increased, agreeing with previous observations made for cysteine [7, 10, 12, 21, 22], and also as required by Eqn. 1. At pH 9.2, the limiting current for homocysteine samples diminished in size compared to values in more acidic buffers (Fig. 5). The rate of autoxidation of thiols increases continuously with increase in pH [17]. For this reason, as

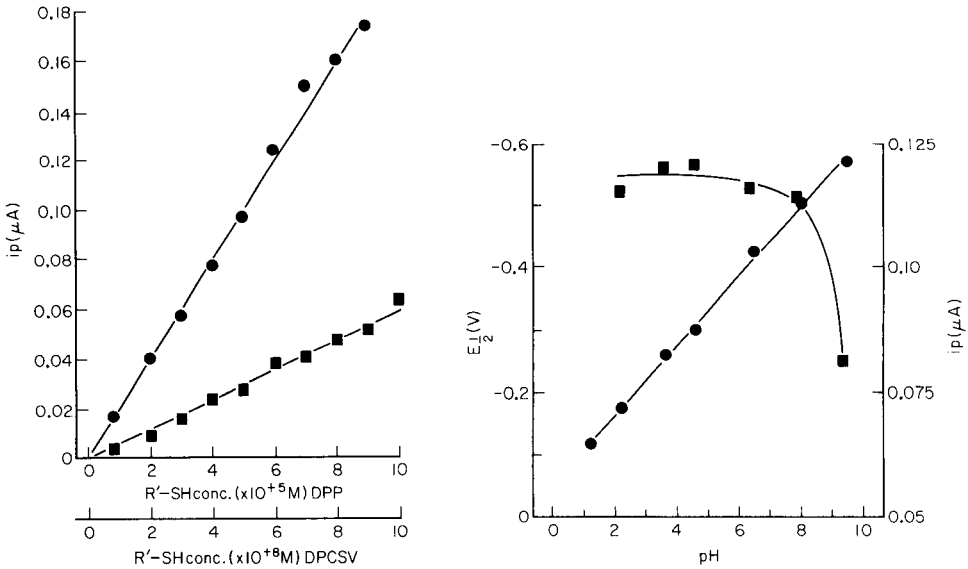

Fig. 4. Peak current vs. homocysteine concentration: (•) d.p. polarography; (▪) d.p. cathodic stripping voltammetry in 0.02 M NaH_2PO_4, pH 2.2. For d.p.c.s.v., deposition time was 90 s at +0.05 V, scan rate 10 mV s^{-1}, pulse 50 mV every 0.5 s.

Fig. 5. $E_{1/2}$ values (•) and peak currents (▪) of 10^{-5} M homocysteine samples vs. buffer pH, using differential pulse polarography (0.5 s drop time, 10 mV s^{-1} scan rate). Buffers used were 0.02 M NaH_2PO_4 up to pH 4.5, and 0.02 M $Na_2B_4O_7$ for higher pH values; pH alterations of the buffers were made with 15 M H_3PO_4.

well as for long-term practical purposes [13, 14], all subsequent polarographic work was done with acidic buffers.

Cathodic stripping voltammetry [23—27] has been used quite extensively to determine cysteine, and a detection limit in the vicinity of 10^{-9} M has been established [26, 27]. As the cyclic voltammograms in Fig. 2 indicated identical reaction mechanisms for cysteine and homocysteine at mercury, d.p.c.s.v. was examined for the determination of homocysteine. Under the deposition and stripping conditions described in the experimental section, a detection limit of 10^{-9} M was found, and also a direct relationship between peak height and homocysteine concentration for concentrations below 10^{-7} M (Fig. 4). Therefore, d.p.c.s.v. could in principle be an extremely useful method for determining microgram concentrations of homocysteine. However, Fig. 2 has shown that cysteine and homocysteine have virtually identical stripping peaks, and in a solution containing both these thiols, discriminatory c.s.v. of either of them in the presence of the other is impossible.

As a consequence of this identical behaviour, in both the polarographic and c.s.v. procedures, any solutions containing both homocysteine and

cysteine require a separation step prior to the electrochemical detection to permit determination of either of the thiols independently. As can be seen in Fig. 6, separation can be achieved by using liquid chromatography as described in the experimental section, the detection of the thiols being done amperometrically at a mercury-coated gold electrode held at +0.10 V versus Ag/AgCl. A detection limit of about 10^{-6} M is possible for both species when this amperometric method is used. If fractions are collected followed by d.p.c.s.v., a much lower detection limit should be attainable.

Disulfides

D.c. polarograms of cystine and homocystine are presented in Fig. 7. As mentioned above, the reduction of cystine at the dropping mercury electrode to give two cysteine molecules

$$R{-}S{-}S{-}R + 2H^+ + 2e^- \rightarrow 2R{-}SH \qquad (2)$$

is well documented [7—10], whereas the reduction of homocystine is not. However, unlike the thiol cases where the electrode reactions were identical, there is a difference with the disulfides: the $E_{1/2}$ values are separated by nearly 200 mV, the value for cystine being —0.455 V and for homocystine

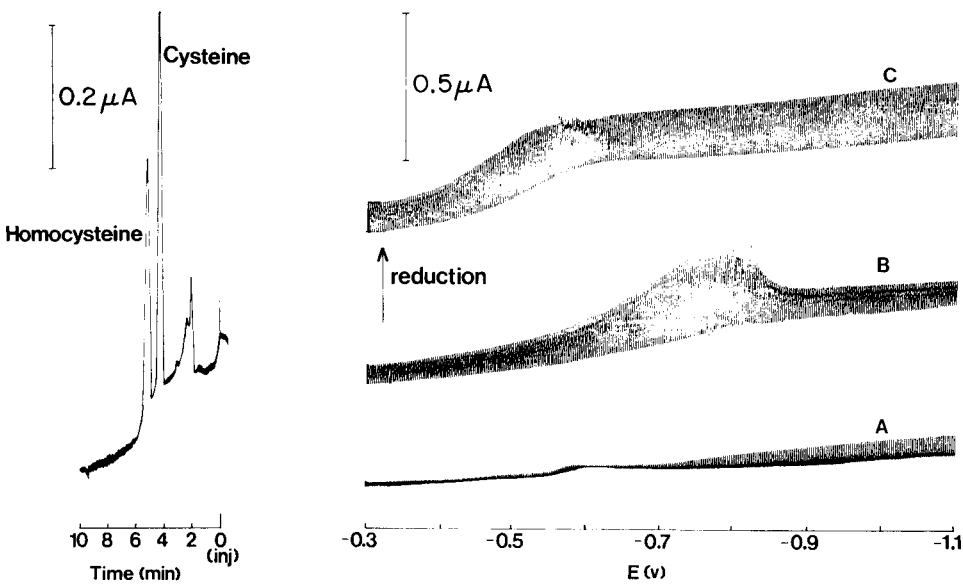

Fig. 6. Cation-exchange liquid chromatography with electrochemical detection of cysteine and homocysteine. Eluting solvent was 0.02 M NaH_2PO_4, pH 2.2, at 0.7 ml min^{-1}, with detection at a mercury-coated gold electrode held at +0.10 V vs. Ag/AgCl. The injected sample contained 5×10^{-5} M concentrations of cysteine and homocysteine in 80 μl of buffer.

Fig. 7. D.c. polarograms (drop time 0.5 s) of: (A) oxygen-free 0.02 M NaH_2PO_4 buffer, pH 2.2; (B) oxygen-free buffer + 10^{-4} M homocystine; (C) oxygen-free buffer + 10^{-4} M cystine.

—0.650 V, at a drop time of 0.5 s. Also, the shapes of the polarograms differ, with homocystine exhibiting a maximum not shown by cystine [28]. Indication of a difference in the electrode kinetics and/or mechanism at mercury for the two disulfides is shown in Fig. 8, where the cyclic voltammograms are presented. The two-electron reduction of cystine occurs as a single wave and the absence of current at appropriate potentials on the backward scan shows that this reduction is irreversible, as expected [7, 10]. However, the forward (reduction) scan of homocystine gives rise to a complex current-voltage curve exhibiting evidence for very strong adsorption. On reversal, the homocystine scan also exhibits irreversibility, as well as a change in double-layer capacitance compared to the supporting electrolyte, again consistent with the influence of adsorption/desorption processes.

The observed differences between cystine and homocystine at mercury must result from differences in the electrochemical and chemical kinetics of the reaction. The overall reaction (i.e., disulfide reducing to 2 thiols) is the same in each case. This conclusion is based upon the observations that in the d.c. polarograms of cystine and homocystine at the same concentrations, the limiting currents per unit concentration for the disulfides are very similar. Controlled potential reductions of the disulfides give single products, the respective thiols, and are two-electron steps confirming that the overall processes are the same.

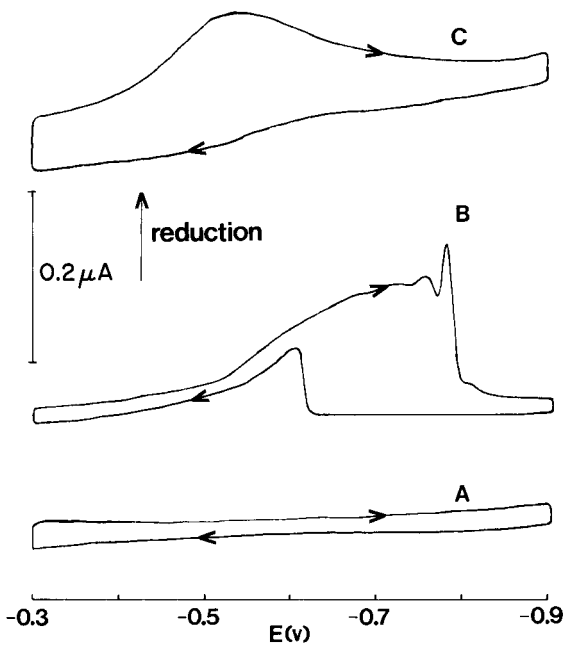

Fig. 8. Cyclic voltammograms (scan rate 100 mV s^{-1}) of: (A) oxygen-free 0.02 M NaH_2PO_4 buffer, pH 2.2; (B) oxygen-free buffer + 10^{-4} M homocystine; (C) oxygen-free buffer + 10^{-4} M cystine.

Conclusions

The oxidation reaction associated with homocysteine at the mercury electrode parallels that for cysteine, and results in the formation of a film of a mercury-thiol, $(RS)_2Hg$, complex. Homocysteine can be determined by d.p.p. at concentrations down to 10^{-6} M; 10^{-9} M and even lower concentrations can be determined when this adsorption film on the electrode is exploited by using d.p.c.s.v. Linearity of response versus homocysteine concentration has been shown for both of these techniques, indicating substantial potential for analytical work on homocysteine. The similarity between the responses of the two thiols at the mercury electrode, however, necessitates the development of a cation-exchange liquid chromatographic separation system to allow the simultaneous determination of each of these amino acids, the detection being done amperometrically at a mercury-coated gold electrode.

Investigation of homocystine indicates that while the kinetics of the reduction at mercury differs from that of cystine, the overall reaction in which two thiol molecules are formed from each disulfide is the same. As a consequence, any analytical work involving determination of these disulfides can utilize prior reduction to form the thiol followed by d.p.c.s.v. Work is currently in progress in these laboratories aimed at applying the above principles to the determination of homocysteine in biological systems.

REFERENCES

1 Soo-Song Kang, P. W. K. Wong and N. Becker, Pediatr. Res., 13 (1979) 1141.
2 D. Valle, G. S. Pai, G. H. Thomas and R. E. Pyeritz, Johns Hopkins Med. J., 146 (1980) 110.
3 R. Griffiths, in J. M. Rattenburg (Ed.), Amino Acid Analysis, E. Horwood, Chichester, 1981.
4 V. J. Gupta and D. E. L. Wilcken, Eur. J. Clin. Invest., 8 (1978) 205.
5 R. W. Hund, E. J. Hammond and B. J. Wilder, Brain Res., 209 (1981) 250.
6 D. E. L. Wilcken and V. J. Gupta, Eur. J. Clin. Invest., 9 (1979) 301.
7 I. M. Kolthoff and C. Barnum, J. Am. Chem. Soc., 62 (1940) 3061.
8 I. M. Kolthoff and C. Barnum, J. Am. Chem. Soc., 63 (1941) 520.
9 W. Stricks and I. M. Kolthoff, J. Am. Chem. Soc., 75 (1953) 5673.
10 I. M. Kolthoff, W. Stricks and N. Tanaka, J. Am. Chem. Soc., 77 (1955) 5211.
11 I. R. Miller and J. Teva, J. Electroanal. Chem., 36 (1972) 157.
12 M. T. Stankovich and A. J. Bard, J. Electroanal. Chem., 75 (1977) 487.
13 D. L. Rabenstein and R. Saetre, Anal. Chem., 49 (1977) 1036.
14 R. Saetre and D. L. Rabenstein, Anal. Biochem., 96 (1978) 684.
15 R. Eggli and R. Asper, Anal. Chim. Acta, 101 (1978) 253.
16 L. A. Allison and R. E. Shoup, Anal. Chem., 55 (1983) 8.
17 P. C. Jocelyn, Biochemistry of the Thiol Group, Academic Press, London, 1972, p. 5.
18 G. L. Ellman, Arch. Biochem. Biophys., 82 (1959) 70.
19 A. F. S. A. Habeeb in S. P. Colowick and N. O. Kaplan (Eds.), Methods in Enzymology, Vol. XXV, Academic Press, London, 1972.
20 A. Fontana and C. Toniolo, in S. Patai (Ed.), The Chemistry of the Thiol Group Part I, Wiley, New York, 1974.
21 C. A. Mairesse-Ducamois, G. J. Patriarche and J. A. Vanderbalck, J. Pharm. Belg., 31 (1976) 169.

22 V. Almagro, M. M. Gomez and J. Sancho, Anal. Quim., 72 (1976) 602.
23 I. E. Davidson and W. F. Smyth, Anal. Chem., 49 (1977) 1195.
24 M. Youssefi and R. L. Birke, Anal. Chem., 49 (1977) 1380.
25 T. M. Florence, J. Electroanal. Chem., 97 (1979) 219.
26 R. A. Grier and R. W. Andrews, Anal. Chim. Acta, 124 (1981) 333.
27 U. Forsman, J. Electroanal. Chem., 122 (1981) 215.
28 L. Meites, Polarographic Techniques, 2nd edn., Wiley, New York, 1965.

Analytica Chimica Acta, 156 (1984) 43—49
Elsevier Science Publishers B.V., Amsterdam — Printed in The Netherlands

CATHODIC STRIPPING VOLTAMMETRY OF THE PEPTIDE FELYPRESSIN IN TRACE AMOUNTS

ULF FORSMAN

Astra Läkemedel AB, Research and Development Laboratories, Pharmaceutical Analysis, S-151 85 Södertälje (Sweden)

(Received 16th March 1983)

SUMMARY

Felypressin, a peptide containing eight amino acids including cystine, is studied by cathodic stripping voltammetry (c.s.v.) at a mercury drop electrode at pH 4.6 in the concentration interval 5×10^{-9}—7×10^{-7} M. Excess of copper(II) ions is required to obtain the c.s.v. activity. The stripping peak potential is —0.55 to —0.70 V vs. SCE depending on the excess of copper(II). The accumulated product is adsorbed both in its oxidized and reduced state. Interference from c.s.v.-active substances which desorb in the reduced state can be eliminated by applying a repetitive cyclic scan and evaluating the second or third scan. Lypressin and somatostatin, two other cystine-containing peptides, are also c.s.v.-active.

Peptides are playing an increasingly important role in pharmacology. In this development, new demands are placed on methods for their determination. The peptide felypressin (I; m.w. 1040) is used in combination with local anaesthetics at a low formulation level (5×10^{-7} M). At present, the

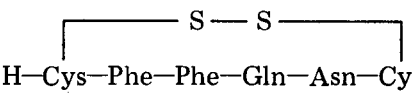

H—Cys—Phe—Phe—Gln—Asn—Cys—Pro—Lys—Gly—NH_2 (I)

bioassay technique comprising measurement of blood pressure in rats [1] is used for the determination of the peptide at this low concentration. Liquid chromatographic methods have been presented for several peptides closely related to felypressin [2, 3]. A detection limit of 30 ng was reported [2]. The development of highly sensitive analytical methods for peptides is naturally of great interest.

Felypressin contains cystine, which suggests that the very sensitive technique of cathodic stripping voltammetry (c.s.v.) should be applicable. Cystine, as well as cysteine, penicillamine and several penicillins have previously been investigated by c.s.v. [4—6]. These substances can accumulate at a mercury electrode in the form of a copper complex when excess of Cu(II) is present. Detection limits as low as 2×10^{-10} M were reported. These compounds can also be accumulated as mercury complexes, but this approach requires solutions extremely free from Cu(II), because this ion,

0003-2670/84/$03.00

even at concentrations much lower than that of the sulphur compound, interferes with the accumulation of the mercury complex.

In the present paper, the c.s.v. characteristics of felypressin are reported. An acetate buffer of pH 4.6 was chosen because felypressin is less stable in neutral and alkaline media.

EXPERIMENTAL

Equipment, sample and reagents

A PAR-174 polarographic analyzer was used. The working electrode was a Metrohm EA-290 hanging mercury drop electrode (HMDE); a drop with a surface area of 0.9 mm^2 was used throughout. A platinum auxiliary electrode and a saturated calomel reference electrode were also used. All potentials given refer to the SCE.

Felypressin (Sandoz, Switzerland) was obtained in solution with a declared concentration of 25 IU ml^{-1} (4.13×10^{-4} M). Solutions diluted to 4.8×10^{-6} M were used as standard solutions.

The acetate buffer, pH 4.6, was composed of equal volumes of 0.05 M acetic acid and 0.05 M sodium acetate in water. Stock solutions of copper(II) nitrate (Merck) were 1×10^{-2}—1×10^{-4} M. Appropriate amounts of stock solution was added to the buffer to produce the desired copper(II) ion concentration. All reagents were of analytical grade.

Procedure

An aliquot of the solution to be investigated was added to 10 ml of deaerated pH 4.6 buffer solution. Accumulation was done at −0.30 V for 1 min, with stirring unless otherwise stated. A repetitive cyclic scan of 100 mV s^{-1}, with an initial cathodic scan direction, was then applied. Scan reversal was done manually at the desired potentials.

RESULTS AND DISCUSSION

Stripping voltammetric pattern

In Fig. 1, cyclic stripping voltammograms obtained from felypressin both before and after the addition of Cu(II) ions are shown. In the 5×10^{-8} M solution, two cathodic peaks, c_1 and c_1', and one anodic peak, a_1, are obtained in the first scan cycle. In the second cycle, the peak c_1' is lost, and the voltammogram shows only one cathodic, c_2, and one anodic, a_2, peak. In the 2×10^{-7} M solution, a hump is obtained at potentials more positive than the peaks described above. This hump is present also during the second scan cycle. The peaks c_1, c_2, a_1, a_2 all increase in height when Cu(II) is added. The peak separation between the anodic and cathodic peaks decreases with increasing excess of Cu(II) and reaches a minimum value of about 20 mV.

The accumulated product responsible for the peak couples c_1/a_1 and c_2/a_2 is adsorbed in both its oxidized and reduced forms, because the anodic

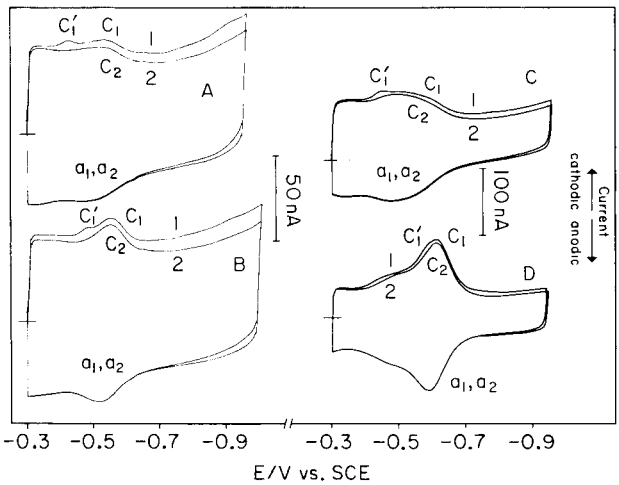

Fig. 1. Cyclic stripping voltammograms: (A) 5×10^{-8} M felypressin; (B) Cu(II) added to A to give a 1×10^{-7} M concentration; (C) 2×10^{-7} M felypressin; (D) Cu(II) added to C to give a 1.4×10^{-6} M concentration. Curves 1 and 2 are the first and second scan cycles, respectively.

and cathodic peaks are of equal height and are obtained on repetitive cyclic scans. The loss of the peak c_1' in the second scan cycle, indicates that the product responsible for this peak desorbs at potentials negative to its peak potential. The stripping procedure for felypressin was mainly based on the peak c_2 obtained in the second cycle, where the influence of c_1' is eliminated. The peak height of c_2 increases linearily with sweep rate, v, ($r^2 = 0.9999$) when examined between 20 and 200 mV s^{-1}, in accordance with the behaviour of a film stripping peak.

An anodic scan, conducted after the accumulation in presence of Cu(II), yields an anodic peak at +0.06 V and a cathodic peak at the same potential upon scan reversal. The peaks are situated close to the peak couple of copper amalgam and are therefore obscured when high excesses of Cu(II) are present. The analytical utility of this peak couple for the determination of felypressin is thus limited, and was not investigated further.

Dependence on the presence of copper(II) ions

The presence of copper ions seems to be essential for obtaining the stripping peaks. The dependence of the peak height, i_p, of peak c_2, on the level of copper(II) ions is shown in Fig. 2. With an increasing excess of Cu(II), a constant value of i_p is approached. Simultaneously, the peak width decreases, and the peak potential, E_p, is displaced in the negative direction (Fig. 1). The peaks c_1, a_1, a_2, follow the same pattern. The E_p value of c_2 from 5×10^{-8} felypressin in the presence of 1×10^{-7} M Cu(II) was —0.55 V, but —0.65 V in the presence of 1×10^{-5} M Cu(II). The influence of the Cu(II) concentration on the peak shape follows the characteristics previously reported for cysteine and penicillamine [5].

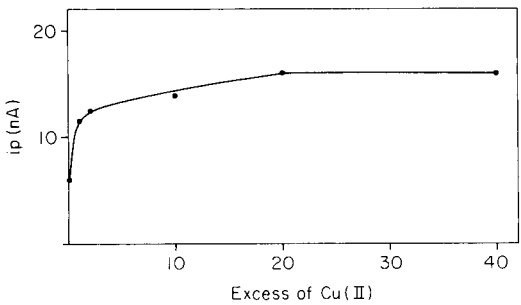

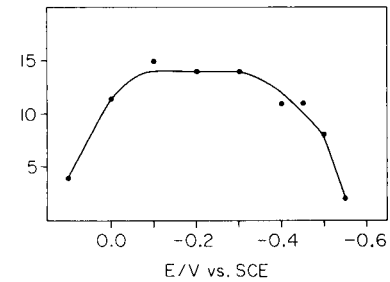

Fig. 2. Peak current of c_2 from 5×10^{-8} M felypressin as a function of the molar excess of copper(II).

Fig. 3. Peak current of c_2 as a function of accumulation potential for 5×10^{-8} M felypressin in the presence of 2×10^{-7} M Cu(II).

It is well-known that cystine, cysteine, and several other sulphur-containing compounds yield cathodic stripping peaks in the absence of Cu(II), because of the reduction of accumulated mercury compounds [4—8]. In the cases of cystine, cysteine and penicillamine, the stripping peak for the mercury compound is well separated from the peak for the copper compound [4—6]. Because the stripping activity is very low when felypressin is in excess over Cu(II) in the solution, it appears that the peptide does not form, or forms only very slowly, an accumulated mercury compound. The peak c_1' probably is not due to a mercury compound of felypressin, because this peak is obtained also in presence of excess of Cu(II).

Accumulation potential

The dependence of i_p of peak c_2 on the accumulation potential, E_{acc}, is shown in Fig. 3. The peak height rapidly decreases at E_{acc} more positive than about 0.0 V. This is also the redox potential of the copper amalgam system, which indicates that the stripping peak is only obtained if copper amalgam is formed from excess of Cu(II) during the accumulation period. This is in accordance with the accumulation of the copper compounds of cysteine, cystine and penicillamine [4, 5]. An increase in the Cu(II) concentration, as stated above, displaces the peak potential in the negative direction. The interval within which i_p is independent of E_{acc} is then simultaneously increased in the negative direction.

Peak current as a function of felypressin concentration

The peak heights of c_1, c_2, a_1, a_2, are linearly related to the felypressin concentration as long as the excess of copper(II) is so large that the height and shape of the stripping peak is unaffected by the Cu(II) concentration (Fig. 2). (A detailed discussion of the dependence of linearity on the Cu(II) concentration has been given in connection with the c.s.v. of cysteine and penicillamine [5].) In the presence of 5×10^{-6} M Cu(II), 4.8×10^{-8}—$2.3 \times$

10^{-7} M felypressin concentrations gave linear calibration graphs for c_2, a_1, a_2; the equation was i_p(nA) = (7.18 ± 0.37 × 10^8)C − 3.0 ± 1.2 with $r^2 \geqslant 0.9995$. Above 2.3 × 10^{-7} M, i_pC^{-1} decreased, and above 5 × 10^{-7} M, only a minor increase in peak height was obtained, indicating that saturation of the electrode surface was approached. The integrated peak area of c_2 from 7 × 10^{-7} M felypressin was about 20 μC cm^{-2}. Increased sensitivity was achieved by increasing the accumulation time. After a 5-min accumulation in buffer solution containing 1 × 10^{-7} M Cu(II), 5 × 10^{-9}—2.0 × 10^{-8} M felypressin gave the following calibration graph: i_p (nA) = (3.68 × 10^9)C − 5.6 with r^2 = 0.9998. The relative standard deviation for 10 determinations in the same solution of 1.5 × 10^{-7} M felypressin in presence of 5 × 10^{-6} M Cu(II) was 2.4%.

Origin of felypressin stripping peaks and degradation of felypressin

The c.s.v. characteristics of felypressin are quite different from those of most previously investigated sulphur compounds. First, the stripping activity in absence of Cu(II) is very low, indicating that the formation of an adsorbable mercury compound of felypressin is negligible. Secondly, the adsorbed product obtained in the presence of Cu(II) is adsorbed both in its oxidized and reduced form. The mechanism discussed for cystine, cysteine and penicillamine [4, 5] is therefore not applicable in this case.

Peptides not containing cystine (e.g., substance P with 11 amino acids) are c.s.v.-inactive. This fact, combined with the requirement that copper must be present for the stripping activity of felypressin to occur, indicates that complex formation between the cystine function of the peptide and copper is vital.

It is of major importance for application of the stripping method to elucidate whether degradation products of felypressin will contribute to the stripping peak or not. Because the degradation pattern of this peptide is unknown, oxidized glutathione was chosen for this investigation as a model compound for smaller peptides possibly formed by hydrolysis of felypressin.

Oxidized glutathione yields a c.s.v. peak at about —0.4 V when Cu(II) is present. Figure 4 shows the influence of this peptide on the c.s.v. of felypressin. In the first cathodic scan, the peak from oxidized glutathione interferes with the peak from felypressin. The accumulated product from oxidized glutathione does, however, desorb in its reduced state. The interference is thus diminished in the second scan cycle. Furthermore, by reversing the scan from the anodic to the cathodic direction at a more negative potential, the peak from oxidized glutathione disappears. An accumulation potential of —0.45 V gives only the felypressin peak. It is evident that the stripping method can separate felypressin and oxidized glutathione.

Lypressin, which is identical to felypressin, with the exception that one phenylalanine is replaced with tyrosine, gives a c.s.v. response identical to that of felypressin. Somatostatin, which contains 14 amino acids, including cystine, yields the peaks c_1, c_2, a_1, a_2 but c_1' is not obtained. No separation is thus possible between these peptides.

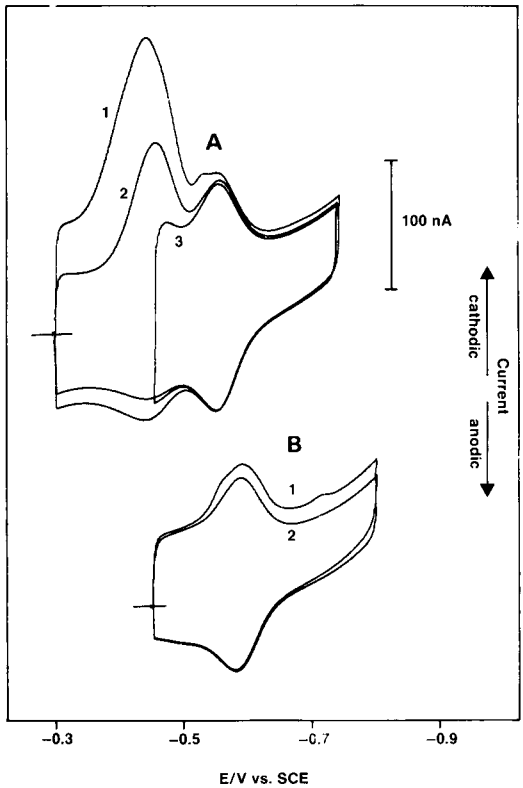

Fig. 4. Cyclic stripping voltammograms of 2×10^{-7} M felypressin and 4×10^{-7} M oxidized glutathione in a mixture; 5×10^{-6} M Cu(II) was present. Accumulation potential: (A) −0.30 V; (B) −0.45 V. Curves 1, 2 and 3 are the first, second and third scan cycles respectively.

Some preliminary investigations were done on felypressin sample solutions treated at 120°C for 20—80 min to produce degradation. The samples were then examined with the stripping method as well as biologically [1]. Both methods showed a decrease in the felypressin concentration with increased time of degradation. The stripping method thus seems to be selective against the degradation products formed. Extended comparative studies are in progress.

Determination in a local anaesthetic formulation

The stripping method was applied for the determination of felypressin in a local anaesthetic formulation containing 5×10^{-7} M felypressin, 0.12 M prilocaine hydrochloride and 6.6×10^{-3} M methyl-*p*-hydroxybenzoate. None of the additional constituents interfered with the stripping procedure. No separation step is thus necessary. At present, the stripping method is being applied in parallel with the biological method for comparison, and a full description will be published later.

Conclusions

Cathodic stripping voltammetry provides a very sensitive method for the determination of felypressin. Extended studies on other peptides are of interest. So far the method seems to be specific for cystine-containing peptides. This, combined with the capability of the method to separate felypressin and smaller peptides such as oxidized glutathione, opens possibilities for the direct determination of mixtures at low concentrations. The application of the method in pharmaceutical analysis for felypressin in local anaesthetics is promising.

REFERENCES

1 U.S. Pharmacopeia XIX, U.S. Pharmacopeial Convention, Inc., 1975, pp. 356, 534.
2 K. Krummen and R. W. Frei, J. Chromatogr., 132 (1977) 27.
3 M. Abrahamsson and K. Gröningsson, J. Liq. Chromatogr., 3 (1980) 495.
4 U. Forsman, J. Electroanal. Chem., 11 (1980) 325; 122 (1981) 215.
5 U. Forsman, J. Electroanal. Chem., 152 (1983) 241.
6 U. Forsman, Anal. Chim. Acta, 146 (1983) 71.
7 T. M. Florence, J. Electroanal. Chem., 97 (1979) 219.
8 R. A. Grier and R. W. Andrews, Anal. Chim. Acta, 124 (1981) 333.

Analytica Chimica Acta, 156 (1984) 51—59
Elsevier Science Publishers B.V., Amsterdam — Printed in The Netherlands

POLAROGRAPHY OF DISODIUM PENTACYANONITROSYLFERRATE(II)

Part 1. Pulse Polarographic Behaviour and Determination at Trace Levels

O. R. LEEUWENKAMP*, H. JOUSMA, E. J. VAN DER MARK, W. P. VAN BENNEKOM and A. BULT

Department of Pharmaceutical Analysis and Analytical Chemistry, Subfaculty of Pharmacy, State University of Leiden, Gorlaeus Laboratories, P.O. Box 9502, 2300 RA Leiden (The Netherlands)

(Received 7th June 1983)

SUMMARY

The pulse polarographic behaviour of disodium pentacyanonitrosylferrate(II) (sodium nitroprusside) was studied in the pH range 0—9. Maximum sensitivity is obtained in 1 M perchloric acid as a result of coincidence of the first two peaks and enhancement of the second peak. Calibration graphs are linear with conventional and high-performance differential pulse polarography at both the dropping mercury and static mercury drop electrode in the range 4—1000 ng ml^{-1} (1.3×10^{-8}—3.3×10^{-6} M). The estimated detection limits are about 2 ng ml^{-1} (7×10^{-9} M). The reduction product(s) are probably adsorbed at the mercury electrode.

Sodium nitroprusside is the common name for disodium pentacyanonitrosylferrate(II) dihydrate ($Na_2[Fe(CN)_5NO] \cdot 2H_2O$). It is frequently administered by infusion to lower blood pressure in cases of severe hypertension, to induce controlled hypotension during anaesthesia, and to improve heart function after myocardial infarction [1]. The drug is, however, toxic by splitting off cyanide [1]. Moreover, wide variability is observed in infusion rate required to attain a therapeutic effect [2, 3]. Therefore, determination of the nitroprusside in body fluids in addition to the observed lowering effect on blood pressure might offer better control of therapy.

Sodium nitroprusside can be determined by direct [4, 5] and indirect [6] spectrophotometry, polarography [7—9] and high-performance liquid chromatography with ultraviolet detection [10]. Two methods have been developed for determination of the drug in plasma [6] and serum [9], respectively. The indirect spectrophotometric method [6] is only applicable at enhanced infusion rates resulting in higher than therapeutic levels, because of the high detection limit (3 μg ml^{-1}). The same is true for the polarographic method [9], which has a similar detection limit.

The main objective of the present study was to achieve a detection limit as low as possible, because determination at therapeutic levels was the ultimate goal. Improvements on the detection limit were expected from both con-

0003-2670/84/$03.00

ventional and high-performance differential pulse polarography (d.p.p. and h.p.d.p.p., respectively) [11, 12]. The latter technique seems more suitable for determination of substances in body fluids [13—15]. It was necessary to investigate the pulse polarographic behaviour over a wide pH range to select the best polarographic medium. Mašek and Máślòva [8] have extensively studied the polarographic reduction mechanism (10^{-3} M nitroprusside) with direct current polarography (d.c.p.) in Britton-Robinson buffers with an ionic strength of 0.3 in the pH range 4—9. The behaviour in the pH range 0—4 was also studied here. In the pH range 0—2, perchloric acid solutions were used, because this acid is very suitable for denaturation of serum and plasma. The behaviour at pH > 9 was not investigated because of conversion of the nitrosyl moiety to a nitrite group by hydroxyl ions [7, 16]. The investigations at pH < 4 showed that maximum sensitivity was obtained in 1 M perchloric acid. In this medium, determination at the ng ml^{-1} level was possible at the dropping mercury electrode or the static mercury drop electrode.

EXPERIMENTAL

Polarographic apparatus and procedure

A polarographic analyzer PAR 174 A (EG & G Princeton Applied Research Corp., Princeton, NJ, U.S.A.), modified for h.p.d.p.p. (electronic diagrams are available on request), was used with a matched drop timer (PAR 174/70) and x-y recorder (Omnigraphic model 2200-4-3).

Measurements were done in a wall-jacketed vessel (Metrohm EA-876-5; 5 ml) wrapped in aluminium foil and thermostatted at 25°C. The three-electrode configuration consisted of a dropping mercury electrode (DME), a sodium chloride-saturated calomel reference electrode (SSCE) (Metrohm EA-402) and a platinum wire auxiliary electrode (Metrohm EA-202). During measurements the height of the mercury column was kept constant at 700 mm. At open circuit the flow rate was 3.28 mg s^{-1} with a corresponding drop time of 2.35 s (1 M $HClO_4$).

A static mercury drop electrode (PAR 303; SMDE) was also used; the large drop size mode (drop weight 5.17 mg) was employed with a cycle time of 1.0 s. For these measurements, the vessel (10 ml) was not thermostatted but it was wrapped in aluminium foil. A sodium chloride-saturated Ag/AgCl reference electrode was used with a platinum wire auxiliary electrode.

Before polarography, the solutions were purged for 10 min with oxygen-free, water-saturated nitrogen that was passed over the solution while scanning the potential. The potential was scanned from 0 to —3000 mV vs. SSCE at a rate of —5 or —2 mV s^{-1}. For d.p.p., the delay time δ was 5 ms and for h.p.d.p.p. the delay times were δ_1 = 5 and δ_2 = 70 ms with a modulation amplitude ΔE of —100 mV, sampling window(s) Δ of 20 ms and a memory time constant of 9.1 ms. These conditions were used unless stated otherwise.

Reagents and materials

Sodium nitroprusside (Merck) and the other chemicals were of analytical grade and were used as received. Water obtained from a Millipore Milli-Q Water Purification System was used for the preparation of all solutions. Britton-Robinson (BR) buffers (pH 2—9) were made with the ionic strength (μ) adjusted to 0.3 (sodium perchlorate). All sodium nitroprusside solutions were wrapped in aluminium foil to prevent light-induced degradation [4]. These solutions, including those of low pH, proved to be stable for a period of at least one week.

RESULTS AND DISCUSSION

Polarography in BR buffers pH 2—9 and in perchloric acid solutions (pH 0—2) at the DME

Polarograms of sodium nitroprusside solutions (10^{-7}—10^{-3} M) in BR buffers pH 2—9 were recorded in the sampled d.c., normal pulse, d.p. and h.p.d.p. modes. Parameters such as drop time, initial potential, delay time and modulation amplitude were varied where relevant. From the results, it was concluded that the electrochemical behaviour of sodium nitroprusside is extremely complex with mechanisms that are difficult to understand completely. Figure 1 shows typical polarograms for 10^{-4} M nitroprusside in BR buffer (pH 7.0), which illustrate the problems. The polarograms exhibit two distinct (I, II) and a third ill-defined reduction process (III) at —360, —610 and —1500 mV vs. SSCE, respectively. These potentials are in fair agreement with the half-wave potentials reported by Mašek and Máślòva [8]. For 10^{-3} M nitroprusside solutions, the third reduction process is much more pronounced. The first peak at E_p = —360 mV vs. SSCE can be ascribed to the one-electron reduction of the positively charged nitrosyl group [7, 8], corresponding to the formation of $[Fe(CN)_5NO^0]^{3-}$. Depending on the pH, this species can be protonated at the reduced nitrosyl moiety or it can lose its axial cyanide [8]. The protonated reduction product and the intermediate formed by loss of the axial cyanide are reduced in a second one-electron process (E_p = —610 mV vs. SSCE), while the primary reaction product is reduced in a third two-electron process (E_p = —1500 mV vs. SSCE) [8].

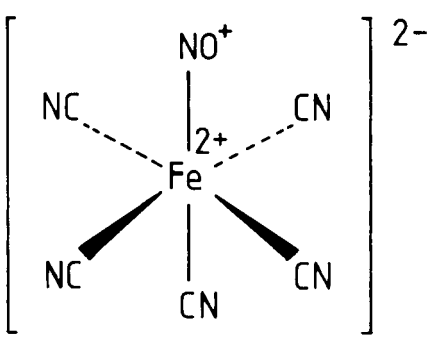

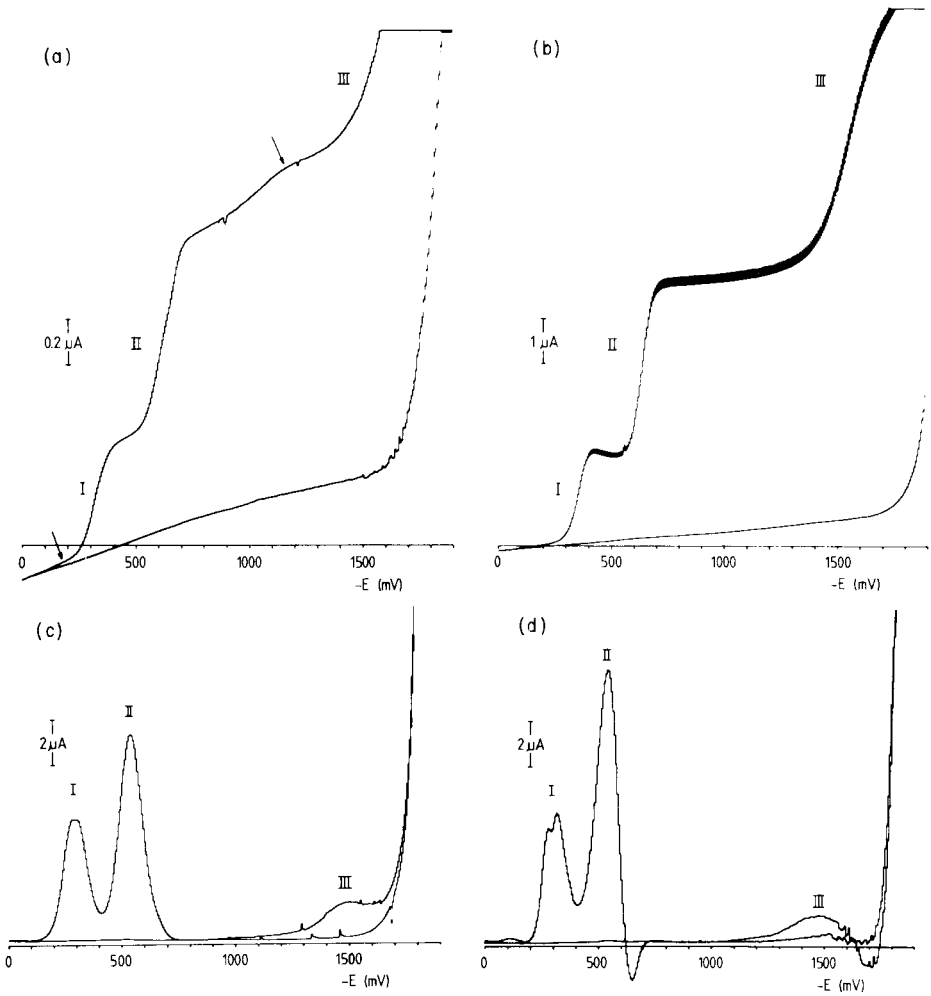

Fig. 1. Polarograms of 10^{-4} M sodium nitroprusside in BR buffer, pH 7.0, μ = 0.3 ($NaClO_4$) at the DME: (a) sampled d.c.; (b) normal pulse (δ = 5 ms); (c) d.p.; (d) h.p.d.p. Conditions as in Experimental; scan rate 5 mV s^{-1}.

In the given polarograms for 10^{-4} M nitroprusside, the second peak is considerably higher than the first peak. At a concentration of 10^{-6} M nitroprusside, the first peak almost vanished, but the second was still observed. The two peaks had about the same height in the case of 10^{-3} M solutions. These observations are in accordance with the fact that for the first peak, linear calibration graphs were obtained at pH 9.0, 7.0, 5.0 and 3.0 over the range 10^{-3}—10^{-5} M, whereas for the second peak the plot curved to the abscissa and intersected the linear plot for the first peak at a concentration of approximately 10^{-3} M (pH 7.0).

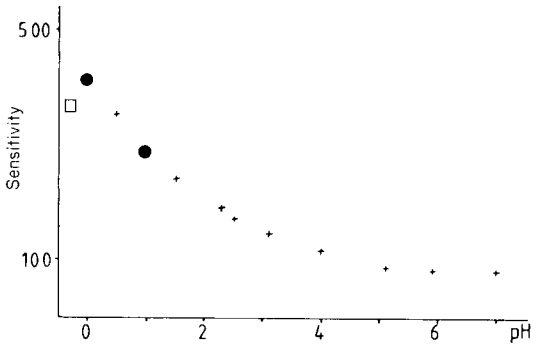

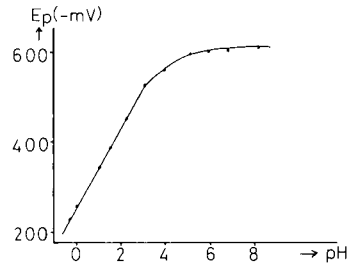

Fig. 2. Sensitivity (mA l mol^{-1}) for the second d.p.p. peak current as a function of pH, measured for 10^{-4} M sodium nitroprusside: (+) BR buffers, μ = 0.3 ($NaClO_4$); (•) μ = 1.0 (1.0 M $HClO_4$; 0.1 M $HClO_4$ + 0.9 M $NaClO_4$); (□) μ = 2.0 (2.0 M $HClO_4$).

Fig. 3. Plot of the second d.p.p. peak potential as a function of the pH (10^{-4} M sodium nitroprusside).

At pH < 6, the second peak current was enhanced (Fig. 2) whereas the first peak current remained nearly constant. Concomitantly, the second peak shifted anodically (Fig. 3). At pH < 3, this shift was linear with pH, (dE_p/pH ≈ −90 mV/pH) (Fig. 3). The first and second peaks coincided at about pH 1.5, and below this pH only one peak was observed. The slope of −90 mV/pH emphasizes the fact that the reduction mechanism is complicated.

At pH > 6 (10^{-4} M nitroprusside) with the sampled d.c. mode, a small prewave precedes the first wave and a post-wave is superimposed on the second wave (Fig. 1a), indicating that adsorption of the reduction product occurs [17]. This may account for the non-linear calibration graphs obtained for the second peak current [17]. Because adsorption can enhance the analytical sensitivity in d.p.p. [18], experiments were done with double potential step chronocoulometry at pH 7.0, electrocapillary and current/time curves to study the adsorption of the reaction product(s). These experiments, which will be described later, showed that products are adsorbed at the mercury electrode. Electrocapillary curves showed that adsorption was involved throughout the pH range (0—9) studied.

For the determination of low concentrations, maximum sensitivity is important; this was obtained in 1 M perchloric acid as a result of coincidence of the first two peaks and enhancement of the current of the second one. Typical polarograms for 10^{-4} M nitroprusside in 1 M perchloric acid are depicted in Fig. 4. As can be seen, there is no prewave in the sampled d.c. mode. However, the dip located anodically to the h.p.d.p.p. peak (arrowed in Fig. 4d) is probably associated with a prewave. There are large maxima on the sampled d.c. and normal pulse peaks. Correspondingly, split h.p.d.p. peaks and somewhat tailing d.p. peaks are observed. At concentrations

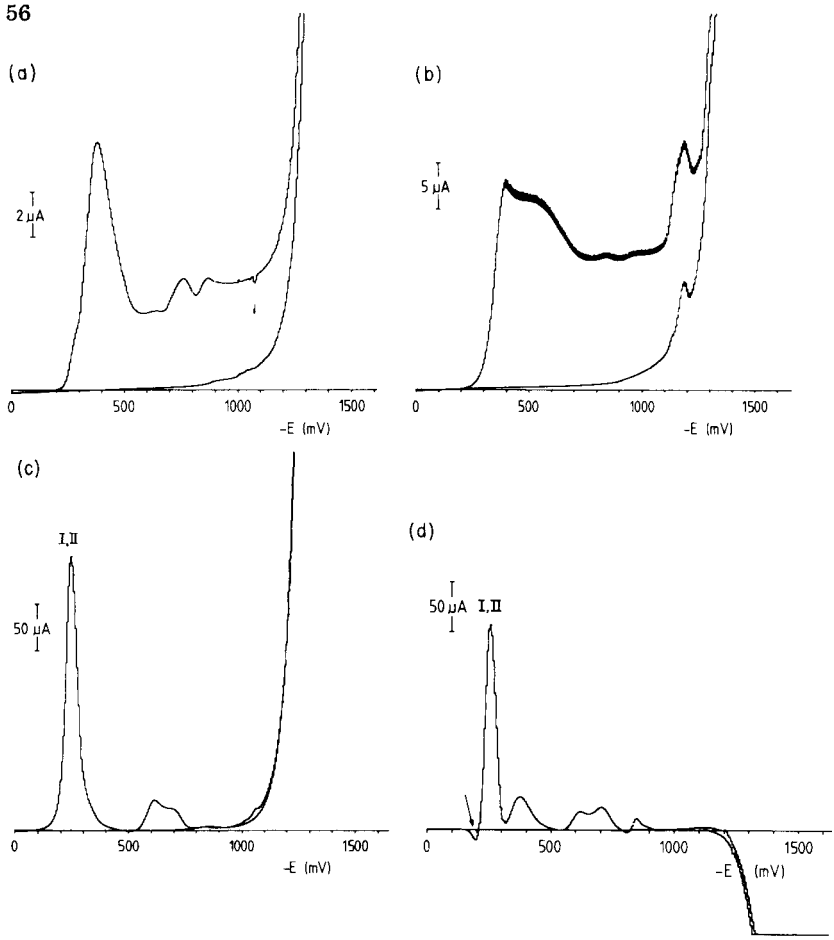

Fig. 4. Polarograms of 10^{-4} M sodium nitroprusside in 1 M $HClO_4$ at the DME: (a) sampled d.c.; (b) normal pulse; (c) d.p.; (d) h.p.d.p. Conditions as in Fig. 1.

lower than 10^{-5} M, in d.p.p. and h.p.d.p.p., a much more regular peak is observed at E_p = —270 mV vs. SSCE. A second, ill-defined peak is present in the given polarograms at about —600 mV vs. SSCE.

The stability of sodium nitroprusside in 1 M perchloric acid was investigated spectrophotometrically. The visible spectrum of the compound is characteristic (λ_{max} = 394 nm, ϵ = 20 l mol^{-1} cm^{-1}; λ_{max} = 550 nm, ϵ = 8) [19]. Therefore spectra for 10^{-3} M sodium nitroprusside in BR buffer pH 7.0 and in 1 M perchloric acid were recorded. These spectra were identical, and it was concluded that the nitroprusside ion remains unaltered in 1 M perchloric acid. After 5 h, no change was observed in the spectrum, indicating that the ion is stable in this medium.

Calibration graphs (peaks I + II) in 1 M perchloric acid, by either the d.p.p. or h.p.d.p.p. mode, were linear in the range 4—1000 ng ml^{-1} (Table 1). For the h.p.d.p. mode, a lower and less steep background was recorded, as

TABLE 1

Calibration data for sodium nitroprusside in 1 M $HClO_4$ in the concentration range 4—1000 ng ml^{-1} (n = 7)

	DME		SMDE	
	D.p.p.	H.p.d.p.p.	D.p.p.	H.p.d.p.p.
Slope[a]	11.16 ± 0.087	8.06 ± 0.076	13.45 ± 0.018	11.31 ± 0.003
Intercept[b]	23.75 ± 13.61	12.30 ± 11.86	−1.74 ± 7.03	−0.28 ± 1.30
Correlation coefficient	0.9998	0.9998	0.9999	0.9999
Calculated slope[c]	1.68	0.97	2.33	1.39
Drop area[d] (m^2)	$1.88 \cdot 10^{-6}$		$2.54 \cdot 10^{-6}$	

[a]Mean slope with standard deviation (nA ml ng^{-1}). [b]Mean intercept with standard deviation (nA). [c]According to [13], taking into account the built-in amplification factor of 10. For sodium nitroprusside, the diffusion coefficient $D = 9.0 \times 10^{-10}$ m^2 s^{-1} [7]. [d]Large drop size mode.

is to be expected theoretically [11—13]. The detection limit for sodium nitroprusside in 1 M perchloric acid was about 2 ng ml^{-1} (7×10^{-9} M). The slopes for the obtained calibration graphs (Table 1) are substantially greater than the theoretical slopes for an uncomplicated two-electron reduction, assuming that n = 2 because of the observed coincidence of the first two peaks in 1 M perchloric acid. Adsorption of the reduction product(s) can at least partially explain the discrepancy between the experimental and theoretical slopes [18].

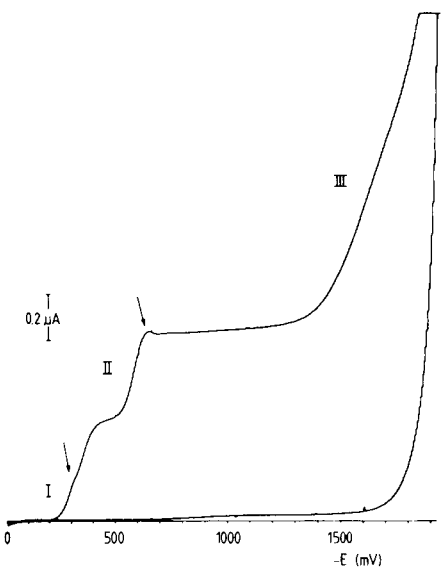

Fig. 5. Sampled d.c. polarogram for 10^{-4} M sodium nitroprusside in BR buffer pH 7.0 (μ = 0.3, $NaClO_4$) at the SMDE. Conditions as in Fig. 1.

Polarography in BR buffers pH 2—9 and in perchloric acid solutions (pH 0—2) at the static mercury drop electrode

The polarograms obtained for 10^{-4} M sodium nitroprusside in BR buffer pH 7.0 and 1 M perchloric acid were essentially the same at the SMDE as reported above for the DME. However, in the sampled d.c. mode at pH 7.0 (BR buffer), a pronounced prewave was observed as well as a small maximum on the second wave (Fig. 5). In 1 M perchloric acid, linear calibration graphs were obtained by d.p.p. and h.p.d.p.p. with greater slopes than those at the DME (Table 1). The larger drop area (Table 1) accounts for the higher slopes obtained; with the SMDE, higher coverage of the drop with the adsorbed product(s) is possible because of the static period of the drop especially when the adsorption process is slow [20]. The above reasoning of a slow adsorption process is supported by the fact that with cycle times of 2.0 and 5.0 s, the limiting and peak currents are enhanced by about 15%. This may explain the more pronounced prewave observed with the sampled d.c. mode for BR buffer solutions at pH 7.0.

Conclusions

The pulse polarographic behaviour of sodium nitroprusside is variable in the pH range 2–9 in Britton-Robinson buffers (μ = 0.3) and in perchloric acid solutions (pH 0—2). For 10^{-3} M nitroprusside solutions, at pH > 2, three main reduction processes are observed; the third process is less pronounced at concentrations $<10^{-3}$ M and the first process is not observable at concentrations $<10^{-6}$ M. The reduction mechanism in these solutions is complicated and not yet fully understood. However, there is evidence for adsorption of reduction product(s) at the surface of the mercury electrode.

In the perchloric acid solutions, at pH < 1.5, the first and second processes coincide, yielding an increased current. Maximum sensitivity is observed in 1 M perchloric acid. In this medium, calibration graphs are linear in the range 4—1000 ng ml^{-1} with d.p.p. and h.p.d.p.p. at both the DME and SMDE. The analytical performance at the SMDE in combination with h.p.d.p.p. is somewhat better. The estimated detection limits are about 2 ng ml^{-1}. The discrepancy between the theoretical and experimental slopes of the calibration graphs can, at least partly, be explained by adsorption phenomena.

Perchloric acid is appropriate for denaturation of plasma and serum, so that nitroprusside at ng ml^{-1} levels might be determined by measurement in the supernatant solutions obtained after suitable treatment of such samples.

We are grateful to Prof. Dr. J. H. Sluyters and Drs. C. J. van Velzen (State University of Utrecht) for offering the facilities for chronocoulometric experiments.

REFERENCES

1 J. H. Tinker and J. D. Michenfelder, Anaesthesiology, 45 (1976) 340.
2 F. Conso, A. Marsac and L. Petit, Bull. Med. Leg. Toxicol. Med., 21 (1978) 215.
3 H. Kruszyna, R. Kruszyna and R. P. Smith, Anaesthesiology, 57 (1982) 303.
4 M. J. Frank, J. B. Johnson and S. H. Rubin, J. Pharm. Sci., 65 (1976) 44.
5 B. Jaselskis and J. C. Edwards, Anal. Chem., 32 (1960) 381.
6 F. L. Rodkey and H. A. Collison, Clin. Chem., 23 (1977) 1969.
7 I. M. Kolthoff and P. E. Toren, J. Am. Chem. Soc., 75 (1953) 1197.
8 J. Mašek and E. Máślòva, Collect. Czech. Chem. Commun., 39 (1974) 2141.
9 M. Alkayer, J. J. Vallon and Y. Pegon, Anal. Lett., 14(B6) (1981) 399.
10 D. M. Baaske, M. D. Smith, N. Karnatz and J. E. Carter, J. Chromatogr., 212 (1981) 339.
11 W. P. van Bennekom and J. B. Schute, Anal. Chim. Acta, 89 (1977) 71.
12 W. P. van Bennekom, Anal. Chim. Acta, 101 (1978) 283.
13 W. P. van Bennekom, Ph.D. Thesis, State University of Leiden, 1981.
14 J. J. van der Lee, W. P. van Bennekom and H. J. de Jong, Anal. Chim. Acta, 117 (1980) 171.
15 W. P. van Bennekom, U. R. Tjaden, E. A. de Bruijn and A. T. van Oosterom, Anal. Chim. Acta, 156 (1984) in press.
16 J. H. Swinehart, Coord. Chem. Rev., 2 (1967) 385.
17 E. Laviron, J. Electroanal. Chem., 52 (1974) 355.
18 F. C. Anson, J. B. Flanagan, K. Takahashi and A. Yamada, J. Electroanal. Chem., 67 (1976) 253.
19 P. T. Manoharan and H. B. Gray, J. Am. Chem. Soc., 87 (1965) 3340.
20 P. Zuman and I. M. Kolthoff, Progress in Polarography, Vol. 1, Wiley-Interscience, New York, 1962, pp. 98—103.

Analytica Chimica Acta, 156 (1984) 61—69
Elsevier Science Publishers B.V., Amsterdam — Printed in The Netherlands

DIRECT DETERMINATION OF TRACES OF SILVER IN MERCURY BY VOLTAMMETRY AT THE HANGING MERCURY DROP ELECTRODE IN ACETONITRILE MEDIUM

STEFAN GŁODOWSKI and ZENON KUBLIK*
Department of Chemistry, University of Warsaw, Pasteura 1, Warsaw 02093 (Poland)
(Received 6th June 1983)

SUMMARY

A direct method for the determination of silver in mercury is described. The sample of mercury is introduced into the container of the hanging mercury drop electrode and the anodic voltammograms are recorded in a 0.1 M lithium perchlorate solution in acetonitrile. The anodic peak of silver obtained under these conditions is well separated from the mercury dissolution current. The peak height is proportional to silver concentration over the wide range 2×10^{-6} mol dm^{-3} (1.6×10^{-6} %) to at least 2.0×10^{-2} mol dm^{-3}. No prior separation is needed; the procedure requires less than 20 min. The diffusion coefficient of silver in mercury was determined at several temperatures. It was found that silver in mercury does not form intermetallic compounds with copper, lead, thallium, cadmium, tin and bismuth.

The use of very pure mercury is essential in various branches of science and technology [1], but there are serious difficulties in determining trace metallic contaminants in mercury. In most methods proposed for the analysis of mercury, preliminary separations are recommended [2—7]. Only Neyman et al. [8] and Głodowski and Kublik [9] have determined copper, lead and cadmium in mercury directly by voltammetric methods. The application of such a direct method for the determination of silver in mercury encounters some difficulties. In the most aqueous supporting electrolytes, the silver peak is severely overlapped by the mercury dissolution current. Only in concentrated thiocyanate solutions has separation of the silver and mercury peaks been observed [10, 11], but their separation is insufficient to exploit for determining silver in the presence of a large excess of mercury. Non-aqueous media seem more promising [10, 12]. Using acetonitrile as the solvent, Hubmann et al. [10] determined silver ions in solution by anodic stripping voltammetry at the hanging mercury drop electrode (HMDE) with a detection limit of 5×10^{-7} mol dm^{-3}.

The aim of the present work was to check whether the procedure described previously for the direct determination of copper, lead and cadmium in mercury [9] could also be applied for the direct determination of silver. Previously, silver has been determined in mercury by a spectrographic

0003-2670/84/$03.00

method [13, 14] after dissolution of the sample in nitric acid and a rather cumbersome extractive separation of constituents or by thermal separation.

EXPERIMENTAL

Voltammograms and chronoamperograms were recorded with a Radelkis OH-105 polarograph. A three-electrode cell was used: an aqueous calomel electrode saturated with sodium chloride was connected with the investigated solution by a salt bridge (0.1 M $LiClO_4$) with Vycor tips; the other electrodes were a 2-cm^2 platinum foil and a HMDE of the type described by Kemula and Kublik [15]. The container of the HMDE was filled with very pure mercury, with the amalgams studied, or with samples of mercury under check. The resistance of the system with 0.1 mol dm^{-3} lithium perchlorate in acetonitrile in the cell was 25 kΩ, measured by means of a Radelkis OK-102/1 conductometer.

Commercially available mercury was further purified and the amalgams were prepared as described earlier [9].

Acetonitrile (u.v. spectroscopic grade; Fluka) was used as received; the p.a. grade (Fluka) was purified as described by O'Donnel et al. [16]. The water content in acetonitrile was titrated with Karl Fischer reagent using a simplified coulometric procedure [17]; the value found was $<2.5 \times 10^{-2}$%. Lithium perchlorate (Merck, p.a.) was used to prepare the supporting electrolytes. Other chemicals were of reagent grade.

In the medium used, oxygen was reduced at potentials distinctly more negative than the silver oxidation potential. Thus, when the curves were recorded from 0 V (i.e., when only silver was determined), air was not removed from solutions. Otherwise, argon was used for deaeration. The experiments were done in a cell thermostated by a water bath, usually at 20°C; other temperatures are indicated specifically in the text.

RESULTS

Preliminary experiments

The effects of various factors on the residual currents and on the stability of silver amalgam were first studied. The residual current curves obtained in acetonitrile and aqueous solutions are compared in Fig. 1. It is evident that the useful potential range is markedly larger in acetonitrile medium than in aqueous solution. Fortunately, the anodic peak of silver occurs in the extended range. Figure 1 also shows that the solvent, supporting electrolyte and mercury used are "clean" in the potential range of interest, though the residual currents obtained in the acetonitrile medium are less regular than those for the aqueous solutions. However, at the sensitivity used to record Fig. 1, it should be possible to determine silver concentrations around 10^{-6} mol dm^{-3}. Prolonged contact of acetonitrile with mercury, particularly in stirred solution, led to small distortions of the residual current in the potential range where silver is oxidized from amalgams.

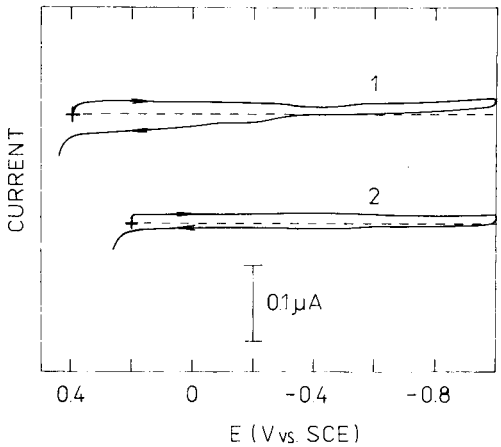

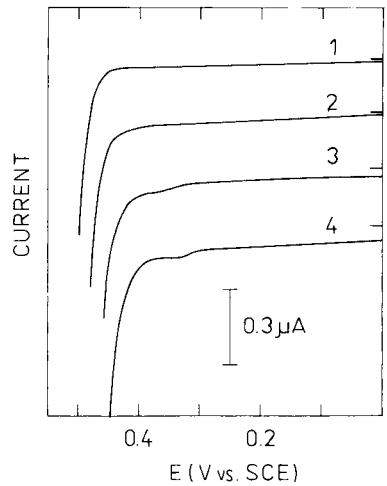

Fig. 1. Residual current curves obtained in 0.1 mol dm^{-3} lithium perchlorate in: (1) acetonitrile, (2) water. HMDE surface area, 0.038 cm^2; voltage scan rate, 1 V min^{-1}; solution deaerated with argon.

Fig. 2. The influence of water on the anodic curves obtained in 0.01 mol dm^{-3} lithium perchlorate in acetonitrile. Water content: (1) 0.025%; (2) 1%; (3) 2%; (4) 3%. HMDE surface area, 0.038 cm^2; scan rate, 0.5 V min^{-1}.

Figure 2 illustrates the influence of water on the residual currents obtained in acetonitrile medium. With increasing water content, the anodic limit shifts towards more negative potentials and the magnitude of the anodic residual current increases. If the water content exceeds 2%, an additional small anomaly appears in the potential range where silver is oxidized (Fig. 2) so that silver could not then be determined in mercury at trace levels.

In order to establish the stability of silver amalgams, a sample of 2×10^{-3} mol dm^{-3} silver amalgam was left in contact with air or aqueous 0.1 mol dm^{-3} perchloric acid. After various times, small portions of the amalgam were placed in the container of the HMDE and the anodic voltammograms were recorded, with 0.1 mol dm^{-3} lithium perchlorate in acetonitrile as the supporting electrolyte. These experiments showed that the height of the anodic peak of silver remained constant even after three months of contact of amalgam with air or the dilute perchloric acid solution. Similar experiments with lead amalgam showed that the concentration of lead decreased by 20% after contact with air for 10 days whereas it decreased to 1% of the initial value on contact with dilute perchloric acid solution for 10 days. Obviously, silver amalgam is significantly more stable than the amalgams investigated previously [9].

The stability of dilute silver amalgams in contact with 0.1 mol dm^{-3} lithium perchlorate in acetonitrile was studied by holding a drop of amalgam, extruded from the container of the HMDE, at open electrical circuit. After various

periods of contact, the anodic voltammograms were recorded. In such an experiment with an amalgam containing 5×10^{-5} mol dm^{-3} silver, the silver peak height remained constant even after 6 min of contact. The presence or absence of air, as well as stirring the solution, had no essential effect on the height of the silver peak. In similar experiments with dilute lead amalgam in contact with aqueous solution, the concentration of lead content decreased to 5% of its initial value after 3 min [9].

Direct determination of silver in mercury

Typical anodic voltammograms obtained for dilute amalgams of silver and several other metals are presented in Fig. 3. The silver peak is well separated from the mercury dissolution current and from the peaks of other metals except for the second peak of the oxidation of tin amalgam. The silver peak is quite well developed. Comparison of the cyclic voltammograms of silver obtained in acetonitrile medium with the reversibility criteria given by Galus [18] and Nicholson [19] showed that the Ag^+—Ag/Hg/ couple behaves reversibly. Variations in the silver concentrations in the amalgam

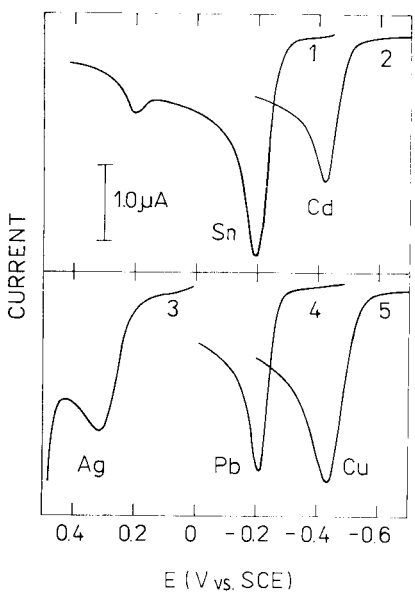

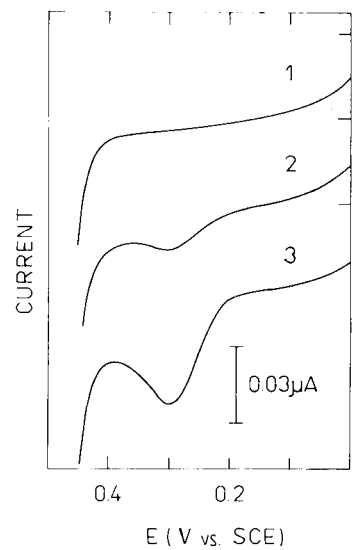

Fig. 3. Anodic voltammograms obtained in 0.1 mol dm^{-3} lithium perchlorate in acetonitrile. The HMDE (surface area 0.038 cm^2) was filled with the following amalgams: (1) 2.2×10^{-4} mol dm^{-3} tin; (2) 1.4×10^{-4} mol dm^{-3} cadmium; (3) 5×10^{-4} mol dm^{-3} silver; (4) 2×10^{-4} mol dm^{-3} lead; (5) 6.5×10^{-4} copper. Scan rate 1 V min^{-1}; solution deaerated with argon.

Fig. 4. Anodic voltammograms obtained in 0.1 mol dm^{-3} lithium perchlorate in acetonitrile. The HMDE (surface area 0.038 cm^2) was filled with: (1) purified mercury; (2) amalgam containing 4×10^{-6} mol dm^{-3} silver; (3) commercially available pure mercury. Scan rate 0.5 V min^{-1}.

have, in practice, little effect on the shape of the silver peak. The peak height was proportional to the silver concentration in amalgam over a wide concentration range from 2×10^{-6} to 2.0×10^{-2} mol dm^{-3}, allowing silver to be determined from appropriate calibration plots. However, handling the large volumes of mercury necessary to prepare the appropriate amalgams is cumbersome. Also the use of the standard addition method is inconvenient. It is much simpler to use the theoretical equation describing the relation between the peak current and the concentration [20]. For this purpose, it is convenient to transform the equation given by Nicholson and Shain [20] to

$$C_{Me(Hg)} = i_{pa}/4.64 \times 10^3 n^{3/2} A(Dv/T)^{1/2} - 72.5\, nDA/r$$

where $C_{Me(Hg)}$ is the concentration of metal in mercury (mol dm^{-3}), i_{pa} is the peak current (A), D is the diffusion coefficient of the metal in mercury (cm^2 s^{-1}), T is the temperature (K), A is the surface area of the electrode (cm^2), r is the radius of the mercury drop (cm), and v is the voltage scan rate (V s^{-1}).

In order to use this equation for the determination of silver, not only the peak height but also the diffusion coefficient of silver in mercury must be known. Several values of the diffusion coefficient of silver in mercury are presented in Table 1; how they were determined is discussed later. The above equation is usually given in the form valid for 25°C. For other temperatures, it is necessary to recalculate not only the diffusion coefficients but also the numerical factors in the equation.

Curve 2 in Fig. 4 was obtained for an amalgam containing 4×10^{-6} mol dm^{-3} silver. Comparison of this curve with the blank test (curve 1) shows that this peak height is readily measurable. The detection limit for silver estimated on the basis of such curves was 2×10^{-6} mol dm^{-3}, i.e., 1.6×10^{-6}%.

Variations in the concentration of lithium perchlorate in the range 0.01—0.2 mol dm^{-3} had no essential influence on the shape and height of the silver peaks. Variations in the voltage scan rate gave peak currents consistent with theoretical prediction for 10^{-4} mol dm^{-3} silver in mercury; for concen-

TABLE 1

Diffusion coefficients of silver in mercury

Temp. (°C)	D_{Ag} in mercury ($\times 10^{-5}$ cm^2 s^{-1})[a]			
	A[b]	B[b]	C	D
15	0.96	0.99	1.11[c]	—
20	1.04	1.09	—	—
25	1.11	1.17	1.25[d]	0.9

[a](A) Values from chronoamperometric experiments; (B) values from voltammetric experiments; (C) literature value [21]; (D) literature value [22]. [b]Mean from 3 experiments. [c]Value for 16°C. [d]Value obtained using the present temperature coefficient.

trations of silver close to the detection limit, high scan rates led to increased residual currents which made the measurement of peak heights difficult.

Table 2 presents the results obtained for the determination of silver in mercury. The silver content in mercury purified in this laboratory was below the detection limit. In contrast, commercially available pure mercury (POCH) contained a significant concentration of silver; curve 3 (Fig. 4) was obtained for such a sample.

Determination of the diffusion coefficient of silver in mercury

Few data are available for the diffusion coefficient (D) of silver in mercury. An experimental value of 1.11×10^{-5} cm^2 s^{-1} at 16°C was given by Schwarz and Stockert [21]. A value of 0.9×10^{-5} cm^2 s^{-1} at 25°C was estimated by Stromberg and Zakharova [22], who found a linear dependence between D and the reciprocals of the densities for several metals and estimated D for silver from this plot, knowing the density of silver.

The good separation of the anodic peak of silver from the mercury dissolution current in acetonitrile medium made it possible to establish the diffusion coefficient of silver in mercury electrochemically. In chronoamperometric experiments, following the original work of Stevens and Shain [23], the amalgam was prepared in situ. Silver was deposited from the usual acetonitrile solution containing 7×10^{-4} mol dm^{-3} silver ions at zero potential; the deposition lasted 3 min with stirring and the radius of the mercury drop was 0.055 cm. The chronoamperometric curves were recorded at a potential 120 mV more positive than the potential of silver oxidation. The mean values obtained from three experiments at each temperature studied are presented in Table 1.

The diffusion coefficient of silver in mercury was also determined from voltammetric curves on the basis of the equation given above. The voltammetric curves were recorded using an amalgam prepared externally from a weighed sample of silver; the concentration of silver in this amalgam was

TABLE 2

The determination of silver in mercury (0.1 mol dm^{-3} $LiClO_4$ in acetonitrile, HMDE surface area 0.038 cm^2, scan rate 0.5 V min^{-1}, 20°C)

Mercury sample	C_{Ag} in Hg (mol dm^{-3})		Relative difference (%)	S.d. (mol dm^{-3})	R.s.d. (%)
	Added	Found[a]			
Pure	0	1.48×10^{-5}	—	0.068×10^{-5}	4.56
Purified[b]	0	—[c]	—	—	—
Purified[b]	1.60×10^{-3}	1.63×10^{-3}	2.06	1.61×10^{-5}	1.0
Purified[b]	2.17×10^{-5}	2.28×10^{-5}	5.1	0.22×10^{-5}	9.6

[a]Mean from 7 measurements. The diffusion coefficient used in the calculations was 1.04×10^{-5} cm^2 s^{-1}. [b]Purified in this laboratory. [c]Below the detection limit.

1.6×10^{-3} mol dm^{-3}. The mean values of D at each temperature studied are also listed in Table 1. The values obtained by both methods agree well but the values obtained in chronoamperometric experiments are probably more reliable.

The temperature coefficient for the diffusion coefficient of silver in mercury, calculated for 15—25°C on the basis of the data in Table 1, is 1.44% K^{-1}. This temperature coefficient was used to recalculate the value of the diffusion coefficient given by Schwarz and Stockert from 16 to 25°C.

Interference studies

The direct voltammetric determination of silver in mercury can be distorted in several ways: (a) by overlap of the silver peak by the peaks of other metals present in mercury; (b) by the formation of intermetallic compounds in mercury; and (c) by the peaks of contaminants present in solution.

Experiments in the acetonitrile medium with amalgams of bismuth, lead, tin, thallium, copper and cadmium showed that the bismuth peak occurring at 0.36 V, i.e., between the peak of silver and the dissolution current of mercury, interferes severely with the silver peak. The peaks of the other metals are well separated from the silver peak (see Fig. 3) but the fact that the silver peak occurs on the descending portion of these peaks can cause difficulties. Thus, when these metals are present, the curves should be recorded very slowly, or the scan should be stopped for some time after the negative peak until the current drops to zero [24].

In order to establish if silver forms intermetallic compounds in mercury, mixed amalgams were prepared containing silver (5×10^{-3} mol dm^{-3}) and lead, tin, thallium, copper or cadmium at a concentration of about 3×10^{-3} mol dm^{-3}. None of the results obtained in these experiments could be interpreted as indicating intermetallic compound formation. In order to separate the peaks of silver and bismuth, the relevant amalgam was examined in aqueous solution; the bismuth peak was not affected by the presence of silver in mercury.

Some batches of acetonitrile, even after thorough purification, gave a small anodic peak in the potential range where silver was oxidized. Attempts to elucidate the cause of this peak were unsuccessful, but it was not formed by hydroxide, chloride or cyanide ions. The anodic currents caused by these ions start at more negative potentials [25, 26].

DISCUSSION

The finding that in acetonitrile medium the silver peak is well separated from the mercury dissolution current makes it possible to study the properties of silver amalgam electrochemically. In contrast to the unstable amalgams studied earlier [9], the silver amalgam could be handled in the presence of air and could be stored for long periods of time without any risk of losses of silver from the amalgam. The value of the diffusion coefficient of silver in

mercury found in this work is considered to be more reliable than the literature values [21, 22].

There is scant information in the literature on intermetallic compounds of silver in mixed amalgams [27]. The present experiments showed clearly that silver does not react in the mercury phase with bismuth, copper, tin, lead or thallium. Literature data [28, 29] on the formation in mercury of the compound AgCd were not confirmed.

Methods proposed previously in the literature for the determination of silver in mercury required awkward separations. The results presented above show that the use of acetonitrile solutions offers good possibilities for the direct voltammetric determination of traces of silver in mercury. Compared with the results obtained for lead and cadmium in aqueous solution [9], the detection limit found in acetonitrile medium for silver is slightly poorer. This can be attributed partly to the one-electron charge transfer of silver and partly to impurities in the solvent used. It should be stressed that the requirements imposed on the purity of solvents for trace analysis are very high. It seems that the residual currents serving as blank tests in previous work with acetonitrile solutions were not recorded at such high sensitivities as were used here.

The detection limit found here (1.6×10^{-6}%) for the determination of silver in mercury is poorer than the detection limit found spectrographically by Tiptsova et al. [14] (2×10^{-7}%). However, the procedure proposed here is very much simpler.

In principle, the proposed method offers the possibility of simultaneous determinations of such metals as lead, tin, thallium, copper and cadmium. However, it is easier to determine these metals in mercury with aqueous solutions as proposed earlier [9].

This work was done as part of Project PMR.I.32.

REFERENCES

1 P. P. Pugatchevitch, Rabota so Rtutju, Khimia, Moscow, 1972.
2 E. Jackwerth, Fresenius Z. Anal. Chem., 206 (1964) 269.
3 J. Meyer, Fresenius Z. Anal. Chem., 219 (1966) 147.
4 E. Jackwerth, Fresenius Z. Anal. Chem., 251 (1970) 353.
5 L. S. Anisimova, W. F. Sliptchenko, W. E. Katjukhin, A. A. Kaplin and K. M. Spector, Zavod. Lab., 44 (1978) 1304.
6 A. A. Kaplin, I. P. Mamontova and A. G. Stromberg, Zavod. Lab., 45 (1979) 484.
7 A. I. Zebreva, R. N. Matakova and R. B. Zholdybaeva, Zh. Anal. Khim., 36 (1981) 405.
8 E. Ya. Neyman, E. D. Kuzniec and L. A. Belova, Zavod. Lab., 35 (1969) 277.
9 S. Głodowski and Z. Kublik, Anal. Chim. Acta, 149 (1983) 137.
10 J. Hubmann, J. Buffle and D. Monnier, Anal. Chim. Acta, 62 (1962) 393.
11 R. Bilewicz and Z. Kublik, Anal. Chim. Acta, 152 (1983) 2030.
12 I. M. Kolthoff and J. F. Coetzee, J. Am. Chem. Soc., 79 (1957) 1852.
13 V. P. Gladyshev, E. I. Savichev, E. V. Shugurov and G. S. Starozhenko, Zh. Anal. Khim., 31 (1976) 1934.

14 V. G. Tiptsova, E. I. Malkina and Z. A. Anisimova, Zh. Anal. Khim., 21 (1966) 459.
15 W. Kemula and Z. Kublik, Anal. Chim. Acta, 18 (1958) 104.
16 J. F. O'Donnel, J. T. Ayres and Ch. K. Mann, Anal. Chem., 37 (1965) 1161.
17 W. Pawłowski and W. Jędral, Chem. Anal. (Warsaw), 25 (1980) 151.
18 Z. Galus, Fundamentals of Electrochemical Analysis, PWN, Warsaw, and Horwood, Chichester, 1976.
19 R. S. Nicholson, Anal. Chem., 37 (1965) 1351.
20 R. S. Nicholson and I. Shain, Anal. Chem., 36 (1964) 706.
21 K. Schwarz and R. Stockert, Monatsh. Chem., 68 (1936) 383.
22 A. G. Stromberg and X. Zakharova, Zh. Fiz. Khim., 40 (1966) 81.
23 W. G. Stevens and I. Shain, J. Phys. Chem., 70 (1966) 2276.
24 W. Kemula, Z. Kublik and S. Głodowski, J. Electroanal. Chem., 1 (1959—60) 91.
25 K. Izutsu, T. Adach and T. Fujinaga, Electrochim. Acta, 15 (1970) 135.
26 M. Wojciechowski and J. Osteryoung, Anal. Chem., 54 (1982) 1713.
27 M. Kozlovsky and A. Zebreva, in P. Zuman and L. Meites (Eds.), Progress in Polarography, Vol. III, Wiley-Interscience, New York, 1972.
28 W. Kemula, Z. Galus and Z. Kublik, Bull. Acad. Polon. Sci. Ser. Sci. Chim., 6 (1958) 661.
29 A. Zebreva, Tr. Inst. Khim. Nauk Akad. Nauk Kaz. SSSR, Ser. Khim., 1 (1959) 33; 9 (1962) 55.

Analytica Chimica Acta, 156 (1984) 71—76
Elsevier Science Publishers B.V., Amsterdam — Printed in The Netherlands

FLOW INJECTION ANALYSIS WITH TENSAMMETRIC DETECTION FOR THE DETERMINATION OF DETERGENTS

M. BOS, J. H. H. G. VAN WILLIGEN and W. E. VAN DER LINDEN*

Department of Chemical Technology, Twente University of Technology, P.O. Box 217, 7500 AE Enschede (The Netherlands)

(Received 19th August 1983)

SUMMARY

A straightforward flow injection method for the tensammetric determination of surfactants is described. The flow-through cell is equipped with a mercury-coated gold electrode as the working electrode. Ionic as well as nonionic surfactants can be determined in the concentration range 10^{-5}—10^{-4} M. The calibration graph is not linear but with an approximation by a polynomial or a cubic spline function, correct results can be obtained with an accuracy of ±4%. The sample rate is about 60 h^{-1}.

The determination of surfactants in aqueous solutions is of great importance both in production control and in the monitoring of, for example, sewage water. There are two types of standard method, both based on ion-pair extraction [1]. Probably the most widely used is the two-phase titration procedure; the other type comprises direct photometric determinations in the organic phase. Because these methods are rather time-consuming, much attention has been given to the development of other methods during the last decade. The most important contributions are in the field of potentiometry, particularly with ion-selective electrodes [2—9], and tensammetry [10—15]. Recently, also automation of existing extraction procedures and subsequent photometric detection has been pursued. These attempts are either based on the continuous flow technique (AutoAnalyzer system) [16, 17] or on flow injection analysis [18, 19]. The elegant phase separation by means of a permeable membrane used by Kawase and coworkers is worth mentioning. Such a phase separator will be superfluous, however, with flow-through detectors based on potentiometry or tensammetry. Because the potentials of surfactant-sensitive electrodes are, in general, not very stable and reproducible, these electrodes are mostly used for end-point indication in titrations; they are not suitable for flow-through detectors.

Detectors based on the tensammetric principle seem to be more promising in this respect. Such a flow-through detector, based on a dropping mercury electrode, has been described for applications in h.p.l.c. [14]. Although it offers the advantage of a clean surface every few seconds, it has the disadvantage that its proper functioning is sensitive to changes in flow conditions.

0003-2670/84/$03.00

The use of a solid electrode not only simplifies the cell construction, but makes the whole system more robust and allows larger variations in the flow rate. Because the object of the present work was the development of a fast procedure for the direct determination of detergents, flow injection in conjunction with tensammetric detection at a solid electrode seemed to be an obvious choice. The feasibility of such a system is assessed here.

THEORY

In tensammetry the capacitance of the electrical double layer of an electrode is measured. The value of this capacitance is strongly influenced by the presence of adsorbing species. In the equilibrium state strongly adsorbing compounds present in sufficiently large concentration tend to cover the surface totally, yielding a constant capacitance value. At lower concentrations the coverage will follow the adsorption isotherm provided that equilibrium between surface and bulk concentration is attained. This equilibrium may not be reached at a relatively fast dropping mercury electrode because the expansion of the surface exceeds the supply of adsorbate from the bulk. Under such circumstances the coverage, and so the actual capacitance value measured, will be controlled by mass transport. This means that for normal polarographic conditions, where mass transport is caused by diffusion only, a linear relationship between capacitance and concentration can be expected [20, 21].

In a flow-through cell with a stationary electrode, no extra transport caused by surface expansion is needed. Convection will assist the pure diffusion process in achieving an equilibrium state between surface and bulk concentration. Therefore, it can be expected that in a flow-through cell with stationary electrode, the capacitance vs. concentration graph will more or less follow the adsorption isotherm, which generally is not linear. To cope with such calibration curves, polynomial functions are often used and cubic spline functions have been suggested [22]. For a polynomial function, the constants are obtained by least-square fitting whereas the degree of the polynomial is determined by trial [23, 24]. A drawback of this approach is that, especially with polynomials of higher degree, there is no guarantee that the curve will be smooth and without oscillations between the calibration points. The use of cubic spline functions can help to circumvent this problem [25], and does not seem to have been used previously for calibration purposes.

EXPERIMENTAL

Chemicals

Sodium dodecylsulphate (puriss.), diisobutylphenoxyethoxyethyldimethylbenzylammonium chloride monohydrate (Hyamine 1622), hexadecylpyridinium chloride (purum), diisobutylcresoxyethoxyethyldimethylbenzylammonium chloride monohydrate (Hyamine 10X), benzalkonium chloride

(purum), hexadecyltrimethylammonium bromide (purum) were from Fluka. Sodium sulphate (zur. Anal.) and dioctyl sodium sulphosuccinate were from Merck. All were used as received. Solutions were prepared with deionized water that was filtered through Millipore Q2 filters.

Equipment

A schematic diagram of the flow injection equipment is shown in Fig. 1. A peristaltic pump (Gilson, Minipuls 2), was used to produce a flow rate of 1.25 ml min^{-1} in each channel. Samples were introduced with a Rheodyne manual injection valve equipped with a 60-μl sample loop. Teflon tubing (0.8 mm i.d.) was used to connect the voltammetric cell (Metrohm EA-1096) with the pump and the injection valve. To avoid trapping air bubbles, the cell was placed with its outlet tubing pointing vertical and upwards.

The working electrode was a gold electrode (5 mm diameter; Metrohm EA-286/3) which has been covered by mercury by dipping it in polarographic-grade mercury and wiping off adhering mercury drops. The smooth mercury surface thus obtained could be used for at least a week without renewal. The reference electrode was a silver/silver chloride electrode filled with 3 M KCl (Metrohm EA-442). An uncoated gold electrode (Metrohm EA-286/3) was used as counter electrode.

The equipment for operating the voltammetric cell as a tensammetric detector consisted of a PAR polarograph, model 174, together with its AC interface and a PAR lock-in amplifier, model 122. The phase angle used was 90°. A Philips PM-8100 chart recorder was used. The measuring system was calibrated in capacitance units with the use of a dummy cell constructed with a standard capacitance decade. The supporting electrolyte was 0.1 M Na_2SO_4 in all experiments.

RESULTS AND DISCUSSION

Although tensammetry is possible at all kinds of electrode surfaces, mercury is the most widely used electrode material and was therefore selected for these experiments. The major problem in preparing a stationary working electrode for tensammetric measurements is the formation of a homogeneous and well-defined surface. In this respect, the mercury film on a gold support obtained by simply dipping in mercury was much easier to prepare and showed a more favourable behaviour than electrochemically deposited mercury films on glassy carbon or carbon paste.

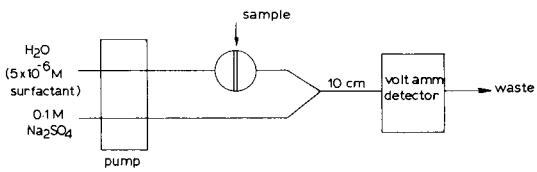

Fig. 1. Schematic diagram of the flow injection equipment for the determination of detergents.

In the present flow injection determinations, all measurements were made at a d.c. potential of −0.85 V vs. Ag/AgCl (3 M KCl) except for the benzalkonium chloride which was measured at −0.40 V. These potentials were chosen in between the two adsorption/desorption peaks where a decrease of the capacitance is generally observed in the presence of specifically adsorbing species.

For some of the surfactants examined, the flow injection peaks (capacitance vs. time curves) had the normal, slightly asymmetric shape; for some others, however, enhanced tailing seemed to occur after the signal had returned to a certain level above the baseline. Nevertheless, the same peak maxima were reached for subsequent injections at various intervals even though the surface was apparently still covered by small, but varying amounts of surfactant molecules from previous injections. This indicates that it is the absolute value of the maximum capacitance that is of importance. It is more attractive, however, to have a steady baseline, thus a small amount of surfactant was added to the carrier stream to make its concentration approximately 5×10^{-6} mol l^{-1}. An additional advantage of maintaining a small concentration of surfactant in the carrier stream is that active sites in the system between injection and detection remain blocked throughout the whole procedure. A similar procedure has been recommended before for potentiometric flow-through detectors [26].

For various detergents (anionic, cationic and nonionic), standard solutions were prepared, generally in the range 10^{-5}—10^{-4} mol l^{-1}. From each stock solution, diluted standards were prepared with concentrations in the ratio 1:2:3:6:8:10. Because the calibration graphs were not linear, the "best" curve had to be calculated. Two procedures were adopted: (i) a polynomial fitting procedure, (ii) a cubic spline approximation with 3 intervals. If the total concentration span of the calibration graph is equal to C_{tot}, the intervals chosen are: $0.1C_{tot}$—$0.3C_{tot}$, $0.3C_{tot}$—$0.6C_{tot}$ and $0.6C_{tot}$—$1.0C_{tot}$. This number of intervals is the maximum that still produces a unique set of cubic splines describing the data with six distinct concentration values. Each calibration solution was measured four times and the complete data set was used in the calculations. The computer programs for the calculations were written in FORTRAN and are based on the corresponding subroutines from the NAG library [24].

A typical cubic spline calibration graph is presented in Fig. 2. The scale of the drawing is too small to show the difference between the polynomial and the cubic spline functions fitting the data, therefore only the spline function is plotted. However, the numerical values for this calibration show that the cubic spline approximation follows the data more closely in the lower concentration range (Table 1).

Test samples were prepared independently for all surfactants. For each sample the average of four measurements was used for calculation of the concentration. The results are presented in Table 2. Because the concentrations of the test solutions were chosen in the middle of the calibration range,

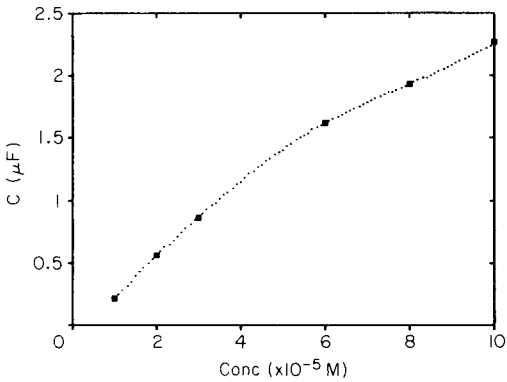

Fig. 2. Calibration plot for Hyamine 1622: (···) cubic spline approximation; (■) experimental points averaged over 4 measurements.

TABLE 1

Calibration data for Hyamine 1622

Conc. ($\times 10^{-5}$ M)	ΔC measured (μF)				ΔC mean (μF)	ΔC polyn. (μF)	ΔC spline (μF)
1.0	0.212	0.219	0.214	0.217	0.215	0.217	0.215
2.0	0.548	0.565	0.565	0.566	0.562	0.556	0.561
3.0	0.873	0.861	0.876	0.885	0.874	0.878	0.873
6.0	1.62	1.62	1.60	1.64	1.62	1.62	1.62
8.0	1.93	1.94	1.94	1.93	1.93	1.94	1.93
10.0	2.27	2.30	2.25	2.23	2.26	2.26	2.26

TABLE 2

Flow injection determination of detergents

Compounds	Concentration ($\times 10^{-5}$ M)			Error (%)	
	Given	Found polyn.	Found spline	Polyn.	Spline
Hyamine 1622[a]	5.00	5.07	5.06	+1.4	+1.2
Hyamine 1622[a,b]	5.00	4.90	4.93	−2.0	−1.4
Sodium dodecylsulphate	50.0	50.0	50.4	+1.0	+0.8
Hyamine 10X[a]	5.00	5.08	5.12	+1.6	+2.4
Benzalkonium chloride[a,c]	30.0	29.7	29.6	−1.0	−1.3
Dioctyl sodium sulfosuccinate[a]	5.00	5.20	5.20	+4.0	+4.0
Hexadecyltrimethylammonium Bromide[a]	5.00	4.90	4.90	−2.0	−2.0
Triton X-100[c]	25.5	24.5	24.4	−3.9	−4.3
Hexadecylpyridinium chloride	5.00	irreversible adsorption			

[a] 5×10^{-6} M detergent in supporting electrolyte. [b] Independent calibration. [c] Concentration in mg l^{-1}.

no significant difference is observed between the values calculated on the base of the polynomial or cubic spline function. The accuracy of the method appears to be about ±4%. In the case of hexadecylpyridinium chloride, the adsorption is irreversible and no return to the baseline occurs even after prolonged waiting times. In such cases, the electrode surface has to be wiped with a tissue and the electrode dipped in mercury again before use for the next sample.

The present flow injection procedure allows the determination of at least 60 samples h^{-1}. As for all tensammetric procedures, it is not possible to differentiate between different kinds of surfactants. Because of this lack of selectivity, the proposed method is only suitable for well-defined samples as is generally the case with, for example, process streams.

The authors thank W. Lengton for carrying out preliminary experiments, Mrs. B. Verbeeten-Van Hettema for preparing the manuscript and R. H. Arends for making the drawings.

REFERENCES

1 H. Konig, Neuere Methoden zur Analyse von Tensiden, Springer-Verlag, Berlin, 1971.
2 K. Vytras, M. Remes and H. Kubesova-Svoboda, Anal. Chim. Acta, 124 (1981) 91.
3 K. Vytras, M. Dajkova and V. Mach, Anal. Chim. Acta, 127 (1981) 165.
4 D. L. Jones, G. J. Moody, J. D. R. Thomas and B. J. Birch, Analyst, 106 (1981) 974.
5 M. Sak-Bosnar and M. S. Jovanovic, Mikrochim. Acta, (I) (1981) 409.
6 T. Kobayashi, M. Kataoka and T. Kambara, Talanta, 27 (1980) 253.
7 W. Selig, Fresenius Z. Anal. Chem., 300 (1980) 183.
8 N. Ciocan and D. F. Anghel, Fresenius Z. Anal. Chem., 290 (1978) 237.
9 S. G. Cutler, P. Meares and D. G. Hall, J. Electroanal. Chem., 85 (1977) 145.
10 M. Bos, Anal. Chim. Acta, 135 (1982) 249.
11 M. J. Rosen, X. Hua, P. Bratin and A. W. Cohen, Anal. Chem., 53 (1981) 232.
12 D. Britz, Anal. Chim. Acta, 115 (1980) 327.
13 D. R. Canterford and R. J. Taylor, J. Electroanal. Chem., 98 (1979) 25.
14 J. Lankelma and H. Poppe, J. Chrom. Sci., 14 (1976) 310.
15 H. Jehring, J. Electroanal. Chem., 20 (1969) 33.
16 J. Kawase and M. Yamanaka, Analyst, 104 (1979) 750.
17 K. W. Petts and I. Sliney, Water Res., 15 (1981) 129.
18 J. Kawase, A. Nakae and M. Yamanaka, Anal. Chem., 51 (1979) 1640.
19 J. Kawase, Anal. Chem., 52 (1980) 2124.
20 J. Koryta, Collect. Czech. Chem. Commun., 18 (1953) 206.
21 D. Britz and D. Knittel, Electrochim. Acta, 20 (1975) 891.
22 W. A. Halang, R. Langlais and E. Kugler, Anal. Chem., 50 (1978) 1829.
23 L. M. Schwartz, Anal. Chem., 49 (1977) 2062.
24 NAG FORTRAN Library Manual, Mark 9, Vol. 2, Numerical Algorithms Group Ltd., Oxford, 1981.
25 C. de Boor, A Practical Guide to Splines, Springer-Verlag, Berlin, 1978.
26 W. E. van der Linden and R. Oostervink, Anal. Chim. Acta, 101 (1978) 419.

Analytica Chimica Acta, 156 (1984) 77—85
Elsevier Science Publishers B.V., Amsterdam — Printed in The Netherlands

COMPUTER METHODS FOR THE CALCULATION OF COMPLEX FORMATION CONSTANTS BY DIFFERENTIAL PULSE POLAROGRAPHY

Modification to the DeFord—Hume Method Applicable to Quasireversible and Irreversible Processes

M. A. GÓMEZ-NIETO, M. D. LUQUE DE CASTRO and M. VALCARCEL*

Department of Analytical Chemistry, Faculty of Sciences, University of Córdoba, Córdoba (Spain)

J. L. CRUZ SOTO

Department of Mathematics, University of Córdoba, Córdoba (Spain)

(Received 10th February 1983)

SUMMARY

The modification to the DeFord and Hume method for differential pulse polarography is applicable to quasi-reversible and irreversible processes and takes into account any change in the reversibility of the system when the concentration of the ligand is altered. Three computer programs for the calculation of the stability constants are outlined: two of them are based in the weighted least-squares and the third is a simulation process.

Polarographic methods for the evaluation of stability constants of complexed metal ions are based on the changes undergone by the reduction waves of cations when their coordination spheres are occupied by molecules other than water. The reduction potential is shifted, almost invariably in the more negative direction, and the diffusion current changes, usually becoming smaller. These phenomena may be attributed to the bulkier complexed ion requiring more energy for reduction at the dropping mercury electrode (DME), and having a different diffusion coefficient compared to the aquated ion, respectively.

Generally, methods for the polarographic evaluation of stability constants of metal complexes depend on the reversibility of the system under study; the three categories of method are those applicable to reversible reductions, those applicable to irreversible reductions, and those applicable to either.

Among the methods applicable to reversible processes are Lingane's, DeFord and Hume's and some modifications to the latter. The Lingane method [1], based on the shift in the reduction potential of the metal ion on complex formation, is applicable to systems in which a single complex species exists over the whole range of ligand concentration, or when one species predominates in a particular interval of ligand concentration. The

0003-2670/84/$03.00

method of DeFord and Hume [2], based on similar principles, partly solves the problems of the Lingane method: it permits simultaneous calculation of the consecutive stability constants of the complexes that exist in a cation-ligand system, taking into account the variation of the current when the ligand concentration is altered. However, possible changes in the diffusion coefficient of the metal species or in the reversibility of the system on complex formation are not considered in this method. Schaap and McMasters [3] developed a logical extension of the DeFord and Hume method in which the metal ions were complexed by two ligand species simultaneously in solution; this required prior knowledge of the stability constants of the simple complexes. Various other early modifications of the DeFord and Hume technique have been suggested but most of these also have disadvantages.

The methods applicable to irreversible processes are more restrictive owing to the need for an indicator ion that must fulfil tight requirements. The most important methods of this type are those of Schwarzenbach and co-workers [4, 5] and Ringbom and Eriksson [6, 7]. The methods applicable to both reversible and irreversible processes are based on the variation of the diffusion coefficient of the electroreducible species when the ligand concentration is altered. The method of Kacena and Matousek [8] is applicable when a single species exists in solution but is subject to high errors. The Crow method [9] starts from the Stokes—Einstein equation, but requires a series of approximations that diminish its applicability. More specialized methods have been developed by Tur'yan and co-workers [10]; these are applicable to systems influenced by the kinetics of complex formation.

The method of DeFord and Hume has been very widely used. The equation was normally solved by graphical extrapolation until the introduction of various computer methods of solving it [11—13]. Almost all of these are based on the application of the least-squares method to the equations derived from the experimental data.

In the present study, the DeFord and Hume method was used, not in its original form but in the modification proposed by Heath and Hefter [14] for differential pulse polarography (d.p.p.) with all the implicit approximations. Three computer programs are used in solution of the equation. The programs are verified by application to classic systems.

EXPERIMENTAL

An ABC microcomputer, model 26, was used with a floppy disk unit, the main memory was 64 kbyte, and Fortran and Basic Compilers were used. A Hewlett-Packard microcomputer (model HP-85; main memory 32 kbyte) was used with a magnetic tape unit and Basic interpreter. A Data-General minicomputer (model Eclipse C/350; AOS operating system; main memory 768 kbyte) was equipped with two 25-Mbyte fixed disk units and Fortran V, Basic and Pascal compilers were used.

RESULTS AND DISCUSSION

Modification proposed

The situation considered is essentially the same as that discussed by DeFord and Hume [2], i.e., the different possible forms of the metal in solution are in equilibrium so that it is impossible to establish which of the species actually reacts at the electrode in the electron-transfer process:

$$\begin{array}{c} M \rightleftharpoons MX \rightleftharpoons \underset{\Downarrow\Uparrow}{MX_2} \rightleftharpoons \ldots \rightleftharpoons MX_N \\ M(Hg) \end{array} \qquad (I)$$

Further, the equilibrium is such that some reactions at the electrode are too slow for the overall process to be completely reversible. (To simplify matters, charges and activity coefficients are not considered in this paper.)

The equation for the half-wave potential is modified to include a term that accounts for the irreversibility of the process, and the half-wave potential, $E_{1/2}$, is replaced by the peak potential, E_p, by means of the equation of Parry and Osteryoung [15]. The following expressions are then obtained:

$$E_{pM} = E_0 - \tfrac{1}{2}\Delta E_{1/2} - [RT/(n\alpha)_0 F] \ln (I_M/I_A) + IRE_1 \qquad (1)$$

$$E_{pC} = E_0 - \tfrac{1}{2}\Delta E_{1/2} - [RT/(n\alpha)_j F] \ln (I_{MX_j}/I_A) \sum_{j=0}^{N} \beta_{MX_j}[X]^j + IRE_2 \qquad (2)$$

where E_{pM} and E_{pC} are the peak potentials for the free and complexed metal, respectively, and the IRE terms are defined as

$$IRE_1 = [RT/(n\alpha)_0 F] \ln 0.886\, k_0\, t^{1/2}/D_0^{1/2}$$

and $$IRE_2 = [RT/(n\alpha)_j F] \ln 0.886\, k_j\, t^{1/2}/D_j^{1/2}$$

The terms $(n\alpha)_0$ and $(n\alpha)_j$ are the number of electrons involved in the reaction at the electrode multiplied by the transfer coefficient for the metal reduction in the absence and presence of the ligand, respectively; k_0 and k_j are the rate constants for the electrode reaction. The other terms have their common meanings.

The change in the peak potential of the cation when the ligand concentration is altered is given by

$$\Delta E_p = E_{pM} - E_{pC} = (RT/F) \ln (I_C^{1/(n\alpha)_j}/I_M^{1/(n\alpha)_0}) + (RT/F)$$
$$\ln I_A^{[(n\alpha)_j - (n\alpha)_0]/(n\alpha)_j(n\alpha)_0} + [RT/(n\alpha)_j F] \ln \sum_{j=0}^{N} \beta_{MX_j}[X]^j + IRE_1 - IRE_2 \qquad (3)$$

In pulse polarography, when the applied pulse is sufficiently small, the peak intensity is given [17] by

$$I_p = [(n\alpha)^2 F^2/4RT]\, AC\Delta E\, (D/\pi t_M)^{1/2} = KIC \qquad (4)$$

where ΔE is the pulse amplitude, t_M is the integration time of the apparatus, I is the d.c. current constant, and K is the conversion constant, i.e., the

ratio between the current constants in d.c. and d.p. polarography. $K = K'(n\alpha) F\Delta E/4.609RT$, where K' is a constant that takes into account the ratio between the characteristics of the capillary in the d.c. and d.p. techniques.

Substituting in Eqn. 3 the I_M and I_C values calculated starting from Eqn. 4 gives

$$\Delta E_p = E_{pM} - E_{pC} = (RT/F) \ln [I_{pC}^{1/(n\alpha)_j}/I_{pM}^{1/(n\alpha)_0}] + [RT/(n\alpha)_j F]$$

$$\ln \sum_{j=0}^{N} \beta_{MX_j}[X]^j + \delta(j) \quad (5)$$

where $\delta(j)$ is defined by

$$\delta(j) = (RT/F) \ln (KCI_A\ 0.886t^{1/2})^{[(n\alpha)_j - (n\alpha)_0]/(n\alpha)_j(n\alpha)_0}$$

$$+ (RT/F) \ln [D_j^{1/2(1/(n\alpha)_j)}/D_0^{1/2(1/(n\alpha)_0)}] + (RT/F) \ln [k_0^{1/(n\alpha)_0}/k_j^{1/(n\alpha)_j}] \quad (6)$$

For systems in which an increase in the ligand concentration does not cause an appreciable change in the $n\alpha$, D and K parameters regardless of the reversibility of the process, the $\delta(j)$ term is of a similar order to the experimental errors. Thus if this term is not considered, the values of the formation constants obtained will not be modified. Thus Eqn. 5 can be used without the $\delta(j)$ term. Manipulation of this form of Eqn. 5 then leads to

$$F_1 = [I_{pM}^{(n\alpha)_j/(n\alpha)_0}/I_{pC}] \exp [\Delta E_p (n\alpha)_j F/RT] = \sum_{j=0}^{N} \beta_{MX_j}[X]^j$$

$$= \beta_0 + \beta_1[X] + \beta_2[X]^2 + \ldots + \beta_N[X]^N \quad (7)$$

This equation is similar to DeFord and Hume's equation but, instead of the theoretical number of electrons involved, the product of the number of electrons by the transfer coefficient is considered; values are calculated for each particular experiment. Obviously if $(n\alpha)_j = (n\alpha)_0 = n$ in Eqn. 7, the equation of DeFord and Hume for differential pulse polarography is obtained.

Description of the computer methods for calculation of the formation constants of chelates

For the calculation of stability constants in a metal/ligand system from polarographic data, the peak current and potential values (for the differential pulse method) and the $(n\alpha)$ product must be known. Generally, the currents and potentials were measured directly from the polarogram obtained in a particular experiment or by the application of the weighted least-squares method.

The method of weighted least-squares, as is well-known, is based on minimizing the expression $S = \Sigma_{j=1}^{N} w_j[y_j - f(x_j)]^2$, where S is the sum of the weighted squares of the residuals, y_j are the experimental measurements and $f(x_j)$ are the calculated values; w_j is the weight of the y_j measured with variance σ_j^2, i.e., $w_j = 1/\sigma_j^2$.

For the calculation of I_p, E_p and $(n\alpha)$, a computer method FØ(I) was

developed, based on applying the weighted least-squares method to the equation of the Tomes' line for a.c. and differential pulse polarography [17]. The equation can be written in the form

$$\ln \{(I_p/I_j)^{1/2} \pm [(I_p - I_j)/I_j]^{1/2}\} = aE_j + b \quad (8)$$

where $E_p = -b/a$, $a = (n\alpha)_j F/2RT$, and $b = E_p(n\alpha)_j F/2RT$; j represents experimental peak values.

The error in the E_j measurement is negligible but the current measurements are of unequal accuracy, thus the weight of the logarithmic term is estimated by applying the law of propagation of errors to Eqn. 8 rewritten as

$$1/W_j = \sigma_j^2 = \{(\delta/\delta I_j)[\ln\{(I_p/I_j)^{1/2} \pm [(I_p - I_j)^{1/2}/(I_j)^{1/2}]\}]\}^2 \sigma_{I_j}^2 + \{\delta/\delta I_p[\ln\{(I_p/I_j)^{1/2} \pm [(I_p - I_j)^{1/2}/(I_j)^{1/2}]\}]\}^2 \sigma_{I_p}^2 \quad (9)$$

Because I_j and I_p are independent of each other, they are probably measured with the same accuracy, thus $\sigma_{I_j}^2 = \sigma_{I_p}^2$. Manipulation of Eqn. 9 gives the expression

$$w_j = 4I_p I_j^2 (I_p - I_j)/I_p^2 + I_j^2 \quad (10)$$

In this manner, using w_j as the weight for the current intensity of each measurement, more accurate values for a and b, and finally for E_p, I_p and $(n\alpha)$, are obtained.

The program FΦ(I) is based on application of the weighted least-squares method to Eqn. 8. The output data for each experiment are the peak potential and current, the $(n\alpha)$ product and the FΦ value (first item of the equation proposed by DeFord and Hume) and F_1 (first item of the equation proposed here). The input data are the current and potential values measured at each point of a recorded peak.

The data obtained by the FΦ(I) program are substituted in Eqn. 7, leading to a system of z equations (experiments done) with N unknowns (constants to be determined). This system was solved by using three computer methods. Two of them (GIP II and FΦW), based on the weighted least-squares method, are adapted from earlier methods [12, 13] and the third is an original method based on obtaining the values of the stability constants by a simulation process.

GIP II (Gaussian iteration program). For application of this program, Eqn. 7 is rewritten in the form

$$\ln (1 + \sum_{j=1}^{N} C_i^j \beta_j) = \ln \begin{Bmatrix} F\Phi(i) \\ F_1(i) \end{Bmatrix} = P_i \quad (i = 1, 2, \ldots k) \quad (11)$$

where i is the number of measurements and N is the number of stability constants. As the weighted least-squares method requires linearity of the equations for the parameters to be calculated, an unknown β_j value is replaced by its approximate value β_j^0 having small deviation $\delta\beta_j$ from the true β_j: $\beta_j = \beta_j^0 - \delta\beta_j$. If $\delta\beta_j$ is very small, Eqn. 11 can be expanded in a Taylor

series, ignoring higher-order terms in the deviations $\delta\beta_j$:

$$\ln\left(1 + \sum_{j=1}^{N} C_i^j \beta_j^0\right) = (C_i \delta\beta_1 + C_1^2 \delta\beta_2 + \ldots + C_i^N \delta\beta_N)/\left(1 + \sum_{j=1}^{N} C_i^j \beta_j^0\right) \qquad (12)$$

A system of linear equations in relation to the deviations, which are now the unknown factors and can be solved by applying the weighted least-squares method, is thus obtained. The program is based on an iterative method by which the deviations $\delta\beta_j$ are calculated and substituted in the equation for β_j to obtain new values of β_j that are again considered as approximates (β_j^0) and substituted in Eqn. 12 to obtain lower deviations and so on until the convergence previously imposed on $\delta\beta$ is attained.

The GIP II program solves the system of equations by Gauss's numerical elimination method in all and each of the iterations (this method appears as a subroutine of the main program). The variances of the most probable values of the final β_j can be calculated easily by the variance matrix of the normal equations, because the β_j variances are equal to those corresponding to $\delta\beta_j$. In this way, the accuracy in the stability constants obtained is calculated from their variance as well as the values of Student's t at 95% level of confidence for an appropriate degree of freedom. For the cases in which the deviations obtained are higher than the corresponding constant, this is considered not significantly different from zero and the calculation is done again by ignoring this stoichiometry.

FØW (weighted FØ). This method is based on calculation of the formation constants directly starting from Eqn. 7, the variance of the term $\Delta E_p(i)$ being twice the variance of the peak potential measurement, because it is assumed that the variance remains constant in all measurements. This method can be used only if it is assumed that the measurement of the concentrations is error-free and that the values of the left-side of Eqn. 7 are corrected starting from the relative weights, which are $w_i = 1/\sigma^2_{F\phi(i)} = 1/F\phi^2(i)$ and $w_i^{1/2} = 1/F\phi(i)$. When these weights are applied, Eqn. 7 takes the form

$$[C_i/F\phi(i)]\beta_1 + [C_i^2/F\phi(i)]\beta_2 + \ldots + [C_i^N/F\phi(i)]\beta_N = 1 - [1/F\phi(i)] \qquad (13)$$

yielding a set of simultaneous equations in $F\phi(i)$ solvable by the weighted least-squares method.

MSE (minimum sum of errors). This program is organized differently but again consists in minimizing the sum of errors. The difference is that this sum is defined as a function of n variables (formation constants) which can be plotted by a surface in an $(n + 1)$ dimensional space. The optimal values of the formation constants are those that represent a minimal part of that surface in this space.

The program involves numerical approximation in which the difference between the theoretical and experimental values is minimized. The input data are the E_p, I_p and $(n\alpha)$ values obtained in each particular experiment and calculated from the program $F\phi(i)$. Two tolerances are considered: a

tolerance of error that is equal to the minimum accumulated error (the one theoretically calculated) and a tolerance at intervals, which is equal to the minimal significant deviation for each constant. When values below the imposed tolerances are obtained in the partial calculations of the program, the program converges and the values of the stability constants obtained are the most probable.

As can be observed from the flow chart (Fig. 1), the intervals at which the constants are explored, undergo continuous rearrangement. The program provides as output data, in addition to the most probable values of the constants, the $\bar{n}$ values (the average ligand number or degree of formation) and the molar fraction of each complex for each ligand concentration. These values, together with the deviation of the constants, provide sufficient data to judge the insignificance of some constant; in this case, the calculations are repeated, imposing the non-existence of this stoichiometry.

In the three methods described, it is assumed that the concentration of free ligand in solution is equal to the initial concentration. This approximation is corrected, once the most probable values for the stability constants have been calculated. With these values and starting from the equations

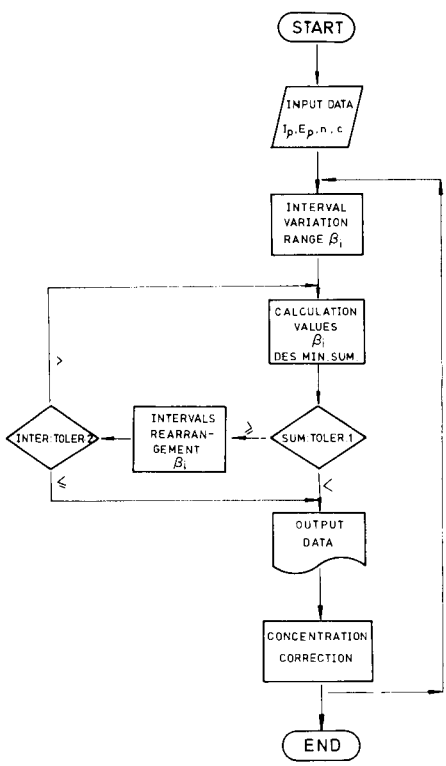

Fig. 1. Flow chart for the MSE program.

TABLE 1

Verification of the program

Method	β_1	β_2	β_3
Cadmium chloride system			
Ref. 14	21.2 ± 1.3	49.0 ± 0.8	34.0 ± 9.0
GIP II	21.2 ± 0.3	54.4 ± 0.8	32.4 ± 0.6
FØW	21.0 ± 0.3	55.2 ± 1.0	31.7 ± 0.8
MSE	21.0 ± 1.0	55.0 ± 1.0	32.0 ± 1.0
Cadmium thiocyanate system			
Ref. 12	13.3 ± 1.9	47.3 ± 5.8	86.2 ± 3.1[a]
GIP II	12.6 ± 2.3	45.3 ± 6.2	81.3 ± 2.5[a]
FØW	12.5 ± 3.1	45.9 ± 5.1	79.5 ± 1.3[a]
MSE	15.0 ± 1.0	42.0 ± 1.0	81.0 ± 1.0[a]
Zinc pyridine system			
Ref.17	8.0 ± 0.5	34.0 ± 1.0	0.0
GIP II	6.8 ± 1.2	33.3 ± 1.0	0.0
FØW	6.7 ± 1.2	33.4 ± 1.8	0.0
MSE	8.0 ± 1.0	32.0 ± 1.0	0.0

[a]Values for β_4.

$$(\sum_{j=1}^{N} C_i^j \beta_j)/(1 + \sum_{j=1}^{N} C_i^j \beta_j) = \bar{n} \text{ and } C_i = (C_i)_0 - \bar{n}\, C_M$$

new more correct values of the free ligand concentration are obtained with which the stability constants are calculated again. (C_M is the metal ion concentration and $(C_i)_0$ is the total concentration of ligand in experiment i).

Verification of the programs

In order to verify the three programs (GIP II, FØW and MSE), each of them was run through with the data for three systems from the literature. The chosen systems were the cadmium chloride system studied by differential pulse polarography [14], and the cadmium thiocyanate [12] and zinc pyridine [17] systems, both studied by classic polarography. The stability constants for each system were estimated by the method of DeFord and Hume. Although these authors did not provide data on peak width or $E_{3/4} - E_{1/4}$, data provided was sufficient to run through the programs. The values of the stability constants obtained are summarized in Table 1. As can be observed, the three programs provided constants very close to those presented in the literature. The MSE program (simulation) usually gave smaller deviations in the values of the formation constants than the GIP II and FØW programs.

The proposed modification of the method of DeFord and Hume has been applied to the Bi(III)—azomethine derivatives of 2-benzoylpyridine (oxime, hydrazone and thiosemicarbazone) systems. The irreversible character of the

reduction processes of these systems makes them suitable for the verification of this modification [18].

REFERENCES

1 J. J. Lingane, Chem. Rev., 29 (1941) 1.
2 D. D. DeFord and D. N. Hume, J. Am. Chem. Soc., 73 (1951) 5321.
3 W. B. Schaap and D. L. McMasters, J. Am. Chem. Soc., 83 (1961) 4699.
4 G. Schwarzenbach and H. Ackermann, Helv. Chim. Acta, 35 (1952) 485.
5 G. Schwarzenbach, R. Gut and G. Anderegg, Helv. Chim. Acta, 37 (1954) 937.
6 A. Ringbom and L. Eriksson, Acta Chem. Scand., 7 (1953) 1105.
7 L. Eriksson, Acta Chem. Scand., 7 (1953) 1146.
8 V. Kacena and L. Matousek, Collect. Czech. Chem. Commun., 18 (1953) 294.
9 D. R. Crow, J. Electroanal. Chem., 16 (1968) 137.
10 See e.g., Ya. I. Tur'yan, N. K. Strizhov, V. N. Gnusin, K. M. Kardailova and L. M. Maluka, Zh. Neorg. Khim., 23 (1968) 2061; Ya. I. Tur'yan, I. N. Loguinov and N. K. Strizhov, Zh. Neorg. Khim., 23 (1978) 1970; Ya. I. Tur'yan, V. N. Gnusin and V. S. Yatsenko, Zh. Neorg. Khim., 23 (1978) 2083.
11 D. J. Leggett, Talanta, 27 (1980) 787.
12 K. Momoki, H. Sato and H. Ogawa, Anal. Chem., 39 (1967) 1072.
13 L. Meites, Talanta, 22 (1975) 733.
14 G. A. Heath and G. Hefter, J. Electroanal. Chem., 84 (1977) 295.
15 E. P. Parry and R. A. Osteryoung, Anal. Chem., 37 (1965) 1634.
16 A. M. Bond, Modern Polarographic Methods in Analytical Chemistry, M. Dekker, New York, 1980, pp. 249, 301.
17 V. K. Sharman and J. N. Gaur, J. Electroanal. Chem., 9 (1965) 321.
18 M. A. Gomez-Nieto, M. D. Luque de Castro and M. Valcarcel, Talanta, (1983) in press.

Analytica Chimica Acta, 156 (1984) 87—101
Elsevier Science Publishers B.V., Amsterdam — Printed in The Netherlands

A KALMAN FILTER FOR CALIBRATION, EVALUATION OF UNKNOWN SAMPLES AND QUALITY CONTROL IN DRIFTING SYSTEMS
Part 1. Theory and Simulations

P. C. THIJSSEN*, S. M. WOLFRUM and G. KATEMAN

University of Nijmegen, Faculty of Sciences, Department of Analytical Chemistry, Toernooiveld, 6525 ED Nijmegen (The Netherlands)

H. C. SMIT

University of Amsterdam, Laboratory for Analytical Chemistry, Amsterdam (The Netherlands)

(Received 14th July 1983)

SUMMARY

The suitability of a Kalman filter for processing slowly varying parameters of a linear calibration graph is described. After calibration, the recursive algorithm predicts the changing parameters in time, which are used for the evaluation of unknown samples. With a preselected precision of the final results as a proper analytical goal, one may decide successively either to do another unknown sample or to calibrate again. The application of the proposed algorithm is demonstrated with a simulated example based on realistic data.

The performance of analytical systems can be assessed in terms of the quality of results and the time for which the system will function properly without breakdowns or disturbances. The systems considered here are complex structures including chemical, mechanical, electrical and optical parts. If the quality of these parts changes in time, the analytical performance may also change. Statistical measures such as reliability, stability, accuracy and signal/noise ratio are necessary for practical evaluation of the quality of results. In general, the quality of a system can be resolved into two main components: a stationary random component associated with fluctuations under normal working conditions, and a semi-random non-stationary component caused by irreversible processes such as contamination, evaporation, wear or aging. All analytical systems have some tendency towards non-stationary behaviour [1]. Varying systematic deviation or time-dependent variance of the analytical errors can occur, or the system may become defective, giving errors beyond some preset limit.

The present paper is concerned with slowly varying parameters in a linear calibration function. Calibration drift with time is a particular problem in

0003-2670/84/$03.00

automated analytical procedures, e.g., those based on flow systems or atomic absorption spectrometry [2—4]. Drift can seriously affect the accuracy of results for unknown samples if it is ignored. Various methods have been proposed to solve the drift problem. Usually, calibration drift is dealt with by putting control standards at fixed positions in the sample sequence. Data are corrected by mathematical manipulation such as graphical solutions and linear regression [2—6]. An alternative involves electronic compensation of the measuring device, which must be applied before the actual experiments are started [7, 8]. These methods always involve off-line drift compensations.

Recently, a Kalman filter was suggested for on-line compensation of linear drift in multicomponent analysis [9]. The drift model is based on a static description and reformulation is required. In accordance with an extended dynamic model, the Kalman filter works by on-line calibration of the changing parameters. Samples are evaluated by using the parameters predicted by a recursive algorithm. Given a preset precision of the final results as the goal, the system may be recalibrated or assessed in some other way.

The proposed design of quality control has the capacity to adapt to the experimental conditions encountered. The algorithm could be a step forward in the development and integration of some intelligence within automated analytical instrumentation.

THEORY

Model structure

The general starting point for the system description is based on a state space model. In many analytical situations, one may consider the linear discrete dynamic system

$$\mathbf{x}(k) = \mathbf{F}(k)\mathbf{x}(k-1) + \mathbf{w}(k-1) \tag{1}$$

$$z(k) = \mathbf{h}^t(k)\mathbf{x}(k) + v(k) \tag{2}$$

Here, k is a discrete variable denoting a particular time or a sequence number; $\mathbf{x}(k)$ is the n-column state vector which denotes, for example, concentrations or sensitivities. The relation between the old state $\mathbf{x}(k-1)$ and new state $\mathbf{x}(k)$ in the sequence is represented by the $n*n$ transition matrix $\mathbf{F}(k)$ and can be a set of difference equations. The state $\mathbf{x}(k)$ is weighted by the n-row measurement vector $\mathbf{h}^t(k)$ to give the measured signal $z(k)$; $\mathbf{w}(k-1)$ is a n-column vector representing the system noise and $v(k)$ is the measurement noise (a scalar) with statistical characteristics that have to be defined. The assumption of the linearity of the state space model implies that the transition matrix $\mathbf{F}(k)$ and measurement vector $\mathbf{h}^t(k)$ have to be known deterministically. The state space model [1, 2] is often designed as a block diagram (Fig. 1).

The current values of the state vector are sufficient to determine the behaviour of the system completely. A given state space model is not unique, because there are infinite possible representations. The various equivalent

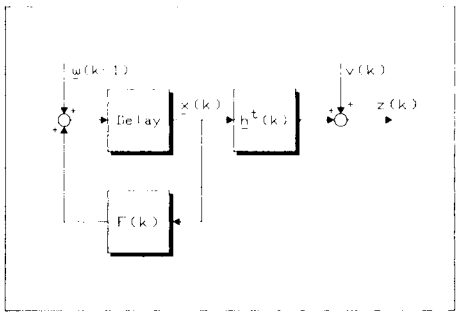

Fig. 1. A linear dynamic system. $\mathbf{x}(k)$ represents the state vector, $\mathbf{F}(k)$ the transition matrix, $\mathbf{h}^t(k)$ the measurement vector, and $z(k)$ the resulting signal; $\mathbf{w}(k)$ and $v(k)$ denote the system noise and measurement noise, respectively.

state descriptions can be interrelated by similarity transformations. Defining a new state vector $\mathbf{x}^*(k)$ by the transformation $\mathbf{x}(k) = \mathbf{T}(k)\mathbf{x}^*(k)$, with $\mathbf{T}(k)$ as a non-singular matrix, generates the alternative state space model [10]

$$\mathbf{x}^*(k) = \mathbf{T}(k)^{-1}\mathbf{x}(k); \quad \mathbf{F}^*(k) = \mathbf{T}(k)^{-1}\mathbf{F}(k)\mathbf{T}(k-1); \quad \mathbf{w}^*(k) = \mathbf{T}(k)^{-1}\mathbf{w}(k);$$

$$\mathbf{h}^{*t}(k) = \mathbf{h}^t(k)\mathbf{T}(k) \tag{3}$$

In general, it is common practice to use models with the lowest dimensional order.

A system can be observed when all states can be determined, directly or indirectly, from the measurements. As an algebraic criterion, a sufficient number of linear independent equations is needed. Hence, when a certain system state or changes in that state cannot affect the output of the system, the system is said to be unobservable. The observability condition is satisfied if the matrix [11]

$$\mathbf{M} = \{\mathbf{h}, \mathbf{F}^t\mathbf{h}, \ldots, (\mathbf{F}^t)^{n-1}\mathbf{h}\} \tag{4}$$

is of rank n or equivalently the determinant $|\mathbf{M}| \neq 0$.

A state space model for a calibration curve can be derived as follows. First, the primary system model is extended with linear drift. Then, a dynamic model structure, which describes the slowly varying parameters as stochastic drift, is investigated. The commonly used calibration graph is based on the linear relationship

$$y = ac + b \tag{5}$$

where a is the sensitivity (slope), b the intercept, c the concentration, and y the corresponding measurement. Some alternatives are easily transformed or extended into a similar mathematical relation [14].

Reformulation of Eqn. 5 to other notation gives

$$y = (c, 1)\begin{pmatrix} a \\ b \end{pmatrix} \tag{6}$$

With the definitions

$$\mathbf{x} = \begin{pmatrix} a \\ b \end{pmatrix}, \mathbf{F} = \begin{pmatrix} 1 & 0 \\ 0 & 1 \end{pmatrix}, \mathbf{h}^t = (c, 1) \text{ and } z = y$$

introduction of system noise and measurement noise, by analogy with Eqns. 1 and 2, gives the state space description

$$\begin{pmatrix} a(k) \\ b(k) \end{pmatrix} = \begin{pmatrix} 1 & 0 \\ 0 & 1 \end{pmatrix} \begin{pmatrix} a(k-1) \\ b(k-1) \end{pmatrix} + \begin{pmatrix} w_1(k-1) \\ w_2(k-1) \end{pmatrix}$$

$$z(k) = (c, 1) \begin{pmatrix} a(k) \\ b(k) \end{pmatrix} + v(k) \tag{7}$$

The practical problem is that the descriptive parameters of the calibration graph vary slowly in time or sequence. In principle, the derived state space model (relation 7) could cover this description by the introduced system noise. However, mathematical interpretation of a slowly varying state indicates time-dependent disturbances. Linear drift can often be used. A single state x affected by linear drift can be described by

$$x(k) = dk + e \tag{8}$$

Here d is the drift parameter and e is the value of $x(k)$ at $k = 0$. The state space model

$$\begin{pmatrix} e(k) \\ d(k) \end{pmatrix} = \begin{pmatrix} 1 & 0 \\ 0 & 1 \end{pmatrix} \begin{pmatrix} e(k-1) \\ d(k-1) \end{pmatrix} + \begin{pmatrix} w_1(k-1) \\ w_2(k-1) \end{pmatrix}$$

$$z(k) = (1, k) \begin{pmatrix} e(k) \\ d(k) \end{pmatrix} + v(k) \tag{9}$$

is based on a static description. A disadvantage of using this model is that the desired state $x(k)$ is based on the additive Eqn. 8, which depends on the index k. Consequently, an alternative representation was developed. Reformulation of Eqn. 8 and straightforward introduction of system noise and measurement noise gives

$$x(k) = d(k-1) + d + e = x(k-1) + d \tag{10}$$

$$\begin{pmatrix} x(k) \\ d(k) \end{pmatrix} = \begin{pmatrix} 1 & 1 \\ 0 & 1 \end{pmatrix} \begin{pmatrix} x(k-1) \\ d(k-1) \end{pmatrix} + \begin{pmatrix} w_1(k-1) \\ w_2(k-1) \end{pmatrix}$$

$$z(k) = (1, 0) \begin{pmatrix} x(k) \\ d(k) \end{pmatrix} + v(k) \tag{11}$$

Important features of this model are that it incorporates a dynamic structure and involves the required parameter directly in the state.

Both state space models (relations 9 and 11) can be related by the non-singular transformation matrix

$$\mathbf{T}(k) = \begin{pmatrix} 1 & -k \\ 0 & 1 \end{pmatrix}$$

into equivalent representations. A drifting parameter can thus be described by using only two random (stochastic) state variables. The alternative model is called random drift, represented by a combination of random constant,

random walk and random ramp [11]. If random drift acts on both the sensitivity a and the intercept b of the calibration graph, the first system model (7) must be expanded with two extra parameters, which describe the slowly varying behaviour of the system completely. This finally yields the discrete linear dynamic system

$$\begin{pmatrix} a(k) \\ b(k) \\ \alpha(k) \\ \beta(k) \end{pmatrix} = \begin{pmatrix} 1 & 0 & 1 & 0 \\ 0 & 1 & 0 & 1 \\ 0 & 0 & 1 & 0 \\ 0 & 0 & 0 & 1 \end{pmatrix} \begin{pmatrix} a(k-1) \\ b(k-1) \\ \alpha(k-1) \\ \beta(k-1) \end{pmatrix} + \begin{pmatrix} w_1(k-1) \\ w_2(k-1) \\ w_3(k-1) \\ w_4(k-1) \end{pmatrix}$$

$$z(k) = (c, 1, 0, 0) \begin{pmatrix} a(k) \\ b(k) \\ \alpha(k) \\ \beta(k) \end{pmatrix} + v(k) \tag{12}$$

The observability (Eqn. 4) of the final state space model for the dynamic calibration graph is

$$\mathbf{M} = \begin{pmatrix} c_1 & c_2 & c_3 & c_4 \\ 1 & 1 & 1 & 1 \\ 0 & c_2 & 2c_3 & 3c_4 \\ 0 & 1 & 2 & 3 \end{pmatrix} \tag{13}$$

The determinant of the matrix **M** is zero if all concentrations c_i ($i = 1, 2, 3, 4$) are the same, but the system is observable if there are two different concentrations, each measured twice.

Two other frequently used representations of random disturbances are exponentially correlated variables and periodic random variables [11]. A disadvantage of these descriptions is that the time constant or periodic constants become involved in the transition matrix of the state space model. For linearity of the model, these characteristics must be known in advance, whereas the drift model does not need them. When a wrong model is chosen, additional errors (system noise) are introduced. If it is assumed that the state varies only slowly, possible model errors will be of minor importance. Hence, the best solution to the practical problem is based first on the random drift model. If this is unsatisfactory another state space model is needed. The preceding paragraphs, based on applied systems theory, outline a useful state space model, which describes a drifting calibration graph in a manner useful in analytical practice.

Calibration

The parameters of a calibration graph are evaluated by taking analytes of known concentration or reference standards through the procedure. Drift can be evaluated by at least four calibrations with two different concentrations, each measured twice, over a period of time. The elements of the transition matrix $\mathbf{F}(k)$ and the measurement vector $\mathbf{h}^t(k)$ are assumed to be non-random quantities. In the state space model (Eqn. 12), $\mathbf{F}(k)$ is known exactly and $\mathbf{h}^t(k)$ is known from the calibration procedure. An implicit assumption is that Eqn. 5 is valid, which requires extensive preliminary test-

ing. In addition, the statistical properties of the system noise and measurement noise must be defined. It is assumed that they are random quantities, which are sequentially uncorrelated and are described by a normal probability density function (i.e., they are white with zero mean and given covariances)

$$E\{\mathbf{w}(k)\} = 0;\ E\{\mathbf{w}(k)\mathbf{w}^t(l)\} = Q(k)\delta(k, l) \quad (k, l = 1, 2, \ldots)$$

$$E\{v(k)\} = 0;\ E\{v(k)v^t(l)\} = R(k)\delta(k, l)$$

$$E\{\mathbf{w}(k)v^t(l)\} = 0 \tag{14}$$

where $\delta(k, l) = 1$ for $k = l$ and $\delta(k, l) = 0$ for $k \neq l$ is the Kronecker delta and $E\{\ \}$ denotes the expected value of the quantity between brackets.

The $n*n$ covariance matrix of the system noise $Q(k)$, and the scalar variance of the measurement noise $R(k)$, remain constant during the entire sequence and are assumed to be known from preliminary experiments.

A recursive procedure is used to estimate the parameters of the calibration graph (i.e., the slope, intercept, and the drift parameters). As a result of the preliminary assumptions, the Kalman filter algorithm is directly applicable [11]

$$\hat{\mathbf{x}}(k/k-1) = \mathbf{F}(k)\hat{\mathbf{x}}(k-1/k-1) \tag{15}$$

$$\mathbf{P}(k/k-1) = \mathbf{F}(k)\mathbf{P}(k-1/k-1)\mathbf{F}^t(k) + Q(k-1) \tag{16}$$

$$\hat{\mathbf{x}}(k/k) = \hat{\mathbf{x}}(k/k-1) + \mathbf{k}(k)\{z(k) - \mathbf{h}^t(k)\hat{\mathbf{x}}(k/k-1)\} \tag{17}$$

$$\mathbf{P}(k/k) = \mathbf{P}(k/k-1) - \mathbf{k}(k)\mathbf{h}^t(k)\mathbf{P}(k/k-1) \tag{18}$$

$$\mathbf{k}(k) = \mathbf{P}(k/k-1)\mathbf{h}(k)\{\mathbf{h}^t(k)\mathbf{P}(k/k-1)\mathbf{h}(k) + R(k)\}^{-1} \tag{19}$$

where $\hat{\mathbf{x}}(k/k)$ is the estimate of $\mathbf{x}(k)$ after k measurements for calibration have been processed; $\mathbf{k}(k)$ is an n-column correction vector, known as the Kalman gain vector. The Kalman filter for the state estimation is shown schematically in Fig. 2.

The $n*n$ matrix $\mathbf{P}(k/k)$ can be interpreted as the error covariance matrix of the difference between the state $\mathbf{x}(k)$ and its estimate $\hat{\mathbf{x}}(k/k)$. In probability terms $\hat{\mathbf{x}}(k/k)$ and $\mathbf{P}(k/k)$ can be interpreted as

$$\hat{\mathbf{x}}(k/k) = E\{\mathbf{x}(k)/Z(k)\}$$

$$\begin{aligned}\mathbf{P}(k/k) &= E\{[\mathbf{x}(k) - \hat{\mathbf{x}}(k/k)]\,[\mathbf{x}(k) - \hat{\mathbf{x}}(k/k)]^t/Z(k)\} \\ &= E\{[\mathbf{x}(k) - \hat{\mathbf{x}}(k/k)]\,[\mathbf{x}(k) - \hat{\mathbf{x}}(k/k)]^t\}\end{aligned} \tag{20}$$

where $Z(k)$ involves all the processed measurements $\{z(i)\}$, $i = 1, 2, \ldots, k$. The covariance matrix $\mathbf{P}(k/k)$ is a measure of the quality of the estimated state vector $\hat{\mathbf{x}}(k/k)$. In general, the diagonal elements $p_{ii}(k/k)$, $i = 1, 2, \ldots, n$ of $\mathbf{P}(k/k)$ can be regarded as the variance in the ith component $\hat{x}_i(k/k)$ of $\hat{\mathbf{x}}(k/k)$.

Starting from index $k = 1$, it is necessary to initialize the algorithm. It is common practice to choose for the estimate $\hat{\mathbf{x}}(0/0)$ and covariance $\mathbf{P}(0/0)$

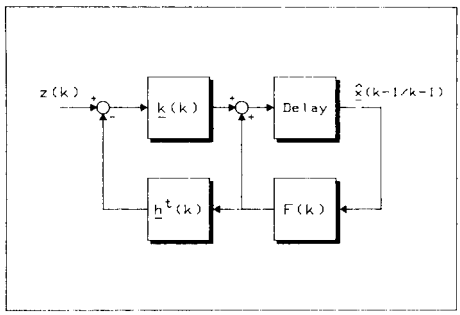

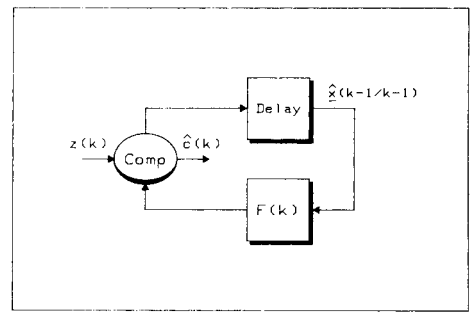

Fig. 2. The scheme for on-line calibration. $\hat{\mathbf{x}}(k-1/k-1)$ represents the last estimated or predicted state vector and $\mathbf{F}(k)$ the transition matrix which is used to predict the new state $\hat{\mathbf{x}}(k/k-1)$. The measurement vector $\mathbf{h}^t(k)$, the gain vector $\mathbf{k}(k)$ and the signal $z(k)$ produce a new estimated state $\hat{\mathbf{x}}(k/k)$.

Fig. 3. A scheme for on-line evaluation of unknowns. $\hat{\mathbf{x}}(k-1/k-1)$ and $\mathbf{F}(k)$ are the same as in Fig. 2. $z(k)$ is the measured signal and $\hat{c}(k)$ the estimated concentration of the sample; Comp denotes a non-linear computation.

the initial values $\hat{\mathbf{x}}(0/0) = 0$ and $\mathbf{P}(0/0) = s_0^2\mathbf{I}_n$ where $\mathbf{I}_n$ is the $n*n$ identity matrix. In general, a large value (e.g., 100) is chosen for the initial variance s_0^2. The a priori filter Eqns. 15 and 16 of the Kalman filter predict the state one step in advance. Because of the system noise present and the dynamics involved, the covariance matrix representing the uncertainty in the state is increased. After a new measurement has been processed, the a posteriori filter Eqns. 17—19 reduce this uncertainty gradually by means of the information supplied by the new calibration.

The innovation $v(k)$ is defined as the difference between the experimental and estimated measurement

$$v(k) = z(k) - \mathbf{h}^t(k)\hat{\mathbf{x}}(k/k-1) \tag{21}$$

The innovation sequence has been shown to be white, with zero mean and given covariance [11]

$$E\{v(k)\} = 0$$

$$E\{v(k)v^t(l)\} = \{\mathbf{h}^t(k)\mathbf{P}(k/k-1)\mathbf{h}(k) + R(k)\}\delta(k,l) \tag{22}$$

Equation 22 describes also the variance of a predicted measurement. In the Appendix, it is shown that when the drift and the system noise are omitted from the model, the proposed formula is equivalent to the relation frequently used for the confidence bands of a linear calibration graph [13—15]. However, the proposed statistical equation is more general. The statistical characteristics of the monitored innovations can be exploited in practice for failure detection, checking a correct model implementation or for identifying unknown noise covariances $Q(k)$ and $R(k)$ [12]. For testing purposes, it is more convenient to consider the standardized innovations

$$n(k) = v(k)\{\mathbf{h}^t(k)\mathbf{P}(k/k-1)\mathbf{h}(k) + R(k)\}^{-1/2} \tag{23}$$

The sample mean of the standardized innovations is estimated as $\bar{n} = 1/N\Sigma_{k=1}^{N}\, n(k)$, where N denotes the sample size. Given the whiteness of the innovations, $\bar{n}$ has a normal distribution with zero mean and variance $1/N$. The weighted sum of the squared innovations or the quantity $\chi^2 = \Sigma_{k=1}^{N}\, n(k)\, n^t(k)$ is a chi-squared random variable with $(N - n)$ degrees of freedom. As a criterion for the optimal nature of the Kalman filter, the autocorrelation of the standardized innovations can be used

$$\phi(\tau) = 1/(N - \tau - 1) \sum_{k=1}^{N-\tau} [n(k) - \bar{n}]\,[n(k + \tau) - \bar{n}]^t \tag{24}$$

For white innovations, it can be shown that the estimated $\phi(\tau)$, $\tau = 1, 2, \ldots$ are normal with zero mean and variance $1/(N - \tau - 1)$.

Evaluation of a constituent in samples

In accordance with the dynamics involved in the calibration model, the Kalman filter predicts the varying state which is used to evaluate a constituent in an unknown sample. Because of the system noise, the uncertainty, represented by the covariance matrix, in the expected systems behaviour increases. When a measurement is processed for evaluating a constituent, the predicted state and the uncertainty in that state remain constant.

The procedure under consideration is described by Eqns. 15 and 16 with simplified versions of Eqns. 17 and 18, i.e., $\hat{\mathbf{x}}(k/k) = \hat{\mathbf{x}}(k/k - 1)$ and $\mathbf{P}(k/k) = \mathbf{P}(k/k - 1)$, respectively. Figure 3 shows a block diagram of the calculation.

The unknown concentration of the constituent in a sample ($\hat{c}_{un}$) is obtained by rewriting the calibration relation (Eqn. 5)

$$\hat{c}_{un} = (z(k) - \hat{b})/\hat{a}$$

$$\mathrm{var}(\hat{c}_{un}) = (1/\hat{a}^2)\{\mathbf{h}_{un}^t \mathbf{P}(k/k - 1)\mathbf{h}_{un} + R_{un}\} \tag{25}$$

with $\mathbf{h}_{un}^t = (\hat{c}_{un}, 1, 0, 0)$ and $\hat{a}$, $\hat{b}$ from $\hat{\mathbf{x}}(k/k - 1)$.

The variance in $\hat{c}_{un}$ is based on a first-order error propagation

$$y = \mathrm{f}(x_1, x_2, \ldots, x_n)$$

$$\mathrm{var}(y) \approx \sum_{i=1}^{N} \sum_{j=1}^{N} (\mathrm{d}f/\mathrm{d}x_i)^t \mathrm{cov}(x_i, x_j)\, (\mathrm{d}f/\mathrm{d}x_j) \tag{26}$$

where $\mathrm{d}f/\mathrm{d}x_i$ is the first derivative of the function with respect to the parameter x_i, and $\mathrm{cov}(x_i, x_j)$ is the covariance between the parameters x_i and x_j. It is further assumed that there is no correlation between a measurement and the parameters of the calibration curve. Straightforward development of Eqn. 26 gives the variance (Eqn. 25). The drift parameters are not directly involved in the variance formula of Eqn. 25. They affect it indirectly by the dynamics of the model. When no system noise is considered, the given formula is equivalent to the commonly used relation for the confidence of an analytical result with a linear calibration graph [13—15].

If the unknown concentration is evaluated from more measurements in the sequence, the different concentration estimates are each weighted by their variance. For higher-order calibration models, the upper and lower concentration boundaries should be computed by solving the resulting equation of the predicted calibration curve with its confidence bands [16].

Quality control

The minimal precision required for the final results obtained for an unknown concentration can be predefined as a proper analytical goal. The proposed design of quality control starts with the decision when to re-calibrate, followed by selection of the standard concentrations which give the best performance. The Kalman filter predicts the varying state of the calibration model, which is used for evaluation of unknown concentrations. Because of the system noise and dynamics that are involved, the uncertainty in the predicted state is increased.

For a hypothetical evaluation of unknown concentrations with use of the predicted calibration graph, the relative imprecision of a concentration c_{un} can be expressed as

$$N_{un} = 2/(c_{un}\,\hat{a})\{\mathbf{h}_{un}^{t}\,\mathbf{P}(k/k-1)\mathbf{h}_{un} + R_{un}\}^{1/2} \qquad (27)$$

with $\mathbf{h}_{un}^{t} = (c_{un}, 1, 0, 0)$. The actual concentration c_{un} that will be obtained from the evaluation is, of course, not known in advance. Therefore, all available calibration standards c_{cal} are used for the computation of Eqn. 27. From a worst point of view, the maximum value N_{max} of the computed relative imprecisions N_{un} is defined as a test criterion. Consequently, a decision is made by comparing the maximum imprecision N_{max} with a predefined imprecision N_{crit}. If $N_{max} \geqslant N_{crit}$, calibration is repeated; if $N_{max} < N_{crit}$, samples are processed.

The entire procedure under consideration is completed before data on unknown samples are evaluated. The decision when to calibrate again enables the state vector and covariance matrix to be predicted one or more steps in advance until the criterion for N_{max} is reached.

The quality control algorithm integrated in the calibration and sample evaluation procedure is shown in Fig. 4. The greatest errors are found at the boundaries of the working range of the linear calibration graph, so that the control algorithm should compute the relative imprecision N_{un} twice. In order to decide which calibration gives the best results, it is probably best to calibrate twice, initially, with the highest and lowest concentration of the available standards. It should be noted that the entire quality control procedure depends not only on the predefined goal for precision but also on the experimental characteristics of the state space model (i.e., system noise covariance, measurement noise variance, current slope, and the standards available for calibration).

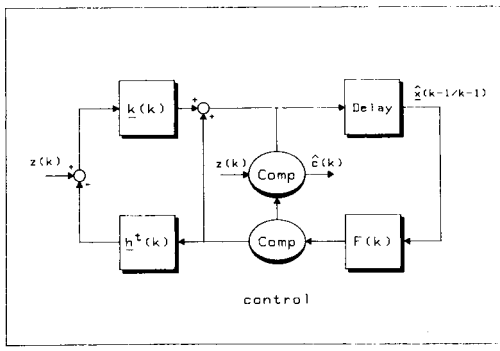

Fig. 4. On-line calibration, evaluation of unknowns and quality control. $\hat{\mathbf{x}}(k-1/k-1)$ and $\mathbf{F}(k)$ are the same as in Fig. 2: $\hat{\mathbf{x}}(k/k)$ is produced as in Figs. 2 and 3. $z(k)$ is the measurement and $\hat{c}(k)$ the estimated concentration of the sample; Comp denotes a non-linear computation.

EXPERIMENTAL

The theory presented above is demonstrated with a simulated application. A standard routine was employed to generate the Gaussian random noise [17]. The drifting state of the system was simulated as in Eqn. 1. For every new state $\mathbf{x}(k)$, white noise $\mathbf{w}(k-1)$ is added to the product of the transition matrix $\mathbf{F}(k)$ and the old state $\mathbf{x}(k-1)$. In order to compute the measurement $z(k)$ in Eqn. 2, random noise $v(k)$ is added to the product of the measurement vector $\mathbf{h}^t(k)$ and the new state $\mathbf{x}(k)$. For calibration, known concentrations $c_{\min}$ and $c_{\max}$ are used, and for evaluation of unknown samples, random values between $c_{\min}$ and $c_{\max}$ are used in the measurement vector. In order to produce the entire sequence, this procedure is repeated for each new sample. Table 1 summarizes some characteristics of the simulation of the system, the initialization of the estimator and the noise statistics. These data were extracted from some experiments on flow injection analysis. The automatic system used for the determination of copper with EDTA is presented in Fig. 5.

A Kalman filter (Eqns. 15—19) was used to process the calibration measurements. The predicted state of the Kalman filter was used for evaluation of

TABLE 1

Some data used for simulation of the system, the noise statistics and the initial values of the Kalman filter

$\mathbf{x}(0) = \begin{pmatrix} 0.15 \\ 0.07 \\ 0.0005 \\ -0.0001 \end{pmatrix}$	$R = 10^{-6}$	$Q = \begin{pmatrix} 0\,0 & 0 & 0 \\ 0\,0 & 0 & 0 \\ 0\,0 & 10^{-8} & 0 \\ 0\,0 & 0 & 10^{-8} \end{pmatrix}$
$\hat{\mathbf{x}}(0/0) = 0$	$\mathbf{P}(0/0) = I_4$	(4*4 identity matrix)
$c_{\min} = 1$	$c_{\max} = 5$	

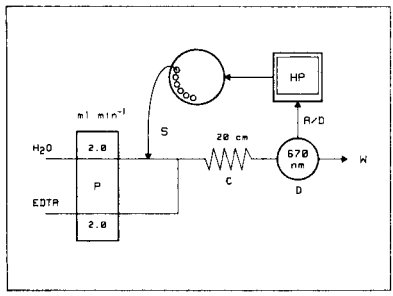

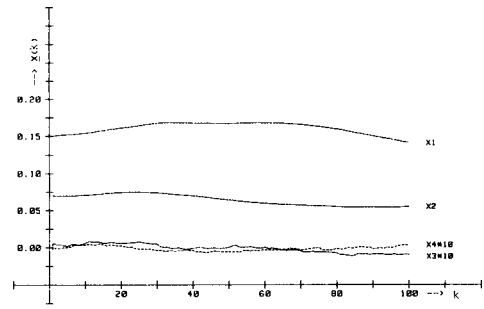

Fig. 5. A flow injection system for the determination of copper with EDTA buffered at pH 5 in water. P, peristaltic pump; S, automatic sampler with injection valve; W, waste; A/D, analog-to-digital converter; HP, computer; C, reaction coil; D, detector at 670 nm.

Fig. 6. An example of the drifting state of a system, based on simulation with the data in Table 1.

unknowns as described by Eqns. 15 and 16 and the simplistic versions of Eqns. 17 and 18. The quality control procedure (Eqn. 27 and N_{max} criterion) was implemented to decide when to recalibrate.

RESULTS

Figure 6 illustrates the drift of a system, based on simulation with the data in Table 1. The drift parameters x_3 and x_4 both vary rapidly between the values -0.001 and $+0.001$, because they are directly affected by the system noise. Its effects on the slope x_1 and intercept x_2 of the calibration graph is smoothed by the dynamics of the system. As a result the slope varies slowly in the range 0.15—0.17 and the intercept between 0.05 and 0.075.

To demonstrate that the Kalman filter based on the model (Eqn. 12) can be applied to process a drifting system as shown in Fig. 6, first all samples are used for calibration purposes.

Figure 7(a) depicts the measurements including measurement noise and the drift of the system. Figure 7(b) shows the concentrations; for calibration purposes they are always c_{min} and c_{max}. The measurements and concentrations are the data used by the Kalman filter to estimate the drift (Fig. 7c). This demonstrates that the Kalman filter can cope with the varying system after a short initial period (compare Figs. 6 and 7c). For a statistical evaluation, the mean $\bar{n}$, chi-squared value χ^2 and the autocorrelation function $\phi(\tau)$ (Eqn. 24) of the standardized innovations are given in Fig. 7(d). The mean and its 95% confidence interval $\bar{n} = -0.09 \pm 0.20$ does not differ significantly from zero. The computed chi-squared value of 103.9 lies between the critical values $\chi^2(96, 0.025) = 75.8$ and $\chi^2(96, 0.975) = 125.0$. The autocorrelation function proves the correctness of the assumption of whiteness of the innovations. The dashed lines around zero represent the 95% confidence

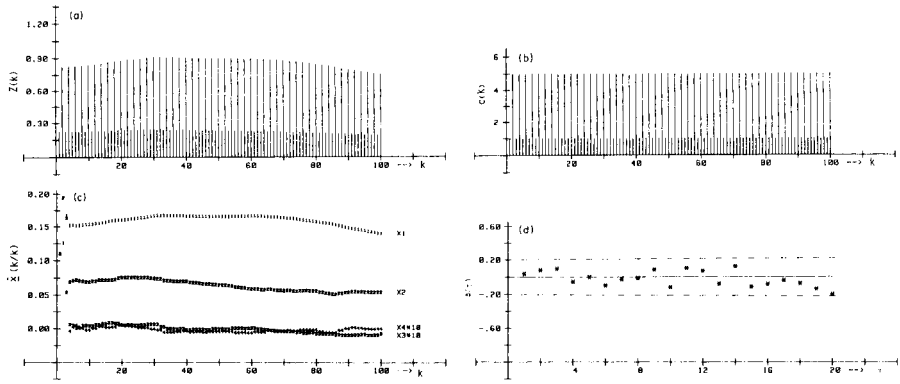

Fig. 7. The situation where all samples are used for calibration. The Kalman filter is employed for the data in Table 1 and the control algorithm uses a critical imprecision N_{crit} = 1%. (a) Measurements including noise and drift; (b) concentrations in the samples; (c) estimates of the state of the system (i = 1, 2, 3, 4 denotes the estimated $\hat{x}_i$); (d) autocorrelation function of the standardized innovations, for 100 entries with mean —0.09, standard deviation 1.02 and chi-square 103.88.

regions of the computed correlations. It is seen that there is only one significant correlation at $\tau = 0$. All these features confirm that a reconstruction produced by the Kalman filter is not significantly different from reality at the 95% confidence level. This is not surprising, because the system noise covariances and measurement noise variance used for the estimator are the same as those used in the simulated system in Fig. 6.

In practical situations, however, the correct values of the noise covariances with the given statistical criteria have to be sought in advance. This will be discussed in more detail in a later paper. Figure 8 shows a situation where the samples are used either for evaluation of unknowns or for calibration with use of the quality control algorithm. Figure 8(a) shows the measurements and Fig. 8(b) the corresponding concentrations. In Fig. 8(c) the estimated and predicted state such as produced by the Kalman filter are shown; the estimator follows the drifting system quite well. Because only a small number of innovations was available, no statistical testing of the system was done. Near the index k = 40, nine unknowns are evaluated before recalibrating. However, near the index k = 100, a lower sensitivity produces seven evaluations only. This observation shows how the sensitivity in Eqn. 27 affects the control algorithm. It should be noted that the algorithm starts with the minimal number of four calibrations with two different concentrations, as required for observability of the system. Figure 8(d) shows a histogram of the relative errors of estimated concentrations of the samples used for evaluation of results compared with their real values. This shows clearly that all experimental errors of the evaluation are below the critical imprecision N_{crit} = 5% as they should be.

An evaluation of the quality control algorithm is given in Fig. 9. Figure 9(a)

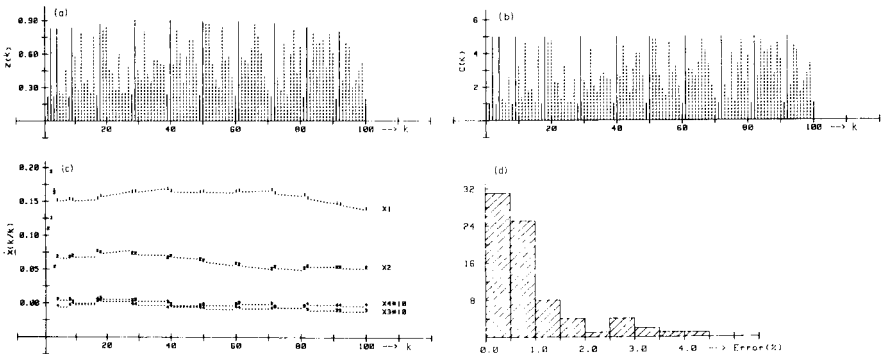

Fig. 8. The situation with samples used for calibration or evaluation of unknowns. The Kalman filter is employed for the data in Table 1 and the control algorithm uses a critical imprecision N_{crit} = 5%. (a) Measurements including noise and drift: (—) used for calibration; (---) used for evaluation. (b) Concentrations of the samples: (—) used for calibration; (---) estimated from the evaluation. (c) Estimates and predictions of the state of the system: (1, 2, 3, 4) estimated state based on calibration; (---) predicted state used for evaluation. (d) Histogram of the relative errors of the estimated concentrations of samples used for evaluation compared with their real concentrations; 77 entries with mean 0.90 and standard deviation 0.91.

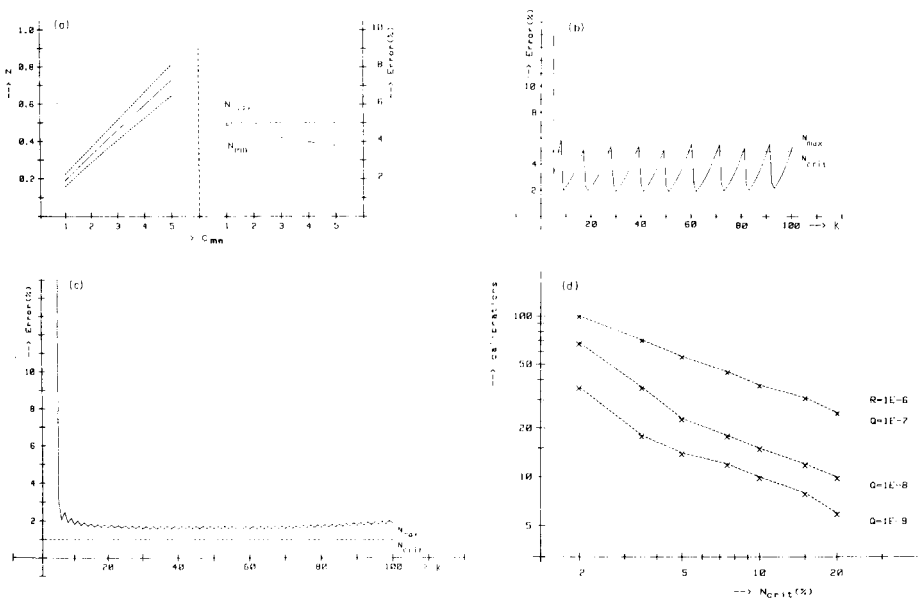

Fig. 9. The quality control algorithm. (a) (left) An estimated calibration curve with its confidence regions (multiplied by a factor 2.5); (right) the critical imprecisions N_{crit} with the computed imprecisions N_{un}. (b) The resulting maximal imprecisions N_{max} with the critical imprecision N_{crit} = 5% (cf. Fig. 8). (c) The resulting maximal imprecisions N_{max} with the critical imprecision N_{crit} = 1% (cf. Fig. 7). (d) The number of calibrations after 100 samples for different values of the system noise covariances; the value of Q represents both $Q(3, 3)$ and $Q(4, 4)$.

shows a calibration graph with its confidence limits as computed by Eqn. 22 and the relative imprecision in the evaluation of unknowns given by Eqn. 27. The maximal value N_{max} of all computed imprecisions N_{un} is used by the control algorithm to decide whether to do an unknown sample or to calibrate again. When the computed imprecision exceeds the preset limit, recalibration is initiated. Figure 9(b) shows the control values of the system with a critical value N_{crit} = 5% (cf. Fig. 8). After an initial phase, the algorithm becomes stable and alternates samples and calibrations regularly. Along with the first 100 samples a total of 23 calibrations is required (see Fig. 8), which is a reasonable investment from an analytical point of view. If the demands on the algorithm are too high, it will decide to calibrate every time again and never evaluate an unknown sample. This situation arises here when the algorithm is processed with a critical value N_{crit} = 1%. The maximal imprecisions N_{max} resulting from Fig. 7 are shown in Fig. 9(c). The sawtooth behaviour is a result of alternating two different concentrations while calibrating.

It can be seen that it is not possible to get a better imprecision than approximately 2% for unknown samples in the system under investigation. To obtain this value, at least 68 calibrations are needed for 100 samples. The effect of the system noise covariance on the number of calibrations for 100 samples is shown in Fig. 9(d) for various values of $Q(3, 3)$ and $Q(4, 4)$. If both system noise covariances are equal to 10^{-7}, it is impossible to get better than 10% imprecision within a reasonable number of calibrations. When both system noise covariances are below 10^{-9}, it is possible to obtain an imprecision less than 1% in the evaluation of unknowns.

CONCLUSIONS

A method for on-line drift compensation is presented. The two drifting parameters that describe a linear calibration graph are processed by a Kalman filter. For the evaluation of unknown samples, the parameters predicted by the recursive algorithm are used. With use of a quality control procedure one can decide after each measurement whether to calibrate again or to do the next sample.

Apart from a pre-defined imprecision in the evaluation of unknowns, the algorithm depends on the system noise covariance, measurement noise variance, the current sensitivity and of the available concentration standards. The system noise can be interpreted as an important quality characteristic. In analytical practice, much effort is expended on minimizing its effects in order to obtain a good system. However, if chemical, technical or instrumental improvements can only be achieved up to a certain limit, computational means are the only feasible means of further progress. The proposed algorithm describes the analytical possibilities completely. It shows that a bad system cannot acquire high precision. The results demonstrate that one could make a reasonable choice from a given minimal precision level. In a following paper, the proposed theory will be applied to real examples.

APPENDIX

Equivalence of the variance formulae of the predicted measurement for the linear calibration graph (5) without drift and system noise. For k calibrations with the measurement vectors $\mathbf{h}_i^t = (c_i, 1)$, $i = 1, 2, \ldots k$ and equal noise variances R, the reciprocal of the covariance matrix $\mathbf{P}_k$ is given by

$$\mathbf{P}_k^{-1} = \sum_{i=1}^{k} \mathbf{h}_i R^{-1} \mathbf{h}_i^t = R^{-1} \begin{pmatrix} \sum_{i=1}^{k} c_i^2 & \sum_{i=1}^{k} c_i \\ \sum_{i=1}^{k} c_i & k \end{pmatrix}$$

Defining the mean value $\bar{c} = 1/k \; \Sigma_{i=1}^{k} c_i$, the inverse yields

$$\mathbf{P}_k = R \left[\sum_{i=1}^{k} (c_i - \bar{c})^2 \right]^{-1} \begin{pmatrix} 1 & -\bar{c} \\ -\bar{c} & 1/k \sum_{i=1}^{k} c_i^2 \end{pmatrix}$$

The variance of the predicted measurement $\tilde{y} = \mathbf{h}^t \hat{\mathbf{x}}$ with $\mathbf{h}^t = (\tilde{c}, 1)$ in the calibration graph is described by the statistical relation

$$\mathrm{var}(\tilde{y}) = \mathbf{h}^t \mathbf{P}_k \mathbf{h} + R$$

$$= R \left[\sum_{i=1}^{k} (c_i - \bar{c})^2 \right]^{-1} \left\{ \tilde{c}^2 - 2\tilde{c}\bar{c} + 1/k \sum_{i=1}^{k} c_i^2 \right\} + R \qquad (22)$$

This finally produces the commonly used formula

$$\mathrm{var}(\tilde{y}) = R \left\{ \left[(\tilde{c} - \bar{c})^2 / \sum_{i=1}^{k} (c_i - \bar{c})^2 \right] + 1/k + 1 \right\}$$

The highest variances are found at the boundaries and the lowest variance in the centre of the range of the calibration graph.

REFERENCES

1 C. Liteanu and J. Rica, Statistical Theory and Methodology of Trace Analysis, Ellis Horwood, Chichester, 1980.
2 J. A. Nisbet and E. Simpson, Clin. Chim. Acta, 39 (1972) 339.
3 J. A. Nisbet and J. A. Owen, Clin. Chim. Acta, 92 (1979) 367.
4 A. Bennet, D. Gartelmann, J. J. Mason and J. A. Owen, Clin. Chim. Acta, 29 (1970) 161.
5 G. Svehla and E. L. Dickson, Anal. Chim. Acta, 136 (1982) 369.
6 A. S. McLelland and A. Fleck, Ann. Clin. Biochem., 15 (1978) 281.
7 C. E. Cox, Anal. Chem., 47 (1975) 1493.
8 W. A. Riggs, Anal. Chem., 43 (1971) 976.
9 H. N. J. Poulisse and P. Engelen, Anal. Lett., 13 (1980) 1211.
10 D. Graupe, Identification of Systems, R. E. Krieger, New York, 1975.
11 A. Gelb (Ed.), Applied Optimal Estimation, MIT Press, Cambridge, MA, 1974.
12 R. K. Mehra and J. Peschon, Automatica, 7 (1971) 637.
13 J. S. Garden, D. G. Mitchell and W. N. Mills, Anal. Chem., 52 (1980) 2310.
14 J. Agterdenbos, Anal. Chim. Acta, 108 (1979) 315.
15 J. Agterdenbos, F. J. M. J. Maessen and J. Balke, Anal. Chim. Acta, 132 (1981) 127.
16 D. G. Mitchell, W. N. Mills and J. S. Garden, Anal. Chem., 49 (1977) 1655.
17 T. H. Naylor, J. L. Balintfy, D. S. Burdick and K. Chu, Computer Simulation Techniques, Wiley, New York, 1966.

Analytica Chimica Acta, 156 (1984) 103—109
Elsevier Science Publishers B.V., Amsterdam — Printed in The Netherlands

MEASUREMENT OF THE ESSENTIAL OIL IN INCLUSION COMPLEXES WITH CYCLODEXTRIN BY MEANS OF CAPILLARY GAS CHROMATOGRAPHY

J. HARANGI* and P. NÁNÁSI
Institute of Biochemistry, L. Kossuth University, H-4010 Debrecen (Hungary)
(Received 14th October 1982)

SUMMARY

The oil content in inclusion complexes of cyclodextrin and essential oils can be determined efficiently by extraction at high temperature followed by capillary gas chromatography of the extracted oil. The total amount of complexed oil is calculated by comparison of the total peak area of the examined material with that of the relevant authentic sample. A computer program is outlined for the calculations.

Cyclodextrins are cyclic oligomers of α-D-glucose having six, seven or eight glucose units in the ring. As the ring cavity has a hydrophobic character, the cyclodextrins easily form inclusion complexes with compounds having an apolar moiety and a molecular size corresponding to the size of the ring cavity [1]. These complexes have become more important as they are potentially useful in the food and pharmaceutical industries for stabilization of the oxidizable or volatile components of essential oils or medicines [2—5]. The complexes are resistant to oxygen and possess rather good thermal stability [6].

Analysis of the cyclodextrin/essential oil complexes involves not only identification of the components of the original oil but also determination of the individual components and of the total amount of the complexed oil. Identification is readily achieved by capillary gas chromatography [7], but quantitative measurements are more difficult. If the complex has only one complexed component exhibiting u.v. or visible absorption, it can be detected by spectrophotometry. However, in the case of essential oils, there may be numerous components forming complexes with different affinities and the quantitative composition of the complexed oil always differs from that of the original one.

Therefore, the oil content of the complexes cannot be measured by spectrophotometry. Because the cyclodextrin complexes show excellent thermal stability, the complexed components leave the complex at relatively high temperatures (200—300°C) depending on the strength of intermolecular interaction. At this temperature, the cyclodextrin usually starts to pyrolyze,

0003-2670/84/$03.00

and so the oil content of the complex cannot be measured by weight. Accordingly, the most practical method of determining the essential oil content in these cyclodextrin complexes is to extract the oil and subject the extract to gas chromatography, comparing the chromatograms of the original and the extracted oils.

The method developed here involves extraction of the oil content of the complex at high temperature and capillary gas chromatography of the extracted oil. The oil content is calculated on the basis of total peak area by comparison to that of the relevant standard oil.

EXPERIMENTAL

Gas chromatography

A Hewlett-Packard 5840A type gas chromatograph equipped with a capillary inlet system, an OV-101-coated silica fused glass capillary column (25 m, 0.2 mm i.d.), and a flame ionization detector was used. The gas chromatograph was connected to a Hewlett-Packard 9825A desktop computer via an RS-232 serial interface (HP 98036A). The operating conditions were as follows: initial oven temperature 70°C, then after 1 min heating at 3°C min^{-1} to 180°C; injector temperature 200°C, flame ionization detector temperature 300°C; carrier gas (nitrogen) flow rate 1.0 ml min^{-1}, split ratio 1:100, detector make-up flow rate 30 ml min^{-1}. Equal volumes of the extracts of the standard oil and sample were injected (see below).

Procedures

Preparation of the solution of the standard oil. This procedure is similar to that for the extraction of the examined complex to reduce the experimental error. Chloroform (2 ml) and 50 ml of water were placed in a separatory funnel, the funnel was closed with a teflon plug, and 10 μl of essential oil was added through the plug. The closed funnel was warmed to 60°C, shaken for 10 min and cooled, and the organic phase was separated and transferred to a sample vial which was then sealed.

Extraction of the cyclodextrin/essential oil complex. Chloroform (2 ml), 50 ml of water and 0.1 g of cyclodextrin/essential oil complex were put in a separatory funnel, and the mixture was heated to 60°C and shaken for 10 min. The cyclodextrin dissolved at this temperature and the oil content of the complex went into the organic layer. The mixture was cooled, and the organic phase was separated and transferred to a sample vial. It is very important to close the separatory funnel tightly during the extraction procedure For this procedure a special separatory funnel with greater wall thickness, teflon plug and teflon valve was used.

RESULTS AND DISCUSSION

The qualitative and quantitative analysis of the samples was achieved by comparing the gas chromatographic data of the examined oil and that of the respective standard oil. A computer program was developed for measurement

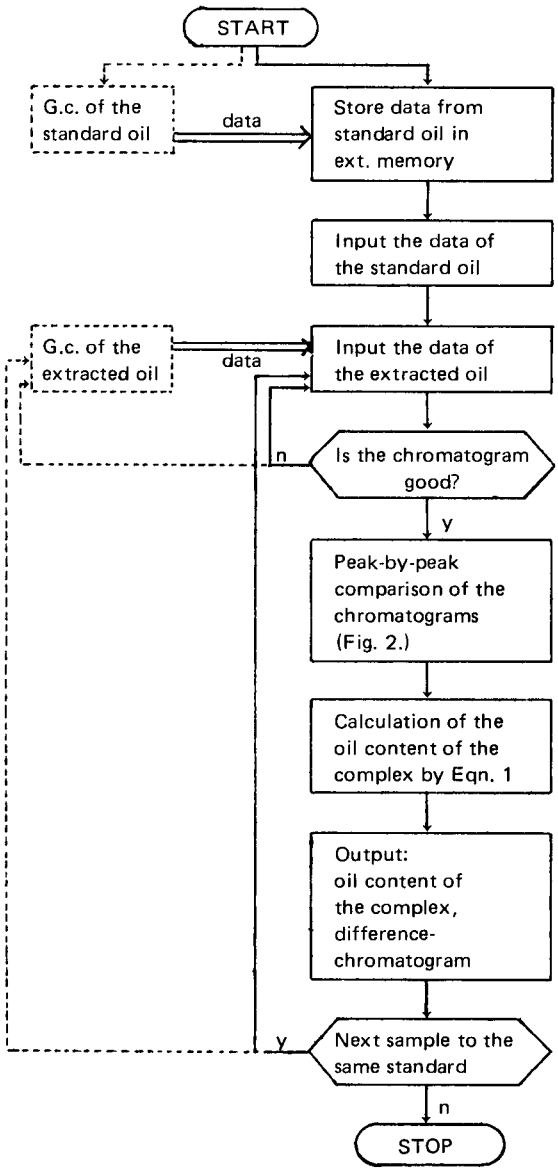

Fig. 1. Flow diagram for the calculation of the oil content of cyclodextrin/essential oil complexes.

of the oil content of cyclodextrin/essential oil complexes and for the required peak-by-peak comparison of the chromatograms. First, the chromatogram of the original essential oil is recorded. The data of this chromatogram (retention times and peak areas) are stored in an external memory (tape cartridge) for later use. If these data have already been stored, they can be

used for the calculation without recording the chromatogram again. The computer reads the data for the original oil from the external memory, and the experimental data found for the given extracted oil are transferred to the computer memory from the gas chromatograph. Then the computer constructs the peak-by-peak difference-chromatogram using the stored data of the standard oil and the algorithm shown in Fig. 1. The difference chromatogram consists of all peaks of both chromatograms. The common peaks appear in it with the mean of the retention times and with the difference of their percentage area. If a peak is detectable in only one of the two samples, it is listed in the difference chromatogram with an annotation indicating the sample in which this peak was found. A positive sign (in practice no sign) shows that the percentage area of the given component is higher in the extracted oil; a negative sign indicates a relative deficit of this component in the extracted oil. On the basis of the percentage area values in the difference chromatogram, the differences between the two oils can quickly be recognized. In the example shown in Fig. 3, there are no important differences

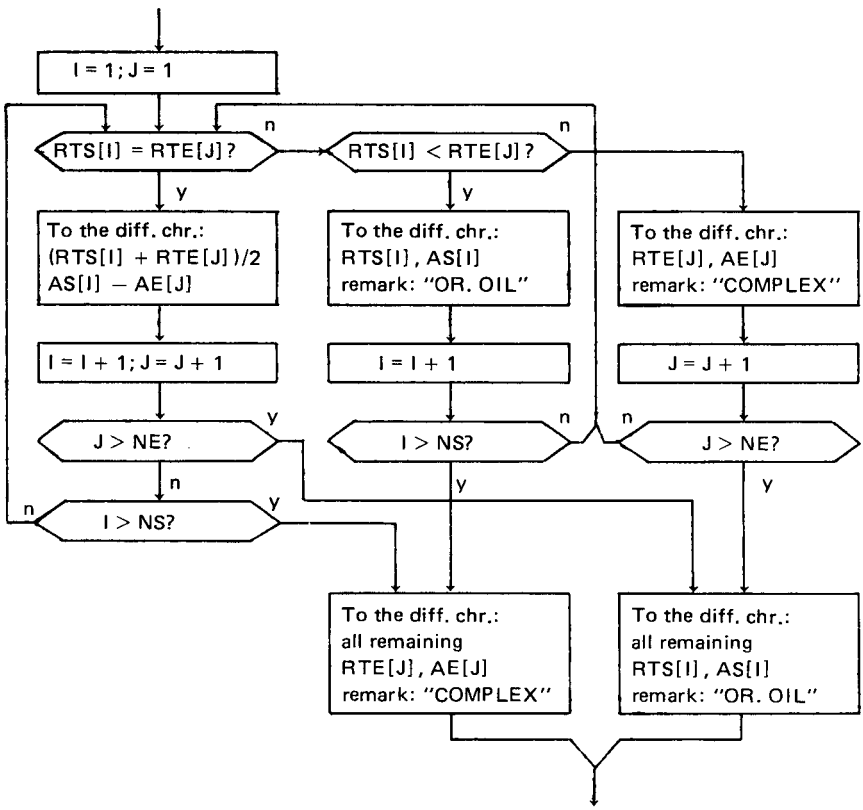

Fig. 2. Flow diagram of the peak-by-peak comparison subroutine of the standard and the extracted essential oils. RTS(I), AS(I) and NS are the retention time, peak area and number of the components of the standard oil. RTE(J) AE(J) and NE are the corresponding data for the components of the extracted oil. RTS(I) must agree with RTE(J) within 1%.

(see also Table 1). The peaks at 4.08 min and 6.28 min were detected only in the chromatogram of the extracted oil; these are marked "COMPLEX" in the list (Table 2). The peak at 10.70 min was found only in the chromatogram of the original oil.

To calculate the total amount of the complexed essential oil, the following input data are necessary: (a) the oil content (% v/v) of the solution of the standard essential oil (S); (b) the specific gravity of the standard essential oil (G); (c) the weight of the extracted complex (W); and (d) the volume of the organic solvent used for the extraction (V). With the data described above, and the total area of peaks in the chromatograms, the total amount of the extracted oil can be calculated using the following function

$$X(\text{w/w \%}) = SGVA_e/WA_s \quad (1)$$

where A_s is the total peak area of the standard essential oil and A_e is the total peak area of the extracted oil.

In this calculation it is assumed that the response factors of the components are nearly the same. Knowledge of the response factors of all components would allow for more accurate calculations. It is assumed, however, that the error originating from any difference in the response factors is lower than that of the extraction procedure.

The extraction procedure given under Experimental was estimated to pro-

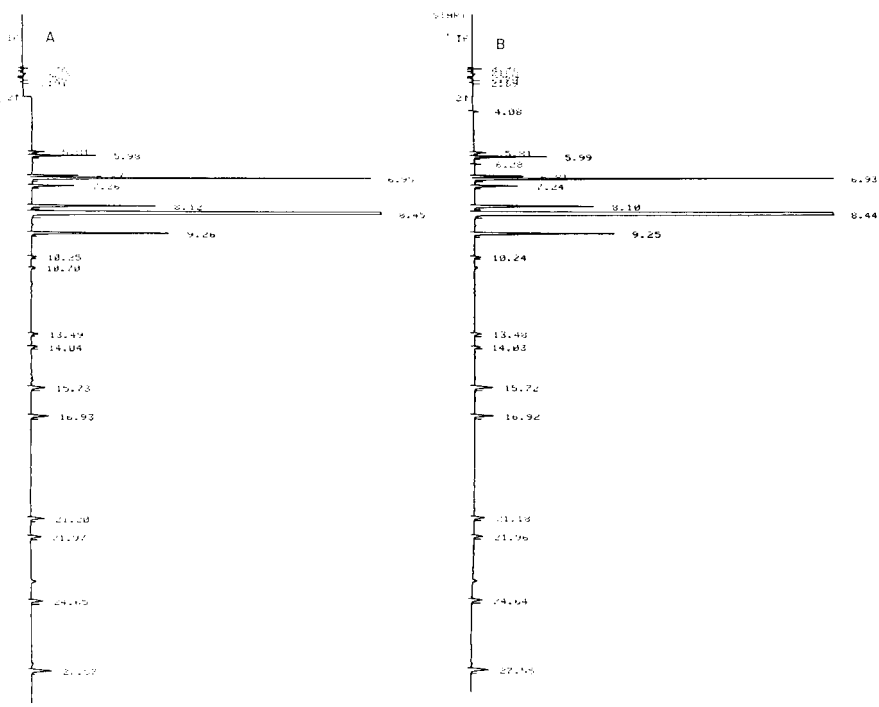

Fig. 3. Gas chromatograms of (A) the standard lemon oil and (B) the extracted oil from a cyclodextrin complex.

TABLE 1

Characteristic data (retention time and peak area) of the gas chromatograms shown in Fig. 3

Standard oil			Extracted oil		
RT	Area	Area (%)	RT	Area	Area (%)
5.81	309	0.309	4.08	35	0.033
5.98	1659	1.659	5.81	330	0.313
6.83	1442	1.442	5.99	1876	1.779
6.95	10950	10.952	6.28	17	0.016
7.26	1276	1.276	6.81	1447	1.372
8.12	4484	4.485	6.93	12570	11.922
8.45	69940	69.954	7.24	1323	1.255
9.26	5179	5.180	8.10	4312	4.090
10.25	139	0.139	8.44	74160	70.338
10.70	62	0.062	9.25	4985	4.728
13.49	228	0.228	10.24	184	0.175
14.04	224	0.224	13.48	233	0.221
15.73	658	0.658	14.03	165	0.156
16.93	764	0.764	15.72	855	0.811
21.20	599	0.599	16.92	882	0.837
21.97	471	0.471	21.18	441	0.418
24.65	599	0.599	21.96	341	0.323
27.57	1037	1.037	24.64	424	0.402
			27.55	854	0.810

vide about 98% extraction of the oil content of the complexes. As water dissolves a certain amount of chloroform, it is necessary to shake with water in the case of the standard oil. There was no measurable difference in the results when cyclodextrin was added to the aqueous phase during the preparation of the standard oil solution.

Gas chromatograms obtained in the analysis of the cyclodextrin/lemon oil are shown in Fig. 3. The results obtained for the total oil content of the lemon oil complexes in three parallel extractions were 8.97, 8.69, 9.73% (w/w), giving an average content of 9.13%.

The extraction method was tested with other organic solvents, but chloroform was found to be the best.

The method for the extraction of the essential oil is also applicable for measuring the essential oil content of the mother liquor of the complexation procedure. In this case, 50 ml of the mother liquor is added instead of water, otherwise the procedure is the same as described above for the extraction of the complexes.

The authors thank the Cyclopack Co. (Budapest, Hungary) for the complexes examined and Ms. K. Molnar for technical assistance.

TABLE 2

Final computer output

OIL CONTENT OF THE COMPLEX: 8.97%

THE COMPONENTS OF THE COMPLEXED OIL COMPARED TO THE ORIGINAL ESSENTIAL OIL:

RT	AREA (%)
4.08	0.033 COMPLEX
5.81	0.004
5.99	0.120
6.28	0.016 COMPLEX
6.82	−0.070
6.94	0.970
7.25	−0.021
8.11	−0.395
8.45	0.384
9.26	−0.452
10.25	0.035
10.70	−0.062 OR. OIL
13.49	−0.007
14.04	−0.068
15.73	0.153
16.93	0.072
21.19	−0.181
21.97	−0.148
24.65	−0.157
27.56	−0.227

REFERENCES

1 F. Cramer and H. Hettler, Naturwissenschaft, 54 (1967) 625.
2 J. Szejtli, Die Starke, 29 (1977) 26.
3 K. H. Fromming and I. Weyermann, Arch. Pharm., (Weinheim, Ger.), 305 (1972) 290.
4 J. Szejtli and E. Banky-Elod, Die Starke, 27 (1975) 368.
5 J. Szejtli, Cyclodextrines and Their Inclusion Complexes, Akadémia Kiado, Budapest, 1982, pp. 239, 245.
6 J. Szejtli, L. Szente and E. Banky-Elod, Acta Chim. Acad. Sci. Hung., 101 (1979) 27.
7 See, e.g., W. Jennings, J. Chromatogr. Sci., 17 (1979) 636.

Analytica Chimica Acta, 156 (1984) 111—120
Elsevier Science Publishers B.V., Amsterdam — Printed in The Netherlands

SUPERSONIC JET FLUORESCENCE SPECTROMETRY OF PERYLENE AND BENZO[a]PYRENE

TOTARO IMASAKA, HIROMI FUKUOKA, TOSHINORI HAYASHI and NOBUHIKO ISHIBASHI*

Faculty of Engineering, Kyushu University, Hakozaki, Fukuoka 812 (Japan)

(Received 11th April 1983)

SUMMARY

A supersonic jet instrument for fluorescence spectrometry is described. It consists of a high-temperature free expansion nozzle for continuous sample introduction and a vacuum chamber equipped with a high-speed pumping system. Rotationally cooled spectra obtained with the supersonic jet are compared with gas-phase spectra measured at high temperature for perylene and benzo[a]pyrene molecules. Each component of the unresolved band structure in the high-temperature spectra was found to be composed of a rotational congestion of several vibrational bands. For a 1:1 mixture of perylene and benzo[a]pyrene, selective detection is possible by using supersonic jet spectrometry. The detection limit for perylene is 100 ng. The advantages of this technique over other low-temperature spectrometric methods based on Shpol'skii and matrix isolation effects are discussed.

Identification and quantification of polycyclic aromatic hydrocarbons (PAHs) are of importance, because some of them are strongly carcinogenic and occur frequently in the environment. Real samples are known to contain many kinds of trace PAHs, and therefore sensitive and selective spectrometric methods are required. Most of the PAHs are strongly fluorescent, and fluorimetry has been conventionally used. Laser fluorimetry is quite attractive because of the sensitivity conferred by the large output power of the laser [1—3]. However, a room-temperature spectrum shows broad structures consisting of unresolved vibrational bands. Therefore, the monochromaticity of the laser is not effectively used for selective identification of the sample, and room-temperature fluorimetry suffers from its poor selectivity.

Low-temperature fluorimetry removes the congestion of rotational lines and gives sharp vibrational lines in the spectrum. It provides the best use of the monochromaticity of the laser for selective identification of the sample. Two types of solid-state fluorimetry based on Shpol'skii and matrix isolation effects have been reported [4]. An alternative method may be low-temperature gas-phase fluorimetry. A molecular jet adiabatically expanded through a small pinhole into a vacuum has a very low temperature, so that rotational freedom decreases and sharp vibrational bands appear in the spectrum

0003-2670/84/$03.00

[5, 6]. This technique has been recently used for spectroscopic studies of PAHs [7—19].

A very few analytical applications of supersonic jet spectrometry have been studied but only for PAHs with two or three aromatic rings. Warren et al. [20] have measured the fluorescence and excitation spectra of naphthalene and its derivatives, and discussed the advantage of the technique for selective detection of the sample species. Hayes and Small [21] combined this technique with gas chromatography. Very recently Amirav et al. [22] studied anthracene and its derivatives, and demonstrated the identification of isotopic species of 9,10-dichloroanthracene. Most of the strongly carcinogenic substances such as benzo[a]pyrene, which is used as a carcinogenic standard, have five or six aromatic rings in the molecule. These molecules have extremely low vapor pressures at room temperature, so that they require an expansion nozzle that can be heated to 400°C and a continuous sample introduction port for convenient use in analytical applications.

In this paper, the construction of a supersonic jet fluorimeter is described. It consists of a high-temperature free expansion nozzle for continuous sample introduction. The high-temperature spectrum is compared with the supersonic jet spectrum and the analytical advantages are discussed. Identification of strongly carcinogenic benzo[a]pyrene ($C_{20}H_{12}$) in mixtures with non-carcinogenic perylene ($C_{20}H_{12}$) from a fluorescence spectrum is demonstrated.

EXPERIMENTAL

Supersonic jet equipment

Figure 1 shows a schematic diagram of the apparatus. The free jet is formed by expanding 400—1500 torr of argon seeded with PAH molecules. The expansion chamber is maintained below 10^{-2}—10^{-3} torr by means of a pumping system consisting of a liquid nitrogen trap equipped with a 6-in diffusion pump (ULVAC, ULK-6; 1400 l s^{-1}) which is backed by a mechanical booster pump (Shimadzu, MB-100; 1500 l min^{-1}) and is further followed by a rotary pump (Shimadzu, DK-300, 300 l min^{-1}).

A home-made nitrogen-laser-pumped dye laser with a spectral resolution of 0.5 nm [23] was used for the measurement of the fluorescence spectrum. In order to record an excitation spectrum, a dye laser (Lambda Physik, FL2002, $\Delta\lambda$ = 0.005 nm) pumped by an excimer laser (Lambda Physik, EMG102E, 170 mJ) was used. The laser beam is crossed by the supersonic jet 10 mm away from a nozzle. All windows of the chamber are made of non-fluorescent quartz. The fluorescence image is expanded five times and introduced onto the entrance slit of a monochromator (Jasco CT-100; 0.8 nm mm^{-1}) to improve the fluorescence collection efficiency. The detected pulse signal from a photomultiplier (Hamamatsu, R928) was integrated by a home-made amplifier with a response time of 2 s and recorded by a strip-chart recorder. The high-temperature supersonic nozzle used in this study

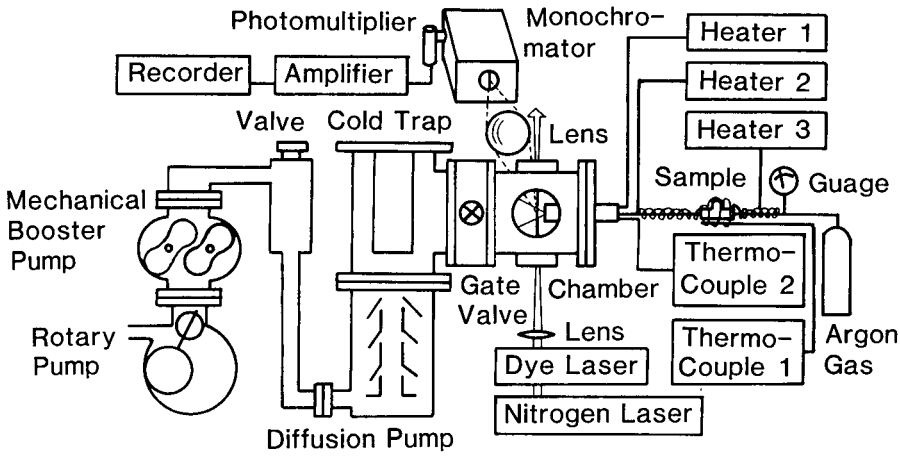

Fig. 1. Apparatus for supersonic jet fluorimetry.

is shown in detail elsewhere [24]. The top of the nozzle is made from a 0.1-mm thick stainless steel sheet with a 0.3-mm pinhole. The constructed nozzle is all made of stainless steel and ceramic, and can be heated to at least 500° C. In order to avoid decomposition and condensation of the sample in the stainless tube, the nozzle was usually heated to 400° C and the stainless tube between the nozzle and the sample was maintained at a slightly lower temperature.

For the measurement of a fluorescence spectrum, 30—100 mg of the sample was placed in a tee-fitting and typically heated to 300°C by tape heaters. This sample lasted about 20 min for the measurement. In order to estimate the limit of detection, the sample in solution was injected into the inlet port of a gas chromatograph (Shimadzu, GC-8A) and introduced from there to the free expansion nozzle. Sample separation was unnecessary in this study, and the packing material was removed in the measurement.

Static cell

The sample was also measured at high temperature in a static cell. The sample cell (2-cm diameter, 4 cm high) was made of pyrex glass. Several milligrams of the solid sample was put into this cell and sealed after evacuation. The sample cell was typically heated to 300°C in a ceramic tube (5-cm diameter) by tape heaters. The arm of the sample cell outside the ceramic tube was kept at a slightly lower temperature so as not to condense the sample on the cell wall.

Reagents. The samples of benzo[a]pyrene (Wako Pure Chemical Co.) and perylene (Aldrich) were used as received.

RESULTS AND DISCUSSION

Temperature and velocity

Fluorescence and excitation spectra measured at room temperature are broad because of congestion of rotational and vibrational levels. Expansion from a jet nozzle into high vacuum results in adiabatic cooling of the molecular flow, which greatly clarifies the spectrum. Under the present experimental conditions (stagnation pressure 1 atm, pinhole diameter 0.3 mm), the achieved terminal Mach number is 33 and the translational temperature is 1.6 K [25], if the sample temperature before expansion is assumed to be 573 K. The rotational temperature may be close to the calculated translational temperature, and the vibrational temperature may be considerably higher because of insufficient vibrational cooling [17]. The velocity of the molecules in the jet is estimated to be 773 m s^{-1} (FWHM = 22 m s^{-1}) which slightly exceeds the root mean square velocity of 598 m s^{-1} (FWHM = 565 m s^{-1}) calculated from the distribution function for the static molecules. It has been noted that uniform velocity distribution of the sample molecules is achieved in the jet flow [17].

Perylene

The electronic structure of perylene in the gas phase has not been investigated in detail, and the wavelength corresponding to the transition from a pure electronic ground state to a pure electronic singlet excited state (0—0 transition) is unknown. Perylene was heated to 290°C, and the fluorescence spectrum was measured in the static cell. The result is shown by the broken line in Fig. 2. There are three unresolved structures which may be composed of congestion of the rotational and vibrational levels. These features are almost identical in the spectrum measured in the solution phase at room temperature. When carefully compared with the solution spectrum, the

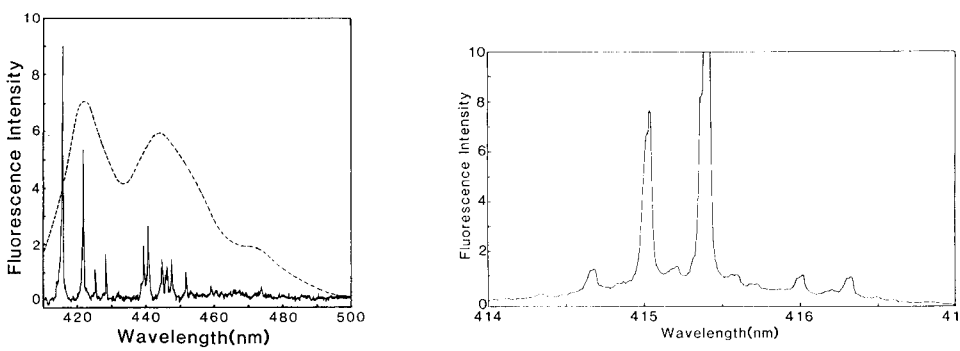

Fig. 2. Fluorescence spectra of perylene: (---) high-temperature spectrum, λ_{ex} = 415.9 nm; (—) supersonic jet spectrum, λ_{ex} = 415.3 nm, $\Delta\lambda_{em}$ = 0.24 nm.

Fig. 3. Supersonic jet excitation spectrum of perylene, $\Delta\lambda_{ex}$ = 0.005 nm, λ_{em} = 440.0 nm.

observed structure in Fig. 2 is found to be more poorly resolved. This seems to be due to hot-band excitation because of the high temperature in the gas phase measurement (573 K). The fluorescence spectrum was also measured at the excitation wavelength of 385.1 nm for gas-phase perylene, but no appreciable change was observed. It is apparent that even a gas-phase spectrum does not provide sharp features and that the wavelength corresponding to the 0—0 transition seems to be located at around 415 nm. The perylene spectrum was also measured under molecular beam conditions by using the present supersonic jet equipment but turning off the argon gas. Still, no appreciable change was observed in the fluorescence spectrum.

The solid line in Fig. 2 shows the supersonic jet fluorescence spectrum of perylene excited at 415.3 nm. Very sharp vibrational lines appear between 410 and 460 nm. This structure is quite similar to the low-temperature Shpol'skii spectrum of perylene in heptane, but obviously the Shpol'skii spectrum shifts 32 nm to longer wavelengths because of the strong solvent effect [26]. In the nitrogen matrix, the spectral shift is 17 nm and is much smaller. The linewidth of the principal peaks in the supersonic jet spectrum is 14 cm^{-1} and is limited by the resolution of the fluorescence monochromator used in this study. The linewidth in the jet spectrum is apparently narrower than the peaks in the nitrogen matrix spectrum (135 cm^{-1}). The jet temperature (1.6 K) is lower than the temperature generated by a conventional cryostat (15 K) [26]. No splitting arising from differences of the site environment in the matrix occurs in the gas-phase spectrum. The linewidth of the peak in the supersonic jet spectrum may be essentially narrower than for the peak in the Shpol'skii spectrum (1.3 cm^{-1}). It is interesting to note that the first and second vibrational structures from the shorter wavelengths in the high-temperature spectrum correspond to the 1—4 and 5—10 sharp vibrational lines in the supersonic jet spectrum. The third structure (shoulder) at around 470 nm may correspond to the small structures in the jet spectrum at 460—480 nm. The fluorescence bands in the high-temperature spectrum are slightly red-shifted, which may be due to excitation to the high rotational levels in the dense excited state and to succeeding transition to the high rotational levels in the sparse ground state.

The excitation spectrum of perylene is shown in Fig. 3. Very sharp vibrational peaks are resolved fairly well. The individual peaks seem to be composed of two or three rotational lines. The linewidth of the peak is 0.06 nm and it is not limited by the linewidth of the exciting laser. The largest peak at 415.42 nm may correspond to the 0—0 transition of perylene. A few vibrational lines at shorter wavelengths shows vibrational overtones (20 cm^{-1}) in the excited state.

Figure 4 shows a supersonic jet fluorescence spectrum of perylene excited at 388.3 nm. The wavelengths of the peaks observed in this spectrum are similar to those observed for 415.3-nm excitation, but its structure becomes broad and continuum emission is superimposed. Line broadening in the fluorescence spectrum may not be due to insufficient cooling in the super-

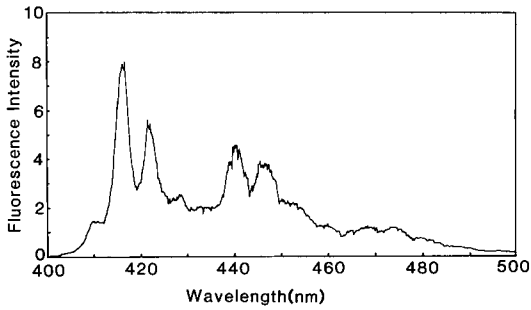

Fig. 4. Supersonic jet fluorescence spectrum of perylene excited at 388.3 nm.

sonic jet. It may be due to the many possible transitions to the ground state with different vibrational quantum numbers because of congestion of the many vibrational levels in the excited state, or it may be caused by rearrangement of the quantum numbers by radiationless transition in the excited state and succeeding transitions to the ground state with various rotational quantum numbers. Such apparent line broadening interferes with selective identification of the sample species.

Benzo[a]pyrene

The fluorescence spectrum of benzo[a]pyrene was measured at 300°C in a static cell to estimate the energy corresponding to the 0—0 transition. The result is shown by the broken line in Fig. 5. Three main features are apparent at 401 nm, 423 nm, and 450 nm, and there is a shoulder at around 393 nm. The wavelength of the 0—0 transition may be shifted several nanometers to shorter wavelengths from either 393 nm or 401 nm. The supersonic fluorescence spectrum measured by exciting benzo[a]pyrene at 386.7 nm, which may correspond to the wavelength of 393 nm in the high-temperature spectrum, is shown by the solid line in Fig. 5. The fluorescence intensity of benzo[a]pyrene was very weak in comparison with that of perylene, and this spectrum was recorded with a spectral resolution of 1.6 nm. The relatively broad linewidths are not intrinsic to benzo[a]-pyrene but are instrumentally limited. Several peaks are clearly resolved in the supersonic jet spectrum. It is apparent that the first vibrational band at 401 nm in the batch spectrum consists of at least four lines between 396 nm and 410 nm in the jet spectrum. The second band at 423 nm may correspond to the lines between 420 nm and 430 nm, and the shoulder at 450 nm to the line at around 446 nm. The baseline of the supersonic jet spectrum increases with increasing wavelength in the fluorescence spectrum, but this was found to be caused by background emission from solid benzo[a]pyrene stuck on the surface of the chamber. Strong scattered emission of the exciting source is superimposed on the fluorescence peak of benzo[a]pyrene at 387 nm, and this band is not considered further in this study. The most intense band appears at 397 nm, and it can be used as a "key" band for identification of benzo[a]pyrene.

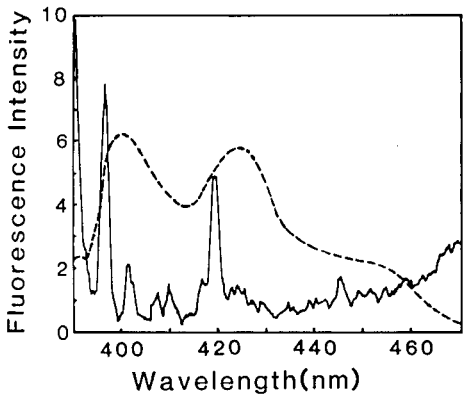

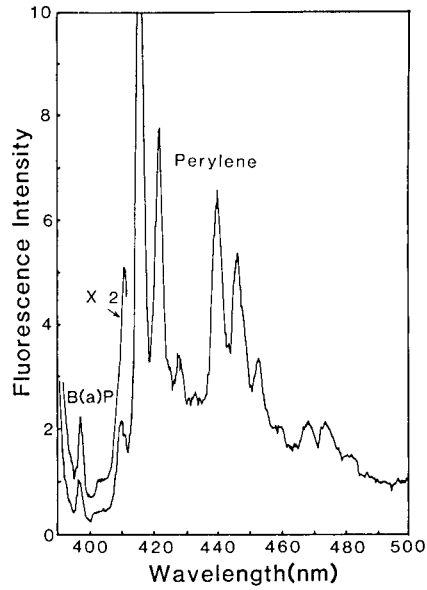

Fig. 5. Fluorescence spectra of benzo[a]pyrene: (---) high-temperature spectrum, λ_{ex} = 386.4 nm; (—) supersonic jet spectrum, λ_{ex} = 386.7 nm, $\Delta\lambda_{em}$ = 1.6 nm.

Fig. 6. Identification of benzo[a]pyrene in a 1:1 mixture with perylene from a fluorescence spectrum based on supersonic jet spectrometry (λ_{ex} = 386.7 nm). The fluorescence band at 397 nm originates from benzo[a]pyrene, and other bands from perylene.

In order to clarify the position of the 0—0 transition, the exciting wavelength was adjusted to 397 nm which probably correspond to the 401-nm band in the high-temperature fluorescence spectrum. But, no appreciable emission was observed at around this wavelength. Benzo[a]pyrene in a batch cell was also excited at around 400 nm, but the fluorescence was much weaker than that observed on exciting at 387 nm. From these results, the 0—0 transition of benzo[a]pyrene may be located at around 387 nm, though this assignment is not conclusive.

The supersonic jet spectrum of benzo[a]pyrene is similar to that measured in a heptane solution. The spectrum seems to be shifted about 6 nm to longer wavelengths by the solvent effect [26]. It is noted that the fluorescence band of benzo[a]pyrene is split in the Shpol'skii fluorescence spectrum, and its intensity distribution is changed by a slight shift of the exciting wavelength [26]. This splitting is assumed to be due to the presence of benzo[a]pyrene molecules in different discrete lattice sites or experiencing different crystal fields. Essentially, such splittings do not exist in supersonic jet spectrometry, so that this technique provides simpler and more reliable information for analytical purposes.

Identification of benzo[a]pyrene

Benzo[a]pyrene is strongly carcinogenic, while perylene is non-carcinogenic. Therefore, these molecules should be determined separately for assessment of carcinogenicity of the sample. However, both benzo[a]pyrene and perylene have an identical chemical formula ($C_{20}H_{12}$), and they have similar spectral properties in the u.v.-visible region. Also, conventional mass spectrometry and fluorimetry do not resolve these compounds easily without using a separation technique. Supersonic jet spectrometry provides very sharp line structures in both excitation and fluorescence spectra, therefore this technique may be very useful for selective identification of these compounds.

The energy of the pure electronic excited state of perylene is lower than that of benzo[a]pyrene. Selective excitation of perylene and detection of the strong perylene fluorescence should be readily achieved without being affected by weak fluorescence from benzo[a]pyrene. The determination of carcinogenic benzo[a]pyrene from a mixture with perylene is more difficult, because the excitation wavelength of 387 nm also excites perylene and its strong fluorescence band superimposes on the weak fluorescence band of benzo[a]pyrene.

A supersonic jet spectrum of a 1:1 mixture of benzo[a]pyrene and perylene is shown in Fig. 6. The exciting wavelength was adjusted to the absorption maximum of benzo[a]pyrene at 386.7 nm. Fluorescence from perylene is very strong and broad, but the sharp fluorescence band of benzo[a]pyrene is clearly observed at 397 nm, and selective identification of benzo[a]pyrene is possible. The fluorescence band at 420 nm for benzo[a]pyrene should be observed in this spectrum, but it is relatively small and may be buried in the broad and strong fluorescence bands of perylene.

Calibration curve and detection limit

A calibration curve was constructed for perylene by injecting the sample solution into a hot carrier gas (argon). The useful range extended from 0 to at least 4 μg, and the detection limit was 0.1 μg. The main noise was background emission from the benzene used as a solvent of the sample. The baseline drift might be coming from a dark current noise of the photomultiplier. Hayes and Small [21] reported detection limits of 60—14 ng for naphthalene and its derivatives by using supersonic jet fluorimetry. The sensitivity of the present apparatus is probably similar to their system when the spectral resolution of the fluorescence monochromator in both studies is taken into account.

Comparison with other low-temperature spectrometric methods

Supersonic jet spectrometry is based on the idea of beam expansion into vacuum with sudden decrease in the sample temperature. It provides a spectrum consisting of a number of sharp vibrational lines, which is very useful for identification of the particular molecules included in the sample.

Low-temperature spectrometry based on the Shpol'skii and matrix isolation effects is now quite widely studied as an analytical technique for traces of PAHs in the environment, because it also gives very sharp vibrational lines in the spectrum and is useful for identification.

Supersonic jet spectrometry has several distinct advantages over solid-phase low-temperature spectrometry. The supersonic jet method is done in vacuum and requires no solvent. Accordingly, there are no solvent effects, i.e., no spectral shift, no line splitting in the band structure, and no Raman scattering from the solvent molecules, and no background emission from solvent impurities. Thus, the observed spectrum includes much purer information and is more reliable for identification. In solid-phase spectrometry, the sample preparation procedure is tedious and time-consuming. Furthermore, this method cannot be combined with flow analysis or a flow separation technique such as gas [21] or liquid chromatography. It is noted that the supersonic jet technique can be used not only for the determination of the PAH molecules but also for many other molecules such as nitrogen dioxide [5, 6], whereas the Shpol'skii and matrix isolation effects are used for the determination of PAH molecules.

Supersonic jet spectrometry has a few disadvantages. It is used under gas-flowing conditions, and the sample is lost during the measurement, whereas the sample is conserved in solid-phase spectrometry. Temperature control is very important for the measurement of the fluorescence spectrum by supersonic jet spectrometry, because the concentration of the sample in the jet is determined by the temperature of the sample in the tee-fitting. This disadvantage may be overcome by measuring the total fluorescence from the sample using a monochromator equipped with an optical multichannel analyzer.

Finally, it is emphasized that the nozzle-beam equipment allows multiphoton ionization and succeeding single ion detection [27]. This method combined with a gas chromatographic system for the selective identification of the sample species will be described at a later date. Such a method would be advantageous in trace analysis for environmental or biochemical substances.

This research was supported by a Grant-in Aid for Scientific Research (Grant No. 57430016) from the Ministry of Education of Japan and by a Grant of Shimadzu Foundation.

REFERENCES

1 T. F. V. Geel and J. D. Winefordner, Anal. Chem., 48 (1976) 335.
2 J. H. Richardson and M. E. Ando, Anal. Chem., 49 (1977) 955.
3 M. Kunitake, T. Imasaka and N. Ishibashi, Nippon Kagaku Kaishi, (1981) 55.
4 E. L. Wehry and G. Mamantov, Anal. Chem., 51 (1979) 643A.
5 R. E. Smalley, B. L. Ramakrishna, D. H. Levy and L. Wharton, J. Chem. Phys., 61 (1974) 4363.

6 R. E. Smalley, L. Wharton and D. H. Levy, J. Chem. Phys., 63 (1975) 4977.
7 S. M. Beck, D. E. Powers, J. B. Hopkins and R. E. Smalley, J. Chem. Phys., 73 (1980) 2019.
8 S. M. Beck, J. B. Hopkins, D. E. Powers and R. E. Smalley, J. Chem. Phys., 74 (1981) 43.
9 F. M. Behlen and S. A. Rice, J. Chem. Phys., 75 (1981) 5672.
10 F. M. Behlen, D. B. McDonald, V. Sethuraman and S. A. Rice, J. Chem. Phys., 75 (1981) 5685.
11 A. Amirav, U. Even and J. Jortner, J. Chem. Phys., 75 (1981) 3151; Chem. Phys., 67 (1982) 1; Chem. Phys. Lett., 72 (1980) 16.
12 S. Leutwyler, U. Even and J. Jortner, Chem. Phys. Lett., 86 (1982) 439.
13 P. S. H. Fitch, L. Wharton and D. H. Levy, J. Chem. Phys., 70 (1979) 2018.
14 P. S. H. Fitch, C. A. Haynam and D. H. Levy, J. Chem. Phys., 74 (1981) 6612.
15 U. Even, J. Jortner and J. Friedman, J. Phys. Chem., 86 (1982) 2273.
16 U. Even, J. Magen and J. Jortner, Chem. Phys. Lett., 88 (1982) 131; J. Chem. Phys., 76 (1982) 5684.
17 A. Amirav, U. Even and J. Jortner, J. Chem. Phys., 51 (1980) 31.
18 I. Raitt, A. M. Griffiths and P. A. Freedman, Chem. Phys. Lett., 80 (1981) 225.
19 A. Amirav, U. Even and J. Jortner, J. Chem. Phys., 75 (1981) 3770; Chem. Phys. Lett., 69 (1980) 14.
20 J. A. Warren, J. M. Hayes and G. J. Small, Anal. Chem., 54 (1982) 138.
21 J. M. Hayes and G. J. Small, Anal. Chem., 54 (1982) 1202.
22 A. Amirav, U. Even and J. Jortner, Anal. Chem., 54 (1982) 1666.
23 K. Mori, T. Imasaka and N. Ishibashi, Anal. Chem., 54 (1982) 2039.
24 T. Imasaka, J. Spectrosc. Soc. Jpn., 32 (1983) 120.
25 N. Mikami, Oyo Butsuri, 49 (1980) 802.
26 J. R. Maple, E. L. Wehry and G. Mamantov, Anal. Chem., 52 (1980) 920.
27 D. M. Lubman and M. N. Kronick, Anal. Chem., 54 (1982) 660.

Analytica Chimica Acta, 156 (1984) 121—127
Elsevier Science Publishers B.V., Amsterdam — Printed in The Netherlands

DETERMINATION OF ARSENIC BY HOLLOW-CATHODE EMISSION SPECTROMETRY

A. ALIMONTI, S. CAROLI* and F. PETRUCCI

Department of Physical Chemistry, Laboratory of Applied Toxicology, Istituto Superiore di Sanità, Viale Regina Elena 299, 00161 Rome (Italy)

C. ALVAREZ HERRERO

Department of Spectrochemistry, Institute of Analytical Chemistry, Consejo Superior de Investigaciones Científicas, Madrid (Spain)

(Received 7th April 1983)

SUMMARY

The applicability of the hollow-cathode discharge source in the emission spectrometric determination of arsenic is described. Neutral and 10% nitric acid solutions, as well as solutions obtained by mineralization of biological materials, all containing 2.5 to 125 μg As cm^{-3}, were introduced into stainless steel cathodes, dried under i.r. radiation, and calcined in a muffle furnace; the loaded cathodes were then subjected to discharge. Acidic solutions were found to leach nickel from the steel of the cathode: this converted the analyte into thermally-stable nickel arsenide, thus minimizing losses. Matrix effects were small, and the r.s.d. was satisfactory (5—8%). The detection limit was 3 μg cm^{-3}.

The toxicity of arsenic is mainly due to its capacity to inhibit various enzyme systems, particularly those regulating the mechanism of cellular energy production [1]. Its reputation as a classic poison dates back to the ancient Egyptians, and forensic records are a clear testimonial to its past popularity for homicides. Nowadays, cases of arsenic poisoning are mostly a consequence of occupational exposures; pesticide manufacture, smelting of metals and burning of coal can be listed among the major sources of this element in ambient air deriving from human activities. A trace amount of arsenic is contained in tobacco and originates from the agricultural use of arsenical insecticides. Average concentration values of this element determined in various brands of cigarettes are normally below 8 ng g^{-1} [1].

Arsenic is also a trace element which is essential for the performance of normal biological functions [2]. Accurate and precise methods are therefore necessary to determine arsenic in biological samples down to the ng g^{-1} level. At present, numerous techniques are available for this purpose, e.g., atomic absorption spectrometry (a.a.s.), neutron activation γ-spectrometry, atomic emission and fluorescence spectrometry, x-ray fluorescence spectrometry, anodic stripping voltammetry and pulse polarography. An excellent critical survey of the advantages and shortcomings of these methods has recently been compiled by Brooks et al. [3].

0003-2670/84/$03.00

By far the preferred technique during the last decade has been hydride generation a.a.s. [4]. However, the argon-hydrogen flame generally used in this procedure, because of its low temperature, makes chemical interferences particularly severe. This difficulty can partly be overcome if the evolved hydride is passed through an electrically heated cell instead of entering the flame. The applicability of a.a.s. with electrothermal atomization for direct determination of arsenic, however, is greatly hampered by the high volatility of arsenic. Losses can be prevented by adding nickel which leads to the formation of stable arsenides [5, 6]. However, matrix effects cannot be ignored in determining arsenic by a.a.s. [7]. Moreover, spectral overlap and background emission are two main drawbacks when arsenic is determined by means of inductively-coupled plasma emission spectrometry.

The above disadvantages are very much decreased in atomic emission spectrometry when a hollow-cathode excitation source is used [8, 9]. The suitability of this source for arsenic determination has been tested qualitatively [10]. A novel analytical method based on the utilization of the hollow-cathode discharge is described in this paper.

EXPERIMENTAL

Instrumentation and solutions

Technical details of the hollow-cathode demountable lamp, vacuum spectrograph and other ancillary apparatus have been reported [11, 12]. Table 1 therefore only summarizes the main information.

Three types of arsenic solutions were analyzed by means of the hollow-cathode discharge in order to test its suitability for the determination. They were KH_2AsO_4 (Carlo Erba RP) in twice-distilled water, KH_2AsO_4 (Carlo Erba RP) in aqueous 10% nitric acid (Merck Suprapur), and solutions resulting from the wet-ashing of biological materials. In this last case, the brains, livers and kidneys of six male rats of similar age and weight were excised

TABLE 1

Experimental facilities employed for the determination of arsenic

Vacuum spectrograph SPV 1m/800 (Paschen-Runge mounting, 30-μm entrance slit)[a]	Concave grating, 1200 grooves mm^{-1}, 1-m radius, blazed at 5° 52'[e]
Glow discharge/hollow-cathode demountable tube[a]	Oil pumps Trivac D 8 A and D 16 A (noble gas flow in the tube)[c]
Stabilized-current source unit HVG 2[a]	Oil pump Trivac D 16 A (prevacuum in the spectrograph)[c]
Digital multimeter 3476 A[b]	Turbomolecular pump THP 900 (high vacuum in the spectrograph)[f]
Vacuum gauge Thermotron TM 14/2[c]	
Microdensitometer MD 100[d]	

[a]RSV, West Germany; [b]Hewlett-Packard, U.S.A.; [c]Leybold Heraeus, West Germany; [d]Jenoptik Jena, East Germany; [e]Bausch & Lomb, U.S.A.; [f]Pfeiffer Vakuumtechnik, West Germany.

after sacrifice and pooled according to type. The organs were digested in concentrated nitric acid (Merck Suprapur) by evaporating the mixture on a small flame until a clear solution was obtained on cooling. Solutions thus obtained were diluted to 150 cm^3 with twice-distilled water. Six aliquots, each of 25 cm^3, were drawn and spiked with the above arsenic standard solutions at increasing concentrations. In each of the three types of solutions mentioned above, the final solutions contained 2.5, 5.0, 12.5, 50 and 125 μg As cm^{-3}. Gallium (as $GaCl_3$) was present at 12.5 μg cm^{-3} in all solutions as a reference element.

Hollow-cathode discharge procedure

According to previous investigations [7], 18/8 stainless steel is the most suitable material for preparing hollow cathodes for liquid samples, owing to its thermal and electrical conductance as well as its resistance to the corrosive action of acidic solutions. Thus 400 μl of each sample was introduced by a micropipette into the cathode cavity (i.d. 6.0 mm, depth 14.8 mm) and slowly dried therein under an infrared lamp. For the entire duration of this process, the cathodes were slowly and continuously rotated at an inclination of 20° from the vertical in order to produce a uniform, reproducible deposit of salt film on the bottom and lower wall of each cathode. Subsequently, the hollow cathodes were placed in a muffle furnace for further thermal treatment. Preliminary measurements showed that the acidity of the arsenate/nitric acid and dissolved tissue solutions was sufficient to leach small amounts of nickel from the cathode inner surface (most likely during the i.r. heating as the acid concentrates and the temperature increases), thus quantitatively forming stable arsenides. This permitted the solutions to be heated at 700°C for up to 60 min with no problems insofar as analyte volatilization was concerned. The non-acidified samples had to be treated much more mildly (200°C for 30 min) in order to minimize volatilization losses of arsenic.

The hollow cathodes thus loaded with solution residues were subjected to discharge, and the spectra were recorded on photographic films; the blackening of the lines of interest was then measured with a microdensitometer and finally converted to the corresponding intensity values. Table 2 sets out the operating parameters adopted.

TABLE 2

Working conditions for the determination of arsenic

Carrier gas, Ar at 440 Pa	Emulsion, Kodak SA-1 films
Applied current, 200 mA	Developer, Kodak D-19 (4 min at 20°C ± 0.1°C)
Resulting voltage range, 280—400 V	Fixer, Kodak Kodafix
Exposure time, 2 min	Ga reference line, 417.21 nm
As analytical line, 234.98 nm	

Optimization studies

Of the four spectral lines of arsenic suitable for measurement (i.e., 216.62, 222.87, 228.81 and 234.98 nm), the last was found to be most sensitive and was therefore selected for use. Though rather far from this, the gallium reference line chosen was that at 417.21 nm, because it adequately reflected discharge oscillations. The optimal intensity-to-background ratio was achieved at a noble gas pressure of 440 Pa, which also provided excellent discharge stability.

In order to establish the most appropriate exposure time in each of the three cases described above, the arsenic emission intensity was measured as a function of time. For all the solutions, independent of their concentration, the peak emission occurred in the first 2 min of discharge. An example of this behaviour is shown in Fig. 1. The behaviour of biological samples containing added arsenic followed the same pattern, the only difference being that the first 30 s of discharge showed a certain instability of the arsenic signal until it reached its full intensity. This is apparently related to the higher mineral content of these samples, which can inhibit the immediate onset of stable sputtering. An exposure time of 2 min was chosen as the best compromise between a sufficiently intense emission and reproducibility of measurements, without increasing the background to unacceptable levels. Insofar as the original inorganic solutions were concerned, however, even a 1-min exposure gave satisfactory results. For each specimen, exposures were

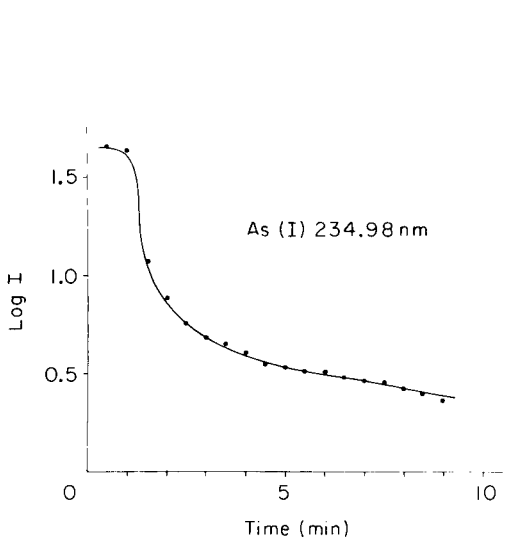

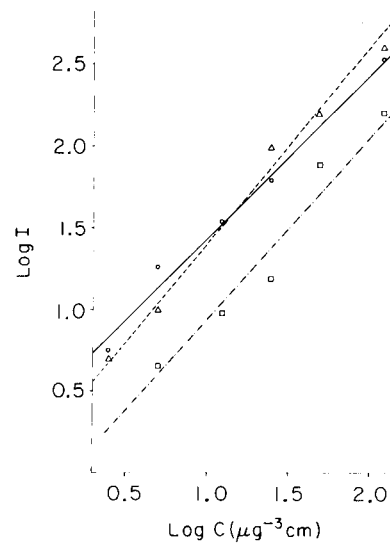

Fig. 1. Burn-off curve for arsenic (12.5 μg cm^{-3}) in aqueous 10% nitric acid. Intensity is given in arbitrary units.

Fig. 2. Log-log plots of emission intensity vs. arsenic concentration (C). Analytical line, 234.98 nm: (○) in twice-distilled water; (△) in aqueous 10% HNO_3; (□) in acidic solutions of wet-ashed biological materials.

done in triplicate and the results averaged. Blackening values of the spectral lines were corrected for background emission as suggested by Slavin [13], which avoids overcorrecting analytical lines of low intensity. Blackenings were finally converted to the corresponding intensities by means of a densitometric curve plotted beforehand.

RESULTS AND DISCUSSION

Though the three types of sample under study were different either in composition or in the dissolution procedure, experimental findings in all cases indicated the advantages of the hollow-cathode discharge for arsenic determinations. The corresponding linear calibration and precision information are summarized in Table 3. The calibration graphs are shown in Fig. 2. From these data, it is apparent that, independent of the acidity of the samples, the potassium arsenate solutions provide calibration results which are very similar. For the dissolved biological materials the signal is obviously lower, as the presence of appreciable amounts of other salts dilutes the bulk concentration of the analyte in the solid phase deposited on the cathode inner wall. This leads to the diminution of arsenic available for the layer-by-layer ablation of the residue films. It should be stressed, however, that notwithstanding this decrease in emission intensity the slope of the calibration plot is very similar to that for potassium arsenate in nitric acid, further supporting the interpretation that matrix effects, if any, are mainly related to surface availability of the analyte and not to specific mutual chemical interferences. Therefore, the utilization of an internal reference element permits the signal decrease easily to be circumvented and the matrix-independent nature of the effect to be demonstrated, as has already been reported in similar cases [7]. In fact, when the As-Ga intensity ratios are considered, all the calibration lines overlap within the standard deviation range.

Interferences, as is usual with low-pressure emission sources, are negligible. Overlapping of spectra is not very likely because of the sharpness of the lines emitted by the hollow cathode as well as the rather limited number of lines present in the spectra in comparison with other emission sources.

TABLE 3

Characteristics of the determination of arsenic by hollow-cathode discharge

Type of sample	Calibration function	Relative standard deviation[a] (%)
Aqueous solutions	$\log C = 0.96 \log I - 0.37$	5—8
Aqueous 10% HNO_3	$\log C = 0.87 \log I - 0.22$	3—6
Wet-ashed biological materials	$\log C = 0.85 \log I + 0.22$	5—8

[a]For 10 measurements.

The plots in Fig. 2 are linear over at least two orders of magnitude. This is one of the more desirable properties of sputtering sources which permits the determination of elements at trace, minor and major concentrations. The precision of measurements is similar to that attained by a.a.s. Precision was calculated as the relative standard deviation (r.s.d.) of a series of 10 measurements. Solutions of 2.5, 12.5 and 125 μg As cm^{-3} for each of the three types of samples investigated were employed. For each solution at each concentration, 10 steel cathodes were simultaneously treated as described above. Cathodes were discharged under exactly the same working conditions, monitoring current and carrier gas pressure with the greatest care. For each solution, the 10 spectra were recorded on an individual strip of film. Each analytical arsenic signal (blackening value) was converted to the corresponding emission intensity and the r.s.d. was calculated. Over the entire concentration range, the r.s.d. was 3—8% (Table 3).

Accuracy is not completely satisfactory, as recovery is subject to appreciable fluctuations around the values of the amounts added. Memory effects in the lamp caused by deposition of trace arsenic on the tube inner surface probably account for concentration values higher than the nominal ones, which indicates the need for more frequent cleaning of the lamp body (generally done after a set of 9—12 discharges). In contrast, random ejection of small particles of the sample from the cathode cavity when the residue layer does not adhere perfectly to the electrode surface apparently should lead to a lower degree of recovery. A better control of these two key factors should result in better accuracy. Though accuracy was determined only on the basis of arsenic recovery after spiking the samples, and not by means of reference materials, the data obtained are sufficient to indicate some of the problems to be expected.

Detection limits, calculated according to the 3σ criterion, are about 3 μg cm^{-3} in the solutions. The low background indicates that the detection limit could be improved by prolonging the exposure so as to integrate the emission signal over the total period of sample discharge. Generally, background intensity increases more slowly with exposure time than spectral line intensity.

The procedure developed was applied to the determination of arsenic in samples from two groups of rats, each of six animals. The first group contained unexposed animals, whose organs showed no detectable arsenic by the technique proposed. The second group was injected intravenously with sodium arsenite and the animals were killed after 2 h. The total content of arsenic in brain, kidney and liver was found to be 0.3, 0.9 and 1.1 $\mu g\, g^{-1}$ (wet weight), respectively, corresponding to 2.3, 6.9 and 8.4 $\mu g\, cm^{-3}$ in the solutions resulting from the wet ashing. These data are in accordance with the fact that kidney and liver accumulate arsenic very quickly after treatment.

In conclusion, the hollow-cathode discharge determination of arsenic does not seem to be subject to many of those disadvantages which can limit, sometimes severely, the performance of other more popular techniques. It

has, however, its own limitations. Solutions cannot be analyzed directly, but must be subjected to preliminary drying, and detection limits are not yet comparable with those achieved, for example, by a.a.s. with electrothermal atomization. Although the proposed method is far from reaching is ultimate performance, nonetheless it offers a valid and advantageous alternative in many instances.

REFERENCES

1 B. A. Fowler, N. Ishinishi, K. Tsuchiya and M. Vahter, in L. Friberg, G. F. Nordberg and V. B. Vouk (Eds.), Handbook on Toxicology of Metals, Elsevier/North-Holland Biomedical Press, Amsterdam, 1979. Ch. 17.
2 B. A. Fowler, in R. A. Goyer and M. A. Mehiman (Eds.), Toxicology of Trace Elements, Hemisphere Publishing Co., Washington, DC, 1977, Ch. 3.
3 R. R. Brooks, D. E. Ryan and H. Zhang, Anal. Chim. Acta, 131 (1981) 1.
4 W. Holak, Anal. Chem., 41 (1969) 1712.
5 H. Freeman, J. F. Uthe and B. Fleming, At. Absorpt. Newsl., 15 (1976) 49.
6 R. M. Hammer, D. L. Lechak and P. Greenberg, At. Absorpt. Newsl., 15 (1976) 122.
7 S. Caroli, O. Senofonte and P. Delle Femmine, Analyst, 108 (1983) 196.
8 S. Caroli, A. Alimonti, F. Petrucci and S. K. Shukla, Anal. Chim. Acta, 136 (1982) 225.
9 S. Caroli, A. Alimonti and K. Zimmer, Spectrochim. Acta, Part B, 38 (1983) 625.
10 G. Milazzo and S. K. Shukla, Rep. ERO, DAJA-37-67-C-0577, 1968.
11 S. Caroli, A. Alimonti and O. Senofonte, Spectrosc. Lett., 13 (1980) 307.
12 S. Caroli and O. Senofonte, Can. J. Spectrosc., 25 (1980) 73.
13 M. Slavin, Appl. Spectrosc., 16 (1962) 173.

Analytica Chimica Acta, 156 (1984) 129—137
Elsevier Science Publishers B.V., Amsterdam — Printed in The Netherlands

THE DIRECT DETERMINATION OF CADMIUM IN URINE BY ELECTROTHERMAL ATOMIC ABSORPTION SPECTROMETRY WITH THE L'VOV PLATFORM[a]

J. J. McAUGHEY and N. J. SMITH*

Health and Safety Executive, Occupational Medicine and Hygiene Laboratory, 403 Edgware Road, London NW2 6LN (Great Britain)

(Received 23rd August 1983)

SUMMARY

A simple, direct procedure for the measurement of cadmium in urine is described. Graphite-furnace atomic absorption spectrometry is used in conjunction with selective atomisation at 800°C from a L'vov platform. Urine samples are diluted with an equal volume of deionised water and 20-μl aliquots are injected. Calibration is done by standard additions. The sensitivity is 0.016 μg Cd l^{-1} for 1% absorption for a 20-μl sample. Within-run precision is 4.9% at 0.84 μg l^{-1}. The detection limit is 0.06 μg l^{-1}, which allows normal unexposed levels of cadmium in urine to be determined. The method is applicable to the determination of urinary cadmium levels of both occupationally non-exposed and exposed populations.

Uptake of cadmium following environmental or occupational exposure results in a gradual accumulation in liver and kidney, with the eventual production of kidney dysfunction [1]. It has been suggested that cadmium workers should be monitored by measuring blood and urinary cadmium to establish the current status of the body's store and by measuring urinary proteins to determine kidney function [1]. However, it is only recently that methods based on atomic absorption spectrometry (a.a.s.) or atomic fluorescence spectrometry [2] have become available for estimating urinary cadmium concentrations, particularly in those subjected to low exposures.

The most widely used method for the determination of cadmium in urine is a.a.s. with electrothermal atomisation. The major problems in measuring cadmium in urine are related to the high ratio of background-to-analyte signal and to the high volatility of cadmium. In order to overcome the matrix problems, some of the early work used chelation and extraction before the a.a.s. step. However, such methods are prone to losses and contamination. More recently, the approach has been towards direct analysis by injection of urine into a graphite furnace, employing a matrix modifier to decrease interference problems. Vesterberg and Wrangskogh [3] diluted

urine (1 + 1) with 0.3 M nitric acid to decrease interferences before placing the mixture on a carbon rod for measurement. Bruhn and Navarrete [4] used matrix modification with phosphate in conjunction with standard addition to determine cadmium in urine. They used temperature-controlled maximum power heating of a furnace to atomise cadmium at 800°C. Similarly, Carmack and Evenson [5] also relied on maximum power heating to atomise cadmium selectively in a graphite furnace, but with molybdenum-coated tubes to decrease interferences.

Recently, the use of Zeeman background correction in conjunction with atomisation from the L'vov platform has been proposed for the direct determination of cadmium in urine [6]. This method uses matrix modification with diammonium hydrogenphosphate and atomisation at 1600°C, with calibration against aqueous standards. Zeeman background correction is used to overcome the high background absorbance (>1.0) reported. The authors state that diammonium hydrogenphosphate from several sources had significant cadmium contamination although a source was eventually found which was essentially cadmium-free. Experience was similar in this laboratory. In order to eliminate time-consuming extraction procedures for the purification of these matrix modifiers, their use has been avoided, and direct injection after simple dilution of urine together with selective atomisation of cadmium from the L'vov platform using the temperature-controlled maximum power heating mode is proposed here. Measurement of cadmium using conventional deuterium background correction is made possible by the temporal separation of the analyte signal from background interferences. The use of gas-stop conditions in the atomisation cycle gives an improvement in sensitivity over previous methods employing selective atomisation, and the sensitivity is comparable to that of Zeeman a.a.s. [6].

EXPERIMENTAL

Apparatus

The Perkin-Elmer Model 4000 atomic absorption spectrometer used was fitted with the Perkin-Elmer HGA-400 or HGA-500 graphite furnace with an optical temperature sensor for maximum power heating. This allows rapid heating of the order of 2000°C s^{-1} to be achieved. This sensor may be pre-set between 800°C and 3000°C. Samples were introduced into the furnace using a Perkin-Elmer AS-40 autosampler. A Perkin-Elmer Model 056 twin-pen recorder was used to monitor simultaneously the peaks of both analyte and background absorption. Data output was recorded remotely via an RS-232C interface board to a Trivector Trilab microcomputer system. Pyrolytic graphite tubes (Perkin-Elmer, 3012-1091) fitted with solid pyrolytic graphite platforms (Perkin-Elmer, 3012-1092) were used for all determinations after initial temperature calibration with an optical pyrometer. Samples were prepared for measurement using a Hamilton Microlab-M programmable dispenser/diluter or Oxford P-7000 series pipettes.

Materials

The only reagents used were deionised double-distilled water, nitric acid (Fisons Primar grade), Triton X-100 (Fisons scintillation grade), and 1000 mg l^{-1} cadmium standard solution (Hopkin & Williams Stan-Ion). The 1000 mg l^{-1} cadmium solution was used to prepare a 1 mg l^{-1} cadmium standard solution in 0.1% nitric acid. Working standards were prepared each week from this solution. These working standards were prepared in 0.1% Triton X-100 solution and were found to be stable for 2—3 weeks when stored at 4°C.

Nitric acid was not used in the preparation of the working standards as it gave unacceptably high cadmium concentrations with respect to the detection limit, even for 0.1% acid. Similarly, commercially available ammonium hydrogenphosphates were found to contain unacceptably high cadmium concentrations of up to 0.5 $\mu g\ l^{-1}$ if used directly, without a previous extraction step.

All glassware used was Grade A and was prepared by soaking in 5% nitric acid followed by two rinses with deionised double-distilled water before use. Subsequent washing was by distilled water rinses only. All disposable pipette tips were rinsed three times with deionised double-distilled water and once with the sample to be dispensed, immediately prior to use. All autosampler cups were prepared by soaking in 10% nitric acid overnight, rinsed twice with deionised double-distilled water, and dried before use.

Sample preparation

Random urine samples from both occupationally exposed and unexposed subjects were collected in polycarbonate bottles, without preservative, and stored at 4°C unless analysed immediately. Samples were diluted (1 + 1) with deionised double-distilled water into cadmium-free 5-ml screw-cap glass bottles and mixed well; 500-μl aliquots of this diluted urine were delivered into the autosampler cups containing 500 μl of 0.0, 1.0 and 2.0 $\mu g\ l^{-1}$ cadmium standard solutions dispensed using the Hamilton Microlab-M. This gave a standard addition series of 0.0, 0.5 and 1.0 $\mu g\ l^{-1}$ cadmium. A 2.0 $\mu g\ l^{-1}$ cadmium standard addition was also used initially, but was found to give no improvement in the precision of the results, and was subsequently omitted. Each standard addition series was run in descending concentration order and the intercept was calculated by the microcomputer system. Standard addition graphs were linear up to a concentration of 4 $\mu g\ l^{-1}$ cadmium in the diluted samples. This is equivalent to 12 $\mu g\ l^{-1}$ in the original urine sample. Urine samples from occupationally exposed workers exceeding this value required further dilution before repeat measurements by standard addition.

Parameters for a.a.s.

Samples were injected in triplicate, using the furnace parameters given in Table 1, and the following instrumental conditions: wavelength 228.8 nm; spectral bandwidth 0.7 nm; spectral source, electrodeless discharge tube at 5 W. Absorbance was measured with deuterium arc background correction,

TABLE 1

Graphite-furnace parameters for cadmium determination

Step	Temperature (°C)	Ramp time (s)	Hold time (s)
Dry	150	25	15
Ash[a]	300	15	60
Atomise[b]	800[c]	0	9
Clean	2500	2	5
Cool	20	1	20

[a]Automatic baseline correction used after 55 s. [b]Gas-stop conditions plus maximum power heating. [c]This may be increased to 850°C without affecting sensitivity.

using peak area integration (5.0 s), for samples of 20 μl. The chart recorder was set at 10 mV full-scale deflection; the purge gas was argon.

RESULTS

Ashing and atomisation temperatures

A suitable ashing temperature was selected from a plot of ashing temperature against absorbance for 20-μl injections of a diluted urine sample. Figure 1 shows a graph comparing the ashing curves for 20-μl injections of an aqueous cadmium sample and a spiked urine sample. There is clearly a difference between the two curves for the maximum permissible ashing temperature before loss of cadmium occurs. However, to allow for variation between urine samples, the ashing temperature selected was 300°C. The HGA-400 and HGA-500 were used in the maximum power heating mode, and the best atomisation temperature was selected from a plot of temperature against absorbance for an ashing temperature of 300°C. In the maximum power heating mode, it is only possible to control the final temperature above 800°C. Figure 2 shows that the cadmium signal falls steadily with increasing temperature beyond 800°C. This is undoubtedly due to the decreased separation of cadmium from the background matrix with increasing temperature. However, because differences can occur between graphite tubes, it was found that an atomisation temperature of up to 850°C could be used without affecting sensitivity unduly.

Analytical performance

Calibration graphs for aqueous cadmium standards and standard addition plots for urine samples were linear up to 4 μg l^{-1} cadmium. Figure 3 shows an aqueous cadmium calibration graph and the plots for a number of urine samples. The urine plots generally show some depression in sensitivity compared with that for aqueous standards. Because of the large variation in matrix composition between urine samples, the method of standard additions was necessary for reasonable accuracy of results.

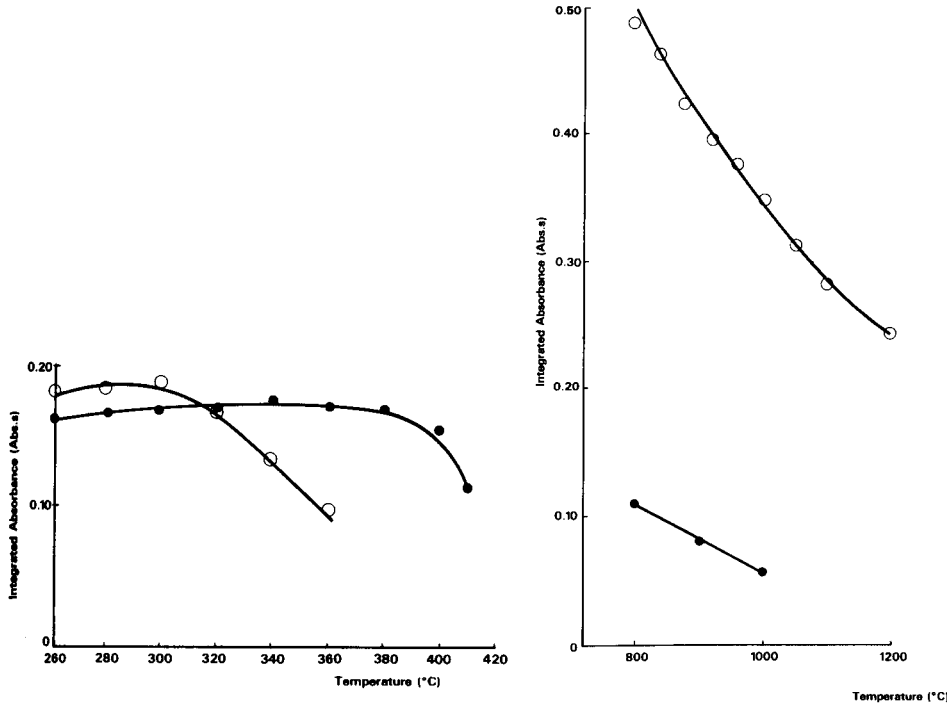

Fig. 1. Effect of ashing temperature on absorbance signal of cadmium in 20-μl samples of: (○) 0.5 μg l^{-1} cadmium standard; (●) diluted urine.

Fig. 2. Effect of atomisation temperature on absorbance signal for cadmium in 20-μl samples of: (○) 1.0 μg l^{-1} cadmium standard; (●) diluted urine.

The absolute sensitivity of the method was calculated as the amount of cadmium in a sample that produced 1% absorption or 0.0044 absorbance sec; this was found to be 0.32 pg. The detection limit, defined as the amount of cadmium required to give a signal twice the magnitude of the variation of a blank sample, was found to be 1.3 pg. The recovery was calculated by spiking an unexposed urine sample at two different levels (2 and 4 μg l^{-1}) and running duplicate determinations. The average recoveries at the two levels were 102.5% and 103%, respectively. The precision of the method for within-run and between-run determinations at two different levels is shown in Table 2.

At present, there is no certified reference material available for urinary cadmium. This means that an assessment of accuracy is difficult to obtain. To try to overcome this, two approaches were adopted. First, various urine samples were analysed by this proposed method and also by a technique based on anodic stripping voltammetry (a.s.v.) which has been used by this laboratory for some considerable time. The latter method is based on that

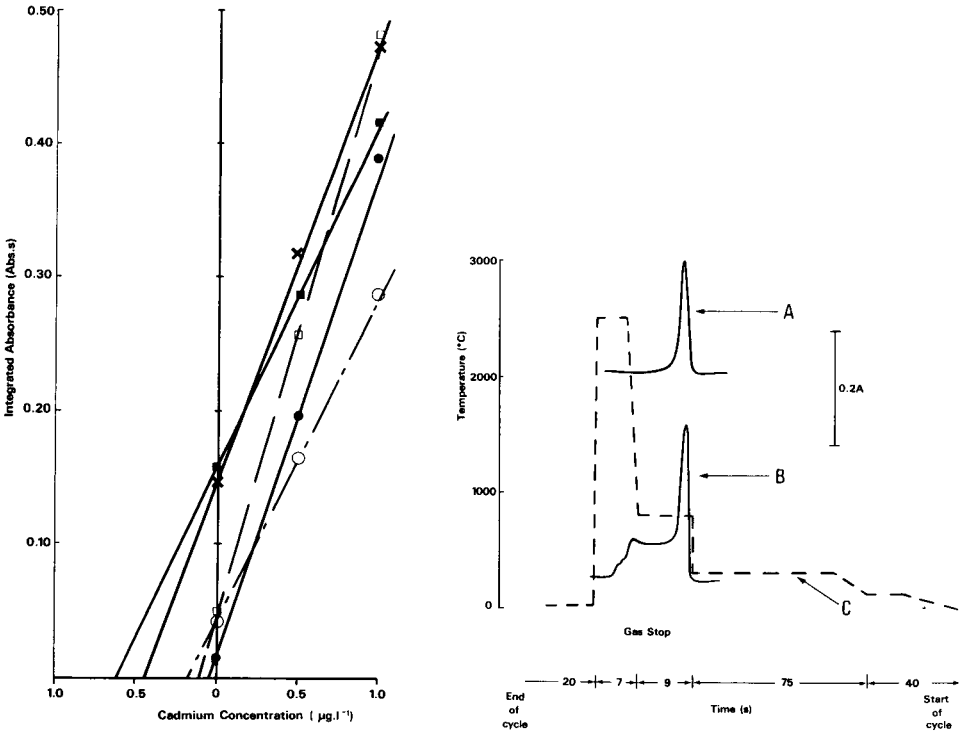

Fig. 3. Calibration graph for aqueous standards (•) and standard addition series for different urine samples (○, □, ■, X).

Fig. 4. Absorption/time profiles for specific and non-specific absorbance: (A) background-corrected cadmium absorbance; (B) non-specific background absorbance; (C) temperature profile.

of Pinchin and Newham [7], but an Environmental Sciences Associates Model 2014 instrument is used; cadmium is plated onto a glassy carbon electrode from a sodium acetate buffer following a nitric acid/perchloric acid digestion. A comparison of the two sets of results is shown in Table 3.

TABLE 2

Precision at occupationally unexposed and exposed concentrations of cadmium

	Conc. ($\mu g\ l^{-1}$)	No. of results	R.s.d. (%)
Within-run	0.84	6	4.9
	10.30	18	3.0
Between-run	0.84	36	11.3
	10.30	27	4.4

TABLE 3

Comparison of urinary cadmium results by a.a.s. and a.s.v.[a]

Sample	Cd found ($\mu g\ l^{-1}$)	
	A.a.s.	A.s.v.
1	1.0	<2.0
2	2.4	2.4
3	16.9	18.5
4	20.9	25.0
5	37.0	42.5

[a]The regression line is $y = 1.17x - 0.46$ ($r = 0.99$).

In the second procedure, seven samples with concentrations ranging from 9 to 65 $\mu g\ l^{-1}$ cadmium were measured after two different dilutions in order to test the effect of the matrix; the dilutions varied from (1 + 1) to (1 + 40). There was very good agreement between results at different dilutions, the equation of the regression line being $y = 0.98x + 0.99$ ($r = 0.99$).

DISCUSSION

Cadmium is a very volatile metal and the determination of this element in biological samples, particularly blood and urine, has posed many problems for some time. Typical levels in urine from occupationally unexposed subjects are usually less than 1 $\mu g\ l^{-1}$ and therefore with such a high background-to-analyte ratio, direct determination has had to wait until improvements and developments in instrumentation became available. The recent developments in graphite-furnace a.a.s. coupled with microprocessor control have brought about improvements that now allow normal levels of cadmium in blood and urine to be measured easily. Furthermore, the capability of graphite furnaces to produce very fast heating rates means that volatile elements can be selectively atomised from their matrix, thus allowing separation of analyte signal from background absorption to be achieved. Many workers have chosen to use either matrix modification techniques as a means of decreasing interference effects or a combination of matrix modification and temperature-controlled maximum power heating of the graphite furnace, to measure urinary cadmium. However, an important development in graphite-furnace a.a.s. has been the introduction of the L'vov platform or stabilised-temperature platform furnace. This is a technique which is gradually gaining widespread acceptance, especially for the more volatile elements, as a means of overcoming or at least decreasing interference effects [8]. This platform approach to the determination of cadmium in urine has been used in the present work, as it avoids the need for sample pretreatment and relies solely on the controlled selection and optimisation of instrumental parameters to minimise interference effects. The critical steps are the optimisation

of the atomisation temperature of cadmium from the L'vov platform and accurate control of the ashing temperature. In this work, an optical pyrometer and thermocouple probe were used to verify the temperatures of the graphite tube.

In normal graphite-furnace a.a.s., atomisation of the analyte takes place from the tube wall, and it is possible that differences in matrix composition of samples can lead to changes in the appearance temperature of the element of interest, thus shifting the analyte signal in time. This variation in appearance temperature can, under changing temperature conditions, cause changes in the efficiency of atomisation and in the residence time of atoms in the furnace, both of which can give rise to differences in analyte absorbance signals whether the peak height or the peak area mode is used [9]. With the L'vov platform, however, the platform is heated solely by radiation from the tube wall. Consequently, sample vaporisation and atomisation are delayed until isothermal conditions are attained within the tube. As vaporisation of the analyte then takes place into a region of higher temperature, there is increased dissociation of molecular species, thus resulting in fewer background interference problems. It is important that isothermal conditions be attained within the tube before the surface of the platform reaches a temperature at which cadmium can be volatilised. At atomisation temperatures exceeding 1000°C, the rate of heating of the platform is such that vaporisation of cadmium from the platform is likely to occur before a constant temperature is achieved within the tube. The instrument used in this study will, in the maximum power heating mode, give controlled temperatures only from 800°C upwards. However, with a different temperature sensing system, a lower atomisation temperature may give greater sensitivity. It was found in this system that, because of individual differences between graphite tubes, an atomisation temperature of up to 850°C could be used without significantly affecting sensitivity. These temperatures are in good agreement with atomisation temperatures used in earlier work involving atomisation from the tube wall [4, 5].

In this work, the temperature of the platform is taken from 300 to 800°C by radiative heating, and under these conditions the analyte is selectively atomised from the matrix. An initial high background absorbance peak, caused mainly by volatilisation of the remaining organic components of the urine matrix, is observed just before the cadmium signal. However, this peak is decreasing as the main analyte peak appears. Background absorption from inorganic salts present in the urine sample is not seen until the final clean-out at 2500°C. These effects are shown in Fig. 4. Hence, as the absorbance of cadmium is measured at a separate time from the main background interferences, these are no longer a limiting factor in the analysis, and cadmium in concentrated matrices can easily be measured after simple dilution of the sample. This relative freedom from background interferences means that gas-stop conditions can be used during atomisation, giving a significant improvement in sensitivity over previous methods. This, in turn, leads to improved

precision at the concentrations found in occupationally unexposed populations. To overcome residual matrix effects in the analysis of urine samples, it is necessary for peak area integration to be used in conjunction with the method of standard addition for each sample.

Under isothermal conditions, the residence time for each atom is the same, and although variations in matrix may affect peak width and so peak height, peak area remains unaffected [8, 9]. It is still necessary, however, that standard addition be used for measurement because of the large matrix variations between urine samples.

The method described has been successfully applied in the analysis of samples from both unexposed and exposed populations, having a concentration range of 0.1—164 $\mu g\ l^{-1}$. Samples with exceptionally high urinary cadmium levels simply require further dilution before spectrometry. The average concentration of cadmium in urine found in a known occupationally-unexposed population (n = 29) was 0.40 $\mu g\ l^{-1}$ (range 0.08—0.94 $\mu g\ l^{-1}$); these values are in good agreement with previous studies. By this method, one sample can be analysed in 20—30 min, and as there is no preliminary digestion or extraction, this is the total time required for analysis, so that 12—15 samples can be analysed per day. This technique provides a simple direct method for the determination of cadmium in urine with the added advantage that it lends itself readily to automated sampling.

REFERENCES

1 R. Lauwerys, in M. Webb (Ed.), The Chemistry, Biochemistry and Biology of Cadmium, Elsevier/North-Holland, New York, 1979, pp. 433—453.
2 R. G. Michel, M. L. Hall, J. M. Ottaway and G. S. Fell, Analyst, 104 (1979) 491.
3 O. Vesterberg and K. Wrangskogh, Clin. Chem., 24 (1978) 681.
4 C. F. Bruhn and G. A. Navarrete, Anal. Chim. Acta, 130 (1981) 209.
5 G. D. Carmack and M. Evenson, Anal. Chem., 51 (1979) 907.
6 E. Pruszkowska, G. R. Carnrick and W. Slavin, Clin. Chem., 29 (1983) 477.
7 M. J. Pinchin and J. Newham, Anal. Chim. Acta, 90 (1977) 91.
8 B. V. L'vov, Spectrochim. Acta, Part B, 33 (1978) 153.
9 F. J. Fernandez, M. M. Beaty and W. B. Barnett, At. Spectrosc., 2 (1981) 16.

Analytica Chimica Acta, 156 (1984) 139—145
Elsevier Science Publishers B.V., Amsterdam — Printed in The Netherlands

DETERMINATION OF SILVER IN SEA WATER BY COPRECIPITATION WITH COBALT PYRROLIDINEDITHIOCARBAMATE AND ZEEMAN GRAPHITE-FURNACE ATOMIC ABSORPTION SPECTROMETRY

N. S. BLOOM* and E. A. CRECELIUS

Battelle, Marine Research Laboratory, 439 West Sequim Bay Road, Sequim, WA 98382 (U.S.A.)

(Received 19th May 1983)

SUMMARY

A preconcentration technique is described for silver, which allows the precise and accurate determination of silver in sea water at nanogram per liter levels. Silver is co-precipitated with cobalt(II) pyrrolidinedithiocarbamate from 200-ml samples. The precipitate is dissolved in concentrated nitric acid and silver is quantified by Zeeman graphite-furnace atomic absorption spectrometry, with acid phosphate matrix modification. The detection limit is 0.1 ng l^{-1}. The method is simple and rapid, and also allows the simultaneous extraction of lead, copper, cadmium, and nickel.

In view of the possible toxicity [1—3] and enrichment [4—6] of silver in the marine environment, it is surprising that so little work has been done on establishing the concentration of silver in sea water. Earlier attempts to quantify silver in sea water have typically led to high values [7], inadequate detection limits [8], or noisy data. In response to the need for a simple and reliable method for accurately quantifying silver in sea water, the following technique was developed. The method represents a refinement of the co-precipitation procedure based on cobalt ions and ammonium pyrrolidine-dithiocarbamate (APDC), which was used by Boyle and Edmond [9, 10] to determine copper, cadmium, and nickel. The extraction parameters were optimized for silver using a radiotracer. Silver was quantified by graphite-furnace Zeeman atomic absorption spectrometry (a.a.s.). Several other metals, including lead, copper, cadmium, and nickel are co-extracted with silver, making the procedure economical for multielement quantitation.

EXPERIMENTAL

Reagents and solutions

Water used for the rinsing of glassware was deionized to a minimum of one megohm resistance. For reagent preparation and sample dilution, double-deionized water from a Millipore Super-Q reagent-water system (18 megohms resistance) was used. Acid used in the washing of glass and plasticware was

0003-2670/84/$03.00

6 M nitric acid (reagent grade). Ultra-high purity nitric acid was used in the preparation of reagents and samples.

Cobalt(II) nitrate solution. A solution containing 200 mg l^{-1} cobalt(II) was prepared by dissolving 200 mg of ultrapure cobalt wire (Ventron) in 5 ml of nitric acid, and diluting to 1 l with water.

Ammonium pyrrolidinedithiocarbamate (APDC) solution. A 2% (w/v) solution of APDC in water was purified by repeated extraction with carbon tetrachloride [10]. This solution was stored in a refrigerator when not in use.

Ammonium acetate buffer. A 4.5 M solution of ammonium acetate was prepared by the reaction of 500 ml of ultra-high purity acetic acid with 590 ml of ultra-high purity aqueous ammonia (28%), and dilution to 2.0 l with water.

Extract diluting solution. The digested precipitates were diluted to volume with a solution containing 0.2% (w/v) high-purity ammonium dihydrogenphosphate and 5% (v/v) nitric acid.

^{110m}Ag tracer. A stock solution containing 40 μCi ml^{-1} ^{110m}Ag and 9.4 mg l^{-1} total silver was prepared by diluting 2 mCi of ^{110m}Ag into 50 ml of 5% nitric acid. A working solution was prepared from this by diluting 2 ml of the stock to 100 ml with 5% nitric acid.

Acid-cleaned filters. The precipitate of cobalt with APDC was filtered through acid-cleaned, 47-mm, 0.4-μm polycarbonate membrane filters. The filters were always handled with acid-cleaned fluorinated polyethylene tongs.

Vials. The filters were digested and the solutions were diluted to volume in acid-cleaned 17-ml fluorinated polyethylene wide-mouth vials (Savillex, Minetonka, MN).

Instrumentation

Atomic absorption measurements were done with a Perkin-Elmer model Z-5000 graphite-furnace atomic absorption spectrometer, with Zeeman background correction. This system includes the HGA-500 furnace controller, Model 10 data station with HGA graphics and the AS-40 autosampler. The operating parameters are listed in Table 1. A hollow-cathode silver lamp was used, and the monochromator was set at 328.1 nm (0.7-nm slit width).

Radioactive decay of the ^{110m}Ag was counted on a Princeton Gamma-tech Ge(Li) detector, using the 658-keV photon peak. Peak separation and quantitation were achieved with a Canberra series 40 multichannel analyzer.

Preliminary work

Sea-water storage. Experiments to evaluate losses of silver to container walls during storage were done at pH values of 8.1, 1.9, and 1.6. Fresh, filtered sea water was placed in 2-l polyethylene bottles. The water in each bottle was brought to the desired pH with nitric acid, and then spiked with ^{110m}Ag equal to 1.0 μg l^{-1} total Ag. The bottles were stored at room temperature, with lights on for approximately 12 h per day.

TABLE 1

Furnace controller parameters for the graphite-furnace a.a.s. measurement of silver in sea-water extracts[a]

Step number	Ramp time (s)	Hold time (s)	Temperature (°C)	Gas flow	Recorder	Zeeman
1	10	0	80	300	off	off
2	50	5	130	300	off	off
3	25	5	250	300	off	off
4	20	15	750	300	off	off
5	0	3	1800[b]	0	on	on
6	1	4	2600	300	off	off

[a]Pyrolytic graphite cylindrical tube, argon purge gas, 25-μl sample. [b]Maximum-power mode of the Perkin-Elmer HGA-500.

Optimization of extraction parameters. The parameters were optimized using 100-ml aliquots of sea water (about 30‰ salinity) that had been spiked with ^{110m}Ag to contain 1.0 $\mu g\ l^{-1}$ total silver. The stock of this solution was kept acidified to pH 1.70, with pH adjustments being made on individual aliquots using the ammonium acetate buffer.

The coprecipitation reactions were carried out in 150-ml beakers, by the addition first of the cobalt solution, thorough mixing, and then addition of a 100-fold excess (mass basis) of APDC. Precipitates were vacuum-filtered through 0.4-μm membrane filters. The filters were placed in 60-ml polyethylene bottles with 5.0 ml of nitric acid to digest the precipitate, and then filled with water. The radioactive decay of these samples was counted to determine total silver recovered.

Recommended procedures

Sea-water samples were collected on the beach or offshore in 2-l polyethylene bottles. The samples are immediately acidified with 2.10 ± 0.05 ml of concentrated nitric acid; this brings the pH to 1.90 ± 0.05. In the laboratory, an aliquot of the sample is transferred to a 250-ml volumetric flask.

From each 250-ml sample, 50 ml is poured off and discarded, leaving 200 ml in the flask which serves as the reaction vessel. To each 200-ml sample is added 1.0 ml of cobalt(II) solution and 1.0 ml of APDC solution, with swirling after each addition to insure thorough mixing.

The samples are then filtered by suction through 47-mm acid-cleaned polycarbonate membrane filters (0.4 μm). The filters are rinsed with about 10 ml of water to remove salts, then folded into quarters, and placed in clean, dry 17-ml vials. To each filter is added 210 μl of concentrated nitric acid and the samples are evaporated to dryness under heat lamps. This digestion destroys the APDC complex, but leaves the polycarbonate filters intact, thus minimizing organic matrix interference in the atomic absorption measurements.

Reagent blanks are prepared by adding one filter, 1.0 ml of cobalt(II) solution, and 1.0 ml of APDC to a vial, and bringing to dryness, as for the samples. The blanks are digested with 420 μl of nitric acid, which represents the amount used to acidify the sea-water samples plus the amount used to digest the sample precipitates.

To the dried filters in the vials, 2.00 ml of the phosphate diluting solution are added. The lids are replaced and the samples are gently heated (70—80°C) to dissolve the metals on the filter. The samples are then stored in the vials until quantitation by graphite-furnace a.a.s. as outlined above.

RESULTS AND DISCUSSION

Sea-water storage conditions

As can be seen in Fig. 1, silver was not lost to container walls from sea water at pH <2.0 whereas losses from unacidified sea water were significant. This confirms the work of Massee et al. [11], Struempler's observation [12] that in distilled water, even acidified samples need shielding from light, does not appear to be true for sea water. It should be noted that, because of the low specific activity of the ^{110m}Ag tracer, it was necessary to work at total silver concentrations 1000-fold those of clean sea water. Thus, these results must be applied tentatively, until a carrier-free radiotracer can be obtained.

Optimization of extraction parameters

Because Boyle and Edmond [10] indicated that pH was the most important parameter for the extraction of several metals (Cd, Fe, Mn), this was the first condition to be optimized for silver. Recovery of ^{110m}Ag was monitored over a range of pH values from 1.70 to 5.50. These data, expressed as percent silver recovered, are illustrated in Fig. 2. At very low pH, the yield drops

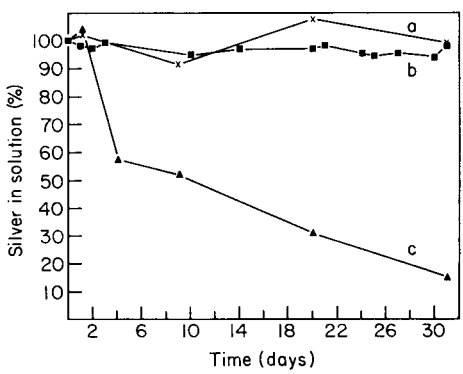

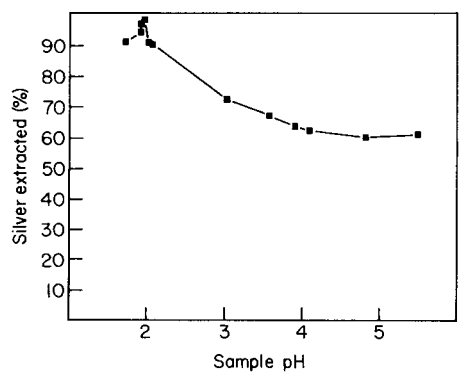

Fig. 1. Loss of ^{110m}Ag from sea water to the walls of acid-cleaned polyethylene sampling bottles as a function of time at different pH values: (a) pH 1.60; (b) pH 1.90; pH 8.10. Total silver concentration in each case was 1.0 μg l^{-1}.

Fig. 2. Extraction efficiency for ^{110m}Ag by the Co-APDC method, as a function of sample pH. Total silver concentration was 1.0 μg l^{-1}.

off, with a maximum yield at pH 1.8—2.0, followed by a rapid decrease with increasing pH.

The minimization of the amount of extraction reagents was also examined because of their potential contribution to the blank. Samples of filtered sea water, at pH 1.90, were spiked with silver (1.0 $\mu g\ l^{-1}$). Varying amounts of cobalt(II) ranging from 0.05 to 1.0 mg l^{-1} were added, along with a proportional 100-fold excess of APDC. The recoveries of silver increased sharply to about 88% as the amount of cobalt(II) was increased to 0.25 mg l^{-1} and then increased gradually to 92% at a cobalt(II) concentration of 1.0 mg l^{-1}. This concentration gave reproducible results (±10%) without admitting excessive amounts of reagents.

The other factors investigated in the optimization of this procedure were: (a) the time of precipitate ageing, from 5 min to 8 h; and (b) the rinse volume for the filters, from 0 to 100 ml of purified water. Neither of these factors influenced the yield of silver recovery to an observable extent.

Radiotracer experiments were also undertaken to ascertain whether the extraction technique was suitable for use over a wide range of silver concentrations. Samples were prepared in filtered Sequim Bay water containing 1.00, 0.1, and 0.010 $\mu g\ l^{-1}$ total silver. These were then extracted using the optimized parameters described above. The results showed consistent yields of 92—95% for all concentrations of silver in sea water.

Atomic absorption parameters

With the use of the 0.2% (w/v) ammonium phosphate matrix sample diluting solution, problems of variable peak shape and multiple peaks are eliminated. The conditions given in Table 1 represent the optimum in terms of precision, accuracy, and graphite tube lifetime for the Perkin-Elmer Z-5000 system. The length of the drying stage is dependent upon the sample volume, and is given for a 25-μl aliquot. Care must be taken that the drying ramp time is not too short as the phosphate matrix is quite prone to spattering at 120—140°C. The 1800°C atomization temperature is made possible by the maximum-power mode of the furnace controller. For an ordinary atomization step, a temperature of 2400°C would be appropriate for this matrix.

In this work, all measurements were done using long-lasting pyrolytic graphite tubes, prepurified argon purge gas, and Zeeman background correction. Under the conditions recommended and with this matrix, repetitive firings of the same sample varied by less than 5%. The linear range was well over 1.0 absorbance. All standards were run by the method of standard additions on the blanks. Under such conditions, a 25-μl sample containing 10 $\mu g\ l^{-1}$ silver gave an absorbance of approximately 0.700.

Application, precision and detection limits

Table 2 summarizes typical results of the complete procedure. The samples were made from clean, unfiltered water from Sequim Bay, Washington. A sample of the water was acidified to pH 1.90 ± 0.05, and divided into three

TABLE 2

Quantitation of silver in spiked sea water by the proposed method

Sample	N	Ag (ng l^{-1})[a]		Yield (%)
		$\bar{x}$	s	
Blanks	5	0.11	0.04	—
Sequim Bay water	3[b]	0.63	0.12	—
SBW + 10 ng l^{-1}	5	10.74	0.29	99.8
SBW + 100 ng l^{-1}	4	94.0	7.9	93.2

[a]Mean of N measurements with standard deviation. [b]Two obviously contaminated values of 5.94 and 1.57 were omitted.

aliquots. One aliquot was spiked with 0.01 μg l^{-1} silver and another with 0.1 μg l^{-1} silver. All three aliquots were then allowed to equilibrate overnight before extraction.

The detection limit is 0.2 ng l^{-1} based on twice the standard deviation of samples near the detection limit. If twice the standard deviation of the blank is taken as the criterion, the detection limit is 0.1 ng l^{-1}. At all levels measured, more than 90% of the silver was recovered with a precision of better than 10%.

Environmental samples. Samples from a variety of Pacific Northwest locations were processed as described above. The data for some of these are summarized in Table 3. Three types of coastal water, as well as the open ocean, are represented in these data. Sequim Bay is a rural area on the well flushed Strait of Juan de Fuca, Elliott Bay is the major harbor for the city of Seattle, and the marina in Tacoma represents a unique local environment, as it is built with slag from a copper smelter. The three depth "profiles" taken in the northeast Pacific shows an increase in silver with depth from about 0.3 ng l^{-1} to 5.8 ng l^{-1}. This trend is essentially identical to two other profiles taken in the same area in the last two years by Battelle.

TABLE 3

Silver concentrations in selected marine samples

Date	Location	Depth	N	Silver (ng l^{-1})	
				$\bar{x}$	s
11-23-82	Sequim Bay	10 cm	3	0.63	0.12
9-13-82	Elliott Bay	10 cm	2	10.0	—
1-6-82	Tacoma (Marina)	10 cm	2	108.0	—
1-20-82	Tacoma (Marina)	10 cm	1	19.0	—
3-3-82	Tacoma (Marina)	10 cm	2	13.5	—
2-12-82	N.E. Pacific Ocean	50 m	3	0.30	0.10
2-12-82	N.E. Pacific Ocean	300 m	2	0.60	—
2-13-82	N.E. Pacific Ocean	3237 m	2	5.82	—

The recent work of Martin and Knauer (personal communication) in the northeast Pacific ocean shows a similar trend for a more detailed profile over the same range.

This work was supported by the U.S. Department of Energy under Contract No. DE-AC06-76RL0 1830. We thank R. A. Feely and G. J. Massoth of NOAA-PMEL for collection of the ocean water samples.

REFERENCES

1 A. Calabrese, R. S. Collier, D. A. Nelson and J. R. MacInnes, Mar. Biol., 18 (1973) 162.
2 D. A. Nelson, A. Calabrese, B. A. Nelson, J. R. MacInnes and D. R. Wenzloff, Bull. Environ. Contam. Toxicol., 16 (1976) 275.
3 A. Calabrese, F. P. Thurberg and E. Goud, Mar. Fish. Rev., 39 (1977) 5.
4 U. Förstner, Chemistry and Biogeochemistry of Estuaries, Wiley-Interscience, New York, 1980, p. 322.
5 G. P. Hershelman, H. A. Schafer, T. K. Jan and D. R. Young, Mar. Pollut. Bull., 12 (1981) 131.
6 R. A. Greig, R. N. Reid and D. R. Wenzloff, Mar. Pollut. Bull., 8 (1977) 183.
7 M. G. Lai and H. V. Weiss, Anal. Chem., 34 (1962) 1012.
8 H. Armannsson, Anal. Chim. Acta, 110 (1979) 21.
9 E. A. Boyle and J. M. Edmond, Anal. Chim. Acta, 91 (1977) 189.
10 E. A. Boyle and J. M. Edmond, Analytical Methods in Oceanography, American Chemical Society, Washington, DC, 1975, p. 44.
11 R. Massee, F. J. M. J. Maessen and J. J. M. de Goeij, Anal. Chim. Acta, 127 (1981) 181.
12 A. W. Struempler, Anal. Chem., 45 (1973) 2251.

Analytica Chimica Acta, 156 (1984) 147—157
Elsevier Science Publishers B.V., Amsterdam — Printed in The Netherlands

DETERMINATION OF TIN AND METHYLTIN SPECIES BY HYDRIDE GENERATION AND DETECTION WITH GRAPHITE-FURNACE ATOMIC ABSORPTION OR FLAME EMISSION SPECTROMETRY

MEINRAT O. ANDREAE* and JAMES T. BYRD
Department of Oceanography, Florida State University, Tallahassee, FL 32306 (U.S.A.)
(Received 13th July 1983)

SUMMARY

A method for the determination of tin and organotin species by hydride generation is described. Tin hydrides are detected by graphite-furnace atomic absorption, quartz-cuvette atomic absorption, or flame emission spectrometry with detection limits of 50, 50, and 20 pg as tin, respectively. Germanium interferences are eliminated with a dual-detector flame photometer with an electronic cancellation circuit.

Tin species in natural waters are generally present at concentrations less than 10 parts per trillion (ng l^{-1}) [1—3]. Quantitation of such trace quantities requires a method that either has extremely low detection limits [1] or involves a preconcentration step [4]. Direct quantitation is preferred because this minimizes the problems of changes in distribution of species and sample contamination, a particularly severe problem with tin.

This paper describes an application of the hydride generation technique coupled with cryogenic trapping and separation to the determination of tin species in natural waters. Inorganic tin, monomethyltin, dimethyltin, and trimethyltin, which are present in aqueous solution as cations or hydroxide complexes, are reduced to the corresponding stannanes with sodium tetrahydroborate. The stannanes are stripped from solution by a helium stream and are trapped at liquid nitrogen temperatures on a chromatographic packing. The trap is then warmed and the stannanes are eluted in order of increasing boiling points. Detection is by one of three methods: quartz cuvette atomic absorption [5], modified graphite furnace atomic absorption [6], or flame photometry [1].

Possible interferences in the flame photometric detector are quantified with respect to their relative importance. A method is given for the simultaneous determination of germanium and reduction of germanium interference in the determination of tin.

0003-2670/84/$03.00

EXPERIMENTAL

Apparatus

The apparatus for the volatilization and trapping of the stannanes is shown in Fig. 1. The reaction vessel is constructed of pyrex glass with a 29/42 ground glass connection for loading the samples into the vessel. Helium enters the vessel through a fritted glass bubbler held in place by a section of 0.25-in. o.d. teflon tubing. The sodium tetrahydroborate is introduced by injection with a polyethylene syringe and a stainless steel needle through a teflon-backed silicone septum held in a teflon Swagelok union.

After the reaction vessel, water vapor is removed from the sample stream by passing it through a pyrex U-tube (7-mm i.d., 28-cm long) which is immersed in a bath of isopropanol. The alcohol is cooled to less than —30°C with a refrigeration probe or with dry ice. The trap for the collection of the stannanes is a 30-cm U-tube of 6-mm o.d. pyrex glass. This tube is filled with 15% OV-3 silicone oil on 60/80 mesh Chromosorb W-AW-DMCS. The trap is wrapped with approximately 0.5 m of Chromel wire (2.3 Ω) which is connected to a variable transformer set at 4.4 V. The outlet of the trap is connected to the detector.

Glass surfaces are deactivated by silylation with 5% dimethyldichlorosilane in toluene (Sylon CT, Supelco, Bellefonte, PA). This deactivation is necessary to prevent tailing of the stannane peaks.

The atomic absorption detector with a quartz cuvette is identical to that described earlier [5]. A quartz tube, 9-mm i.d. and 7-cm long, is held in the beam path of the atomic absorption spectrophotometer by a stainless steel support. Air is introduced through an inlet in the back. A branched inlet in the front introduces both the sample stream and hydrogen, which are mixed before entering the burner. A tin atom population is created by

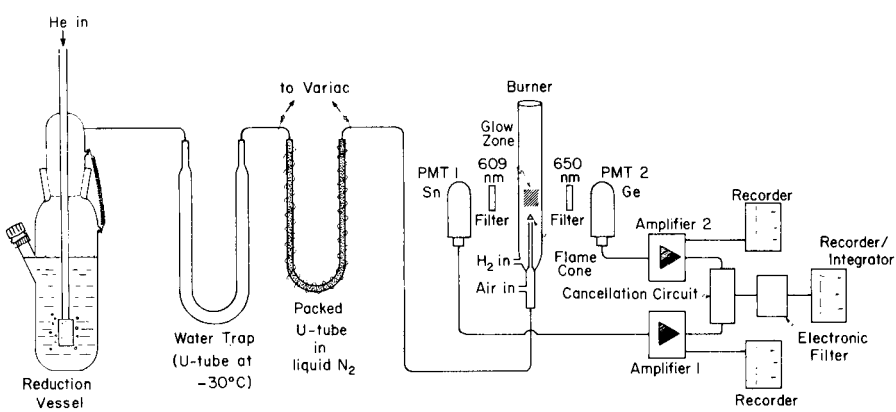

Fig. 1. Hydride generation apparatus and dual-channel photometric detector.

the hydrogen-rich flame burning in the tube. Gas flows were 90 ml min^{-1} helium, 200 ml min^{-1} air, and 330 ml min^{-1} hydrogen.

A Perkin-Elmer HGA-400 graphite furnace was modified as reported earlier [6]. The hydride generation system is connected to the internal purge opening of the graphite furnace by a 1-mm i.d. thick-walled tube. The sample stream is mixed with argon before entering the graphite furnace. Gas flows were set at 100 ml min^{-1} helium and 70 ml min^{-1} argon.

Both the quartz-cuvette and graphite-furnace detectors were used with a Perkin-Elmer 5000 atomic absorption spectrometer. The light source was a Perkin-Elmer electrodeless discharge lamp run at 8 W. The lamp was used at a wavelength of 224.7 nm with a slit width of 0.2 nm.

The flame photometric detector (Fig. 1) is similar to that described by Braman and Tompkins [1]. The burner is made of quartz tubing. The sample stream and air enter through 7-mm o.d. tubing and mix before passing through the 4-mm o.d. burner jet. The hydrogen enters through 7-mm o.d. tubing into the 9-mm o.d. burner jacket. The burner is held in an aluminum housing by a 5/8-in. Swagelok to 3/8-in. pipe thread fitting that has been bored to accept the burner. Teflon ferrules are used in the Swagelok fitting. Stray light is eliminated by blacking the burner connections and enclosing the top of the burner in a bag of black photographic cloth. Light from the flame passes through an interference bandpass filter centered on 610 nm (8-nm bandwidth; Pomfret Research Optics, Stamford, CT). The burner housing and filter are mounted on a photomultiplier module (EMI-Gencom model S-HSG) with a Hamamatsu R928 photomultiplier tube set at 700 V. The signal from the photomultiplier module is amplified with a Pacific Instruments model 3A27 electrometer.

The germanium emission signal is measured with an identical system placed 180° from the tin detector. Here the interference filter is centered on 650 nm with an 11-nm bandpass. After amplification, the germanium signal is electronically subtracted from the tin signal. Inorganic germanium standards were used to establish the correct amplification of the germanium signal for a one-to-one subtraction of the germanium peaks from the tin signal. Flame noise is filtered from the background-corrected signal with a Spectrum model 1021A electronic filter with a cut-off frequency of 0.05 s. The filtered signal is then integrated with a Hewlett-Packard model 3390A electronic integrator/recorder. Both the unfiltered, uncorrected tin signal and the germanium signal are recorded on a Houston Instruments dual-pen recorder.

Standards and reagents

Inorganic tin standards were prepared by dissolving 0.19 g of $SnCl_2 \cdot 2H_2O$ (Baker Analyzed Reagent) in 10 ml of concentrated hydrochloric acid, adding 8 g of citric acid, and diluting to 100 ml. This solution contains 1000 mg l^{-1} tin and is stable for over one month. Serial dilutions in 1 M nitric acid are made daily.

Methyltin chloride standards (Alfa-Ventron, Danvers, MA) were prepared to contain 1000 mg l^{-1} tin in deionized water and kept refrigerated. These standards are stable for up to six months. Serial dilutions of these stock solutions are prepared as needed.

Sodium tetrahydroborate (Fisher Scientific, Pittsburgh, PA) is dissolved in quartz-distilled water (Q-water) to make a 4% solution. The inorganic tin blank in the sodium tetrahydroborate is reduced significantly by adding 1 ml of 2 M sodium hydroxide to 100 ml of the tetrahydroborate solution and letting the reagent stand overnight to allow the tin to adsorb to the container walls. The sodium hydroxide solution must be precleaned by coprecipitation with lanthanum nitrate as described by Lee [7].

Water containing low concentrations of tin was prepared by distilling deionized water in a subboiling quartz still (Quartz et Silice, Paris). The outflow of the still was piped to a polyethylene carboy without contact with room air. This Q-water can be prepared with undetectable tin blanks.

The lowest tin blanks in acid were found in nitric acid which was double-distilled in Vycor (G. F. Smith, Columbus, OH). The concentrated acid was diluted to 5 M with Q-water.

Methods

The reaction vessel is filled with 100 ml of sample and is acidified to pH 2 with 0.2 ml of 5 M nitric acid. The air and volatile gases in the sample are sparged for 2—12 min, shorter times for distilled water, longer times for samples containing large amounts of dissolved carbon dioxide. The stannane trap is immersed in liquid nitrogen and 1 ml of the tetrahydroborate solution is injected with a plastic syringe and a disposable stainless steel needle. During this injection, the air flow is boosted to 200 ml min^{-1} by using a by-pass valve arrangement. This is necessary to prevent extinction of the flame by the surge in hydrogen pressure generated by the reaction. The air flow is returned to normal several minutes before removal of the liquid nitrogen to allow the baseline to stabilize. After reacting for 6—8 min, the liquid nitrogen is removed and the variable transformer is switched on (4.4 V, 1.9 A). The recorder and/or integrator is started and the detector output(s) recorded. In the case of the graphite furnace, a 60-s atomization burn is initiated simultaneously with the removal of the liquid nitrogen.

RESULTS AND DISCUSSION

All detection limits and concentrations are quoted in terms of the tin content of samples.

Hydride generation

Buffering. The yield of stannanes from solution is greatest in the pH range 5—7. As seen in Fig. 2, 0.02 M acetic acid, 0.01 M nitric acid, and 0.01 M Tris/HCl all gave good response. Tris/HCl, as used by Braman and Tompkins

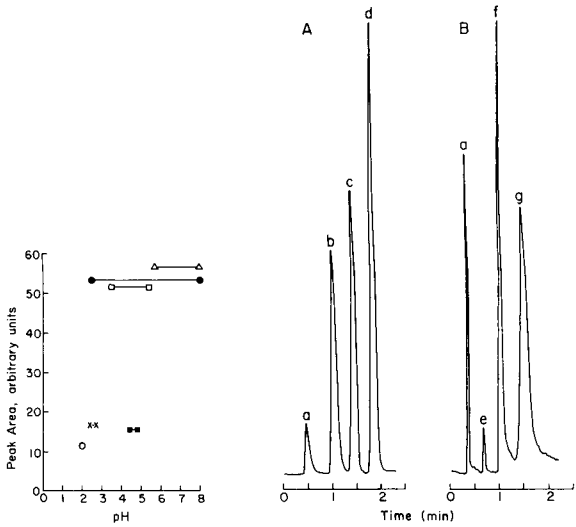

Fig. 2. Influence of pH on the reduction efficiency for 1 ng of tin in 100 ml of Q-water. Buffer systems: (•) 0.01 M HNO_3; (△) 0.01 M Tris/HCl; (□) 0.02 M acetic acid; (×) 0.01 M oxalic acid; (▪) 0.05 M potassium hydrogenphthalate; (○) 0.1 M HNO_3.

Fig. 3. (A) Chromatographic peaks for separation of stannane and the methylstannanes on 15% OV-3 on Chromosorb W-AW DMCS, 60/80 mesh, 30 cm. (B) Separation of butylstannanes on silanized glass wool. Peaks: (a) Sn(IV); (b) $(CH_3)SnH_3$ (1.0 ng); (c) $(CH_3)_2SnH_2$ (1.0 ng); (d) $(CH_3)_3SnH$ (1.6 ng); (e) $BuSnH_3$; (f) Bu_2SnH_2 (10 ng); (g) Bu_3SnH (10 ng).

[1], gave the best response, but had a large reagent blank. Tin blanks in Tris/HCl can be reduced by lanthanum hydroxide coprecipitation, but blanks still remain unacceptably high. Acetic acid in the same concentration used by Hodge et al. [2] gave almost identical response to 0.01 M nitric acid. Nitric acid was chosen as the preferred buffer because it is easier to purify and because the initial pH is lower than acetic acid. This reduces hydrolysis of the tin species and loss to container walls. Under these reaction conditions, there is no differentiation between Sn(II) and Sn(IV), as both are equally reduced to stannane.

Blank determination. Because of the presence of trace amounts of tin in reagents, great care must be taken in measuring the tin blank. The amount of tin added with the nitric acid and sodium tetrahydroborate is measured by adding increasing amounts of each reagent and determining the slope of the response to increasing reagent concentrations. A typical blank using purified sodium tetrahydroborate and ultra-pure nitric acid is 30 pg per determination. However, this number varies with the reagent batch and distilled water batch used and must be determined daily.

Trapping and separation. For the stannane trap, 15% OV-3 on Chromosorb W-AW-DMCS was chosen because it collects the stannanes without

irreversible adsorption losses and gives good separation of the stannane and methylstannane peaks. As CO_2 was an interferent in the flame photometric system, a fully packed 30-cm trap was used to separate CO_2 from stannane. The trap was heated slowly by applying 4.4 V across the Chromel wire wrapping. A typical chromatogram is shown in Fig. 3A. Although monobutyltin is detected using the OV-3 Chromosorb trap, the other butyltins do not elute from this packing. These butyltins can be quantified by using a trap packed with silanized glass wool (Fig. 3B).

As the atomic absorption systems have no CO_2 interference, the trap is only half-packed with the OV-3 Chromosorb and heated at a faster rate (12 V). The water trap can then be omitted.

Atomic absorption with the quartz cuvette. Samples with large concentrations of dissolved carbon dioxide are difficult to process with the flame photometric system because of spectral interference. The atomic absorption system with a quartz cuvette used earlier for the determination of arsenic [5] was therefore investigated. This system gave good results for inorganic tin, with detection limits of the order of 50 pg. This is an improvement of almost an order of magnitude over the detection limits found by Hodge et al. [2] with a similar system. However, a set of unidentified peaks eluted along with each methyltin, interfering with the quantitation of the other methyltins. These spurious peaks rendered this method useless for methyltin determination. For this reason, the quartz-cuvette burner was abandoned in favor of the graphite furnace, which does not produce these spurious peaks.

Graphite furnace

Temperature selection. Peak-height response with varying atomization temperature was determined. As seen in Fig. 4, the response increases rapidly with increasing temperature, reaches a maximum at 2500°C, then drops only slightly with increasing temperature. Because the life of the graphite tube is shortened by high furnace temperatures, a temperature of 2450°C was selected, within the plateau region of the curve.

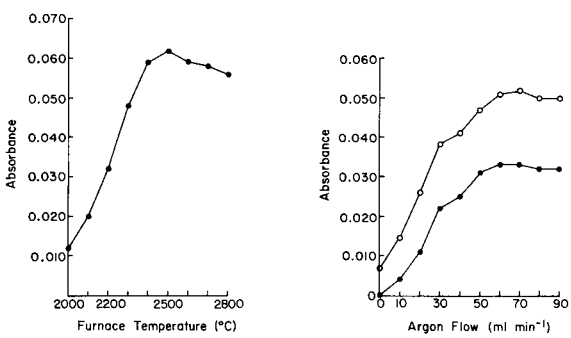

Fig. 4. Effect of furnace temperature on peak absorbance of 3 ng (as Sn) of tetramethyltin.

Fig. 5. Effect of argon flow on peak absorbance of 3 ng (as Sn) of tetramethyltin with helium flows of 50 ml min^{-1} (•) and 100 ml min^{-1} (○).

Carrier gas composition. It is necessary to use helium as the carrier gas, because other gases such as argon would condense in the liquid nitrogen trap. However, helium decreases the sensitivity of the graphite-furnace atomic absorption and causes rapid destruction of the graphite tube; argon is therefore mixed into the gas stream immediately ahead of the furnace. Peak height responses with different argon/helium mixes are plotted in Fig. 5. From these data, gas flows of 100 ml min^{-1} helium and 70 ml min^{-1} argon were chosen. Use of greater helium flow rate leads to a loss of peak separation.

Sensitivity, detection limits, and linearity. The sensitivity of this system (in terms of absorbance) is 0.034 ng^{-1}. This is about four times less sensitive than direct injection of aqueous standards with stopped flow (0.126 ng^{-1}). This loss of sensitivity is due to the need for continuous helium flow and the resulting peak broadening.

Baseline noise levels correspond to an absorbance of 0.0010. This yields a noise-limited detection limit of 50 pg. The stannane calibration graph is linear from the detection limit to 50 ng (0.630 absorbance). This gives a working range of 0.5—500 ng l^{-1} with a 100-ml sample.

Flame photometric detection

The flame photometric detection of tin is based on the molecular emission by the diatomic species SnH which is formed in a highly reducing hydrogen/air flame. This emission has a bandhead at 609.5 nm and overlaps slightly with a GeH emission band with a bandhead at 615 nm. In addition, GeH has an emission band near 650 nm [8]. The spectral overlap between the SnH and GeH band leads to a substantial interference in the determination of tin in natural waters if no background correction system is used.

Signal optimization. Gas flows and burner position were optimized by repeated injections of approximately 1 ng of gaseous tetramethyltin. The optimum burner position was found to be where the burner jet tip was even with the bottom of the interference filter. Flame noise decreases with a decrease in gas flows, but a compromise has to be made between the level of noise and the stability of the flame. Gas flows used were 75 ml min^{-1} helium, 85 ml min^{-1} air, and 270 ml min^{-1} hydrogen. A two-fold improvement in the signal-to-noise ratio results from the addition of the electronic filter.

Detection limits and precision. Detection limits for inorganic tin are limited by the variation in the blank determination. The detection limit with the flame photometric detector, defined as twice the standard deviation of the blank, is 20 pg. Detection limits for the methyltins, defined as twice the baseline noise, are 15 pg.

Calibration graphs for the tin species are linear from the detection limits to 10 ng. With a 100-ml sample, this gives a working range of 0.15—100 ng l^{-1}. This range covers all natural water samples except those from extremely polluted sources.

Precision of the method was calculated at the 2 ng l^{-1} level with replicate measurements. The relative standard deviation for six samples was 4%.

Detector selection

Selection of the graphite-furnace atomic absorption detector or the flame photometric detector depends on the nature of the sample. The furnace method provides higher detection limits than the flame photometric detector, but is useful for highly polluted samples, as the linear working range is almost an order of magnitude higher than for the flame emission detector. The graphite-furnace detector is also useful for samples with large background interferences, such as digested sediment or aerosol samples.

The flame photometric detector is most useful for unpolluted samples, because the concentrations of the methyltins are generally at or below the limits of detection. The portability of the flame system makes possible analysis in the field, eliminating the need for long storage times. The system has been used at sea on several cruises with excellent results [3].

A great advantage of the flame-photometric dual-channel system is the ability to determine both tin and germanium simultaneously. Inorganic germanium is easily quantified from the output of the 650-nm channel, with a detection limit of about 50 pg. Results obtained with this system compare well with the results for the same samples by hydride-generation/graphite-furnace a.a.s. [6]. Organic germanium compounds have been quantified, but optimum reaction conditions for tin are not the same as those for the methylgermanium compounds.

Interferences

The hydride-generation process can be inhibited by high concentrations of several metals [1] as well as by volatile nitrogen oxides [9]. To test for the presence of such interferences, standard additions of tin were made to sea water. No reduction in sensitivity was detected as compared to Q-water.

Possible interferences in the flame emission system are dissolved gases such as carbon dioxide, hydrocarbons, and sulfur gases. Selectivity ratios, the amount of substance in question that is necessary to give the same response as 1 ng of tin, are listed in Table 1. Even though tin is at least two orders of magnitude more sensitive than these compounds, care must be taken with natural samples, because these compounds can be found in concentrations many orders of magnitude greater than the tin concentrations. Without the germanium channel, the detector is not suitable for the direct quantitation of dissolved volatile tin hydrides in natural waters using a purge and trap technique. In contrast, when the hydrides are produced by reduction with tetrahydroborate from nonvolatile, ionic, or hydrolyzed species, these interferences are relatively easy to overcome in most samples by increasing the sparging time before reduction.

One compound that cannot be removed by sparging is dimethylsulfoxide

TABLE 1

Selectivity ratios and ratios of the emission intensities at 610 and 650 nm of selected compounds

Compound	Selectivity[a]	610/650 nm ratio
Inorganic tin	1.0	4.5
Inorganic germanium	—	0.16
Methane	Not trapped	—
Ethane	7×10^5	0.49
Carbon dioxide	34×10^6	0.56
Carbon disulfide	224	0.70
Dimethylsulfide	443	0.70
Carbonyl sulfide	302	0.72

[a]Mass (ng) of substance that gives response equivalent to 1 ng of tin.

(DMSO). However, DMSO can be reduced to dimethylsulfide by reduction with tetrahydroborate [10]. As seen in Table 1, dimethylsulfide is a relatively strong interferent in the flame detector. However, under the reaction conditions used here, the reduction of DMSO is not very efficient. It is therefore a problem only when present in large concentrations, such as in highly productive waters [11].

As indicated above, germanium compounds can be a very serious interference in the determination of tin. This is especially true for the methylgermanium compounds, which are found in many natural samples and which elute with retention times very similar to those of the methyltin compounds. This makes the differentiation of methyltin and methylgermanium peaks virtually impossible with a single-channel system.

The dual-channel system turns these liabilities into an advantage. By measuring the output of each channel as well as the corrected signal, the compound can be identified by the ratio of its responses on each channel. These ratios for tin, germanium, and the most commonly found dissolved gases are shown in Table 1. Thus an eluting peak can be identified by a combination of retention time and this characteristic response ratio.

Accuracy

In the absence of certified standard reference materials for tin species in natural waters, the accuracy of the method described here is difficult to evaluate. In order to reduce the possibility of systematic errors, calibration should be done by addition of known amounts of tin standards to a water matrix similar to the sample. In order to check for systematic differences between the three procedures described in this paper, a sea-water sample to which known amounts of mono-, di-, and trimethyltin salts (10 ng Sn l^{-1} for each species) had been added (Table 2) was taken through the procedures. For inorganic tin, the differences between the results of the three methods are near the precision and not greater than the typical day-to-day

TABLE 2

Comparison of the determination of tin species in sea water with three different methods (Known amounts of mono-, di-, and trimethyltin (10 ng l^{-1} each) were added to the sample. The results are given as ng l^{-1} tin)

Detector	Inorganic tin	Methyl-tin	Dimethyl-tin	Trimethyl-tin
Quartz furnace	3.65 ± 0.15	—	—	—
Graphite furnace	3.84 ± 0.23	8.8 ± 0.3	8.6 ± 0.7	11.4 ± 1.4
Flame photometric	3.43 ± 0.12	10.0 ± 0.2	10.5 ± 0.3	10.5 ± 0.4

variability of replicate runs on the same sample with the same method. For the organic species, the results were within ±15% of the known concentration with the graphite furnace method and within ±5% for the flame emission procedure.

Sample acquisition and storage

One must exercise care when taking samples not to use any material containing poly(vinyl chloride). Organotins used as plasticizers in this material leach out, contaminating the sample with inorganic tin and all of the methyltins and butyltins. Polyethylene, teflon, or polycarbonate are the preferred sampler materials.

Storage of environmental samples also presents a problem. Samples should be filtered as soon as possible to avoid large losses of tin to particles (up to 40% over several hours) and subsequent desorption of tin from particles. Samples can be filtered with no detectable contamination through

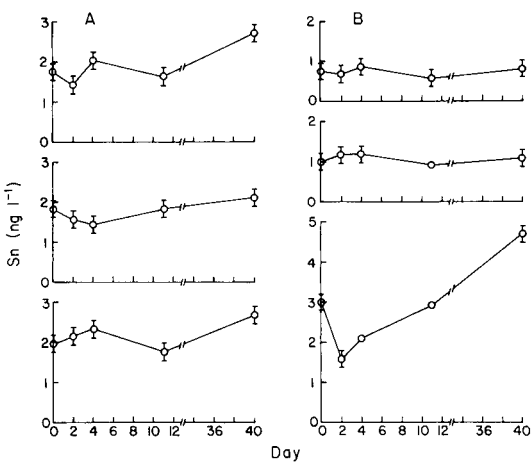

Fig. 6. Effect of storage on the concentration of inorganic tin found in sea-water samples by the flame photometric method. (A) Filtered samples, no acid added. (B) Samples filtered and acidified to pH 2 with nitric acid.

acid-washed 0.45-μm Millipore HAWP filters in a Sartorius polycarbonate pressure filtration vessel.

Long-term storage of sea-water samples was tested by preparing six 2-l splits of Gulf Stream water sample. These samples were filtered, three of the six samples were acidified, and all were subdivided into 250-ml aliquots in acid-washed linear polyethylene bottles. The results for tin in these subsamples after storage are shown in Fig. 6. The samples which were acidified to pH 2 with nitric acid gave poorly reproducible results and showed suppression of the tin signal which is probably due to volatile reaction products between the nitric acid and naturally occurring organic compounds in the samples [9]. Analysis of variance of the data from the unacidified samples showed that no significant change had occurred during storage of up to 11 days, but suggested an increase of some 30% in inorganic tin concentration after 40 days storage. This may be due to leaching of tin from the container walls or to breakdown of colloid forms of tin. In all cases, samples should be processed as soon as possible after collection.

We are grateful to A. P. Woodard and D. Hunley for help with the design and construction of parts of the apparatus. This work was supported in part by National Science Foundation grants OCE-7920183 and OCE-8200931.

REFERENCES

1 R. S. Braman and M. A. Tompkins, Anal. Chem., 51 (1979) 12.
2 V. F. Hodge, S. L. Seidel and E. D. Goldberg, Anal. Chem., 51 (1979) 1256.
3 J. T. Byrd and M. O. Andreae, Science, 218 (1982) 565.
4 J. A. Jackson, W. R. Blair, F. E. Brinckman and W. P. Iverson, Environ. Sci. Technol., 16 (1982) 110.
5 M. O. Andreae, Anal. Chem., 49 (1977) 820.
6 M. O. Andreae and P. N. Froelich, Jr., Anal. Chem., 53 (1981) 287.
7 D. S. Lee, Anal. Chem., 54 (1982) 1682.
8 C. G. Flinn and W. A. Aue, J. Chromatogr., 186 (1979) 299.
9 R. M. Brown, Jr., R. C. Fry, J. L. Moyers, S. J. Northway, M. B. Denton and G. S. Wilson, Anal. Chem., 53 (1981) 1560.
10 M. O. Andreae, Anal. Chem., 52 (1980) 150.
11 M. O. Andreae, Limnol. Oceanogr., 25 (1980) 1054.

Analytica Chimica Acta, 156 (1984) 159—168
Elsevier Science Publishers B.V., Amsterdam — Printed in The Netherlands

DETERMINATION OF TRACE LEVELS OF HEAVY METALS IN WATERS BY EXTRACTION WITH AMMONIUM TETRAMETHYLENEDITHIOCARBAMATE AND HEXAMETHYLENEAMMONIUM HEXAMETHYLENEDITHIOCARBAMATE INTO XYLENE FOLLOWED BY INDUCTIVELY-COUPLED PLASMA EMISSION SPECTROMETRY

HIROAKI TAO*, AKIRA MIYAZAKI, KENJI BANSHO and YOSHIMI UMEZAKI

National Research Institute for Pollution and Resources, Yatabe, Ibaraki 305 (Japan)

(Received 4th March 1983)

SUMMARY

The determination of Cd, Co, Cr, Cu, Fe, Mn, Mo, Ni, Pb, V and Zn in river and sea water by inductively-coupled plasma emission spectrometry after extraction with a mixture of ammonium tetramethylenedithiocarbamate (APDC) and hexamethyleneammonium hexamethylenedithiocarbamate into xylene is described. All these elements are simultaneously concentrated 100-fold in a single extract and directly introduced into the plasma. The pH dependences of the extraction and the stabilities of the complexes are reported. The limits of detection of the method range from 0.017 ng ml^{-1} (cadmium) to 0.5 ng ml^{-1} (lead). With 100-fold concentration factors, calibration graphs are linear up to 30 ng ml^{-1} or more.

Determination of traces of heavy metals in natural waters is important because these elements play important roles in the aquatic environment. Inductively-coupled plasma emission spectrometry (i.c.p.e.s.) has been widely used for this purpose. However, it has been reported that preconcentration techniques such as liquid-liquid extraction [1—3], coprecipitation and flotation [4] or resin chelation [5] are necessary for the determination of trace elements in natural water.

Liquid-liquid extraction is superior to other methods because of its simplicity, speed and low blank levels. For simultaneous multi-element analysis, a chelating agent which can complex with as many of the required metals as possible under the same conditions is most suitable for i.c.p.e.s. In addition, organic solvents which can be directly introduced into the plasma are preferable to save time in sample preparation. Diethyldithiocarbamate (DDC) [1], ammonium pyrrolidinedithiocarbamate (APDC) [2] and combinations of these [3] have been applied with i.c.p.e.s. An APDC-8-quinolinol combination has been proposed for atomic absorption spectrometry [6]. However, these combinations have the common disadvant-

0003-2670/84/$03.00

ages that manganese is not extracted with the other metals and the pH dependences of molybdenum and vanadium extraction tend to be critical. Determination of these elements is useful for evaluation of aquatic environments, because these metals are biochemically and geochemically important.

The aim of this work was to develop a modified extraction system with a combination of chelating reagents and organic solvent for the rapid simultaneous multi-element determination of trace elements in natural water. The best mixture found was ammonium tetramethylenedithiocarbamate (pyrrolidinedithiocarbamate, APDC) and hexamethyleneammonium hexamethylenedithiocarbamate (HMAHMDC).

EXPERIMENTAL

Instrumentation

The i.c.p.e.s. instrument and its operating conditions are described in Table 1. The spectrometer was equipped with 14 fixed slits and a movable slit. It was also capable of selecting different wavelengths by changing the angle of the grating. Because the spectrometer used was not equipped with fixed slits for cobalt and nickel, these emission line intensities were measured by changing the angle of the grating so that the Ni 221.65-nm line entered the fixed slit for the Cd 226.50-nm line and the Co 238.89 nm line entered the movable slit, after the simultaneous measurements of other elements.

Reagents

Distilled-deionized water was used throughout. Diisobutyl ketone (DIBK) and xylene were shaken twice with nitric acid in a separatory funnel and then washed 3 times with water. Aqueous solutions of APDC (Wako Pure Chemicals Co.) and sodium DDC (Wako) were shaken with DIBK to remove contaminating metals. Hexamethyleneammonium hexamethylenedithiocarbamate (HMAHMDC; Tokyo Kasei Co.) was dissolved in methanol. An aqueous solution of 8-quinolinol (Wako) was also prepared. The HMAHMDC and 8-quinolinol solutions were used without purification, because these chelating reagents were dissolved in DIBK if the aqueous solutions were to be shaken with DIBK. An ammonium acetate—acetic acid buffer solution was used for pH 3.2—6.2 and an ammonium phosphate buffer for pH 6.3—8.2. The buffer solutions were purified by a double extraction with the mixture of APDC and HMAHMDC into xylene.

Stock solutions (1000 μg ml^{-1}) of the elements except for molybdenum and chromium(VI) were prepared by dissolving the high-purity metals and oxides in nitric acid so that the final acid concentration was 0.1 M. Molybdenum and chromium(VI) stock solutions (1000 μg ml^{-1}) were prepared by dissolving ammonium molybdate and potassium dichromate in water. Multi-element working standard solutions were prepared from single-element stock solutions by appropriate mixing and dilution.

TABLE 1

Instrumentation and operating conditions

Plasma source	Shimadzu ICPS-2H	
Operating frequency	27.12 MHz, crystal controlled	
Load coil	2-turn copper tubing with teflon coating	
Nebulizer and spray chamber	Glass pneumatic nebulizer (concentric type) into dual-tube spray chamber	
Plasma torch assembly	Fused quartz with capillary injector	
Spectrometer	Shimadzu GEW 170, 1.7-m Ebert	
Grating	2160 lines mm^{-1}	
Entrance slit-width	30 μm	
Exit slit-width	50 μm	
Reciprocal linear dispersion	0.26 nm mm^{-1} (1st order)	
Plasma operating conditions	Xylene extract	DIBK extract[a]
Forward power (kW)	1.45	1.5
Reflected power (W)	<10	<5
Argon flow rates (l min^{-1})		
coolant	13	13
plasma	1.2	1.2
carrier	0.65	0.65
Observation height above load coil (mm)	14	16

[a]From [2].

Extraction procedure

A 500-ml portion of sample, acidified with nitric acid to pH 1, was heated gently on a hot plate for 1 h. After cooling, the pH was adjusted to about 5.2 with ammonia solution, then 2.5 ml of 2% APDC, 2.5 ml of 2% HMAHMDC and the 0.1 M acetate buffer (pH 5.2) solutions were added. The pH was adjusted again to 5.2 ± 0.1 with dilute nitric acid or ammonia solution. The solution was transferred to a 500-ml separatory funnel and 5 ml of xylene was added. The mixture was shaken for 10 min and was allowed to stand for 15 min for phase separation. The organic phase was collected in a dry, stoppered test tube for the determination by i.c.p.e.s. Calibration graphs were prepared by using the above extraction for 500 ml of solutions containing appropriate amounts of the multi-element working standard.

RESULTS AND DISCUSSION

Selection of chelating agent and organic solvent

It has already been demonstrated that the APDC/DIBK extraction system had a good multi-element extraction capability [2]. To increase this capability, various combinations of chelating agents (APDC/DDC, APDC/8-quinolinol, APDC/HMAHMDC) were studied in detail. Solutions (10 ng

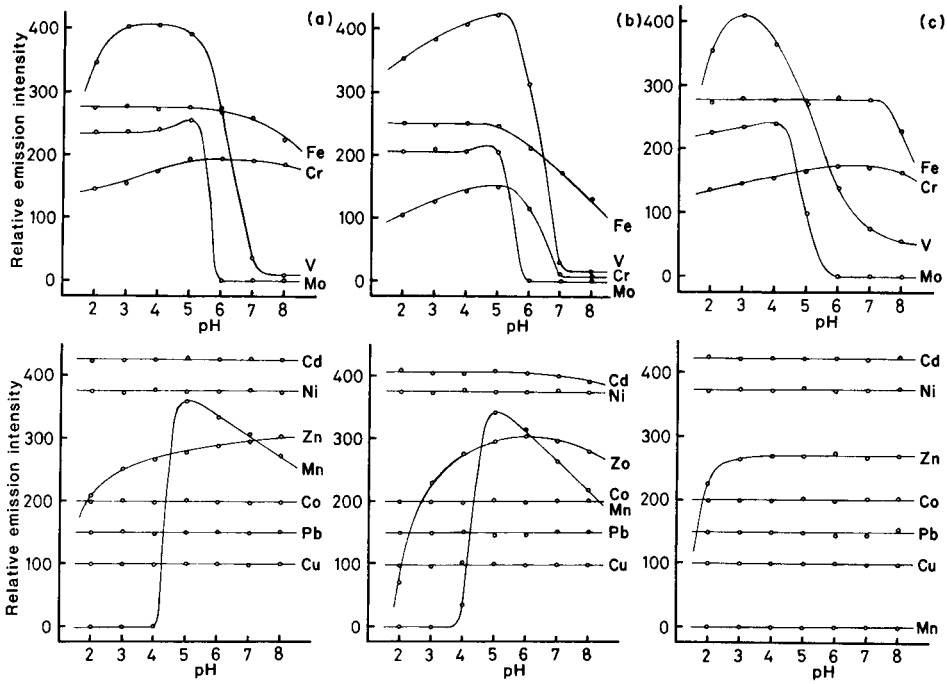

Fig. 1. Effect of pH on extraction of various metals into DIBK with: (a) APDC/HMAHMDC; (b) HMAHMDC; (c) APDC/DDC. Samples (500 ml) contained a 10 ng ml^{-1} concentration of each metal except for 40 ng ml^{-1} Pb; 5 ml of DIBK was used.

ml^{-1} of each metal except for 40 ng ml^{-1} of lead in a 500-ml solution in the pH range 2—8) were extracted into 5 ml of DIBK using 2.5 ml of each of the 2% chelating agent solutions. Figure 1 shows the extraction curves for APDC/HMAHMDC, APDC/DDC, and HMAHMDC alone. The combination APDC/DDC is reported to extend the pH range over which metals are extracted [7]. However, for molybdenum and vanadium the extraction efficiency was sensitive to pH, as reported by McLeod et al. [3]. The combination APDC/8-quinolinol allowed extraction of manganese above pH 8, but this pH range was different from those for other metals. Moreover, the extraction efficiencies for molybdenum and vanadium did not change, compared with those of APDC alone. With the combination APDC/HMAHMDC, manganese was extracted at pH >4. In comparison to APDC alone, the pH range over which molybdenum and vanadium are extracted equally well was extended to the higher pH range, and, in comparison to HMAHMDC alone, the extraction efficiencies of Cd, Cr, Fe, V and Zn were less dependent on the pH of the solution.

These characteristics indicate that the APDC/HMAHMDC combination gives the possibility of simultaneous extraction of these elements under the same conditions. However, the optimum pH range for all these elements is so

narrow that application of this combination to actual samples is difficult. To solve this problem, xylene was tested instead of DIBK. Extraction curves with xylene and DIBK are compared in Fig. 2. In comparison to DIBK, molybdenum and vanadium were extracted into xylene over a wider pH range and manganese was extracted equally well at pH >5.2. Extraction efficiency for zinc became constant over the pH range tested. Hence, extraction with APDC/HMAHMDC into xylene was used in subsequent experiments.

To establish the time required for distribution equilibrium of metal complexes between the aqueous and organic phases, solutions (10 ng ml^{-1} of each metal in 500 ml of solution at pH 5.2) were shaken with 5 ml of xylene for 0.5—15 min and allowed to stand for 15 min. Equilibrium was achieved when the solutions were shaken for at least 10 min. No complex showed any decomposition after 15-min shaking. Therefore, the shaking time was set to 10 min in subsequent experiments.

Stability of metal complexes in the organic phase

To investigate the effects of temperature and contact with water on the stability of metal complexes in the present system, identical solutions (10 ng ml^{-1} for each metal in 500 ml of solution at pH 5.2) were extracted into 25 ml of xylene, and four types of sample treatment were carried out after the phase separation. These were storage at room temperature (25°C) or in a refrigerator (—12°C) with or without contact with water. Determinations were made from 2 to 240 h after phase separation. On each occasion, just before these solutions were to be analyzed, two new identical solutions were extracted and their emission intensities were compared to those of the stored solutions each time. The results at 25°C are shown in Table 2. The solutions stored at —12°C were stable for at least 240 h independent of the presence of water.

Metal carbamate complexes except for the molybdenum, vanadium and cobalt carbamates were stable for at least 24 h, regardless of the type of sample treatment. The solutions left at room temperature in contact with water became cloudy after 24 h, but the other solutions remained clear even after 240 h. The molybdenum and vanadium carbamate complexes in cloudy solutions decomposed first, but after 48 h the rates of decomposition of most of the metal carbamates were faster in the clear solutions at room temperature than those in the cloudy solutions. This is contrary to an earlier report on the stability of metal carbamates in contact with or without water [8], but this is probably because the experimental conditions such as chelating reagents, organic solvent and the ratio of extract to water are different. The reason for the lesser decomposition rate in the cloudy solution might be that the aqueous phase dispersed in xylene contains some decomposed metal carbamate complex which may be adsorbed on the container wall in the pure extract. For analytical work, it is recommended that the extract without water be analyzed within 6 h of phase separation. All the metal carbamate solutions stored in the refrigerator were stable for at least 240 h. Thus, for

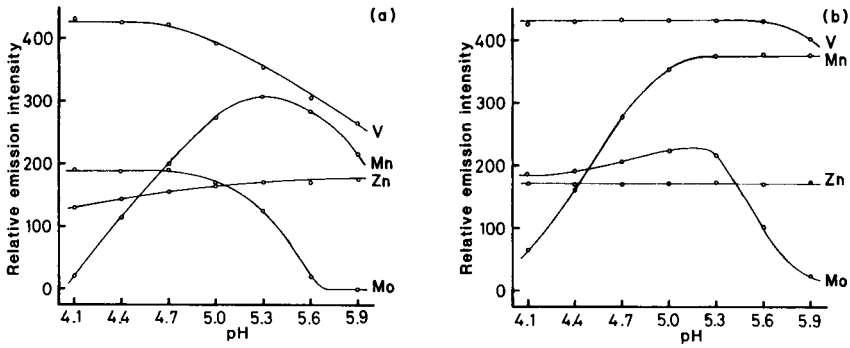

Fig. 2. Effect of pH on extraction of some metals with APDC/HMAHMDC into: (a) DIBK; (b) xylene. Samples were the same as for Fig. 1; a mixture of 2.5 ml of 2% APDC and 2.5 ml of 2% HMAHMDC was used.

storage for long periods, it is recommended that the extracts are kept in the refrigerator.

To demonstrate the stability of the recommended extracts it was compared with that of the APDC/DIBK extracts at room temperature, not in contact with water. The rate of decomposition decreased in the order

TABLE 2

Stability (%) of metal/APDC/HMAHMDC complexes in xylene at 25°C

Element		Time (h)						
		2	4	6	24	48	96	240
Cd	A[a]	100	100	100	100	100	94	65
	B	100	100	100	100	100	100	100
Co	A	100	100	100	85	84	81	76
	B	100	100	100	100	100	100	100
Cr, Cu, Ni	A	100	100	100	100	100	100	100
	B	100	100	100	100	100	100	100
Fe	A	100	100	100	100	100	91	21
	B	100	100	100	100	100	100	100
Mn	A	100	100	100	100	47	16	5
	B	100	100	100	100	100	87	79
Mo	A	100	100	100	83	24	7	46[b]
	B	100	100	100	48	46	31	3
Pb	A	100	100	100	100	100	77	22
	B	100	100	100	100	100	100	100
V	A	100	100	100	91	28	13	5
	B	100	100	92	52	38	24	2
Zn	A	100	100	100	100	100	100	5
	B	100	100	100	100	100	100	100

[a] A: after phase separation. B: after phase separation followed by the addition of 1 ml of water.

[b] The abrupt increase was unaccountable, but was reproducible. The results of the duplicate tests were 43% and 49%.

Mo > V > Pb > Zn > Fe > Cd > Cr > Cu for the APDC/DIBK system. Metal carbamate complexes in the recommended extraction system are more stable than those in the APDC/DIBK system for up to 48 h. Compared with the APDC/MIBK [8—11], APDC/DDC/MIBK [7] and APDC/DDC/Freon TF [12] systems, the stability of the extracts obtained by the recommended system is at least as great.

Optimization of the i.c.p.e.s. measurements of the xylene extracts

Five parameters (output power, observation height and the three gas flow rates) were optimized by using a univariate search method based on net signal intensity-to-background ratio (S/B) measurements. Table 3 shows the five optimized values for xylene and DIBK extracts. There is no tendency resulting from the difference of organic solvent in the optimum output power or flow rates of carrier gas and coolant gas. The optimum observation height for xylene was lower than that for DIBK, possibly because the smaller primary droplet diameter or the higher evaporation rate of xylene increased the transport efficiency in the lower region of the i.c.p. [13]. The better S/B ratio was gained at the lower plasma gas flow rate except for zinc and manganese. However, as xylene deposited carbon on the wall of the torch at the lower flow rate, it was set at 1.2 l min^{-1}. Optimum operated conditions for xylene extracts were therefore selected as follows: forward power, 1.45 kW; observation height, 14 mm; carrier gas flow rate, 0.65 l min^{-1}; coolant gas flow rate, 13.0 l min^{-1}; plasma gas flow rate, 1.2 l min^{-1}.

Detection limits and ranges of linearity

The detection limits for the elements based on 3 times the standard deviation of the blank signals and a 100-fold concentration factor are presented in Table 4. The concentration ranges of these elements in sea

TABLE 3

Optimized operating conditions for xylene and DIBK[a] extracts

Element	Power (kW)	Carrier gas (l min^{-1})	Plasma gas (l min^{-1})	Coolant gas (l min^{-1})	Obs. height (mm)
Cd	1.70 (1.55)	0.65 (0.65)	0.50 (1.15)	12.0 (12.5)	14 (14)
Co	1.20	0.70	0.50	18.0	15
Cr	1.50	0.70	0.50	16.5	13
Cu	1.10 (1.35)	0.75 (0.80)	0.50 (0.90)	9.0 (13.0)	13 (18)
Fe	1.45 (1.55)	0.70 (0.65)	0.50 (1.15)	14.0 (12.5)	13 (16)
Mn	1.35	0.65	1.30	18.0	13
Mo	1.25 (1.50)	0.75 (0.70)	0.50 (1.25)	14.0 (14.5)	16 (14)
Ni	1.25 (1.50)	0.70 (0.70)	0.50 (0.80)	18.0 (15.5)	15 (14)
Pb	1.50 (1.55)	0.65 (0.65)	0.50 (1.15)	14.0 (13.5)	15 (16)
V	1.30 (1.20)	0.70 (0.75)	0.50 (0.75)	14.0 (14.5)	15 (19)
Zn	1.60 (1.55)	0.65 (0.70)	0.75 (1.10)	13.0 (13.0)	14 (16)

[a]Figures in parentheses are values for DIBK extract from [2].

TABLE 4

Detection limits and approximate concentrations in natural waters

Element	Wavelength (nm)	Detection limit[a] (ng ml^{-1})	Sea-water conc. (ng ml^{-1}) [14]	River-water conc. (ng ml^{-1}) [14]
Cd	226.50	0.017	<0.01—9.4	0.01—3
Co	238.89	0.24	0.01—4.1	0.04—8
Cr	267.71	0.068[b]	0.2—50	0.1—6
Cu	324.75	0.047	0.05—12	0.2—30
Fe	259.94	0.048	0.03—70	10—1400
Mn	257.61	0.029	0.03—21	0.02—130
Mo	202.03	0.088	4—10	0.03—10
Ni	221.65	0.13	0.13—43	0.02—27
Pb	220.35	0.52	0.03—13	0.06—120
V	311.07	0.036	0.9—2.5	0.01—20
Zn	202.55	0.11	0.2—48	0.2—100

[a]Based on 3 times the standard deviation of the blank signal and a 100-fold concentration factor. [b]For Cr(VI).

and river waters are given for comparison. The detection limits of the proposed extraction method are sufficient for the determination of metals in natural waters, although higher sensitivity would be desirable for Cd, Co, Cr(VI) and Pb. The relatively high detection limit for zinc might be due to contamination from the nitric acid, ammonia solution and HMAHMDC used in sample preparation.

The linearity of the calibration graph after 100-fold concentration was observed from the detection limit up to at least 30 ng ml^{-1} (15 μg) for most elements. For iron, manganese and molybdenum the linearity extended to 100 ng ml^{-1} (50 μg). The ranges proved to be wide enough to encompass the concentrations found in most natural waters. Deviations from linearity at high concentrations probably arise because the metal carbamates cannot be extracted completely into xylene. However, for only a 20-fold concentration the linearity, as expected, extends to about 5 times the values for 100-fold concentration.

Applications

Table 5 shows the results obtained for the determination of 10 elements in river and sea waters. The results are considered to be equivalent to the dissolved fraction plus the particulate and colloidal metals leached into the solution during the gentle heating of the sample with nitric acid. Some species of dissolved heavy metals in natural waters are organically bound [15] and may show different extractability. Heating of sample with nitric acid is necessary to decompose such bound compounds [2]. Sample C, which showed an extraordinarily high concentration of molybdenum, was taken from a severely polluted area of Tokyo Bay. Because the Cr(VI)/Cr(III) ratio may

TABLE 5

Results obtained for trace elements in river and sea waters (ng ml^{-1})
(Sample A was taken from Kitakami river and samples B and C from Tokyo Bay)

Element	River	Sea	
	A	B	C
Cd	0.05 (38.0)[a]	0.02 (63.5)	0.05 (18.8)
Co	0.45 (17.3)	0.41 (8.5)	n.d.[b]
Cu	2.22 (3.6)	1.35 (3.2)	1.05 (3.3)
Fe	130 (2.7)	66.9 (9.7)	5.07 (5.3)
Mn	7.68 (4.9)	11.8 (4.4)	9.93 (2.5)
Mo	0.12 (21.7)	9.34 (1.1)	168 (4.9)
Ni	0.62 (1.4)	1.6 (2.7)	2.1 (6.7)
Pb	1.1 (9.0)	0.7 (43.3)	0.9 (41.8)
V	0.92 (2.9)	2.98 (1.5)	2.07 (2.5)
Zn	1.03 (7.5)	5.25 (3.3)	5.55 (1.4)

[a]Figures in parentheses are relative standard deviations (%) obtained for duplicate measurements of the emission intensities for three identical samples (n = 6). [b]Not detected.

be changed from its natural value in the heating process, the results for chromium(VI) are not presented here. However, the present extraction might be suitable for the determination of the dissolved fraction of chromium(VI).

The relative standard deviations were 3—5% for all the elements except for cadmium, cobalt and lead, the lack of precision for which arises from the very low concentrations in natural waters; but even for these elements the recommended method might be applicable to polluted waters.

CONCLUSIONS

The above study demonstrates that the APDC/HMAHMDC/xylene extraction system followed by i.c.p.e.s. is useful for the determination of ng ml^{-1} levels of metals in natural waters. The main advantages of this method are the simultaneous extraction of Cd, Co, Cr, Cu, Fe, Mn, Mo, Ni, Pb, V and Zn in a single extract and simultaneous multi-element measurements by direct introduction of the organic phase into the plasma, without back-extraction or evaporation of the extract which is liable to increase contamination and losses by adsorption or evaporation. In this experiment, nitric acid and ammonia solution were super-special grade and HMAHMDC was used without purification. If these reagents are purified, the blank will be decreased and better detection limits will be achieved. Further studies of the extraction of other metals with this system are now underway.

REFERENCES

1 A. Sugimae, Anal. Chim. Acta, 121 (1980) 331.
2 A. Miyazaki, A. Kimura, K. Bansho and Y. Umezaki, Anal. Chim. Acta, 144 (1982) 213.
3 C. W. McLeod, A. Otsuki, K. Okamoto, H. Haraguchi and K. Fuwa, Analyst, 106 (1981) 419.
4 M. Hiraide, T. Ito, M. Baba, H. Kawaguchi and A. Mizuike, Anal. Chem., 52 (1980) 804.
5 W. B. Kerfoot and R. L. Crawford, ICP Inform. Newsl., 2 (1977) 289.
6 R. E. Sturgeon, S. S. Berman, A. Desaulniers and D. S. Russell, Talanta, 27 (1980) 85.
7 J. D. Kinrade and J. C. Van Loon, Anal. Chem., 46 (1974) 1894.
8 I. Dellien and L. Persson, Talanta, 26 (1979) 1101.
9 A. D. Shendrikar, V. Dharmarajan, H. W. Merrick and P. W. West, Anal. Chim. Acta, 84 (1976) 409.
10 R. F. Roberts, Anal. Chem., 49 (1977) 1862.
11 R. R. Brooks, B. J. Presley and I. R. Kaplan, Talanta, 14 (1967) 809.
12 L. G. Danielsson, B. Magnusson and S. Westerlund, Anal. Chim. Acta, 98 (1978) 47.
13 A. W. Boorn and R. F. Browner, Anal. Chem., 54 (1982) 1402.
14 H. J. M. Bowen, Environmental Chemistry of the Elements, Academic Press, London, 1979, p. 16.
15 Y. Sugimura, Y. Suzuki and Y. Miyake, Deep-Sea Res., 25 (1978) 309.

Analytica Chimica Acta, 156 (1984) 169—180
Elsevier Science Publishers B.V., Amsterdam — Printed in The Netherlands

LINEAR CALIBRATION IN ION CHROMATOGRAPHY BY CALCULATING TOTAL AMOUNTS OF SAMPLE FROM MEASURED CONDUCTIVITY DATA

M. J. VAN OS* and J. SLANINA

Netherlands Energy Research Foundation (ECN), Petten, N.H. (The Netherlands)

C. L. DE LIGNY and J. AGTERDENBOS

Laboratory for Analytical Chemistry, State University, Croesestraat 77A, Utrecht (The Netherlands)

(Received 9th May 1983)

SUMMARY

Calibration graphs in ion chromatography are generally not linear, if a suppressor column and a conductivity detector are employed. The main reason for this is that the dissociation equilibrium of the eluent (which is a weak acid after eluent suppression) is shifted by H^+ ions from the sample, which are formed in the suppressor column. Therefore a formula is derived in which the suppression of the eluent dissociation by the sample is considered. Application of this formula for chloride, nitrate and sulphate samples in succinate and carbonate eluents results in linear calibration graphs in the range 0—40 mg l^{-1} when peak areas are used.

Ion chromatography, introduced by Small et al. in 1975 [1], is a useful and sensitive method for the determination of inorganic anions, and has found widespread application, especially in environmental analyses [2]. When a conductometric cell is used as a universal detector, the use of a suppressor column improves sensitivity and detection limit. Unfortunately, in the eluate from the suppressor column, the eluent is a weak acid and the sample is a strong acid, the H^+ ions of which suppress the ionization of the weak acid. Consequently, the contribution of the eluent to conductivity is not constant, but decreases with increasing sample concentration. As a result, calibration graphs, whether based on peak heights or peak areas, cannot be expected to be linear. This was observed in earlier work [3].

In this report a formula is derived, by which the sample concentration can be calculated from the measured conductivity. The displacement of eluent ions from the separator column by sample ions and the eluent dissociation after suppression are considered in the calculation of linear calibration graphs.

0003-2670/84/$03.00

THEORETICAL CONSIDERATIONS

In ion chromatography with eluent suppression and conductivity detection, the following processes take place. A mixture of anions X^-, Y^- and Z^- is injected into an eluent stream which flows through an anion-exchange column, where the separation occurs. If the sample anions are eluted with a salt of a dibasic acid, H_2B, then in the eluate from the separator column X^-, Y^- and Z^- are present as the sodium salts NaX, NaY and NaZ, together with an excess of Na_2B, NaHB (and a small amount of H_2B). To reduce the eluent contribution to the conductivity, a second column (suppressor column) is inserted between separator column and detector. This is a cation-exchange column in the H^+-form, where all cations are exchanged for H^+. In the eluate from the suppressor column, the sample ions are present as strong acids (HX, HY and HZ) and the eluent as a weak acid H_2B. Since the equivalent conductance of H^+ is 7× higher than that of Na^+, the contribution of the sample ions (X^- together with H^+) to the conductivity signal is increased, but the contribution of the eluent (determined by the degree of ionization of the weak acid H_2B) is reduced. Thus, eluent suppression improves the sensitivity and reduces the background conductivity. Consequently, the detection limit also is improved.

It has been shown [4] that the elution of the sample ions is governed by the concentration of divalent B^{2-} ions in the eluate. Thus the ion-exchange column can be considered as in dynamic equilibrium with the divalent eluent ions B^{2-}. After sample injection on the top of the column (Fig. 1a), a dynamic equilibrium is set up in which the sample ions partition between the mobile phase and the stationary phase, an equivalent number of eluent ions B^{2-} being displaced from the stationary phase. Thus the eluent concentration in the stationary phase is locally reduced and the eluent concentration in the mobile phase is locally increased (Fig. 1b). When $\Delta C_{B^{2-},s}$ is the decrease of eluent concentration and $C_{X^-,s}$ is the sample concentration in the stationary phase, then

$$\Delta C_{B^{2-},s} = 1/2 C_{X^-,s} \tag{1}$$

The local deficit of eluent ions in the stationary phase equals the local excess of eluent $\Delta C_{B,m}$ (where $\Delta C_{B,m} = \Delta C_{B^{2-},m} + \Delta C_{HB^-,m} + \Delta C_{H_2B,m}$) in the mobile phase, hence

$$\Delta C_{B^{2-},s}\ V_s = \Delta C_{B,m}\ V_m \tag{2}$$

where $\Delta C_{B,m}$ is the increase of the eluent concentration in the mobile phase and V_s and V_m are the volumes of the stationary and mobile phases in the column, respectively. The eluent ions in the mobile phase are not retarded by the resin in the B^{2-} form and the eluent peak is eluted after V_m ml of eluent has been added (Fig. 1c). Transport of the sample ions through the column is accompanied by the transport of the local deficiency of eluent ions in the stationary phase (Fig. 1c). When the sample ions X^- are eluted

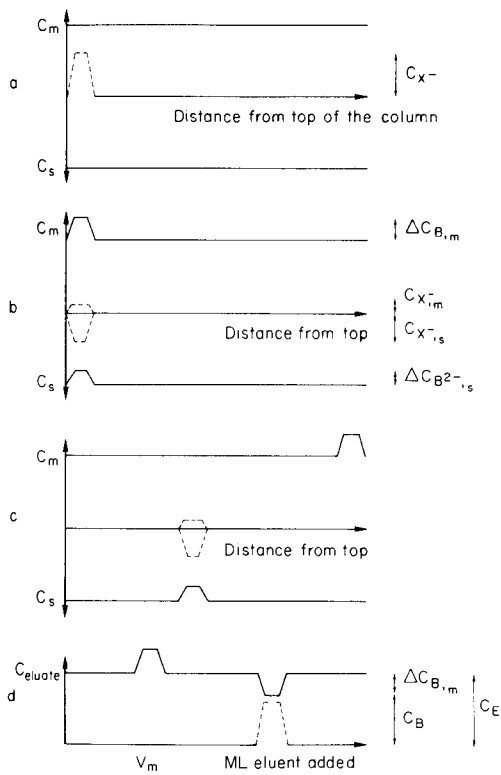

Fig. 1. Displacement of eluent ions from the separator column by sample ions: (—) eluent; (---) sample. (a) Situation in the column after injection of the sample and before equilibration; (b) after equilibration; (c) after the addition of V_m ml of eluent; (d) situation in the eluent after elution of the sample.

from the separator column, the concentration of X^- in the eluate (C_{X^-}) can be calculated as follows. For the last section of the column, containing a volume dV_m of mobile phase and a volume dV_s of stationary phase, and $dn_{X^-,m}$ moles of sample ions in the mobile phase and $dn_{X^-,s}$ moles of sample ions in the stationary phase, it holds that

$$dn_{X^-,m} + dn_{X^-,s} = c_{X^-,m}dV_m + c_{X^-,s}dV_s \quad (3)$$

Division by dV_m gives

$$dn_{X^-,tot}/dV_m = c_{X^-,m} + c_{X^-,s}V_s/V_m \quad (4)$$

If the increase in peak width that occurs during elution of the sample peak is neglected, then when a volume dV_m of eluent flows into (and out of) the column, $dn_{X^-,tot}$ moles of ions leave the last section and enter the eluate (while $dn'_{X^-,tot}$ moles of ions enter the last section from the preceding section). The concentration of the sample ions in the eluate c_{X^-} is equal to $dn_{X^-,tot}/dV_m$, so that $c_{X^-} = c_{X^-,m} + c_{X^-,s}V_s/V_m$. The capacity factor k' is defined as

$k' = c_{X^-,s}V_s/c_{X^-,m}V_m$. Combination of the expressions for c_{X^-} and k' yields

$$c_{X^-,s} = [k'/(k'+1)]c_{X^-}V_m/V_s \tag{5}$$

Then $\Delta c_{B^{2-},m}$ can be calculated as a function of c_{X^-}, by using Eqns. 1, 2 and 5: $\Delta c_{B,m} = 0.5[k'/(k'+1)]c_{X^-} = \gamma c_{X^-}$, with $\gamma = 0.5[k'/(k'+1)]$. When c_B is the actual eluent concentration in the eluate, (where $c_B = c_{B^{2-}} + c_{HB^-} + c_{H_2B}$), the sum of c_B and $\Delta c_{B,m}$ is equal to the original eluent concentration c_E (Fig. 1d):

$$c_E = c_B + \Delta c_{B,m} = c_B + \gamma c_{X^-} \tag{6}$$

It should be realized that Eqn. 6 is valid not only in the absence but also in the presence of sample ions X^-.

In the situation considered, a sample anion X^- is eluted with B^{2-} and, in the eluate of the suppressor column, the sample anion is present as a strong acid HX and the eluent is present as a weak acid H_2B.The equilibrium for the weak acid is $H_2B \rightleftharpoons H^+ + HB^-$, with the equilibrium constant $K_{a1} = c_{H^+}c_{HB^-}/c_{H_2B}$. The second ionization step is neglected (see below). After eluent suppression, the total eluent concentration c_E can be written (see Eqn. 6) as $c_E = c_{HB^-} + c_{H_2B} + \gamma c_{X^-}$. Further, because of electroneutrality, $c_{H^+} = c_{X^-} + c_{HB^-}$. In the eluate of the suppressor column, c_{OH^-} is negligibly small (see below). Thus, from these expressions for K_{a1}, c_E and c_{H^+},

$$c_{H^+} = 0.5\{c_{X^-} - K_{a1} + [(c_{X^-} + K_{a1})^2 + 4K_{a1}(c_E - \gamma c_{X^-})]^{1/2}\} \tag{7}$$

$$c_{HB^-} = 0.5\{-c_{X^-} - K_{a1} + [(c_{X^-} + K_{a1})^2 + 4K_{a1}(c_E - \gamma c_{X^-})]^{1/2}\} \tag{8}$$

The conductivity detector measures the sum of the conductivities of all the ions in the eluate. When c_i is the concentration of ion i in the eluate, Λ_i is its equivalent conductance and S_T is the measured total conductivity, including the contribution of the eluent, S_T is given by

$$\sum_i c_i\Lambda_i = c_{X^-}\Lambda_{X^-} + c_{H^+}\Lambda_{H^+} + c_{HB^-}\Lambda_{HB^-} = PS_T \tag{9}$$

where P is the cell constant of the conductivity cell. If S_E is the eluent conductivity (with zero sample concentration), then $PS_E = c_{H^+}\Lambda_{H^+} + c_{HB^-}\Lambda_{HB^-}$, which can be rewritten, using the expressions for K_{a1} and c_E, as

$$PS_E = 0.5(\Lambda_{H^+} + \Lambda_{HB^-})[-K_{a1} + (K_{a1}^2 + 4c_EK_{a1})^{1/2}] \tag{10}$$

If S_N is the conductivity, compensated for the background eluent conductivity, then $S_N = S_T - S_E$ and S_N is equal to

$$S_NP = c_{X^-}\Lambda_{X^-} + c_{H^+}\Lambda_{H^+} + c_{HB^-}\Lambda_{HB^-} - 0.5(\Lambda_{H^+} + \Lambda_{HB^-})[-K_{a1} + (K_{a1}^2 + 4c_EK_{a1})^{1/2}] \tag{11}$$

When c_{H^+} and c_{HB^-} are both expressed in terms of c_{X^-} (with Eqns. 7 and 8), then

$$S_NP = c_{X^-}\Lambda_{X^-} + 0.5\Lambda_{H^+}\{c_{X^-} - K_{a1} + [(c_{X^-} + K_{a1})^2 + 4K_{a1}(c_E - \gamma c_{X^-})]^{1/2}\}$$

$$+ 0.5\Lambda_{HB^-}\{-c_{X^-} - K_{a1} + [(c_{X^-} + K_{a1})^2 + 4K_{a1}(c_E - \gamma c_{X^-})]^{1/2}\}$$
$$-0.5(\Lambda_{H^+} + \Lambda_{HB^-})[-K_{a1} + (K_{a1}^2 + 4c_E K_{a1})^{1/2}] \quad (12)$$

Equation 12 can be rearranged to a quadratic equation in the unknown concentration c_{X^-}

$$Ac_{X^-}^2 + Bc_{X^-} + C = 0 \quad (13)$$

$$\text{where } A = (\Lambda_{H^+} + \Lambda_{X^-})(\Lambda_{X^-} - \Lambda_{HB^-}) \quad (14)$$

$$B = -0.5(2\Lambda_{X^-} + \Lambda_{H^+} - \Lambda_{HB^-})(\Lambda_{H^+} + \Lambda_{HB^-})(K_{a1}^2 + 4c_E K_{a1})^{1/2}$$
$$-S_N P(2\Lambda_{X^-} + \Lambda_{H^+} - \Lambda_{HB^-}) - 0.5K_{a1}(\Lambda_{H^+} + \Lambda_{HB^-})^2(1 - 2\gamma) \quad (15)$$

$$C = (S_N P)^2 + S_N P(\Lambda_{H^+} + \Lambda_{HB^-})(K_{a1}^2 + 4c_E K_{a1})^{1/2} \quad (16)$$

c_{X^-} is calculated with the square root formula:

$$c_{X^-} = -B + (B^2 - 4AC)^{1/2}/2A \quad (17)$$

This means that c_{X^-} can be calculated from the measured conductivity S_N with Eqns. 14—17. The physical constants Λ_{H^+}, Λ_{HB^-}, Λ_{X^-} and K_{a1}, the eluent concentration c_E, the cell constant P and the value of γ (or the capacity factor k') must be known. The capacity factor is calculated from chromatographic retention data and P is determined by calibrating the conductivity cell with KCl solutions of known concentrations.

The effect of the suppression of the ionization of the weak acid is illustrated for two weak acids, succinic acid and carbonic acid. These acids originate after suppression of succinate and carbonate eluent, respectively. Figure 2 shows the effects of increasing chloride concentration (c_{Cl^-}) in the suppressor eluate on the H^+ concentration (c_{H^+}) and on the concentrations of the monobasic eluent ions hydrogensuccinate (c_{HSu^-}) and hydrogen carbonate ($c_{HCO_3^-}$), respectively. The value of c_{H^+} is calculated with Eqn. 7; c_{HSu^-} and $c_{HCO_3^-}$ are calculated from Eqn. 8 with $c_E = 1.4 \times 10^{-3}$ mol l^{-1} and $c_E = 3 \times 10^{-3}$ mol l^{-1}, respectively (eluent concentrations commonly used in ion chromatography). The pK_{a1} values applied were 4.16 for succinic acid and 6.37 for carbonic acid. Capacity factors for chloride were 1.26 in 1.4×10^{-3} mol l^{-1} sodium succinate and 1.52 in 3×10^{-3} mol l^{-1} sodium carbonate.

Some results are as follows. First, as carbonic acid is a much weaker acid than succinic acid, both c_{HB^-} and c_{H^+} are smaller in carbonic acid. Second, the pH in the succinic acid eluate is 3.56 or lower and in the carbonic acid eluate 4.45 or lower. It is clear that c_{OH^-} is extremely small and can be neglected in the equation $c_{H^+} = c_{X^-} + c_{HB^-}$. Third, the pK_{a2} values for succinic and carbonic acids are 5.61 and 10.25, respectively, and the pH of the two eluates is $\leqslant 3.56$ and $\leqslant 4.45$, respectively, which means that the ratio $c_{B^{2-}}/c_{HB^-}$ for both eluates is less than 1%. For this reason, the second ionization step, $HB^- \rightleftharpoons H^+ + B^{2-}$, of the weak acid H_2B is not considered in the equation $c_E = c_{HB^-} + c_{H_2B} + \gamma c_{X^-}$.

In Fig. 3, the total ionic conductivities $\Sigma_i c_i \Lambda_i$ in succinic and carbonic

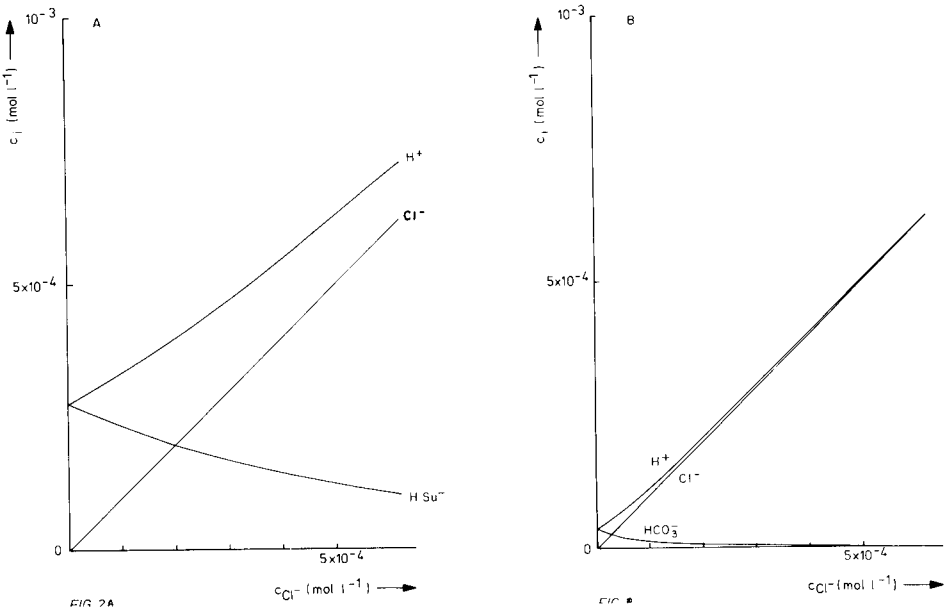

Fig. 2. Dissociation of (A) 1.4 × 10^{-3} mol l^{-1} succinic acid and (B) 3 × 10^{-3} mol l^{-1} carbonic acid as a function of chloride concentration.

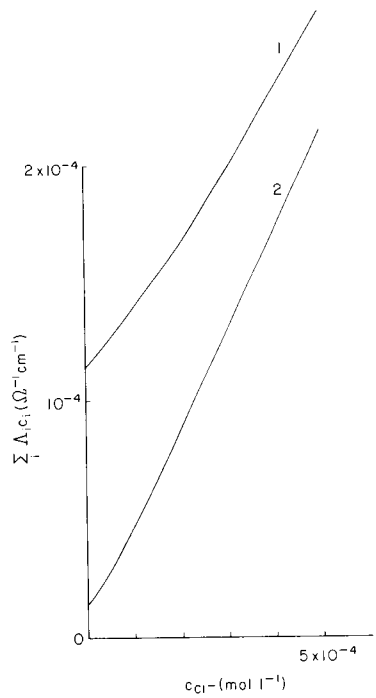

Fig. 3. Total ionic conductivity in 1.4 × 10^{-3} mol l^{-1} succinic acid (curve 1) and 3 × 10^{-3} mol l^{-1} carbonic acid (curve 2) as a function of chloride concentration.

acids are calculated as a function of c_{Cl^-}, using Eqn. 9. The Λ_i values applied were 76.3 Ω^{-1} cm^2 eq^{-1} for chloride, 350 for H^+, 60 for hydrogensuccinate and 44.5 for hydrogencarbonate ions [5]. As can be seen, both plots are curved.

EXPERIMENTAL

Chemicals

Zipax SAX, a pellicular anion exchanger with a particle diameter of 25—37 μm and a capacity of about 12 μeq g^{-1} dry material (DuPont de Nemours) was used in the separation column. The cation exchanger AG 50W-X16 (BioRad), with a capacity of about 5 meq g^{-1} dry resin was used in the suppressor columns. Sodium succinate ("Baker grade") and sodium carbonate (99.6%) were obtained from Baker Chemicals.

Column packing and measuring procedure

The ion chromatograph and column packing apparatus are described in detail elsewhere [4]. A 200 × 4.5 mm column was packed with Zipax SAX beads and two 150 × 2.0 mm suppressor columns were packed with AG 50W-X16 using the slurry technique [4]. A 100 × 4.0 mm glass column was packed by pumping over Dionex anion-exchange material from a 250 × 4.5 mm prepacked Dionex column. The separation column, suppressor column and detector cell were thermostated at 25.0°C.

Eluents were prepared by dissolving 1.0599 g of sodium carbonate and 2.7015 g of sodium succinate hexahydrate, respectively, in 1 l of deionized water. These solutions were then diluted to 3×10^{-3} mol l^{-1} sodium carbonate and 1.4×10^{-3} mol l^{-1} sodium succinate, respectively.

A FORTRAN computer program (available on request) was written to calculate the total amount of sample in the eluate from conductivity data. The program consists of the following parts. First, conductivity is measured at regular time intervals. This time interval is increased after each peak, because the peak width increases with the retention time. Second, a peak search routine indicates the start, maximum and end of each peak. The baseline is determined before and after the peak and the mean value of the baseline is subtracted from each point on the chromatogram. Third, the sample concentration in each point is calculated with Eqn. 17. Finally, the total amount of sample is obtained by integrating the calculated sample concentrations over the total eluted peak volume.

RESULTS AND DISCUSSION

The cell constant P was determined by measuring the conductivity S of 10^{-4} mol l^{-1} KCl at 25.0°C. The response of the conductivity cell was linear up to 5×10^{-4} mol l^{-1} KCl according to the relation $S \times P = 10^3\, c(\Lambda_{K^+} + \Lambda_{Cl^-})$ wherein Λ_{K^+} and Λ_{Cl^-} are 73.5 and 76.3 Ω^{-1} eq^{-1} cm^2, respectively, c is

the KCl concentration (mol l^{-1}) and S is the conductivity (μmho). P was found to be 1.69 cm^{-1}.

Capacity factor data for chloride, nitrate and sulphate were calculated with the equation $k' = (V_R - V_M)/V_m$, wherein V_R and V_M are the retention volumes of the retarded component and water, respectively, in the separator-suppressor column combination. The k' values, listed in Table 1, were determined by injecting 2 μg of each sample ion.

Calibration graphs for chloride, nitrate and sulphate were prepared for both a 200 × 4.5 mm Zipax SAX column and a 100 × 4.0 mm Dionex column. The eluents were 1.4 × 10^{-3} mol l^{-1} sodium succinate and 3 × 10^{-3} mol l^{-1} sodium carbonate, respectively. A 150 × 2.0 mm AG 50W-X16 suppressor column was used in both cases. Samples with concentrations ranging from 1 to 40 mg l^{-1} were injected with a 200-μl or 500-μl loop.

In Table 2, experimental plate heights are listed for chloride, as well as the ratios S_p/c_0 and c_p/c_0, where c_0 is the known chloride concentration in the sample, S_p is the conductivity at the peak maximum, and c_p is the calculated chloride concentration at the peak maximum. It appears that on the Zipax column, S_p/c_0 increases with c_0 for c_0 = 1 to 10 mg l^{-1} and decreases for $c_0 > 10$ mg l^{-1}. Obviously the Zipax column is overloaded if more than 10 mg l^{-1} is injected and as a result the eluted peak is broadened. This is

TABLE 1

Capacity factors (k') for chloride, nitrate and sulphate on a Zipax SAX column and a Dionex column
Eluents: 1.4 × 10^{-3} mol l^{-1} sodium succinate and 3 × 10^{-3} mol l^{-1} Na_2CO_3, respectively)

Ion	Cl^-	NO_3^-	SO_4^{2-}
k' (Zipax)	1.26	5.46	8.38
k' (Dionex)	1.52	6.23	13.21

TABLE 2

Calibration for chloride on a Zipax SAX column and a Dionex column, based on conductivity data at the peak maximum[a]

c_0	Zipax SAX			Dionex		
	H	S_p/c_0	$10^5\ c_p/c_0$	H	S_p/c_0	$10^5\ c_p/c_0$
1	0.12	6.88	2.37	0.18	8.70	2.66
2	0.13	7.03	2.38	0.18	9.55	2.63
5	0.13	7.18	2.33	0.18	11.01	2.58
10	0.13	7.21	2.20	0.19	11.82	2.53
20	0.17	6.77	1.91	0.21	12.19	2.47
40	0.25	5.73	1.49	0.25	11.63	2.29

[a] c_0: concentration of chloride injected (mg l^{-1}). H: plate height (mm). S_p: peak height (μmho). c_p: peak height (mol l^{-1}). Injected sample volume: 200 μl.

affirmed by the measured plate heights: H is constant (0.13 mm) for c_0 = 1 to 10 mg l^{-1} but increases for $c_0 > 10$ mg l^{-1}. Consequently, c_p/c_0 is constant only for c_0 = 1 to 5 mg l^{-1} and decreases when $c_0 > 5$ mg l^{-1}. The same reasoning applies for the Dionex column. It is concluded that, because of peak broadening, a calibration based on calculated sample concentrations at the peak maximum is not linear over the range 1—40 mg l^{-1}.

The effect of peak broadening on the calibration is eliminated if the total amount of constituent under the peak is determined. Total amounts of chloride, nitrate and sulphate were so determined from conductivity measurements and the results are listed in Table 3 (n_1 data). For convenience, the amounts of sample injected (n_0) and the n_1/n_0 ratios are also given, as well as the conductivities at the peak maximum S_p and the S_p/c_0 ratios. The results in Table 3 indicate again that calibration graphs based on peak heights are curved. It can be seen that the n_1/n_0 ratios are all about 1.0. Thus the amount of sample that is injected can be accurately determined by conductivity. In principle, no standards are required once the cell constant has been measured, but this kind of absolute calibration can be applied successfully only if the eluent flow rate, the loop volume and the capacity factors are all accurately known and if the temperature remains constant. In practice, the capacity factors vary somewhat whenever a fresh eluent or a fresh suppressor column is used. Therefore a relative calibration with two standards is advisable.

The linear regression technique was used to test the calibration graphs. Inspection of the n_1/n_0 values in Table 3 shows that 6 out of the 12 data at the lowest concentration are rather low. Therefore, the results obtained at c_0 = 1 mg l^{-1} were not considered for the regression. The n_1 values obtained at the other values of c_0 are probably beset with a constant relative error. (The main contribution to the error of n_1 stems from the error of the conductivity measurements; generally, the relative error of conductivity measurements is constant.) The error in n_0 is negligible, and the values of n_1/n_0 are about constant. Therefore, if the relative error of n_1 is constant, the absolute error of n_1/n_0 is constant. Accordingly, the regression equation used was $n_1/n_0 = a + bc_0$. The results are shown in Table 4. It appears that the intercepts a are just significant statistically, so that a single-point calibration is not warranted. Two-point calibration gives values of s_{n_1/n_0} of about 0.02, i.e., an accuracy of 2%. Thus a linear calibration graph with a standard deviation of 2% can be obtained when the proposed formula is applied.

Conclusions

In ion chromatography with eluent suppression, non-linear relations between sample concentrations and conductivity values are found if the usual procedures are applied. Linear relations are found if three modifications are applied: consideration of the suppression of the eluent dissociation by the sample ions, consideration of the displacement of eluent ions in the separator column by the sample ions, and integration of the calculated

TABLE 3

Calibration of chloride, nitrate and sulphate on Zipax SAX and Dionex columns, based on integration of conductivity data over the peak volume[a]

Ion injected	c_0 (mg l^{-1})	n_0 (μg)	S_p (μmho)	S_p/c_0 (μmho mg^{-1} l)	n_1 (μg)	n_1/n_0
(a) Zipax SAX (1.4×10^{-3} mol l^{-1} sodium succinate eluent at 1.86 ml min^{-1}; 200 μl injected)						
Chloride	1	0.2	6.88	6.88	0.194	0.97
	2	0.4	14.07	7.03	0.398	0.99
	5	1.0	35.90	7.18	0.990	0.99
	10	2.0	72.05	7.21	1.983	0.99
	20	4.0	135.4	6.77	4.00	1.00
	40	8.0	229.0	5.73	8.02	1.00
Nitrate	1	0.2	1.03	1.03	0.188	0.94
	2	0.4	2.08	1.04	0.390	0.98
	5	1.0	5.20	1.04	0.981	0.98
	10	2.0	10.27	1.03	1.989	0.99
	20	4.0	19.83	0.99	4.05	1.01
	40	8.0	37.40	0.94	8.10	1.01
Sulphate	1	0.2	0.96	0.96	0.209	1.05
	2	0.4	1.93	0.97	0.425	1.06
	5	1.0	4.85	0.97	1.045	1.05
	10	2.0	9.84	0.98	2.07	1.04
	20	4.0	20.06	1.00	4.16	1.04
	40	8.0	40.54	1.01	8.29	1.04
(b) Zipax SAX (1.4×10^{-3} mol l^{-1} sodium succinate as eluent at 1.85 ml min^{-1}; 500 μl injected)						
Chloride	1	0.5	16.50	16.50	0.490	0.98
	2	1.0	33.39	16.70	0.983	0.98
	5	2.5	81.26	16.25	2.464	0.99
	10	5.0	148.6	14.86	4.92	0.98
	20	10.0	250.7	12.54	9.90	0.99
	40	20.0	379.3	9.48	19.81	0.99
Nitrate	1	0.5	2.55	2.55	0.477	0.96
	2	1.0	5.11	2.56	0.985	0.99
	5	2.5	12.45	2.49	2.459	0.98
	10	5.0	23.77	2.38	4.96	0.99
	20	10.0	44.73	2.24	9.98	1.00
	40	20.0	84.17	2.10	19.93	1.00
Sulphate	1	0.5	2.42	2.42	0.512	1.02
	2	1.0	4.87	2.44	1.031	1.03
	5	2.5	12.42	2.48	2.578	1.03
	10	5.0	25.29	2.53	5.15	1.03
	20	10.0	51.82	2.59	10.24	1.02
	40	20.0	104.6	2.62	20.26	1.01

TABLE 3 (continued)

Ion injected	c_0 (mg l^{-1})	n_0 (μg)	S_p (μmho)	S_p/c_0 (μmho mg^{-1} l)	n_1 (μg)	n_1/n_0
(c) Dionex (3×10^{-3} mol l^{-1} sodium carbonate as eluent at 1.91 ml min^{-1}; 200 μl injected)						
Chloride	1	0.2	8.70	8.70	0.206	1.03
	2	0.4	19.09	9.55	0.414	1.03
	5	1.0	55.05	11.01	1.022	1.02
	10	2.0	118.2	11.82	2.05	1.02
	20	4.0	243.7	12.19	4.09	1.02
	40	8.0	465.3	11.63	8.09	1.01
Nitrate	1	0.2	1.14	1.14	0.194	0.97
	2	0.4	2.30	1.15	0.400	1.00
	5	1.0	5.76	1.15	1.013	1.01
	10	2.0	11.66	1.17	2.04	1.02
	20	4.0	23.98	1.20	4.10	1.02
	40	8.0	50.37	1.26	8.16	1.02
Sulphate	1	0.2	0.84	0.84	0.200	1.00
	2	0.4	1.71	0.86	0.414	1.04
	5	1.0	4.45	0.89	1.025	1.02
	10	2.0	9.35	0.94	2.05	1.03
	20	4.0	19.99	1.00	4.12	1.03
	40	8.0	40.56	1.01	8.17	1.02
(d) Dionex (3×10^{-3} mol l^{-1} sodium carbonate as eluent at 1.92 ml min^{-1}; 500 μl injected)						
Chloride	1	0.5	23.41	23.41	0.507	1.01
	2	1.0	52.13	26.06	1.015	1.02
	5	2.5	139.3	27.90	2.531	1.01
	10	5.0	273.1	27.31	5.03	1.01
	20	10.0	494.4	24.72	9.98	1.00
Nitrate	1	0.5	2.74	2.74	0.492	0.98
	2	1.0	5.48	2.74	1.005	1.01
	5	2.5	13.81	2.76	2.513	1.01
	10	5.0	28.51	2.85	5.03	1.01
	20	10.0	60.69	3.03	9.96	1.00
	40	20.0	126.9	3.17	19.96	1.00
Sulphate	1	0.5	2.11	2.11	0.503	1.01
	2	1.0	4.35	2.18	1.012	1.01
	5	2.5	11.72	2.34	2.542	1.02
	10	5.0	24.44	2.44	5.06	1.01
	20	10.0	48.87	2.44	9.97	1.00
	40	20.0	92.83	2.32	19.87	0.99

[a] n_0: amount of sample injected. n_1: amount of sample found. Further legend as in Table 2.

concentrations over the total eluted peak area. Linear calibration based on peak heights cannot be obtained as the peak width increases with the sample concentration when constant volumes are injected. With these modifications, linear calibration graphs were obtained for chloride, nitrate and sulphate ions in both succinate and carbonate eluents.

TABLE 4

Results obtained in calibration for chloride, nitrate and sulphate on Zipax and Dionex columns

Separation column/ injection loop	Chloride			Nitrate			Sulphate		
	a	b	s_{n_1/n_2}	a	b	s_{n_1/n_2}	a	b	s_{n_1/n_2}
Zipax/200 µl	0.99	0.0003	0.005	0.98	0.0010	0.018	1.05	—0.0005	0.011
Zipax/500 µl	0.98	0.0002	0.004	0.99	0.0004	0.007	1.03	—0.0005	0.008
Dionex/200 µl	1.03	—0.0005	0.009	1.01	0.0004	0.010	1.03	—0.0002	0.005
Dionex/500 µl	1.02	—0.0010	0.008	1.01	—0.0002	0.005	1.02	—0.0006	0.010

REFERENCES

1 M. Small, T. S. Stevens and W. C. Bauman, Anal. Chem., 47 (1975) 1801.
2 J. D. Mulik and E. Sawicki (Eds.), Ion Chromatographic Analysis of Environmental Pollutants, Vol. 2, Ann Arbor Science Publishers, Ann Arbor, 1979.
3 J. Slanina, F. P. Bakker, P. A. C. Jongejan, L. van Lamoen and J. J. Möls, Anal. Chim. Acta, 130 (1981) 1.
4 M. J. van Os, J. Slanina, C. L. de Ligny, W. E. Hammers and J. Agterdenbos, Anal. Chim. Acta, 144 (1982) 73.
5 W. A. Roth and K. Scheel (Eds.), Landolt-Bornstein Physikalisch-Chemische Tabellen, dritter Ergänzungsband, Springer Verlag, Berlin, 1935, p. 2060.

Analytica Chimica Acta, 156 (1984) 181—192
Elsevier Science Publishers B.V., Amsterdam — Printed in The Netherlands

ION CHROMATOGRAPHIC DETERMINATION OF COMMON IONS AT ULTRATRACE LEVELS IN ANTARCTIC SNOW AND ICE

M. LEGRAND, M. DE ANGELIS and R. J. DELMAS*

Laboratoire de Glaciologie et Géophysique de l'Environnement B.P. 68, F38402 St Martin d'Heres-Cedex (France)

(Received 22nd February 1983)

SUMMARY

The simultaneous determination of major impurities present in Antarctic snow and ice at ng g^{-1} (ppb) concentrations by ion chromatography is described. Calibration data are presented for ammonium, sodium, potassium, chloride, nitrate and sulphate ions. Special attention is paid to the different ways of removing field contamination from ice and snow cores and suitable equipment is described. The results provide evidence against the validity of published sets of concentration data for nitrogen-containing compounds (NO_3^- and NH_4^+) in Antarctic snow, and demonstrate a crucial contamination problem in the determination of ammonium ions.

Antarctic aerosol is mainly composed of sea salt particles and gas-derived ultrafine secondary aerosol [1]. There is increasing interest in the major soluble impurity records in snow and ice layers, because they reflect the changes in the chemical composition of polar aerosol with time. Some of the impurities detected in polar ice are involved in biochemical cycles and are therefore of global concern. In recent years, several publications have been devoted to the determination of trace elements in polar snow and ice [2—5]. In this paper, results are presented for the concentrations of major cations (Na^+, K^+, NH_4^+) and anions (Cl^-, NO_3^-, SO_4^{2-}) at the ppb level (ppb is defined as ng g^{-1}).

The determination of such low concentrations requires the use of special sampling and measurement techniques. Furthermore, this study was intended to establish not only the concentrations of the different ions, but also their chemical form (i.e., the ionic balance in the atmospheric aerosol). Ultratrace analysis for metals at concentrations lower than 1 ppb generally requires a tedious preconcentration step [6]. The use of ion chromatography made it possible to measure all the ions listed above at the ppb level in a relatively small (10—20 ml) amount of meltwater without any preconcentration. In the same sample, acidity (or H^+ concentration) was determined by titration [7].

Snow (or firn) and ice must be considered as two different materials. Snow and superficial firn are soft and can easily be sampled in snow pits by

0003-2670/84/$03.00

pushing plastic vessels in the pit walls by hand. Deep firn cores may be collected by using plastic augers equipped with plastic knives.

The risk of contaminating firn cores is high because dust easily penetrates into the pores. An original recoring device was designed in order to recover the inner part of these cores. In contrast, ice must be sampled with the aid of metal tools. Related contamination remains superficial and can be removed by rinsing with pure water, a method that cannot be used in the case of snow or firn.

This paper covers the field sampling precautions taken to avoid contamination and the analytical procedure followed to determine accurately and rapidly the six ions which form the bulk of the soluble deposited matter in central Antarctic precipitation. The results of test and calibration experiments are given along with actual sample measurements. The advantages of ion chromatography with respect to other methods of determination are discussed.

EXPERIMENTAL

Ion chromatographic and acidity measurements

Cleaning of sample flasks and vials. The polyetheylene flasks (60 or 120 ml) used to store meltwater samples were pre-cleaned. First, they were filled with double-deionized water (resistivity >18 MΩ) and put into a microwave oven for 5 min to desorb impurities. After this step, each flask was rinsed several times and filled with double-deionized water, and left for 12 h on a clean air bench (class 100) before use. Meltwater samples were always placed in sealed polyethylene bags, refrozen and stored at -15°C between two series of measurements. Precleaned disposable 30-ml polystyrene vials (Coulter Accuvettes) were sometimes used in the field to sample superficial snow layers. In this case, the snow was melted in the laboratory just before the determination. All flasks or vials containing a sample were opened only inside a clean air bench.

Recoring devices. The recoring device (Fig. 1A) used for contaminated snow and firn cores was assembled and operated in a clean air bench located in a cold room (-20°C). The drilling system (diameter, 2 cm), made of PTFE and equipped with three molybdenum bits, is mounted at the top of a plexiglas cylindrical box into which the core falls. The assembly is fastened to a slowly rotating axle. All parts of this system in contact with cores were thoroughly washed with double-deionized water before use. After collection, the small firn cores were broken into several parts and put into plastic flasks.

The thermal probe (Fig. 1B) [8] was used for melting and collecting the inner part of ice cores. Different diameters (2.4 or 6 cm) were used, depending on the size of the initial ice core and the amount of meltwater needed for the quantitative method. This device was also operated in a clean air bench located in a refrigerated ($+5^{\circ}$C) clean air room. In this case, only liquid water samples were collected.

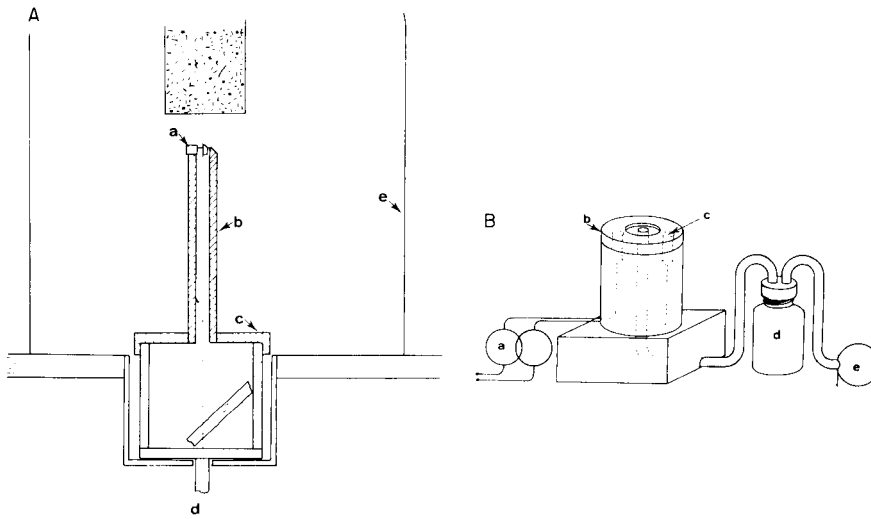

Fig. 1. (A) Recoring system for firn cores: (a) molybdenum bits; (b) PTFE core drill; (c) plexiglas box; (d) gear motor; (e) clean air bench. (B) Recoring system for ice core: (a) variable potentiometer; (b) heating head; (c) resistances; (d) Accuvettes vials; (e) vacuum pump.

Instrumentation. Cations (Na^+, NH_4^+ and K^+) and anions (Cl^-, NO_3^- and SO_4^{2-}) were measured by using a Dionex (Model 10) ion chromatograph. Working conditions are given in Table 1. A linear recorder was used to trace chromatograms; the chart speed was 0.25 cm min^{-1}. The sample was introduced into the chromatograph with the aid of a syringe (10 ml). The volume of the internal sample loop was 5 ml except for chloride measurements

TABLE 1

Working conditions for the Dionex Model 10 ion chromatograph

	Separator column		Suppressor column		Eluent	Flow rate (ml h^{-1})	Regeneration[a]
	I.d. (mm)	Length (mm)	I.d. (mm)	Length (mm)			
Na^+, NH_4^+, K^+	6	250	9	100	0.005 M HCl	280	0.5 M NaOH
SO_4^{2-}, NO_3^-	4	250	6	250	0.002 M Na_2CO_3 0.0025 M $NaHCO_3$	280	0.5 M H_2SO_4
Cl^-	4	125	6	250	0.003 M Na_2CO_3 0.002 M NaOH	250	0.5 M H_2SO_4

[a]At a rate of 140 ml h^{-1}, then rinsing with double-deionized water for 90 min.

(1.5 ml). Between two injections, the loop was rinsed with 10 ml of double-deionized water.

Standard solutions. Five 0.1 M standard solutions (NaCl, NH_4Cl, KCl, KNO_3 and Na_2SO_4), supplied by Orion, were used to prepare stock solutions containing 5 mg l^{-1} Na^+, 1 mg l^{-1} NH_4^+ and 1 mg l^{-1} K^+ (cation determination) or 5 mg l^{-1} Cl^-, 5 mg l^{-1} SO_4^{2-} and 1 mg l^{-1} NO_3^- (anion determination). All dilutions were made with double-deionized water. The concentration ratios in these solutions were chosen to be similar to those in Antarctic snows. The different test solutions used for calibration were prepared by diluting these stock solutions.

Neutron activation (n.a.) measurements

Frozen meltwater samples were melted within a clean air bench (class 100) and transferred to 30-ml polyethylene vials which had been rinsed first with dilute nitric acid and hydrofluoric acid (both Suprapur, Merck) and then with double-deionized water (from a Millipore Milli-Q system). The vials were sealed in individual polyethylene bags and re-frozen. They were then allowed to melt at room temperature just before irradiation at the High Flux Reactor of the Laue Langevin Institute, Grenoble. A bag containing a 30-ml vial was placed in a polyethylene "rabbit", which carried the sample through the pneumatic system to a position near the reactor core. Irradiation was done for 5 min at a thermal neutron flux of 1.6×10^{13} n cm^{-2} s^{-1}.

After irradiation, the samples were returned to the laboratory in 30 s and transferred manually to a counting box where the γ-peaks were counted with a 50-cm^3 Ge—Li detector coupled to a Plurimat 20 calculator (Intertechnique). The observed resolution was 2.5 keV for the ^{60}Co 1332-keV peak and the peak-to-Compton ratio was 40. The γ-peaks used were 1642.0 keV for ^{38}Cl and 1368.4 keV for ^{24}Na. The counting times were 10 min for ^{38}Cl and 30 min for ^{24}Na. The peak activity was computed by Cowell's method. Because of the large sample volume required (30 ml), the sample and the standard were not placed in the same rabbit. Flux monitors (20 μg of Na) were irradiated with each sample to check irradiation flux.

Standards were pure solutions of chloride and sodium ions with concentrations varying from 20 to 500 ng g^{-1}. They were irradiated and counted under the same conditions as samples. The error on counting rates per unit mass was estimated from the dispersion of the experimental data around the calibration regression line (typically 7% for ^{38}Cl, 1% for ^{24}Na). Average analytical error (the sum of the statistical counting error of both samples and flux monitor and of the calibration error) varied from 8 to 13% for ^{38}Cl and from 2 to 5% for ^{24}Na, depending on the concentration. The maximum blank values related to laboratory work were generally <3 ng g^{-1} for chloride and <1 ng g^{-1} for sodium. The validity of the sodium measurements was checked by irradiating dilute solutions of sodium ion prepared from the NBS standard "Trace element in water" samples, containing 9 ng g^{-1} sodium.

RESULTS AND DISCUSSION

Optimum conditions for ion chromatography

The volume of the internal sampling loop of the ion chromatograph is chosen as a function of the concentration level to be measured. For measurements at concentrations higher than 100 ng g^{-1}, a sample volume smaller than 500 μl is generally sufficient. Before this study was started, it was believed that the measurement of low concentrations (<10 ng g^{-1}) would require the use of a concentrator column [9] in order to avoid loss of sensitivity by peak broadening when large loops were used. In fact, preliminary tests showed that this effect was not very important, probably because of the high eluent flow used (55—60% of the maximum flow rate, 460 ml h^{-1}, available with the Dionex chromatograph). Table 2 is a comparison of measurements of 20 ng g^{-1} sodium ion when either a large sampling loop or a concentrator column was used. Peak height to sample volume ratios were found to be much the same (about 2.9 and 3.1 cm ml^{-1}, respectively). Consequently, the use of large loops (5 to 10 ml) was preferred to mounting a concentrator column, which increases the pressure of sample loading.

The minimum detectable quantity of an element is generally defined as a function of the baseline fluctuations. In order to obtain reasonably stable baselines conditioning of columns by the eluent requires particular attention. It was observed that a correct stabilization was reached in 60 min for cations, 4 h for chloride and 6 h for nitrate and sulphate measurements. Under these conditions, it was possible to obtain a detection limit of 1 ng g^{-1} for all elements and to measure 20—25 samples for cations, 30 for chloride and 20 for nitrate and sulphate, before saturation of the suppressor column. For some elements (especially Na^+), the detector response may change appreciably depending on room temperature changes, or on the state of the columns; it was therefore necessary to calibrate at the beginning of each set of measurements.

The 4 × 250-mm separator column supplied by Dionex for anion determinations was not suitable for chloride because at ng g^{-1} levels, the peak of this element starts in the so-called "water dip". Recently, a new separator

TABLE 2

Peak heights as a function of injected volumes when a large loop or a concentrator column was used. When a sampling loop was used, the volume injected corresponded to the volume of the loop

	Large sampling loop			Concentrator column		
Sample volume (ml)	1.0	2.6	4.8	1.0	3.0	5.0
Peak height (cm)	2.7	7.1	13.8	2.5	9.25	15.0

column (S_2) specially designed for chloride measurements became available. When this column is used, the chloride peak appears after the water dip. In this manner, it was possible to achieve a good detection limit (≈ 2 ng g^{-1}). Typical ion chromatograms (obtained on standard solutions) are shown in Fig. 2.

Calibrations

The ion chromatographic procedures were calibrated with standard solutions. Calculated regression lines, estimated errors, correlation coefficients and minimum detection limits are given in Table 3.

An intercalibration of the neutron activation and chromatographic techniques was done for the Na^+ and Cl^- concentrations in 18 ice samples collected in East Antarctica. The agreement (as can be seen in Fig. 3) between both sets of data is excellent. It must be kept in mind that the chromatographic method measures only chloride whereas neutron activation measures total chlorine. However, the neutron activation results are not systematically higher than the chromatographic results, which suggests that chlorine is not present in inorganic or organic forms other than chloride at any significant concentration.

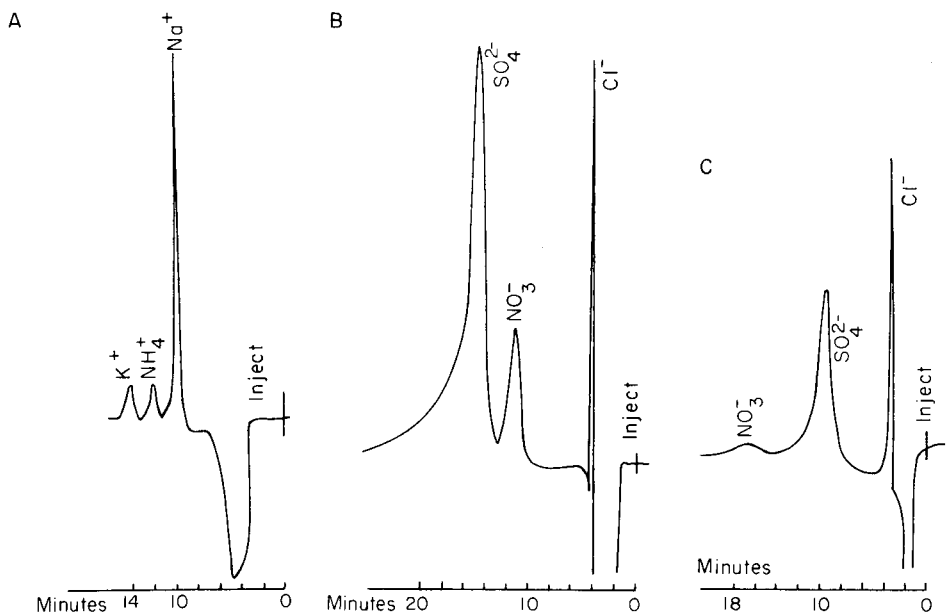

Fig. 2. Typical ion chromatograms. (A) Na^+ (8 ng g^{-1}), NH_4^+ (1 ng g^{-1}) and K^+ (4 ng g^{-1}); meter setting 3 μS, expansion 4, sample volume 6 ml. (B) Cl^- (80 ng g^{-1}), NO_3^- (15 ng g^{-1}) and SO_4^{2-} (50 ng g^{-1}); meter setting 10 μS, expansion 20, sample volume 6 ml. (C) Cl^- (30 ng g^{-1}), SO_4^{2-} (100 ng g^{-1}) and NO_3^- (30 ng g^{-1}) with S_2 separator column; meter setting 10 μS, expansion 20, sample volume 2 ml.

TABLE 3

Parameters of calibration lines and estimation of precision for the ion chromatographic measurement of the six major ions (Na^+, NH_4^+, K^+, Cl^-, NO_3^- and SO_4^{2-}) in Antarctic precipitation

	Na^+	NH_4^+	K^+	Cl^-	NO_3^-	SO_4^{2-}
Range (ng g^{-1})	0—30	0—10	0—10	0—50	0—40	0—250
Regression line[a]	$h = 0.132 + 1.0807\ C$	$h = -0.032 + 0.7818\ C$	$h = -0.014 + 0.2354\ C$	$h = 0.305 + 0.2391\ C$	$h = -0.041 + 0.1855\ C$	$h = -0.197 + 0.7151\ C$
Error[b] (ng g^{-1})	±1.3	±0.7	±1.0	±2.7	±1.3	±11.0
r[c]	0.998	0.996	0.992	0.998	0.999	0.998
Detection limit	0.5	0.5	1.0	2.0	1.0	2.0

[a] h is peak height and C is concentration. [b] Estimated at 95% confidence limits. [c] Correlation coefficient.

Contamination problems by atmospheric trace gases

Several different experiments demonstrated clearly that measurements of ammonium ion at ng g^{-1} levels could be widely erroneous if stringent precautions were not taken for sample handling and melting. First, several Accuvettes were filled with double-deionized water within a clean air bench and left open over variable time periods (5—520 min); ammonium ion was then

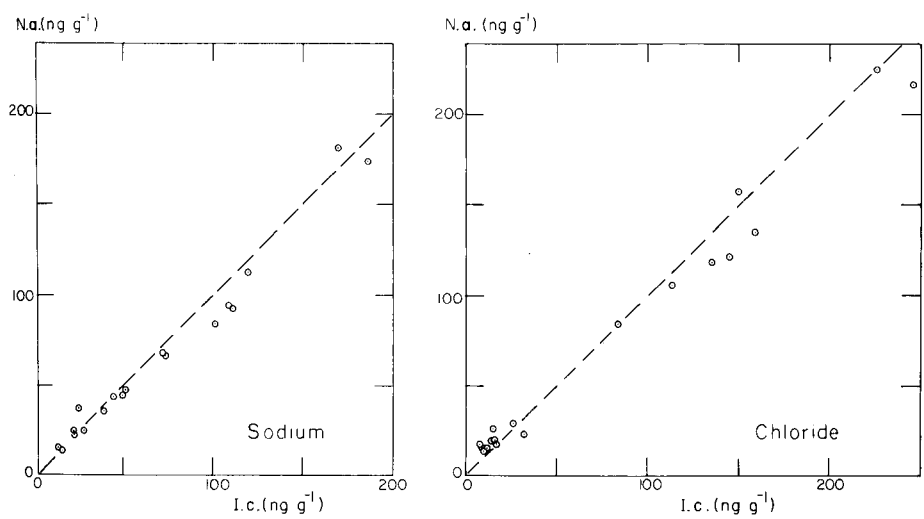

Fig. 3. Intercalibration between ion chromatography (i.c.) and neutron activation (n.a.) for Na^+ and Cl^- in Antarctic snow samples. The dashed lines are the theoretical regression lines of unit slope.

TABLE 4

Increasing concentrations of ammonium ion in double-deionized water samples exposed to ambient air in a clean air bench

Time (min)	5	18	33	60	92	124	342	517
NH_4^+ found ($ng\ g^{-1}$)	1	2	3	8	10	16	31	49

measured in each. Results given in Table 4 show that the ammonium ion concentration reached 49 ng g^{-1} after less than 9 h; this uptake was not observed when the vials were closed immediately after filling with ultrapure water. A standard solution (5 ng g^{-1} NH_4^+) was measured 3 times; the results showed increasing concentrations of NH_4^+ (5, 8 and 12 ng g^{-1}).

The results concerning two sets of samples collected side by side in the same snow pit are reported in Fig. 4. All samples were collected in Accuvettes and transported in sealed plastic bags from the Antarctic to Grenoble. One batch suffered inadvertent but limited melting en route; this obviously had a dramatic effect on the ammonium ion concentrations.

This sort of contamination has been noted by Hayes et al. [10], who showed that sulphuric acid particles deposited on filters collected in the stratosphere were readily neutralized by ammonia and converted to ammonium sulphate when stored in laboratory air. The obvious explanation for this contamination is the ready dissolution of atmospheric ammonia traces into meltwater: $NH_3 + H_2O \rightleftharpoons NH_4^+ + OH^-$. Another contamination hazard seems to be linked to the methyl chloride used in refrigeration circuits of cold rooms, which may leak accidentally. In such cases, a strong chlorine signal was measured by neutron activation in samples stored in cold rooms. This signal was not detected by ion chromatography, which shows the non-ionic nature of the chlorine contamination.

A few cases of meltwater contamination by nitrite were observed, possibly because of dissolution of the atmospheric traces of nitrogen dioxide: $2\ NO_2 + H_2O \rightleftharpoons HNO_2 + HNO_3$.

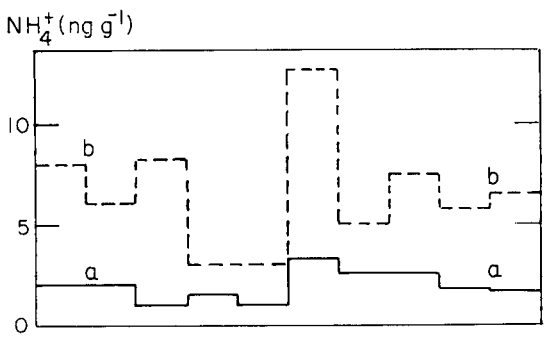

Fig. 4. Comparison of NH_4^+ profiles on samples of Antarctica snow (South Pole): (a) correct samples; (b) accidentally melted samples.

Contamination problems during sample collection and recoring

The different techniques used to collect snow and ice may appreciably contaminate the samples. The importance of this contamination was assessed in order to determine the best of the five procedures used during this study: (1) direct sample collection in plastic vials (Accuvettes); (2) surface decontamination of firn cores with the aid of a handsaw; (3) "dry" recoring; (4) "wet" recoring; (5) sample rinsing (wet cleaning).

Sampling in plastic vials is tedious, but this method, which can be used only up to about 10 m depth in Central Antarctica, gave excellent results for the major trace elements. Blank values were negligible as long as stringent precautions were taken (e.g., clean clothes when working in the snow pit, Accuvettes closed immediately with plastic caps and then wrapped in double sealed polyethylene bags). At depths greater than about 10 m, firn was so hard that a drill was needed. Surface contamination of firn or ice cores is then inevitable. The surface layers of firn cores can be removed with a teflon (PTFE)-coated handsaw. Another means of eliminating the outer part of the core is to recore using the small drilling device shown in Fig. 1A. At Dome C, snow sample series were collected and decontaminated by these three procedures. The depth of the samples was from 2.3 to 2.8 m both in a pit (samples collected in Accuvettes) and in two parallel snow cores drilled side by side about 1 km away from the snow pit. The results of this comparison are reported in Fig. 5 for the seven major soluble anions and cations (NH_4^+, K^+, NO_3^-, SO_4^{2-}, Na^+, Cl^- and H^+). Generally, they agree quite well. However, for NH_4^+ and K^+, it can be seen that handsaw cutting is less efficient than the two other methods, probably because of slight dragging of contaminants from the surface into the inner part of the core. The best decontamination procedure of a firn core is therefore a "dry" recoring.

The above methods cannot be used for ice cores; decontamination by rinsing or recoring with the aid of the thermal probe (Fig. 1B) is then needed. The efficiency of rinsing with double-deionized water was tested on an ice core section (at 359 m depth) taken in the 906-m ice core of Dome C, Antarctica. The sample was slowly melted in a plastic funnel in a clean air bench. Successive meltwater fractions (ca. 20 ml) were recovered and measured by ion chromatography and acid titration. Between each 20-ml fraction, the remaining ice piece was rinsed with double-deionized water and introduced into a new clean plastic funnel. These operations were repeated until the ice core was completely melted. The operator wore a mask and plastic gloves for transferring the ice pieces. The results (Fig. 6) clearly show that there was very significant superficial contamination of the ice, except for nitrate and ammonium ions. Concentrations decreased rapidly from the outside to the inside of the ice core, the inner part (less than 50% of the core) probably being free of contamination. Moreover, major contamination by atmospheric trace gases is evident for NO_3^-, NH_4^+ and even NO_2^-. Only the heart of the core (which was melted directly in a clean flask) was completely free of this effect (see above). It can therefore be

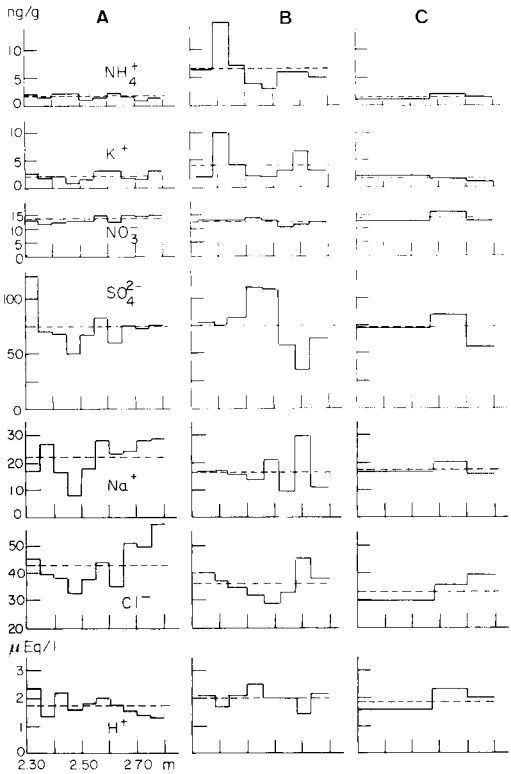

Fig. 5. Comparison of three profiles in Dome C snow: (A) in a pit; (B) core cutting with handsaw; (C) core recoring with drill. Concentrations are given as a function of depth (m).

concluded that for these seven major elements, satisfactory decontamination of the ice cores can be achieved by rinsing with double-deionized water and 50% removal of the material.

When thin ice layers (<1 cm thick) must be studied, e.g., to obtain the exact ice-print of a volcanic event, rinsing is not suitable. In this case, it is necessary to use the special thermal probe (Fig. 1B) which melts the contamination-free inner part of the ice core for collection.

CONCLUSION

These efforts to understand and to reduce contamination problems in snow and ice sample collection and processing lead to the conclusion that reliable results can only be obtained for major anions and cations if certain stringent sampling conditions or sample decontamination procedures are followed. These results are generally in agreement with those recently obtained by other research workers. However, discrepancies are

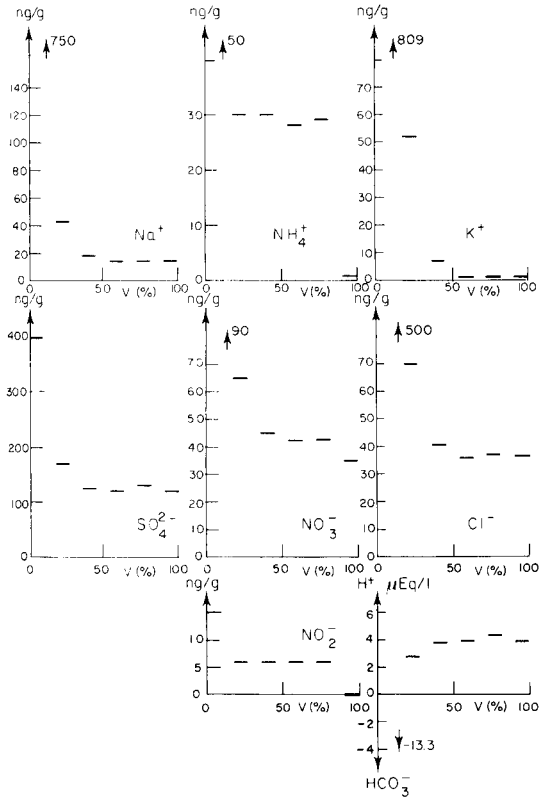

Fig. 6. Demonstration of the external contamination of an ice core. Measurement of meltwater after successive washings with double-deionized water. Concentrations (ng g^{-1}) are given as a function of the melted fraction of the ice sample (V, %).

TABLE 5

Concentrations of nitrogen-containing compounds obtained in Antarctic snow and ice (in ng g^{-1}, NO_3^- or NH_4^+) by different authors. At each of the three Antarctic stations, the results presented here correspond to the same period

Site and time period or depth	This study[a]		Other studies[a]		Ref.
	NO_3^-	NH_4^+	NO_3^-	NH_4^+	
Dome C 1969—1979	28 (10—57)	1.3 (0.5—3.5)	27 (11—102)	18 (12—40)	11
South Pole 1958—1970	89 (63—130)	3.0 (0.5—8.0)	133 (80—290)	8 (4—27)	12
Vostok 50—950 m	54 (15—190)	2.0 (0.5—4.0)	530 (49—2340)	25 (8—46)	11

[a]Mean values with ranges in parentheses.

large for nitrate and overall ammonium ion concentrations (Table 5). The different cases of sample contamination outlined above probably explain the excessive concentrations which were found for these ions. Compared with other analytical methods, ion chromatography is the most efficient, even for Na^+ and K^+ determinations. The amount of meltwater required is about an order of magnitude less than for neutron activation and two orders less than for atomic absorption spectrometry. Along with acid titration, ion chromatography is particularly suitable for measuring all the major ions of the ionic balance in Antarctic precipitation.

We are very grateful to D. Donnou for designing the recoring system for firn cores. Field work was supported by Terres Australes et Antarctiques Françaises, Expéditions Polaires Françaises and the U.S. National Science Foundation. CNRS (ATP "Nuisances chimiques") and the Ministère de l'Environnement sponsored jointly the purchase of the ion chromatograph.

REFERENCES

1 W. C. Cunningham and W. H. Zoller, J. Aerosol. Sci., 12 (1981) 367.
2 C. Boutron and C. Patterson, Geochim. Cosmochim. Acta, 47 (1983) 1355.
3 M. M. Herron, J. Geophys. Res., 87 (1982) 3052.
4 C. U. Hammer, in E. D. Goldberg (Ed.), Atmospheric Chemistry, Dahlem Konferenzen, Springer-Verlag, Berlin, 1982, 119.
5 R. J. Delmas, M. Briat and M. Legrand, J. Geophys. Res., 84 (1982) 4314.
6 C. Boutron and S. Martin, Anal. Chem., 51 (1979) 140.
7 M. R. Legrand, A. J. Aristarain and R. J. Delmas, Anal. Chem., 54 (1982) 1336.
8 A. J. Aristarain, Thèse de 3e cycle, Grenoble, 1980; Publ. No. 322 du Laboratoire de Glaciologie et Géophysique de l'Environnement.
9 R. A. Wetzel, C. L. Anderson, H. Schluder and G. D. Grook, Anal. Chem., 51 (1979) 1532.
10 D. Hayes, K. Snetsinger, G. Ferry, V. Oberbeck and N. Farlow, Geophys. Res. Lett., 7 (1980) 974.
11 E. J. Zeller and B. C. Parker, Geophys. Res. Lett., 8 (1981) 895.
12 B. C. Parker and E. J. Zeller, Antarct. J. U.S., 14 (1980) 80.

Analytica Chimica Acta, 156 (1984) 193—199
Elsevier Science Publishers B.V., Amsterdam — Printed in The Netherlands

THE EXTRACTION OF GOLD(III) FROM NITRIC ACID MEDIUM

Z. MARCZENKO* and T. KOWALSKI
Department of Analytical Chemistry, Technical University, 00-664 Warsaw (Poland)
(Received 31st May 1983)

SUMMARY

The extraction of gold(III) from nitric acid solutions by means of oxygen-containing solvents (di-isopropyl, diethyl and dichlorodiethyl ethers, methyl isobutyl and methyl isopropyl ketones, n-amyl acetate and n-amyl alcohol) is described. The most effective of these extractants are di-isopropyl ether (in the range 5.5—10 M nitric acid) and diethyl ether (4—10 M nitric acid). In both cases, maximum extraction is ca. 95% in a single pass. Salting-out agents (ammonium, magnesium and aluminium nitrates) have little effect on the extraction of gold(III) with di-isopropyl ether. Uranium(VI), thorium(IV), cerium-(IV) and chromium(VI) are extracted to different degrees with di-isopropyl ether under the optimal conditions for gold (7 M nitric acid). The method for extracting gold from strong nitric acid medium with di-isopropyl ether is applied in the analysis of anode copper and copper concentrate.

Gold is generally separated by extraction of chloroauric and bromoauric acids by means of oxygen-containing solvents such as methyl isobutyl ketone (MIBK), ethyl acetate, amyl acetate, mesityl oxide, di-isopropyl, diethyl or dichlorodiethyl ethers, tri-n-butyl phosphate (TBP) or tri-n-octyl phosphine oxide (TOPO) solutions in cyclohexanone. Gold can also be separated from chloride medium as acetylacetonate, dithizonate, diethyldithiocarbamate, thiooxinate, thionaphthoate and as a complex with di-(2-ethylhexyl)phosphoric acid (HDEHP) [1—4].

Sometimes it is necessary to extract gold from media other than chloride [1, 3, 4]. Extractive separation of gold from nitric acid medium is useful in the analysis of materials containing significant amounts of silver which interferes with the extraction of gold as its chloride complex. Nørström and Sillén [5] and Bock and Bock [6] extracted gold(III) as its nitrate complex from nitric acid medium with diethyl ether. Gold has also been extracted from nitric acid medium with petroleum ether [7], dibenzylsulphoxide in benzene [8], TBP in carbon tetrachloride [9], TOPO in cyclohexane [10], isooctylthioglycolate [11], tetrabutylmethylenediphosphonate or tetrabutyl ethylenediphosphonate [12], and 5-(4-pyridyl)nonane *N*-oxide in xylene [13].

In view of the need to separate gold from nitric acid medium in the analysis of samples obtained during processing of copper ores, and because of the lack of data concerning such methods, a detailed study of the extraction

0003-2670/84/$03.00

of gold with oxygen-containing solvents from nitric acid medium was undertaken.

EXPERIMENTAL

Reagents and apparatus

A standard solution of gold(III) (chloride-free, 200 μg ml^{-1}) was prepared by dissolving 20 mg of gold metal in aqua regia, evaporating the solution twice to dryness on a water bath, dissolving the dry residue in concentrated nitric acid, adding silver nitrate solution and filtering off the precipitated silver chloride. The results of gravimetric determinations showed that under the conditions applied a three-fold (molar) amount of silver chloride (relative to the gold present in the solution) was formed; this indicates that silver ions quantitatively remove chloride from the coordination sphere of gold(III) (after evaporation to dryness of a gold(III) chloride solution, gold is present as $AuCl_3$). The concentration of nitric acid in the standard solution of gold(III) was about 11 M and the concentration of silver ions was 0.1 M. The solution was stable for one week; after that, a brown precipitate, hydrated gold(III) oxide [14], appeared. Lower nitric acid concentrations in the gold solution decreased the stability.

A standard solution of gold(III), containing chloride only in the gold complex (200 μg ml^{-1}) was prepared by dissolving 20 mg of gold in aqua regia, evaporating the solution to dryness with nitric acid on a water bath several times, and dissolving the dry residue in water.

Dichlorodiethyl ether was purified from chloride by shaking with 1 M silver nitrate solution and filtering off the silver chloride. Di-isopropyl and diethyl ethers, methyl isobutyl and methyl isopropyl ketones, n-amyl acetate and n-amyl alcohol were used without special purification.

Gold-198 was used as the gold(III) chloride complex. Chloride-free nitric acid and water were used.

The atomic absorption spectrometric (a.a.s.) measurements were done with a Unicam SP-90A Series 2 spectrometer. For the radiometric measurements, a well-type scintillation counter was used with a high voltage supply and a scaler manufactured by POLON (Poland).

General procedures

Examination of the gold extraction by a.a.s. An aqueous nitrate solution of gold(III) (10 ml) was shaken with 10 ml of organic solvent for 30 s. After phase separation, the organic phase was transferred to a beaker. The solvent was evaporated and the dry residue was dissolved in aqua regia. After dilution with water, the solution was transferred to a 10-ml volumetric flask and diluted with water to the mark. The gold content was determined by the standard addition technique.

Radiometric examination of the gold extraction. A chloride-free standard solution of gold(III) was prepared as described above after addition of a

suitable amount of gold-198. After extraction and treatment of the extract as above, gold was determined in the aqueous and organic phases by measuring the activity of 1 ml of the phases placed in polyethylene vials.

Recommended procedures for materials

Anode copper. A sample of anode copper (10 g) was heated with 50 ml of 2 M nitric acid at a temperature close to boiling in a covered beaker (periodically, concentrated nitric acid was added to replace the acid used in the reaction with copper). The residue was filtered off (filtrate A, precipitate B).

To filtrate A, sufficient concentrated nitric acid was added to give a final concentration of about 7 M. The solution was shaken twice with half its volume of di-isopropyl ether. The aqueous phase was separated and the organic phase was transferred to a beaker. The ether was evaporated and the dry residue was dissolved in aqua regia. After removal of nitrate by several evaporations to dryness with hydrochloric acid (on a water bath), gold was coprecipitated with tellurium collector [2]. The precipitate of tellurium and gold was filtered off and dissolved in aqua regia. Nitrate was removed from the solution as described above and gold was determined by using the extractive-spectrophotometric method with rhodamine B [2] (with benzene as extractant).

Precipitate B was dissolved in aqua regia and gold was determined as described above after separation with tellurium.

Copper concentrate. The sample of copper concentrate (10 g) was first ignited at about 500°C, and then leached by heating with 50 ml of nitric acid (1 + 1) for about 2 h. Centrifugation gave solution C and precipitate D. Gold was determined in solution C as described above for filtrate A. Precipitate D was dissolved by heating with a mixture of 30 ml of concentrated hydrochloric acid and 20 ml of hydrofluoric acid (40%). The solution was evaporated to dryness. The dry residue was dissolved in aqua regia and the solution was diluted with water as to give a final solution 2 M in hydrochloric acid. The solution was shaken twice with an equal volume of di-isopropyl ether. In the extract, gold was determined as described above for filtrate A.

RESULTS AND DISCUSSION

Conditions for the extraction of gold

The effect of the concentration of nitric acid on the extraction of gold-(III) from chloride-free medium with the above-mentioned solvents was examined. The extraction curve for gold with di-isopropyl ether (Fig. 1, curve a) has a maximum in the range 5.5—10 M nitric acid, the maximum extraction being about 95%. The decrease in the extraction at nitric acid concentration exceeding 10 M is presumably due to mutual solubility of water and ether. Curves b, c and d in Fig. 1 represent the extraction of gold-(III) from nitric acid medium in the presence of chloride ions. (In these three

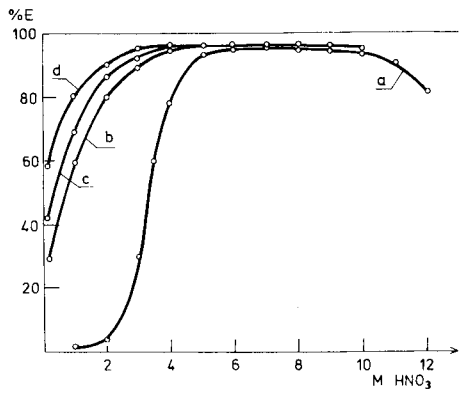

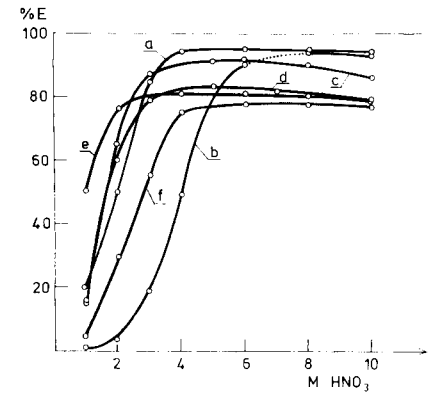

Fig. 1. Dependence of the di-isopropyl ether extraction of gold(III) on the nitric acid concentration for 20 μg Au ml^{-1}. Curves: (a) chloride-free medium; (b) chloride in stoichiometric amounts of gold; (c) 0.5 M HCl; (d) 1 M HCl.

Fig. 2. Dependence of the extraction of gold(III) with different solvents on the nitric acid concentration for 20 μg Au ml^{-1}. Curves: (a) diethyl ether; (b) dichlorodiethyl ether; (c) MIBK; (d) methyl isopropyl ketone; (c) n-amyl alcohol; (f) n-amyl acetate.

cases, the standard solution of gold(III) was free from chloride not bound in the gold complex.) The presence of chloride ions, even in stoichiometric amounts with respect to gold, clearly has a significant effect on the course of the extraction curve.

Effective extraction of gold(III) (ca. 95%) was also obtained by using diethyl ether in the range 4—10 M nitric acid (curve a, Fig. 2). Again, the percentage extraction decreased at nitric acid concentrations above 10 M. Dichlorodiethyl ether (curve b, Fig. 2) could be used to extract gold(III) in the range 8—10 M nitric acid, the maximum extraction being ca. 94% (at these acidities, the organic phase is less dense than the aqueous phase). In the range 6—8 M nitric acid, the densities of the aqueous and organic phases are similar which makes extraction impossible. At nitric acid concentrations less than 6 M, the extraction does not exceed 90% (the organic phase is then more dense than the aqueous phase).

Methyl isobutyl ketone (MIBK) is a good extractant for gold(III) in the range 4—8 M nitric acid (curve c, Fig. 2), the maximum extraction being ca. 92%. The other extractants examined were less effective. The maximum extraction of gold(III) was about 82% (curve d) for methyl isopropyl ketone, 81% (curve e) for n-amyl alcohol, and 78% (curve f) for n-amyl acetate.

Attempts were made to enhance the extraction of gold(III) by using salting-out agents. Gold (20 μg Au ml^{-1}) was extracted with di-isopropyl ether from 7 M nitric acid in the presence of 1 M aluminium nitrate or 1.5 M magnesium nitrate (these salt concentrations were close to their solubility in 7 M nitric acid at room temperature). In both cases, the effect of the salting-out cations was small; the extraction attained ca. 97%. The effect

of salting-out agents (ammonium, magnesium or aluminium nitrates) was more pronounced at nitric acid concentrations less than the optimal (Fig. 3). Nitrate salts in sufficient concentration allowed gold to be extracted with good efficiency from solutions with lower nitric acid concentrations.

The effect of the gold(III) concentration on its extraction with di-isopropyl ether from 7 M nitric acid medium was examined. The extraction percentage was practically constant (93—97%) within the gold concentration range 0.1 μg ml^{-1}— 1 mg ml^{-1}. A brown hydrated gold(III) oxide precipitated quickly from the solution of 10 mg Au ml^{-1} in 7 M nitric acid.

The following elements were effectively extracted with oxygen-containing solvents from nitric acid medium: uranium(VI), thorium(IV), cerium(IV) and chromium(VI). Extraction of these metals with di-isopropyl ether under optimal conditions for gold extraction (7 M nitric acid, 30 s shaking time) was evaluated, with the results shown in Table 1.

Determination of gold in materials

Gold traces were determined in anode copper and copper concentrate from the electrolytic refining of copper. In order to separate the interfering elements, the samples were dissolved in nitric acid. The gold metal in the

TABLE 1

Di-isopropyl ether extraction of uranium(VI), thorium(IV), cerium(IV) and chromium(VI) from 7 M nitric acid medium (phase volumes ratio 1:1)

Concentration (mg ml^{-1})	Extraction (%)			
	U(VI)	Th(IV)	Ce(IV)	Cr(VI)
10	31	11	63	10
0.1	29	12	6	2
0.01	28	10	<1	<1

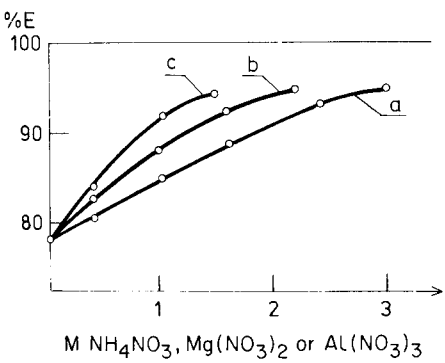

Fig. 3. Effect of concentration of NH_4NO_3, $Mg(NO_3)_2$ or $Al(NO_3)_3$ on extraction of gold(III) (20 μg Au ml^{-1}, 4 M HNO_3). Curves: (a) NH_4NO_3; (b) $Mg(NO_3)_2$; (c) $Al(NO_3)_3$.

TABLE 2

Results obtained for gold in samples (10 g) of anode copper (Nos. 1 and 2) and copper concentrate (No. 3)

Sample	Gold (μg) added to		Gold (μg) found[c] in	
	sample[a]	filtrate[b]	residue	filtrate
1	—	—	1.47 ± 0.15	—
	5.00	—	5.81 ± 0.57	—
	—	5.00	—	4.70 ± 0.24
2	—	—	2.05 ± 0.25	—
	5.00	—	6.36 ± 0.72	—
	—	5.00	—	4.74 ± 0.30
3	—	—	1.68 ± 0.19	—
	5.00	—	6.32 ± 0.65	—
	—	5.00	—	4.83 ± 0.31

[a]As metal (after precipitation with tellurium collector and ignition) to the weighed sample before treatment with nitric acid. [b]As chloride-free gold solution. [c]Mean and confidence limits (probability level 0.90) for three determinations.

samples should remain in the residue. However, it is quite probable that any gold present as compounds (e.g., sulphide, selenide, telluride) or as the chloride complex would pass to the solution. Therefore gold must be determined in the filtrate as well. The results presented in Table 2 were obtained by applying the procedures described in the Experimental section. Gold was determined in the three samples without and with addition of gold. These data prove that during the treatment of samples with nitric acid, very little gold passes to the solution. Trace amounts of gold added to the nitrate filtrate were almost completely recovered (about 95%) when the proposed extraction separation was applied.

Conclusions

Extraction from a nitric acid medium makes it possible to separate small amounts of gold(III) from many metals. Of the extractants examined, the most effective are di-isopropyl ether (in the range 5.5—10 M nitric acid) and diethyl ether (in the range 4—10 M nitric acid). In both cases, quantitative separation of gold can be achieved by double extraction. Di-isopropyl ether is more convenient in use, owing to its lower volatility and weaker reducing properties.

Dichlorodiethyl ether and MIBK are good extractants of gold(III) in the range 8—10 M and 4—8 M nitric acid, respectively. Quantitative separation of gold(III) with methyl isopropyl ketone, n-amyl alcohol and n-amyl acetate is possible only by multiple extractions.

Extraction of gold(III) from nitric acid medium makes possible its separation from most elements. When di-isopropyl ether and 7 M nitric acid are used, only uranium(VI), thorium(IV), cerium(IV) and chromium(VI) are extracted, but the extractions are less effective than that of gold(III).

REFERENCES

1 N. R. Das and S. N. Bhattacharyya, Talanta, 23 (1976) 535.
2 Z. Marczenko, Spectrophotometric Determination of Elements, Ellis Horwood, Chichester, 1976.
3 G. H. Morrison and H. Freiser, Solvent Extraction in Analytical Chemistry, Wiley, New York, 1957.
4 E. B. Sandell and H. Onishi, Photometric Determination of Traces of Metals. General Aspects, Wiley, New York, 1978.
5 A. Nφrström and L. G. Sillén, Sven. Kem. Tidskr., 60 (1948) 227.
6 R. Bock and E. Bock, Z. Anorg. Chem., 236 (1950) 146.
7 Tseng Chia Lian, Radiochem. Radioanal. Lett., 26 (1976) 165.
8 P. Markl, Mikrochim. Acta, (1973) 907.
9 V. R. Negina, V. N. Zamyatnina, M. A. Presnyakova and L. A. Chikisheva, Radiokhimiya, 3 (1961) 473.
10 C. A. Horton and J. C. White, Anal. Chem., 30 (1958) 1779.
11 J. S. Fritz, R. K. Gillette and H. E. Mishmash, Anal. Chem., 38 (1966) 1869.
12 T. Ishimóri, K. Kimura, E. Nakamura, J. Akatsu and T. Kobune, Nippon Genshiryoku Gakkaishi, 5 (1963) 663; Chem. Abstr., 61 (1964) 10102d.
13 M. Ejaz, Talanta, 23 (1976) 193.
14 D. T. Burns, A. Townshend and A. H. Carter, Inorganic Reaction Chemistry. Vol. 2. Reaction of the Elements and Their Compounds. Part A: Alkali Metals to Nitrogen, Ellis Horwood, Chichester, 1981.

Analytica Chimica Acta, 156 (1984) 201—206
Elsevier Science Publishers B.V., Amsterdam — Printed in The Netherlands

KOMPLEXBILDUNG UND EXTRAKTION VON KUPFER UND EISEN SOWIE GALLIUM MIT ISOMEREN LANGKETTIGEN ALKYLCHINOLIN-8-OLEN

E. UHLEMANN* und W. WEBER

Pädagogische Hochschule "Karl Liebknecht", DDR-1500 Potsdam (Deutsche Demokratische Republik)

C. FISCHER

Akademie der Wissenschaften der DDR, Zentralinstitut für Festkörperphysik und Werkstofforschung, DDR-8027 Dresden (Deutsche Demokratische Republik)

M. RAAB

Akademie der Wissenschaften der DDR, Zentralinstitut für Ernährung, DDR-1500 Potsdam-Rehbrücke (Deutsche Demokratische Republik)

(Eingegangen den 26. Juli 1983)

SUMMARY

(Complex formation and liquid-liquid extraction of copper, iron and gallium with isomeric long-chain alkylquinolin-8-ols)

The extraction of copper(II) and iron(III) with the 5-nonyl-, 5- and 7-decyl- and 5-chloro-7-decyl derivatives of quinolin-8-ol was studied with chloroform, benzene or toluene as the organic solvent. Isomeric extractants show only small differences and are very suitable for the extraction of copper and its separation from iron, similarly to Kelex 100 (7-dodecenylquinolin-8-ol). With these derivatives log K_{ex} values are —5.18 to —6.08 for iron(III) with $pH_{0.5}$ = 4.5 to 5, whereas log K_{ex} values are 1.54 to 1.82 for copper(II) with $pH_{0.5} \approx 1.35$. The chelates of copper, iron and gallium with isomeric ligands, isolated as the solids, have characteristic differences in melting points and solubilities. To extract gallium from alkaline solution, only 7-alkyl-8-quinolinols proved as favourable.

ZUSAMMENFASSUNG

Es wurde die Extraktion von Kupfer(II) und Eisen(III) mit 5-Nonyl-, 5- und 7-Decyl- sowie 5-Chlor-7-decylchinolin-8-ol im System Chloroform/Wasser bzw. Benzin(Toluen)/Wasser untersucht. Isomere Extraktionsmittel weisen dabei nur geringfügige Unterschiede auf und sind wie Kelex 100 sehr gut für die Extraktion von Kupfer und seine Trennung von Eisen geeignet. Die in Substanz isolierten Chelate isomerer Liganden mit Kupfer, Eisen und Gallium zeigen charakteristische Abstufungen von Schmelztemperatur und Löslichkeit. Für die Galliumextraktion aus alkalischer Lösung sind danach lediglich 7-Alkylchinolin-8-ole geeignet.

Als Derivat des Chinolin-8-ols wird Kelex 100 für die Extraktion von Kupfer und seine Trennung von Eisen im technischen Maßstab angeboten. Dabei übt der Alkenylrest in 7-Stellung nur einen schwachen Einfluß auf das

0003-2670/84/$03.00

Verhältnis der relativen Komplexstabilitäten der Kupfer- und Eisenchelate aus [1]. Im Gegensatz dazu bestehen bei der Extraktion von Gallium aus Bayerlauge größenordnungsmäßige Unterschiede zwischen den isomeren 5- und 7-Nonylchinolin-8-olen [2]. Es stellt sich daher die Frage, welchen Einfluß die Position eines langkettigen Alkylsubstituenten auf die Komplexbildung und das Extraktionsverhalten von Alkylchinolin-8-olen hat. In Anlehnung an Kelex 100, das als wirksame Substanz ein 7-Dodecenylchinolin-8-ol enthält [3] wurden als Modellsubstanzen für die Untersuchungen 5- und 7-Nonylchinolin-8-ol, 5- und 7-Decylchinolin-8-ol und 5-Chlor-7-decylchinolin-8-ol ausgewählt, die Komplexbildung mit Kupfer, Eisen und Gallium, sowie die Extraktion von Kupfer und Eisen untersucht.

EXPERIMENTELLES

Extraktionsmittel und Extraktionsuntersuchungen

Die benötigten Alkylchinolin-8-ole wurden nach Literaturangaben [2, 4, 5] durch Friedel—Crafts-Acylierung von Chinolin-8-ol bzw. 5-Chlorchinolin-8-ol, Trennung der nebeneinander gebildeten 5- und 7-Acylchinolin-8-ole und Reduktion nach Wolff—Kishner synthetisiert.

Die Untersuchungen erfolgten in den Systemen Wasser/Chloroform und Wasser/Benzin. Für die wäßrige Phase wurden 5 ml Metallnitratlösung ($8 \cdot 10^{-3}$ g l^{-1}) vorgelegt, der pH-Wert durch Zusatz von verdünnter Salzsäure bzw. Kalilauge variiert und mit Wasser auf 20 ml aufgefüllt. Die Ionenstärke der Stammlösung war mit Natriumnitrat auf 0,1 M eingestellt. Das Volumen der organischen Phase betrug ebenfalls 20 ml, die Ligandkonzentration erreichte einen 200-fachen (Cu) bzw. 300-fachen Überschuß. Die Extraktionszeit war auf 15 min festgelegt. Die Messung des pH-Wertes erfolgte nach der Extraktion mit dem pH-Meßgerät MV-84 (VEB Präcitronic Dresden) unter Verwendung einer Einstabmeßkette EGA-501-N (Forschungsinstitut Meinsberg).

Zur Bestimmung des Extraktionsgrades wurde der Metallgehalt der wäßrigen Phase atomabsorptionsspektrometrisch am Gerät Perkin-Elmer 2380 bestimmt, und der Gehalt der organischen Phase durch Differenzbildung ermittelt. Daneben kamen auch radiometrische Messungen mit ^{64}Cu und ^{59}Fe nach der AKUFVE-Technik [6] zur Anwendung.

Die Bestimmung der Zeitabhängigkeit der Extraktion erfolgte beim jeweils optimalen pH-Wert. Die Abhängigkeit des Extraktionsgrades von der Ligandkonzentration wurde bei günstigster Extraktionszeit und günstigstem pH-Wert untersucht. Die organische Phase bestand aus einer vorgelegten Menge Ligandlösung, die mit dem Verdünnungsmittel entsprechend aufgefüllt wurde, während die wäßrige Phase konstant blieb. Das Metall/Ligand-Verhältnis variierte zwischen 1:1 und 1:200.

Zur Untersuchung der Trennmöglichkeiten enthielt die wäßrige Phase jeweils $2 \cdot 10^{-3}$ g l^{-1} Kupfer und Eisen.

Darstellung von Metallchelaten

Die Metallchelate der Alkylchinolin-8-ole wurden durch Umsetzung gesättigter alkoholischer Lösungen der Liganden mit konzentrierten alkoholischen Metallnitratlösungen unter Pufferung mit Natriumacetat hergestellt. Dabei fallen die Kupferchelate meist sofort aus und können durch Waschen mit Ethanol gereinigt werden. Die Eisen- und Gallium-chelate müssen mit Wasser ausgefällt werden. Zur Reinigung löst man zweckmäßigerweise in Chloroform und kristallisiert aus Chloroform/Petrolether bzw. Petrolether um.

ERGEBNISSE UND DISKUSSION

Extraktionsuntersuchungen

Die Untersuchungen erfolgten auf der Grundlage des vereinfachten Extraktionsmodells nach Markel [7]. Als abhängige Größen wurden der Extraktionsgrad (R in %), der Verteilungskoeffizient (log D) und die Extraktionskonstante (log K_{ex}) bestimmt.

Die Ergebnisse der Extraktion von Kupfer(II) und Eisen(III) mit 5-Nonylchinolin-8-ol sind für Chloroform/Wasser bzw. Benzin/Wasser in Abb. 1 dargestellt. Kupfer wird bereits aus saurer Lösung in kurzer Zeit (5 min) maximal extrahiert, während die Extraktion von Eisen(III) höhere pH-Werte erfordert. Der Rückgang des Extraktionsgrades oberhalb pH 7 ist offensichtlich auf die Bildung nichtextrahierbarer Hydroxoverbindungen zurückzuführen. Verglichen mit dem Kupfer erfolgt die Extraktion des Eisens deutlich langsamer. Die notwendige Extraktionszeit für eine maximale Extraktion beträgt 10 min.

Für die unterschiedlichen Alkylchinolin-8-ole sind die log D/pH-Abhängigkeiten der Extraktion von Kupfer und Eisen in Abb. 2 wiedergegeben. Danach hat die Stellung der Substituenten im Liganden nur geringen Einfluß auf die Extraktion. In den extrahierten Eisen(III)-chelaten sind entsprechend dem Anstieg der log D/pH-Geraden nur zwei Ligandmoleküle gebunden. Einige Kenngrößen der Extraktion sind in Tab. 1 zusammengestellt.

Nach den vorliegenden Ergebnissen sind die isomeren 5- und 7-Alkylchinolin-8-ole für die Extraktion von Kupfer und seine Abtrennung von

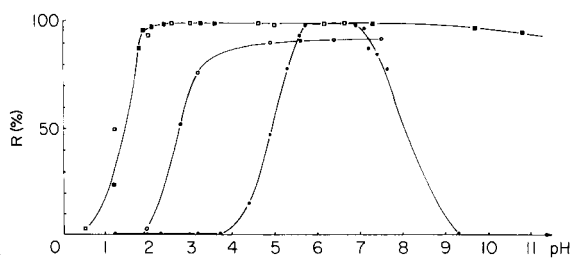

Abb. 1. Extraktionskurven für Kupfer und Eisen mit 5-Nonylchinolin-8-ol im System Chloroform/Wasser [(■) Cu, (●) Fe] bzw. Benzin/Wasser [(□) Cu, (○) Fe].

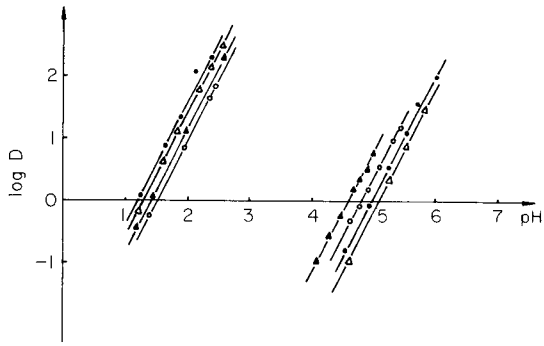

Abb. 2. Log D/pH-Darstellung für die Extraktion von Kupfer und Eisen mit verschiedenen n-Alkylchinolin-8-olen im System Chloroform/Wasser: (•) 5-Nonylchinolin-8-ol; (△) 5-Decylchinolin-8-ol; (○) 5-Chlor-7-decylchinolin-8-ol; (▲) 7-Decylchinolin-8-ol.

Eisen gleich gut geeignet. In den Werten der Extraktionskonstante offenbaren sich sogar Vorzüge gegenüber Kelex 100 (K_{ex} = 12,3): für 5-Nonylchinolin-8-ol, K_{ex} = 66,38. Da das System Chloroform/Wasser jedoch in der industriellen Praxis unüblich ist, wurden weitere Untersuchungen im System Benzin/Wasser mit den Liganden 5-Decylchinolin-8-ol und 7-Decylchinolin-8-ol vorgenommen. Während bei der Extraktion des Kupfers keine größeren Änderungen gegenüber dem System Chloroform/Wasser vorliegen, ist bei der Extraktion des Eisens in Benzin eine starke Verschiebung der Extraktionskurve in den sauren Bereich festzustellen (vgl. Abb. 1). Damit erhöht sich aber auch die für eine maximale Eisenextraktion erforderliche Ligandmenge. Die Abhängigkeit des Extraktionsgrades von der Zeit bleibt annähernd gleich. Als günstigste Bedingungen für die Extraktion von Kupfer bei gleichzeitiger Anwesenheit von Eisen erwiesen sich bei einer Extraktionszeit von 5 min pH 2,5 und ein 100-facher Überschuß an Extraktionsmittel bezogen auf vorhandenes Kupfer. Dabei konnten Trennfaktoren $\alpha_{Cu/Fe}$ von

TABELLE 1

Extraktionsparameter für die Extraktion von Kupfer(II) und Eisen(III) mit n-Alkylchinolin-8-olen[a]

Alkyl-substituent	pK_{s1}[b]	pK_{s2}[b]	Cu(II)		Fe(III)	
			$pH_{0,5}$	log K_{ex}	$pH_{0,5}$	log K_{ex}
5-Nonyl-	3,31	10,21	1,29	1,82	4,91	−5,88
5-Decyl-	3,31	10,32	1,30	1,80	5,01	−6,08
7-Decyl-	2,70	11,00	1,41	1,58	4,55	−5,18
5-Chlor-7-decyl-	2,0	10,41	1,43	1,54	4,75	−5,56

[a] $c_{Cu} = 2 \cdot 10^{-3}$ g l^{-1}, c_{HL} = 6,294 mol l^{-1}; $c_{Fe} = 2 \cdot 10^{-3}$ g l^{-1}, c_{HL} = 10,743 mol l^{-1}; I = 0,1 M, t = 15 min, T = 20°C. [b] A. Friedrich, unveröffentlichte Ergebnisse (berechnet für wäßrige Lösungen).

TABELLE 2

Extraktion von Kupfer und Eisen mit substituierten Chinolin-8-olen in aromatischen Verdünnungsmitteln (t = 3 min; c_{HL} = 0,15 M)

Extraktionsmittel	Verdünnungsmittel	pH	D_{Cu}	D_{Fe}
5-Nonylchinolin-8-ol	Toluen	1,70	620	2,9
		2,80	760	4,1
5-Chlor-7-decyl-chinolin-8-ol	Benzen/Hexan	2,60	435	0,08
		2,90	1121	0,08
Kelex 100 [1]	Toluen	1,0	13	0,16
		2,0	200	1,0[a]

[a]pH = 2,7.

TABELLE 3

Eigenschaften der Metallchelate von langkettigen n-Alkylchinolin-8-olen

Substituent	Farbe	Schmelztemperatur (°C)	C (%)		H (%)		N (%)	
			Ber.	Gef.	Ber.	Gef.	Ber.	Gef.
Kupferchelate (CuL_2)								
5-Nonyl-	goldgelb	171—73	71,7	71,7	8,0	7,8	4,6	5,0
7-Nonyl-	goldgelb	144—45	71,7	71,5	8,0	8,3	4,6	5,0
5-Decyl-	goldgelb	170—72	72,2	72,4	8,3	8,7	4,4	4,4
7-Decyl-	dunkelgelb	135—37	72,2	72,5	8,3	8,2	4,4	4,4
5-Chlor-7-decyl-[a]	hellocker	117—19	65,1	65,0	7,2	7,2	4,0	4,0
Eisen(III)-Chelate (FeL_3)								
5-Nonyl-	schwarzgrün	80—82[b]	74,8	75,2	8,4	8,5	4,85	4,7
7-Nonyl-	schwarz	52—55[c]	74,8	74,3	8,4	8,2	4,85	4,9
5-Decyl-	schwarzgrün	78—79[b]	75,3	74,95	8,7	9,0	4,6	4,5
7-Decyl-	schwarz	60—63[c]	75,3	75,0	8,7	8,45	4,6	4,6
5-Chlor-7-decyl-[c]	schwarz	186—88[d]	67,6	67,8	7,5	7,0	4,15	4,2
Galliumchelate (GaL_3)								
5-Nonyl-	rotbraun	57—58[c, d]	73,6	73,8	8,25	8,1	4,8	5,0
7-Nonyl-	gelb	80—81[c]	73,6	73,4	8,25	8,1	4,8	5,0
5-Decyl-	rotbraun	53—55[c, d]	74,2	74,5	8,5	8,3	4,55	4,75
7-Decyl-	gelb	76—78[c]	74,2	74,3	8,5	8,2	4,55	4,6
5-Chlor-7-decyl-	rotbraun	—[f]	66,7	67,0	7,4	7,2	4,1	4,3

[a]Cl: ber. 9,1; gef. 9,5%. [b]Ethanol. [c]Petrolether (wachsartig). [d]Chloroform. [e]Cl: ber. 10,5; gef. 10,6%. [f]Kein scharfes Schmelzen.

TABELLE 4

Extraktion von Gallium aus simulierter Bayerlauge mit 0,3 M Lösungen von Alkylchinolin-8-olen in Benzen/Hexanol (1:1) (t = 2 Std)

Alkylsubstituent	5-Nonyl-	7-Nonyl-	5-Chlor-7-decyl-	Kelex 100
D_{Ga}	0,05	1,03	0,05	1,05 [8]

mindestens 70 bis 90 erreicht werden. Die Rückextraktion des Kupfers ist innerhalb von 30 s mit 1 M H_2SO_4 möglich.

Für einige weitere Systeme sind die Ergebnisse der Extraktion von Kupfer und Eisen in Tab. 2 erfaßt.

Eigenschaften der Metallchelate

Die beobachtete Abhängigkeit der Eisenextraktion von verschiedenen Verdünnungsmitteln war Anlaß, Metallchelate der Alkylchinolin-8-ole in Substanz zu isolieren und ihre Eigenschaften zu untersuchen. Die wesentlichen Angaben sind in Tab. 3 zusammengefaßt. Bei den Schemelztemperaturen ist eine deutliche Abhängigkeit von der Position des Alkylsubstituenten am Liganden zu erkennen; die Chelate der 7. Alkylchinolin-8-ole mit Kupfer/Eisen schmelzen niedriger als die Chelate der 5-Isomeren. Eine ähnliche Abhängigkeit ist auch bei der Löslichkeit der Eisen(III)-chelate in diversen organischen (Lösungsmitteln festzustellen. Die bessere Löslichkeit der Chelate von 7-Alkylchinolin-8-olen bietet die Erklärung für die deutlich größeren Extraktionskonstanten.

Bei den Galliumchelaten nähert sich dieser Trend dem Extremfall. Galliumchelate der 5-Alkylchinolin-8-ole sind in Benzin fast unlöslich, während sich die entsprechenden 7-Alkylverbindungen in diesem Lösungsmittel relativ gut lösen. Damit wird die Eignung von 7-Nonylchinolin-8-ol [2] und Kelex 100 für die Galliumextraktion aus Bayerlauge verständlich, 5-Chlor-7-decylchinolin-8-ol ist dafür dagegen wieder nicht geeignet (vgl. Tab. 4).

LITERATUR

1 D. S. Flett, J. A. Hartlage, D. R. Spink und D. N. Okuhara, J. Inorg. Nucl. Chem., 37 (1975) 1967.
2 E. Uhlemann, W. Mickler und C. Fischer, Anal. Chim. Acta, 130 (1981) 177.
3 A. W. Ashbrook, Hydrometallurgy, 1 (1975) 93.
4 E. Uhlemann und W. Weber, Z. Chem., im Druck.
5 E. Uhlemann, W. Mickler, E. Ludwig und G. Klose, J. prakt. Chem., 323 (1981) 521.
6 K. Gloe und P. Mühl, Isotopenpraxis, 15 (1979) 236.
7 P. Markel, Methoden der Analyse, Bd. 13, Verlag Chemie, Weinheim, 1979.
8 J. Helgorsky und A. Leveque, Franz. Pat. 7, 424, 263 (1976); BRD-Pat. 2, 743, 475 (1978).

Analytica Chimica Acta, 156 (1984) 207—219
Elsevier Science Publishers B.V., Amsterdam — Printed in The Netherlands

APPLICATION OF STEAM DISTILLATION IN THE DETERMINATION OF PETROLEUM HYDROCARBONS IN WATER AND MUSSELS (*Mytilus edulis*) FROM DOSING EXPERIMENTS WITH CRUDE OIL

P. DONKIN* and S. V. EVANS

Institute for Marine Environmental Research, Prospect Place, The Hoe, Plymouth, PL1 3DH (Great Britain)

(Received 28th June 1983)

SUMMARY

Steam distillation is shown to provide recoveries in excess of 80% for petroleum hydrocarbons in the volatility range encompassed by toluene and pyrene from water and mussel tissues. These recoveries were achieved with an apparatus based on Dean and Stark water estimators which are commercially available at low cost. Saponification is shown to aid hydrocarbon recovery from mussel tissue. The steam distillates derived from tissues were analysed by u.v. spectrophotometry after clean-up on alumina, or directly by gas-liquid chromatography or normal- and reverse-phase high-performance liquid chromatography (h.p.l.c.). Steam distillates of water did not require prior clean-up. Normal-phase h.p.l.c. of steam distillates on an amino-cyano phase provided a particularly convenient method for petroleum-derived aromatic hydrocarbons. These techniques were examined extensively in laboratory experiments with crude oil, but preliminary results suggest that they may be used also in environmental monitoring of hydrocarbons.

The objective of these investigations was to develop a procedure for determining some of the major components of crude oil known to be important in oil spills and chronic oil pollution, with emphasis on the particularly toxic aromatic compounds. The extraction procedure should permit rapid screening of numerous samples without excluding the possibility of subsequent detailed examination of the extracts. The techniques most commonly used for the extraction of hydrocarbons tend to be complex, give poor recoveries of alkylbenzenes and some naphthalenes, and perform badly in interlaboratory comparisons [1—3].

Steam distillation has been used successfully to extract hydrocarbons from water, sediment and biota [4—13] and forms the basis of the proposed method.

EXPERIMENTAL

Apparatus

The apparatus comprised a 2-l round-bottom flask fitted with a 12.5-ml capacity Dean and Stark water estimator (for heavy entrainers) the riser part

0003-2670/84/$03.00

of which was wrapped in aluminium foil for insulation, and a Liebig condenser of 50-cm overall length; all items were Quickfit products (Fig. 1). The extraction systems were heated on a six-place electric mantle. Cooling water at 16 ± 2°C was passed through the six condensers linked in series at a flow rate of 1.7 l min^{-1}.

Extraction of hydrocarbons from water

The water was placed in the round-bottom flask followed by extracting solvent (4—10 ml) and boiling chips and then the apparatus was assembled as shown in Fig. 1. Suitable distillation rates were within the range 0.9—1.4 ml min^{-1} for the water condensing, but for each batch of extractions the distillation rates in each of the six apparatus were adjusted to within 0.08 ml min^{-1} of each other. At the end of the distillation period, the recovered solvent was removed from the water estimator which was then rinsed with <1 ml of solvent to recover residual traces of hydrocarbon. Extracts were stored at —17°C.

The efficiency of extraction of crude oil components from water by steam distillation was compared with that of direct extraction by extracting 20-ml samples of the water-accommodated fraction (w.a.f.) of North Sea crude oil [14], or w.a.f. dilutions, with three successive 3.3-ml aliquots of 2,2,4-trimethylpentane (TMP), or by extracting 1-l samples of oil-contaminated aquarium water with four successive 5-ml aliquots of TMP (see Table 2).

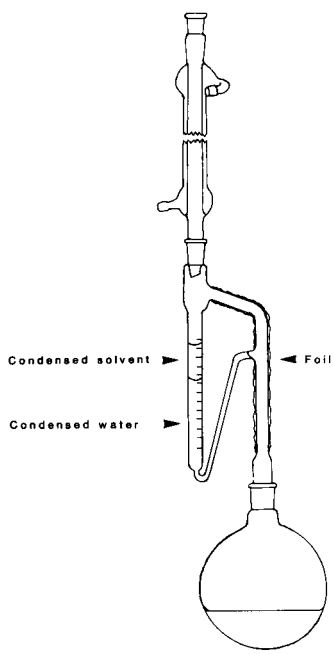

Fig. 1. Steam-distillation apparatus.

Extraction of hydrocarbons from tissues

Homogenised wet tissue, usually not more than 20 g, was added to the round-bottomed flask which already contained boiling chips, 100 ml of distilled water and organic solvent (4—10 ml). Then 10 ml of sodium hydroxide solution (4 M) was added, followed by water to a total volume of 400 ml. The apparatus was then heated sufficiently to maintain the temperature of the aqueous homogenate at 80 ± 5°C for 2 h, after which time 50 ml of 0.68 M hydrochloric acid was added by pouring down the condenser, followed by a rinse of 50 ml of distilled water. The acid addition should reduce the pH of the homogenate to between 7.5 and 11; acidification increased the recovery of non-petroleum u.v.-absorbing material.

Distillation was then continued and the distillate recovered as described above. For many aromatic hydrocarbons, distillation rates of 0.9—1.4 ml min^{-1} for water condensing proved satisfactory, but the recovery of chrysene and involatile alkanes, the latter prior to gas-liquid chromatography (g.l.c.), was improved by higher rates.

Spiking experiments. Standard compounds were dissolved in acetone and spike volumes of 100 or 200 μl of solution were added directly to water in the distillation flask before solvent addition, or to the tissue homogenate before transfer to the flask.

Treatment of distillates

Gas-liquid chromatography. Distillates, concentrated by evaporation if required, could be injected directly. G.l.c. was conducted as described elsewhere [14].

For routine g.l.c. of petroleum-contaminated mussel tissue, the homogenate, plus internal standards [14], was saponified and distilled along with 4 ml of hexane at a distillation rate of approximately 1 ml min^{-1} for water condensing. The distillation was stopped after 2 h, the hexane removed, 5 ml of hexane/cyclohexane (4:1, v/v) added to the cooled distillation flask, and the distillation was then continued for a further 14 h at a rate of 1.7—2.0 ml min^{-1} for water condensing to recover involatile alkanes. Benzenes with three or fewer alkyl carbons were measured directly in the first distillate, and then the distillates were fractionated on 2.5-g, 4% water-deactivated silica columns [15]. Alkanes were recovered in 7 ml of pentane and aromatics in 10 ml of 10% (v/v) diethyl ether in pentane.

U.v. spectrophotometry. Distillations were done with either hexane or TMP (h.p.l.c. grade). Distillates of aquarium water were measured directly. The u.v. spectrum was recorded in the range 200—350 nm.

For u.v. spectrophotometric determination of oil in mussels, a maximum wet weight of 6 g of tissue was used, and the maximum distillation time, after a preliminary 2-h saponification, was 2 h. Biogenic interferences were removed by chromatography on 2-g alumina columns [16]. Distillate (10 ml) previously dried over anhydrous sodium sulphate was loaded onto each column and the column was eluted with the same solvent as used for the

distillation until 15 ml was recovered. Alternatively, 5 ml of distillate was run onto the column, and elution was continued until 10 ml was collected.

The u.v. spectrum of the product, diluted if necessary to give an absorbance of less than 1 in the 220—225 nm region, was then recorded against an appropriate solvent blank.

High-performance liquid chromatography (h.p.l.c.). Both normal-phase and reverse-phase systems were used. Tissue weights distilled ranged from 1 to 6 g; extracting solvent was generally hexane (5 ml).

The normal-phase system comprised a Shandon column (250 mm long, 5 mm bore) and precolumn, packed with Partisil-10 PAC (polar amino-cyano; Whatman). The mobile phase was hexane at a flow rate of 2 ml min^{-1}. Eluting aromatic hydrocarbons were detected by means of a Perkin-Elmer LC-75 u.v. spectrophotometric detector with wavelength settings of 225 nm or 254 nm and sensitivity set at 0.01 to 0.04 absorbance for f.s.d. At least 200 injections of distillate could be made into the PAC system without noticeable deterioration of column performance. Procedures for regenerating contaminated columns have been devised [17—19].

For reverse-phase h.p.l.c., a column of the same dimensions as that described above was packed with 5-μm ODS-Hypersil (Shandon) and eluted with 20% (w/v) water in methanol; u.v. detection was used as above. Prior to injection into this system, methanol was added to the distillates, and the hexane was evaporated off.

Samples were injected with a syringe via a Rheodyne valve fitted with loops of 100- or 200-μl capacity. The larger loop was used with the normal-phase system only.

RESULTS AND DISCUSSION

Recovery of hydrocarbons by steam distillation

Recovery of specific hydrocarbons from water. The results in Table 1 show that good recoveries can be obtained for hydrocarbons which are major components of aqueous dispersions of crude and fuel oils [20]. A distillation time of 1 h was adequate to recover hydrocarbons encompassing a wide range of volatility.

Recovery of u.v.-absorbing components of North Sea (Auk Field) crude oil from water. The u.v. spectrum of Auk crude oil in hydrocarbon solvents (Fig. 2) has a broad peak with a maximum at approximately 225 nm, largely from alkylnaphthalenes, and a less strongly absorbing shoulder, partly from phenanthrenes and benzenes, at approximately 257 nm. The region of high absorbance below 220 nm which is predominant in w.a.f. of the oil is due mainly to the high concentration of benzenes [14].

Typically, more than 70% of the components absorbing at 220—225 nm could be recovered within 1 h (Table 2). Recovery at 255 nm was less than at 220—225 nm.

TABLE 1

Recovery of hydrocarbons from water by steam distillation

Hydrocarbon	Hydrocarbon concentration in water[a] ($\mu g\ l^{-1}$)	Distillation time[b] (h)	Hydrocarbon recovery[c] (%)
Aromatics			
Toluene	50	2	90.3 ± 3.5 (3)
	130	0.5, 1 and 2	100.9 ± 2.8 (6)
	870	2	98.5 ± 3.4 (4)
	4,320	3	84.6
o-Xylene	50	2	92.5 ± 3.7 (3)
	130	0.5, 1 and 2	110.0 ± 4.9 (6)
	4,380	1 and 3	98.9 ± 4.2 (2)
n-Propylbenzene	230	3	93.1
Naphthalene	1	1	99.5 ± 1.7 (3)[d]
	6	1	95.1 ± 1.7 (3)[e]
	2,510	1	95.7 ± 7.2 (3)
2-Methylnaphthalene	2,510	1 and 3	93.1 ± 2.2 (4)
1,5-Dimethylnaphthalene	530	2	90.2 ± 9.2 (4)
	2,640	1 and 3	87.7 ± 5.2 (4)
Biphenyl	250	3	92.3
	2,420	1 and 3	93.2 ± 1.4 (4)
Phenanthrene	1	1	89.0 ± 8.3 (3)[d]
	650	2	89.7 ± 8.7 (4)
	2,700	1 and 3	97.9 ± 3.5 (4)
Pyrene	1	1	88.4 ± 6.2 (3)[d]
	4	1	102.0[f]
	10	1	97.2 ± 8.1 (2)[e]
Chrysene	1	2	87.7 ± 1.4 (3)[d]
Alkanes			
Undecane (n-C_{11})	3,690	1	95.4 ± 2.2 (2)
Eicosane (n-C_{20})	130	3	80.3
	220	2	86.9 ± 2.9 (4)

[a]The hydrocarbons were spiked into 0.4 l or 1 l of filtered sea water and steam-distilled with either 4 ml or 10 ml of hexane or TMP or 10 ml of pentane. Pentane was not used for the extraction of toluene, xylene or undecane. [b]Where more than one distillation time is indicated, recoveries obtained with each individual distillation are averaged; no account is taken of distillation time. [c]Mean ± range where $n = 2$ or ± standard deviation where $n > 2$; n, the number of determinations is shown in parentheses. Distillates were analysed by g.l.c. except where denoted otherwise. [d]H.p.l.c. [e]U.v. spectrophotometry. [f]U.v. fluorescence.

Hydrocarbon recovery from mussel tissues. The results presented in Table 3 show that alkaline saponification can substantially increase the recovery of hydrocarbons from mussel tissue by steam distillation. This observation is consistent with other evidence that the presence of lipids in biota can adversely affect recovery of non-polar compounds by vapour-phase procedures [21, 22].

TABLE 3

Effect of saponification on the recovery of hydrocarbons from mussel tissues by steam distillation

Hydrocarbon	Hydrocarbon added to tissue ($\mu g\ g^{-1}$ wet wt.)	Hydrocarbon recovery[a] (%)		Relative increase in recovery[b] (%)
		+NaOH	−NaOH	
Specific hydrocarbons[c]				
Toluene	57.7	93.3 ± 5.5	85.9 ± 12.3	8.6
1,5-Dimethylnaphthalene	35.0	97.4 ± 3.2	86.1 ± 4.6	13.1
Phenanthrene	43.0	90.5 ± 6.8	73.7 ± 3.3	22.8
Chrysene	29.8	23.2 ± 2.1	16.9 ± 2.8	37.3
		Concentration in tissue ($\mu g\ g^{-1}$ wet wt.)		
		+NaOH	−NaOH	
Crude oil[d]				
Alkylnaphthalenes		1.86 ± 0.18	1.31 ± 0.14	42.0
Alkylphenanthrenes		0.99 ± 0.11	0.57 ± 0.11	73.7

[a]Recoveries and tissue concentrations are means ± standard deviation for 3 replicate determinations on the tissue homogenates. Analysis of "control" (i.e., uncontaminated) tissues was also triplicated and the results were used to correct the concentrations given for w.a.f.-exposed tissues. [b]$[R_{(+NaOH)} - R_{(-NaOH)}/R_{(-NaOH)}] \times 100$, where R denotes recovery. [c]6 g of spiked tissue (all wet tissue bulked) was saponified for 2 h in the presence of 6 ml of hexane and then steam-distilled for 2 h; procedural details were as described under Experimental; g.l.c. was used. [d]Distillation was done as described above, using tissues from mussels which had been exposed to a diluted w.a.f. of North Sea crude oil for in excess of 1 month. Normal-phase h.p.l.c. was quantified by reference to 2,3-dimethylnaphthalene (225 nm detection) or 1-methylphenanthrene (254 nm detection).

Compound recoveries achieved from both water and tissues by the water estimator-based apparatus were comparable with those obtained with more specialised equipment [8—10, 12, 13, 23].

Measurement techniques applicable to steam distillates containing petroleum hydrocarbons

Gas-liquid chromatography. Here, g.l.c. was used to examine mussel distillates for hydrocarbons with volatilities in the range encompassed by toluene and C_1-alkylnaphthalenes. However, the chromatographic peaks of less volatile hydrocarbons are masked by biogenic compounds which increase in concentration with distillation time. These biogenics are eluted from silica clean-up columns with the aromatic hydrocarbons; removal requires gel-permeation chromatography [24] or normal-phase h.p.l.c. [22].

If 20 g (wet weight) of mussel tissue is extracted by steam distillation and

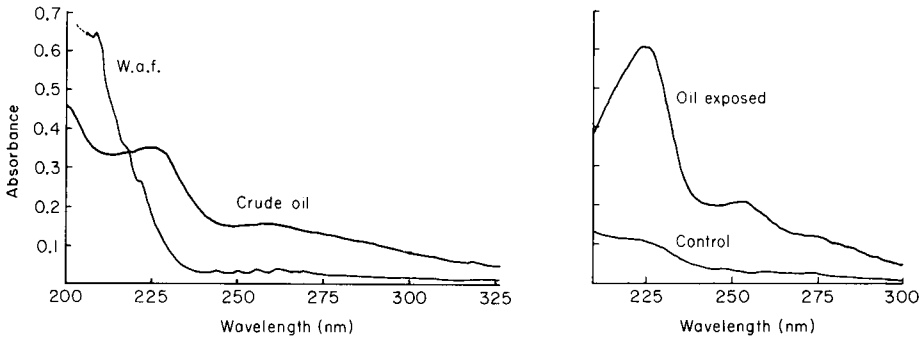

Fig. 2. U.v. absorbance spectra in 2,2,4-trimethylpentane: spectrum of North Sea (Auk Field) crude oil and spectrum of a 2,2,4-trimethylpentane extract of water-accommodated fraction (w.a.f.) of Auk Field crude oil [14].

Fig. 3. U.v. absorbance spectra of alumina cleaned-up steam distillates of mussel tissue (all remaining tissues after removal of the digestive glands); mussels exposed for 1 month to Auk Field w.a.f. with a total hydrocarbon content of 30 $\mu g\ l^{-1}$ [14] and "control" animals. Estimated aromatic hydrocarbon content of the oil contaminated tissue was 9.3 $\mu g\ g^{-1}$ wet weight. Solvent, 2,2,4-trimethylpentane.

Table 4 shows that the proposed saponification/steam distillation procedure is capable of efficient recovery of a range of hydrocarbons known to be accumulated by oil-contaminated mussels [3]. The less volatile compounds proved difficult to recover within 2 h, but recovery could be improved by extending the distillation time (see chrysene, eicosane and tetracosane) and/or increasing the distillation rate.

TABLE 2

Recovery of crude oil from water[a]

Form of oil	Conc. in water ($\mu g\ l^{-1}$)	Vol. of water (l)	Dist. time (h)	λ used (nm)	Recovery[b] (%)
Crude	1,580	0.2	0.75, 2.0	224	72.3 ± 1.8 (5)
				255	49.4 ± 4.7 (5)
W.a.f.[c]	4,200[d]	0.4	1.0	221	72.0 ± 5.0 (2)
Diluted w.a.f.	1,400[d]	1.0	1.0	221	68.2
			2.0 more	221	9.7
Aquarium[e]	25[d]	1.0	1.0	221	125.1 ± 22.6 (3)
	20[d]	1.0	1.0	221	107.0 ± 4.6 (2)

[a]Filtered sea water was extracted by steam distillation with 10 ml of 2,2,4-trimethylpentane and the distillates were examined by u.v. spectrophotometry. [b]Mean ± range where n (in parentheses) = 2 or ± standard deviation where $n > 2$. 100% recovery was considered to be that achieved by direct partition extraction into TMP (see Experimental). [c]Water-accommodated fraction of crude oil. [d]Hydrocarbon concentrations determined by g.l.c. [e]Aquarium containing mussels and dosed with w.a.f. plus algae [14].

TABLE 4

Recovery of hydrocarbons from mussel tissues by steam distillation[a]

Hydrocarbon	Hydrocarbon concentration in tissue ($\mu g\ g^{-1}$ wet wt.)	Mass of tissue (g wet wt.)	Time[b] (h)	Hydrocarbon recovery[c] (%)
Aromatics				
Toluene	14	6	1 (0.5)	104.3 ± 4.4 (3)
	30	6		85.8 ± 4.3 (2)
o-Xylene	15	6	1 (0.5)	109.3 ± 4.4 (3)
	90	20		83.3
Naphthalene	1	6		88.8 ± 4.2 (3)[d]
	50	20		85.1
2-Methylnaphthalene	50	20		92.3
1,5-Dimethylnaphthalene	20	6		94.5 ± 2.5 (2)
	50	20		94.3
Biphenyl	5	20	1 (1)	100.6
	40	15		103.5 ± 4.7 (6)
	40	2		95.5
Phenanthrene	1	6		85.6 ± 9.5 (3)[d]
	20	6		97.0 ± 2.0 (2)
	50	20		102.0
Pyrene	1	6		84.0 ± 9.4 (5)[d]
Chrysene	1	6	2 (2)	29.4 ± 5.0 (3)[d]
			14 more	47.6 ± 5.7 (3)[d]
Alkanes				
Undecane (n-C_{11})	70	20		86.7
Tetradecane (n-C_{14})	2	15	14 (2)	89.1 ± 1.2 (2)[e]
	30	6		105.2 ± 1.9 (2)
Hexadecane (n-C_{16})	30	6		91.3 ± 5.9 (5)
Eicosane (n-C_{20})	3	15	14 (2)	77.5 ± 6.5 (3)[e]
	7	6		31.9 ± 5.7 (3)
Tetracosane (n-C_{24})	15	15	2 (2)	5.3 ± 0.9 (6)
			14 more	43.6 ± 0.1 (2)

[a]Either all tissues were combined for analysis or digestive glands were removed and the remaining tissues were combined. Extraction was with 4 ml of either hexane or hexane/cyclohexane (2:1, v/v) mixture; the latter was used for 14-h distillations. [b]Saponification time was 2 h and distillation time (in parentheses) was 2 h unless otherwise tabulated. [c]See Table 1. [d]H.p.l.c. [e]Recovery after steam distillation and silica-gel column chromatography.

column fractions are reduced to 1 ml, individual hydrocarbons can be measured down to a concentration of 0.1 $\mu g\ g^{-1}$ (wet weight) with a precision generally within ±10% when quantification is by reference to internal standards.

Steam-distillation extraction of 1.5 l of water followed by concentration of the distillate to 1 ml enables individual hydrocarbons to be determined with acceptable precision by g.l.c. at concentrations down to 1 $\mu g\ l^{-1}$.

U.v. spectrophotometry. Aromatic hydrocarbons can be detected selectively in a matrix of biogenic compounds by measuring their characteristic u.v. absorbance/fluorescence; this enables clean-up procedures to be simplified. Englehardt et al. [11] quantified petroleum hydrocarbons in distillates of seal tissue by u.v. fluorescence, but did not provide recovery data for the fluorescent components. Present observations suggest that recovery by steam distillation of hydrocarbons fluorescing at long wavelengths is incomplete. By combining steam-distillation extraction with u.v. spectrophotometry, it proved possible to measure the naphthalenes, a petroleum component efficiently recovered from mussel tissue, with better precision than could be achieved with an alternative spectrophotometric procedure [25].

Aromatic hydrocarbons ranging in molecular weight from benzene to pyrene were recovered with an efficiency of more than 90% from the alumina clean-up column. Recovery of u.v.-absorbing components of crude oil from this column was 76.7 ± 1.3% at 225 nm and 68.5 ± 0.0% at 256 nm (mean ± s.d., $n = 3$ in each case).

The u.v. spectrum of a typical cleaned-up distillate of mussels experimentally exposed to Auk field crude oil is shown in Fig. 3, along with a distillate from control animals. Comparison of these spectra with that derived from a w.a.f. extract (Fig. 2), demonstrates more efficient accumulation of diaromatics by the mussel than monoaromatics.

The spectrophotometric results were quantified by calibrating against naphthalene, readings from both sample and standard spectra being taken at the peak wavelength for naphthalene (221 nm). The measurements were then related to aromatic hydrocarbon concentrations determined simultaneously by g.l.c. on a limited number of samples [14, 25]. Because of selectivity of hydrocarbon accumulation [3, 14], reference to a di- or tri-alkyl substituted naphthalene at 225—230 nm is more appropriate for tissue analysis.

The detection limit for experimental hydrocarbon contamination of mussels is controlled by the variability of the background signal measured in groups of "control" animals. Twice the error (standard deviation) of measurement of an average "control" background gave a detection limit of 0.2—0.8 $\mu g\ g^{-1}$ wet weight when expressed in naphthalene equivalents or 1.3—5.2 $\mu g\ g^{-1}$ wet weight expressed as aromatic hydrocarbons, determined by g.l.c. intercalibration [14]. Precision of duplicate hydrocarbon results corrected by means of associated duplicate control results was generally better than ±10% (range) at tissue hydrocarbon concentrations greater than 2—3 $\mu g\ g^{-1}$ wet weight expressed as naphthalene. The detection limit for u.v. spectrophotometric analysis of oil-dosed aquaria based on the precision of results for uncontaminated water (500-ml samples) was approximately 0.2 $\mu g\ l^{-1}$ expressed as naphthalene of 3 $\mu g\ l^{-1}$ expressed as oil w.a.f. The relative standard deviation at ten times this detection limit was better than ±5% ($n = 3$).

Phthalates absorb strongly at 220—230 nm and were efficiently recovered by steam distillation. However, they were not eluted from the alumina clean-up columns so could only interfere with measurements of aromatic hydrocarbons where clean-up was omitted (i.e., water analysis).

High-performance liquid chromatography. By combining u.v. spectrophotometric and spectrofluorimetric detection with h.p.l.c., the procedure for aromatic hydrocarbon can be made compound-specific or compound-group specific. Reverse-phase h.p.l.c. has been applied in this way to steam distillates of industrial effluents [7]. A reverse-phase chromatogram of a steam distillate of an oil-contaminated mussel tissue and of its associated "control" is shown in Fig. 4, along with a chromatogram of the oil w.a.f. used for experimental dosing (see [14]). The detection wavelength is 222 nm, selective for naphthalenes. The increase in biological concentration factor with increasing alkyl substitution of naphthalene is clearly demonstrated [3,

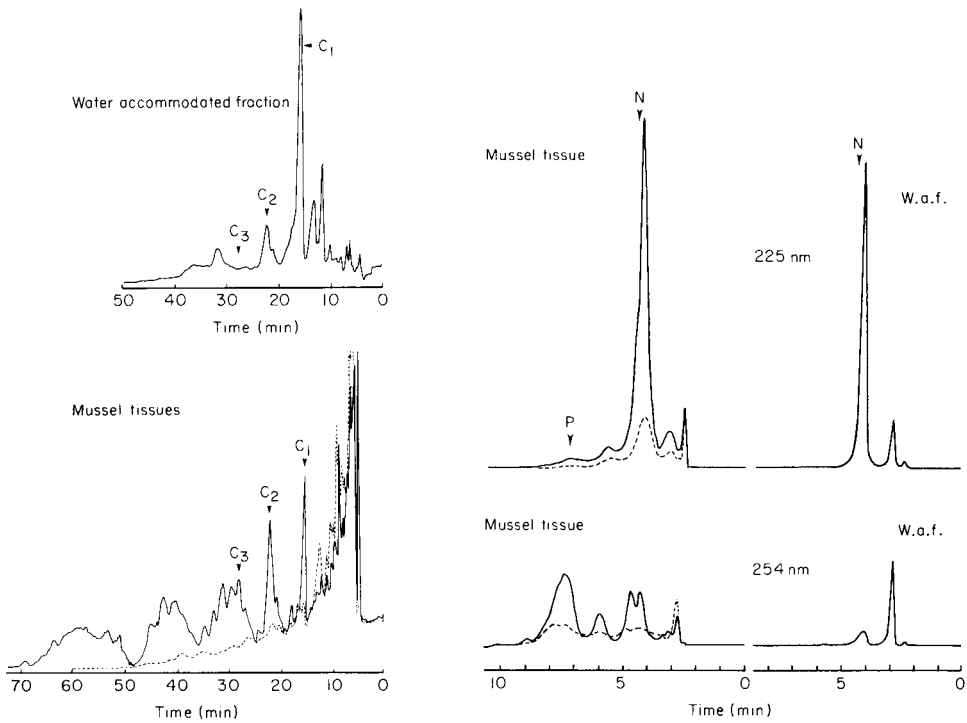

Fig. 4. Reverse-phase h.p.l.c. of a hexane extract of a w.a.f. of Auk Field crude oil and of steam distillates of mussel tissue (tissues as for Fig. 2). Mussels were exposed for 1 month to w.a.f. containing 36 $\mu g\ l^{-1}$ hydrocarbons and had a tissue aromatic hydrocarbon content of 12.6 $\mu g\ g^{-1}$ wet weight [14]. A chromatogram of a distillate derived from "control" mussels is shown by the broken line. C_1, C_2 and C_3 denote the retention times of 1-methylnaphthalene, 1,5-dimethylnaphthalene and 2,3,5-trimethylnaphthalene standards, respectively. Detection wavelength was 222 nm.

Fig. 5. Normal-phase h.p.l.c. of a hexane extract of w.a.f. of Auk Field crude oil and of a steam distillate of mussel tissue (mantle). Mussels were exposed for 20 days to w.a.f. with a total hydrocarbon content of 30 $\mu g\ l^{-1}$. A chromatogram of a distillate derived from "control" mussels is shown by the broken line. N and P denote the retention times of 2,3-dimethylnaphthalene and 1-methylphenanthrene standards, respectively. Detection wavelengths are shown.

14]. Phenanthrenes may be detected more selectively at 254 nm [26]. In this work, such chromatograms were quantified by reference to naphthalene, and representative C_1, C_2 and C_3 alkylnaphthalenes or phenanthrene and 1-methylphenanthrene, as appropriate to the monitoring wavelength. However, quantification is difficult because of the complexity of the chromatograms.

Shorter retention times and chromatograms of simpler form may be obtained by using normal-phase h.p.l.c. on amino or amino-cyano phase columns [19, 27—30]. Typical normal-phase (PAC) chromatograms derived from steam distillates of oil-contaminated mussels and an associated "control" are shown in Fig. 5, along with a chromatogram of a hexane extract of the oil w.a.f. to which the mussels were exposed [14]. The preferential accumulation of C_3-alkylnaphthalenes by the mussels is indicated by the broadening of the naphthalenes peak in comparison to that derived from the w.a.f. The quantity of u.v.-absorbing material detected by h.p.l.c. increased linearly with tissue weight extracted over a range 1—6 g wet weight for both experimentally contaminated and control animals.

The detection limit for experimental hydrocarbon contamination was determined in the same way as described for u.v. spectrophotometry. Expressed in terms of 2,3-dimethylnaphthalene and 1-methylphenanthrene equivalents, detection limits with PAC h.p.l.c. were always less than 1 $\mu g\ g^{-1}$ wet weight for naphthalenes, and less than 0.1 $\mu g\ g^{-1}$ wet weight for phenanthrenes; relative standard deviations were better than ±10% at concentrations 10 times the detection limit. Chromatograms may be quantified by reference to these standard compounds at the appropriate monitoring wavelengths (225 nm for alkylnaphthalenes, 254 nm for alkylphenanthrenes). The error introduced by using a single aromatic hydrocarbon to quantify a multicomponent peak may be estimated in selected samples by analysing appropriate h.p.l.c. fractions by g.l.c. [31].

Phthalates could not be recovered from the PAC column under the elution conditions described, so could not interfere with the analysis.

Application of steam distillation to analysis of environmental hydrocarbon residues

Although the procedures described above have been evaluated in laboratory experiments, they have also been applied successfully to a comparison of hydrocarbon contamination of mussels from a polluted dock and an estuary [32]. Examination of the steam distillates by u.v. fluorescence has enabled the distribution of aromatic hydrocarbons in an estuarine water column to be mapped [33].

We are grateful to Dr. J. Widdows and Dr. R. F. C. Mantoura for critically reading the manuscript. This work forms part of the experimental ecology programme of the Institute for Marine Environmental Research, a component of the Natural Environment Research Council. It was commissioned in

part by the Department of the Environment (U.K.) (Contract No. DGR 480/683) and the European Economic Community (Contract No. 401-80 Env. U.K. (B)).

REFERENCES

1 S. A. Wise, S. N. Chesler, F. R. Guenther, H. S. Hertz, L. R. Hilpert, W. E. May and R. M. Parris, Anal. Chem., 52 (1980) 1828.
2 H. Awad, Mar. Chem., 10 (1981) 417.
3 J. W. Farrington, A. C. Davis, N. M. Frew and K. S. Rabin, Mar. Biol., 66 (1982) 15.
4 R. G. Ackman and D. Noble, J. Fish Res. Board. Can., 30 (1973) 711.
5 K. Grob, J. Chromatogr., 84 (1973) 255.
6 L. Dalla Venezia and V. U. Fossato, Mar. Biol., 42 (1977) 233.
7 R. D. Smillie and D. T. Wang, in A. Bjorseth and A. J. Dennis (Eds.), Aromatic Hydrocarbons: Chemistry and Biological Effects, Battelle Press, Columbus, OH, 1980, p. 863.
8 T. L. Peters, Anal. Chem., 54 (1982) 1913.
9 M. Cooke, G. Nickless, A. Povey and D. J. Roberts, Sci. Total Environ., 13 (1979) 17.
10 A. A. Belisle and M. L. Gay, Bull. Environ. Contam. Toxicol., 29 (1982) 539.
11 F. R. Engelhardt, J. R. Geraci and T. G. Smith, J. Fish. Res. Board Can., 34 (1977) 1143.
12 A. Tanaka, N. Nose, T. Suzuki, A. Hirose and A. Watanabe, Analyst (London), 103 (1978) 851.
13 D. W. Kuehl, M. J. Whitaker and R. C. Dougherty, Anal. Chem., 52 (1980) 935.
14 J. Widdows, T. Bakke, B. L. Bayne, P. Donkin, D. R. Livingstone, D. M. Lowe, M. N. Moore, S. V. Evans and S. L. Moore, Mar. Biol., 67 (1982) 15.
15 P. Donkin, S. V. Mann and E. I. Hamilton, Sci. Total Environ., 19 (1981) 121.
16 P. Donkin, S. V. Mann and E. I. Hamilton, Anal. Chim. Acta, 88 (1977) 289.
17 B. A. Tomkins, R. R. Reagan, J. E. Caton and W. H. Griest, Anal. Chem., 53 (1981) 1213.
18 D. Karlesky, D. C. Shelly and I. Warner, Anal. Chem., 53 (1981) 2146.
19 R. Miller, Anal. Chem., 54 (1982) 1742.
20 J. W. Anderson, J. M. Neff, B. A. Cox, H. E. Tatem and G. M. Hightower, Mar. Biol., 27 (1974) 75.
21 M. Cooke, D. J. Roberts and M. E. Tillett, Sci. Total Environ., 15 (1980) 237.
22 S. N. Chesler, B. H. Gump, H. S. Hertz, W. E. May and S. A. Wise, Anal. Chem., 50 (1978) 805.
23 M. Godefroot, M. Stechele, P. Sandra and M. Verzele, J. High Res. Chromatogr. Chromatogr. Commun., 5 (1982) 75.
24 P. R. Mackie, R. Hardy, K. J. Whittle, C. Bruce and A. S. McGill, in A. Bjørseth and A. J. Dennis (Eds.), Polynuclear Aromatic Hydrocarbons: Chemistry and Biological Effects, Battelle, Columbus, OH, 1980, p. 379.
25 J. M. Neff and J. W. Anderson, Bull. Environ. Contam. Toxicol., 14 (1975) 122.
26 J. Grimalt and J. Albaiges, J. High Res. Chromatogr. Chromatogr. Commun., 5 (1982) 255.
27 S. A. Wise, S. N. Chesler, H. S. Hertz, L. R. Hilpert and W. E. May, Anal. Chem., 49 (1977) 2306.
28 J. C. Suatoni, in K. H. Altgelt and T. H. Gouw (Eds.), Chromatography in Petroleum Analysis, M. Dekker, New York, 1979, p. 121.
29 R. Amos, J. Chromatogr., 204 (1981) 469.
30 M.-L. Angelin, A. Collignan, J. Bellocq, J.-L. Oudin and M. Ewald, C. R. Acad. Sci. Paris Ser. II, 296 (1983) 705.

31 F. Berthou, Y. Gourmelun, Y. Dreano and M. P. Friocourt, J. Chromatogr., 203 (1981) 279.
32 J. Widdows, P. Donkin, P. N. Salkeld, J. J. Cleary, D. M. Lowe, S. V. Evans and P. E. Thomson, Mar. Ecol. Progr. Ser., (1984) in press.
33 A. R. D. Stebbing, J. J. Cleary, L. Brown and M. Rhead, in P. Kilho Park (Ed.), Wastes in the Ocean, Vol. 10: Monitoring Strategies for Ocean Waste Disposal, Wiley-Interscience, Chichester, 1984, in press.

Analytica Chimica Acta, 156 (1984) 221—233
Elsevier Science Publishers B.V., Amsterdam — Printed in The Netherlands

THE DETERMINATION OF NITROGEN TRICHLORIDE IN LIQUID CHLORINE

A REPORT PREPARED BY THE MERCURY ANALYSIS WORKING PARTY OF THE BUREAU INTERNATIONAL TECHNIQUE DU CHLORE[a]

BITC, 250 Avenue Louise, Bte. 72, B-1050 Bruxelles (Belgium)

(Received 13th December 1982)

SUMMARY

Methods are described for the determination of nitrogen trichloride over the range of concentrations at which it exists in chlorine manufacture and handling. The methods are based on the conversion of nitrogen trichloride to ammonium chloride by hydrochloric acid and the determination of ammonium by spectrophotometry as the indophenol complex or by potentiometry with an ammonia gas-sensing electrode; higher levels of nitrogen trichloride are determined by titration. For liquid chlorine, a sample is taken in a refrigerated trap containing hydrochloric acid. After that, the chlorine is slowly evaporated at atmospheric pressure. Results of tests are given to prove the reliability of the methods.

ZUSAMMENFASSUNG

Es werden Verfahren beschrieben zur Bestimmung von Stickstofftrichlorid in Konzentrationen, wie sie bei der Herstellung von Chlor und dessen Weiterverarbeitung auftreten können. Diesen Methoden ist die Umwandlung von Stickstofftrichlorid in Ammoniumchlorid durch konzentrierte Salzsäure gemeinsam. Die Bestimmung des Ammoniumions erfolgt spektrophotometrisch als Indophenolkomplex oder elektrochemisch durch Anwendung einer ionselektiven Elektrode; höhere Ammoniumkonzentrationen werden durch Titration bestimmt. Flüssiges Chlor wird in ein gekühltes Gefäss gebracht, dass Salzsäure enthält. Das Chlor wird verdampft bei Atmosphärischem Druck. Die Eignung dieser Analysenverfahren wird durch Testergebnisse belegt.

RÉSUMÉ

On décrit des méthodes permettant la détermination du trichlorure d'azote à la teneur dans laquelle qu'il est présent dans les fluides de fabrication du chlore et la mise en oeuvre. Les méthodes sont basées sur la conversion du trichlorure d'azote dans la chlorure d'ammonium par acide chlorhydrique et la détermination d'ammonium par spectrophotométrie comme le complexe d'indophénol ou par électrode d'ion spécifique; les concentrations plus élevées sont déterminées par titration. En cas de chlore liquide, l'échantillon est introduit dans un piège refroidi contenant de l'acide chlorhydrique. Après, le chlore est évaporé à pression atmosphérique. Les résultats des essais sont donnés pour vérifier la fidélité des méthodes.

---

[a]The members of the Working Party responsible for this report were R. Ankersmit, G. W. Ashley, W. T. Carter, M. Garcia, T. Jonsson, Ch. Killens, H. J. Ostmann, H. Romeis, K. Schüller and A. Yllana.

0003-2670/84/$03.00

After the standardization of analytical methods for the determination of mercury in products, process streams and wastes of the chlorine manufacturing, the European chlorine manufacturers started work to standardize a method for the determination of nitrogen trichloride in liquid chlorine. Nitrogen trichloride is an unstable compound which can be formed during the electrolytic production of chlorine from salt solutions which contain ammoniacal compounds. Nitrogen trichloride decomposes spontaneously and explosively at various concentrations, depending on the temperature, but usually at concentrations of >3% (w/w). Therefore, all necessary precautions must be taken to avoid appreciable amounts and concentrations of nitrogen trichloride; the chlorine industry tries to avoid amounts greater than a few grams at any point of the system and concentrations greater than 1% (w/w). These recommendations are also given to customers, because many customers evaporate the liquid chlorine before they use it and nitrogen trichloride is enriched in the residue.

From the above, it is clear that a reliable analytical method for the determination of nitrogen trichloride in liquid chlorine is necessary. The method also has to be very sensitive because of the large enrichment of nitrogen trichloride when liquid chlorine is evaporated.

METHODS FOR THE DETERMINATION OF NITROGEN TRICHLORIDE

When methods for the determination of nitrogen trichloride are considered, it is important to realise that nitrogen trichloride exists in equilibrium with ammonium chloride in liquid chlorine systems [1, 2]

$$NCl_3 + 4HCl \rightleftharpoons NH_4Cl + 3Cl_2 \quad (1)$$

Therefore, during processing of samples for the determination of nitrogen trichloride, problems can be caused by a shift in this equilibrium. Another problem in determining nitrogen trichloride is that nitrogen trichloride can decompose under numerous conditions, e.g., on exposure to u.v. radiation, at temperatures higher than 90°C, or in contact with grease, organic matter or some metals, notably copper and copper alloys such as Monel. Nitrogen trichloride can also decompose autocatalytically at concentrations as low as 4% (w/w). All these causes of loss must be eliminated during sampling and sample storage, otherwise the final results for nitrogen trichloride concentration will have a low bias.

Published methods for the determination of nitrogen trichloride are either instrumental techniques or chemical determinations based on conversion to ammonium ions. The instrumental techniques are based on the absorption of ultraviolet or infrared radiation [3] or gas chromatography [4]. Nitrogen trichloride can be determined very selectively by these methods, but this has the disadvantage that any nitrogen trichloride that has decomposed to ammonium chloride will not be detected. Other disadvantages are that these methods are not applicable over the whole concentration range that is

necessary and require the preparation of solutions of nitrogen trichloride in carbon tetrachloride for calibration purposes. (The preparation and analysis of solutions of nitrogen trichloride in carbon tetrachloride is safe by the procedure given by Noyes [1]; an outline procedure based on infrared spectrometry and used by a BITC member laboratory is given at the end of this paper.)

The chemical determinations of nitrogen trichloride are based on the determination of the ammonium ions that are formed when the equilibrium (1) is moved to the right. This can be done by using a hydrochloric acid matrix of at least 4 M [5]. If the dissolved chlorine is removed before the hydrochloric acid is neutralized or diluted below 4 M, a stable solution of ammonium chloride equivalent to the original concentration of nitrogen trichloride is obtained. The ammonium ion in this solution may be determined in several ways depending to some degree on the concentration present. If the concentration is high enough, the simplest procedure is to distil the ammonia into a known volume of standard acid solution and measure it by titration [6]. For lower levels, it is necessary to use either a spectrophotometric procedure or an ammonia. For the lowest levels (<5 mg NH_3 kg^{-1}) a spectrophotometric method is preferred because of the non-linear response of the potentiometric method at these levels. The two most widely used spectrophotometric procedures are those based on either Nessler's reagent [7] or the indophenol reaction sensitized by sodium nitroprusside [8, 9]. Neither of these methods is entirely satisfactory because they both suffer from interference and the Nessler method is also affected by high concentrations of electrolytes. These problems can be overcome by distilling the ammonia out of the hydrochloric acid solution but this increases the time required for analysis and may also lead to difficulties in achieving acceptably low blanks. Experience with the potentiometric ammonia gas-sensing electrode for this application is limited but the method appears to have advantages over the spectrophotometric procedure: it has an acceptable tolerance to dissolved electrolytes and can be used over a wider concentration range because of the logarithmic response.

Of the various methods outlined above, the chemical principle is preferred and the methods that will be described below are of this type. The most important features of these methods are as follows: (1) they are applicable to the determination of nitrogen trichloride in the concentration range 0.2—20 000 mg kg^{-1} for NCl_3 in chlorine; (2) the sampling procedure avoids contact with copper-containing metal components and grease; (3) evaporation of the sample in the presence of 8 M hydrochloric acid prevents autocatalytic decomposition of nitrogen trichloride; (4) the sample flask and absorbers are protected from light during evaporation and absorption; (5) the system of blank control is designed to achieve realistic results at low nitrogen trichloride levels, which enables a laboratory to judge whether the results obtained at low levels are meaningful with reference to the repeatability and absolute value of the blanks which are achieved.

DESCRIPTION OF METHODS

(For technical reasons, the text of the methods has been modified and shortened in certain places; those interested in the original text can obtain it in French, German or English, on application to the BITC.)

Scope and field of application

These methods are suitable for the determination of nitrogen trichloride in chlorine in the ranges 0.2—200 and 200—20 000 mg kg^{-1} nitrogen trichloride. The lower limit of detection varies with the laboratory doing the analysis and the source of the chlorine, but should not be higher than 1 mg kg^{-1} nitrogen trichloride.

Principle

The liquid chlorine is evaporated in the presence of hydrochloric acid (8 M) and the gas is scrubbed by hydrochloric acid (12 M) with which nitrogen trichloride reacts to form ammonium chloride. After removal of the dissolved chlorine, the hydrochloric acid solution is carefully neutralized and the ammonium ion is determined either by spectrophotometry of the indophenol complex or by an ammonia gas-sensing electrode for levels up to 200 mg kg^{-1} nitrogen trichloride or by distillation and titration for higher levels. For the lowest levels of nitrogen trichloride (less than 5 mg kg^{-1}) the spectrophotometric method is preferred.

Apparatus (Note 1)

A liquid chlorine sample cylinder, made of special steel (e.g., 18/8) resistant to chlorine, nitric acid (7 M) and to pressure [10] is required, e.g., Hoke HS 500. The sample capacity is 500 ml. This cylinder is subject to the pressure vessel regulations. The sample flask for taking a sample of liquid chlorine is shown in Fig. 1.

The all-glass ammonia distillation apparatus consists of a 1-l round-bottom flask with short neck and boiling rod, a multiple adapter (two necks parallel), a splash head with vertical joints, a dropping funnel (cylindrical, stem with cone), a double surface or coil condenser, and a conical flask as receiver with straight delivery adaptor with glass bubbler.

Also required are a pH meter and magnetic stirrer, and a spectrophotometer capable of making measurements at 625 nm, fitted with 1-cm cells.

For the potentiometric method, an ammonia electrode and digital pH/mV meter reading to 0.1 mV are needed. Suitable models are the Orion Ammonia Electrode Model 95-10 and Digital pH/mV Meter Model 701A. Gran's plot paper (e.g., Orion catalogue 90-00-90) is used.

Reagents (Note 1)

Methyl red/methylene blue indicator. Dissolve 0.1 g of methyl red in 65 ml of ethanol and dilute to 100 ml with water. Dissolve 0.1 g of methylene

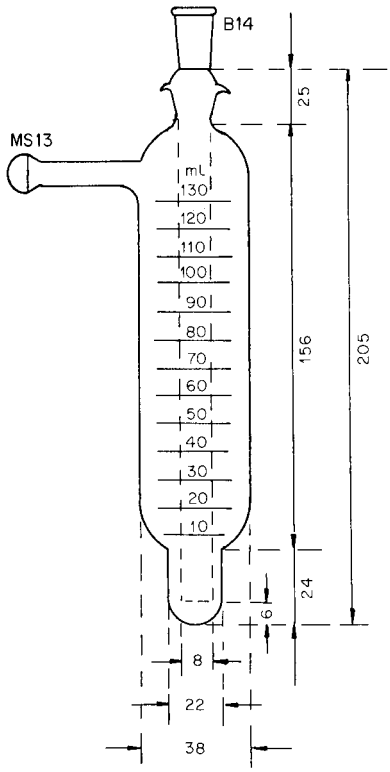

Fig. 1. Sample flask for liquid chlorine (dimensions in mm).

blue chloride in 10 ml of ethanol and 30 ml of 0.01% (w/v) potassium hydroxide. Mix both solutions.

Phenol reagent. Dissolve 5 g of phenol and 0.05 g of sodium nitroprusside, $Na(Fe(CN)_5NO) \cdot 2H_2O$, in 500 ml of water. Store in an amber glass bottle and replace every month.

Sodium hypochlorite. Dissolve 2.5 g of sodium hydroxide and 4.2 ml of sodium hypochlorite (50 g l^{-1} available chlorine) in 500 ml of water. Store in a brown bottle in a refrigerator and replace at monthly intervals. It is important to ensure that the available chlorine content of the sodium hypochlorite is at the stated value.

Standard ammonia solutions. Dissolve 3.15 g of ammonium chloride in water and dilute to 1 l in a volumetric flask; this solution contains 1000 μg ml^{-1} ammonia (if the solution is required for use with the ammonia electrode, dissolve the ammonium chloride in sodium chloride solution (2 M) and dilute to 1 l with this solution). Prepare from it by appropriate dilution with water, freshly as required, a series of standard solutions containing 100.0, 10.0 and 4.0 μg ml^{-1} ammonia.

Sampling and evaporation of the sample

Collect the sample taking care to purge all connecting lines and the sample cylinder before collecting the final sample (Note 2). Ensure that the cylinder is not overfilled. Continue the analysis immediately after collection of the sample, unless it has been established that nitrogen trichloride does not decompose at a significant rate when liquid chlorine is stored in the cylinder.

For evaporation of the sample, fill the sample flask (Fig. 1) with 10 ml of hydrochloric acid (8 M). Place the cylinder with liquid chlorine in an efficient fume chamber and connect the bottom valve of the cylinder with the sample flask via a glass wool filter. Cool the sample flask to −60°C by adding small pieces of solid carbon dioxide to trichloroethylene contained in the Dewar flask surrounding the sample flask. (WARNING: Do not allow the temperature to fall below −60°C, otherwise the 8 M hydrochloric acid may solidify.)

Slowly open the cylinder valve and collect 100 ml of sample in the cooled sample flask at a rate which allows no more than small quantities of gas to escape from the flask. Close the cylinder valve, disconnect the cylinder and store it with the valve uppermost. Attach to the sample flask two Drechsel (gas-washing) bottles, with sintered glass discs, each containing 5 ml of hydrochloric acid (12 M). Attach the second bottle to the chlorine absorption system (see Fig. 3 in [6]), consisting of two Drechsel bottles, each containing 1 l of sodium hydroxide (about 5 M). Connect the inlet of the sample flask to a supply of nitrogen, closed off by a glass tap with a small scrubber containing dilute sulphuric acid incorporated into the nitrogen line to remove traces of ammonia. Turn on the water ejector and adjust the air bleed so that the absorption train is under a slight suction and air is passing freely through the absorbers. Connect the exit from the sample flask to the first absorber, remove the Dewar flask from around the sample flask and replace it with a glass beaker. Allow the liquid chlorine to evaporate to give a gas rate of 50—100 l h^{-1}. Add water at 30°C to the beaker surrounding the sample flask as necessary to maintain the evaporation rate. Shield the evaporation flask and the absorbers from light by loosely covering them with dark coloured paper or cloth.

When all of the chlorine has evaporated, pass a slow stream of nitrogen through the sample flask and absorption system. Continue to pass nitrogen until chlorine can no longer be detected at the outlet from the second absorber using a moistened starch iodide paper.

Spectrophotometric determination of nitrogen trichloride at concentrations in the range 0.2—200 mg kg^{-1}

Neutralization of the absorbent solution. Carefully transfer the contents of the sample flask and the absorbers to a 150-ml beaker. Wash each sparingly with water and add the washings to the beaker. Place the beaker in an ice/water bath and using a magnetic stirrer, agitate the solution slowly.

Suspend a pH electrode in the cooled solution and add (x −0.5 ml) of

sodium hydroxide solution (ca. 10 M) slowly and continuously from a burette with the delivery below the liquid level in the beaker; the addition should take 4—5 min. Thereafter add the alkali in very small increments up to pH 2.5, and complete the neutralization using a dilute sodium hydroxide solution (0.1 M). In order to avoid losses of ammonia during neutralization it is essential to avoid overshooting in this titration. A trial titration may be done on 20 ml of the mixed acid but this will give a higher titration than the actual absorbing solution which loses some hydrogen chloride during passage of the chlorine gas.

Transfer the neutralized solution completely to a 100-ml standard flask, allow the solution to reach room temperature, dilute to volume with water and mix. (If the liquid chlorine sample is contaminated with iron(III) chloride, hydrous iron(III) oxide will be precipitated and should be filtered off and washed before diluting the solution to volume.)

Prepare a reagent blank by neutralizing a solution containing 10 ml of hydrochloric acid (ca. 8 M), 10 ml of hydrochloric acid (ca. 12 M) and 30 ml of water in the same manner and make up to 100 ml.

Preparation of the calibration graphs. Into a series of six 50-ml volumetric flasks, transfer 0, 1.0, 2.0, 2.5, 7.5 and 10.0 ml of standard ammonia solution (4 μg ml^{-1} NH_3). Dilute to 25 ml, add 5 ml of phenol reagent and 5 ml of sodium hypochlorite solution and mix after each addition. Dilute to volume, mix and, with the stoppers set loosely in position, place the flasks in a boiling water bath so that the test solution is covered by the boiling water. After 10 min in the bath, allow to cool to room temperature. Measure the absorbance of each solution at 625 nm using water as the reference liquid. Deduct the absorbance of the solution containing no added ammonia from the absorbance of each of the others and plot a graph of corrected absorbance against μg of ammonia added.

Examination of the test solution. Measure a suitable volume of test solution (25 ml maximum), containing not more than 30 μg of ammonia, into a 50-ml standard flask and dilute to 25 ml if necessary. Measure an equal volume of the reagent blank solution into a second volumetric flask and again dilute to 25 ml if necessary. Complete the development and measurement of the indophenol complex as described above (Note 3). Deduct the absorbance of the reagent blank solution from the absorbance of the sample and refer the corrected value to the calibration graph.

Blank monitoring. For nitrogen trichloride determinations at the lowest levels, check the daily blank value as described earlier [11] and calculate the corresponding limit of detection. A typical value of the confidence interval (*CI*) is 0.15 mg of nitrogen trichloride in a 100-ml sample.

Calculation.

$$\text{mg } NCl_3 \text{ kg}^{-1} \text{ } Cl_2 = m \times 100 \times 120.4/M \times V \times 17 = 707 \times m/(M \times V)$$

where m is the ammonia content of test solution aliquot (μg), V is the volume of the aliquot of test solution (ml), and M is the mass of sample taken (160 g for 100 ml of liquid chlorine).

Determination of nitrogen trichloride at concentrations greater than 200 mg kg^{-1} by distillation and titration

Procedure for test solution. Combine the contents of the sample flask and absorbers in a 100-ml standard flask, dilute to volume and mix.

Place 20 ml of sodium hydroxide solution (ca. 10 M) and 200 ml of water in the ammonia distillation apparatus. Distil 50 ml and reject the distillate. Into the conical flask accurately measure 25.0 ml of hydrochloric acid (0.1 M for nitrogen trichloride concentrations up to 2000 mg kg^{-1} and 1.0 M for up to 20 000 mg kg^{-1}) and place the flask in position so that the end of the condenser is immersed in the solution. Transfer 50.0 ml of the test solution to the distillation apparatus via the tap funnel and rinse through the tap funnel with a small amount of water. Distil about 100 ml of distillate into the conical flask and then lower it so that the final 5 ml of condensate washes out the delivery tube. Rinse the outside of the delivery tube into the conical flask with a small amount of water and stop the distillation.

Titrate the contents of the conical flask with sodium hydroxide solution (0.1 M or 1.0 M) using screened methyl red indicator. If the content of the conical flask is alkaline, repeat the determination with a smaller volume of test solution.

Calculation.

$$\text{mg } NCl_3\,kg^{-1}\ Cl_2 = (25.0 - V_1) \times N \times 1.205 \times 10^7/M \times V_2$$

where V_1 is the volume of standard alkali used in the back-titration (ml), N is the normality of standard acid and alkali used, M is the mass of sample taken (160 g for 100 ml of liquid chlorine), and V_2 is the volume of the aliquot of test solution (ml).

Determination of nitrogen trichloride at concentrations in the range 5—200 mg kg^{-1} with an ammonia gas-sensing electrode (Note 4)

Ammonia is determined by the standard addition method followed by evaluation by Gran's plot [12]. Prior to making the measurement in the sample solution, the electrode is calibrated in sodium chloride (2 M) to establish the slope over the anticipated working range of ammonia concentrations. If for a tenfold change in concentration, the slope is found to be within the range 58.5 ± 1 mV, the results may be evaluated on the special Gran's plot paper; if not, the alternative method of plotting on linear paper must be used.

The procedure is not recommended for the lowest levels of nitrogen chloride (less than 5 mg kg^{-1}) because at these levels the response of the electrode is slow and non-linear in sodium chloride solution (2 M).

Electrode calibration. Dip the electrode system into 500 ml of sodium chloride solution (2 M), add 5.0 ml of sodium hydroxide solution (ca. 10 M) and stir the solution slowly with a magnetic stirrer without creating a vortex. Add from a burette increments of 0.5, 1.0, 3.5, 10.0 and 100.0 ml of standard ammonia solution (1000 μg ml^{-1} ammonia in 2 M sodium chloride solution) and record the potential (to 0.1 mV) after each addition, after equilibrium

has been attained. Plot the potentials on the linear axis of semilogarithmic graph paper against ammonia concentration on the logarithmic axis. The concentrations are 1.0, 3.0, 9.9, 29.1 and 47.6 mg kg^{-1} ammonia, respectively.

Examination of test and blank solutions. Combine and neutralize the contents of the sample flask and absorbers and also neutralize a reagent blank solution as detailed above under *Neutralization of the absorbent solution.* Transfer the neutralized solutions to 100-ml standard flasks, adjust to 20°C, dilute to the mark and mix.

Pipette 50.0 ml of sample solution into a 100-ml beaker and stir slowly using a magnetic stirrer without creating a vortex. Add 0.5 ml of sodium hydroxide solution (ca. 10 M), place the electrode in the solution, wait for equilibrium to be established, and record the electrode potential. Refer this value to the calibration graph to give an approximate indication of the concentration of ammonia present and measure the slope of the calibration curve at about this level. Prepare a standard ammonia solution in sodium chloride solution (2 M) containing approximately forty times the approximate ammonia concentration present in the sample solution. (If this value indicates an ammonia concentration greater than 50 mg kg^{-1} ammonia, take a smaller sample aliquot and dilute to 50 ml with the 2 M sodium chloride solution.) Make three to five additions of 0.50-ml increments of the prepared standard ammonia solution, wait for equilibrium and read off the electrode potential to 0.1 mV after each addition.

Take an equal volume of reagent blank solution and examine in a similar manner using a 4 μg ml^{-1} ammonia standard solution, prepared in sodium chloride solution (2 M), for the additions.

If the slope of the calibration plot, produced as described above, at the concentration of the test solution, is found to be within the range 58.5 ± 1 mV, prepare a Gran's plot using the special graph paper and read off the ammonia content in mg kg^{-1} ammonia. Prepare a similar plot for the blank test solution and deduct the ammonia concentration of the blank from that of the sample.

If the value of the slope at the approximate concentration of ammonia in the test solution deviates from the theoretical value, prepare a Gran's plot on linear graph paper in the following manner. Calculate values for $10^{E/S}$ $(V + v)$ and Av/V for each addition, including zero ml and with the former displayed on the x axis and the latter on the y axis, project the plot to intercept the y axis. The negative intercept is equal to the concentration of ammonia. In these calculations, A is the concentration of the standard ammonia solution (μg ml^{-1}) in NaCl (2 M) used, v is the volume of the standard solution added (ml), V is the sample volume when the e.m.f. is measured (ml), E is the observed e.m.f. (mV) at equilibrium, and S is the change in e.m.f. (mV) for a tenfold change in ammonia concentration at the working level in NaCl (2 M). S is positive if E increases with increasing concentration of ammonia and negative if it decreases with increasing ammonia levels.

Calculation.

mg NCl_3 kg^{-1} Cl_2 = $m \times 707/M$

where m is the concentration of ammonia (mg kg^{-1}) in the 100 ml of test solution, and M is the mass of sample taken (160 g for 100 ml of liquid chlorine).

The determination of nitrogen trichloride by infrared spectrometry

Infrared spectrometry can be used for the specific determination of nitrogen trichloride at concentrations of 0.1% w/w and above, particularly in chlorine distillation residues (still boilers, chlorine evaporators, etc.).

For the determination, the "residue" is dissolved in carbon tetrachloride (1—10 g in 100 g of carbon tetrachloride) and then the carbon tetrachloride solution is analysed in the region 750—550 cm^{-1}. Nitrogen trichloride gives an absorption band at 640 cm^{-1} and the intensity of this band can be compared with bands obtained from standard solutions of nitrogen trichloride in carbon tetrachloride. These may be prepared by the procedure given by Noyes [1] and standardized by any of the chemical procedures given. The concentration of nitrogen trichloride in the prepared solutions should not exceed 1% (w/w).

Notes

1. If a laboratory is required to analyse for the complete range of nitrogen trichloride concentrations, it is essential to have two complete sets of equipment, one of which is used for nitrogen trichloride concentrations below 200 mg kg^{-1} and the other for higher levels. This applies both to the sample cylinders and connections and to the glassware which, in the case of concentrations below 200 mg kg^{-1}, should be reserved exclusively for this purpose and stored in dilute hydrochloric acid when not in use.

All reagents must be of analytical reagent quality, selected for low ammonia content. All references to water imply distilled water deionized immediately before use by passage through a cationic deionizing cartridge such as the "Elgacan" C114.

To obtain blank values low enough to make it possible to measure nitrogen trichloride concentrations at about the mg kg^{-1} level, considerable care is necessary in choosing and storing reagents and ensuring that the laboratory background ammonia level is low enough. The ammonia levels of alkaline reagents can often be reduced by boiling and cooling in an ammonia-free atmosphere. It is difficult to obtain hydrochloric acid with a suitably low ammonia content and it may be necessary to prepare this reagent by absorbing dry hydrogen chloride in water. All reagents may be protected during storage by the use of liquid dispensers pre-set to deliver the volume required in the procedures.

2. It is important to avoid materials of construction which cause the catalytic decomposition of nitrogen trichloride, notably those containing copper.

The sampling system should also be designed so that the cylinder can be purged with sample and it is essential to use a sampling procedure which avoids overfilling the cylinder.

3. If the colour of the test solution complex is different from that of the calibration solutions, interfering bodies other than iron are present. Distil 50 ml of the test and reagent blank solutions separately using a boiled-out ammonia distillation apparatus containing 5 ml of sodium hydroxide solution (ca. 10 M). Collect 49 ml of distillate in a 50-ml standard flask containing 1 ml of hydrochloric acid. Mix the contents of the flasks and repeat the development and measurement of the colour.

4. Ion-selective electrodes. Manufacturers of ion-selective electrodes supply detailed instructions on the use, care and maintenance of their products. It is essential that these instructions are read in conjunction with the procedures detailed above. Attention is particularly drawn to the following points: (a) all test, blank and standard solutions should be measured at the same temperature; (b) the electrode should be kept in alkaline standardizing solution between measurements and in ammonium chloride solution (1000 μg ml^{-1} ammonia, without added sodium hydroxide) when not in use.

The Gran's plot paper catalogue number quoted is the appropriate paper for the addition volumes specified in this paper. If different addition ratios are used the appropriate plotting paper must be substituted. When plots are made, the e.m.f. values should be plotted in such a manner that the slope of the plot is always positive.

In work with solutions with electrolyte concentrations higher than 0.1 M, there is a danger of changing the composition of the electrode reference solution by osmosis. If this is suspected, the performance of the electrode should be checked and it should be reconditioned if necessary.

EVIDENCE FOR THE RECOMMENDED PROCEDURES

Member laboratories of BITC have carried out many different experiments in order to prove the validity of the methods given. One of the problems with these experiments is that nitrogen trichloride decomposes slowly in some qualities of liquid chlorine, so these qualities cannot be used as such in these experiments (Tables 1 and 2). This decomposition of nitrogen trichloride is probably related to the reasons given in the introduction. Therefore, recovery experiments were carried out with chlorine that was vaporized and recondensed (distilled). All additions of nitrogen trichloride were made as a solution in carbon tetrachloride.

From the recovery experiments, given in Table 3, it can be observed that added nitrogen trichloride can be recovered and that the methods give excellent results, even below 1 mg kg^{-1}. Some other results on recoveries of added nitrogen trichloride have been given by de Vries et al. [13]. The results given in Table 4 indicate that the indophenol method and the ammonia gas-sensing electrode give comparable results.

TABLE 1

Stability of nitrogen trichloride in liquid chlorine after sampling in mild steel cylinders. All samples were taken from the same factory

Time after sampling (days)	1	4	6	7	13	14	15	18	21	28
NCl_3 found (mg kg^{-1})										
Sample 1[a]	66	67	—	65	—	66	—	—	—	—
Sample 2[b]	24	22	17	15	2.5	—	2	1	—	—
Sample 3[b]	18	20.5	21.5	19.5	14	—	13.5	14	8	4.5

[a]Analysis by distillation and titration (experiments done in 1954). [b]Analysis by the indophenol blue method (experiments done in 1978).

TABLE 2

Recoveries of nitrogen trichloride (50 mg kg^{-1}) added to chlorine manufactured in different factories. The indophenol blue method was used

Factory[a]	2	2	3	4	5
NCl_3 recovered (mg kg^{-1})	46	55	53	40	3

[a]Chlorine from factories 4 and 5 gave quantitative recovery of nitrogen trichloride if the nitrogen trichloride was added after the chlorine had been distilled.

TABLE 3

Recoveries of nitrogen trichloride added to distilled chlorine

Distillation and titration								
NCl_3 added (mg kg^{-1})	32	57	79	94	132	173	192	244
NCl_3 recovered (mg kg^{-1})	38	59	79	95	139	179	188	244
Indophenol blue method								
NCl_3 added (mg kg^{-1})	1.0	2.5	5.0	10.0	25	50		
NCl_3 recovered (mg kg^{-1})	1.0	2.3	4.8	9.0	26	56		
Indophenol blue method[a]								
NCl_3 added (mg kg^{-1})	0	0.10	0.10	0.50	1.00	5.0		
NCl_3 recovered (mg kg^{-1})	0	0.10	0.10	0.50	0.94	4.1		

[a]During distillation of the chlorine, the chlorine vapour was led through concentrated hydrochloric acid.

TABLE 4

Results for nitrogen trichloride (mg kg^{-1}) by indophenol method and ammonia gas-sensing electrode

Chlorine sample	1	2	3	4
Indophenol method	0.20	0.8	2.3	6.0
Ammonia gas-sensing	0.15	1.0	1.8	4.7

REFERENCES

1 W. A. Noyes, Inorganic Synthesis, Vol. 1, McGraw-Hill, New York, 1957, p. 65.
2 Th. Seliwanow, Chem. Ber., 27 (1894) 1012.
3 F. W. Czech, R. J. Fuchs and H. F. Antczak, Anal. Chem., 33 (1961) 705.
4 J. Drahonovsky, J. Hovorka and A. Capek, Chem. Prûm., 27 (1977) 62.
5 R. M. Chapin, J. Am. Chem. Soc., 53 (1931) 912.
6 British Standard 3947: 1965, Specification for Liquid Chlorine.
7 J. P. Riley, Anal. Chim. Acta, 9 (1953) 575.
8 W. T. Bolleter, C. J. Bushman and P. W. Tidwell, Anal. Chem., 33 (1961) 592.
9 B. Lubochinsky, J.-P. Zalta, Bull. Soc. Chim. Biol., 36 (1954) 1363.
10 Mercury Analysis Working Party of BITC, Anal. Chim. Acta, 87 (1976) 276.
11 Mercury Analysis Working Party of BITC, Anal. Chim. Acta, 109 (1979) 219.
12 G. Gran, Analyst, 77 (1952) 661.
13 T. de Vries, C. P. Savariar and M. M. Chakrabarthy, J. Am. Water Works Assoc., 54 (1962) 858.

Analytica Chimica Acta, 156 (1984) 235—243
Elsevier Science Publishers B.V., Amsterdam — Printed in The Netherlands

EXTRACTION STUDIES OF METAL COMPLEXES WITH SOME MACROCYCLIC TETRAAZA LIGANDS AND XANTHENE DYES
Spectrophotometric determination of Cadmium(II) with Tetramethyltetraazacyclotetradecane and Erythrosin A

WALENTY SZCZEPANIAK*, BERNARD JUSKOWIAK and WANDA CISZEWSKA

Department of Instrumental Analysis, Faculty of Chemistry, A. Mickiewicz University, ul. Grunwaldzka 6, 60-780 Poznań (Poland)

(Received 3rd January 1983)

SUMMARY

The liquid-liquid extraction of ion-pair complexes of zinc(II), copper(II) and cadmium(II) is described. The macrocyclic ligands 1,4,8,11-tetramethyl-1,4,8,11-tetraazacyclotetradecane (4Me-cyclam-14) and rac-5,7,7,12,14,14-hexamethyl-1,4,8,11-tetraazacyclotetradecane (Tet b) are used with xanthene dyes as the counter ions. The apparent extraction constants (D'_c) are reported. The sequences of extraction efficiency of both ligands are related to the structure of the complexes. The apparent molar absorptivity of the Cd(4Me-cyclam-14)—erythrosin A ion-associate is 1.1×10^5 l mol^{-1} cm^{-1}. The calibration graph is linear over the range 0—10^{-5} M, which allows even 0.05 μg ml^{-1} cadmium to be determined in a 0.5 M sodium hydroxide medium. No interference was observed from Ni^{2+}, Pb^{2+}, Zn^{2+}, Mg^{2+}, Sn^{4+}, Ga^{3+}, Al^{3+} and Fe^{3+}. Interferences were Cu^{2+}, Hg^{2+}, Ag^{+} and large anions.

The extraction properties of macrocyclic ligands have been widely studied in recent years. Several metals can be determined by extraction of the ion-pairs formed between the cationic metal/macrocyclic compound and an anionic dye [1—6]. In a previous paper from this laboratory, an extraction-spectrophotometric determination of lead(II) with cryptand (2.2.2.) and eosin was reported [7]. The high sensitivity of that method ($\epsilon = 1.1 \times 10^5$ l mol^{-1} cm^{-1}) and its relative freedom from interferences indicated that studies of other macrocyclic ligands as complexing agents would be worthwhile.

Macrocyclic tetraaza ligands, which form stable cationic complexes with heavy metal ions seem to be very useful for application in ion-pair extraction. The selectivity of complex formation principally depends on cavity size within the ligand molecule and on steric factors. Apart from papers by Luo and Chung [8] and Luo et al. [9], which were devoted to the extraction of copper complexes with Tet a and Tet b ligands as ion-pairs with halides, there seem to be no reports concerning the subject. This paper deals with the ion-pair extraction of the complexes of Cu(II), Zn(II) and

0003-2670/84/$03.00

Cd(II) with rac-5,7,7,12,14,14-hexamethyl-1,4,8,11-tetraazacyclotetradecane (Tet b) or 1,4,8,11-tetramethyl-1,4,8,11-tetraazacyclotetradecane (4Me-cyclam-14) as the ligand and a xanthene dye as the counter ion. A selective determination of traces of cadmium(II) is presented.

EXPERIMENTAL

Reagents and equipment

The ligands Tet b (Parish) and 4Me-cyclam-14 (Ventron) were used as received. Ligand solutions (10^{-2} M in 10^{-2} M sodium hydroxide) were stored in polyethylene flasks.

Chloroform was purified by distillation (60—62°C). All other chemicals were of analytical grade and were used as received. Redistilled water was used throughout.

The instrumentation included a Specord u.v.-visible recording spectrophotometer and a VSU-2P spectrophotometer (both from Zeiss, Jena) with quartz cells (10-mm path), and an AAS-1 atomic absorption spectrometer (Zeiss Jena). A Thys-2 (VEB MLW Labortechnik, Ilmenau, E. Germany) shaker with a time switch was used for horizontal shaking of stoppered polyethylene tubes.

Preliminary extraction studies

The aqueous phase for a typical test of extraction contained 1×10^{-3} M metal ion, 1×10^{-3} M dye and 1×10^{-3} M macrocyclic ligand; 0.1 M sodium hydroxide was used to provide a 10^{-2} M hydroxide ion concentration. Toluene, chloroform and nitrobenzene were examined as the solvents. No extraction was observed with toluene and high blank values were obtained when nitrobenzene was used. Chloroform was therefore selected for further work.

Sulphonephthaleins (bromophenol blue, bromocresol green, bromocresol purple, bromothymol blue) and xanthenes (eosin, erythrosin A, erythrosin B) were tested as the counter ions. The low extractability of the sulphonephthaleins eliminated them from further consideration. Various degrees of extraction were obtained with xanthene dyes for Ag^{+}, Cd^{2+}, Co^{2+}, Cu^{2+}, Hg^{2+}, Zn^{2+}. The following cations were examined: Ag^{+}, Tl^{+}, Ba^{2+}, Be^{2+}, Ca^{2+}, Cd^{2+}, Co^{2+}, Cu^{2+}, Hg^{2+}, Mn^{2+}, Mg^{2+}, Ni^{2+}, Pb^{2+}, Pd^{2+}, Sn^{2+}, Zn^{2+}, Al^{3+}, Cr^{3+}, Fe^{3+}, Ga^{3+} and In^{3+}. The extractions of Ag^{+} and Co^{2+} could not be made quantitative; the cobalt(II) complexes may have been oxidized to Co(III) complexes [10]. Mercury(II) complexes were extracted, but a maximum occurred when the effect of increasing reagent concentration was examined (i.e., the absorbance decreased as the dye concentration increased above a certain level), which did not bode well for quantitative work. Detailed extraction studies were therefore restricted to the zinc(II), copper(II) and cadmium(II) complexes.

Determination of apparent molar absorptivities

Apparent molar absorptivities (ϵ_{app}) were evaluated from the expression

$$\epsilon_{app} = \Delta A_i/(C_0^M - C_i^M)$$

where ΔA_i is the absorbance of the organic phase measured against the reagent blank, C_0^M is the total initial metal ion concentration, and C_i^M is the metal ion concentration in the aqueous phase after extraction, determined by atomic absorption spectrometry.

The results are collected in Table 1.

Recommended procedure for determination of cadmium(II)

To 1 ml of sample solution containing no more than 5 μg of cadmium(II) in a polyethylene separatory funnel, add 0.5 ml of 1×10^{-2} M 4Me-cyclam-14 in 1×10^{-2} M sodium hydroxide, 2.5 ml of 1 M sodium hydroxide to give a final hydroxide concentration of 0.5 M and 1 ml of 1×10^{-3} M erythrosin A solution. Shake with 5 ml of chloroform for 10 min, and then centrifuge for 5 min at 2000 rpm. Measure the absorbance of the organic phase at 550 nm against a reagent blank.

RESULTS AND DISCUSSION

Absorption spectra

Figure 1 shows the absorption spectra of the ion-pair formed between Cd-(4Me-cyclam-14)$^{2+}$ and erythrosin A and of the reagent blank. The shapes of the spectra of other extracts were very similar but the maxima were shifted slightly. Absorbances were measured at the wavelengths where there was the largest difference between absorbances of ion-pair and the reagent blank.

TABLE 1

Extraction equilibrium constants (log D'_c) and apparent molar absorptivities (ϵ_{app}) for ion-pairs of metal tetraaza complexes with xanthenes

Cation	Ligand	Eosin[a]		Erythrosin B[c]		Erythrosin A[d]	
		Log D'_c	ϵ[b]	Log D'_c	ϵ	Log D'_c	ϵ
Cu(II)	Tet b	4.7	7×10^4	4.9	6.6×10^4	—	—
	4Me-cyclam-14	2.6	3×10^4	3.8	6.1×10^4	3.8	5.8×10^4
Cd(II)	Tet b	4.3	7×10^4	—	—	—	—
	4Me-cyclam-14	4.8	8.5×10^4	5.6	1.2×10^5	5.6	1.2×10^5
Zn(II)	Tet b	5.6	9×10^4	5.6	8.2×10^4	—	—
	4Me-cyclam-14	2.3	5.1×10^4	3.4	8.5×10^4	3.4	7.4×10^4

[a]Tetrabromofluorescein. [b]ϵ_{app} in l mol^{-1} cm^{-1}. [c]Tetraiodofluorescein. [d]Triiodofluorescein.

Extraction equilibria

Equilibrium constants were calculated as described earlier [7]. The apparent distribution constant (D'_c) is defined as

$$D'_c = A_i/[(C^0_M - A_i)(C^0_A - A_i)] \quad (2)$$

where $A_i = \Delta A_i/\epsilon_{app}$, ΔA_i being the absorbance of the organic phase measured against the reagent blank, and $C^0_M(C^0_A)$ is the total metal ion (dye) concentration.

The values of log D'_c (Table 1) are in good accord with the extraction curves for the Zn(II), Cu(II) and Cd(II) complexes shown in Fig. 2. Generally, the complexes of Tet b are extracted better than the corresponding 4Me-cyclam-14 complexes. The better extractibility of the Tet b complexes is caused by

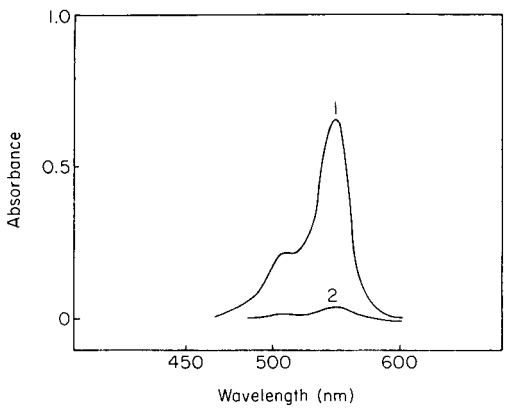

Fig. 1. Absorption spectra: (1) the extracted ion-pair, Cd(4Me-cyclam-14)$^{2+}$(erythrosin A)$^{2-}$; (2) its blank value. Conditions: 6 × 10^{-6} M Cd, 5 × 10^{-4} M 4Me-cyclam-14, 2 × 10^{-4} M erythrosin A, 0.5 M NaOH.

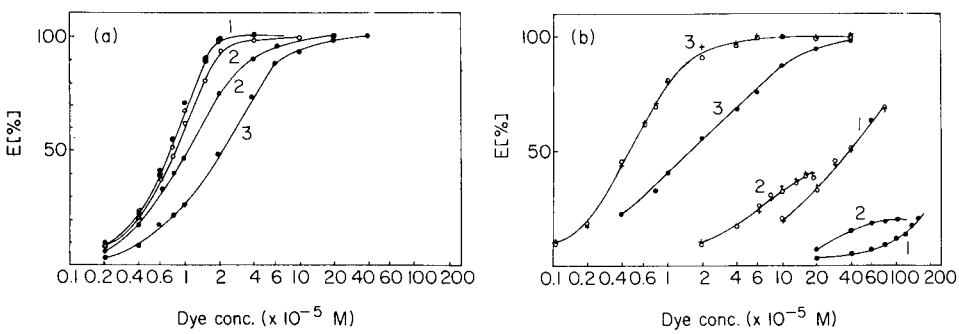

Fig. 2. Effect of dye concentration on extractions: (a) metal–(Tet b) complexes; (b) metal–(4Me-cyclam-14) complexes. Dye: (•) eosin; (○) erythrosin B; (+) erythrosin A. Metal: (1) zinc; (2) copper; (3) cadmium.

differences in the quantity and mode of substitution of methyl groups in the macrocyclic rings in the two ligands. Despite the similarity of the cavity sizes in the ligands, two different sequences of log D_c' values were obtained: Zn > Cu > Cd for Tet b and Cd ≫ Cu > Zn for 4Me-cyclam-14. That means that the extraction properties depend not only on the structure of the complexes, but on the possibility of interactions with solvent molecules and co-extracting dye anions.

Literature data on the structure relate mainly to the crystal structures in the solid state. Polarographic [11, 12] and n.m.r. [13, 14] studies have provided some information concerning the structures in solution. The structures of copper(II) macrocyclic complexes have been fairly thoroughly investigated [15—18]. Tetragonally distorted octahedral coordination of copper ion, the "*trans* III" geometry of Bosnis et al. [19], was reported for the red complex of Cu(Tet b)$^{2+}$ which exists in alkaline media. Slightly distorted tetrahedral coordination was reported [11, 12] for the Zn(Tet b)$^{2+}$ complex. To date, the Cd(Tet b)$^{2+}$ complex has not been considered in detail but several contrary reports concerning the cyclam/cadmium complex have been published.

Kodama and Kimura [20] found no complex formation between cadmium nitrate and the cyclam. The authors concluded that the Cd(II) ion (ionic radius 0.97 Å) was too large to fit within the plane of the cyclam cavity. In contrast, Alcock et al. [14] reported the formation of a mixture of two pentacoordinated isomeric Cd/cyclam complexes. One isomer contained a planar set of donor atoms with the cadmium ion displaced from the plane towards the fifth monodentate ligand (*trans* I). The other isomer has a dynamically folded trigonal bipyramidal configuration (t.b.p.) with the monodentate ligand in the equatorial plane.

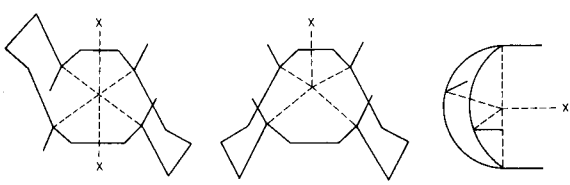

trans III *trans* I t.b.p.

The M(4Me-cyclam-14)$^{2+}$ complexes exist in both the square planar pyramid (*trans* I) and trigonal bipyramid (t.b.p.) configurations. Such coordination is possible because of the four methyl groups substituted at nitrogen atoms in the cyclam ring. In solution, the complexes take the t.b.p. configuration [13, 14]. Distortion then depends on the metal ion size; the larger the ion, the greater the degree of distortion.

Because the interactions in ion-pair formation are essentially electrostatic, there should not be considerable differences in the D_c' values for such similar

anions as erythrosin and eosin. The results for the Cu(Tet b)$^{2+}$ and Zn-(Tet b)$^{2+}$ ion-pairs with eosin and erythrosin confirm this statement.

However, in these tests, the extraction of the 4Me-cyclam-14 complexes of Cd, Zn and Cu by ion-pair formation with the iodo derivatives of fluorescein (erythrosin A and B) was much better than that with the bromo derivative (eosin). This indicates the occurrence of other than electrostatic interactions between the dye anion and the complexed cation. The additional interactions may depend on the "soft" or "hard" properties of the dye anions and the accessibility of the complexed cations. A "softer" anion and a readily accessible metal cation (i.e., a cation that does not fit fully within the macrocycle cavity) will form adducts with stronger interactions than those in pure ion-pair formation. In particular cases, the additional interaction causes the collection of the ion-associate at the phase boundary; this was observed for the Cd(Tet b) adduct with erythrosin B.

Another factor controlling the rate of extraction is a competition of monodentate anions in aqueous solution. Given the presence of a monodentate anion (the most likely is OH^-) in the coordination sphere of the complexed metal, the extraction mechanism could be

$$MLOH^+ + A^{2-} \rightleftharpoons MLA + OH^- \quad (\rightleftharpoons MLA_o)$$

where subscript o indicates the organic phase. If so, then the extraction (D'_c value) will depend on the replacement of the hydroxyl by the dye anion. Again, the "softer" anion will possess a greater ability to replace the hydroxyl in the $MLOH^+$ complex.

The results obtained for the extractions confirm the above considerations. Thus the metal coordinations in the tetrahedral Zn(Tet b)$^{2+}$ and the distorted tetrahedral Cu(Tet b)$^{2+}$ complex cations do not allow for any additional interactions of the metal ion with the dye anion; only pure electrostatic interactions will occur in ion-pair formation. In contrast, pentacoordinated complexes with trigonal bipyramid configuration can form adducts and their extraction depends on the soft and hard properties of the ions. Cadmium-(4Me-cyclam-14)$^{2+}$ is much better extracted than the corresponding copper and zinc complexes because the cadmium ion is larger and so offers greater possibilities for additional interaction with the dye anion. Finally, precipitation of an adduct at the interface was observed for the Cd(Tet b)$^{2+}$ complex with erythrosin B. This behaviour may be caused by the combined contribution of all the factors mentioned above: t.b.p. configuration, relative accessibility of the metal ion and softness of the erythrosin B.

Effect of pH

The influence of pH on the extraction was investigated only for pH > 11 to avoid the protonation of the ligand. The H_2L form of tetraaza ligands is known to be unreactive compared to the HL and L forms; the kinetic constants for the copper(II) reaction with 4Me-cyclam-14 are $k^{Cu}_{H_2L} = 1.3 \times$

10^{-4} M^{-1} s^{-1} and k_{HL}^{Cu} = 2.9 × 10^5 M^{-1} s^{-1} [21]. Further, the protonated ligand can be responsible for high reagent blank values by formation of the ion-pair H_2L^{2+} A^{2-}. An increase in the hydroxide concentration decreased the reagent blank value. The protonation constants (pK_1, pK_2, pK_3, pK_4) are (11.6, 10.7, 2.7, 2.3) [22] and (10.1, 9.35, 3.45, 2.7) [21] for Tet b and 4Me-cyclam-14, respectively.

The influence of the hydroxide concentration on the extraction of the Zn(II), Cu(II) and Cd(II) complexes of 4Me-cyclam-14 by ion-association with erythrosin A is shown in Fig. 3. The decrease in extraction with increasing hydroxide concentration is caused by competitive formation of hydroxo complexes. All extraction studies were therefore done at a sodium hydroxide concentration of 1 × 10^{-2} M; no hydroxo complex formation was observed up to that alkalinity.

Formation of the hydroxo complex might be useful for masking Cu and Zn ions in the determination of cadmium. The absorbance of Cd(4Me-cyclam-14)$^{2+}$ extracted from 0.5 M NaOH decreased only slightly while the absorbance of the copper(II) complex decreased significantly and that of the zinc(II) complex became almost negligible (Fig. 3).

The effect of metal hydrolysis on the formation of complex ML^{2+} can be expressed by $[ML^{2+}] = \alpha C_M^0$, where

$$\alpha = \{1 + (K\,[L])^{-1} + \sum_{i=1}^{n} (\beta_i^{OH}[OH]^i / K\,[L])\}^{-1}$$

K being the stability constant of the complex, β_i^{OH} the stability constant of the hydroxo complex, and C_M^0 the total metal concentration.

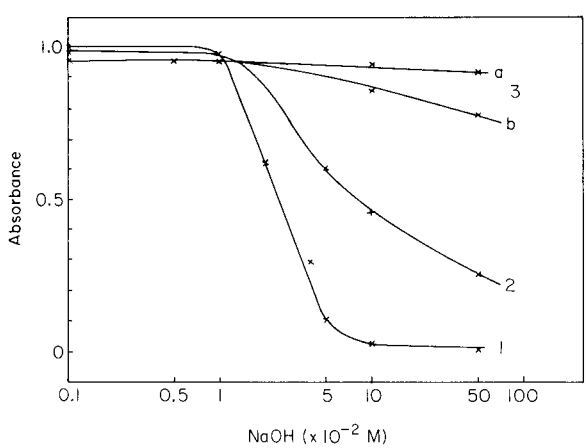

Fig. 3. Effect of the alkalinity of the aqueous phase on extraction: (1) 2 × 10^{-5} M Zn^{2+} with 2 × 10^{-4} M 4Me-cyclam-14 and 8 × 10^{-4} M erythrosin A; (2) 2 × 10^{-5} M Cu^{2+} with 1 × 10^{-4} M 4Me-cyclam-14 and 2 × 10^{-4} M erythrosin A; (3) 8 × 10^{-6} M Cd^{2+} with 2 × 10^{-4} M erythrosin A and (a) 2 × 10^{-3} M 4Me-cyclam-14, (b) 2 × 10^{-5} M 4Me-cyclam-14.

The stability constants of the Cd(Tet b) and Cd(4Me-cyclam-14) complexes are not available in the literature. They were estimated here from the influence of the hydroxide concentration on extraction, by means of the above expressions. The approximate values are: $\log K \approx 9$ and $\log K \approx 13$ for the Cd(II) complexes with Tet b and 4Me-cyclam-14, respectively.

Determination of cadmium and interference study

The high D'_c value, negligible reagent blank value and beneficial masking effect of hydroxyl ions enable extraction of the cadmium(II) complex, Cd-(4Me-cyclam-14)—erythrosin A, to be applied for trace determination of the metal. A calibration graph was prepared according to the procedure described under Experimental. It was linear in the $0—1 \times 10^{-5}$ M cadmium concentration range. The apparent molar absorptivity (ϵ_{app}) of the extracted cadmium complex at 550 nm was 1.1×10^5 l mol^{-1} cm^{-1} which allowed 0.05 μg ml^{-1} cadmium to be determined.

The following metal ions in 100-fold excess over the cadmium concentration (0.5 μg ml^{-1} Cd) were examined in a study of interference: Ag^+, Tl^+, Be^{2+}, Pd^{2+}, Mg^{2+}, Mn^{2+}, Pb^{2+}, Cu^{2+}, Co^{2+}, Hg^{2+}, Ni^{2+}, Zn^{2+}, Al^{3+}, Bi^{3+}, Cr^{3+}, Fe^{3+}, Ga^{3+}, In^{3+}, Sn^{4+}. Copper, mercury and silver appeared to be the ions that can interfere significantly. Copper and mercury in amounts equal to cadmium and 10-fold amounts of silver increased the absorbance by 10%; Bi^{3+}, Co^{2+}, Tl^+ interfered slightly. The lack of interference from zinc may be explained by the masking effect of hydroxide. Bulky, monovalent anions (I^-, ClO_4^-, Br^-, NO_3^-) lowered the absorbance as a result of competitive extraction of the Cd(4Me-cyclam-14) complex with the colourless counter ions.

The usefulness of the proposed method was confirmed by determining cadmium ions in mixtures with Mg^{2+}, Zn^{2+}, Pb^{2+}, Ni^{2+}, Al^{3+}, Ga^{3+} (5×10^{-4} M each). The results were 1.69 μg Cd (1.71 μg Cd taken, $n = 10$, r.s.d. = 2%) and 3.93 μg Cd (3.91 μg Cd taken, $n = 10$, r.s.d. = 2%) which were considered satisfactory given the low concentrations.

Further studies on the determination of cadmium in various materials are in progress and will be published later.

REFERENCES

1 H. Sumiyoshi and K. Nakahara, Talanta, 24 (1977) 763.
2 K. Kenyu, S. Katsuhiko and I. Nobuhiko, Bunseki Kagaku, 27 (1978) 291.
3 A. Yu. Nazarenko and I. V. Pyatnitskii, Zh. Neorg. Khim., 25 (1980) 1064.
4 A. Yu. Nazarenko, I. V. Pyatnitskii and T. A. Stolyarchuk, Zh. Anal. Khim., 36 (1981) 1719.
5 A. Sanz-Medel, D. B. Gomis and J. R. G. Alvarez, Talanta, 28 (1981) 425.
6 M. Takagi, H. Nakamura, Y. Sanui and K. Ueno, Anal. Chim. Acta, 126 (1981) 185.
7 W. Szczepaniak and B. Juskowiak, Anal. Chim. Acta, 140 (1982) 261.
8 C. L. Luo and C. S. Chung, Proc. Natl. Sci. Counc. ROC, 3 (1979) 136; Chem. Abstr., 91 (1979) 113105 k.
9 C. L. Luo, C. H. Chen and C. S. Chung, J. Chin. Chem. Soc. Taipei, 26 (1979) 61; Chem. Abstr., 91 (1979) 113164 d.

10 G. McLendon and M. Mason, Inorg. Chem., 17 (1978) 362.
11 K. B. Yatsimirskii, V. P. Vasilev, T. D. Orlova and V. V. Pavlishchuk, Zh. Neorg. Khim., 26 (1981) 2937.
12 K. B. Yatsimirskii and V. V. Pavlishchuk, Zh. Neorg. Khim., 26 (1981) 1812.
13 N. W. Alcock, N. Herron and P. Moore, J. Chem. Soc., Dalton Trans., (1978) 1282.
14 N. W. Alcock, E. H. Curson, N. Herron and P. Moore, J. Chem. Soc., Dalton Trans., (1979) 1987.
15 R. A. Bauer, W. R. Robinson and D. W. Margerum, Chem. Commun., (1973) 289.
16 R. W. Hay and C. R. Clark, J. Chem. Soc., Dalton Trans., (1977) 1148.
17 R. Clay, J. Murray-Rust and P. Murray-Rust, J. Chem. Soc., Dalton Trans., (1979) 1135.
18 B. F. Liang, D. W. Margerum and C. S. Chung, Inorg. Chem., 18 (1979) 2001.
19 B. Bosnis, C. K. Poon and M. L. Tobe, Inorg. Chem., 4 (1965) 1102.
20 M. Kodama and E. Kimura, J. Chem. Soc., Dalton Trans., (1977) 2269.
21 R. Buxtorf and Th. A. Kaden, Helv. Chim. Acta, 57 (1974) 1035.
22 N. F. Curtis, J. Chem. Soc., (1964) 2644.

Analytica Chimica Acta, 156 (1984) 245—252
Elsevier Science Publishers B.V., Amsterdam — Printed in The Netherlands

SOLID-PHASE LUMINESCENT CATALYST IMMUNOASSAY FOR HUMAN SERUM ALBUMIN WITH HEMIN AS LABELING CATALYST

YOSHIHITO IKARIYAMA[a] and SHUICHI SUZUKI

Research Laboratory of Resources Utilization, Tokyo Institute of Technology, 4259 Nagatsuta, Midori-ku, Yokohama 227 (Japan)

MASUO AIZAWA*

Institute of Materials Science, University of Tsukuba, Sakura-mura, Ibaraki 305 (Japan)

(Received 13th May 1983)

SUMMARY

A solid-phase luminescent catalyst immunoassay is described for the determination of human serum albumin (HSA) in solution; hemin is used as a label which catalytically amplifies the sensitivity. The method is essentially a non-radioactive and non-enzymatic sandwich immunoassay. Anti-HSA antibody is covalently bound to a transparent plate, which then undergoes the immunochemical reaction with HSA in the test solution, and with the fixed amount of hemin-labeled anti-HSA antibody. After the two-step immunoreaction, the immunochemically-adsorbed hemin—antibody conjugate is quantified by means of the luminescence produced in a solution containing luminol and hydrogen peroxide. The luminescence intensity is correlated with the amount of HSA. The limit of detection for HSA is 1 ng ml^{-1}.

Quantitative radio-immunoassay techniques are now standard practice [1, 2]. However, the drawbacks of radio-isotopic handling such as high costs, health and environmental hazards, limited variety of usable isotopes, short half-life of the radio-labeled antigens and difficult introduction of the radio-isotopes onto the substances to be determined, have stimulated the search for non-isotopic methods in immunological assays. Of the many non-isotopic immunoassays, enzyme immunoassay has been proved as an alternative to radio-immunoassay for determining antigens and antibodies in clinical medicine [3—12], as it can claim easy preparation, simplified handling and relatively low cost.

Immunoassay coupled to light-emitting systems can be used to determine some biologically important molecules with a sensitivity that cannot be easily achieved by other methods [13, 14]. Puget et al. [15] used the luminol reaction catalyzed by horseradish peroxidase covalently bound to antibody to measure cell surface antigen. Solid-phase luminescence immunoassays have been developed with horseradish peroxidase as a labeling agent

[a]Present address: Institute of Materials Science, University of Tsukuba, Sakura-mura, Ibaraki 305, Japan.

0003-2670/84/$03.00

[8, 16]. Because of their large molecular weight, however, enzyme labels inevitably lead to steric hindrance against antigen-antibody reaction.

In a previous paper [17], a novel non-isotopic and non-enzymatic luminescent immunoassay was proposed. The basic concept of this luminescent immunoassay is the use of hemin as a small molecular catalyst in place of a labeling enzyme such as peroxidase. Human serum albumin (HSA) was chosen as a model compound for determination. In this method, anti-HSA antibody is covalently bound to a transparent plate; HSA in the test solution reacts, in the presence of a known amount of hemin-labeled HSA, with the immobilized antibody plate. The labeling agent catalyzes the luminol/hydrogen peroxide reaction

$$\text{Luminol} + H_2O_2 \xrightarrow{\text{Hemin}} \text{Aminophthalate} + N_2 + H_2O + h\nu$$

and the hemin molecules fixed immunochemically on the plate are quantified by counting the photons emitted. This method was termed luminescent catalyst immunoassay in an analogous manner to enzyme immunoassay.

The purpose of this paper is to present experimental evidence that the luminescent catalytic immunoassay is possible by a sandwich-binding method as well as by the competitive-binding method described previously [17]. The antibody is labeled with hemin whereas the antigen was labeled in the previous work. The species to be determined (HSA) is sandwiched between the plate-bound antibody and the hemin-labeled antibody via two steps of immunochemical reaction. The labeling molecule is quantified by luminescence measurement. Such a small molecular catalyst as hemin is expected to provide not only a simple labeling procedure but long-term stability.

Though the catalytic activity of hemin can be determined sensitively by its luminescence, it may also be detected with an electrochemical detector. Another catalytic immunoassay system, characterized by continuous flow immunoassay coupled with electrochemical detection, is described in another paper [18].

EXPERIMENTAL

Chemicals

Hemin (Tokyo Kasei; Tokyo) was washed with distilled water before every use, and dissolved in dimethylsulfoxide. Water-soluble carbodiimide [1-cyclohexyl-3-(2-morpholinoethyl)carbodiimide *p*-methyltoluene sulfonate] was obtained from Kokusan Kagaku (Tokyo). The poly(vinylbenzyl chloride) used (PVBC; Aldrich, Milwaukee, WI) contained the *ortho* and *para* isomers in a ratio of 60:40. 1,8-Diamino-4-aminomethyloctane was courteously supplied by Asahi Kasei Industries (Tokyo).

Human serum albumin (HSA; Kabi AB, Sweden) and anti-HSA rabbit serum containing the specific antibody at a level of 3.2 mg ml^{-1} (Miles-Yeda, Israel) were used. The immunoglobulin fraction was separated by DEAE-cellulose chromatography with 15 mM phosphate buffer of pH 8.3.

Then the antibody was dialyzed against 1 l of 1% NaCl solution for 1 h; dialysis was repeated five times. The antibody thus obtained is hereafter termed anti-HSA antibody.

Preparation of hemin-labeled anti-HSA antibody

Anti-HSA antibody was conjugated to hemin with carbodiimide as a coupling agent as follows. Having been washed with distilled water, 2 mg of hemin was dissolved in 1 ml of dimethylsulfoxide, and 11 mg of the morphocarbodiimide [1-cyclohexyl-3-(2-morpholinoethyl)carbodiimide *p*-methyltoluene sulfonate] was added. The mixture was incubated for 10 min at 25°C with magnetic stirring. Then 23 mg of anti-HSA antibody dissolved in 4 ml of 1% (w/v) sodium chloride solution was added and the mixture was maintained at 25°C for 3 h with magnetic stirring. The pH of the solution was maintained at 4.5 ± 0.5 by the addition of dilute solutions of hydrochloric acid and sodium hydroxide during the coupling reaction. The mixture was blended with 10 ml of distilled water to retrieve soluble product, and centrifuged at 4°C. To the resulting precipitate was added 10 ml of 0.1 M phosphate buffer of pH 7.0 for thorough retrieval of soluble product; this was followed by blending and centrifugation at 4°C. The whole retrieved product was collected and mixed with enough ammonium sulfate to give a solution saturated with the latter. This solution was left at 4°C overnight. The precipitate was then dialyzed against 1 l of 0.1 M phosphate-buffered solution (pH 7.0) at 4°C for 1 h; this dialysis was repeated five times. The end product, a pale brown solution, was evaporated to 2 ml. Then the whole sample was passed through a Sepharose CL-6B column (17 mm i.d.; 100 ml volume) and eluted with 0.1 M phosphate buffer (pH 7.0). This solution contained 2.5 mg of the hemin-labeled antibody per ml.

Anti-HSA serum was also coupled to hemin in a manner similar to that outlined above, except that the serum (25 mg) was dissolved in 2 ml of distilled water. Coupling of hemin to anti-HSA serum was done for 6 h at the same temperature.

Luminescent catalytic activity of the hemin moiety of the anti-HSA antibody conjugate

The catalytic activity of the hemin moiety of the conjugated antibody was studied in the luminol/hydrogen peroxide system by fixing the luminol and hydrogen peroxide concentrations at 0.34 and 120 mM, respectively. Luminol was prepared in dimethylsulfoxide solution, so that 5% of dimethylsulfoxide was present in the luminescent medium. The hemin conjugate was diluted in 0.1 M phosphate buffer (pH 7.0). Luminol and hydrogen peroxide were added to 0.1 M phosphate buffer of pH 7.0, and incubated at room temperature for 30 min to minimize background luminescence. A portion of this mixture and a known amount of the hemin conjugate (total volume 0.5 ml) was placed in a cuvette (5 mm i.d., 50 mm tall). The cuvette

was shaken vigorously, and set within 2 s in a photometer (Chem-Glow photometer, American Instrument Co., Silver Spring, MD). The emitted light was integrated for 1 min.

Preparation of immobilized antibody plate

The PVC plates were treated with poly(vinylbenzyl chloride), 1,8-diamino-4-(aminomethyl)octane, and glutaraldehyde in exactly the same way as described previously [17]. After thorough washing with 0.1 M phosphate buffer (pH 7.0), the plates were placed in a solution of anti-HSA antibody (14 mg of antibody per 10 ml of 0.1 M phosphate buffer, pH 7.0), and left there at 4°C overnight. The plate being cut into 4 × 15-mm pieces, the pieces were washed with the 0.1 M phosphate buffer and stored in the buffer for use. In the preparation of antiserum-immobilized plate, the chemically activated plate was in contact with anti-HSA serum (20 mg of antiserum per 10 ml of the 0.1 M phosphate buffer) at 4°C overnight.

Immunoassay

The procedure of sandwich assay is shown diagrammatically in Fig. 1. The immobilized antibody plate (4 × 15 mm) is here called an immunoplate. The immunoplate was treated with a known amount of HSA dissolved in 500 μl of 0.1 M phosphate buffer (pH 7.0) in the presence of 1% bovine serum albumin (BSA) at 20°C for 4 h, and was then washed several times with the 0.1 M phosphate buffer. Hemin-conjugated anti-HSA antibody (20 μg) was contained in 500 μl of phosphate buffer (0.1 M, pH 7.0) in the presence of 1% BSA. The washed immunoplate was placed in this solution at 20°C for 4 h. The immunoplate was then washed three times with 0.1 M phosphate buffer (pH 7.0), and placed in a cuvette containing 500 μl of 0.1 M phosphate buffer (pH 7.0) with luminol and hydrogen peroxide added to make the solution 0.34 mM in luminol and 0.12 M in peroxide. The intensity of emitted light was measured as described above.

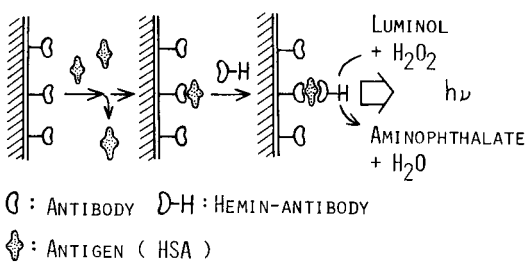

Fig. 1. Representation of the solid-phase luminescence catalyst immunoassay for antigen (HSA) with hemin as labeling catalyst. The anti-HSA IgG is covalently immobilized on a solid support (PVC) coated with PVBC.

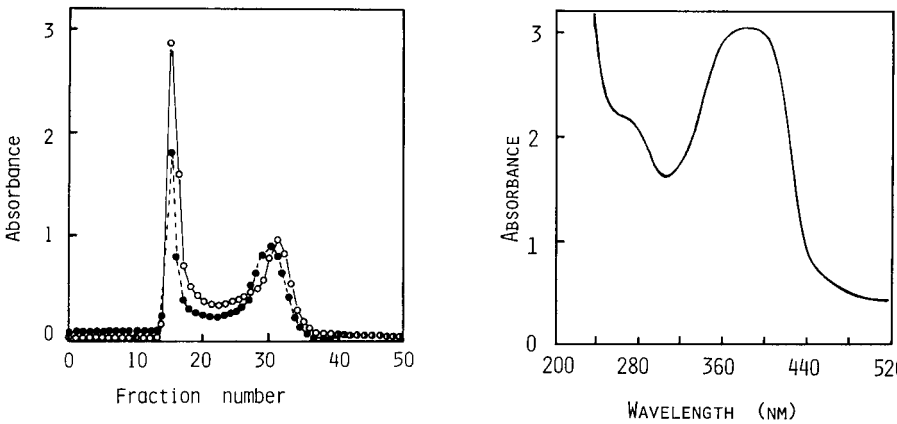

Fig. 2. Fractionation of hemin-conjugated anti-HSA antibody on a Sepharose CL-6B column. Each fraction (3 ml) was monitored at 390 nm (○) and 280 nm (●).

Fig. 3. Absorption spectrum of hemin-labeled antibody (fraction 15).

RESULTS AND DISCUSSION

Luminescent catalytic activity of antibody-conjugated hemin

Sepharose CL-6B chromatography of the anti-HSA antibody-conjugated hemin gave two peaks (Fig. 2). Each fraction (3 ml) was monitored at 390 nm for the hemin moiety and at 280 nm for the protein and hemin moieties. The first peak (fraction 15) was estimated to contain oligomerized immunoglobulin conjugated with hemin, whereas the second peak (fraction 31) contained monomeric antibody conjugated with hemin. This was estimated by the elution patterns of such molecular weight markers as urease (m.w. = 470 000) and immunoglobulin G (m.w. = 150 000) from the same Sepharose CL-6B column. Free hemin was eliminated by thorough ammonium sulfate salting-out and dialysis prior to chromatography.

Figure 3 shows the absorption spectrum of fraction 15. The fraction shows a broad peak at 395 nm and a shoulder at 280 nm. The hemin/antibody molar ratio of the conjugate was estimated for fractions 15 and 31 from the corresponding absorption spectra on the assumption that the $E^{1\%}_{280}$ value for the antibody, and the molar absorptivities of hemin at 280 nm and 390 nm were 15, 3.0×10^4 and 9.3×10^4 l mol^{-1} cm^{-1}, respectively [19]. The approximate molar ratios were 7 for fraction 15 and 4 for fraction 31. Fraction 15 was used for further investigations because of its higher hemin/antibody molar ratio; this fraction is referred to as conjugated hemin in the following description.

The luminescent reaction catalyzed by the conjugated hemin was first monitored at varying concentrations of hydrogen peroxide. The sample volume was adjusted to 0.5 ml. Mixtures of luminol and hydrogen peroxide were stood at room temperature (20°C) for 30 min to make non-catalytic

background luminescence negligible, i.e., 20 cpm. The concentrations of conjugated-hemin and luminol were 20 ng ml^{-1} and 340 μM, respectively. The luminescence of the luminol/H_2O_2 system increased remarkably when the peroxide concentration was increased, but the increase in luminescence levelled off when the peroxide concentration exceeded 120 mM. When the luminol and hydrogen peroxide concentrations were kept constant at 340 μM and 120 mM, respectively, there was good linearity between the luminescence and the hemin-conjugate concentration in the ng ml^{-1} range (Fig. 4). Thus conjugated hemin can be quantified in this concentration range by measuring the luminescence under the above conditions. The precision was good (±2%); thus the limit of detection for conjugated hemin was about 1 ng ml^{-1}. This result indicates the utility of hemin as a sensitive label in immunoassay, because hemin shows excellent amplification in the luminol/hydrogen peroxide system. Conjugated hemin was reacted with HSA (antigen) in a solution and assayed for the catalytic activity in antigen-bound form. There was no noticeable difference in catalytic activity between the antibody-conjugated hemin and the hemin in antigen-bound form.

Sandwich catalyst immunoassay of HSA with hemin-labeled anti-HSA antibody

After the two-step immunoreaction, the intensity of emitted light from the immunoplate was recorded for 2 min under the conditions described above. Immediately the immunoplate in the luminescent medium was placed in the photometer, a sharp luminescence was observed (data not shown). The intensity of the luminescence as well as the integrated luminescence

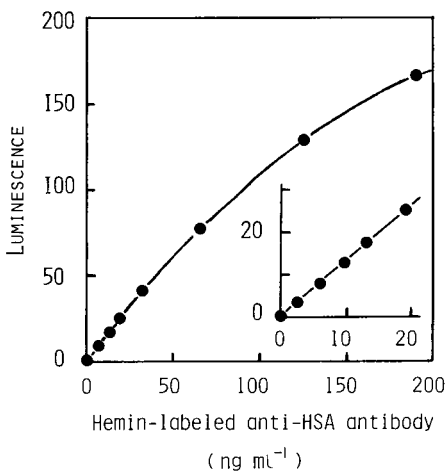

Fig. 4. Catalytic activity of the hemin-HSA conjugate. Conditions: 340 μM luminol, 120 mM H_2O_2, 0.5 ml sample. Luminescence was integrated for 1 min and is given in arbitrary units.

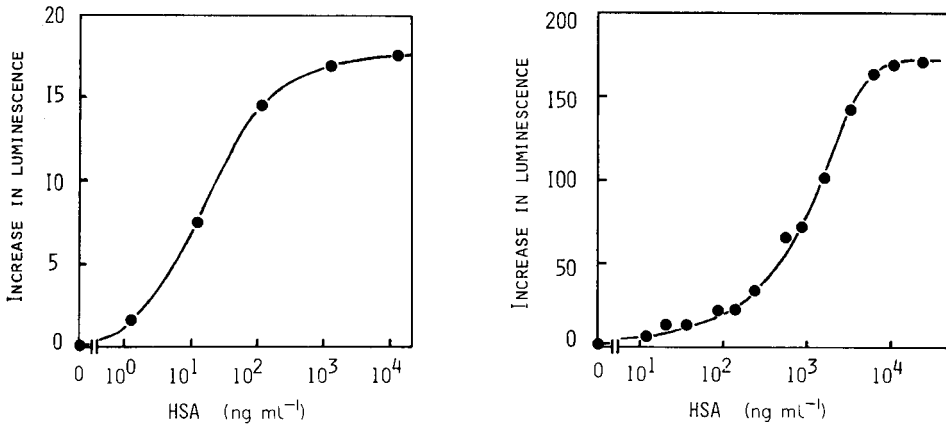

Fig. 5. Calibration curve for HSA with hemin-conjugated antibody. Hemin-conjugated antibody (20 μg/0.5 ml) was used in the second reaction. Each immunoplate was placed in a cuvette (0.5 ml) containing luminol (340 μM) and H_2O_2 (120 mM), and the generated photons were integrated for 2 min; luminescence is expressed in arbitrary units.

Fig. 6. Calibration curve for HSA with hemin-conjugated antiserum. Hemin-conjugated antiserum (11 μg/0.5 ml of medium) was used in the second reaction. Other conditions are the same as for Fig. 5.

changed drastically, depending on the amount of HSA added. In such a binding assay as this, the activity of a ligand immunochemically bound on an immunoplate is expected to increase with increasing concentration of the species being determined. Figure 5 represents a response curve (calibration curve) for the analyte (HSA) with a constant concentration of 20 μg of hemin—anti-HSA antibody conjugate per 0.5 ml. The increase in luminescence for 2 min was plotted on the ordinate; this meant that the luminescence at an HSA concentration of 0 ng ml^{-1} had to be set to zero, and the corrected luminescence was plotted. Figure 5 shows that the luminescence (in arbitrary units) increased when the concentration of HSA was raised from about 1 ng ml^{-1} to 10^4 ng ml^{-1}. A typical sigmoidal curve was obtained. The HSA concentration at the midpoint of the response curve was 20 ng ml^{-1}. If the 100% response level is defined by the saturated luminescence at an HSA concentration of 10^4 ng ml^{-1}, the 90% and 10% response levels were 1 ng ml^{-1} and 500 ng ml^{-1}, respectively.

In these tests, the hemin—antiserum conjugate was also examined instead of the hemin—antibody conjugate. The antiserum (anti-HSA)-immobilized immunoplate was treated with antigen (HSA) and thereafter with hemin—anti-HSA conjugate (11 μg ml^{-1}) in a similar manner as described under Experimental. The results, plotted analogously to Fig. 5, are shown in Fig. 6. Under these conditions, the useful range of the immunoassay with hemin—antiserum was from 50 ng ml^{-1} (10% response level) to 5000 ng ml^{-1} (90% response level). The HSA concentration at the midpoint of the response curve was 700 ng ml^{-1}. The precision was determined at an HSA concentration of 100 ng ml^{-1} with a constant hemin-conjugated antibody

concentration of 40 ng ml^{-1}; the relative standard deviation was about ±8% (n = 10). Solutions containing as little as 1 ng ml^{-1} antigen can be assayed by the proposed luminescent catalyst immunoassay.

The proposed catalyst label can amplify the sensitivity in immunoassay. The sensitivity can also be improved by the photon-counting measurement. The solid-phase technique described gives a very convenient separation of bound reactant from free reactant. Thus, solid-phase luminescent immunoassay appears to be a very effective method.

However, it should be emphasized that the conditions outlined here do not necessarily represent the highest limit of sensitivity of this method. The use of a conjugate with a greater hemin catalytic activity would increase the sensitivity of the assay. Sensitivity might also be improved by using organometallic compounds and complexes as luminescence catalytic labels.

Conclusions

The combination of the high catalytic activity of hemin and the sensitive luminescent reaction provides a very sensitive luminescence catalyst immunoassay.

The excellent stability of the labeling catalyst and the extremely small interference with the antigen-antibody reaction from low-molecular-weight iron porphyrin complex were naturally attained. The simple and inexpensive labeling was achieved via the two carboxyl groups in the hemin structure. The assay can be simplified by using a transparent solid matrix to which the antibody is covalently immobilized.

REFERENCES

1 R. S. Yalow and S. A. Berson, in W. D. Odell and W. H. Daughaday (Eds.), Principles of Competitive Protein-Binding Assays, J. B. Lippincott, Philadelphia, 1971.
2 C. W. Parker, Radioimmunoassay of Biologically Active Compounds, Prentice-Hall, New York, 1976.
3 E. Engvall and P. Perlmann, Immunochemistry, 8 (1971) 871.
4 B. K. van Weemen and A. H. W. M. Schuurs, FEBS Lett., 15 (1971) 232.
5 G. B. Wisdom, Clin. Chem., 22 (1976) 1243.
6 M. Halman, B. Velan and T. Sery, Anal. Environ. Microbiol., 34 (1977) 473.
7 G. L. Rowley, K. E. Rubenstein, J. Huisjen and E. F. Ullman, J. Biol. Chem., 250 (1975) 3759.
8 T. Olsson, G. Brunius and A. Thore, J. Immunol. Methods, 25 (1979) 127.
9 M. Aizawa, A. Morioka, H. Matsuoka, S. Suzuki, Y. Nagamura, R. Shinohara and I. Ishiguro, J. Solid-Phase Biochem., 1 (1976) 319.
10 M. Aizawa, A. Morioka and S. Suzuki, J. Membrane Sci., 3 (1978) 221.
11 M. Aizawa, A. Morioka, S. Suzuki and Y. Nagamura, Anal. Biochem., 94 (1979) 22.
12 M. Aizawa, A. Morioka and S. Suzuki, Anal. Chim. Acta, 115 (1980) 61.
13 R. J. Carrico, K. K. Yeung, H. R. Schroeder, R. C. Boguslaski, R. T. Buckler and J. E. Christner, Anal. Biochem., 76 (1976) 95.
14 H. R. Schroeder, R. J. Carrico, R. C. Boguslaski and J. E. Christner, Anal. Biochem., 72 (1976) 283.
15 K. Puget, A. M. Michelson and S. Avrameas, Anal. Biochem., 79 (1977) 447.
16 M. Aizawa, S. Suzuki, T. Kato, Y. Fujiwara and Y. Fujita, J. Appl. Biochem., 2 (1980) 190.
17 Y. Ikariyama, S. Suzuki and M. Aizawa, Anal. Chem., 54 (1982) 1126.
18 I. Karube, T. Matsunaga, T. Satoh and S. Suzuki, Anal. Chim. Acta, 156 (1984) 283.
19 T. Yamakawa (Ed.), Handbook of Biochemistry, Vol. I, Tokyo Kagaku Dojin Co. Ltd., Tokyo, 1979, p. 97.

Analytica Chimica Acta, 156 (1984) 253—261
Elsevier Science Publishers B.V., Amsterdam — Printed in The Netherlands

FLUORIMETRIC ASSAY FOR MONOAMINE OXIDASES A AND B BY MEANS OF *p*-SULFAMOYLBENZYLAMINE AND BENZYLAMINE

HITOSHI NOHTA, KIYOSHI ZAITSU, YASUTO TSURUTA[a] and YOSUKE OHKURA*

Faculty of Pharmaceutical Sciences, Kyushu University 62, Maidashi, Higashi-ku, Fukuoka 812 (Japan)

(Received 26th May 1983)

SUMMARY

p-Sulfamoylbenzylamine and *p*-hydroxybenzylamine are shown to be substrates for monoamine oxidase A and for monoamine oxidases A and B, respectively. This was established by studies on the selectivity of benzylamine derivatives as substrates using monoamine oxidase inhibitors. A sensitive fluorimetric method for the separate assay of monoamine oxidases A and B is described. *p*-Sulfamoylbenzaldehyde and benzaldehyde formed enzymatically from *p*-sulfamoylbenzylamine and benzylamine, a known substrate for monoamine oxidase B, are quantified by means of the selective fluorimetric determination of aromatic aldehydes with 2,2'-dithiobis(1-aminonaphthalene). The limits of detection for the *p*-sulfamoylbenzaldehyde and benzaldehyde formed enzymatically are, respectively, 300 and 150 pmol per assay tube. Monoamine oxidases A and B in rat brain mitochondrial tissue and human platelets were assayed.

Monoamine oxidases (MAO; monoamine:oxygen oxidoreductase, EC 1.4.3.4) occur in many tissues and catalyze the oxidative deamination of monoamines. The enzyme is classified into two types, MAO A and MAO B by their substrate specificity and sensitivity to MAO inhibitors [1—5]. Monoamine oxidase A acts on norepinephrine and 5-hydroxytryptamine and is strongly inhibited by MAO inhibitors such as clorgyrine, while MAO B deaminates benzylamine and β-phenylethylamine and is inhibited by MAO inhibitors such as deprenyl or pargyline [2, 5]. Dopamine and tyramine are deaminated by both these oxidases [2, 3, 5]. Because MAO A and MAO B share the deamination of the neurotransmitters in biological tissues, separate assays of the two oxidases are required.

Many assay methods for MAO in biological materials have been reported: manometric [6], spectrophotometric [7—9], fluorimetric [10—12], and radioisotopic [13, 14] methods have been produced. However, only the radioisotopic methods permit separate assays of MAO A and MAO B, based on ^{14}C-5-hydroxytryptamine and ^{14}C-β-phenylethylamine as substrates, respectively.

---

[a]Present address: Faculty of Pharmacy and Pharmaceutical Sciences, Fukuyama University, Sanzo, Higashimuramachi, Fukuyama 729-02, Japan.

0003-2670/84/$03.00

Benzylamine is known to be a useful substrate for MAO B [2]. 3,4-Dimethoxybenzylamine and *N*-methylbenzylamine have been described as substrates for MAO [15], but their specificity to MAO A or MAO B has not been reported, nor has any specific substrate for MAO A among the benzylamine derivatives.

In the present work, several benzylamine derivatives including the above-mentioned substrates were screened as substrates for MAO A and MAO B by means of inhibition techniques with clorgyline, a specific inhibitor of MAO A [2, 3], and pargyline, a fairly selective inhibitor of MAO B [2]. *p*-Sulfamoylbenzylamine and *p*-hydroxybenzylamine were found to be suitable substrates for MAO A and for both MAO A and MAO B, respectively. The specificity and potency of several MAO inhibitors were also checked against these amines as substrates. A fluorimetric method for the separate assay of MAO A and MAO B was thus developed by using *p*-sulfamoylbenzylamine and benzylamine. This is based on determination of the *p*-sulfamoylbenzaldehyde and benzaldehyde formed enzymatically from the corresponding benzylamine derivatives by means of a fluorimetric procedure for aromatic aldehydes with 2,2′-dithiobis(1-aminonaphthalene) (DTAN), a selective fluorigenic reagent for aromatic aldehydes, with some modifications [16]. In these studies, a rat brain mitochondrial preparation was used as a model enzyme preparation, because both the monoamine oxidases are present in brain mitochondria and the deactivation of neurotransmitters in the brain is the major role of these oxidases [1]. Human platelet MAO activity was also measured by this method.

EXPERIMENTAL

Reagents, solutions and instrumentation

All chemicals were of reagent grade, unless otherwise noted. Deionized and distilled water was used. DTAN was obtained from the Dojin Institute of Chemistry, Kumamoto 862, Japan. *p*-Hydroxybenzylamine hydrochloride was prepared from *p*-methoxybenzylamine by the method of Salkowski [17]. *p*-Sulfamoylbenzaldehyde was synthesized by the method of Momose and Ueda [18].

Rat brain mitochondrial preparation. Donryu rats (male, 4 weeks old) were killed by decapitation, the brains were removed and the mitochondria were isolated by the method of Johnston [1] with minor modifications as follows. The brains were chilled on ice, weighed and homogenized with 4 volumes of ice-cold 0.25 M sucrose solution in a Potter-Elvehjem homogenizer. The homogenate was centrifuged at 800 g for 5 min and the supernatant liquid was then centrifuged at 25000*g* for 15 min. The precipitate was suspended in water. The protein concentration was adjusted to ca. 1 mg ml^{-1}, and measured by the method of Lowly et al. [19] using bovine serum albumin as a standard protein.

Human blood platelet preparation. Human blood platelets were collected from platelet concentrates, which were obtained from venous blood at the

Japan Red Cross, Fukuoka, Japan, as described by Zaitsu et al. [11]. The platelets were suspended in water. The protein concentration was adjusted to ca. 1 mg ml^{-1} as in the rat brain mitochondrial preparation.

Apparatus. Fluorescence was measured with a Hitachi MPF-4 spectrofluorimeter (quartz cells). The spectral bandwidths were set at 10 nm in both the excitation and emission monochromators. A Hitachi-Horiba M-7 pH meter was used to measure pH at 37°C.

Procedure for screening of benzylamine derivatives (Procedure A)

To 0.7 ml of 0.1 M Tris-HCl buffer (pH 8.0), 0.1 ml of the mitochondrial preparation was added. The mixture was pre-incubated at 37°C for 5 min, and then incubated at 37°C for 15 min after addition of 0.1 ml of 1×10^{-7} M clorgyline solution or 1×10^{-6} M pargyline solution (both in the Tris-HCl buffer). At the end of the incubation, 0.1 ml of a 10 mM solution (in the Tris-HCl buffer) of one of the benzylamine derivatives (see Table 1) was added, and the mixture was again incubated at 37°C for 30 min. The enzyme reaction was stopped by the addition of 0.2 ml of 3 M perchloric acid, and the mixture was centrifuged at 1000*g* for 10 min. To the supernatant solution (0.5 ml), 1.0 ml of DTAN solution was added. The mixture was maintained at 37°C for 40 min to develop fluorescence. To the mixture, 2.0 ml of 1 M sulfuric acid/acetone (1:1, v/v) was added to enhance and stabilize the fluorescence. The fluorescence intensity of the reaction mixture was then measured by using the following wavelengths: the excitation and emission maxima of the fluorescence were 358 and 498 nm for *p*-sulfamoylbenzaldehyde, 356 and 473 nm for benzaldehyde (from benzylamine or *N*-methylbenzylamine), 374 and 462 nm for *p*-methoxybenzaldehyde, 382 and 462 nm for 4-hydroxy-3-methoxybenzaldehyde, and 382 and 463 nm for 3,4-dimethoxybenzaldehyde), respectively.

To prepare the blank, the same procedure was followed except that the substrate solution was added after the addition of perchloric acid.

TABLE 1

Inhibition of MAO activity towards benzylamine derivatives by clorgyline and pargyline[a]

Substrate	Inhibition (%) of MAO activity	
	Clorgyline (1×10^{-8} M)	Pargyline (1×10^{-7} M)
p-Sulfamoylbenzylamine	85	18
p-Hydroxybenzylamine	35	68
Benzylamine	0	95
p-Methoxybenzylamine	0	95
4-Hydroxy-3-methoxybenzylamine	0	95
3,4-Dimethoxybenzylamine	0	95
N-Methylbenzylamine	0	95

[a]Portions (0.1 ml) of the mitochondrial preparation were treated as in procedure A.

Procedure for testing the effect of inhibitor concentrations on MAO activities towards p-*sulfamoylbenzylamine, benzylamine and* p-*hydroxybenzylamine (Procedure B)*

To 0.7 ml of 0.05 M Tris-HCl buffer (pH 8.5), 0.1 ml of the mitochondrial preparation was added. The mixture was pre-incubated at 37°C for 5 min, and incubated again at 37°C for 15 min after the addition of 0.1 ml of a MAO inhibitor solution (0—10^{-3} M) in the Tris-HCl buffer. At the end of the incubation, 0.1 ml of a substrate solution in the Tris-HCl buffer (*p*-sulfamoylbenzylamine, 191 mM; benzylamine, 0.95 mM; *p*-hydroxybenzylamine, 15 mM) was added, and the mixture was treated in the same way as in procedure A. The blank was prepared as described in procedure A.

Standard procedure for the assay of MAO A and MAO B (Procedure C)

To 0.8 ml of 0.05 M Tris-HCl buffer (pH 8.5), 0.1 ml of the enzyme preparation (mitochondria or platelet preparation) was added. The mixture was pre-incubated at 37°C for 5 min, and incubated again at 37°C for 30 min after addition of 0.1 ml of 191 mM *p*-sulfamoylbenzylamine solution for MAO A assay or 0.95 mM benzylamine solution for MAO B assay. The mixture was then treated in the same way as in procedure A. *p*-Hydroxybenzylamine solution (see procedure B) was used when required.

The blank was prepared by treating the enzyme preparation in the same way but the substrate solution was added after the addition of perchloric acid. To obtain calibration graphs, 0.1 ml of the substrate solution was replaced with 0.1 ml of a standard solution (10—100 nmol ml^{-1}) of the corresponding aldehyde (*p*-sulfamoylbenzaldehyde or benzaldehyde).

RESULTS AND DISCUSSION

Inhibition of the enzymes

Specificity for the benzylamine derivatives was investigated by estimating the inhibitory effect of clorgyline and pargyline on the rat brain mitochondrial monoamine oxidases according to procedure A. The enzyme reaction conditions of procedure A was tentatively selected from those described in the literature [11, 15]. The concentrations of the MAO inhibitors prescribed in the procedure were selected from the reported data [1, 11]. The data in Table 1 suggest that *p*-sulfamoylbenzylamine is a substrate of MAO A, *p*-hydroxybenzylamine of both MAO A and MAO B, and the others of MAO B. *p*-Sulfamoylbenzylamine, benzylamine and *p*-hydroxybenzylamine were thus used for further studies as substrates for MAO A, MAO B and both oxidases, respectively.

The effect of the inhibitor concentrations towards these benzylamine derivatives was investigated by applying procedure B. Figure 1 shows the effect of the concentrations of clorgyline and pargyline on the activities of these oxidases. The oxidizing activity of *p*-sulfamoylbenzylamine is inhibited at low concentrations of clorgyline and at relatively high concentrations of

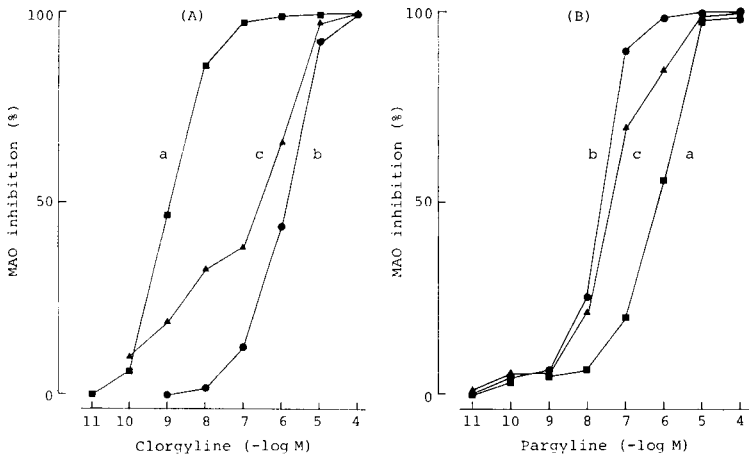

Fig. 1. Effect of the concentrations of (A) clorgyline and (B) pargyline as inhibitors of the monoamine oxidases towards: (a) *p*-sulfamoylbenzylamine; (b) benzylamine; (c) *p*-hydroxybenzylamine. Portions (0.1 ml) of the mitochondrial preparation were treated as in procedure B.

pargyline, whereas the situation is reversed for the oxidizing activity of benzylamine. These inhibition curves show that *p*-sulfamoylbenzylamine is highly selective for MAO A, and benzylamine for MAO B. The curves show that 1×10^{-8} M clorgyline and 1×10^{-7} M pargyline in the enzyme reaction mixture in procedure A are suitable concentrations. The inhibition curve of clorgyline obtained with *p*-hydroxybenzylamine is biphasic. The inhibition curves of other MAO inhibitors were also investigated; the I_{50} values (the concentration of inhibitor required to cause 50% inhibition of the MAO activity) are shown in Table 2. Harmine, an inhibitor of MAO A [3] shows potent inhibition of the oxidizing activity of *p*-sulfamoylbenzylamine in the

TABLE 2

I_{50} values of MAO inhibitors against the oxidizing activities of *p*-sulfamoylbenzylamine, benzylamine and *p*-hydroxybenzylamine[a]

Inhibitor	I_{50} (M)		
	p-Sulfamoyl-benzylamine	Benzylamine	*p*-Hydroxy-benzylamine
Clorgyline	2×10^{-9}	2×10^{-6}	2×10^{-7}
Pargyline	7×10^{-7}	2×10^{-8}	3×10^{-8}
Harmine	1×10^{-8}	3×10^{-7}	5×10^{-7}
Imipramine	$>1 \times 10^{-4}$	2×10^{-5}	5×10^{-5}
Iproniazid	1×10^{-5}	1×10^{-5}	8×10^{-6}
Tranylcypromine	2×10^{-5}	1×10^{-8}	3×10^{-8}

[a]Portions (0.1 ml) of the mitochondrial preparation were treated as in procedure B.

same manner as clorgyline. This confirms the selective behaviour of *p*-sulfamoylbenzylamine for MAO A. Imipramine has been reported as an inhibitor of MAO B [5] and inhibits the oxidizing activity of benzylamine strongly but that of *p*-sulfamoylbenzylamine weakly. Iproniazid and tranylcypromine are both non-specific MAO inhibitors, but the latter has a strong effect on the benzylamine reaction. *p*-Hydroxybenzylamine proved to be a substrate for both MAOs but seemed to be oxidized by a MAO B-mediated reaction rather than a MAO A-mediated reaction.

p-Hydroxybenzylamine is not required as substrate in the procedure for the assay of MAO A and MAO B, but it was examined as a reference substrate in investigations of the best conditions for the enzyme reactions.

Optimum pH conditions and substrate concentrations

The pH of the enzyme reaction mixture affects the Michaelis constant (K_m) values for the substrates (Fig. 2A); the K_m values decrease more or less exponentially with increasing pH. This agrees with earlier results for benzylamine, *N*-methylbenzylamine and 3,4-dimethoxybenzylamine [15]. The K_m values at pH 8.5 were 3.82 mM for *p*-sulfamoylbenzylamine, 0.019 mM for benzylamine, and 0.299 mM for *p*-hydroxybenzylamine. The maximum velocities (V_{max}) for MAO-mediated reactions with the substrates are almost maximal at pH 8.0—9.0 (Fig. 2B). The V_{max} values (nmol of aldehyde formed/mg of protein/min) of the reactions at pH 8.5 were 0.79 with *p*-sulfamoylbenzylamine, 1.35 with benzylamine and 1.00 with *p*-hydroxybenzylamine. The Tris-HCl buffer (pH 8.5) gave constant results at concen-

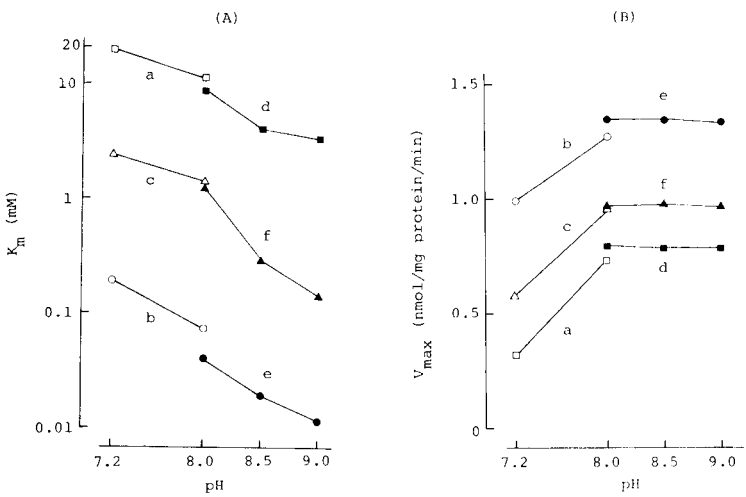

Fig. 2. Effect of pH on (A) K_m values for *p*-sulfamoylbenzylamine, benzylamine and *p*-hydroxybenzylamine and (B) V_{max} values of the enzyme reactions. Portions (0.1 ml) of the mitochondrial preparation were treated as in procedure C with (a, b and c) 0.05 M phosphate buffer or (d, e and f) 0.05 M Tris-HCl buffer at various pH values. (a, d) *p*-sulfamoylbenzylamine; (b, e) benzylamine; (c, f) *p*-hydroxybenzylamine.

trations of 0.01—0.1 M, and a 0.05-M Tris-HCl solution was therefore used in the assay of MAOs and in procedures A and B. Substrate concentrations five times the K_m values at pH 8.5 were selected as saturating concentrations for the enzyme reactions in procedures B and C.

The amounts of *p*-sulfamoylbenzaldehyde, benzaldehyde and *p*-hydroxybenzaldehyde formed enzymatically from the corresponding substrates were proportional to the amounts of protein in the mitochondrial preparation up to 400 μg. The enzyme activity was linear with time up to at least 60 min in each case for incubation at 37°C (Fig. 3).

The fluorimetric method

The fluorescence reaction of aromatic aldehydes with DTAN, conditions for which were established by using *p*-hydroxybenzaldehyde as model compound, required sodium sulfite and sodium phosphite as accelerators [16]. Unfortunately, sulfite and phosphite interfered with the reactions of *p*-sulfamoylbenzaldehyde and benzaldehyde. The fluorescence intensities from these aldehydes (1×10^{-6} M each) reached peak values after reaction for ca. 15 min at 37°C in the presence of sulfite and phosphite but the peaks corresponded to only about 70% of the values obtained in the absence of these ions after reaction for 40 min. The reactions of these aldehydes, without sulfite and phosphite, were complete within 25 min at 37°C and the resulting fluorescence was stable for more than 1 h at 37°C. *p*-Hydroxybenzaldehyde gave a constant, almost maximum fluorescence intensity after reaction for 40 min without sulfite and phosphite. Thus sulfite and phosphite are omitted and a reaction time of 40 min is prescribed in the procedures.

β-Mercaptoethanol, which was used to stop the fluorescence development

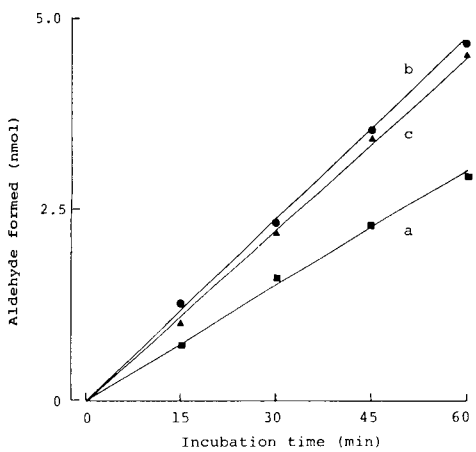

Fig. 3. Effect of incubation time on the amount of aldehyde formed. Portions (0.1 ml) of the mitochondrial preparation were treated as in procedure C with different incubation times for the enzymatic reaction. (a) *p*-Sulfamoylbenzylamine; (b) benzylamine; (c) *p*-hydroxybenzylamine.

from *p*-hydroxybenzaldehyde [16], decreased the fluorescence intensity from *p*-sulfamoylbenzaldehyde and benzaldehyde by about 70%. Acetone stopped the fluorescence reaction abruptly when added at concentrations greater than 13%, and the fluorescence of the final reaction mixture was unchanged for more than 6 h; a concentration of 28% in the mixture is recommended.

The calibration graphs for *p*-sulfamoylbenzaldehyde, *p*-hydroxybenzaldehyde and benzaldehyde were linear up to 100 nmol ml^{-1}, the highest concentrations examined.

The recoveries of 2 nmol of *p*-sulfamoylbenzaldehyde or benzaldehyde added to the enzymatic reaction mixtures of the blank in procedure C were 100 ± 1% (mean ± standard deviation (SD), $n = 10$ in each case). The limits of detection for *p*-sulfamoylbenzaldehyde and benzaldehyde formed enzymatically were 100 and 50 pmol/mg protein/min (300 and 150 pmol per assay tube), respectively. The limit was defined as the concentration giving a fluorescence intensity twice the blank.

In a study of the precision (repeatability), the relative standard deviations for procedure C with *p*-sulfamoylbenzylamine and benzylamine were 1.1 and 1.9%, for mean activities of 0.72 nmol of *p*-sulfamoylbenzaldehyde/mg protein/min and 1.16 nmol of benzaldehyde/mg protein/min, respectively ($n = 10$ in each case).

Application of the method

The activities of MAO A and MAO B in the rat brain mitochondrial preparations corresponded to 0.67 ± 0.16 nmol of *p*-sulfamoylbenzaldehyde/mg protein/min and 1.05 ± 0.33 nmol of benzaldehyde/mg protein/min (mean ± SD, $n = 5$ in each case), respectively.

Procedure C permitted the assay of human platelet monoamine oxidases. This oxidase in platelets is mainly of the B type [20, 21], and acts only slightly on *p*-sulfamoylbenzylamine. The MAO B activity of normal adult platelets corresponded to 1.04 ± 0.37 nmol of benzaldehyde/mg protein/min (mean ± SD, $n = 9$). The MAO A activity could not be measured exactly because the amounts of *p*-sulfamoylbenzaldehyde formed were less than the detection limit.

This study provides the first fluorimetric method for the assay of MAO A and MAO B. The method is simple and sensitive, and should be useful for the assay of MAOs in other biological samples. The method also may permit estimations of MAO inhibitory specificity and potency of inhibitors, and should be suitable for the development of selective MAO inhibitors.

A Grant-in-Aid for Scientific Research from the Ministry of Education, Science and Culture of Japan is gratefully acknowledged. We also thank the staff of the Central Clinical Laboratory of Kyushu University Hospital for the kind supply of platelet concentrates, and Miss Yuki Imaishi and Miss Miyuki Takahashi for valuable technical assistance.

REFERENCES

1 J. P. Johnston, Biochem. Pharmacol., 17 (1968) 1285.
2 N. H. Neff and H.-Y. T. Yang, Life Sci., 14 (1974) 2061.
3 M. D. Houslay and K. F. Tipton, Life Sci., 19 (1976) 467.
4 M. Jain, Life Sci., 20 (1977) 1925.
5 H. Kinemuchi and K. Kamijo, Tanpakushitsu Kakusan Koso, 25 (1980) 1069.
6 N. H. Creasy, Biochem. J., 64 (1956) 178.
7 C. W. Tabor, H. Tabor and S. M. Rosenthal, J. Biol. Chem., 208 (1954) 645.
8 C. M. McEwen and J. D. Cohen, J. Lab. Clin. Med., 62 (1963) 766.
9 T. Nagatsu and K. Yagi, J. Biochem., 60 (1966) 219.
10 M. Harada and T. Nagatsu, Anal. Biochem., 56 (1973) 383.
11 K. Zaitsu, H. Nagai, K. Ohtsubo, S. Eto, K. Kohashi and Y. Ohkura, Chem. Pharm. Bull., 26 (1978) 3471.
12 M. Yamaguchi, H. Nohta and Y. Ohkura, Chem. Pharm. Bull., 30 (1982) 3803.
13 S. Ohtsuka and Y. Kobayashi, Biochem. Pharmacol., 13 (1963) 995.
14 J. Fowler, B. Ekstedt, T. Egashira, H. Kinemuchi and L. Oveland, Biochem. Pharmacol., 28 (1979) 3063.
15 C. M. McEwen, Jr., G. Sasaki and W. R. Lenz, Jr., J. Biol. Chem., 243 (1968) 5127.
16 Y. Ohkura, K. Ohtsubo, K. Zaitsu and K. Kohashi, Anal. Chim. Acta, 99 (1978) 317.
17 H. Salkowski, Berichte, 22 (1889) 2141.
18 T. Momose and Y. Ueda, Yakugaku Zasshi, 67 (1947) 23.
19 O. H. Lowly, N. J. Rosebrough, A. L. Farr and R. J. Randall, J. Biol. Chem., 193 (1951) 265.
20 D. J. Edwards and S.-S. Chang, Life Sci., 17 (1975) 1127.
21 C. H. Donnelly and D. L. Murphy, Biochem. Pharmacol., 26 (1977) 853.

Analytica Chimica Acta, 156 (1984) 263—271
Elsevier Science Publishers B.V., Amsterdam — Printed in The Netherlands

FLUORESCENCE INVESTIGATION OF ISOCHLOROTETRACYCLINE: GROUND-STATE AND EXCITED-STATE ACID-BASE EQUILIBRIA

B. M. AHMED and R. D. JEE*

The School of Pharmacy, University of London, 29—39 Brunswick Square, London WC1N 1AX (Great Britain)

(Received 22nd June 1983)

SUMMARY

The fluorescence emission from isochlorotetracycline is shown to be associated with the hydroxyphthalide portion of the molecule. Neutral, anionic, zwitterionic and cationic forms of the fluorophore are proposed to account for the fluorescent behaviour in aqueous and organic media of different acidities. In strongly acidic aqueous solution intermolecular photoautomerism is observed, while in chloroform intramolecular phototautomerism occurs. In aqueous solution an excited-state pK_a of 3.3 was observed for the fluorophore. From a study of the pH vs. fluorescence profile with excitation at 350 nm, the ground-state microscopic dissociation constants for isochlorotetracycline hydrochloride were calculated. The optimum conditions for the fluorimetric determination of isochlorotetracycline are an alkaline medium (pH > 10) with λ_{ex} = 350 nm and λ_{em} = 415 nm.

Numerous procedures for the determination of chlorotetracycline based on fluorimetry have been presented [1—16]. A few of the early methods reported [2, 3, 6] were based on what was considered to be the native fluorescence of this compound, but the conditions of measurement used strongly suggest that the compound being measured was isochlorotetracycline. Kelly et al. [10] and Hall [15] have shown that the native fluorescence is minimal. A recent study of the natural fluorescence of chlorotetracycline has been reported by Mathew and Balaram [17].

Chlorotetracycline rapidly (half-life approximately 5 min at pH 12 and 298 K) undergoes degradation in alkaline solution to give isochlorotetracycline (I) which shows very intense fluorescence. It is generally agreed that

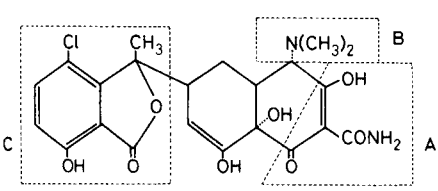

(I)

the fluorescence emission at approximately 415 nm should be measured in alkaline solution, but the exact nature of the fluorescing species and the

0003-2670/84/$03.00

detailed pH/fluorescence profile have not been reported. In this paper, a detailed study and analysis of the pH/fluorescence behaviour of isochlorotetracycline is presented. The fluorescent properties of this compound are particularly interesting because of the excited-state acid-base equilibria observed and the need to use microscopic dissociation constants to explain the pH/fluorescence profile.

EXPERIMENTAL

Isochlorotetracycline hydrochloride was prepared from chlorotetracycline hydrochloride by the method of Waller et al. [18]. Solutions of isochlorotetracycline for absorption and fluorescence measurements at different pH values over the range 2.4—12 were prepared using an acetic, phosphoric and boric acid universal buffer adjusted to an ionic strength of 0.1 mol dm^{-3} using potassium chloride. In the pH range 1.2—2.4, hydrochloric acid/potassium chloride solutions were used. All pH measurements were made using a Corning-Eel 110 digital pH meter with a Russell CJ74 combination electrode.

Ultraviolet-visible absorption spectra were measured on a Cecil CE595 double-beam spectrophotometer for an isochlorotetracycline concentration of 20 $\mu g\ cm^{-3}$ with a 1-cm path length. Fluorescence was measured with a Perkin-Elmer 204 spectrofluorimeter and a 1-cm square cross-section silica cell. The stability of the fluorimeter was checked at regular intervals throughout the work by using a 0.5 $\mu g\ cm^{-3}$ quinine sulphate solution in 0.25 M sulphuric acid.

RESULTS

Isochlorotetacycline shows fluorescence at all pH values. However, the exact pH vs. fluorescence intensity relationship depends on the wavelength of excitation. Preliminary studies showed that the fluorescence intensity was insensitive to potassium chloride used for ionic strength adjustment of the buffers and that the concentration vs. fluorescence intensity dependence was linear over the range 0.001—5 $\mu g\ cm^{-3}$. All subsequent measurements were made at 0.25 $\mu g\ cm^{-3}$. The isochlorotetracycline solutions showed good stability at all pH values and were not particularly sensitive to photodecomposition. All measurements reported were taken on freshly prepared solutions.

Three pK_a values of approximately 3.1, 6.7 and 8.2 have been determined for isochlorotetracycline hydrochloride [18—20] and, by analogy with the parent molecule, chlorotetracycline, the first pK_a value can be assigned to the tricarbonyl methane system (site A). The assignments of the second and third pK_a values are not known.

At low pH values, the long-wavelength absorption band of isochlorotetracycline shows a maximum at 315 nm while in alkaline solution the band moves to 350 nm. In the parent molecule, chlorotetracycline, absorption

above 300 nm is considered to be associated with the phenolic β-diketone site [21, 22]. From this and comparison with a model compound, 7-hydroxy-3-methylphthalide [23], the 315-nm and 350-nm peaks may be associated with the hydroxyphthalide portion of the isochlorotetracycline molecule. The 350-nm peak obtained in alkaline solution corresponds to the ionized form of the compound.

Irrespective of the wavelength (315 or 350 nm) used for excitation, the fluorescence emission spectrum in the pH range 1—12 exhibits only a single band at 415 nm (Fig. 1). Above pH 10, regardless of the assignment of the ground-state pK_a values, the only absorbing species in solution is the ionized form of the compound. Hence the fluorescence emission at 415 nm may be associated with this species. In the pH range 1—5 the predominant form of the compound is the protonated form yet the fluorescence observed is still characteristic of the ionized compound. This can be accounted for by dissociation in the excited state.

Figures 2 and 3 show the pH vs. fluorescence intensity profiles for isochlorotetracycline at the two different excitation wavelengths. Excitation at 315 nm, corresponding to the absorption maximum of the protonated compound (HC), gives in the low pH region (1—4) a rising segment which can be explained by the photo-dissociation of the excited species HC* to C^-*. The inflection point of this part of the curve corresponds to pK_a*. At higher pH values the fluorescence intensity again increases because of the direct excitation of C^- produced by the ground-state dissociation of HC. An examination of the values for the molar absorptivities at 315 nm for HC ($\approx$5400 l mol^{-1} cm^{-1}) and C^- ($\approx$4500 l mol^{-1} cm^{-1}) would, however, have suggested an expected decrease in fluorescence intensity at high pH values. The observed increase can be accounted for by assuming that only 40% of HC* is photodissociated. This is not unreasonable as prototropic equilibrium in the excited state in the mid-pH region is virtually never observed [24].

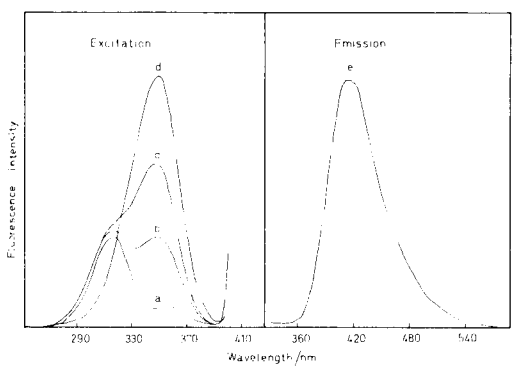

Fig. 1. Uncorrected excitation and emission spectra of isochlorotetracycline in aqueous solution at pH: (a) 5; (b) 6; (c) 6.5; (d) 7.5—12 (half sensitivity); (e) 1—12 (intensity varies with pH).

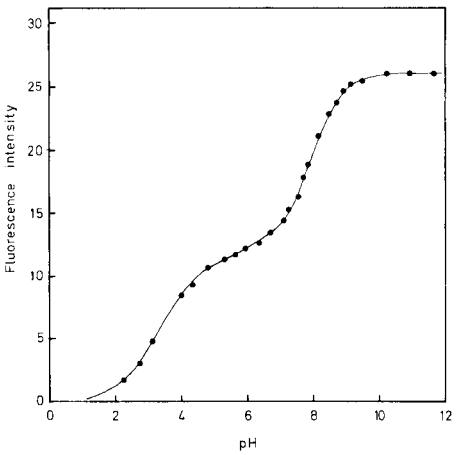

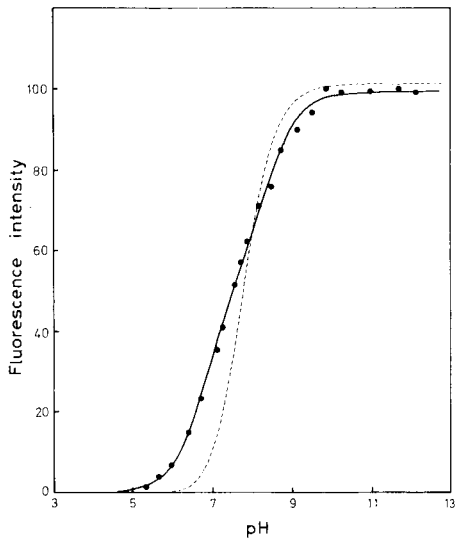

Fig. 2. Fluorimetric titration curve for isochlorotetracycline (λ_{ex} = 315 nm; λ_{em} = 415 nm).

Fig. 3. Fluorimetric titration curve for isochlorotetracycline (λ_{ex} = 350 nm, λ_{em} = 415 nm: (•) experimental points; (---) model based on macroscopic dissociation constants; (——) model based on microscopic dissociation constants.

With excitation at 350 nm, C^- is the only species which significantly absorbs (the molar absorptivity at 350 nm is 7140 l mol^{-1} cm^{-1}; that for HC at 350 nm is <200 l mol^{-1} cm^{-1}). Figure 3, curve (a), therefore simply represents the titration of the ground state of the compound, with the inflection occurring at pK_a.

The fluorescence behaviour of isochlorotetracycline in the pH range 1—12 can be summarized by the following scheme

$pH < pK_a^* < pK_a$

$HC + h\nu_1 \longrightarrow HC^*$ (λ_{ex} = 315 nm)

$HC^* \longrightarrow HC$ (radiationless)

$pK_a^* < pH < pK_a$

$HC + h\nu_1 \longrightarrow HC^*$ (λ_{ex} = 315 nm)

$HC^* \overset{pK_a^*}{\rightleftharpoons} C^{-*} + H^+$

$C^{-*} \longrightarrow C^- + h\nu_2$ (λ_{em} = 415 nm)

$C^- + H^+ \underset{pK_a}{\rightleftharpoons} HC$

$pH > pK_a$

$$C^- + h\nu_1 \longrightarrow C^{-*} \quad (\lambda_{ex} = 315 \text{ nm})$$

$$C^- + h\nu_3 \longrightarrow C^{-*} \quad (\lambda_{ex} = 350 \text{ nm})$$

$$C^{-*} \longrightarrow C^- + h\nu_2 \quad (\lambda_{em} = 415 \text{ nm})$$

The first inflection point in the pH vs. fluorescence intensity curve with λ_{ex} = 315 nm (Fig. 2) gives a value of 3.3 for pK_a*. This value must be considered approximate; the curve is drawn out because the excited-state prototropic equilibrium is not fully established. Examination of the corresponding curve for λ_{ex} = 350 nm (Fig. 3) shows this also to be drawn out more than expected. However, as excited-state equilibria are not involved, there must be another reason. The dotted line in Fig. 3 indicates the best fit of a model based on the three ground-state macroscopic dissociation constants to the experimental data. The experimental curve can be better accounted for by using an ionization scheme based on microscopic dissociation constants such as that proposed for tetracycline [25] in which the first deprotonation step is considered to be exclusively from site A. The superscripts refer to the charge on each acid-base site.

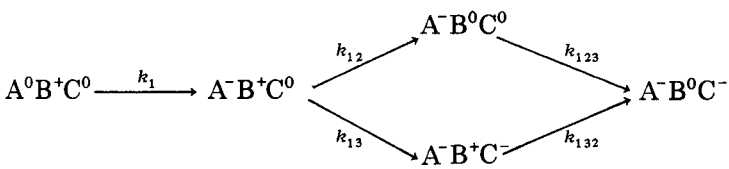

It is clear from this scheme that there are two species, $A^-B^+C^-$ and $A^-B^0C^-$, in which the C group is ionized and therefore expected to show fluorescence. The measured fluorescence, F, can therefore be expressed by

$$F = klI_0(\epsilon_{A^-B^+C^-}\phi_{A^-B^+C^-}C_{A^-B^+C^-} + \epsilon_{A^-B^0C^-}\phi_{A^-B^0C^-}C_{A^-B^0C^-})$$

where ϵ, ϕ and C are the molar absorptivity, quantum efficiency and concentration of the subscripted species, respectively, and k, l and I_0 are the instrument constant, path-length and excitation intensity, respectively. As the hydroxyphthalide portion of the isochlorotetracycline molecule is quite separate from sites A and B it is not unreasonable to take the corresponding ϵ and ϕ values for each species as equal. The concentrations of $C_{A^-B^+C^-}$ and $C_{A^-B^0C^-}$ may be expressed in terms of the total isochlorotetracycline concentration, C_T, and the various microscopic and macroscopic dissociation constants describing the equilibria in solution. Making these substitutions gives

$$F = (klI_0\epsilon\phi C_T/D)\{(K_1k_{13}/[H^+]) + (K_1K_2K_3/[H^+]^3)\} \quad (1)$$

where $D = 1 + (K_1/[H^+]) + (K_1K_2/[H^+]^2) + (K_1K_2K_3/[H^+]^3)$, K_1, K_2 and K_3 are the macroscopic dissociation constants and k_{13} is a microscopic dissociation constant as shown in the microionization scheme given above.

The pH vs. fluorescence intensity data for λ_{ex} = 350 nm were fitted to Eqn. 1, using non-linear least squares with the parameters k_{13}, K_3 and $klI_0\epsilon\phi C_T$ floated. Potentiometrically measured values for pK_1 (3.08) and pK_2 (6.68) [19] and a value of 0.777 for the hydrogen ion activity coefficient were used. The resulting fit is extremely good, as can be seen from the solid line in Fig. 3. The predicted values for pK_3 and pk_{13} were 8.24 and 6.95, respectively. The value for pK_3 agrees well with the values of 8.1 and 8.3 in the literature [18, 20]. Table 1 summarizes the macroscopic and microscopic pK_a values for isochlorotetracycline hydrochloride which were calculated from the values for pK_1, pK_2, pK_3 and pk_{13} using the known interrelationships between the constants.

Fluorescence in strong protic and aprotic media

Below pH 1 a long-wavelength fluorescence band at 460 nm begins to appear at the expense of the 415-nm emission; in 2.5 M hydrochloric acid only the 460-nm emission is observed. Increasing the acid concentration to 10 M results in a blue shift of the fluorescence to 432 nm and doubling in intensity (Fig. 4). In contrast, the excitation spectrum is unaffected by all these changes in conditions and remains at 315 nm, indicating that the undissociated molecule is the absorbing species. All these fluorescence emissions are of low intensity, being only a few percent of the fluorescence emission observed in alkaline solution.

As both the new emission wavelengths are red-shifted with respect to the C^-* fluorescence, they most probably entail protonation of the electron acceptor group C=O, which becomes more basic in the excited state than in the ground state. Moreover, longer wavelength emission is most likely to be the result of the dissociation of the electron donor group (the phenolic OH). Therefore, the 460-nm and the 432-nm emissions can be assigned to the zwitterionic, Z*, and cationic, C^+*, forms of the fluorophore, respectively.

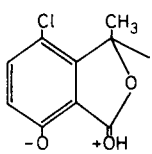

Z*

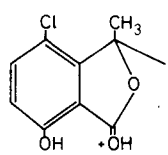

C^+*

HC* must be ruled out as one of the fluorescent species, as this would be inconsistent with the large increase in fluorescence intensity on going from

TABLE 1

Macroscopic and microscopic pK_a values for isochlorotetracycline hydrochloride

Macroscopic constants	pK_1 = 3.08 [19]	pK_2 = 6.68 [19]	pK_3 = 8.24		
Microscopic constants	pk_1 = 3.08	pk_{12} = 7.01	pk_{13} = 6.95	pk_{123} = 7.91	pk_{132} = 7.97

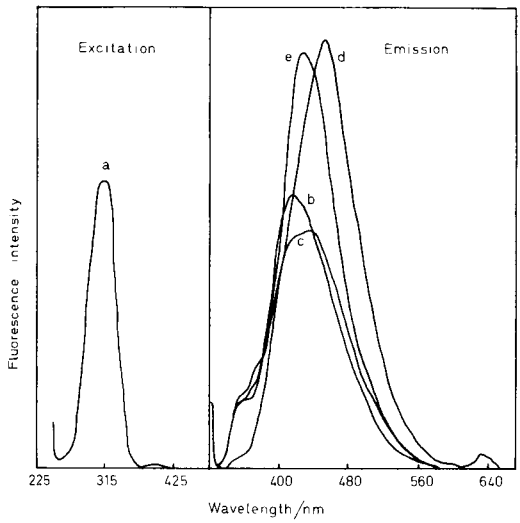

Fig. 4. Uncorrected excitation and emission spectra of isochlorotetracycline in aqueous HCl. HCl concentration (mol dm^{-3}): (a) 0.1—10 (intensity varies with concentration); (b) 0.1; (c) 0.25; (d) 2.5; (e) 10 (half sensitivity).

0.1 to 2.5 M hydrochloric acid (Fig. 4). The formation of Z* must have occurred by intermolecular phototautomerism of HC* so as to account for the increase in Z* concentration (hence fluorescence intensity) with increasing acidity. The conversion of HC* to Z* therefore comprises the protonation of the carbonyl group as a first step, followed by a fast dissociation from the hydroxyl group.

In chloroform, and in chloroform containing 2% (v/v) trifluoracetic acid, the only excitation and emission bands observed were those at 315 and 465 nm, respectively. Here the formation of Z*, of which the 465-nm emission is characteristic (the small red shift compared to aqueous media being due to solvent effects), must have occurred by the fast intramolecular phototautomerism of HC*. Figure 5 shows the excitation and emission spectra in chloroform rendered basic with different quantities of morpholine. With 2% (v/v) morpholine there is only the excitation peak at 360 nm and the emission peak at 415 nm, indicating that C^- is the ground-state absorbing chromophore. In the presence of smaller concentrations of morpholine (0.2%, 0.1% and 0.07%), the emissions of both C^-* and Z* are observed, the intensity and therefore concentration of each form being dependent on the morpholine concentration. In contrast to the aqueous systems investigated, the excited-state dissociation of HC* to C^-* was not observed and is presumably due to the much faster intramolecular phototautomerism compared to dissociation in aprotic solvents.

For analytical purposes, it is clear that alkaline conditions (pH >10) and excitation at 350 nm should be used for maximum sensitivity. The liter-

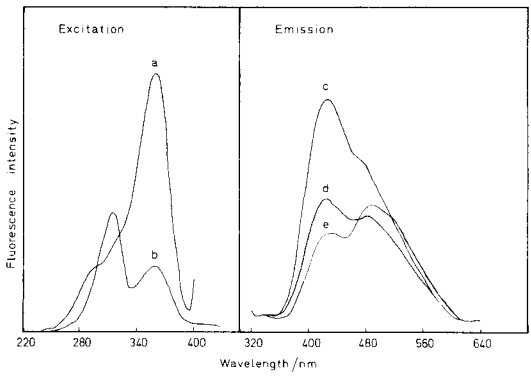

Fig. 5. Uncorrected excitation and emission spectra of isochlorotetracycline in chloroform/morpholine mixtures. Morpholine concentration (%, v/v): (a) 0.07 (λ_{em} = 415 nm); (b) 0.07 (λ_{em} = 460 nm); (c) 0.2 (λ_{ex} = 315 nm); (d) 0.1 (λ_{ex} = 315 nm); (e) 0.07 (λ_{ex} = 315 nm).

ature indicates that these optimum conditions have not always been used. The now somewhat dated procedures proposed by Levine et al. [1] and Feldman et al. [5] used a pH of approximately 7.5 for the fluorescence measurements, while Saltzman [2] used pH 8.5. More recent papers [4, 8, 9, 11, 12, 15] have used sodium hydroxide (>0.1 M) as the medium of measurement.

B.M.A. thanks the University of Khartoum for financial support. The authors thank Lederle Laboratories, Cyanamid of Great Britain Ltd., for providing the chlorotetracycline hydrochloride sample.

REFERENCES

1 J. Levine, E. A. Garlock and H. Fischbach, J. Am. Pharm. Assoc., Sci. Ed., 38 (1949) 473.
2 A. Saltzman, J. Lab. Clin. Med., 35 (1950) 123.
3 S. Renato, Bull. Soc. Ital. Biol. Sper., 26 (1950) 497.
4 F. S. Chiccarelli, P. van Gieson and M. H. Woolford, J. Am. Pharm. Assoc., Sci. Ed., 45 (1956) 418.
5 D. H. Feldman, H. S. Kelsey and J. C. Gavagnol, Anal. Chem., 29 (1959) 1697.
6 S. Udenfriend, D. E. Duggan, B. M. Vasta and B. B. Brodie, J. Pharmacol. Exp. Ther., 120 (1957) 26.
7 K. W. Kohn, Anal. Chem., 33 (1961) 862.
8 J. Spock and S. E. Katz, J. Assoc. Off. Agric. Chem., 40 (1963) 434.
9 S. E. Katz and J. Spock, J. Assoc. Off. Agric. Chem., 47 (1964) 203 and 1157.
10 R. G. Kelly, H. A. Floyd and K. D. Hoyt, Antimicrobial Agents and Chemotherapy, (1966) 216.
11 R. G. Kelly and K. D. Hoyt, Z. Klin. Chem. Klin. Biochem., 7 (1969) 152.
12 I. A. Buga and F. V. Babilev, Zaravook-hranenie, 16 (1973) 55.
13 R. Andrzej, Acta Pol. Pharm., 31 (1974) 259.
14 D. Hall, J. Pharm, Pharmacol., 27 (1975) 33P (Suppl.).

15 D. Hall, J. Pharm. Pharmacol., 28 (1976) 420.
16 H. Poiger and Ch. Schlatter, Analyst, 101 (1976) 808.
17 M. K. Mathew and P. Balaram, J. Inorg. Biochem., 13 (1980) 339.
18 C. W. Waller, B. L. Hutchings, C. J. Wolf, A. A. Goldman, R. W. Broschard and J. H. Williams, J. Am. Chem. Soc., 74 (1952) 4981.
19 B. M. Ahmed, Ph.D. Thesis, University of London, 1982.
20 C. R. Stephens, K. Murai, K. J. Brunings and R. B. Woodward, J. Am. Chem. Soc., 78 (1956) 4155.
21 L. H. Conover, Chemical Society (London), Spec. Publ. No. 5, p. 73.
22 J. R. D. McCormick, S. M. Fox, L. L. Smith, B. A. Bitler, J. Reichental, V. E. Origoni, W. H. Muller, R. Winterbottom and A. P. Doershuk, J. Am. Chem. Soc., 79 (1957) 2849.
23 F. A. Hochstein and R. Pasternack, J. Am. Chem. Soc., 74 (1952) 3905.
24 S. G. Schulman and A. C. Capomacchia, J. Phys. Chem., 79 (1975) 1337.
25 G. L. Asleson and C. W. Frank, J. Am. Chem. Soc., 98 (1976) 4745.

Analytica Chimica Acta, 156 (1984) 273—277
Elsevier Science Publishers B.V., Amsterdam — Printed in The Netherlands

Short Communication

A HIGHLY SENSITIVE LASER TWO-PHOTON IONIZATION DETECTOR FOR LIQUID CHROMATOGRAPHY

SUNAO YAMADA, ATSUSHI HINO and TEIICHIRO OGAWA*

Department of Molecular Science and Technology, Graduate School of Engineering Sciences, Kyushu University, Kasuga-shi, Fukuoka 816 (Japan)

(Received 4th May 1983)

Summary. A highly sensitive detector for liquid chromatography using the laser two-photon ionization technique is described. Detection limits for several aromatic molecules, such as pyrene and chrysene, with a nitrogen laser (337 nm) are in the range 5—30 pg, which is considerably below the limits attainable with a commercial u.v. absorption detector.

Although a multitude of detectors has been developed for liquid chromatography, there is yet to be invented a universal and sensitive detector. Several laser-based detectors for liquid chromatography have offered better sensitivity and selectivity than commercial detectors [1]. The laser two-photon ionization technique is new and quite sensitive in a liquid phase [2—5], and an application of this technique for liquid chromatographic measurements is very attractive. A windowless flow cell has been constructed [2, 3]; its sensitivity is almost identical with that of a commercial u.v. absorption detector.

The two-photon ionization detection of aromatic molecules in a flow system has been reported; the minimum detectable concentration of pyrene was 6 ng l^{-1} [5]. In this communication, it is shown that the laser two-photon ionization system is useful as a detector of liquid chromatography. The sensitivity is substantially improved compared with the commercial u.v. detector.

Experimental

Instrumentation. The laser photoionization detection system has been described [4, 5]. A Molectron UV-12 nitrogen laser was used at a repetition rate of 10 Hz. A quartz lens (50 cm focal length) focused the laser beam at the central point between two electrodes. The photocurrent was converted to voltage with a home-made current-to-voltage converter (ICH 8500A; gain = 10^9 VA^{-1}, time constant $\approx$1 ms). The voltage output was monitored by a Iwatsu SS-5416A oscilloscope (40 MHz) and was averaged for 1 s by a NF BX-530A boxcar integrator (gate width 200 ns—10 ms, time constant 100 μs—100 s, time base 5 μs—1 s), and the boxcar output was recorded on a RDK R-02 recorder.

0003-2670/84/$03.00

Photoionization cell. As shown in Fig. 1, the photoionization cell has two stainless steel tubes (1.8 mm o.d.); one is the solution inlet (0.25 mm i.d.) and the other is the outlet (1.5 mm i.d.). The ends of the two tubes are cut and planed thinly to serve as electrodes. The cell is made of a teflon plate (10 × 10 × 2.7 mm) through which 1.8-mm diameter holes are drilled to insert the tubes. Teflon sheets with 2 × 1-mm holes in the center and quartz plates are fastened to the cell. The internal volume of the cell is about 5 μl. A bias voltage of 500 V is applied to one electrode (the solution inlet) through a 10-MΩ current limiting resistor. The other electrode (the solution outlet) collects the resultant photocurrent. The cell is shielded by placing it inside a grounded aluminium box.

Materials. Pyrene (Nakarai Chemicals) [4], hexane (reagent grade, Wako Pure Chemicals) [5], and 1-chloroanthracene [5] were purified as described previously. Other compounds (reagent grade) were used as received.

Chromatographic measurements. The chromatographic system (Hitachi 655; 4.6 × 150 mm column with Shodex Silicapak E-411 (5-μm packing)) was interfaced to a commercial u.v. absorption detector (Hitachi 638-41; 17.7-μl cell volume, 195—350 nm) or the photoionization cell. The sample injection was 10 μl and the flow rate was 1.5 ml min^{-1} in all measurements. The effluent from the column was routed to the photoionization cell through 20 cm of 0.25-mm i.d. teflon tubing. Sample solutions were prepared from freshly prepared stock solutions (10^{-2}–10^{-3} M).

Results and discussion

Characteristics and performance of the laser photoionization cell. The signal/noise ratio of the photoionization detection system depends pro-

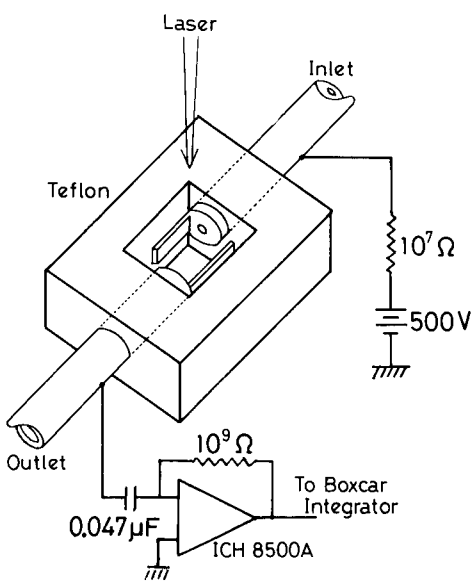

Fig. 1. Schematic diagram of the photoionization cell.

foundly on the cell design [5]. Because the scattered light of the laser does not affect the sensitivity, a photoionization cell with windows was constructed; the use of windows settles the problem of solvent volatilization from a windowless cell. The electrodes should be placed as close as possible while avoiding electrical breakdown and direct illumination of the electrodes. In the present case, the electrode spacing was less than 1 mm and the optimum bias voltage was 500 V.

The internal volume of the cell should be as small as possible to increase the selectivity of the detector. The internal volume of the present cell (about 5 μl) is considerably smaller than that of the commercial u.v. detector (17.7 μl). The laser irradiation volume is estimated to be 10^{-4}—10^{-3} cm^3, so that further decrease of the internal volume is essentially a mechanical problem.

In order to compare the present apparatus with those of previous reports, the detection limit for pyrene was evaluated by introducing its solutions directly into the cell. The detection limit (S/N = 2) was 0.1 $\mu g\ l^{-1}$; this value is one order of magnitude worse than that of the previous work [5] mainly because of the decrease in the laser irradiation volume of the present cell. It is, however, one order of magnitude better than that of the windowless flow cell [2]; this improvement is attributed to the new cell design as well as optimization of several factors affecting the sensitivity.

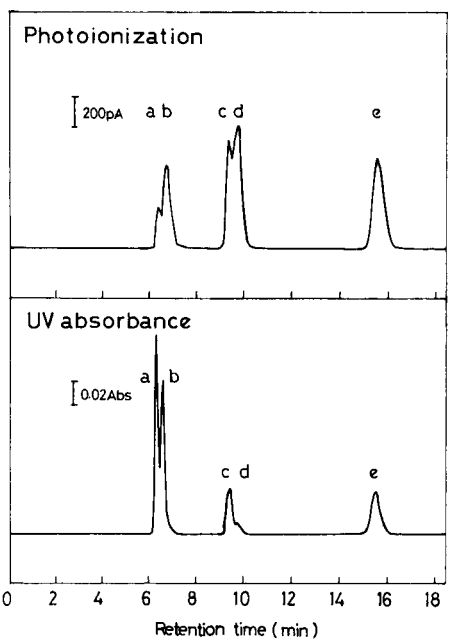

Fig. 2. Photoionization (337 nm) and u.v. absorption (254 nm) chromatograms of a mixture of aromatic molecules in hexane. Peaks: (a) 9-bromoanthracene (injected quantity 64 ng); (b) 1-chloroanthracene (43 ng); (c) anthracene (16 ng); (d) pyrene (20 ng); (e) tetraphene (91 ng).

Chromatographic measurements. Photoionization and u.v. absorption chromatograms for a mixture of pyrene, tetraphene, anthracene, 1-chloroanthracene, and 9-bromoanthracene in hexane are shown in Fig. 2. The photoionization peaks are somewhat wider than the u.v. peaks, probably because of the cell design; the cross-section of the cell suddenly becomes large at the connection with the inlet tube.

The detection limit for pyrene obtained from a chromatogram was evaluated by comparing the peak-to-peak blank noise with the least-square slope of the plot of chromatographic peak heights versus quantities of injected pyrene (0—2 ng). Detection limits for pyrene (S/N = 2) were 6 pg for photoionization method and 160 pg for the u.v. method. Comparison of peak heights of known quantities of several aromatic molecules with those of pyrene gave the detection limits summarized in Table 1. The present detector is much more sensitive than the commercial u.v. absorption detector (Table 1), except for 9-bromoanthracene, especially if the comparison is made at the same wavelength (337 nm). The present detector is also better than a one-photon ionization detector where detection limits for pyrene and tetraphene were reported to be 20 pg and 50 pg, respectively [6]. It is also more sensitive than a three mode (fluorescence, photoacoustic, and photoionization) detector [7].

The sensitivity of the u.v. detector depends on the molar absorptivity of the analyte and is better at 254 nm than at 337 nm (Table 1). The sensitivity of the photoionization detection tends to increase with increasing molar absorptivity of the analyte [5]. The increase of photoionization efficiency arising from increased photon absorption indicates a good chance of improving the sensitivity of the photoionization detector by using a laser tuned to the wavelength of the largest molar absorptivity of the analyte. Voigtman and Winefordner [7] used an excimer laser (308 nm) and found the minimum detectable concentration of anthracene to be 0.2 mg l^{-1} (S/N = 3) in 70:30 acetonitrile/water.

In conclusion, the proposed two-photon ionization detector is more

TABLE 1

Comparison of detection limits in liquid chromatography

Compound	Detection limit (pg)		
	Photoionization 337 nm	U.v. absorbance	
		254 nm	337 nm
Anthracene	5	17	120
1-Chloroanthracene	12	15	180
9-Bromoanthracene	23	15	160
Pyrene	6	160	100
Tetraphene	18	110	160
Chrysene	32	47	1700

sensitive than the commercial u.v. detector or the one-photon ionization detector. The quartz windows used settle the problem of solvent volatilization from windowless cells.

The authors thank Drs. J. D. Winefordner and E. Voigtman for sending their results prior to publication.

REFERENCES

1 R. B. Green, Anal. Chem., 55 (1983) 20A.
2 E. Voigtman, A. Jurgensen and J. D. Winefordner, Anal. Chem., 53 (1981) 1921.
3 E. Voigtman and J. D. Winefordner, Anal. Chem., 54 (1982) 1834.
4 S. Yamada, K. Kano and T. Ogawa, Bunseki Kagaku, 31 (1982) E247.
5 S. Yamada, A. Hino, K. Kano and T. Ogawa, Anal. Chem., 55 (1983) 1914
6 D. C. Locke, B. S. Dhingra and A. D. Baker, Anal. Chem., 54 (1982) 447.
7 E. Voigtman and J. D. Winefordner, J. Liq. Chromatogr., 5 (1982) 2113.

Analytica Chimica Acta, 156 (1984) 279—282
Elsevier Science Publishers B.V., Amsterdam — Printed in The Netherlands

Short Communication

ION-INTERACTION CHROMATOGRAPHY OF DITHIOCARBAMATES ON μBONDAPAK CN AND LICHROSORB RP-8 STATIONARY PHASES IN THE PRESENCE OF TETRAALKYLAMMONIUM SALTS

G. F. KIRKBRIGHT* and F. G. P. MULLINS

Department of Instrumentation and Analytical Science, University of Manchester Institute of Science and Technology, Manchester M60 1QD (Great Britain)

(Received 15th August 1983)

Summary. Dithiocarbamates are examined by high-performance liquid chromatography on μBondapak CN and LiChrosorb RP-8 bonded phases using ion-interaction with tetraalkylammonium salts. The effects of the tetraalkylammonium cation and its inorganic co-anion on solute retention are considered. The response for sodium diethyldithiocarbamate is linear over the range 1—500 μg ml^{-1}, with a detection limit of 0.1 μg ml^{-1}.

Dithiocarbamate insecticides pose unique problems in residue analysis. Dithiocarbamate salts are highly polar, very soluble in water and are thermally unstable [1]. In addition, dithiocarbamates are pH-sensitive; dithiocarbamates decompose on acidification [2—4], the products usually being carbon disulphide and an amine. Moreover, dithiocarbamates are commonly metabolised to products that may be of toxicological significance in water and other samples [5]; such products would include ethylenethiourea, ethylenethiuram monosulphide and ethylenebisisothiocyanate.

High-performance liquid chromatography (h.p.l.c.) is ideally suited to the separation of dithiocarbamate salts owing to its low operating temperatures, high selectivity and high efficiency within a single column. Methods useful in analyses for dithiocarbamates have been reviewed elsewhere [6]. Kepple [7] has reported a method which uses hydrolysis of the dithiocarbamates followed by measurement of the amine as its trifluoroacetate by gas chromatography with electron-capture detection. These methods are susceptible to interferences and require careful sample clean-up procedures prior to derivatisation before accurate and reproducible results may be obtained. The methods are specific only for the dithiocarbamate group and cannot distinguish between compounds with different *N*-alkyl substituents.

Smith et al. [8] reported a method for the h.p.l.c. of dithiocarbamates, using transition metal ions as ion-interaction reagents. Bond and Wallace [9] used dithiocarbamates to detect copper by h.p.l.c. with electrochemical detection. Kirkbright and Mullins [6] used cetrimide above its critical micelle concentration to achieve separation of five dithiocarbamates. This communication reports the effect of tetraalkylammonium salts (R_4N^+),

0003-2670/84/$03.00

and the effect of the inorganic co-anion on the retention of dithiocarbamate salts on both μBondapak CN and LiChrosorb RP-8 stationary phases.

Experimental

Apparatus. For liquid chromatography, a Waters μBondapak CN column (3.9 × 300 mm; 10 μm, or a Pye-Unicam LiChrosorb RP-8 column (4.6 × 250 mm; 5 μm) was used with a Rheodyne 7125 valve injector with a 20-μl loop. The eluates were detected with a 480 variable-wavelength u.v. detector (Lambda-Max Waters Associates) operated at 253 nm. Retention times and peak areas were obtained using either a Hewlett-Packard Model 3390 integrator or an LDC Model 308 computing integrator.

Reagents. The sodium salts of dimethyl- and diethyl-dithiocarbamates (Fluorochem, Glossop, and Robinson Bros., West Bromwich) and the tetraalkylammonium salts (Fluorochem, Glossop) were used as recieved. Methanol was h.p.l.c. grade (Rathburn Chemicals, Scotland). Deionised water, distilled from glass, was further deionised using a Water I deioniser (Gelman Sciences). Disodium hydrogenphosphate (Fisons Scientific Apparatus, Loughborough) and potassium dihydrogenphosphate (BDH Chemicals) were of analytical-reagent grade.

Procedure. Solutions of dithiocarbamates (100 μg ml^{-1}) were injected onto the column. The mobile phase used was water/methanol (70:30, v/v). The mobile phases were buffered to pH 6.4 with phosphate buffer (0.01 M). The solutions were filtered using a 0.45-μm filter (Millipore). The flow rates were 2 ml min^{-1} or 1 ml min^{-1}, as indicated. The column was conditioned by passage of the buffered mobile phase containing the tetraalkylammonium salt through the column at 1.5 ml min^{-1} for 90 min. This gave reproducible retention times for the injected solutes. Capacity factor (k') was used as a measure of the degree of retention of the solute; $k' = (t_r - t_m)/t_m$ where t_r is the retention time of the solute and t_m is the retention time of unretained solute.

Results and discussion

Dithiocarbamates are eluted at the solvent front ($k' = 0$) on a cyano-bonded stationary phase or on an octyl-bonded stationary phase if an ion-interaction reagent is not included in the mobile phase [8]. Bidlingmeyer et al. [10, 11] reported a model in which the addition of a hydrophobic cation (tetraalkylammonium cation) to the mobile phase is assumed to occupy the primary layer sorbed onto the bonded stationary phase while the coanion occupies the secondary layer. As the mobile phase always contains the hydrophobic cation, a dynamic equilibrium is established between the double layer, the hydrophobic salt and the analyte anion. This overall process is known as ion-interaction chromatography. Bidlingmeyer [10] reported the separation of weak acids on reverse-phase octadecylsilane columns using ion-interaction reagents. Smith et al. [8] reported that the addition of tetrabutylammonium hydroxide resulted in degradation of the dithiocarbamates. Similar decomposition with tetraalkylammonium salts was not noted here.

As discussed by Kirkbright and Mullins [6], pH control is very important in the h.p.l.c. of dithiocarbamates.

Table 1 shows that the retention of dithiocarbamates increases on μBondapak CN or LiChrosorb RP-8 as the number of carbon atoms in the tetraalkylammonium salt (i.e., hydrophobicity) increases. The concentration of tetraalkylammonium salt in the mobile phase was 5×10^{-3} M at pH 6.4 (phosphate buffer) to ensure that the dithiocarbamates were in anionic form; Iskandarani and Pietrzyk [12] reported similar findings.

Few studies have considered the effect of the co-anion accompanying the tetraalkylammonium salt on the retention of the solute. Table 2 lists the k' values for the retention of several dithiocarbamates on the μBondapak CN stationary phase in the presence of tetrabutylammonium salts with dif-

TABLE 1

Effect of variation of carbon number in tetraalkylammonium salt on retention of dithiocarbamates on μBondapak CN and LiChrosorb RP-8[a]

Dithiocarbamate	Capacity factor, k'					
	TMACl	TBACl	THACl	TMACl	TBACl	THACl
	μBondapak CN			LiChrosorb RP-8		
Sodium diethyldithiocarbamate	0.26	0.52	2.70	2.15	6.2	9.10
Sodium dimethyldithiocarbamate	0	0.20	2.30	1.22	4.18	8.18
Ammonium tetramethylene-dithiocarbamate	0	0.13	1.86	1.14	4.46	8.92
Disodiumethylenebis-dithiocarbamate	0	0.04	Retained	2.09	—	—
Ethylenethiourea	0.21	0.21	0.21	—	—	—

[a]30:70 methanol/water, 0.01 M in phosphate buffer (pH 6.4) containing 5×10^{-3} M tetramethylammonium chloride (TMACl), tetrabutylammonium chloride (TBACl) or tetrahexylammonium chloride (THACl). Flow rate 2 ml min^{-1} for μBondapak and 1 ml min^{-1} for LiChrosorb.

TABLE 2

Effect of different co-anions in the tetrabutylammonium salt on the retention of dithiocarbamates on μBondapak CN[a]

Dithiocarbamate	Capacity factor, k'					
	NO_3^-	PO_4^{3-}	Br^-	Cl^-	HSO_4^-	F^-
Sodium diethyldithio-carbamate	0.30	0.38	0.39	0.50	0.66	0.73
Sodium dimethyl-dithiocarbamate	0.04	0.06	0.20	0.210	0.22	0.22
Sodium tetramethylene-dithiocarbamate	0.07	0.104	0.22	0.24	—	0.25

[a]Other conditions as for Table 1.

ferent inorganic co-anions. This demonstrates that not only is the effect of co-anion significant, but it appears to follow a regular pattern. Although there are small variations for individual solutes, the effect of the added anion in reducing the solute retention follows the order $NO_3^- > PO_4^{3-} > Br^- > Cl^- > HSO_4^- > F^-$.

Gibson and Weatherburn [13] reported on the distribution of various inorganic anion—organic quaternary cation pairs. They demonstrated that for most of the anions studied, the distribution ratio generally increased with the size of the anion, the order of extraction of the anion being similar to the above, and to that reported by Iskandarani and Pietrzyk [12].

A calibration graph prepared for sodium diethyldithiocarbamate with tetrabutylammonium bromide as the interacting reagent was linear over the range 1—500 $\mu g\ ml^{-1}$, with a detection limit of 0.1 $\mu g\ ml^{-1}$. The plot of concentration against peak area had a slope of 2.07 with an intercept of 6.075 (r = 0.997). The relative standard deviation obtained for 10 injections of 20-μl aliquots of sample solutions containing 10 $\mu g\ ml^{-1}$ of diethyldithiocarbamate was 0.042.

It is apparent from the results obtained that ion-interaction chromatography with tetraalkylammonium ions may be used to detect and determine trace levels of dithiocarbamates. Particular determinations may be optimised by careful selection of the ion-interaction reagent, the bonded stationary phase and the inorganic co-anion.

We are grateful to Thames Water Authority for support of the work reported here.

REFERENCES

1 G. D. Thorn and R. A. Ludwig, Can. J. Chem., 32 (1954) 872.
2 R. G., Joris, K. I. Aspila and C. L. Chakrabarti, Anal. Chem., 41 (1969) 1441.
3 R. G. Joris, K. I. Aspila and C. L. Chakrabarti, J. Phys. Chem., 74 (1970) 860.
4 K. I. Aspila, V. S. Sastri and C. L. Chakrabarti, Talanta, 16 (1969) 1099.
5 W. H. Newsome, in G. Zweig and J. Sherma (Eds.), Analytical Methods for Pesticides and Plant Growth Regulators, Vol. 3, Academic Press, New York, 1964, p. 197.
6 G. F. Kirkbright and F. G. P. Mullins, Analyst, (1983) in press.
7 G. E. Kepple, J. Assoc. Off. Anal. Chem., 52 (1969) 162.
8 R. M. Smith, R. L. Morarjii and W. G. Salt, Analyst, 106 (1981) 129.
9 A. M. Bond and G. G. Wallace, Anal. Chem., 53 (1981) 1209.
10 B. A. Bidlingmeyer, J. Chromatogr. Sc., 18 (1980) 525.
11 B. A. Bidlingmeyer, S. N. Denning, W. P. Price, B. Sachok and M. Petrusek, J. Chromatogr., 186 (1979) 419.
12 Z. Iskandarani and D. J. Pietrzyk, Anal. Chem., 54 (1982) 1065.
13 N. A. Gibson and D. C. Weatherburn, Anal. Chim. Acta, 58 (1972) 149, 158.

Analytica Chimica Acta, 156 (1984) 283—287
Elsevier Science Publishers B.V., Amsterdam — Printed in The Netherlands

Short Communication

A CATALYTIC IMMUNO-REACTOR FOR THE AMPEROMETRIC DETERMINATION OF HUMAN SERUM ALBUMIN

ISAO KARUBE*, TADASHI MATSUNAGA, TAKERU SATOH and SHUICHI SUZUKI

Research Laboratory of Resources Utilization, Tokyo Institute of Technology, Nagatsuta-cho, Midori-ku, Yokohama 227 (Japan)

(Received 24th June 1983)

Summary. A catalytic immuno-reactor for the determination of human serum albumin (HSA) was constructed by using immobilized antibody and an amperometric detector. A sandwich assay with hemin-labeled antibody to catalyze the decomposition of hydrogen peroxide was used, the catalytic activity of the hemin-antibody conjugate being determined by measuring the decrease in hydrogen peroxide concentration. The reaction of hemin-labeled antibody with antigen was complete within 30 min and the current decrease was correlated with the HSA concentration. The relative standard deviation was about 9% at an HSA concentration of 1 mg ml^{-1}.

Various sensors consisting of bio-active substances (enzymes, micro-organisms, organella, antigens and antibodies) and electrochemical devices have been developed for clinical analysis [1—4]. Substances such as glucose and lactic acid may be specifically determined by these devices, but few sensors have been developed for determining macromolecules. Enzyme immunoassays based on antigens, haptens or antibodies labeled with enzymes form a group of binding assays in which the molecular recognition properties of antibodies are used. Recently, such methods have been applied in histochemistry and cytochemistry, and they are regarded as alternatives to radioimmunoassay [5]. Aizawa et al. [6] developed a new "enzyme immuno-sensor", by combining enzyme immunoassay and electrochemical measurements. This sensor utilized catalase as the label. Catalase reduces hydrogen peroxide to oxygen, thus the catalase-labeled antigen bound to an immobilized antibody can be measured from the rate of oxygen generation or hydrogen peroxide consumption. However, a long incubation time is required, possibly because the immunochemical reaction is hindered by the large enzyme molecule.

In this communication, the low-molecular-weight catalyst, hemin, replaces the enzyme. Hemin has been shown to be effective for labeling the antibody in a non-enzymatic luminescent immunoassay [7]. Hemin also catalyzes the reduction of hydrogen peroxide, a process that is frequently followed electrochemically. A catalyst immuno-reactor system constructed from the immobilized antibody and an amperometric cell was examined for the determination of human serum albumin (HSA).

0003-2670/84/$03.00

Experimental

Materials. Human serum albumin (HSA; Kabi AB, Sweden) and anti-HSA rabbit serum (Miles Laboratories, Israel) were used. The immunoglobulin fraction anti-HSA IgG was separated by DEAE-cellulose chromatography with 15 mM phosphate buffer (pH 8.3). Then, the antibody was dialyzed against 1 l of 1% NaCl solution for 1 h; this dialysis was repeated five times. Hemin (Tokyo Kasei, Tokyo) was washed with distilled water before use. Other chemicals were analytical- or laboratory-grade reagents. Deionized water was used throughout.

Preparation of immobilized anti-HSA. Small pellets (0.5 mm diameter, 5 mm long, 1 g) of molecular sieve 5A were washed with water, and placed in 2 ml of γ-aminopropyltriethoxysilane. The mixture was left for 10 min, and then the pellets were washed with water and suspended in 5 ml of 1% (w/v) glutaraldehyde solution (in 0.05 M phosphate buffer, pH 7.0) for 1 h at room temperature. The pellets were washed again with water and added to 1 ml of antibody solution containing 10 mg of anti-HSA. This mixture was stirred for 12 h at 4°C. After reaction, the pellets were washed with water, and stored in 0.1 M phosphate buffer, pH 7.0, at 5°C.

Preparation of hemin-labeled anti-HSA antibody. Water-soluble carbodiimide [1-cyclohexyl-3-(2-morpholinoethyl)-carbodiimidemetho-*p*-toluene sulfonate] (10 mg) was added to 1 ml of dimethylsulfoxide containing 5 mg of hemin; the mixture was stirred magnetically for 10 min at 20°C. Then, anti-HSA antibody (23 mg) in 4 ml of water was added, and the mixture was stirred for 3 h at 20°C. After centrifugation twice at 4°C, ammonium sulfate was added to the supernatant liquid and the precipitate was dialyzed for 1 h against 0.1 M phosphate buffer (pH 7.0). The resulting solution (5 ml) was applied to a Sepharose CL-6B column and eluted with 0.1 M phosphate buffer, pH 7.0. The hemin-anti-HSA antibody conjugates were assayed for catalytic activity and protein content.

Catalyst immuno-reactor system. Figure 1 is a schematic diagram of the system. Immobilized anti-HSA (50 mg) was placed in a glass reactor (1.8 mm i.d., 3.5 cm long). The hydrogen peroxide concentration was monitored amperometrically; in the 3-electrode cell the working electrode (platinum, 0.5 cm^2) was used with a silver counter electrode (5 cm^2) and a saturated (KCl) calomel electrode (SCE). A potentiostat (Hokuto Denko, Model HA-104) applied +0.6 V vs. SCE and the current was measured by a milliammeter (TOA Electronics, Model 18N) and displayed on a recorder (TOA Electronics, Model EPR-200A). The volume of the cell was 0.4 ml; temperature was maintained at 30°C.

Procedure for electrochemical determination of HSA. The sandwich method [7] was employed. The phosphate buffer (0.1 M, pH 7.0) was continuously transferred to the system by the peristaltic pump (Model SJ-1211H, Atto Co.). When the baseline current became steady, 100 μl of hydrogen peroxide solution (9.8×10^{-5} mol l^{-1}) was injected at the sample inlet (1) and the current (I_0) was recorded. Then, a 500-μl sample solution

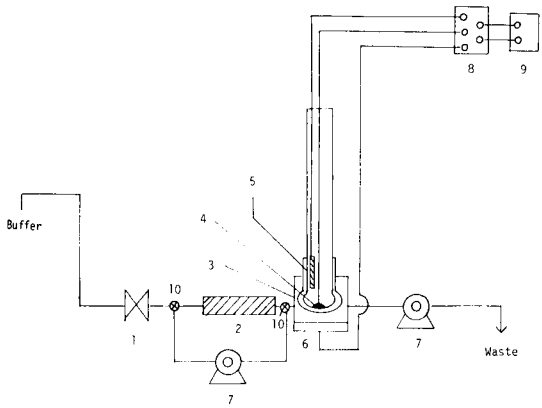

Fig. 1. Schematic diagram of the sensor system: (1) sample inlet; (2) immobilized antibody reactor; (3) flow cell; (4) anode (Pt plate); (5) SCE; (6) cathode (Ag plate); (7) peristaltic pump; (8) monitoring system; (9) recorder.

containing HSA was injected into the system. This was cycled through the reactor for 30 min; the reactor was then washed with phosphate buffer (pH 7.5) containing 1 mM glycine to remove non-specifically adsorbed HSA. Next, 200 μl of hemin-labelled anti-HSA antibody was injected and cycling was continued for 30 min. The system was washed to remove unreacted hemin-anti-HSA IgG conjugates. Then, 100 μl of the peroxide solution was injected again, and the current (I_1) was recorded. The current difference ($\Delta I = I_0 - I_1$) was used as the measure of HSA concentration.

Results

Relationship between current and hydrogen peroxide concentration. The current measured was linearly related to the hydrogen peroxide concentration over the range 0.1 M—1 $\times$ 10^{-5} M peroxide when 100 μl of hydrogen peroxide solution was injected. As the decrease in peroxide concentration was actually measured, a 9.8 $\times$ 10^{-5} M hydrogen peroxide solution was used to enhance sensitivity.

Screening of possible catalysts for labeling antibody. The catalytic activities of hemin (m.w. 652), ferrocene (m.w. 186), and vitamin B_{12} (m.w. 1355) were examined. Catalysts (0.1 mmol) were dissolved in the hydrogen peroxide solution (1 ml) and incubated at 30°C for 3 min. The initial decomposition rates of hydrogen peroxide by hemin, ferrocene, and vitamin B_{12} were in the ratio 1.00:0.22:0.15. The catalytic activity of hemin is thus substantially higher than those of ferrocene and vitamin B_{12}. Anti-HSA antibody was therefore labeled with hemin. The activity of the hemin—anti-HSA IgG conjugate was determined. The decomposition rate of hydrogen peroxide by the conjugate was 63% of that obtained with free hemin; thus the conjugate can be used as a labeled antibody.

Time course of the immunochemical reactions. Figure 2 shows the time course of the reaction of the immobilized HSA with hemin- or catalase-labeled anti-HSA antibody. The HSA solution (2 ml, 1 mg ml^{-1}) was injected into the system and cycled for 30 min. After thorough washing, 200 μl of hemin- or catalase-labeled anti-HSA IgG (20 μM) was injected and recycled for 5 min. Then, 100 μl of hydrogen peroxide (9.8×10^{-5} mol l^{-1}) was injected and the current was measured. This procedure was repeated ten times. The immunochemical reaction increased with time, reaching a steady state after 30 min in the case of hemin-labeled antibody, but 1 h with the catalase-labeled antibody. Hemin-labeling was therefore preferred.

Response curves. Figure 3 shows a typical response obtained when a 1 mg ml^{-1} HSA solution was used. The first peak is the reference current before the immunochemical reaction; the second peak is the current obtained after binding of hemin-labeled anti-HSA IgG to HSA. The peak current was obtained within 2 min, and a complete assay could be completed within 1 h, which is much less than the time needed with the enzyme immunosensors reported previously [6, 8].

Determination of HSA. Figure 4 shows the relationship between the current difference and HSA concentration. The current difference was correlated with HSA concentration over the range 1—10 mg ml^{-1}. The current difference (ΔI) showed a relative standard deviation of about 9% for a 1 mg ml^{-1} HSA solution.

Discussion

Immunochemical, catalytic and electrochemical reactions were used in this assay. The catalytic and electrochemical reactions are rapid, and the immunochemical reaction is the rate-determining step. The enzyme immunosensor with the enzyme-labeled antigen or antibody [6] requires a lengthy

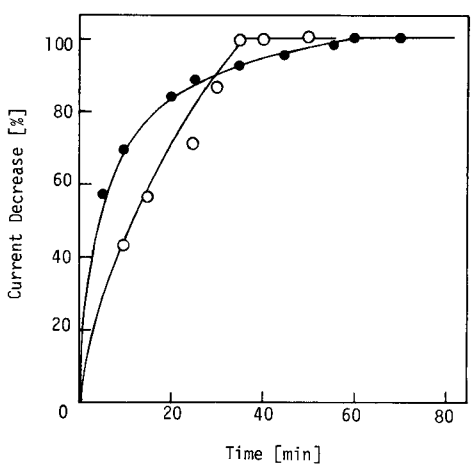

Fig. 2. Time course of the immunochemical reaction. Labeling reagent: (○) hemin; (●) catalase. HSA concentration, 1 mg ml^{-1}.

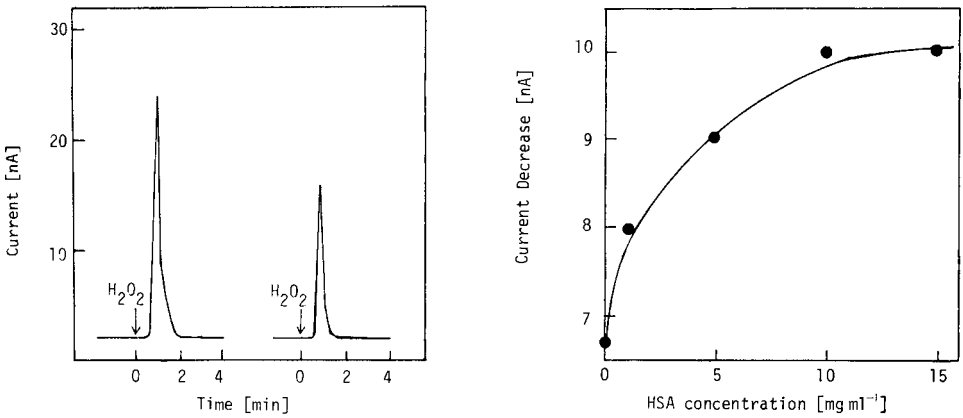

Fig. 3. Response curves of the sensor system: (1) before immunochemical reaction; (2) after immunochemical reaction.

Fig. 4. Calibration curve for HSA.

incubation, probably because the large enzyme molecule hinders the immunochemical reaction. The low-molecular-weight catalyst used here provides a much faster assay.

Further, this catalyst immuno-reactor allows a simple and effective removal of antigen—antibody complexes; because HSA reacts with immobilized anti-HSA antibody, the HSA—anti-HSA IgG complex can be removed by simply washing the reactor, which can then be re-used. The serum of normal individuals contains about 5 mg ml^{-1} HSA. The minimum detectable concentration of this sensor was 1 mg ml^{-1}. As 500 μl of sample solution is needed for the assay, 100 μl of serum has to be sampled and diluted.

The HSA—anti-HSA IgG system was chosen as a model system. Ongoing studies are directed toward applying the reactor to the determination of other proteins and steroids.

REFERENCES

1 G. G. Guilbault, Handbook of Enzymatic Methods of Analysis, M. Dekker, New York, 1976.
2 T. M. S. Chang (Ed.), Biomedical Applications of Immobilized Enzymes and Proteins, Plenum, New York, 1977.
3 A. Arnold and G. A. Rechnitz, Anal. Chem., 52 (1980) 1170.
4 S. Chen, S. S. Kuan and G. G. Guilbault, Clin. Chim. Acta, 100 (1980) 21.
5 G. B. Wisdom, Clin. Chem., 22 (1975) 243.
6 M. Aizawa, A. Morioka and S. Suzuki, Anal. Biochem., 94 (1979) 22; Anal. Chim. Acta, 106 (1979) 150; Anal. Chim. Acta, 115 (1980) 61.
7 Y. Ikariyama, S. Suzuki and M. Aizawa, Anal. Chim. Acta, 156 (1984) 243.
8 M. E. Meyerhoff and G. A. Rechnitz, Anal. Biochem., 95 (1979) 483.

Analytica Chimica Acta, 156 (1984) 289—294
Elsevier Science Publishers B.V., Amsterdam — Printed in The Netherlands

Short Communication

DETERMINATION OF MITOMYCIN C IN HUMAN BLOOD PLASMA AND URINE BY HIGH-PERFORMANCE DIFFERENTIAL PULSE POLAROGRAPHY

W. P. VAN BENNEKOM* and U. R. TJADEN

Department of Pharmaceutical Analysis and Analytical Chemistry, Subfaculty of Pharmacy of the University of Leiden, Gorlaeus Laboratories, P.O. Box 9502, 2300 RA Leiden (The Netherlands)

E. A. DE BRUIJN

Leiden University Medical Center, Department of Pharmacology, Leiden (The Netherlands)

A. T. VAN OOSTEROM

Leiden University Medical Center, Department of Clinical Oncology, Leiden (The Netherlands)

(Received 6th June 1983)

Summary. High-performance differential pulse polarography is used for determining the antitumor antibiotic mitomycin C in human blood plasma and urine. The limit of determination (2-ml samples) is 25 ng ml^{-1} when the substance is isolated by means of Amberlite XAD-2, and 200 ng ml^{-1} when samples are not pretreated. The method was applied in a pharmacokinetic experiment; no metabolites of mitomycin C were observed in urine or plasma.

Several papers have appeared dealing with the determination of the antitumor antibiotic mitomycin C in body fluids [1—7]. Mitomycin C (I) is currently used in the treatment of various tumors [8] and is most selectively determined by reversed-phase high-performance liquid chromatography (h.p.l.c.) with ultraviolet or electrochemical detection [5]. So far, the

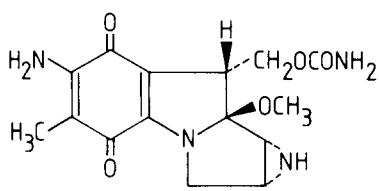

(I)

possible presence of metabolites or degradation products of mitomycin C in biological specimens has been reported only once [4]. In the procedures used, these substances were mostly not isolated and/or detected [5]. The present study was therefore concerned with the possibility of monitoring therapeutic levels of mitomycin C with no or limited pretreatment of biological samples.

0003-2670/84/$03.00

It is known [9, 10] that mitomycin C is polarographically active. As polarography often shows good selectivity with respect to endogenous substances, a polarographic assay for mitomycin C in biological fluids was studied. In particular, high-performance differential pulse polarography (h.p.d.p.p.) seemed promising, because detection limits ranging from 1 to 10 ng ml^{-1} have been reported [11—13]. Moreover, polarography offers additional discriminating power to detect possible metabolites or degradation products. A polarographic procedure for the determination of mitomycin C in biological fluids applied in a pharmacokinetic experiment, is described here.

Experimental

Polarographic apparatus and procedure. A polarographic analyzer PAR 174A (EG & G Princeton Applied Research, Princeton, NJ), modified for h.p.d.p.p. (electronic schematics are available on request), was used with matched drop timer (PAR 174/70) and x-y recorder (Omnigraphic model 2200-4-3). A wall-jacketed polarographic cell (Metrohm EA-876-5, 5 ml) was thermostatted at 25°C. The three-electrode configuration consisted of a dropping mercury electrode (DME), a platinum wire auxiliary electrode (Metrohm EA-202), and a saturated calomel reference electrode (SCE) (Metrohm EA-404).

During the measurements the height of the mercury column was kept constant at 700 mm. At open circuit, the flow rate was 4.04 mg s^{-1} with a corresponding natural drop time of 2.50 s. Before measurements, the solution was purged for 10 min with a stream of oxygen-free and water-presaturated nitrogen, which was passed over the solution while the potential was scanned. The standard parameters of h.p.d.p.p., employed throughout the experiments, were: scan range from 0 to —1500 mV vs. SCE, scan rate —5 mV s^{-1}, drop time 2 s, modulation amplitude ΔE = —100 mV, delay times δ_1 = 5 and δ_2 = 61 ms, sampling window Δ = 20.0 ms, and memory time constant = 110 ms.

Reagents and materials. Mitomycin C was obtained either as Mutamycin (Bristol Myers Nederland B.V., Weesp, The Netherlands) or as Mitomycine (Kyowa, Tokyo, Japan) and was used as received.

Britton-Robinson (BR) buffers (pH 2—12) were prepared from analytical-grade chemicals (Merck). Water was obtained from a Millipore Milli-Q Water Purification System. Servachrom Amberlite XAD-2 (100—200 μm) was purchased from Brunschwig Chemie B.V. (Amsterdam, The Netherlands).

Biological fluids were obtained from apparently healthy volunteers and patients prior to and during chemotherapy. Blood samples were taken in heparinized tubes and centrifuged at 1000*g* for 5 min.

Polarographic measurements. Mitomycin C was dissolved in the BR buffers, directly before use. Biological fluids were spiked by dissolving known amounts of mitomycin C in BR buffer (pH 7.0) prior to addition. Peak currents were measured with respect to polarographic blanks or using tangent fits.

Isolation of mitomycin C. Mitomycin C was isolated from plasma or urine by means of an Amberlite XAD-2 resin, of which 150 mg (100—200 μm) was transferred to a Pasteur pipette in which a plug of glass wool had been inserted. The resin was pretreated with acetone (three 5-ml aliquots) and water (15 ml). Then 2 ml of sample was pulled into the resin. The resin was washed with water (three 5-ml aliquots) after which mitomycin C was eluted with acetone (three 5-ml aliquots). The acetone fractions were collected in a conical flask and the acetone was evaporated at reduced pressure at about 60°C. The residue was dissolved in 5.0 ml of BR buffer (pH 7.0) by thoroughly mixing it on a whirlmixer for about 2 min. Aliquots (4.0 ml) were transferred to the polarographic vessel.

Results and discussion

Polarography in BR buffers. Polarograms of mitomycin C (about 10^{-5} M in BR buffer pH 7.0) were recorded from 0 to −1500 mV vs. SCE in the d.c., sampled d.c., normal pulse, d.p. and h.p.d.p. modes. Typical polarograms (Fig. 1) show that the response to mitomycin C depends on the technique used. The recorded sensitivity in h.p.d.p.p. was better than that in d.p.p., so that h.p.d.p.p. was the method of choice (Fig. 1c). Moreover, as was expected, the recorded baseline was much lower, resulting in improved signal-to-background ratios.

In h.p.d.p.p. three peaks were observed at −315, −415 and −710 mV vs. SCE. The peak current at −315 mV was not linear with concentration and this peak was not present at concentrations smaller than 3 μg ml^{-1}. The peak at −415 mV can be attributed to the reduction of the quinone moiety in the molecule, while the mechanism for the third peak is unknown. In the BR buffers (pH 2—12) the peak potentials (E_p) in h.p.d.p.p. were linear with pH,

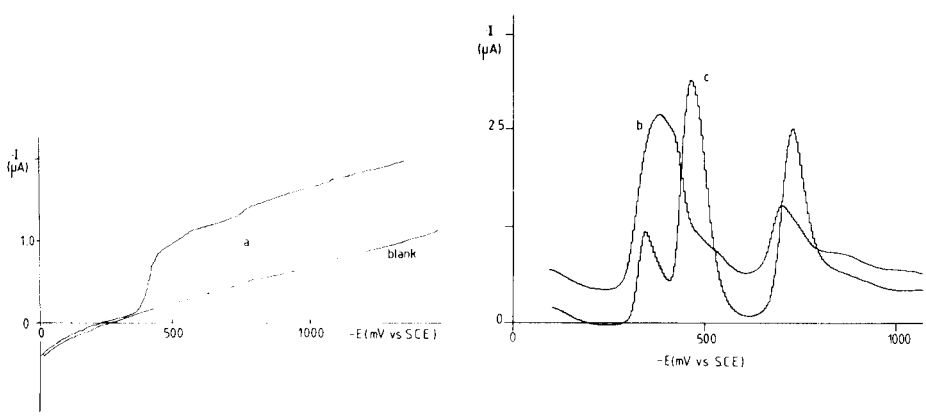

Fig. 1. Typical sampled d.c. (a), d.p. (b) and h.p.d.p. (c) recordings of mitomycin C in BR buffer pH 7.0. Experimental parameters for h.p.d.p.p. are given under *Experimental.* In d.p.p. the delay time δ is 40 ms and in sampled d.c.p. the drop time is 2 s, while the other parameters are unchanged.

with slopes of about 60 mV pH^{-1}. From these data, it was concluded that the electrochemical behaviour of mitomycin C is rather complex and has still to be solved.

It was found that mitomycin C solutions were unstable outside the pH range 5—8. This was confirmed with both ultraviolet spectrophotometry and polarography. The chemical behaviour is also complex. However, mitomycin C in BR buffers of pH 7.0 are stable for at least a week. Calibration graphs were therefore recorded in BR buffers of pH 7.0. These calibration plots for the peaks at —415 and —710 mV vs. SCE were linear over the range 0—10 μg ml^{-1} with correlation coefficients of 0.999 and 0.998, respectively. The detection limit in these solutions was better than 5 ng ml^{-1} (at E_p = —415 mV vs. SCE). This lower limit, imposed by a high inclination of the baseline, is probably due to interfering electroactive impurities and residual charging current. The repeatability at the 100-ng ml^{-1} level was within 3% (n = 6).

Measurements in biological fluids. Direct polarographic assays in biological fluids like serum, plasma, urine and saliva were tested. After the biological blank had been recorded, each of the fluids was spiked with mitomycin C (about 10 μg ml^{-1}) without and with adjustment of the pH (to 7.0). A typical polarogram of spiked plasma is shown in Fig. 2. Direct measurements in these fluids appeared to be possible but, probably because of surface-active substances in the biological matrix, the peak pattern changed. Only reduction of the quinone moiety was observed in these fluids.

Calibration graphs, recorded in plasma and urine, were linear for concentrations up to 10 μg ml^{-1}. However, the minimum detectable amount in plasma was only about 200 ng ml^{-1}. To obtain lower limits in these biological samples, the isolation procedure with Amberlite XAD-2 was employed. Aqueous solutions of mitomycin C were measured directly and via the isolation procedure. From calibration graphs, the recovery was about 95%. Biological fluids were spiked and subjected to direct measurements as well as column isolation. These solutions were measured directly and by standard addition of mitomycin C (BR buffer, pH 7.0). Calibration graphs for the drug in plasma and urine were linear, both with correlation coefficients of 0.999, in the range 25—1000 ng ml^{-1}. From these results it was

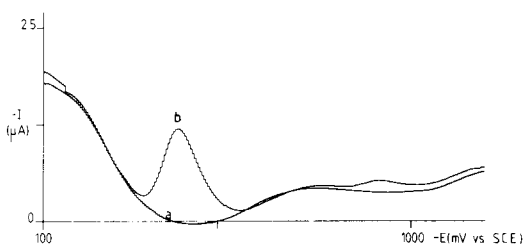

Fig. 2. Typical h.p.d.p. recordings of blank (a) and mitomycin C spiked (b) plasma. The drug concentration is 12 μg ml^{-1} (standard h.p.d.p.p. conditions).

concluded that the recovery from biological samples was about 90% for urine and 85% for plasma. The lowest detectable amount, after isolation, was 25 ng ml^{-1} present in 2 ml of biological fluid. This makes the procedure applicable for routine analysis. Smaller amounts might be determined if larger quantities of biological fluids or smaller polarographic vessels were used.

Stability of mitomycin C in biological samples on storage. The stability of mitomycin C in spiked biological materials (about 10 μg ml^{-1}) was tested. Mitomycin C in plasma was stored at −20°C; the peak current was constant within the polarographic precision for at least one month. The polarographic background of frozen plasma was notably cleaner than that of directly measured plasma, possibly because of denaturation of proteins during the freezing. Plasma from patients was stored at −20°C.

Samples of a patient treated with mitomycin C. A 36-year old female with histologically proven, rapidly progressive liver metastases of breast cancer in whom no other metastases could be found, was treated by a 10-min infusion of 20 mg of mitomycin C into the hepatic artery as described by Kinami and Miyazaki [14]. The treatment proceded uneventfully and caused no side effects. No bone marrow toxicity was observed. Progression was stopped and after four weeks the treatment was repeated with 30 mg of mitomycin C. Again, no side effects were seen, while after four weeks a slight decrease in liver span was observed. After the 30-mg dosage, plasma and urine samples were taken. The samples were analyzed as described with the results presented in Fig. 3. These correlate well with the h.p.l.c. method described earlier [5]. During the first three hours, mitomycin C was monitored in plasma. Relatively large amounts of the drug were excreted in the urine, a process described as being dose-dependent [8]. No metabolites of mitomycin C were observed in the potential range from 0 to −1500 mV vs. SCE.

It can be concluded that high-performance differential pulse polarography is suitable for the determination of mitomycin C in biological fluids and

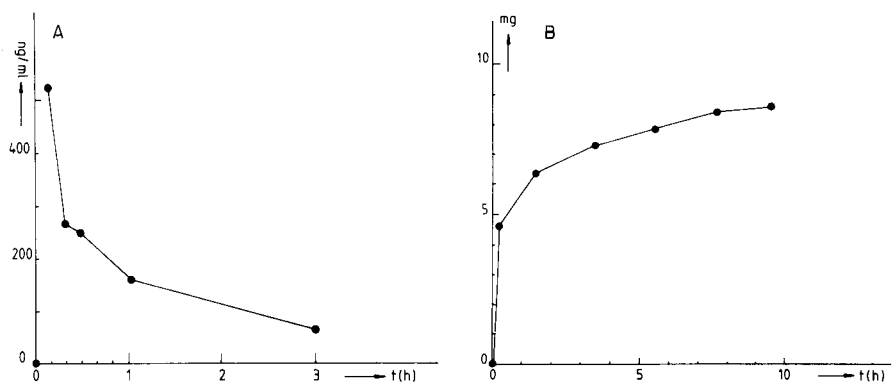

Fig. 3. Monitoring of mitomycin C during therapy: A, concentration/time curve in plasma; B, cumulative excretion curve in urine.

can be applied in pharmacokinetic experiments for simple and fast screening of concentration profiles.

The authors thank Rolien de Ru for secretarial and editorial help, and the nursing staff of the University Hospital for collecting the samples.

REFERENCES

1 S. C. Srivastava and U. Hornemann, J. Chromatogr., 161 (1978) 393.
2 D. Edwards, A. B. Selkirk and R. B. Taylor, Int. J. Pharm., 4 (1979) 21.
3 A. Kono, Y. Hara, E. Eguchi, M. Tanaka and Y. Matsushima, J. Chromatogr., 164 (1979) 404.
4 J. den Hartigh, W. J. van Oort, M. C. Y. M. Bocken and H. M. Pinedo, Anal. Chim. Acta, 127 (1981) 47.
5 U. R. Tjaden, J. P. Langenberg, K. Ensing, W. P. van Bennekom, E. A. de Bruijn and A. T. van Oosterom, J. Chromatogr., 232 (1982) 355.
6 G. U. van Hazel and J. S. Kovach, Cancer Chemother. Pharmacol., 8 (1982) 189.
7 H. S. Schwarz and F. S. Philips, J. Pharm. Exp. Ther., 133 (1961) 335.
8 S. K. Carter and S. T. Crooke (Eds.), Mitomycin C: Current Status and New Developments, Academic Press, London, 1979.
9 S. Kinoshita, K. Uzu, K. Nakano, M. Shimizu, T. Takahashi, S. Wakaki and M. Matsui, Progr. Antimicrob. Anticancer Chemother., II (1970) 1058.
10 S. Kinoshita, K. Uzu, K. Nakano, M. Shimizu, T. Takahashi, S. Wakaki and M. Matsui, J. Med. Chem., 14 (1971) 103.
11 W. P. van Bennekom and J. B. Schute, Anal. Chim. Acta, 89 (1977) 71.
12 W. P. van Bennekom, Anal. Chim. Acta, 101 (1978) 283.
13 J. J. van der Lee, W. P. van Bennekom and H. J. de Jong, Anal. Chim. Acta, 117 (1980) 171.
14 Y. Kinami and I. Miyazaki, Cancer, 41 (1978) 1420.

Analytica Chimica Acta, 156 (1984) 295—299
Elsevier Science Publishers B.V., Amsterdam — Printed in The Netherlands

Short Communication

DETERMINATION OF TRACES OF MERCURY AND BARIUM IN MINERAL-CONTAINING WATER BY SELECTIVE RETENTION ON ION-EXCHANGE PAPERS AND X-RAY FLUORESCENCE SPECTROMETRY

P. CLECHET* and G. ESCHALIER

Laboratoire de Physicochimie des Interfaces, Ecole Centrale de Lyon, 69131 Ecully Cedex (France)

(Received 18th March 1983)

Summary. Mercury(II) is collected from dilute hydrochloric acid solutions on anion-exchange paper disks; barium ions are collected on cation-exchange paper disks after separation by coprecipitation with lead chromate and dissolution of the precipitate in 1,2-diaminocyclohexanetetraacetic acid which also serves as masking agent. The disks are then subjected to x-ray fluorescence spectrometry. The method is satisfactory for mg kg^{-1} levels of the two ions in the presence of large amounts of sodium, calcium and magnesium ions (e.g., in synthetic sea water and Contrexeville water). Various procedural modifications are discussed.

A combination of ion-exchange collection and x-ray fluorescence spectrometry (x.r.f.) makes it possible to determine traces of metal ions in aqueous solutions, with a detection limit of a few $\mu g\ kg^{-1}$ [1, 2]. The use of ion-exchange resin-loaded papers instead of granular resin eliminates the tricky compacting process. These ion-exchange papers are also well suited for storing samples; percolation through the disks is easy and is readily adjusted, which is important for routine analysis. From the point of view of x.r.f., the disks (about 0.35 mm thick) can be considered as thin samples, because of the low absorption by the organic matrix. Interelement effects are also negligible, because of the small quantities collected and their low concentrations in the cellulose matrix.

If the solution only contains a single cation, or if this cation is associated only with elements which have concentrations and affinities for the resin similar to the required cation, preconcentration is simple, several percolations through the exchange paper providing virtually total retention [1, 2]. Under the real conditions of water analysis, however, traces of heavy elements (e.g., lead, barium, mercury, chromium) are always associated with large amounts of sodium, potassium, calcium and magnesium ions. Selectivity is then achieved by using a suitable complexing agent before retention of the ions of interest (either as complexed or free ions). These possibilities have been examined for mercury(II) ions (complexed by chloride) [3] and barium

0003-2670/84/$03.00

ions [4] in the presence of 1,2-diaminocyclohexanetetraacetic acid (DCTA) [5, 6]. Low concentrations ($\mu g\ kg^{-1}$) of these two metals could easily be distinguished, even in the presence of 10—100-fold concentrations of sodium, potassium, calcium and magnesium ions. Clearly, when traces of several metals with very similar properties are present, a more complicated process is needed. The problem is discussed here in the context of mercury and barium traces in natural waters.

Experimental

Apparatus. The percolation apparatus has been described [3]. The ion-exchange cellulose disks (36 mm diameter) analyzed with a Hilger and Watts Plurovac III-EB x-ray spectrometer; LiF_{200} (Ba $L\alpha 1$ and Hg $L\alpha 1$) and PET (S $K\alpha$) served as analysing crystals. A vacuum of about 10^{-3} torr was maintained in the spectrometer chamber during measurements. For present purposes, P is defined as the mean fluorescence intensity for the element calculated from five successive 100-s measurements, and F is the equivalent mean background intensity. All results here are expressed in net fluorescent intensities ($\overline{P - F}$, in counts/100 s) which are the means of measurements made on both sides of each disk, to allow for irregular distribution of elements in the disk. The confidence interval adopted in all statistical calculations is 95%.

Conditions of individual fixation for the mercury and barium ions. Mercury [3] was fixed on Reeve-Angel type SB2 anion-exchange paper as tetrachloromercurate(II) ions. The alkali and alkaline-earth ions are not complexed and so are not collected; this was checked by ten successive passages of a 50-ml sample in 0.2 M HCl media (RP, Normapur). The mercury solutions were prepared by dilution of a stock solution (100 mg Hg kg^{-1}) of mercury-(II) nitrate (Merck, analytical grade).

Barium ions [4] were collected as such on Reeve-Angel SA2 cation-exchange paper (ammonium form) which exhibits a very strong affinity for barium ions [7]. Sodium, potassium, calcium and magnesium ions were eliminated by applying the procedure of Sixta et al. [5, 6] which involves coprecipitation of barium and lead chromates and redissolution of the precipitate of 0.2 M DCTA (Merck, analytical grade) at pH 5.5. In this solution, barium is present in the free ionic state [5, 7] whereas the lead and any coprecipitated calcium or magnesium ions form strong anionic complexes. In the procedure, the SA2 paper disks are washed with 6 M nitric acid, to eliminate all traces of calcium (checked by x.r.f.) and converted to the ammonium form by soaking in 3 M ammonia solution. Although five successive percolations sufficed to assure good retention of barium, the same percolation procedure as for mercury was used, i.e., ten successive passages of a 50-ml sample. The barium solutions were prepared by dilution of a stock solution (100 mg Ba kg^{-1}) of barium chloride dihydrate (RP Normapur, analytical grade).

Results and discussion

Before selective fixation was considered, it was established that the presence of one cation did not interfere with measurement of the other at similar levels of concentration (10—20 mg kg^{-1}). To accomplish this, suitable solutions were percolated through SA2 and SB2 disks inserted together in the percolation apparatus. This is the O—O arrangement where the two ion-exchange disks are placed one on top of the other in the percolation apparatus. In order to check that collection was total, the solutions were then passed ten times through another disk of the same type; in no case was any retention observed on these control disks. The results (Table 1) show that barium and mercury ions do not influence the fixation of each other and that collection is complete on the relevant disk when they are placed together. The above procedures are thus satisfactory for the determination of the individual ions in mixtures. In considering the detection limits of the method, the criterion used was that the analytical signal should be three times the standard deviation of the background noise. Thus, for 50-ml samples and counting times of 100 s, the detection limit is about 0.1 mg kg^{-1} for each element. The precision of the measurements is about 3% at the 10 mg kg^{-1} level.

It was then necessary to establish if the two cations could be retained simultaneously and selectively in the presence of large amounts of sodium, potassium, calcium and magnesium ions. The simplest procedure, involving one complexing medium and one percolation sequence on a single disk, is obviously useless; with the SA2 cation-exchange paper and a non-complexing acid medium (e.g., nitric acid) collection of barium and mercury traces must be limited by the large quantities of other cations present. In a chloride-containing medium, the chloromercurate ions are not fixed by the exchanger. With the procedure of Sixta et al. barium ions are collected quantitatively but mercury ions are not because they are masked by DCTA at pH 5.5 [4].

TABLE 1

Spectroscopic measurements of mercury and barium collected in O—O arrangement from demineralized water
(Standard deviation for background noise ≈50 cp100s for mercury and ≈35 cp100s for barium)

Element measured (medium)	Amount (mg kg^{-1})	Other element	Amount (mg kg^{-1})	$\overline{P-F}$ ± 2 s/cp100s	
				on SA2 disk	on SB2 disk
Hg^{2+} (HCl)	10	Ba^{2+}	0	85 ± 92	12456 ± 238
	10	Ba^{2+}	10	103 ± 95	11984 ± 236
	10	Ba^{2+}	20	105 ± 100	11936 ± 234
Ba^{2+} (DCTA)	20	Hg^{2+}	0	9786 ± 212	53 ± 68
	20	Hg^{2+}	10	9774 ± 212	53 ± 67
	20	Hg^{2+}	20	9676 ± 220	84 ± 73

On SB2 disks simultaneous retention is again impossible; in a chloride medium only mercury is captured, whereas in DCTA medium only the fraction of the mercury ions still present in the solution when DCTA is added is captured as the anionic DCTA/Hg^{2+} complex. Moreover, the excess of chromate ion present competes for the exchanger. Tests showed that only 40% of the mercury was collected under such conditions. Placing the SA2/SB2 disks together in an O—O arrangement does not improve the situation.

Further tests were done in which the two masking operations were applied successively to a given solution, with passage through the dual SA2/SB2 disks each time. When barium ions were fixed first on the SA2 paper from DCTA medium, and then hydrochloric acid was added to the effluent which was passed through the disks again, some barium ions were lost from the SA2 disk. Some mercury ions were also lost during the DCTA treatment. This procedure is not sufficiently reliable for quantitative work. If the procedure is reversed, so that mercury is first fixed from 0.2 M HCl on the SB2 disk and then the method of Sixta et al. [5, 6] is used prior to fixation of barium ions, chromate tends to displace chloromercurate(II) ions from the SB2 disk. Again, the procedure is unreliable.

The last possibility for simplification of the procedure consists of using successive complexation for the same water sample, each followed by passages through the appropriate individual disk. If the method of Sixta et al. is used initially, an SA2 disk collects barium ions but some mercury ions are lost during the treatment. If the order is reversed, the collection of mercury ions on an SB2 disk is quantitative, but some barium ions may be lost during the coprecipitation.

The failure of all the above sequential treatments to provide reliable results meant that the two ions must be determined individually as described under Experimental. The results thus obtained from solutions containing a given quantity of one cation and progressively larger quantities of the other cation in distilled water, in Contrexeville water and in a synthetic sea water are presented in Table 2. The Contrexeville water has a mineral salt concentration of 2.1 g kg^{-1} (mass percentage of the principal ions: SO_4^{2-} 49%; Ca^{2+} 21%; HCO_3^- 18%; Mg^{2+} 0.7%; Na^+ 0.4%; Cl^- 0.3%). The synthetic sea water

TABLE 2

Spectroscopic measurements for mercury and barium from different aqueous media

Element measured (medium)	Amount (mg kg^{-1})	Other element	Amount (mg kg^{-1})	P — F ±2 s/cp100s		
				Distilled water	Contrexeville water	Sea water
Hg^{2+} (HCl)	10	Ba^{2+}	0	25573 ± 254	25328 ± 220	25306 ± 251
	10	Ba^{2+}	10	25559 ± 252	25258 ± 248	25276 ± 246
	10	Ba^{2+}	20	25347 ± 251	25284 ± 247	25223 ± 248
Ba^{2+} (DCTA)	10	Hg^{2+}	0	10472 ± 214	1625 ± 208	9984 ± 210
	10	Hg^{2+}	10	10351 ± 213	1601 ± 296	9868 ± 212
	10	Hg^{2+}	20	10245 ± 214	1553 ± 205	9859 ± 211

had a mean mineral salt concentration of 35.0 g kg^{-1} (mass percentage of the principal ions: Cl^- 54%; Na^+ 30%; Mg^{2+} 3.8%; SO_4^{2-} 1.7%; Ca^{2+} 1.2%).

The collection of mercury ions is obviously unaffected by the concentration of barium ions or by the mineral content of the water. The same is true for barium ions in distilled or sea water. However, in the Contrexeville water, the collection of barium ions is very inefficient, undoubtedly because barium was precipitated by the sulfate and hydrogencarbonate ions present. An x.r.f. determination on the white precipitate collected on a filter paper placed above the SA2 disk in the percolation apparatus, showed that sulfur and barium were present; the quantity of barium corresponded roughly to the missing 85%. Obviously, this is a purely academic case, but it emphasizes the need for care in complicated analyses.

Conclusions

Preconcentration on ion-exchange paper followed by x.r.f. is appropriate for the determination of traces of cations if their complexing properties are similar [1, 2]. The presence of mineral salts in large concentrations is not a major impediment in that a single masking operation usually suffices [3, 4]. The case described above is more difficult in that a heavy cation (Hg^{2+}) with an alkaline-earth cation (Ba^{2+}) are determined in the presence of calcium, magnesium and sodium ions. The method can nonetheless be extended to such mixtures of cations with different properties. The process becomes more complicated, but a judicious choice of ion-exchange paper and masking agents allows cations to be fixed in groups that can then be subjected to x.r.f. spectrometry for accurate and precise measurement.

REFERENCES

1 W. J. Campbell, E. F. Spano and T. E. Green, Anal. Chem., 38 (1966) 987.
2 W. J. Campbell, T. E. Green and S. L. Law, Am. Lab., June (1970) 28.
3 P. Clechet, G. Eschalier, C. Rampon and C. Vallouy, Analusis, 7 (1977) 366.
4 P. Clechet and G. Eschalier, Analusis, 4 (1981) 125.
5 V. Sixta, M. Miksovsky and Z. Sulcek, Collect. Czech. Chem. Commun., 38 (1973) 3418.
6 V. Sixta, M. Miksovsky and Z. Sulcek, Z. Anal. Chem., 273 (1975) 193.
7 A. Ringbom, Les Complexes en Chimie Analytique, Dunod, Paris, 1967.

Analytica Chimica Acta, 156 (1984) 301—305
Elsevier Science Publishers B.V., Amsterdam — Printed in The Netherlands

Short Communication

DETERMINATION OF BISMUTH IN GEOLOGICAL MATERIALS BY AUTOMATED HYDRIDE GENERATION AND ELECTROTHERMAL ATOMIC ABSORPTION SPECTROMETRY

SHIGERU TERASHIMA

Geological Survey of Japan, 1-1-3 Higashi, Yatabe, Tsukuba, Ibaraki 305 (Japan)

(Received 26th July 1983)

Summary. The rapid and precise determination of bismuth (> 5 μg kg^{-1}) in geological materials is described. The sample is decomposed with a $HClO_4/HNO_3/HF$ mixture; interferences are eliminated by addition of aluminium chloride, ascorbic acid and thiourea. Bismuth hydride is introduced into a quartz cell atomizer.

Although atomic absorption spectrometry (a.a.s.) based on hydride generation has been applied to the determination of bismuth in steel [1, 2], coal and fly ash [3], the sensitivity of the method is inadequate for the determination of bismuth at the μg kg^{-1} level common to geological materials. Lee [4] reported a more sensitive method based on hydride generation for a.a.s. with a carbon rod atomizer, but the procedures for hydride generation and collection seem rather complicated.

Recently, an electrically-heated quartz cell atomizer and an automated, continuous hydride generator were described [5], which provided highly sensitive and rapid results. Some fundamental conditions were investigated [5, 6]. In the present study, the effect of concomitant elements, elimination of interferences and dissolution of samples were examined so that the method could be applied to a variety of geological materials.

Experimental

Apparatus. The Nippon Jarrell-Ash Model AA-781 atomic absorption spectrometer used was equipped with a Nippon Jarrell-Ash Model HYD-1 automated hydride generator [5, 6], a HYD-2 heated quartz cell atomizer [5], a bismuth hollow-cathode lamp and a deuterium background corrector.

Reagents. Bismuth standard solutions (0.005, 0.05 and 0.5 μg ml^{-1}) were prepared by consecutive dilution of a 1 mg ml^{-1} atomic absorption standard with 1.2 M hydrochloric acid. The sodium tetrahydroborate (Wako Pure Chemical Ind.) was dissolved in water and made up to a 1% solution in 0.5% sodium hydroxide. All other reagents were of analytical-reagent grade.

Procedure. Weigh accurately 0.1—0.5 g of powdered sample into a teflon beaker. Add 3 ml of perchloric acid (60%), 3 ml of concentrated nitric acid,

0003-2670/84/$03.00

and 8 ml of hydrofluoric acid (46%), and mix. After letting stand for 15—20 min, evaporate the mixture to dryness on a sand bath at about 220°C. Dissolve the residue by heating with 5 ml of 3 M hydrochloric acid. For samples such as iron and manganese ore, dissolve 0.1 g by heating with 5 ml of concentrated hydrochloric acid; later add 1 ml of the perchloric acid and 1 ml of the hydrofluoric acid. Transfer all the solution (if the content is less than 5 μg Bi) or a portion of the solution to a 25-ml volumetric flask. Adjust the final acidity to about 0.6 M hydrochloric acid, and add 5 ml of aluminium chloride solution (20 mg Al ml^{-1} in water). After diluting the solution with water to about 20 ml, add 2 ml of aqueous 10% (w/v) ascorbic acid and mix to reduce iron(III). Then add 2 ml of aqueous 8% (w/v) thiourea. Make up to volume and mix.

Introduce the solution into the hydride generator for 30—40 s, and determine bismuth under the operating conditions given in Table 1. Calculate the bismuth concentration directly from a calibration graph based on peak heights obtained by taking 0—5 μg of bismuth in 25-ml volumetric flasks, and proceeding as described above.

Results and discussion

Study of analytical conditions. When the high concentration mode of the instrument was used, reasonable linearity was obtained for the calibration graphs up to 2 μg at the 223.1-nm absorption line, and up to 5 μg at the 306.8-nm line. The conditions (0.5—2% sodium tetrahydroborate and 0.5—6 M hydrochloric acid in the hydride generator, and 900—1100°C for the hydride atomizer) were not critical. The sensitivity for bismuth increased with the feed rate of the sample solution; the maximum feed rate was selected.

Interferences and their elimination. Interferences from various elements in the determination of bismuth by hydride generation/a.a.s. have been eliminated by the presence of iron [1]. In this study, however, there was a clear

TABLE 1

Operating conditions for bismuth determination

Wavelength		223.1 or 306.8 nm
Lamp current		10 mA
Hydride generator (HYD-1)		
$NaBH_4$ solution,	feed rate	12 ml min^{-1}
	concentration	1% in 0.5% NaOH
HCl solution,	feed rate	12 ml min^{-1}
	concentration	2 M
Sample solution,	feed rate	20 ml min^{-1}
Argon flow,	carrier I	0.1 l min^{-1}
	carrier II	1.0 l min^{-1}
Hydride atomizer (HYD-2)		
Temperature		1000 ± 20°C

difference between the effects of iron(II) and iron(III) in the elimination of interferences. The interferences from 500 μg of copper or nickel were eliminated by the addition of 50 mg of iron(III); but the same amount of iron(II) was ineffective. The addition of large amounts of iron(III) was undesirable because of increasing noise and the presence of high blanks. Therefore, after some preliminary experiments, ascorbic acid and thiourea were selected as suitable for the elimination of interferences from various elements (Table 2). The enhancing effects on bismuth absorbance from aluminium and iron(II) can be minimized by the addition of 100 mg of aluminium to both samples and calibration standards.

For other elements, at the maximum amount tested, no interference was observed from 1000 mg of perchloric acid or phosphoric acid, 100 mg of sodium, potassium, magnesium, calcium or manganese, 20 mg of titanium, or 1 mg of chromium, lead, vanadium or zinc, for 0.25 μg of bismuth. Background absorbance was not detected.

Decomposition of samples. For samples such as bauxites and clays, small amounts of a white suspension remained in the sample solution, but the quantity of bismuth in the suspension was negligible. When the organic carbon content of the sample was high, an ashing procedure was used to destroy the organic material [7]. In this study, the ashing procedure was omitted, so that non-carbonate carbon was not completely removed from samples such as shale and coal fly ash, but the residue did not have any effect on the bismuth absorbance.

Precision and recovery. Known amounts of standard bismuth were added to 0.1 or 0.5 g of reference rock samples (JA-1 andesite, JB-2 basalt and JG-1 granodiorite). The relative standard deviations for the determination of 0.005—10 μg of bismuth were less than 17%, and recovery was 98—102%, as shown in Table 3.

TABLE 2

Effect of various elements on bismuth absorbance (0.25 μg Bi)

Element	Compound	Amount (mg)	Absorbance change (%)	
			Without ascorbic acid or thiourea	With ascorbic acid and thiourea
Cu	$CuCl_2$	1	−92	0
Ni	$NiCl_2$	0.5	−69	−3
		1	−81	−12
Co	$CoCl_2$	1	−28	−6
Ag	$AgNO_3$	0.1	−65	0
Pt	H_2PtCl_6	1	−94	0
Al	$AlCl_3$	50	+12	+10
		100	+20	+17
		200	+27	+21
Fe	$FeCl_3$	100	+16	+12

TABLE 3

Precision and recovery for the determination of bismuth

Samples	Taken (g)	Bi (μg)		R.s.d. (%)	Recovery (%)
		Added	Found[a]		
JA-1	0.5	0.0	0.0046	17.4	—
	0.5	0.5	0.498	3.0	99
	0.1	10.0	10.08	2.2	101
JB-2	0.5	0.0	0.0165	9.1	—
	0.5	0.5	0.506	2.2	98
	0.1	10.0	9.95	2.1	100
JG-1	0.5	0.0	0.258	2.1	—
	0.1	10.0	10.23	1.8	102

[a]Average value of 5 determinations.

TABLE 4

Results for bismuth (μg kg^{-1}) in geological reference samples and some reported values

Samples		This work[a]	Reported values		
			Heinrichs [8]	Kane [7]	Others
USGS	AGV-1 Andesite	53	59	51.9	54 [9]
	BCR-1 Basalt	45	46	44.1	46 [9]
	DTS-1 Dunite	5.8	9	<10	5.2 [9]
	G-2 Granite	35	36	32.6	41 [9]
	GSP-1 Granodiorite	32	47	31.7	39 [9]
	MAG-1 Marine mud	354	300	331	
	PCC-1 Peridotite	6.4	13	<10	9 [9]
	SGR-1 Oil shale	930	—	1030	
ANRT	AN-G Anorthosite	9.0	—	—	21 [10]
	BE-N Basalt	15	—	—	42 [10]
	MA-N Granite	1770	—	—	1660 [10]
	VS-N Synthetic glass	915[b]	—	—	900?[b] [11]
NBS	1a Limestone	57	—	—	—
	69A Bauxite	668	—	—	—
	97a Clay, flint	733	—	—	—
	98a Clay, plastic	790	—	—	—
	120b Phosphate	197	—	—	—
	1633a Coal fly ash	1110	—	—	—
BCS	176/2 Manganese ore	1160	—	—	—
	301/1 Iron ore	1380	—	—	—
GSJ	JB-1 Basalt	31	33	—	—
	JG-1 Granodiorite	516	410	—	—
JSS	800-3 Iron ore	222[b]	—	—	230 ± 15[b,c]

[a]Average of 3—5 determinations. [b]Results in mg kg^{-1}. [c]Certificate value, Iron and Steel Institute of Japan.

Analysis of geological samples. Results obtained for bismuth in 23 international geological reference samples (rocks, sediments, minerals, and ores) are given in Table 4, and compared with reported values. The reported values were obtained by a.a.s. with a graphite furnace atomizer after volatilization by heating [8] or liquid-liquid extraction [7], or are consensus [9] or compiled [10, 11] values. The satisfactory agreement with the reported values indicates that the method is accurate for the various types of geological materials examined.

The sensitivity of the present method (1% absorption) was evaluated as 3 ng of bismuth, and the limit of detection was 5 $\mu g\ kg^{-1}$ for 0.5 g of a given sample at the 2 standard deviation confidence level. The proposed method is rapid and convenient, and allows the analysis of 40 samples per 8-h man-day.

REFERENCES

1 H. D. Fleming and R. G. Ide, Anal. Chim. Acta, 83 (1976) 67.
2 P. K. Hon, O. W. Lau, W. C. Cheung and M. C. Wong, Anal. Chim. Acta, 115 (1980) 355.
3 R. A. Nadkarni, Anal. Chim. Acta, 135 (1982) 363.
4 D. S. Lee, Anal. Chem., 54 (1982) 1682.
5 M. Ikeda, J. Nishibe and T. Nakahara, Bunseki Kagaku, 30 (1981) 368, 545.
6 M. Ikeda, J. Nishibe, S. Hamada and R. Tujino, Anal. Chim. Acta, 125 (1981) 109.
7 J. S. Kane, Anal. Chim. Acta, 106 (1979) 325.
8 H. Heinrichs, Fresenius Z. Anal. Chem., 294 (1979) 345.
9 E. S. Gladney, C. E. Burns and I. Roelandts, Geostand. Newsl., 7 (1983) 3.
10 K. Govindaraju, Geostand. Newsl., 4 (1980) 49.
11 S. Abbey, Geol. Surv. Can. Pap., 80-14 (1980) 1.

Analytica Chimica Acta, 156 (1984) 307—312
Elsevier Science Publishers B.V., Amsterdam — Printed in The Netherlands

Short Communication

COMPARISON OF MERGING ZONES, INJECTION OF REAGENT AND SINGLE-LINE MANIFOLDS FOR ENTHALPIMETRIC FLOW INJECTION ANALYSIS

CELIO PASQUINI and WALACE A. DE OLIVEIRA*

Instituto de Química, Universidade Estadual de Campinas, C.P. 6154, Campinas, SP (Brazil)

(Received 20th April 1983)

Summary. A flow enthalpimeter suitable for all flow injection manifolds is described. The apparatus includes the injection valve immersed in an equilibration water bath which improves sensitivity and sampling rate. Detection limits for quantitation of hydrochloric acid range from 0.4 to 0.07 mM at 80—90 samples per hour.

Several flow enthalpimeters have been described in the literature. The first apparatus was built by Priestley et al. [1] and works with continuous addition of sample and reagent, yielding a constant thermometric signal at steady state. This and other instruments [2, 3] based on the same principle give a low sampling frequency. Censullo et al. [4] introduced the peak enthalpimeter which utilizes a transient signal generated by the injection of a discrete volume of sample into the flow stream. This instrument embodies all requirements established [5] for the flow injection technique. A similar enthalpimeter with a packed column reactor has been described [6]; this apparatus was designed to work with an immobilized enzyme reactor and was later modified to use two fluid streams, and applied to various types of reactions [7]. Although this approach is very useful for routine work, it does not allow the use of some flow manifolds frequently used in flow injection methods (e.g., single line [5], merging zones [8], and the recently introduced reverse flow injection [9]). Moreover, temperature equilibration after the injection of the sample decreases the sensitivity and the use of a packed reactor hinders work with precipitation reactions.

This report describes a flow enthalpimeter that permits the use of all flow injection manifolds, allows solid materials to be used in suspension, and avoids the disadvantages with post-equilibration. This was accomplished by placing the injection valve, coils, connectors, and other manifold components in a water bath and by using an open tube reactor. Results based on the neutralization reaction of hydrochloric acid with sodium hydroxide are discussed.

0003-2670/84/$03.00

Experimental

The apparatus consists of a peristaltic pump (Ismatec G13) that impels the reagent (in the present case, a sodium hydroxide solution, as specified later), sample and carrier streams toward an insulated 8-l water bath. The equilibration coils (stainless steel tubes, 0.5 mm i.d.), a home-made acrylic proportional injector [10], the reactor tubing, and the flow cells are immersed in the bath. At the top cover of the bath there are two crevices, one for the injector control lever and the other for the overhead stirrer stem. The flow cells consist of home-made acrylic blocks modeled as a T-connector, with the thermistor mounted perpendicular to the fluid stream. The total cell volume is about 17 μl. The reactor, the sample loops, and all other flow conductors are made of polyethylene tubing (0.8 mm i.d. and 1.5 mm o.d.). The twin thermistors (Thermometrics, 2.2 kΩ at 25°C) are connected to opposite arms of a d.c. Wheatstone bridge which has a sensitivity of 11.6 mV K^{-1} at 298 K. The voltage was monitored with a strip-chart recorder (Sargent-Welch Scientific Co., model SRG). Pulsation in the fluid streams that pass through the flow cells is suppressed with a pulse damper similar to that described earlier [7].

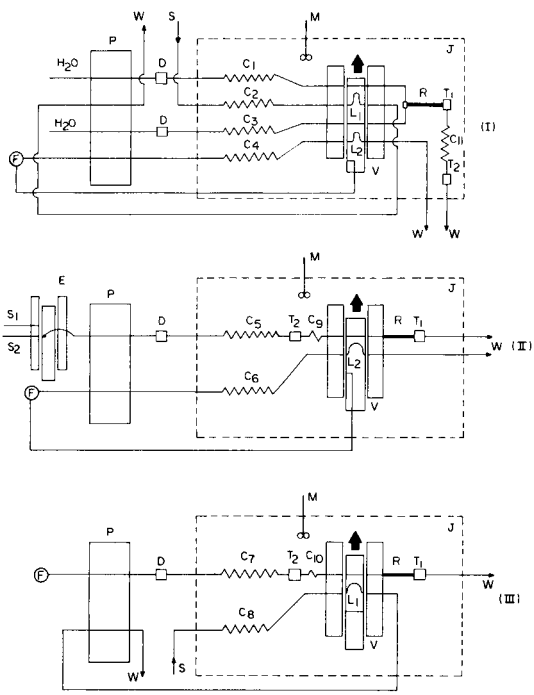

Fig. 1. Flow injection manifolds: I, merging zones; II, reverse flow injection; III, single line. J, Insulated water bath; P, peristaltic pump; D, pulse dampers; M, overhead stirrer; V, injection valve; R, reactor tube; C_1—C_{11}, equilibration coils; T_1 and T_2, indicator and reference thermistor cells; L_1 and L_2, sample and reagent loops; E, sample commuter; S, sample inlet; F, reagent reservoir; W, waste.

Figure 1 shows the manifolds used in the enthalpimeter. The equilibration coils C_1 to C_8 are 1 m long and are needed to promote temperature equilibrium of all fluids that will be mixed. In the reverse flow injection (II) and single line (III) systems, a 25-cm long coil (C_9 and C_{10}, respectively) is used after the reference cell, in order to achieve temperature equilibrium in the carrier stream that may be heated by dissipation on the reference thermistor. In the merging zones manifold (I), the differential detector system is built with the reference cell placed after the indicator thermistor to fulfil the requirement of equal flow rate in both cells; a 1.0-m long coil (C_{11}) is then used to provide temperature equilibration. In this manifold, the reagent and the sample streams, at the same flow rate, pass through a stainless steel conductor (0.5 mm i.d., 3 cm long) from the injector towards an acrylic T-connector where they merge at 180°. The reactor tubing (R) in all manifolds and also the sample and reagent loops (L_1 and L_2) in the single line (III) and reverse flow injection (II) systems were insulated by coating the polyethylene tubing with tygon tubing (1.5 mm i.d., 3.5 mm o.d.).

For comparison purposes, an additional manifold was constructed resembling one described earlier [7]. In this case, the injector was outside the water bath and the sample path was a 95 cm, 0.5-mm i.d. stainless steel equilibration coil placed inside the bath and reaching the confluence point with the reagent stream that flowed continuously.

Results and discussion

An overall thermometric dispersion factor, D_0, is used in this work, for comparison between the manifolds and flow parameters studied. This factor is defined as $D_0 = \Delta T_0/\Delta T_p$, where ΔT_p is the peak maximum temperature change observed when a solution is injected and undergoes reaction in the manifold and ΔT_0 is the largest temperature change obtained for the same reaction assuming that the reaction is complete without dispersion. This value can be found from $\Delta T_0 = (\Delta H[X])/C$, where ΔH is the molar enthalpy of the reagent-sample reaction (kcal mol^{-1}), [X] represents the molar concentration of the sample species, and C is the sample solution heat capacity (kcal l^{-1} K^{-1}). The D_0 value includes the physicochemical dispersion and physical factors like heat exchange in the reactor path. Values of ΔT_0 for the neutralization reaction were found using a ΔH value of 13.3 kcal mol^{-1} and 1 kcal l^{-1} K^{-1} for heat capacity of the diluted hydrochloric acid solution.

Figure 2 shows the effect of flow parameters on the dispersion factor and indicates the best conditions for quantitative work. The occurrence of double peaks, as shown in this figure, appears to be due to poor mixing of sample and reagent. Inefficient mixing was always observed with reverse flow injection and in a few cases with the single line system, because it was necessary to work with very short reactors. The experimental conditions used for the reverse flow system which gave single peaks (see Fig. 3) truly should give double peaks. The occurrence of double peaks was never observed with merging zones, probably because the confluence of sample and

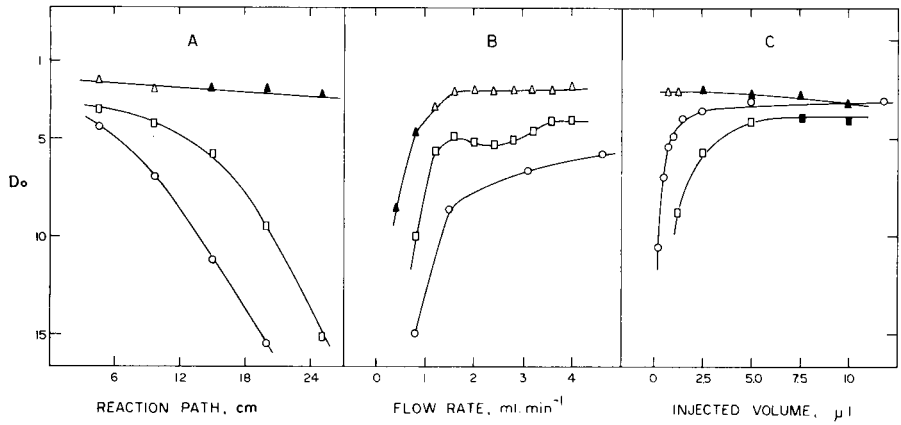

Fig. 2. Effect of flow parameters on the overall dispersion factor: A, reaction path length; B, flow rate; C, sample volume. (△) Reverse flow injection; (□) single line; (○) merging zones. Filled symbols indicate the occurrence of double peaks. Injected volume $\times 10^{-2}$ for merging zones and $\times 10^{-1}$ for single line and reverse flow. Flow rate, 3.4 ml min^{-1} for single line; other flow parameters as in Table 1 for all manifolds.

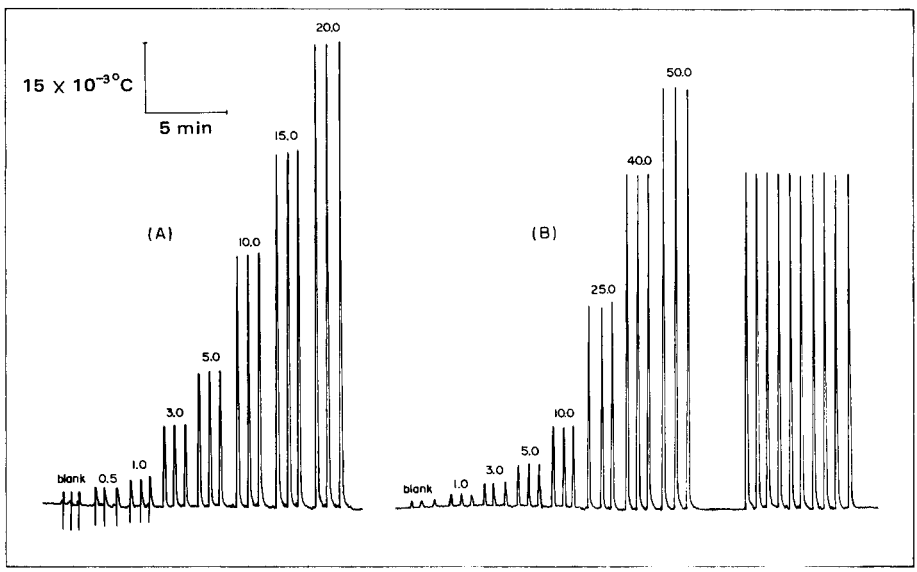

Fig. 3. Calibration runs for the enthalpimetric methods: A, reverse flow injection; B, merging zones. The numbers over the signals are the HCl concentrations (mM). The peaks to the right indicate the reproducibility of the signals for 40 mM HCl with the merging zones system. All flow parameters as in Table 1.

reagent promotes efficient mixing. The absence of double peaks with merging zones indicates that the effect is not thermal in nature. Although slow heat transfer with the reactor wall certainly occurs to some extent and actually

TABLE 1

Overall comparison of calibration graphs and system parameters for the flow manifolds[a]

Manifold	Intercept ± s.d. (10^{-3}°C)	Slope ± s.d. (10^{-3}°C mM^{-1})	HCl range (M)	Corr. coeff.
Merging zones	−2.04 ± 0.60	1.85 ± 0.02	0—0.1	0.9998
Single line	−1.94 ± 0.60	2.54 ± 0.03	0—0.05	0.9997
Reverse flow	−1.20 ± 1.01	4.96 ± 0.09	0—0.02	0.9990
Ref. 7	−1.88 ± 0.69	0.92 ± 0.02	0—0.1	0.9996

Manifold	D_0	Sampling rate (h^{-1})	Sample volume (μl)	Reagent used (μl)
Merging zones	7.2	85	50	50
Single line	5.2	90	50	1600[b]
Reverse flow	2.7	80	1800[b]	7.5
Ref. 7	14.5	50	50	1920[b]

[a]Intercept and slope refer to $\Delta T = a + b$ [HCl], where ΔT is the thermometric signal. Concentration of NaOH pumped was 1.0 M for reverse flow and 0.3 M for the other manifolds. Flow rate was 3.1 ml min^{-1} for the merging zones and ref. 7 manifolds and 2.4 ml min^{-1} for the reverse flow and single line manifolds. [b]Values obtained using the average time needed for one injection and the flow rate of the reagent or sample. Reaction path equal to 10 cm for all manifolds.

hinders the improvement of sampling rate, it is not the source of the double peaks. The profile of the curve for the single line system (Fig. 2B) can probably be understood by considering competition between the greater dispersion caused by mass transport [5] and the simultaneous decreased overall dispersion caused by the drop in heat transfer.

Table 1 shows an overall comparison between the three enthalpimetric manifolds. The best values of flow parameters were used and the results were obtained with eight samples of diluted hydrochloric acid injected in triplicate. Comparison of results obtained with the manifold as described by Schifreen et al. [7] with the merging zone results shows that elimination of the post-equilibration coil for the sample [7] resulted in substantial increase in sensitivity and sampling rate.

Results for the reproducibility of the thermometric signals are presented in Table 2, which includes the relative standard deviations for the blank and for the most precise point, using ten replicates. Typical calibration runs for the reverse flow injection and merging zones systems are shown in Fig. 3. The negative signals found with lower acid concentrations and blank do not affect the reproducibility. Detection limits for the neutralization reaction were estimated from the standard deviation of the blank and the sensitivities at 99.7% confidence level. Values of 0.4, 0.2 and 0.07 mM hydrochloric acid were found for the merging zones, single line and reverse flow injection manifolds, respectively.

The flow enthalpimeter described here shows the capability to work

TABLE 2

Precision of results with the flow injection manifolds[a]

	Merging zones		Single line		Reverse flow	
HCl conc. (M)	0.0	0.07	0.0	0.04	0.0	0.02
Average signal (10^{-3}°C)	2.70	130.29	3.83	104.28	1.40	100.68
R.s.d. (%)	9	0.5	5	0.4	8	0.5

[a]Experimental conditions as in Table 1.

with all flow injection manifolds, with an increase in sensitivity and sampling rate over previously reported instruments. Precipitation, oxidation-reduction and complexation reactions have been used successfully with the open tube reactor. Moreover, all configurations have potential applications for methods based on the heat of dilution.

The authors are grateful to the staff at CENA, Piracicaba, SP, Brazil, for the help received in the beginning of this work.

REFERENCES

1 P. T. Priestley, W. S. Sebborn and F. W. Selman, Analyst, 90 (1965) 589.
2 J. J. Christensen, L. D. Hansen, D. J. Eatough, R. M. Izatt and R. M. Hart, Rev. Sci. Instrum., 47 (1976) 730.
3 G. Peuschel and F. Hagedorn, Fresenius Z. Anal. Chem., 277 (1975) 177.
4 A. C. Censullo, J. A. Lynch, D. H. Waugh and J. Jordan, in R. S. Port and J. F. Johnson (Eds.), Analytical Calorimetry, Vol. 3, Plenum Press, New York, 1979, p. 217.
5 J. Růžička and E. H. Hansen, Flow Injection Analysis, Wiley, New York, 1981.
6 R. S. Schifreen, D. A. Hanna, L. D. Bowers and P. W. Carr, Anal. Chem., 49 (1977) 1929.
7 R. S. Schifreen, C. S. Miller and P. W. Carr, Anal. Chem., 51 (1979) 278.
8 H. Bergamin F°, E. A. G. Zagatto, F. J. Krug and B. F. Reis, Anal. Chim. Acta, 101 (1978) 17.
9 K. S. Johnson and R. L. Petty, Anal. Chem., 54 (1982) 1185.
10 H. Bergamin F°, J. X. Medeiros, B. F. Reis and E. A. G. Zagatto, Anal. Chim. Acta, 101 (1978) 9.

Analytica Chimica Acta, 156 (1984) 313—317
Elsevier Science Publishers B.V., Amsterdam — Printed in The Netherlands

Short Communication

SPECTROPHOTOMETRIC DETERMINATION OF SULPHATE IN SODIUM HYDROXIDE SOLUTIONS BY FLOW-INJECTION ANALYSIS

E. A. JONES

Council for Mineral Technology (Mintek), Private Bag X3015, Randburg 2125 (South Africa)

(Received 28th June 1983)

Summary. A spectrophotometric flow-injection procedure is described for the determination of sulphate in sodium hydroxide solutions. Sulphate catalyses the reaction between zirconium and methylthymol blue to form a complex measured at 586 nm. Optimal reaction conditions are discussed. The calibration graph is linear over the range 0.05—0.5 g l^{-1} sulphate with a relative standard deviation of 0.02. The sample throughput is 20 h^{-1}. Sulphate is easily determined in 1 M sodium hydroxide; the results agree with those obtained by the conventional gravimetric method and by ion chromatography.

Sulphate in natural waters has been determined by flow-injection analysis (f.i.a.) based on measurement of the turbidity of a barium sulphate suspension [1—5]. One of the problems associated with these methods is the accumulation of the barium sulphate precipitate in the flow-through cuvette [5].

Hems et al. [6] described a direct spectrophotometric determination of sulphate by catalysis of the zirconium—methylthymol blue (MTB) reaction. Certain anions (e.g., fluoride, phosphate, and sulphate) form labile complexes with zirconium that can react more rapidly with the ligand (MTB) than the polymerized zirconyl species that normally persist in weakly acidic solutions [7]. Hems et al. [6] found that a freshly prepared zirconyl chloride solution instantly formed a colour with MTB, a day-old solution formed the colour only slowly and weakly, and a solution several weeks old formed no colour other than that of the MTB. Conditions can be so arranged that the anion-catalysed reaction proceeds at a reasonable rate, whereas the uncatalysed reaction (blank) proceeds only to a limited extent. Thus, a time plateau is formed during which the quantitative effect of the catalysis can be measured. In this dynamic measurement, it is essential for the reaction conditions to be strictly controlled, and for the change of reactant or product concentration as a function of time to be measured as accurately as possible. This can be achieved by f.i.a.

In this communication, a rapid determination of sulphate concentrations $\geqslant 0.05$ g l^{-1} in sodium hydroxide solutions is reported. The method is based on the above catalysis.

0003-2670/84/$03.00

Experimental

Reagents. All chemicals used were of analytical-reagent grade.

Methylthymol blue solution (8×10^{-5} M) was prepared by dissolution of 0.0329 g of the reagent in 500 ml of 0.6 M hydrochloric acid; it was discarded after 5 days. The zirconium reagent solution (10^{-2} M) was prepared by dissolution of 1.611 g of zirconium oxychloride ($ZrOCl_2 \cdot 8H_2O$) in 0.012 M hydrochloric acid, and dilution to 500 ml with the same acid. This solution polymerizes at a convenient rate for use between 2 and 10 days. A working solution of 8×10^{-4} M $ZrOCl_2$ was prepared by suitable dilution and made 0.05 M in hydrochloric acid, the acidity that was found to effect the least change in polymerization as the solution ages [7]. A stock sulphate solution (50 mg l^{-1}) was prepared by dissolution of 7.3933 g of anhydrous sodium sulphate in water, and dilution to 100 ml. Working standards in the range 0.1—0.5 g l^{-1} were prepared by suitable dilution with water.

Apparatus and manifold. The manifold (Fig. 1) was made of teflon tubing (0.5 mm i.d.) with teflon connectors. The peristaltic pump was a Gilson Minipuls 2. The sample injector was a Cheminert R6031SV rotary valve with interchangeable sample loops of varying capacity. A Beckman Model 25 spectrophotometer equipped with a Hellma-type 178 flow-through cuvette (light path 10 mm, inner volume 80 μl) was connected to a Beckman stripchart potentiometric recorder.

Procedure. In the flow system (Fig. 1), the methylthymol blue carrier solution (8×10^{-5} M in 0.6 M hydrochloric acid) was pumped at a flow rate of 1.2 ml min^{-1}. The sample solution (100 μl) was injected into this stream, which was then merged with the zirconium solution (8×10^{-4} M) also flowing at 1.2 ml min^{-1}. The catalytic effect of sulphate on the zirconium—MTB reaction proceeded in the mixing coil (4 m long, 0.5 mm i.d.), and the absorbance of the complex was monitored at 586 nm.

Results and discussion

The labile complex between sulphate and zirconium reacts with MTB to form a complex that exhibits an absorption maximum at 586 nm, the molar absorptivity being 2×10^4 l mol^{-1} cm^{-1}. The rate of complex formation is slow so that 1 hour is usually required for batchwise determination of

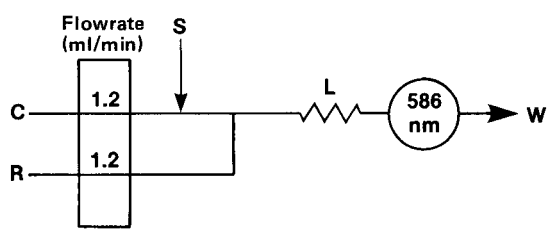

Fig. 1. Flow diagram for determination of sulphate. C, 8×10^{-5} M MTB in 0.6 M HCl; R, 8×10^{-4} M $ZrOCl_2$ in 0.05 M HCl; L, 4-m reaction coil; S, sample injection; W, waste.

the sulphate. Conversion to a flow-injection procedure allows the controlled sequential photometric detection of the colour complex to proceed even while the reaction is in progress, thus yielding a higher throughput with simple apparatus. The fact that the measurement is made at a stage when colour development is not complete does, however, have a limiting effect on the sensitivity of the method as used.

Optimization of the flow-injection system. Parameters that affect the reaction rate and the reaction time of the f.i.a. system, such as the length of the reaction coil, the flow rate, and reagent concentration, are important owing to the slow rate of reaction. These parameters affect the sensitivity, precision, and throughput of samples and require optimization.

The effect of coil length was tested by varying the length of the coil between 1 m and 6 m while the flow rates of the carrier (8×10^{-5} M in 0.4 M hydrochloric acid) and reagent (8×10^{-4} M in 0.05 M hydrochloric acid) were maintained at 1.2 ml min^{-1}. The peak height increased with increasing coil length (Fig. 2, curve B). At a coil length of less than 2 m, the residence time was too short for colour development and, at a length of more than 4 m, the peak height increased more slowly because, though the residence time increased for colour development, the dispersion also increased, resulting in a lower peak height. The effect of the flow rate is also shown in Fig. 2

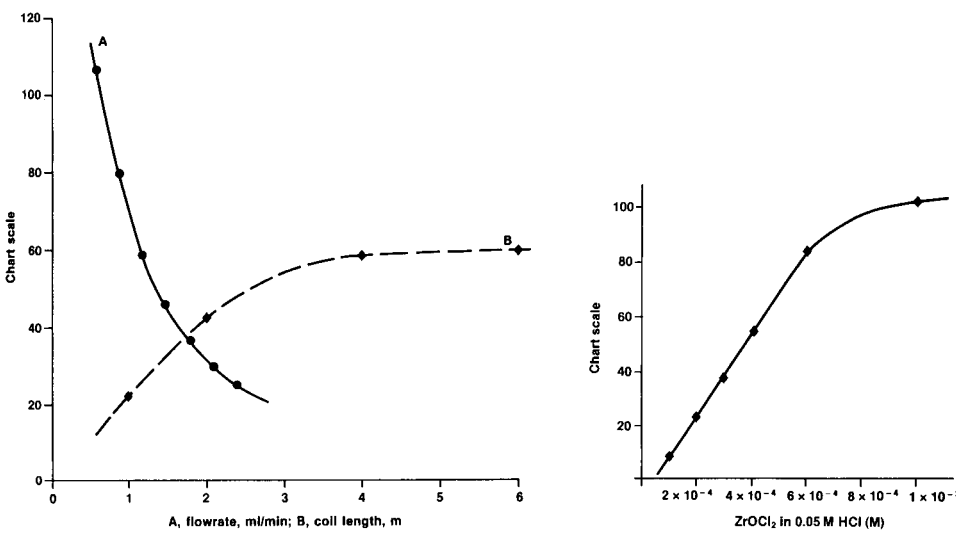

Fig. 2. Effect of flow rate (curve A) and length of reaction coil (curve B). Conditions: 8×10^{-4} M $ZrOCl_2$ in 0.05 M HCl; 8×10^{-5} M MTB in 0.6 M HCl; sample volume, 100 μl; sample concentration, 0.5 g l^{-1} SO_4^{2-}. Coil length for curve A, 4 m. Flow rate for curve B, 1.2 ml min^{-1}.

Fig. 3. Effect of molarity of $ZrOCl_2$. Conditions: 8×10^{-5} M MTB in 0.6 M HCl; sample volume, 100 μl; sample concentration, 0.5 g l^{-1} SO_4^{2-}; flow rate 1.2 ml min^{-1}; coil length, 4 m.

(curve A). The slow catalytic reaction led to a considerable decrease in peak height with higher flow rates, indicating that there was insufficient residence time as well as increased dispersion. A flow rate of 1.2 ml min^{-1} was therefore chosen, which gave an acceptable peak height as well as a larger throughput of samples.

The effect of different molarities of zirconium solution in 0.05 M hydrochloric acid is shown in Fig. 3. The optimum range of molarity to yield linearity was between 6×10^{-4} and 1×10^{-3}, and an 8×10^{-4} M zirconium solution was chosen. Increasing molarity of MTB had little effect on the peak height, though there was a slight enhancement at 8×10^{-5} M. When the molarity of hydrochloric acid in the MTB was plotted against the absorbance measured, it was found that the peak height increased in a smooth curve as the hydrochloric acid molarity increased from 0.2 to 1.0 M. A 0.6 M solution was chosen because this gave reasonable absorbance values, and because at higher molarities of hydrochloric acid, the zirconium depolymerizes, and the blank reaction proceeds more rapidly [6].

Range of determination. Varying amounts of sulphate were injected successively as a check on the reproducibility and linearity of the response at a low chart speed. The catalytic effect of sulphate on the reaction between zirconium and MTB was observed in the sulphate concentration range of 0.05 to 0.5 g l^{-1}, where the calibration graph was linear. Below 0.05 g l^{-1}, the sulphate content was too low, whereas above 0.5 g l^{-1}, the formation of the zirconium—MTB complex was inhibited owing to the production of a more stable zirconium—sulphate complex [6].

Analysis of sodium hydroxide solutions. Concentrations of sodium ion to a maximum of 4 g l^{-1} (the sodium concentration in 1 M sodium hydroxide solution) had no effect on the recovery of the sulphate.

A series of 1 M sodium hydroxide solutions was measured for sulphate

TABLE 1

Determination of sulphate in a batch of sodium hydroxide solutions (comparative analysis)

1 M NaOH solutions	Sulphate concentration (g l^{-1})		
	F.i.a.	Ion chromatography	Gravimetry
1	10.1		9.9
2	10.3	10.0	10.1
3	10.0		10.1
4	10.6	10.9	10.2
5	10.1		10.4
6	10.1	10.5	10.4
7	10.1		10.3
8	10.1	10.0	10.3
9	10.4		10.3
10	10.1		10.3

by the f.i.a. procedure, gravimetrically as barium sulphate, and by ion chromatography. The results are given in Table 1. The three methods of measurement are in good agreement, there being no bias between the f.i.a. and gravimetric methods, for which a similar number of results are available. On a routine basis, 20 samples per hour were analysed for sulphate by the f.i.a. method with a relative standard deviation of 0.02. The time required for the determination of sulphate in solution by f.i.a. represents a saving of the order of 80% on the time required for the conventional gravimetric determination. To ensure that the acidity was maintained at 0.6 M in the MTB carrier solution, a calculated amount of hydrochloric acid was added before the sample was injected to neutralize the 1 M sodium hydroxide. For samples where the sodium hydroxide molarity is not known, the pH value can be adjusted to 7 with hydrochloric acid.

This paper is published by permission of the Council for Mineral Technology (Mintek).

REFERENCES

1 J. F. van Staden, Fresenius Z. Anal. Chem., 310 (1982) 239.
2 J. F. van Staden, Fresenius Z. Anal. Chem., 312 (1982) 438.
3 J. Růžička and E. H. Hansen, Flow Injection Analysis, Wiley-Interscience, New York, 1981.
4 F. J. Krug, H. Bergamin F°., E. A. G. Zagatto and S. S. Jorgensen, Analyst, 102 (1977) 503.
5 S. Baban, D. Beettestone, D. Betteridge and P. Sweet, Anal. Chim. Acta, 114 (1980) 319.
6 R. V. Hems, G. F. Kirkbright and T. S. West, Talanta, 16 (1969) 789.
7 M. L. Cabello-Tomas and T. S. West, Talanta, 16 (1969) 781.

Analytica Chimica Acta, 156 (1984) 319—322
Elsevier Science Publishers B.V., Amsterdam — Printed in The Netherlands

Short Communication

SELECTIVE SPECTROPHOTOMETRIC KINETIC DETERMINATION OF COPPER WITH 2-METHYL-1, 3-CYCLOHEXANEDIONE BIS(4-PHENYL-3-THIOSEMICARBAZONE)

J. RODRÍGUEZ, A. GARCÍA DE TORRES and J. M. CANO-PAVON*

Department of Analytical Chemistry, Faculty of Sciences, University of Malaga, Malaga-4 (Spain)

(Received 1st April 1983)

Summary. A non-catalytic kinetic method is described for the determination of copper(II), based on the slow rate of complexation between the metal ion and 2-methyl-1,3-cyclohexanedione bis(4-phenyl-3-thiosemicarbazone), which is due to the slow *syn/anti* equilibration of the reagent. The reaction at pH <2 is followed by measuring the rate of change of the absorbance at 480 nm. The calibration graph is linear over the copper range 2—10 $\mu g\ ml^{-1}$, with relative standard deviations of 1.20% (tangent method), 1.85% (fixed-time method) and 1.75% (fixed-absorbance method). The only serious interferences are from Pd, Sb, Mo, Hg and periodate.

Uncatalysed reactions are rarely used in kinetic analysis because their selectivity and sensitivity are generally poor. The present communication reports a selective kinetic uncatalysed determination of copper based on the slow formation of a complex between copper(II) and 2-methyl-1,3-cyclohexanedione bis(4-phenyl-3-thiosemicarbazone) (2-Me-1,3-CDPT). Although some other metal ions slowly form complexes with this reagent, few do so at pH <2, so that this determination of copper is quite selective. The analytical properties of 2-Me-1,3-CDPT have been described previously [1]; their properties, and those of the bisthiosemicarbazones and bisphenylthiosemicarbazones of β-diketones, are quite different from those of the corresponding α-diketone compounds. In general, thiosemicarbazones have been little used in kinetic analysis, and only in catalysed oxidation-reduction reactions followed by photometry [2—4] or fluorimetry [5, 6].

Experimental

Reagents. All solvents and reagents were of analytical grade. The standard copper(II) solution was prepared from the sulphate (Merck) and standardized iodimetrically; it was diluted as required before use. A 0.2% (w/v) solution of 2-Me-1,3-CDPT in dimethylformamide was used. This reagent was synthesized as described previously [1].

Apparatus. The Pye-Unicam SP-8000 spectrophotometer used was equipped with an Ultrathermostat Techne-Circulator C-100, and 1.0-cm glass

0003-2670/84/$03.00

cells. All pH measurements were made with a Philips PW-9408 meter and a combined glass/calomel electrode.

Procedure. To a 1-ml portion of 0.2% 2-Me-1,3-CDPT solution in dimethylformamide, in a 10-ml volumetric flask, add 5 ml of dimethylformamide, adjust the pH to 1—2 with hydrochloric acid, and add the sample containing 20—100 μg of copper. Dilute to the mark with water, mix and after 30 s, transfer a portion to a 1-cm glass cell maintained at 37°C. Measure the absorbance at 480 nm as a function of time. The reaction rate is calculated from the difference in the slope of the absorbance/time plots.

Results and discussion

Formation of the copper complex. Copper(II) forms a 1:1 metal ion/reagent complex with 2-Me-1,3-CDPT; this complex is formed slowly in acidic medium, and has an absorption maximum at 480 nm (Fig. 1a). The formation of this copper complex is complete in about 11 h (Fig. 1b). Other metal ions react similarly, but the complexes are not formed at pH < 2.

The slow rate of complexation of copper(II) with 2-Me-1,3-CDPT is unusual, compared with other related compounds, such as the thiosemicarbazones [7] and phenylthiosemicarbazones [1] of 1,3-cyclohexanedione, or α-diketone bithiosemicarbazones. Solutions of 2-Me-1,3-CDPT are stable in storage, whereas with 1,3-cyclohexanedione bis(phenylthiosemicarbazone), the absorptivities of the chelates were greater when the reagent was at least two days old; this may be due to prototropic equilibrium in solution with the methylene proton at C_2 modifying the configuration of the imine double bond, so that a stereoisomer is formed from the initial *syn* form; the *anti* form should be more suitable for coordination [1]. In 2-Me-1,3-CDPT, this modification does not occur spontaneously, owing to steric hindrance by the methyl group. However, in the formation of stable complexes with certain metal ions, the related *syn/anti* equilibrium may be displaced slowly so that the complexes are formed quantitatively only after several hours.

For the kinetic determination of copper(II), the tangent method, fixed-time method and fixed-absorbance method can be used. Conventionally, in these methods, the initial copper concentration is plotted against Δ(CuR)/

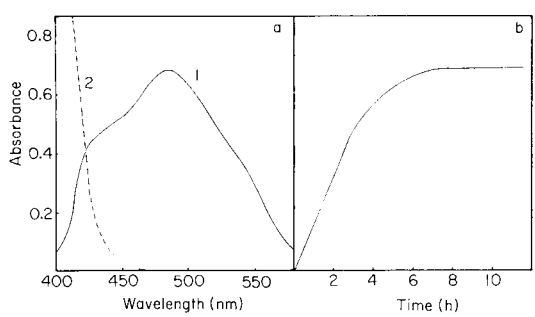

Fig. 1. (a) Absorption spectra of the copper(II)—2-Me-1,3-CDPT complex (5 mg l^{-1} Cu). (b) Variation of absorbance with time in the formation of the copper complex (5 mg l^{-1} Cu).

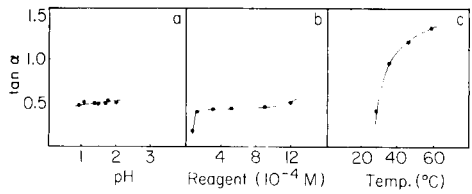

Fig. 2. Influence of experimental variables on the reaction between Cu(II) and 2-Me-1,3-CDPT: (a) influence of pH; (b) influence of reagent concentration; (c) influence of temperature. (Concentration of copper in all cases was 5 mg l^{-1}; other conditions as in Procedure.)

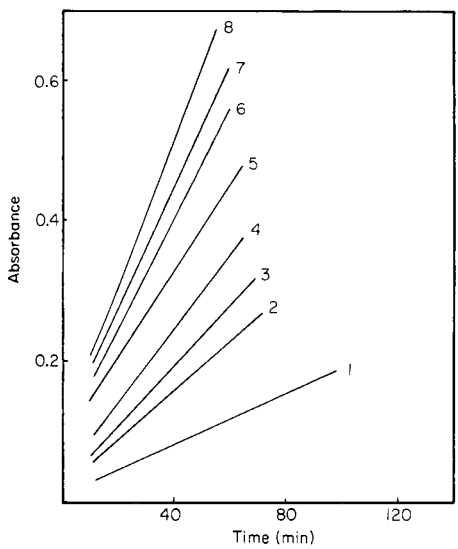

Fig. 3. Absorbance vs. time plots for different copper concentrations under the recommended conditions: (1) 2; (2) 3; (3) 4; (4) 5; (5) 6; (6) 7; (7) 8; (8) 9 mg l^{-1} copper(II).

Δt, the increase of absorbance at constant Δt, and $1/\Delta t$ for constant absorbance, respectively. A detailed study of the theoretical and experimental factors influencing the accuracy of analytical rate measurements has been made by Ingle and Crouch [8].

Effect of reaction variables. Results of the optimization of pH are given in Fig. 2(a). There was little effect in the pH range 1.0—2.0, which was therefore chosen. As shown in Fig. 2(b), the reaction rate was practically unaltered when the reagent was varied from 2×10^{-4} to 10^{-3} M; 1 ml of 0.2% reagent in a total volume of 10 ml was found satisfactory. Figure 2(c) shows that the reaction proceeded quickly at $\geqslant 60°C$; a temperature of 37°C was chosen for the final procedure.

An examination of the dimethylformamide/water ratio showed that when the percentage of dimethylformamide was small, the reaction rate was very slow. In practice, the range from 50 to 70% dimethylformamide was convenient, thus a 60% concentration was chosen in all cases.

TABLE 1

Concentrations of diverse ions tolerated for 8.2 μg ml^{-1} copper(II)

Concentration tolerated (μg ml^{-1})	Ion
100	Co(II), Ni(II), Zn(II), Mn(II), Pb(II), Cd(II), Cr(III), Al(III), In(III), Sn(II), U(VI), W(VI), Ce(IV), Ti(IV), Zr(IV), alkaline, alkaline-earths, F^-, $C_2O_4^{2-}$, PO_4^{3-}, SCN^-, $S_2O_3^{2-}$, EDTA, ClO_3^-, citrate and tartrate.
50	Bi(III), Os(VIII), Se(IV), Fe(II) and (III), ClO_4^-, IO_3^-, BrO_3^-
10	Mo(VI), Hg(II), IO_4^-
5	Pd(II), Sb(III)

Kinetic determination of copper. The absorbance/time curves for solutions containing different amounts of copper(II) were recorded against a water-blank (Fig. 3). The initial slopes indicate a first-order reaction with respect to copper. Copper can be determined in the interval 2—10 μg ml^{-1}.

The relative errors (P = 0.05) in the different methods of measurement, evaluated from 14 samples, were: 1.20% (tangent method), 1.85% (fixed-time method), and 1.73% (fixed-absorbance method).

A study of interferences is summarized in Table 1. From these results it can be concluded that the procedure suffers from few interferences; only Mo(VI), Hg(II), Sb(V), and Pd(II) are likely to interfere. EDTA, nitrate and tartrate do not interfere at the level investigated.

REFERENCES

1 J. Rodríguez, A. García de Torres and J. M. Cano-Pavon, Talanta, 28 (1981) 131.
2 M. D. Perez-Bendíto, M. Valcarcel, M. Ternero and F. Pino, Anal. Chim. Acta, 90 (1977) 405.
3 M. Ternero, F. Pino, M. D. Perez-Bendíto and M. Valcarcel, Microchem. J., 25 (1980) 102.
4 R. P. Igov, M. D. Jaredic and T. G. Pecev, Talanta, 27 (1980) 361.
5 A. Moreno, M. Silva, D. Perez-Bendíto and M. Valcarcel, Talanta, 30 (1983) 107.
6 J. Vazquez Ruiz, A. García de Torres and J. M. Cano-Pavon, Talanta, (1984) in press.
7 J. J. Berzas Nevado, J. A. Muñoz Leyva and R. Roman Ceba, Talanta, 23 (1976) 257.
8 J. D. Ingle and R. S. Crouch, Anal. Chem., 43 (1971) 697.

Analytica Chimica Acta, 156 (1984) 323—327
Elsevier Science Publishers B.V., Amsterdam — Printed in The Netherlands

Short Communication

SEQUENTIAL SPECTROPHOTOMETRIC DETERMINATION OF RHODIUM AND IRIDIUM WITH 1,5-DIPHENYLCARBAZIDE

KRYSTYNA BRAJTER* and URSZULA KOZICKA
Department of Chemistry, University of Warsaw, Warsaw 02-093 (Poland)
(Received 6th June 1983)

Summary. Rhodium and iridium in mixtures are determined sequentially with 1,5-diphenylcarbazide at pH 5.0. The rhodium complex is formed at 70°C and is extracted into isobutanol for measurement. The iridium complex is then formed by heating for 45 min and measured in aqueous solution. Beer's law is obeyed over the ranges 0.56—2.8 $\mu g\ ml^{-1}$ for rhodium and 0.53—3 $\mu g\ ml^{-1}$ for iridium. Pt, Pd, Sn, Co, Ni and Cr can be tolerated in small amounts.

Few reagents are commonly used for the spectrophotometric determination of iridium [1—3] and there are deficiencies in the methods which allow simultaneous determinations of iridium and rhodium in solution [1, 4—15]. The usefulness of 1,5-diphenylcarbazide for the extractive-spectrophotometric determination of rhodium and iridium is described here; the method is based on the different kinetic properties of rhodium and iridium in complex formation with diphenylcarbazide and the different extractive behaviour of the complexes formed. 1,5-Diphenylcarbazide, as far as platinum metals are concerned, has been used only for the determination of osmium [15, 16], though the carbazone has been used spectrophotometrically for iridium [17].

Experimental

Reagents. The iridium solution was obtained by diluting a standard solution of hexachloroiridic acid containing 3.42% of iridium. Rhodium solution was obtained by dissolving $RhCl_3 \cdot 3H_2O$ in 10 ml of concentrated hydrochloric acid, evaporating to low bulk and diluting; it was standardized gravimetrically with thionalide. 1,5-Diphenylcarbazide (Institute of Organic Chemistry, Warsaw) and 1,5-diphenylcarbazone (CIECH, Poland) were purified [18]. Both reagents were used as 0.6% (w/v) solutions in acetone. Other organic reagents were of reagent grade.

Apparatus. A Specord UV—VIS recording spectrophotometer and a Specol ZV spectrophotometer (Carl Zeiss, Jena) were used with 5.0- and 1.0-cm cells.

Procedure. To the rhodium and iridium test solution, add 2 ml of freshly prepared aqua regia and evaporate to dryness. Add 1 ml of concentrated

0003-2670/84/$03.00

hydrochloric acid and evaporate. Dissolve the dry residue in 1 ml of 1 M hydrochloric acid and transfer to a 25-ml flask; add 3 ml of 8% (w/v) ammonium acetate solution and 2 ml of 0.6% (w/v) diphenylcarbazide solution. Heat on a water bath at 70°C for 7—10 min. Cool and transfer to a separating funnel, washing the flask with 1-ml portions of isobutanol. In all, add 8.0 ml of isobutanol and shake for 1 min. Repeat this extraction twice. The amount of platinum metals should not exceed 30 μg; if the amount is larger, repeat the extraction 3 times with 7.0-ml portions of isobutanol. Transfer the organic layers to a 25-ml volumetric flask and dilute to the mark with isobutanol. Measure the absorbance at 570 nm in 1.0-cm cells against a reference blank taken through the entire procedure. The absorbance corresponds to the rhodium content.

Transfer the aqueous phase to a 25-ml volumetric flask and add 1 ml of 1 M hydrochloric acid, 3 ml of the ammonium acetate solution and 2 ml of the diphenylcarbazide solution. Heat for 45 min in a boiling water bath, shaking the solution occasionally after adding 2-ml portions of ethanol. Cool to room temperature, add 10 ml of ethanol, mix well, dilute to the mark with water, and measure the absorbance in 5.0-cm cells at 570 nm against a reference blank taken through the whole procedure. This absorbance corresponds to the iridium content.

Prepare calibration graphs in the same way for 0—3 μg ml^{-1} iridium.

Results and discussion

Complex formation. Rhodium and iridium react only slowly with 1,5-diphenylcarbazide to form coloured complexes, thus heating is necessary. Heating for 7—10 min at 70°C sufficed to form the rhodium complex, which was then stable for 1.5 h. The results of experiments done to establish the kinetics of the reaction between rhodium(III) and diphenylcarbazide are presented in Fig. 1. Maximum absorbance was reached in 10 min at 80°C; the linear relationships indicate a first-order reaction. The mean rate constants found from five separate determinations were $k_1 = 4.35 \times 10^{-4}$ s^{-1} (40°C), $k_2 = 1.38 \times 10^{-3}$ s^{-1} (60°C) and 2.87×10^{-3} s^{-1} (80°C). The activation energy (found from a log k vs. T^{-1} plot) and standard entropy change were $E_a = 50.02$ kJ mol^{-1} and $\Delta S^0 = -145.1$ J mol^{-1} K^{-1}, respectively. Owing to the very slow reaction between iridium and diphenylcarbazide, the complex was produced only after heating for 45 min on a boiling water bath.

The formation of the complexes with diphenylcarbazide depended on the pH of the solution. At about pH 5.0, the absorbance of the complexes was greatest and the blank was smallest. When absorption spectra were measured over the pH range 5.0—11.4, a diphenylcarbazide solution had very high absorbance around 500 nm at pH 10—11.4, but negligible absorbance at pH 5.0 over the range 400—600 nm (Fig. 2). The spectra of complexes are shown in Fig. 2. In these tests, the pH was adjusted with sodium hydroxide or hydrochloric acid.

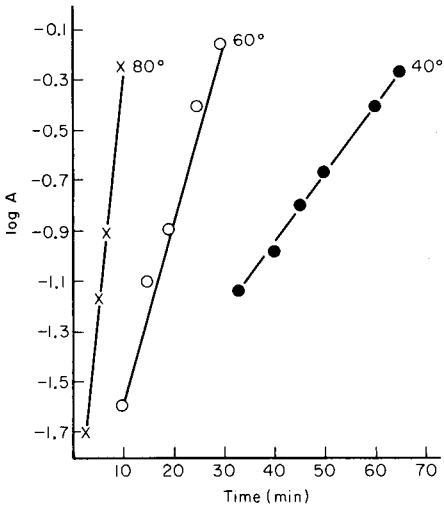

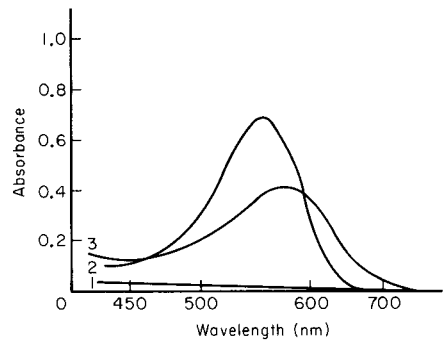

Fig. 1. Variation of ln A (absorbance) with time for the Rh(III) complex at different temperatures: (•) 40°C; (○) 60°C; (×) 80°C.

Fig. 2. Absorption spectra of: (1) Diphenylcarbazide, (2) Ir(IV)—diphenylcarbazide complex, (3) Rh(III)—diphenylcarbazide complex. pH of all three solutions was 5.05.

A large molar excess of diphenylcarbazide was necessary to develop maximum absorbance. At least a 245-fold excess of reagent was necessary for rhodium, and a 500-fold excess for iridium before the coloured complexes were fully developed.

Extraction. To find the most convenient solvent for the extraction, ethyl acetate, dichloroethane, dichloromethane, tri-n-butylphosphate, benzyl alcohol, di-isobutyl ketone, methyl isobutyl ketone, isobutanol, benzene and chloroform were examined. The first five solvents were unsatisfactory. The rhodium complex was extracted with isobutanol but not with the ketones, benzene or chloroform. The iridium complex was not extracted with isobutanol, but could be extracted with benzene, methyl isobutyl ketone or chloroform.

The extraction separation of rhodium from iridium was done after heating the test solution containing both platinum metals for 7—10 min so that only the rhodium complex was formed. This complex was then extracted with isobutanol. Extensive studies showed that the recommended procedure is most convenient; if the solution is heated long enough to ensure the formation of both complexes and iridium is then extracted with chloroform or methyl isobutyl ketone, the results for Ir(IV) and Rh(III) are much less precise.

Calibration graphs obtained by the recommended procedure followed Beer's law over the concentration ranges 0.56—2.8 μg ml^{-1} for rhodium and 0.53—3 μg ml^{-1} for iridium, passing through the origin in both cases. The

TABLE 1

Results obtained for mixtures of iridium and rhodium

Test	Rhodium (μg)		Iridium (μg)		Error (%)		Rh:Ir weight ratio
	Taken	Found	Taken	Found	Rh	Ir	
1	14.00	14.30	17.62	18.04	+2.14	+2.38	1:1
2	28.01	27.80	26.43	25.96	−0.75	−1.77	1:1
3	42.02	43.00	35.23	33.92	+2.33	−3.71	1:1
4	56.03	54.90	52.85	52.00	−2.01	−1.60	1:1
5	21.01	20.84	61.60	59.90	−0.80	−2.75	1:3
6	14.00	14.80	70.40	72.60	+5.71	+3.12	1:5
7	56.03	56.80	26.43	27.07	+1.37	+2.42	2:1
8	63.03	64.86	44.04	43.00	+2.90	−2.36	1.4:1
9	14.00	13.60	61.60	59.90	−2.85	−2.36	1:4
10	56.03	55.00	61.60	60.70	−1.83	−1.55	1:1
11	70.04	69.10	26.43	27.31	−1.34	+3.32	2.6:1
12	21.01	21.85	61.60	60.70	+3.99	−1.42	1:3
13	56.03	54.99	26.43	27.19	−1.85	+2.87	2:1
14	56.03	55.28	13.21	14.00	−1.33	+5.98	4:1
15	49.02	47.99	17.62	18.28	−2.10	+3.74	2.9:1

apparent molar absorptivities were 1.74×10^4 l mol^{-1} cm^{-1} for rhodium and 1.06×10^4 l mol^{-1} cm^{-1} for iridium.

Solutions containing known amounts of iridium and rhodium were taken through the procedure. The results obtained (Table 1) show satisfactory recoveries.

Interferences. Interferences were tested on the sequential determination of rhodium (14 μg) and iridium (13 μg). The tolerance limits were as follows: 50 μg Pd(II), 35 μg Pt(IV), 10 μg Au(III), 50 μg Co(II), 10 μg Ni(II), 5 μg Cu(II), 5 μg Cr(III). Ruthenium, osmium and mercury were not tolerated.

Tests with 1,5-diphenylcarbazone. Rhodium and diphenylcarbazone form a purple complex; the diphenylcarbazide complex is violet. In isobutanol the purple becomes more intense so that the sensitivity with diphenylcarbazone is increased almost 25-fold. However, the precision is worse than that attained with diphenylcarbazide because of the very adhesive properties of the rhodium complex with diphenylcarbazone. Also the colour is less stable, fading after 15 min. The reaction of iridium(IV) with diphenylcarbazone is less sensitive than that with the carbazide. At higher temperatures, iridium forms a precipitate with the carbazone, which dissolves easily in organic solvents. However, when diphenylcarbazone is used, Ir(IV) and Rh(III) cannot be determined by the procedure given for diphenylcarbazide.

REFERENCES

1 F. E. Beamish and J. C. Van Loon, Recent Advances in the Analytical Chemistry of the Noble Metals, Pergamon, Oxford, 1972.
2 Z. Marczenko, Spectrophotometric Determination of Elements, Horwood, Chichester, 1976.
3 Z. Marczenko and K. Kalinowski, Anal. Chim. Acta, 144 (1982) 173.
4 G. A. Vorobyeva, Yu. A. Zolotov, L. A. Izosenkova, A. V. Karjakin, L. I. Pavlenko, O. M. Petrukhin, I. V. Seryakova, L. V. Simonova and V. N. Shevchenko, Zh. Anal. Khim., 29 (1974) 497.
5 J. E. Rakovskij, N. W. Shvedova and L. D. Berliner, Zh. Anal. Khim., 30 (1975) 1775.
6 V. P. Ionov, S. A. Potapova, Z. N. Dubrovina and N. M. Zavoronkov, Zh. Anal. Khim., 30 (1975) 955.
7 V. M. Savostina, O. A. Shpigun, V. A. Parmenova, A. A. Val'shin and V. M. Peshkova, Zh. Anal. Khim., 31 (1976) 2154.
8 V. M. Savostina, O. A. Shpigun, V. A. Parmenova and V. M. Peshkova, Zh. Anal. Khim., 32 (1977) 556.
9 O. M. Petrukhin, V. N. Shevchenko, I. A. Zacharova and V. A. Prochorov, Zh. Anal. Khim., 32 (1977) 897.
10 Yu. A. Zolotov, O. M. Petrukhin, V. N. Shevchenko, V. V. Dunina and E. G. Rukhadze, Anal. Chim. Acta, 100 (1978) 613.
11 G. G. Horoshko, Yu. M. Dedkov and A. N. Jermakov, Zh. Anal. Khim., 33 (1978) 1114.
12 E. G. Koleva and Ta Chong Ngat, Zh. Anal. Khim., 34 (1979) 2207.
13 B. Roy, R. P. Singh and A. K. Singh, Indian J. Chem., 20A (1981) 930.
14 V. M. Savostina, O. A. Shpigun and T. V. Chebrikova, Zh. Anal. Khim., 37 (1982) 285.
15 Z. Marczenko and J. Kuťaga, Chem. Anal., 24 (1979) 841.
16 S. Yaya and T. V. Ramakrishna, Talanta, 29 (1982) 619.
17 G. S. Manku, Mikrochim. Acta, (1973) 341.
18 P. Krumholz and F. Hönel, Mikrochim. Acta, 2 (1937) 177.

Analytica Chimica Acta, 156 (1984) 329—333
Elsevier Science Publishers B.V., Amsterdam — Printed in The Netherlands

Short Communication

SPECTROPHOTOMETRIC DETERMINATION OF COBALT BY EXTRACTION OF TETRATHIOCYANATOCOBALTATE(II) WITH PROPYLENE CARBONATE

D. THORBURN BURNS* and S. KHEAWPINTONG

Department of Analytical Chemistry, The Queen's University of Belfast, Belfast BT9 5AG (Northern Ireland)

(Received 6th September 1983)

Summary. Cobalt is extracted as ammonium tetrathiocyanatocobaltate(II) propylene carbonate. The effects of pH and diverse ions and masking are reported. The system is applied to the determination of cobalt (0.01—0.20%) in mild steels without prior separation of iron.

The tetracyanatocobaltate(II) ion can be extracted as an ion-pair with onium [1, 2] or other cations [3, 4] into chlorinated hydrocarbons. It may also be extracted into alcohols, ketones and esters, e.g., amyl alcohol [5], acetylacetone [6, 7], cyclohexanone [8] and tributyl phosphate [9]; the nature of the extracted species has not been fully elucidated in these cases. This latter group of solvents suffer from the practical disadvantage, in liquid-liquid extraction, of being less dense than water. Propylene carbonate has been used previously as an extracting solvent for a variety of ion-association chelated metal complexes [10—14], condensed molybdate species [15] and also for the tetrathiocyanatocuprate(II) anion [16]. The solvent has the advantages of being denser than water, practically odourless and of low toxicity [17]. Tetrathiocyanatocobaltate(II) ion may be extracted into propylene carbonate as its solvated ammonium salt.

Experimental

Apparatus. Pye Unicam SP8-400 and SP6-550 u.v.-visible spectrophotometers were used for recording absorption spectra and for routine absorbance measurements, respectively, using matched quartz 1-cm cells. A Radiometer TTT-IC pH meter was used to measure pH. Infrared spectra were obtained with a Perkin-Elmer 598 spectrometer.

Solutions. A stock 1000 mg l^{-1} cobalt(II) solution was prepared by dissolving 2.630 g of anhydrous cobalt(II) sulphate (analytical grade dried to constant weight at 400°C) in 1 l of distilled water. More dilute standard solutions were prepared as required. A pH 5 buffer solution was prepared by mixing 49.0 ml of 0.1 M citric acid with 51.0 ml of 0.2 M disodium hydrogen

0003-2670/84/$03.00

phosphate. Propylene carbonate (99%; Aldrich) was used as supplied. All other reagents were of analytical grade; twice-distilled water was used throughout.

Inert salt effect. The solubility of propylene carbonate in water is affected by the presence of inert salts such as sodium chloride [10]. In the present work ammonium sulphate was used to avoid competition between chloride with thiocyanate in complexation of cobalt(II). The optimum amount under the conditions in the general procedure was found to be 1 ml of saturated ammonium sulphate; below this amount extraction was incomplete whereas above 5 ml the absorbance of the extract decreased owing to dilution effects.

Effects of pH. The effect of pH was examined by adjusting the pH of the aqueous solutions prior to extraction by addition of 2 M hydrochloric acid or 2 M ammonia solution. The absorbance was constant over the pH range 2.5—6.2. Solutions were buffered at pH 5 for all further work. A variety of buffer systems was examined; citric acid/disodium hydrogenphosphate gave the lowest blank, and provided good pH control.

Optimum amounts of reagents. The effects of varying the amounts of reagents were examined for 40 μg of cobalt(II). For extraction by 10 ml of propylene carbonate, the optimum amounts of reagents were 3.0 ml of 5 M ammonium thiocyanate, 1.0 ml of buffer and an aqueous phase volume of 15 ml. Absorbances were measured at 320 and 625 nm against a reagent blank; they were stable for at least one month.

Analysis of steel samples. For steel samples containing 0.05—0.2% or 0.005–0.02% cobalt, dissolve 0.2 or 2.0-g samples placed in 250-ml conical flasks as follows. Moisten the sample with 1 or 2 ml of distilled water, and add slowly 4 or 25 ml of concentrated hydrochloric acid followed by 2 or 8 ml of concentrated nitric acid; warm if necessary to complete dissolution. The volumes relate to the two sample sizes mentioned. Boil off oxides of nitrogen and evaporate to 2—5 ml. Cool, transfer quantitatively to a 50-ml volumetric flask, dilute to volume with distilled water and mix thoroughly. Place a 5-ml aliquot of the solution in a 100-ml separating funnel, add 2 ml of 30% (w/v) ammonium fluoride solution, 3 ml of 5 M ammonium thiocyanate, 1 ml of saturated ammonium sulphate solution and 1 ml of pH 5 buffer, and dilute to 15 ml with water. Swirl gently to mix (the pH should be <6). Extract with 10 ml then 2 ml of propylene carbonate. Allow the phases to separate each time and drain the lower (organic) phase through a Whatman No. 42 filter paper (previously moistened with solvent) into a 10-ml volumetric flask. Make up to volume with propylene carbonate, mix and measure the absorbance at 625 nm in a 1-cm quartz cell against pure solvent. Prepare a calibration graph over the range 0—50 μg of cobalt from the results obtained by adding 2 ml of iron(III) nitrate solution containing 0.02 or 0.2 g of iron to the cobalt solutions, followed by the other reagents as for the steel samples, and proceeding as above.

Results and discussion

The composition of the complex anion was confirmed by Job's method and the mole ratio method to be $[Co(CNS)_4]^{2-}$. The role of propylene carbonate was studied by Job's method with nitrobenzene as the extracting phase. Propylene carbonate forms part of the extracted species which corresponds to $(NH_4)_2[Co(CNS)_4] \cdot C_4H_6O_3$ in solution; it was not possible to isolate the solid. The interaction is by hydrogen bonding to the ammonium ions via the carbonyl group, which was confirmed by an i.r. spectral procedure, as described by Murata and Ikeda [15].

Beer's law was obeyed for solutions containing up to 50 and 300 μg of cobalt in the final 10-ml extract at 320 and 620 nm, respectively, with apparent molar absorptivities of 1.15×10^4 and 1.8×10^3 l mol^{-1} cm^{-1}. For 40 μg of cobalt, the coefficients of variation were 1.06 and 0.64 at 320 and 625 nm, respectively, based on 7 replicates. The detection limit was therefore 1 ng of cobalt at 620 nm.

The possible interferences of a number of cations and anions on the ex-

TABLE 1

Effect of diverse ions on the determination of cobalt (20 μg)[a]
(Ions causing a change in absorbance of less than 5% are regarded as non-interfering)

Ion[b]	Ratio to Co (w/w)	Change in absorbance (%)		Ion[b]	Ratio to Co (w/w)	Change in absorbance (%)	
		320 nm	625 nm			320 nm	625 nm
Al^{3+}	250	+6[c]	—	Ascorbate	1250	+15	—
Cr^{3+}	250	+125	—		250	—	—
	250[d]	+10	—	Cl^-	450	—	—
Cu^{2+}	250	+104	+245	NO_3^-	1250	−9	−13
	250[e]	—	—		250	—	—
Fe^{2+}	250	very high	+113	SiO_3^{2-}	1250	−37	−43
	5	+48	—		35	—	—
Fe^{3+}	250	+1913[c]	+851	SO_4^{2-}	1250	+12	—
Hg^{2+}	50	+319	—		250	—	—
	50[f]	+26	—	WO_4^{2-}	1250	−63	−76
Nb(V)	250	+76[c]	+11		250	—	—
Ni^{2+}	250	+12	—				
	50	—	—				
Pd^{2+}	5	+485	—				
	5[e]	+184	—				
Ru(III)	50	very high	+995				
	50[f]	—	—				
Zr(IV)	250	+10[c]	—				

[a] K^+, Mn^{2+}, Na^+, U(IV), Zn^{2+}, MnO_4^-, VO_4^{3-} (250-fold), and acetate, ClO_4^-, $S_2O_3^{2-}$, F^-, HPO_4^{2-}, NO_3^-, and PO_4^{3-} (1250-fold) were without effect. [b] Cations added as chloride or sulphate, anions added as sodium salts. [c] There is no interference in the presence of ammonium fluoride. [d] In the presence of ammonium tartrate. [e] In the presence of sodium thiosulphate. [f] In the presence of hydrazine hydrate.

TABLE 2

Results of analysis for cobalt (%) in B.C.S. mild steels

B.C.S. No.	Cobalt content (% w/w)	
	Certified[a]	Found[b]
456	0.048 (0.043—0.050)	0.046 ± 0.001
457	0.018 (0.017—0.019)	0.018 ± 0.001
458	0.16	0.160 ± 0.003
459	0.077 (0.073—0.080)	0.079 ± 0.0004
460	0.009 (0.008—0.009)	0.0081 ± 0.001

[a]Certified value with range in parentheses. [b]At 625 nm, mean ± 95% confidence limits for 7 replicates.

traction of 20 μg of cobalt were examined. As for other cobalt/thiocyanate methods, the interferences by iron(III), copper(II), mercury(II) and chromium(III) were significant but could be masked by the addition of 2 ml of 30% (w/v) ammonium fluoride solution for 2 mg of iron, 2 ml of 0.2 M sodium thiosulphate for 5 mg of copper, and 2 ml of 1% (w/v) ammonium tartrate for 5 mg of chromium. At high levels of iron, a slightly decreased extraction was noted (2% reduction for 0.02 and 0.2 g of Fe); this effect may be allowed for by adding amounts of iron equivalent to those in samples to the standards used to prepare the calibration graph. Cobalt may be determined in the presence of highly adverse ratios of nickel (1:5000) by using three 10-ml portions of 2 M sulphuric acid to destroy the nickel(II) thiocyanate complex in the organic phase [18]. For the steels examined, it was not necessary to mask copper or nickel. The results for the interference and masking studies are summarised in Table 1.

Results for the determination of cobalt in five British Chemical Standard Steels (7 replicates for each sample) are in excellent agreement with the certified values (see Table 2).

The main advantage of the method is in the use of an almost odourless, non-toxic solvent which is readily and safely disposable after dilution with excess of water.

REFERENCES

1 A. J. Bowd, D. T. Burns and A. G. Fogg, Talanta, 16 (1969) 719.
2 A. G. Fogg, C. T. Higgens and D. T. Burns, Mikrochim. Acta, (1969) 546.
3 D. T. Burns and P. Hanprasopwattana, Anal. Chim. Acta, 115 (1980) 389.
4 D. T. Burns, P. Hanprasopwattana and B. P. Murphy, Anal. Chim. Acta, 134 (1982) 397.
5 F. P. Treadwell, Z. Anorg. Chem., 26 (1901) 1081.
6 W. B. Brown and J. F. Steinback, Anal. Chem., 31 (1959) 1805.
7 J. O. Hibbits, A. F. Rosenberg and R. T. Williams, Talanta, 5 (1960) 250.
8 H. Specker and G. Werding, Z. Anal. Chem., 200 (1964) 337.

9 E. Jackwerth and E. L. Schneider, Z. Anal. Chem., 207 (1965) 188.
10 B. G. Stephens and H. A. Suddeth, Anal. Chem., 39 (1967) 1478.
11 B. G. Stephens and F. Lindstrom, Anal. Chem., 36 (1964) 1308.
12 B. G. Stephens and H. A. Suddeth, Analyst, 95 (1970) 70.
13 B. G. Stephens, J. C. Loftin, W. C. Looney and K. A. Williams, Analyst, 96 (1971) 230.
14 B. G. Stephens, H. L. Felkel, Jr. and W. M. Spinelli, Anal. Chem., 46 (1974) 692.
15 K. Murata and S. Ikeda, J. Inorg. Nucl. Chem., 32 (1970) 267.
16 B. G. Stephens and H. L. Felkel, Jr., Anal. Chem., 47 (1975) 1677.
17 N. I. Sax, Dangerous Properties of Industrial Materials, 5th edn., Van Nostrand, New York, 1979, p. 942.
18 G. Takashi and O. Takiji, Mizu Shori Gijatsu, 20 (1979) 1169.

Analytica Chimica Acta, 156 (1984) 335—338
Elsevier Science Publishers B.V., Amsterdam — Printed in The Netherlands

Short Communication

EXTRACTION-SPECTROPHOTOMETRIC DETERMINATION OF TUNGSTEN AS TUNGSTEN BLUE

NOBUTAKA YOSHIKUNI

Laboratory of Analytical Chemistry, Faculty of Engineering, Chiba University, Yayoi-cho 1-33, Chiba City (Japan)

(Received 24th May 1983)

Summary. Tri-n-butyl phosphate (TBP) is used to extract tungsten(VI) from 0.5 M hydrochloric acid containing molybdenum(VI) and other metals. Tungsten(VI) in the TBP solution is reduced by tin(II) chloride and n-butyl acetate is used for dilution. The tungsten blue formed in the TBP/n-butyl acetate medium (1:1) is measured at 615 nm. The apparent molar absorptivity is about 1000 l mol^{-1} cm^{-1}; calibration graphs are linear in the range 0.1—1.5 mg of tungsten.

In a well known qualitative test for tungsten, tungstate is reduced by tin(II) chloride in strongly acidic solutions to form "tungsten blue" [1], but the reaction has not been used quantitatively because of interferences. However, tri-n-butyl phosphate (TBP) can extract tungstate quantitatively from 0.5 M hydrochloric acid solutions or from the solutions at pH 0.5—2.0 if enough calcium chloride is added for salting-out. Many metal ions and molybdates can be removed by TBP extraction from 0.5 M hydrochloric acid media [2, 3]. A selective extraction of tungstate ions and their spectrophotometric determination is possible on this basis.

Experimental

Apparatus. A Hitachi 124 spectrophotometer with 1 cm quartz cells and a Hitachi-Horiba pH meter Model M-7 were used.

Reagents. Reagent grade chemicals were used unless otherwise mentioned. Deionized water was used throughout. A tungsten(VI) stock solution (1.187 mg ml^{-1}) was prepared by dissolving 0.5325 g of $Na_2WO_4 \cdot 2H_2O$ in about 200 ml of 0.03 M hydrochloric acid, adjusting pH 5.35 with a few milliliters of dilute sodium hydroxide solution, and diluting to 250 ml with water. A molybdenum(VI) stock solution (5.14 mg ml^{-1}) was prepared by dissolving 0.9642 g of $H_2MoO_4 \cdot H_2O$ in a few milliliters of dilute sodium hydroxide solution, diluting with deionized water to about 90 ml, acidifying slightly with hydrochloric acid (pH 5.5), and diluting to 100 ml with water. This solution was diluted to 1.03 mg ml^{-1} molybdenum(VI) with water.

Procedure. To the sample solution containing 0.1—1.5 mg of tungsten(VI),

0003-2670/84/$03.00

add 5—10 ml of 0.1 M sodium hydroxide solution. Heat on a steam bath for 5 min. Cool and add 1 ml of 1 M sodium acetate (and 1 ml of 1 M sodium nitrate for faster determination). Adjust the pH to about 1.3 with hydrochloric acid. Transfer the solution quantitatively to a 50-ml separating funnel, washing the beaker with 3 ml of water. The total volume of the aqueous solution should be about 15 ml. Add 5.0 ml of TBP and shake for 5 min. Add 15 ml of aqueous 50% (w/v) calcium chloride solution and shake vigorously for another 5 min. Discard the aqueous phase. Immediately add 20 ml of 25% (w/v) tin(II) chloride in concentrated hydrochloric acid followed by 5.0 ml of n-butyl acetate. Shake vigorously for 10 min and discard the aqueous phase. Leave the organic phase at room temperature for 1.5 h (or 30 min if nitrate is added). Measure the absorbance of the organic phase at 615 nm against a reagent blank which has been taken through the same procedure. Obtain the calibration graph by taking aliquots containing 0.1—1.5 mg of tungsten(VI) through the procedure.

Results and discussion

The spectrum of the tungsten blue (Fig. 1) shows a broad absorption band at 615 nm. Changes in pH in the range 0.5—2.5 had no effect on the color development from 595 μg of tungsten(VI) when the acetate system was used, but the absorbance decreased at higher or lower pH values because of incomplete extraction of tungstate. Calcium chloride proved to be an effective salting-out agent for the extraction of tungstate from the 0.1 M acetate system. The absorbance finally produced remained constant for 20—30% of calcium chloride in the aqueous phase under the above-specified conditions.

In tests of the color development in the TBP/n-butyl acetate (1+1) medium, the absorbance remained constant when 20 ml of 20—40% (w/v) tin(II)

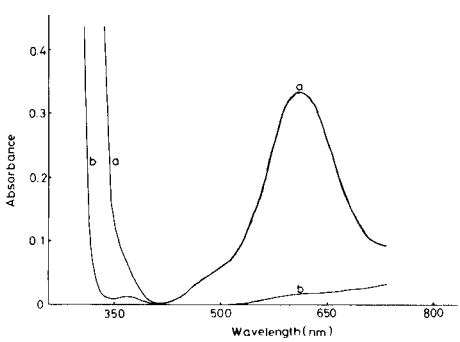

Fig. 1. Absorption spectra: (a) tungsten blue in TBP/n-butyl acetate against the reagent blank (595 μg W(VI), pH 1.30); (b) reagent blank against (1 + 1) TBP/n-butyl acetate.

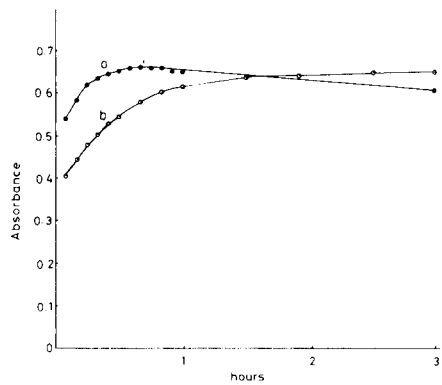

Fig. 2. Effect of standing time of the organic phase for 1.19 mg of W(VI): (a) aqueous phase with sodium nitrate (1 mM); (b) without sodium nitrate.

chloride solution in concentrated hydrochloric acid was used; with less tin(II), the absorbance decreased rapidly whereas with more tin(II) it decreased gradually. Maximum absorbance was obtained only when this solution was prepared in 12 M hydrochloric acid. The development time was important; color development was faster when nitrate was added earlier in the procedure than when no nitrate was added (Fig. 2). With the specified amount of sodium nitrate, the absorbance was constant over a 30—50 min standing time whereas without nitrate, complete color development required 3 h (the funnel was tightly closed meantime). Under the specified conditions (with nitrate), the calibration graph was linear in the range 0.1—1.5 mg of tungsten(VI) and the apparent molar absorptivity was about 1×10^3 l mol^{-1} cm^{-1}. For 10 determinations of 0.595 mg of tungsten(VI), the relative standard deviation was 2.8%.

Interferences. To determine the effect of various ions on the proposed method, solutions containing 595 μg of tungsten(VI) and the potential interference were treated exactly as in the above procedure. There was no interference (when nitrate was present) from 10^{-2} M chloride, or 10^{-4} M sulfate or bromide. Molybdate in equivalent amounts to tungstate ruined the method. Phosphate was tolerated at a 10^{-6} M level but at 10^{-4} M recoveries of tungstate were only about 13%.

Separation of tungsten(VI) from molybdenum(VI) and other metals. Because of the interference from molybdenum and some other metal ions, a prior separation of tungstate was essential. To this end, the sample solution was adjusted to 15 ml, 0.5 M in hydrochloric acid, and shaken for 5 min with 5.0 ml of TBP which had been equilibrated with 0.5 M hydrochloric acid—25% calcium chloride solution (white milky TBP); the aqueous phase was discarded. The organic phase was shaken with 15 ml of 0.5 M hydrochloric acid for 5 min, and again the aqueous phase was discarded. After addition of 5 ml of 4 M sodium hydroxide and 5 ml of chloroform, the mixture was shaken for 5 min and the chloroform phase was discarded. The aqueous phase was washed with 2 ml of chloroform by shaking for 1 min and then treated as in the recommended procedure.

Table 1 shows the recoveries obtained for tungsten(VI) in presence of molybdenum(VI). The effects of other metals, added as chloride or oxy-

TABLE 1

Effect of molybdenum on recovery of tungsten

W(VI) added (mg)	Mo(VI) added (mg)	W recovery (%)
0.119	1.03	99.2
0.595	1.03	99.6
1.19	1.03	100.0
1.19	5.14	73.7

anion, were investigated for 595 μg of tungsten. There was no interference from 10 mg of Cd(II), Co(II), Cr(III), Cu(II), Hg(II), Ni(II), Se(VI), Te(VI), U(IV), V(IV), La(III), Mg(II) or Zn(II); these ions were not extracted into TBP from 0.5 M hydrochloric acid. Gold(III) was extracted under these conditions but 1 mg of gold did not interfere. Palladium(II) and rhenium(VI) (0.1 mg each) did not interfere. Even 0.1 mg of iron(III) interfered with the determination of tungsten, but prior filtration of the solution of iron(III), made alkaline with sodium hydroxide, removed this interference.

REFERENCES

1 F. Feigl and V. Anger, Spot Tests in Inorganic Analysis, 6th Engl. edn., Elsevier, Amsterdam, 1972, p. 495.
2 T. Ishimori and E. Nakamura, JAERI Rep., 1047 (1963).
3 Y. Marcus and A. S. Kertes, Ion Exchange and Solvent Extraction of Metal Complexes, Wiley-Interscience, New York, 1969, p. 954.

Analytica Chimica Acta, 156 (1984) 339—343
Elsevier Science Publishers B.V., Amsterdam — Printed in The Netherlands

Short Communication

THE DETERMINATION OF PHOSPHATE IN TURBID AQUEOUS SAMPLES BY DERIVATIVE SPECTROPHOTOMETRY

JOOP HARMSEN
Institute for Land and Water Management Research (ICW), Wageningen (The Netherlands)
(Received 5th July 1983)

Summary. Phosphate can be determined in turbid solutions by applying a conventional spectrophotometric molybdenum blue method if the first derivative spectrum is used. Turbidity does not interfere if the absorbance caused by turbidity is $\leqslant 0.8$. Calibration graphs are linear for the range 0—3 mg l^{-1} phosphate. Precautions to avoid errors arising from higher concentrations are outlined. Recovery tests gave satisfactory results with imprecision of $\leqslant 4\%$.

In most laboratories, phosphate in water is measured by some version of the molybdophosphate method. In one such procedure, ammonium molybdate and antimony potassium tartrate react in an acidic medium with phosphate to form a mixed antimony molybdophosphate complex, which is reduced by ascorbic acid to an intensely blue complex. The absorbance at 886 nm is proportional to the phosphate concentration.

In practice, samples can be turbid or become turbid after addition of the reagents. Consequently, the absorbance of turbid samples will be too high and the results unreliable. This often happens in total phosphate determinations when the samples are not filtered before reagent addition. Filtration after complex formation often does not remove the turbidity.

With modern spectrophotometers, derivative spectra can be measured; these make it possible to correct for light scattering in turbid solutions. In this communication first derivative spectra are utilized for the determination of phosphate in turbid aqueous samples.

Experimental

All chemicals used were of analytical-reagent grade.

A standard procedure, NEN 6479 [1], was applied to determine phosphate. In this method the sample is pipetted into a 50-ml volumetric flask and diluted to 40 ml. Then 5 ml of reagent (9.6 g of ammonium molybdate and 0.2 g of antimony potassium tartrate in 1 l of 2 M sulphuric acid) is added followed by 2 ml of a freshly prepared 2% (w/v) ascorbic acid solution, and the solution is diluted to 50 ml. The absorbance at 886 nm or the spectrum is measured between 12 and 20 min after mixing.

The spectrophotometer used was a Perkin-Elmer 550-s model. The

0003-2670/84/$03.00

conditions for taking the first-derivative spectrum were as follows: scanning from 910 to 670 nm at 120 nm min^{-1}, response factor 5, range of $dA/d\lambda$ values from −0.020 to +0.020, recorder velocity 15 mm min^{-1}.

For testing, turbidity was caused by adding a 1% (w/v) barium chloride solution to the samples. This gave a very fine precipitate with the sulphate present in the molybdate reagent.

Standards were prepared from potassium dihydrogenphosphate.

Results and discussion

Spectra. The spectrum of the reduced antimony molybdophosphate complex is presented in Fig. 1; there are maxima at 720 and 886 nm. The first derivative spectrum is also shown; this spectrum is shifted slightly compared with the normal spectrum, because of the large response factor involved; the derivative is not zero at the top of the absorption peak. The distance between the maximum and minimum in the derivative spectrum (B—C) can serve as a measure of the amount of phosphate in solution. This distance is not influenced by turbidity, because the latter influence is almost linear in the wavelength region used. The derivative of the turbidity, therefore, is a constant value which affects the position of the derivative value but not the distance between B and C.

Influence of turbidity. The influence of turbidity is not easy to investigate,

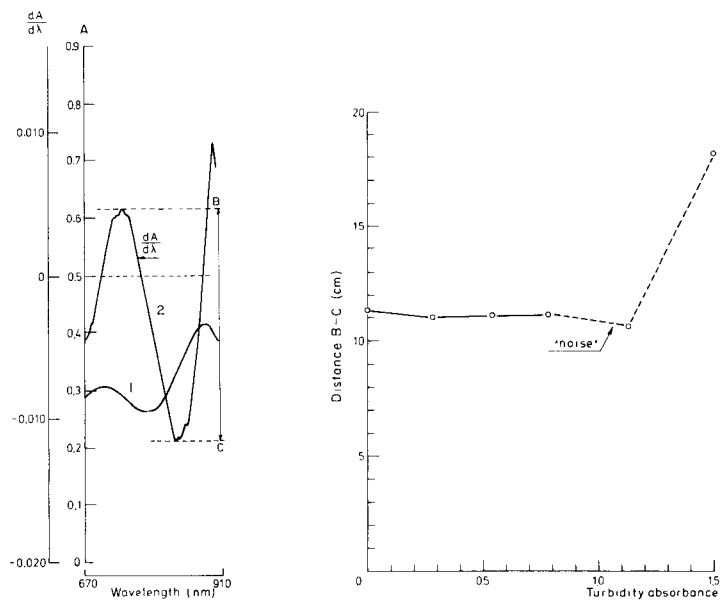

Fig. 1. Spectrum (curve 1) and first derivative spectrum (curve 2) of the reduced complex. Distance B—C is the measure of the phosphate amount present.

Fig. 2. Influence of the absorbance caused by turbidity on the distance B—C in the first derivative spectrum.

because phosphate in the sample may be adsorbed irreversibly to solid particles added to simulate turbidity. For this reason, clay minerals are unsuitable, although they are often present in naturally turbid samples. A good alternative is the finely divided barium sulphate that precipitates when barium chloride is added to the sample.

To investigate the influence of turbidity, various amounts of barium chloride solution were added to equal parts of the same sample, to give barium concentrations of 50—400 $\mu g\ ml^{-1}$ in the final solution. The derivative spectra were taken and the absorptions at 886 nm were measured. The absorbance caused by turbidity was obtained by subtracting the absorbance of an analogous phosphate solution without barium from the total absorbance. The results obtained in this way are presented in Fig. 2. It can be seen that absorbances up to 0.8 caused by turbidity do not affect the distance B—C in the derivative spectrum. Above the turbidity absorbance of 0.8, the noise becomes too high to obtain precise values.

Linearity of response. Derivative spectra were measured for solutions with phosphate concentrations in the range 0—4 mg l^{-1}. One series consisted of clear samples. The other series had enough barium chloride solution added to give an absorbance of 0.360 caused by turbidity at 886 nm. The results are given in Fig. 3. For both series, the relation between the distance B—C

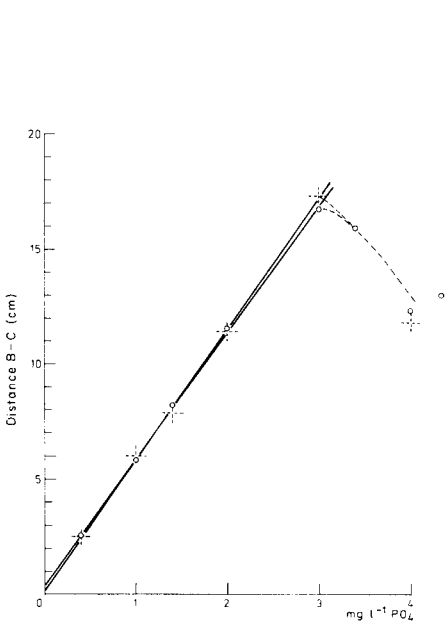

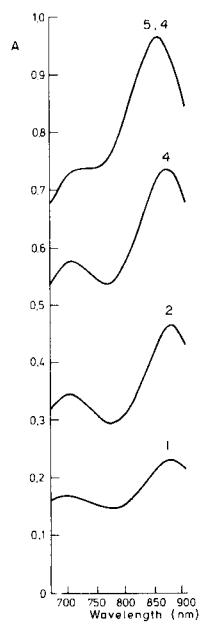

Fig. 3. Linearity of response for the first derivative method with 95% confidence intervals. For turbid solutions (+), $y = (5.67 \pm 0.32)x + (0.17 \pm 0.67)$. For clear solutions (○), $y = (5.47 \pm 0.22)x + (0.40 \pm 0.40)$.

Fig. 4. Absorbance spectra at the different phosphate concentrations (mg l^{-1}) indicated on the curves.

and phosphate concentrations is linear up to a concentration of 3 mg l^{-1}. Turbidity does not affect this relation. Unfortunately, errors may be introduced by measuring phosphate concentrations exceeding 3 mg l^{-1}; for instance, a sample with 4 mg l^{-1} gives the same B—C value as a sample with about 2.2 mg l^{-1}.

Application of the following precautions makes it possible to avoid such errors. First, with some experience, visual checking of the colour intensity allows a rough estimate of the phosphate concentration. Secondly, in a correct measurement, the $dA/d\lambda$ value at B will be about 0.4 times the absolute value at C (see Fig. 1). With turbidity present, this factor may change a little, but the value at B will never be less than 0.4 times the absolute value at C for phosphate concentrations of up to 3 mg l^{-1}. At phosphate concentrations exceeding 3 mg l^{-1}, the absorption peak at 720 nm in the spectrum decreases (Fig. 4); this lowers the value for $dA/d\lambda$ at B which will then be less than 0.4 times the absolute value at C. If possible, concentrations exceeding 2.5 mg l^{-1} should not be measured because checking is more difficult in that range. Of course, in cases of doubt, the determination can be repeated with a diluted sample; a sample diluted to half its phosphate concentration ought to give half the B—C value.

Recovery and accuracy. To a few samples which were turbid even after filtration, phosphate was added and the percentage recovery was calculated. The results presented in Table 1 show that recoveries are almost 100% with a standard deviation of 3%.

As mentioned above, the sample may sometimes become turbid after addition of the reagent. This happened in a sample of which a portion was acidified; the unacidified portion remained clear. With the method described, the turbid portion gave a phosphate concentration of 5.13 mg l^{-1}. The clear sample was analyzed normally, showing a concentration of 5.19 mg l^{-1}. This again shows that reliable results can be obtained by using the first derivative spectrum.

TABLE 1

Recovery of phosphate added to turbid water samples

Initial concentration (mg l^{-1})	Added phosphate (mg l^{-1})	Measured concentration (mg l^{-1})	Recovery (%)
7.8	5.00	12.9	101
1.33	1.00	2.28	98
0.05	0.80	0.86	101
0.05	1.20	1.25	100
0.05	1.60	1.67	101
0.04	0.80	0.82	98
0.04	1.20	1.18	95
0.04	1.60	1.71	104

The imprecision of the method described is about 4% which is more than that of the normal method (1—2%). However, turbid samples cannot be measured reliably by the normal method, so that the greater imprecision must be accepted.

REFERENCE

1 NEN 6479 (in Dutch), Nederlands Normalisatie Instituut, Delft, The Netherlands, November, 1981.

Analytica Chimica Acta, 156 (1984) 345—349
Elsevier Science Publishers B.V., Amsterdam — Printed in The Netherlands

Short Communication

A PROBLEM IN THE SPECTROPHOTOMETRIC DETERMINATION OF DISSOLVED TOTAL PHOSPHORUS IN BRACKISH ANOXIC WATERS

N. ICHINOSE*, H. KANAI and K. NAKAMURA

Department of Chemistry, Hamamatsu University School of Medicine, 3600 Handa-cho, Hamamatsu 431-31 (Japan)

C. SHIMIZU, H. KUROKURA and K. OKAMOTO

Fisheries Laboratory, Faculty of Agriculture, The University of Tokyo, Bentenjima Hamana-gun, Shizuoka-ken 431-02 (Japan)

T. INUI

Shizuoka Prefectural Industrial Research Institute, 550 Makigaya, Shizuoka 421-21 (Japan)

(Received 7th June 1983)

Summary. When dissolved total phosphorus in anoxic brackish waters was determined spectrophotometrically by the heteropoly molybdenum blue method after oxidation with potassium peroxodisulfate, negative dissolved organic phosphorus contents were obtained from the differences between the total phosphorus and inorganic phosphorus contents. A major cause of this inconsistency is coprecipitation of phosphate with the colloidal hydrated iron(III) oxide produced from iron in these waters, or the formation of iron(III) phosphate during the oxidation process. The problem can be avoided by oxidation with nitric and perchloric acids.

The bottom layer of brackish water (about 12 m down) around the center of Lake Hamana (Japan) is connected to a sea basin. Anoxic waters appear from this sea basin in summer because the hydrosphere in the basin becomes reducing as a result of few tidal currents and decomposition of dead marine organisms on the sea floor. Then, relatively large amounts of dissolved inorganic and organic phosphorus (0.02—0.20 mg l^{-1} as dissolved total phosphorus) appear in the anoxic waters. It was shown [1] that the content of dissolved organic phosphorus in such waters, calculated from the difference between the concentrations of the dissolved total phosphorus and inorganic phosphorus, was negative when the total phosphorus was determined by spectrophotometry [2] after oxidation with potassium peroxodisulfate [3, 4], which is a common procedure for natural waters. Later it became apparent from subsequent surveys of the anoxic waters that significant amounts of iron, particularly iron(II), as well as phosphates are washed from the sediments. A thorough examination was therefore undertaken to clarify the cause of the inconsistent errors obtained for dissolved organic phosphorus contents.

0003-2670/84/$03.00

Experimental

Apparatus. A Hitachi Model 100-50 double-beam spectrophotometer with 5-cm glass cells was used.

Reagents. An aqueous orthophosphate stock solution (100 mg l^{-1} P) was prepared from potassium dihydrogenphosphate (0.4349 g l^{-1}); working standards were prepared by appropriate dilution with water. For color reagent A, 62.5 ml of 2.5 M sulfuric acid and 18.75 ml of 4% ammonium molybdate solution were mixed thoroughly with 37.5 ml of an ascorbic acid solution (0.66 g of ascorbic acid, 12.5 mg of EDTA and 0.25 ml of formic acid per 250 ml), and 6.25 ml of potassium antimonyl tartrate solution (0.2743 g of the salt carefully dissolved and diluted to 100 ml with water). Color reagent B was the same as reagent A except that 62.5 ml of 1.25 M sulfuric acid was used. These reagents do not keep for more than 24 h.

Recommended procedures for anoxic waters. Filter the sample solution (1 l) through a Millipore filter (type HA, pore size 0.45 μm). Dry the precipitate on the filter at 110°C in air for 1 h, and weigh it to give a value for suspended solids (mg l^{-1}). Use this precipitate to determine suspended phosphorus (mg l^{-1}) by the method described below for total dissolved phosphorus.

To determine dissolved inorganic phosphorus, take 20.00 ml of the above filtrate in a 25-ml volumetric flask, add 4 ml of reagent A and dilute to the mark with water. Within 10—60 min, measure the absorbance of the solution at 867 nm in 5-cm glass cells against a reference containing 20 ml of the same filtrate diluted to 25 ml with water. For the calibration graph, the reference solution is pure water.

To determine dissolved total phosphorus, heat 20.00 ml of the above filtrate in a covered 50-ml glass beaker with 5 ml of concentrated nitric acid and 5 ml of 60% perchloric acid. After 30 min, remove the watch glass and heat until perchloric acid fumes have been removed. Cool the beaker to room temperature, and add 10 ml of water and 1 ml of 2.5 M sulfuric acid. Warm to dissolve the residue and transfer the solution to a 25-ml volumetric flask, washing with water. Dilute to about 20 ml with water, add 4 ml of reagent B, dilute to the mark with water, and mix thoroughly. Measure the absorbance at 867 nm.

Dissolved organic phosphorus is evaluated from the difference between the total and inorganic phosphorus contents.

Determination of dissolved total phosphorus by the peroxodisulfate method [1]. A portion (20.00 ml) of the above filtrate is heated with 10 ml of fresh 2% (w/v) potassium peroxodisulfate solution in a boiling water bath for 1 h. The color development is the same as outlined above.

Results and discussion

Co-existing iron in the anoxic waters was considered in examining the decomposition of dissolved organic phosphorus by the different procedures. The results obtained by applying the peroxodisulfate and nitric/perchloric

TABLE 1

The results obtained for anoxic waters at different water depths at the same station (No. 2, July 24, 1982) by different methods

Depth (m)	DO[a] (%)	pH	Temp. (°C)	Salinity (‰)	Fe found		Dissolved phosphorus found (μg P l^{-1})							
					Fe^{2+} (μg l^{-1})	Fe^{3+} (μg l^{-1})	Inorg.	Total		Organic		H.p.l.c.		
								$K_2S_2O_8$	$HNO_3/HClO_4$	$K_2S_2O_8$	$HNO_3/HClO_4$	Inorg.	Total	Org.
0	142	8.56	24.2	24.8	10	14	2	8	10	6	8	—	—	—
1	140	8.60	24.2	24.8	17	12	4	8	9	5	5	—	—	—
2	124	8.53	24.2	25.8	13	16	3	11	14	8	11	—	—	—
3	44	8.18	23.2	27.6	13	18	2	10	12	8	10	—	—	—
4	54	8.02	23.1	28.4	13	12	5	8	19	3	14	—	—	—
5	44	7.96	22.7	28.9	20	16	9	5	19	4	10	—	—	—
6	38	7.99	22.5	29.5	27	18	13	13	24	0	11	—	—	—
7	3	7.72	22.4	30.2	31	23	44	17	55	17	11	46	62	16
8	2	7.77	22.2	30.7	59	23	65	25	76	40	11	67	82	15
9	2	7.53	21.5	31.0	80	33	104	48	109	56	5	104	108	4
10	2	7.63	20.8	31.5	90	73	157	56	175	101	18	175	175	15

[a]Relative percent of dissolved oxygen in brackish water against a brackish water saturated by air.

acid oxidations are compared in Table 1. The samples were taken at different depths at the same station. Results obtained by high-performance liquid chromatography (h.p.l.c.) [5] are also given. As can be seen, dissolved organic phosphorus values obtained by oxidation with potassium peroxodisulfate are negative at the water depths of $\geqslant 5$ m, as reported previously [1]. With increasing depth, the concentrations of iron(II), iron(III) and dissolved inorganic phosphorus increase gradually, whereas the dissolved oxygen (DO) content decreases. In contrast, the dissolved organic phosphorus values obtained by oxidation with nitric/perchloric acids are positive regardless of the water depth and the values obtained after this oxidation generally agree closely with those obtained by the h.p.l.c. procedure; the latter was useful only for phosphorus contents exceeding 0.025 mg l^{-1}. On the basis of these results, the dissolved organic values obtained by oxidation with acids can be considered accurate and reliable.

The accuracy of the values for total phosphorus after the two oxidation procedures was tested by processing 20-ml portions of the anoxic waters, rich in iron, taken at a depth of 10 m, to which different amounts of orthophosphate and disodium phenylphosphate were added. The results in Table 2 show that the relative recoveries of total phosphorus after the peroxodisulfate oxidation were unsatisfactory; reproducibility was poor. Results obtained by acid oxidation were satisfactory.

To confirm the effect of iron, 20-ml portions of a synthetic aqueous solution containing iron(II) and different amounts of disodium phenylphosphate were taken through the procedures with peroxodisulfate and mixed acids. The results (Table 3) show that the peroxodisulfate oxidation was inaccurate even in the synthetic aqueous solution, though the control

TABLE 2

Recoveries of dissolved total phosphorus in anoxic waters[a] after addition of known amounts of phosphates

P added as	Amount added (μg P)	Dissolved total phosphorus					
		$K_2S_2O_8$ method			Mixed acids method		
		Found (μg P)	Initially present (μg l^{-1} P)	Recovery[b] (%)	Found (μg P)	Initially present (μg l^{-1} P)	Recovery[b] (%)
—	—	1.12	56	100.0	3.50	175	100.0
KH_2PO_4	0.25	1.74	75	134.0	3.73	174	99.4
KH_2PO_4	0.50	1.84	67	120.0	4.06	178	101.7
KH_2PO_4	0.75	2.34	80	143.0	4.23	174	99.4
KH_2PO_4	1.00	2.48	74	132.2	4.60	180	102.9
DPP[c]	0.25	1.70	73	130.4	3.77	176	100.6
DPP	0.50	2.18	84	150.0	4.10	180	102.9
DPP	0.75	2.18	72	128.6	4.25	175	100.0
DPP	1.00	2.28	64	114.3	4.46	173	98.9

[a]The sample solution used was from a depth of 10 m (Table 1); 20-ml portions were taken. The pH of each test solution after adding phosphorus to the sample solution was approximately 7.6. [b]Recovery of added phosphorus. [c]Disodium phenylphosphate.

TABLE 3

Recoveries of phosphorus from aqueous solutions with sodium diphenylphosphate and iron(II) added[a]

P added[b] (μg)	Fe added[c] (μg)	Phosphorus found			
		$K_2S_2O_8$ method		Mixed acids	
		(μg)	Recovery (%)	(μg)	Recovery (%)
0.00	—	—	—	—	—
0.25	—	0.23	92.0	0.24	96.0
0.50	—	0.50	100.0	0.52	104.0
0.75	—	0.76	101.0	0.75	100.0
1.00	—	0.97	97.0	1.00	100.0
0.00	3.26	—	—	—	—
0.25	3.26	0.14	56.0	0.24	96.0
0.50	3.26	0.35	70.0	0.49	98.0
0.75	3.26	0.42	56.0	0.73	97.3
1.00	3.26	0.52	52.0	1.02	102.0

[a]Each solution (20 ml) was adjusted to pH 7.6 with buffer solution (H_3BO_3/KCl/NaOH) before oxidation with peroxodisulfate or the mixed acids. This pH value and the amount of iron added corresponded to those in the anoxic waters at a depth of 10 m at Station 2 (Table 1). [b]As disodium phenylphosphate. [c]As iron(II) ammonium sulfate.

experiments without iron for both oxidations gave good recoveries. It is therefore clear that the main cause of the negative dissolved organic phosphorus obtained by the peroxodisulfate oxidation procedure was co-existing iron(II) and iron(III). Either iron(III) phosphate ($K_{so} = 10^{-17.3}$) was precipitated during the oxidation with peroxodisulfate, or some orthophosphate ion was adsorbed by hydrated iron(III) oxide formed during the oxidation. The problem can be avoided by using oxidation with mixed nitric and perchloric acids.

We thank Professor K. Yoshimura, Hamamatsu University School of Medicine, for his kind guidance, and Mr. H. Kumagaya for useful advice. This research was supported by a grant in aid of scientific research (1-R16-2) from the Japanese Government.

REFERENCES

1 N. Ichinose, C. Shimizu, H. Kurokura, T. Inui and K. Kadohata, Jpn. Analyst, 31 (1982) 532.
2 J. Murphy and J. P. Riley, Anal. Chim. Acta, 27 (1962) 31.
3 D. W. Mentzel and N. Corwin, Limnol. Oceanogr., 10 (1965) 280.
4 Japanese Government Office of Weather, Kaiyokansokushishin, Japanese Society of Weather, 1970, p. 191.
5 N. Sakurai, K. Kadohata and N. Ichinose, Z. Anal. Chem., 314 (1983) 634.

ANALYTICA CHIMICA ACTA, VOL. 156 (1984)

AUTHOR INDEX

(Continued from inside back cover)

0003-2670/84/$03.00

Printed in The Netherlands

(Continued from outside back cover)

(Continued on p. 356)

CONTENTS

(Abstracted, Indexed in: Anal. Abstr.; Biol. Abstr.; Chem. Abstr.; Curr. Contents Phys. Chem. Earth Sci.; Life Sci.; Index Med.; Mass Spectrom. Bull.; Sci. Citation Index; Excerpta Med.)

(Continued on inside back cov